

7. UNSATURATED- AND SATURATED-ZONE FLOW AND TRANSPORT

*S. David Sevougian, Srikanta Mishra, Yanyong Xiang, Bryan E. Dunlap,
James O. Duguid, James E. Houseworth*

7.1 INTRODUCTION

The unsaturated- and saturated-zone flow and transport models used in TSPA-1995 are described in this chapter. Results from detailed process-level models were used to develop abstractions (response surfaces) for implementation in RIP. Section 7.2 presents the process-level modeling and abstraction of those results for the mountain-scale, unsaturated-zone flow system. Details of the drift-scale, unsaturated-zone hydrologic modeling of "dripping fractures" at the repository level are presented in Section 7.3, including a discussion of how this is incorporated into the RIP TSPA model. In Section 7.4, the unsaturated-zone transport model for TSPA-1995 is presented. Because the process-level transport model for Yucca Mountain was incomplete at the time TSPA-1995 simulations were conducted, the TSPA-1995 transport model is implemented directly in the RIP simulator. The TSPA-1995 transport model includes some abstractions based on the process-level flow model (e.g., the matrix and fracture steady-state velocity fields and the partitioning of total flow between fractures and matrix). It also includes a fracture/matrix interaction model to represent matrix imbibition and intra-unit fracture connectivity, and retardation models to represent chemical interactions between matrix and pore water. A brief comparative study of the TSPA RIP transport model with the FEHM process-level transport model is included at the end of Section 7.4. Transport of gas-phase radionuclides is discussed in Section 7.5. A brief discussion of the saturated-zone model is included in Section 7.6, though this has not changed substantially since TSPA-1993. Finally, a climate change model implemented in TSPA-1995 is described in Section 7.7.

As indicated in Figure 7.1-1, the results of the response surfaces described in the present chapter feed into the determination of engineered-barrier-system releases as well as the determination of cumulative releases and peak doses at the accessible-environment boundary.

7.2 UNSATURATED-ZONE AMBIENT HYDROLOGY

7.2.1 Introduction

If radionuclides are released from the engineered barrier system, they may be advectively transported first through the unsaturated zone and then the saturated zone to the accessible environment. Section 7.2 describes the process-level model used to simulate the flow of ground water in the unsaturated zone (UZ) at Yucca Mountain. The results from this model of UZ flow are abstracted to provide response surfaces of the aqueous flux in the unsaturated zone as a function of infiltration, and the distribution of this flux between fractures and matrix.

As indicated in Figure 7.1-1, the fundamental sources of information used to construct the unsaturated-zone flow model are derived from the results of site investigations that have been summarized in Chapter 2. The quantitative analyses presented in this section are carried out

using 1-D and 2-D submodels extracted from the 3-D site-scale model of the unsaturated zone at Yucca Mountain (Wittwer et al., 1995).

7.2.2 Abstraction Strategy for TSPA-1995

Within the context of TSPA-1995, it is not possible to directly incorporate process-level models, in general, and unsaturated- and saturated-zone flow and transport models, in particular, explicitly in the analyses. Although this is possible conceptually by using "call" statements to the process-level model, in practice this is prohibited by the tremendous increase in computational requirements when conducting multiple stochastic realizations. As a result, a limited set of process-model representations are constructed and the resulting predictions of flow are abstracted for input to the total-system simulation software, RIP. These abstractions are presented in the form of response surfaces describing the relation between the key dependent variables (whether flux or velocity or percent of total flux in different flow regimes) and the primary independent variables (infiltration rate or hydrogeologic properties). In using abstracted model results as input to the total-system model, it is important to demonstrate that the results of the detailed process model and the abstracted model are reasonably similar. A paradigm for the testing of process-model abstractions is illustrated in Figure 7.2-1 (Nelson, 1995).

Figure 7.2-2 presents a schematic representation of the distribution of the applied infiltration over Yucca Mountain which is the basis for the abstraction strategy used in TSPA-1995. This figure identifies those components of flux that may impact the total system performance. Starting with the average annual-precipitation value (q_{ppt}), the spatially variable infiltration rate (q_{inf}) is derived from the distributions presented by Flint and Flint (1994). The infiltration rate is redistributed across each major hydrostratigraphic interface into the percolation flux (q_{perc}). The percolation flux is considered to be spatially variable across the repository area and may be uncertain because of anisotropy and heterogeneity within the unsaturated hydrostratigraphic units between the surface and the repository horizon [in particular within the basal vitrophyre of the Tiva Canyon welded unit (TCw) and the Paintbrush nonwelded unit (PTn)]. As described in Section 7.3, this uncertainty is evaluated in TSPA-1995 by using two separate percolation-flux distributions: one representing a spatially integrated average percolation flux (caused by significant lateral spreading of the infiltrating ground water); and the other representing a local percolation flux equivalent to the local infiltration rate (caused by a predominantly vertical flow).

The percolation flux is used to define the distribution between the fracture and matrix components of flow in the unsaturated zone beneath the repository; shown as q_{frac} and q_{mat} , respectively, on Figure 7.2-2. This distribution is based on process-model results described in this section. Additionally, the distribution of percolation flux at the repository horizon has been used to define the likelihood and magnitude of localized flow which might intersect the drifts; termed q_{drip} on Figure 7.2-2. The determination of the q_{drip} distribution is based on stochastic representations of both q_{perc} and the saturated hydraulic conductivity, K_{sat} , of the Topopah Spring welded unit (TSw), as described in Section 7.3.

The abstraction strategy employed in the previous iteration of TSPA (TSPA-1993: Andrews et al., 1994) is briefly reiterated here to provide a framework for changes made in the current iteration. The percolation flux through the unsaturated zone, q_{perc} , was sampled in TSPA-1993

from an exponential distribution with a mean value of 0.5 mm/yr. Assuming an equivalent continuum model for flow and transport, the matrix pore velocity (v_{mat}) was then determined as:

$$v_{mat} = q_{perc} / [A\phi S_{liq}] \quad (7.2-1)$$

where A is the cross-sectional area of the pathway of interest, ϕ is porosity and S_{liq} is liquid saturation. For each hydrostratigraphic interval, porosity was sampled from a normal distribution with prescribed mean and variance, while an "average" liquid saturation was calculated from the late-time ($t > 10,000$ yr) results of a far-field thermohydrologic model. The main limitation of this approach is that the physical relationships between the key variables are not rigorously honored, in as much as q_{perc} and ϕ are sampled independently, and S_{liq} is obtained from another set of calculations. Furthermore, parametric uncertainties (e.g., saturated conductivity, van Genuchten parameters), as well as conceptual uncertainties (e.g., alternative conceptual models of fracture-matrix flow), cannot be taken into account when using Equation 7.2-1.

The abstraction strategy for TSPA-1995 is designed to overcome the shortcomings identified in TSPA-1993 via the application of detailed process-level modeling to develop a functional relationship between v_{mat} and q_{inf} . Also developed in this strategy is a partitioning of the imposed flux between the fracture and matrix, characterized by the fractional fracture flux, f_{frac} . Multiple unsaturated-flow simulations are conducted to account for: (i) a range of infiltration scenarios, (ii) uncertain/variable matrix hydrologic properties, and (iii) variable fracture-flow initiation rules. The abstracted results are shown in terms of "bands" for v_{mat} and f_{frac} as functions of the imposed infiltration flux, q_{inf} .

The application of this abstraction strategy is shown in Figure 7.2-3. Within RIP, infiltration rate, q_{inf} , is treated as a stochastic parameter with a prescribed statistical distribution and its moments. For a given sampled value of q_{inf} , the types of relationships shown in Figure 7.2-3 are used to determine the corresponding minimum and maximum values for v_{mat} (or f_{frac}). Treating these as the lower and upper bounds for a uniform distribution, a second random sampling between the minimum and maximum provides the value for v_{mat} (or f_{frac}). (A more detailed explanation of the implementation in RIP is given in Section 7.4.4).

Implicit in this strategy is the assumption that descriptions of ambient hydrology are adequate for modeling geosphere flow and transport. This implies that thermohydrologic perturbations due to waste emplacement have dissipated before the arrival of radionuclides from breached waste packages at the EBS/geosphere boundary. Consequently, functional relationships between v_{mat} (or f_{frac}) and q_{inf} derived from ambient-state simulations, with appropriate modifications for climate change, can be used to simulate the flow of water in the unsaturated zone, and can be incorporated into models of the migration of radionuclide from breached waste packages.

7.2.3 Testing of the Proposed Abstraction Methodology

In order to demonstrate that the abstraction methodology as outlined in the previous section provides reasonable bounds on system behavior, it is necessary to "test" the methodology by comparing the abstracted model results against a more detailed representation. As an initial step in this testing, the results of a two-dimensional (2-D) flow model for the unsaturated zone are compared against the one-dimensional (1-D) simplification used in RIP. The performance

measure for comparison will be the travel time of an unretarded species from the repository to the base of the unsaturated zone (water table).

The detailed process model is a 2-D cross-section extracted from the LBL-USGS site-scale model of the unsaturated zone (Wittwer et al., 1995), described in detail in Section 7.2.4. Deterministic steady-state simulations were carried out for three different infiltration rates (0.1, 0.5 and 1.0 mm/yr) using the expected values of the material properties given in Section 2.4. Column 153 was then picked as a representative one-dimensional pathway from the 2-D cross-section (Figure 7.2-4). For each hydrostratigraphic unit below the proposed repository horizon, the simulated ranges in the matrix pore velocity, v_{mat} , and fractional fracture flux, f_{frac} were extracted (Table 7.2-1). Also calculated, based on the velocity information, was the advective travel time from the proposed repository horizon to the water table.

A 1-D pathway, consistent with that section of Column 153 between the proposed repository horizon and the water table, was setup within RIP. This pathway was broken up into four layers as follows: TSw - 111.2 m, TSv - 8.4 m, CHnv - 80.7 m, and CHnz - 121.2 m. The advective transport of a tracer pulse was simulated for each of the three chosen infiltration rates using the abstracted information (v_{mat} and f_{frac}) for each hydrostratigraphic unit. The choice of a finite pulse (with $\Delta t=100$ yr) was dictated by the need to start with a finite time-step size which could then be progressively increased so as to efficiently simulate transport over extremely long time periods ($\sim 10^5$ years). The minimum and maximum arrival times of the pulse were determined by examining its breakthrough curve at the water table.

A comparison between the single-point arrival time calculated by TOUGH2 and the minimum and maximum arrival times calculated by RIP is tabulated in Table 7.2-2, and also shown graphically in Figure 7.2-5. In all cases, the RIP results bracket the arrival times calculated by TOUGH2, and the agreement was found to be better for higher infiltration rates. These calculations indicate that using TOUGH2-derived functional relationships of v_{mat} and f_{frac} vs. q_{inf} to simulate solute transport within RIP is an expedient way of retaining the essential features of the unsaturated-flow process. The calculations also provide a verification for the proposed abstraction methodology.

7.2.4 Process-level Model Description

Background

A three-dimensional site-scale model of the unsaturated zone is currently under development by Lawrence Berkeley Laboratory (LBL) and the United States Geological Survey (USGS) (Wittwer et al., 1995). The model covers an area of about 30 km² (Figure 7.2-6), and is composed vertically of four hydrogeologic units: TCw (Tiva Canyon welded), PTn (Paintbrush nonwelded), TSw (Topopah Spring welded), and CHn (Calico Hills nonwelded). These four layers have been further subdivided into seventeen layers to represent additional lithologic detail (Figure 7.2-4). Based on the work of Klavetter and Peters (1986), the fractured units TCw and TSw are treated as equivalent continua with specified threshold saturations for triggering liquid flow in fractures. Using a "best-guess" set of hydrologic properties for the matrix and fractures, Wittwer et al. (1995) have investigated the impact of uniform/non-uniform surface infiltration patterns and the

role of major faults on the distribution and movement of moisture at Yucca Mountain in one, two, and three dimensions.

As pointed out by Andrews et al. (1994), some of the major uncertainties associated with the description of the hydrologic system in total system performance assessments include: (i) uncertainty in the assumed infiltration scenarios for both current and future climatic conditions, (ii) the impact of uncertain and/or spatially variable matrix hydrologic properties, and (iii) conceptualizations of fracture-matrix flow using both equilibrium and non-equilibrium assumptions. These uncertainties have not been explicitly addressed in the ongoing studies of ambient UZ hydrology being carried out by the LBL-USGS scientists. A suite of simulations has therefore been carried out with the LBL-USGS model to incorporate the effects of these uncertainties on the ambient unsaturated-flow regime, and to provide the abstractions of unsaturated hydrology needed by the geosphere-transport module of RIP.

Geometry and Boundary Conditions

A series of simulations will be discussed, based on one- and two-dimensional models. The one-dimensional model is a vertical column, and the two-dimensional model is a vertical cross-section, extracted from the LBL-USGS three-dimensional site-scale model (Wittwer et al., 1995). The cross-sectional model, as shown in Figure 7.2-4, passes through the potential repository area and the Ghost Dance Fault. The left and right boundaries represent the Solitario Canyon fault and the Bow Ridge fault, and are assumed to be of the no-flow type. The one-dimensional model is chosen as Column 153 shown in Figure 7.2-4.

The top boundary (ground surface) is treated as a single-phase air surface at constant pressure and temperature. The bottom boundary (water table) is treated as a single-phase liquid surface also at constant pressure and temperature. Note that the constant pure-air condition at the ground surface precludes any possibility of moisture flow above the mountain, which may induce errors that are negligible for moderate infiltration rates but can become significant for very small infiltration rates. The water-table boundary condition implies that the saturated zone acts as a sink of infinite capacity, which may be inconsistent for relatively high infiltration rates depending on the transmissive properties of the saturated zone.

Infiltration Scenarios

As noted in Section 2.6, developing a reasonably representative estimate of the average infiltration rate in any particular area of an arid environment is uncertain. At present, a range of estimates exists depending primarily on the hydrogeologic characteristics of the outcropping hydrostratigraphic units. The uncertainty in these estimates has, to date, not been quantified, nor has the effect of other surficial characteristics (including slope, vegetation, and soil cover to name a few) been quantified. Several methods are being used to better represent the spatial-infiltration distribution, including (1) development of a map of current net infiltration based on ten-year average field observations, (2) development of a numerical model based on both deterministic and stochastic processes that can best reproduce that map, and (3) using this model to predict the effects of past and future climate scenarios with changeable soil, vegetation and atmospheric conditions (Flint, 1995). The results of these methods are expected to be completed and documented in the coming fiscal year.

In the absence of definitive estimates of spatial infiltration rates, preliminary estimates documented in Flint and Flint (1994) have been used. As shown in Figure 2.6-2, these inferred infiltration rates range from 0.02 mm/yr, where the welded Tiva Canyon (TCw) unit outcrops, to 13.4 mm/yr in areas where the Paintbrush nonwelded (PTn) unit outcrops. Neglecting the Paintbrush outcrop along the escarpment of the Yucca Crest, the bulk of the area above the repository block is dominated by the outcrop of the Tiva Canyon. If the predominant flow direction is vertical, then the average percolation flux through the repository block, assuming the inferred infiltration rates presented in Flint and Flint (1994), would be 0.02 mm/yr—a value quite consistent with liquid saturations predicted using one-dimensional flow models and representative hydrogeologic properties. If, on the other hand, the predominant flow direction is not vertical but has a significant lateral component due to hydrogeologic property heterogeneity and/or anisotropy and the sloping nature of the hydrostratigraphic unit contacts, then the average net infiltration rate over the repository block could be as high as some weighted average of the infiltration rates inferred from Flint and Flint (1994). Again, neglecting the area of Paintbrush outcrop along the Yucca Crest escarpment, the average spatially integrated infiltration rate is about 1.2 mm/yr. Most of this infiltration occurs along the Paintbrush outcrop in the washes north of the repository block.

Based on the above discussion, TSPA-1995 assumes two possible infiltration regimes. At one extreme (the "low" infiltration case), the infiltration rate at the surface is expected to be uniformly distributed between 0.01 and 0.05 mm/yr—assuming roughly a factor of 2 uncertainty around the mean value of 0.02 mm/yr. At the other extreme (the "high" infiltration case), the surface infiltration rate is expected to be uniformly distributed between 0.5 and 2.0 mm/yr—also assuming roughly a factor of 2 uncertainty around the mean value of 1.2 mm/yr. In order to bound the effect of these ranges of infiltration scenarios, hydrologic simulations have been carried out for six discrete cases corresponding to the limits described above, i.e., at 0.01, 0.02, 0.05, 0.5, 1.0 and 2.0 mm/yr.

Matrix and Fracture Properties

The hydrogeologic database developed by Schenker et al. (1995), which is described in greater detail in Section 2.4, is used as the source for matrix and fracture properties for the hydrogeologic units at Yucca Mountain. Because the Schenker et al. data set includes the latest available information from ongoing site characterization activities, it has been chosen in preference to the "best-guess" hydrologic parameter set used in the LBL-USGS site-scale model (Wittwer et al., 1995).

In order to account for the uncertainty/variability in matrix hydrologic properties, ten random sets of properties have been generated using the summary statistics presented in Chapter 2.4. Figure 7.2-7 shows the values of the sampled variables together with the range and the expected values (arithmetic mean or geometric mean, as appropriate). In the hydrologic simulations, the properties for the hydrogeologic units above the repository horizon (TCw, PTn) are kept fixed at their expected values. As discussed in Section 2.4, residual saturation is treated as a constant for each unit, and fracture properties are treated as constants for all the units.

Fracture Flow Initiation Rules

The LBL-USGS site-scale model conceptualizes the fractured units at Yucca Mountain as equivalent continua with thermal and hydraulic equilibria between fracture and matrix (Wittwer et al., 1995). The equivalent continuum model (ECM) assumes the existence of enormous disparity in capillary suction between the matrix and the fractures. Thus, during drainage, matrix desaturation does not begin until the fractures are almost completely drained, whereas during imbibition, the fractures remain dry until the matrix is almost completely saturated. In the TOUGH2 implementation of the ECM (Tsang and Pruess, 1989), liquid flow in the fractures is assumed to be initiated only after bulk-liquid saturation exceeds a threshold value corresponding to full saturation of the matrix. This rule can be expressed as follows: if the matrix liquid saturation equals 1.0, then fracture flow may occur (i.e., the fracture liquid saturation is greater than 0.0), otherwise the fracture liquid saturation equals 0.0.

There is growing evidence to suggest that episodic water flow at Yucca Mountain may take place along "fast paths" (Wittwer et al., 1995). Such a situation, which possibly results from non-equilibrium fracture flow, cannot be represented by the equivalent continuum model (ECM). By forcing the fractures to remain dry until the matrix is fully saturated, the ECM formulation artificially inhibits the episodic (and rapid) movement of water along these fast paths. The rigorous approach to incorporating such non-equilibrium flow aspects would require at least the use of a dual-continuum model. An alternative approach would be a relaxation of the fracture-flow initiation rule in the ECM in order to allow fracture flow to commence before complete matrix saturation.

With a view to approximating non-equilibrium fracture-matrix flow, Xiang et al. (1995) have proposed an empirical modification to the ECM fracture-flow initiation rule, viz., if the matrix liquid saturation is greater than or equal to σ , then fracture flow occurs (fracture liquid saturation greater than 0), otherwise the fracture liquid saturation equals 0.0. Here σ (≤ 1) is an empirical parameter, hereafter referred to as the "satiated" matrix saturation. This σ -based formulation forces the fractures to conduct water even before the matrix is fully saturated. However, it does not represent the complete dynamics of non-equilibrium flow because matrix imbibition is neglected. In any case, allowing the fractures to transmit fluids without requiring the matrix to be completely saturated is a more conservative model for fracture flow than the equivalent continuum model, from the standpoint of performance assessment.

The σ -based formulation is thus a preliminary method to simulate non-equilibrium fracture flow. In the present study, σ is treated as a sensitivity parameter, and provides an extra degree of freedom for the analyst to investigate the effects of a relaxed fracture-flow initiation criterion. However, it must be pointed out that this formulation does not include any consideration of matrix imbibition to retard fracture flow. It is intended to be merely a surrogate for a detailed representation of non-equilibrium fracture flow.

Further details of the σ -based formulation are discussed in Xiang et al. (1995), along with the results from numerical experiments which investigate the sensitivity to σ . Also presented therein is a comparison between 1-D calculations using a conventional dual-permeability model (Ho, 1995) and the empirical σ -based formulation. Based on these analyses, two values of σ (1.0 and 0.95) have been chosen as the two variants for fracture flow initiation in TSPA-1995. Numerical

experiments with σ values lower than 0.95 appear to result in an exaggeration of fracture flow (Xiang et al., 1995). For the purposes of this study, the value of $\sigma=0.95$ is taken to be a reasonable compromise in order to mimic the non-equilibrium flow effects of fracture flow initiation prior to full matrix saturation. Note that the value of 1.0 represents the classical ECM conceptualization, in which no fracture flow occurs until the matrix is fully saturated. A value for σ of 0.95 implies the onset of fracture flow as soon as matrix saturation equals 0.95.

7.2.5 Abstraction Results and Sensitivity Analyses

Results

Using the one-dimensional model corresponding to Column 153 in Figure 7.2-4, a total of 120 steady-state TOUGH2 simulations were carried out to develop the hydrologic abstractions. Note that the effects of dimensionality in the development of these abstractions is presented later in this section. As discussed previously, the cases considered here include: (i) ten random realizations of matrix hydraulic properties (Figure 7.2-7), (ii) six infiltration rates, i.e., 0.01, 0.02, 0.05, 0.5, 1.0 and 2.0 mm/yr, and (iii) two fracture flow initiation rules, i.e., σ values of 1.0 and 0.95. Matrix pore velocity, v_{mat} , and fractional fracture flux, f_{frac} along Column 153 are taken as the two performance measures. For each of the four hydrostratigraphic units below the potential repository horizon (TSw, TSv, CHnv, CHnz), ranges for v_{mat} and f_{frac} are tabulated as a function of the infiltration rate (q_{inf}) in Table 7.2-3 and Table 7.2-4. These results are also shown in Figure 7.2-8 through Figure 7.2-11.

The minimum and maximum values of v_{mat} for each infiltration rate are determined from the range of values resulting from simulations using the ten random sets of material properties and the two fracture-flow initiation rules. On the other hand, regarding f_{frac} , it is evident that its maximum value would always correspond to a σ value of 0.95, whereas its minimum value would always correspond to a σ value of 1.00. This argument is based on the following rationale. The ECM assumption regarding fracture-flow initiation only after full matrix saturation (i.e., $\sigma=1.0$) tends to minimize fracture flow, whereas using the lower value for σ of 0.95 as the fracture-flow initiation rule in the modified ECM formulation provides a more favorable condition for the onset and continuation of fracture flow. The minimum and maximum f_{frac} for a given infiltration rate are calculated by averaging over the simulations corresponding to the ten sets of random material properties. Given that not all realizations produce fracture flow, an ensemble average is necessary to provide an "expected" and unbiased measure of the fractional fracture flow for a given infiltration rate.

Sensitivity to Dimensionality of Flow

Wittwer et al. (1995) have investigated possible patterns of moisture flow within Yucca Mountain for assumed average infiltration rates, uniform/variable infiltration distribution and hydrologic characteristics of the major faults. Their simulations suggest that flow below the Paintbrush nonwelded (PTn) unit is mostly vertical, except in the immediate vicinity of the major faults. Although preliminary, these results provide some justification to the assumption of one-dimensional vertical flow routinely used in previous TSPA calculations (e.g., Andrews et al., 1994; Wilson et al., 1994).

To further examine the persistence of vertical one-dimensional flow in the vicinity of the proposed repository block, one- and two-dimensional steady-state flow simulations have been conducted for uniform infiltration rates of 0.01, 0.5, and 1.0 mm/yr. The two-dimensional model is the cross-section extracted from the LBL-USGS model as shown in Figure 7.2-4, from which Column 153 is extracted as the one-dimensional model. These deterministic calculations use the expected values of the hydrologic properties as tabulated in Table 7.2.1. Figures 7.2-12 and 7.2-13 demonstrate the general agreement between both sets of calculations in predicting liquid saturation in fracture/matrix, fraction of liquid flowing in the fractures, and liquid velocity in the matrix. These results provide further justification for using one-dimensional models of unsaturated flow in the vicinity of the repository block, albeit for steady-state conditions alone.

Representativeness of Column 153

In TSPA-1995, it is assumed that the ranges of matrix pore velocity and fractional fracture flux as derived for Column 153 (Figure 7.2-4) are representative of the entire repository block. In order to verify this assumption, the response of Column 157—located to the east of the Ghost Dance Fault as shown in Figure 7.2-4—is compared to that of Column 153. Simulations were carried out for two infiltration rates, 0.01 and 1.0 mm/yr, using the expected values of the matrix hydraulic properties tabulated in Section 2.4. As shown in Figure 7.2-14, matrix pore velocities for Column 153 and Column 157 are in excellent agreement for all four hydrostratigraphic units. Although not shown here, similar results have been obtained in comparisons between Column 153 velocities and those of columns located to the west of the Ghost Dance Fault within the repository block.

7.2.6 Abstraction Caveats

In the above sections, a methodology for developing abstractions of the ambient unsaturated-zone hydrology at Yucca Mountain has been described, tested, and implemented. The methodology is customized to the input needs of the total system simulator, RIP, and as such, provides "response functions" for matrix pore velocity and fractional fracture flow. These variables are required inputs to the geosphere-transport module of RIP. Using multiple deterministic simulations, the methodology provides tables of minima and maxima for uniform distributions of the variables of interest as functions of infiltration rate. The distributions account for the uncertainty in material properties, as well as the uncertainty in describing fracture-matrix flow.

The methodology presented herein is a preliminary attempt at rigorously developing and applying abstractions which are based on detailed process-level model calculations. However, several simplifications inherent in these calculations need to be improved in order to further enhance the realism of the unsaturated-zone hydrologic abstractions for future TSPAs. Some of these issues are identified below:

- Although a modified ECM formulation facilitating earlier initiation of fracture flow was used in these analyses, better models are needed to describe non-equilibrium fracture-matrix interaction.
- The assumption that ambient hydrologic models are adequate to model radionuclide transport at late time, because thermal effects due to waste emplacement are likely to have

dissipated, needs further examination. In particular, comparing the onset of unidirectional flow from the repository horizon to the water table predicted by thermohydrologic models with typical waste-package failure-time distributions should provide a sound basis for evaluating this assumption.

- Preliminary model calculations show that flow from the repository horizon to the water table is predominantly one-dimensional in the vertical direction (Wittwer et al., 1995). The actual flow paths are likely to be somewhat more tortuous under the effects of material heterogeneity and/or nonuniform infiltration rate at the surface. Incorporation of the resulting flow-path geometry directly into the TSPA calculations, or indirectly via appropriate abstractions, needs to be included in future analyses.
- The validity of the abstractions depends on the representativeness of the stratigraphy and hydrologic properties. This could be enhanced—especially in the expansion areas—by using more detailed hydrogeologic information (if and when available).

7.3 DRIFT-SCALE HYDROLOGY

Besides the model for unsaturated-zone flow at the "mountain-scale", a flow model is required to describe groundwater movement at the "drift-scale". This model predicts spatial variability of fracture flux (or "drips") intersecting potential repository drifts, and quantifies the probability of "drips" and the magnitude of any "drips" that are predicted to occur.

Water saturation in the EBS (backfill/invert) and near-field tuff matrix surrounding the repository drifts is determined from thermohydrologic process-level simulations conducted using FEHM (see Chapter 4). For the high thermal loading case (83 MTU/acre), there is an extended dryout period during which no stagnant fluid phase is present adjacent to the waste package. Therefore, no aqueous-phase radionuclide transport to the geosphere is possible through the rock matrix surrounding the waste packages. During this period, the only possible transport of radionuclides from waste packages to the geosphere will be a result of water dripping through fractures onto the packages. Once the rewetting front has returned to the packages (at $T < 100^{\circ}\text{C}$), or if the EBS never dries out (low thermal load, 25 MTU/acre), then transport to the geosphere is by a combination of both dripping fractures and diffusive matrix flow. Of course, the packages must first suffer corrosion failure before any radionuclides are released. [Note that transport from the packages to the geosphere by advective matrix flow is not considered possible because of the capillary pressure differential between the drift and the surrounding rock.]

The conceptual model for dripping water on the waste packages simulates spatial variability of fracture flow in the near-field rock surrounding the repository drifts. Thus, while the statistical variation in the process-level conceptualization of geosphere fracture flow (discussed in the previous section) is primarily attributable to property *uncertainty*, the variation in the conceptualization of WP/EBS dripping fracture flow is conceived to arise primarily from property *spatial variability*. This conceptual difference is appropriate because of the distance scale at which the processes are simulated. For the WP/EBS, effects are modeled at the scale of the package dimensions, whereas in the geosphere the variability in flow at the package level has been upscaled (averaged) to a much greater area. This is done, in part, because of computational constraints, in that it is not possible to simulate small-scale (on the order of the package

dimensions) heterogeneities over the entire repository within a TSPA model—given the large number of realizations required. Thus, in the geosphere we only consider the average fracture flow at the column scale—which does incorporate uncertainty, as described in the previous section on hydrological process abstractions.

In the WP/EBS fracture-flow conceptualization (see Figure 7.2-2), it is assumed that a given infiltration flux, q_{inf} , can be represented at depth as percolation flux, q_{perc} , log-normally distributed over the area of a given column. The logarithmic q_{perc} distribution is defined with a mean equal to the given q_{inf} and an assumed standard deviation of 0.5. Furthermore, from Schenker et al. (1995)—as tabulated in Table 2.4-3—we have the moments of the saturated matrix conductivity, K_{sat} , for TSw as: $E[\log_{10}K_{sat}] = 4.07$, and $S.D.[\log_{10}K_{sat}] = 0.9$. (Note that K_{sat} is now expressed in mm/yr.) Suppose there are 10,000 waste packages and that each has a different degree of fracture flow because of variability in the local matrix material properties. Both the q_{perc} and K_{sat} distributions are sampled 10,000 times to form a distribution for $(q_{perc} - K_{sat})$. For any individual package, if $(q_{perc} - K_{sat}) > 0$, then there is dripping flow on that package, and the value of $(q_{perc} - K_{sat}) = q_{drip}$ is the dripping flux in mm/yr. In this way, we develop empirical distributions for the advective dripping flux, q_{drip} , at various infiltration rates; plus a corresponding fraction (i.e., number, *not* distribution) of waste packages, f_{drip} , that experience dripping flow. Figures 7.3-2 and 7.3-4 show the q_{drip} distributions for typical "high" and "low" values of q_{inf} , and Figures 7.3-1 and 7.3-3 show the corresponding K_{sat} distributions. (K_{sat} would equal the matrix flux in the drift for this simple unit-gradient model, but because of the assumed capillary effect, matrix flow directly on the packages is presumed to be zero.) As an example of the meaning of these CDFs, in Figure 7.3-4, which is for $q_{inf} = 0.05$ mm/yr, 91% of the packages have a dripping flux less than 10^{-4} mm/yr, i.e., essentially zero dripping flux.

Because the RIP model does not allow f_{drip} to be a random variable, we could not use a random distribution to represent $q_{perc} - K_{sat}$, i.e., we could not regenerate it for every realization. Therefore, the q_{perc} and K_{sat} distributions were sampled 10^6 times for a given value of q_{inf} . The mean of this sample is an estimate of the expected value, $E[q_{drip}]$, of q_{drip} for the given q_{inf} and the fraction of waste packages with dripping is an estimate of the expected value, $E[f_{drip}]$, of f_{drip} . This was done for about 10 values of q_{inf} over both the low and high q_{inf} ranges, and the functional relationships $E[q_{drip}]$ versus q_{inf} and $E[f_{drip}]$ versus q_{inf} were found to be nearly linear for each range. Based on these samples, Figures 7.3-5 and 7.3-6 show the average dripping flow, $E[q_{drip}]$ vs. q_{inf} , that was used in the TSPA-1995 simulations using the Schenker et al. (1995) K_{sat} distribution and $S.D.[\log_{10}q_{inf}] = 0.5$. Figures 7.3-7 and 7.3-8 show the average fraction of packages with drips, $E[f_{drip}]$ vs. q_{inf} .

Using $E[q_{drip}]$ for every package results in approximately the same releases as applying the distribution of q_{drip} to the packages. To demonstrate this, six values of q_{drip} were selected which would represent the range of advective drip rates corresponding to the range of infiltration flux considered in the low- and high-infiltration rate cases (see Figures 7.3-5 and 7.3-6). Using 41 m² for our "catchment area" (see below), these advective drip rates correspond to advective flow rates, Q_{drip} , of 4×10^{-1} , 4×10^{-2} , 4×10^{-3} , 4×10^{-4} , 4×10^{-5} , and 4×10^{-6} m³/yr for each of the waste packages that sees dripping. RIP was run with each of these advective flow rates (with $f_{drip} = 0.5$, i.e., half of the packages dripping) and a diffusive release rate of 6.1×10^{-5} m³/yr, and two radionuclides were considered: ²³⁹Pu, which has a relatively low solubility, and ⁹⁹Tc, which has a relatively high solubility.

For solubility-limited radionuclides, such as ^{239}Pu , Figure 7.3-9 shows that the release rate is proportional to the total flow rate. Thus, averaging the total flow rate over the packages that see dripping will be equivalent to averaging the release rate over these packages, showing that the release rate is not affected by using $E[q_{\text{drip}}]$ for all packages.

Figure 7.3-10 shows the release rates for ^{99}Tc , a radionuclide that is not solubility-limited. The three curves corresponding to the high infiltration rates superimpose. This shows that for high infiltration rates the release rate is bounded by the amount of available ^{99}Tc , i.e., it is controlled by the waste-form dissolution rate. Thus, the total flow rate does not matter, and using $E[q_{\text{drip}}]$ will have little effect. For the three curves corresponding to the low infiltration cases, it can be seen that the curve corresponding to the middle flow rate is generally about equidistant between the other two curves. This suggests that averaging the total flow rates will have an effect close to averaging the release. Therefore, when the release is either flow-rate controlled or dissolution-rate controlled, or in between these two extremes, Figure 7.3-10 suggests that using $E[q_{\text{drip}}]$ for all packages is reasonable.

To get the total volumetric flow, Q_{drip} , onto each waste package, the effective "catchment area" is computed as twice the package length times twice the package diameter. Therefore, $Q_{\text{drip}} = 4A_{\text{wp}}q_{\text{drip}}$, where A_{wp} is the maximum cross-sectional area of the waste package, perpendicular to flow. Once the first pit goes through both the inner and outer waste-package containers (and also the cladding), it is assumed that all of the waste-form area is exposed to dripping flow. This is the assumption made in the so-called "drips-on-waste-form" model of EBS transport—the default model used for all RIP simulations (see Chapter 9). This is a more conservative (pessimistic) assumption than the diffusive-release model, for which diffusive release is a function of the pitted area. For other models of EBS transport, specifically, the "drips-on-waste-container" model (see Chapters 6 and 9), the drips do not contact the waste directly, but only the waste-package outer surface—pits in the waste container are assumed to be filled with corrosion products that do not allow direct contact of the dripping flux with the waste form. Thus the radionuclides must first diffuse through the corrosion-filled pits in the waste package before they interact with the dripping flow. A sensitivity analysis comparing these two models is presented in Chapter 9.

As discussed in Chapters 8 and 9, without dripping fractures, aqueous-phase radionuclides leave the near-field environment at very low concentrations. This is because diffusive releases are quite low. It shows that, if an effective capillary barrier could be constructed (one that could intercept even dripping fractures), then the repository would reduce releases/doses by several orders of magnitude compared to the drip scenario. (**Note:** There is still diffusive transport across the EBS when dripping water is present, however, it is negligible when compared to the advective releases. The diffusion model used is discussed in Section 6.5.)

The effect of climate change on dripping flow in the near-field is discussed in Section 7.7.

7.4 UNSATURATED-ZONE TRANSPORT

7.4.1 Introduction

At the time of the TSPA-1995 simulations, the Yucca Mountain process-level aqueous-transport model was incomplete (Robinson et al., 1995). Thus, unlike the TSPA-1995 UZ flow model, which is based on abstracted process-level model results, the TSPA transport model is incorporated directly into the RIP TSPA model. It is partly based on the abstractions from the process-level flow model (i.e., the matrix and fracture velocity fields and the partitioning of volumetric flow between fractures and matrix), but also includes a fracture-matrix interaction model (to represent intra-unit fracture connectivity and matrix imbibition) and a radionuclide retardation model (to represent chemical interaction between the matrix and pore water), neither of which is based on process-level transport modeling (although the chemical retardation model is based on LANL experiments on whole tuff samples).

7.4.2 Unsaturated-Zone Transport Stratigraphy and Model Dimensionality

For TSPA-1995, transport simulations have been conducted using the stratigraphy from the USGS/LBL unsaturated-zone site-scale model (Wittwer et al., 1995). Because of the intensive computational nature of performing multiple realizations, the numerical grid of the USGS/LBL process-level model must be averaged to a much larger scale for use in the RIP TSPA model. This involves both areal and vertical spatial averaging. The vertical averaging is natural, since although the USGS model has 8 units below and including the repository horizon, the material properties assigned to several units are about the same, and lead to a natural division into four hydrogeologic units below the repository—TSw (Topopah Spring welded-devitrified), TSv (Topopah Spring welded-vitrophyre), CHnv (Calico Hills nonwelded-vitric, and CHnz (Calico Hills nonwelded-zeolitic). These are the hydrogeologic units used within the process-level flow simulations that provide velocity distributions for RIP transport simulations (see Figure 7.2-2). Although this division of units within the site-scale flow model is sufficient for simulating water movement, there is a significant amount of Prow Pass (PP) formation below the CHnz and above the water table, which has different sorption properties than the CHnz. Therefore, for the purposes of radionuclide transport, the CHnz from the USGS/LBL model is subdivided into CHnz and Ppn (nonwelded-devitrified) units (see Table 7.4-1).

7.4.3 RIP Geosphere Pathways

The RIP TSPA code considers radionuclide transport to be one-dimensional (1-D), i.e., the RIP transport abstraction solves an advection-only or an advection/dispersion equation in 1-D. However, many 1-D aqueous-transport paths may be included in the problem domain to approximate 2-D or 3-D aqueous transport. For the RIP simulations in this report, 3-D aqueous transport in the unsaturated zone is simulated by either six 1-D vertical columns (high thermal load) or ten 1-D vertical columns (low thermal load), covering the area of the potential repository (see Section 3.8 for details regarding pathway geometry). As discussed in Section 7.2, 2-D effects on flow were considered when deriving the velocity and fracture-flow abstractions.

Each of the UZ vertical columns in RIP is represented as a series of "stacked" flow pathways (Figure 7.4-1). As described in Table 7.4-1, each UZ column consists of five pathways of

differing thickness from column to column: TSw, TSv, CHnv, CHnz, and PPN. All columns empty into one saturated-zone (SZ) pathway (devitrified), which connects with the accessible-environment (AE) boundary—the regulatory "fence" at 5 km downstream of the repository. The SZ pathway runs horizontally in the direction of the regional flow gradient from below the repository to the boundary. For purposes of dose calculations, a biosphere (or dose) pathway is connected to the end of the SZ pathway and converts the concentrations at the accessible environment into dose. The TSPA model does not account for the fact that different UZ columns will be at differing distances from the AE boundary. However, this is a conservative assumption, if the AE boundary is 5 km from the outer perimeter of the repository footprint.

The 1-D advection/dispersion (or advection-only) radionuclide mass-transport equation is solved in each individual pathway using finite differences. Input/output of each pathway is determined by its connections to other pathways, and defines the path over which the nuclides travel from the repository to the accessible environment. In summary, each pathway in RIP is similar to a coarse grid block in a process-level simulation. This "grid block" represents an areal average of a certain portion of the repository footprint (either 1/6 or 1/10) plus a vertical average over an entire hydrogeologic formation (e.g., the TSw).

7.4.4 Fracture/Matrix Interaction in the Geosphere

Process-level conceptual model

In TSPA-1993, Andrews et al., (1994) considered only matrix transport of radionuclides; however, as shown by the Calico Hills System Study (M&O, 1995d), fracture flow through the unsaturated zone can significantly reduce travel time to the accessible environment. Thus, in TSPA-1995, both fracture and matrix flow and transport are included.

In order to simulate particle transport in the RIP TSPA model, velocity fields for both fracture and matrix transport are required. The process-level model (and its abstraction to the TSPA model) for these velocity fields is discussed in detail in Section 7.2. A brief summary of how this model affects transport is given here. In this conceptualization of fracture/matrix aqueous-phase flow, the TOUGH2 process-level flow model is applied to a representative vertical column from the LBL-USGS model to determine the percent fracture flow and the matrix velocity as a function of depth—for an unsaturated-zone column that has an area (perpendicular to flow) of about $5 \times 10^5 \text{ m}^2$ (i.e., 1/6 of the repository area for the 83 MTU/acre case). The simulations are for ambient conditions only (i.e., not thermally perturbed) and are carried to steady state in order to determine fraction of flow through fractures, $f_{\text{frac}} = Q_{\text{frac}}/Q_{\text{tot}}$; matrix interstitial velocity, v_{mat} ; and matrix water saturation, S_w , as functions of a given infiltration flux, q_{inf} . The 1-D simulations have been spot-checked against results from 2-D cross-section simulations to make sure any important component of horizontal velocity is not missed.

From these simulations, which use the equivalent continuum model (ECM), two families of curves (v_{mat} vs. q_{inf} and f_{frac} vs. q_{inf}) were generated. The range in uncertainty of v_{mat} or f_{frac} for any given q_{inf} was determined by a range in the following parameters: material properties, including K_{mat} , ϕ , and van Genuchten parameters; fracture/matrix coupling as represented by σ , the "satiated" matrix-water saturation for fracture flow; and vertical spatial variability within a given hydrogeologic unit. For water saturation, only a single curve was determined for average

S_w vs. q_{inf} , rather than a family of curves. This is because it has much weaker variability with material properties compared to the variability in f_{frac} and v_{mat} . The minimum and maximum from each family of curves for v_{mat} and f_{frac} are shown in Figures 7.2-8 to 7.2-11 and the raw data are shown in Tables 7.2-3 and 7.2-4. These minimum and maximum curves are used in the TSPA model to describe the entire family (see next section).

TSPA abstracted model

Based on the above discussion, the infiltration rate, q_{inf} , is the primary independent variable for geosphere transport in the aqueous phase. In particular, during a stochastic simulation, RIP will sample from a q_{inf} distribution (see below) to determine the q_{inf} at repository closure (i.e., the initial q_{inf}). For this value of q_{inf} , there will be stochastic distributions of v_{mat} and f_{frac} (as functions of depth or pathway). These distributions are described by the minimum and maximum values of the given parameter at that q_{inf} , as illustrated by the minimum/maximum curves on Figures 7.2-8 to 7.2-11. Random uniform sampling between these minimum and maximum values is used to determine a stochastic initial v_{mat} and f_{frac} for a given realization (see Figure 7.2-3). During any given simulation (realization), q_{inf} may change due to climatic variations, and thus, f_{frac} and v_{mat} will be time dependent. (The time dependence of S_w is not considered because RIP does not allow time-varying retardation factors—the S_w distribution is only used in the retardation factors.)

Let us designate $U(0,1)$ to be the random fraction (uniformly sampled) between the minimum and maximum value of f_{frac} at any given value of q_{inf} . Then we find the corresponding value of f_{frac} (designated as f) as follows (see Figure 7.2-3):

$$\frac{f - f_{min}}{f_{max} - f_{min}} = U(0,1) \quad (7.4-1)$$

and the corresponding value of v_{mat} (designated as v) as follows:

$$\frac{\log_{10} v - \log_{10} v_{min}}{\log_{10} v_{max} - \log_{10} v_{min}} = 1 - U(0,1) \quad (7.4-2)$$

Regardless of climate change (i.e., changing q_{inf}), the initially sampled fraction, $U(0,1)$, is used throughout the simulation for each new value of q_{inf} , i.e., at all values of time, t . This maintains the same distance between the minimum and maximum curves throughout the simulation.

To model geosphere transport in fractures and/or faults, RIP divides the flow on a volume basis between matrix and fracture "flow modes", according to a user-defined percentage, i.e., according to f_{frac} . Then RIP uses a plug-flow solution (i.e., pure advection) for mass transport in each flow mode. Except for the CHnv pathways at low infiltration rates (0.01 - 0.05 mm/yr), all pathways exhibit some degree of transport through fractures (see Table 7.2-3). Velocity in the matrix-flow

mode, v_{mat} , is given by v from Equation 7.4-2, and velocity in the fracture-flow mode, v_{frac} , is taken to be

$$v_{frac} = \frac{f_{frac} a_{inf}}{\phi_{frac}} \quad (7.4-3)$$

where ϕ_{frac} represents the fracture porosity and is assumed to be equal to 0.001.

Dispersion between fracture- and matrix-flow modes is simulated by a Markovian process algorithm that randomly transitions particles between fracture and matrix modes (Golder, 1994), with a distribution equal to the natural logarithm of a random uniform sample between 0 and 1 (Figure 7.4-2). The transition rate, λ , is a user input. For TSPA-1995, the default particle-transition rate for the Markovian dispersion process between fracture and matrix is set equal to the inverse of the pathway length. This means that on average a radionuclide particle will travel the length of the pathway (e.g., through the TSw) within a fracture, before transitioning to the matrix-flow mode or vice-versa. For a slug input through a single pathway (i.e., one hydrogeologic unit), this will result in some smearing of the two peaks (fracture and matrix) in the breakthrough curve, but will retain much of the bimodal character of the breakthrough curve. For a series of connected pathways, however, most of the bimodality is lost—not necessarily because of the Markovian process, however, but because of the connections between paths.

Consider, as an example only, four connected pathways (of approximately the same length) with 50% of the flow through fractures in each pathway (Figure 7.4-3); and suppose an initial pulse input of mass is injected into the beginning of the first pathway (e.g., TSw). The 50% of the slug that enters the fractures will exit the first pathway much sooner (in general) than the 50% in the matrix. When this fracture-transported mass enters the beginning of the second pathway (e.g., the TSv), 50% of it will enter the fracture flow mode of the second pathway and 50% will enter the matrix flow mode. Thus, only $0.5 \times 0.5 = 0.25$ or 25% of the initial part of the slug will pass through the fractures of the second pathway. Thus, for the fourth pathway (e.g., the CHnz), only $(0.5)^4$ or 6% of the initial slug will pass through fractures in the fourth pathway. This means that the initial arrival of nuclides through fractures to the accessible environment will have a much lower mass release than if the fractures in each unit were connected directly with each other. Although this is apparently not a conservative assumption, it does seem more realistic. Similar to a slug input, this same effect will be visible at the beginning of a breakthrough curve resulting from a continuous input. In either case, if the fraction of fracture flow is much less than 50%, the initial arrival of nuclides will be less by the corresponding fraction raised to an exponent equal to the number of connected pathways (assuming the same fracture-flow fraction and the same pathway length for each formation). Thus, fracture flow in TSPA-1995 has less of an impact than might at first be suspected. In order for it to have a much greater effect, it would be necessary to assume a fault pathway with a more direct connection to the accessible environment. (Note: The value of 50% is only used for illustrative purposes. The actual value is f_{frac} , which is different for each formation.)

For most simulations the matrix/fracture particle transition rate is $\lambda=1/L$, where L is the formation thickness. However, because λ is uncertain, a sensitivity case comparing various values of λ has been conducted (see Sections 9.2.3 and 9.3.3).

Geosphere pathways are assumed to be at ambient temperature conditions at all times. The only modification to other ambient conditions during the course of a simulation (i.e., a realization), will be the time-dependent change in infiltration rate and water table height caused by climate change (see Section 7.7). This will in turn cause a change in fracture flux, matrix flux and velocity, and pathway length in the unsaturated zone.

7.4.5 Comparison of UZ Transport Models in RIP and FEHM

As outlined in the previous sections, the representation of unsaturated-zone transport implemented in RIP is based primarily on "lumped" descriptive parameters, in particular, the fracture/matrix transition rate. Such an approach utilizes information regarding the flow field from calculations external to RIP (e.g., fractional fracture flow and matrix pore velocity), and then solves the transport problem using an empirical Markovian algorithm within RIP. Li et al. (1995) have recently examined the validity of this hybrid approach in RIP *vis-a-vis* detailed process modeling of coupled unsaturated flow and transport with FEHM (Zyvoloski et al., 1995).

The basic approach used in the Li et al. study was to simulate steady-state flow and transient transport with FEHM, and then compare the transport simulations with those from RIP. A one-dimensional vertical column, similar to that used by Ho (1995), was utilized for the simulations, with hydrogeologic properties taken from Schenker et al. (1995). For the FEHM model, a saturated boundary condition was applied at the bottom and a constant flux boundary was applied at the top. Solute transport was simulated by injecting a conservative tracer of constant concentration at the top, and monitoring the breakthrough curve at the bottom. The flow calculations were carried out using the dual porosity/dual permeability (*dpdf*) option in FEHM. Since RIP does not have the ability to simulate flow, steady-state velocity profiles in both fractures and matrix blocks were abstracted from FEHM and input into RIP. The matrix/fracture transition rate parameter was varied to get a visual match between the breakthrough curves predicted by RIP and FEHM. This process was repeated for multiple infiltration rates and solute diffusion coefficients. (Note: The velocity profiles from FEHM, generated during this comparative study, were *not* used in TSPA-1995 simulations. Velocity profiles for TSPA-1995 came from the TOUGH2 simulations described in Section 7.2.)

Information regarding the models and parameters, together with results for infiltration rates of 0.5, 1.0 and 4.0 mm/yr, and for matrix diffusion coefficients of 0, 1×10^{-12} and 1×10^{-10} m²/s, are discussed in detail by Li et al. (1995). For reasons of brevity, we present here only the results for an infiltration rate of 4.0 mm/yr assuming no matrix diffusion (Figure 7.4-4). The breakthrough curve labelled 'FEHM' represents a composite of the fracture and matrix breakthrough curves weighted by the component porosities. The other curves are RIP predictions (also for the composite medium) corresponding to a range of values for the transition rate parameter, λ . Note that the general character of the RIP- and FEHM-predicted breakthrough curves are quite similar, and a value of $\lambda \cong 1/L$ appears to provide a reasonable match between the two curves. The first arrival time predicted by RIP is much later than that predicted by FEHM, primarily due to the use of a large initial time step size ($\Delta t = 175$ yr), which was necessary to simulate a time period of 10^6 years without violating the constraint on the allowable number of time steps in RIP.

These results from the Li et al. (1995) study indicate that properly accounting for the pore velocities, and the partitioning of flow between the fractures and the matrix, in the RIP transport simulations (via abstractions from FEHM, or TOUGH2, flow simulations) helps provide a sound basis in predictions of geosphere transport. Furthermore, these results suggest that the Markovian transport algorithm implemented in RIP provides results which are comparable to those from detailed flow and transport simulations with FEHM.

7.4.6 Radionuclide Retardation

In TSPA calculations all rock/water interactions that can serve to retard the transport of radionuclides are modeled with a simple, equilibrium (infinite capacity), distribution-coefficient (K_d) model.

Consider a simple equilibrium sorption reaction where species A_i in the aqueous phase reacts with species \bar{A}_i sorbed onto the rock matrix:



The differential material-balance equations (per bulk volume) for A_i and \bar{A}_i are:

$$\frac{\partial(\phi S_w c_i)}{\partial t} + u_w \frac{\partial c_i}{\partial x} = R \quad (7.4-5)$$

$$\frac{\partial[\bar{c}_i \rho_s (1-\phi)]}{\partial t} = -R \quad (7.4-6)$$

where

$$c_i = \frac{\text{moles of radionuclide } i \text{ in aqueous phase}}{\text{liter of aqueous phase volume}}$$

$$\bar{c}_i = \frac{\text{moles of radionuclide } i \text{ on solid phase}}{\text{g of solid phase}}$$

$$S_w = \frac{\text{liters of aqueous phase volume}}{\text{liter of pore volume}}$$

$$\phi = \frac{\text{liters of pore volume}}{\text{liter of bulk volume}}$$

$$1-\phi = \frac{\text{liters of solid volume}}{\text{liter of bulk volume}}$$

$$\rho_s = \frac{\text{g of solid phase}}{\text{liter of solid phase volume}}$$

$$u_w = \frac{\text{liters of aqueous phase volume}}{(\text{dm}^2 \text{ of bulk area}) \times \text{time}} = \text{Darcy velocity of aqueous phase}$$

$$R = \frac{\text{moles of radionuclide } i \text{ in reaction}}{(\text{liter of bulk volume}) \times \text{time}}$$

x = decimeters (dm) of bulk length

Combining the above two equations gives the total material balance for species i :

$$\frac{\partial}{\partial t} [\phi S_w c_i + \bar{c}_i \rho_s (1 - \phi)] + u_w \frac{\partial c_i}{\partial x} = 0 \quad (7.4-7)$$

Defining the sorption (or distribution) coefficient, K_d , as

$$K_d = \frac{\text{moles of radionuclide } i \text{ per g of solid phase}}{\text{moles of radionuclide } i \text{ per ml of aqueous phase}} = \frac{1000 \bar{c}_i}{c_i} \quad (7.4-8)$$

and combining with the above equation gives

$$\frac{\partial}{\partial t} [\phi S_w c_i + \rho_m (1 - \phi) K_d c_i] + u_w \frac{\partial c_i}{\partial x} = 0 \quad (7.4-9)$$

where $\rho_m = \rho_s / 1000$ and has units of g/cm^3 . Factoring out ϕS_w and rearranging, gives

$$\left[1 + \frac{\rho_m (1 - \phi)}{\phi S_w} K_d \right] \frac{\partial c_i}{\partial t} + \frac{u_w}{\phi S_w} \frac{\partial c_i}{\partial x} = 0 \quad (7.4-10)$$

The definition of bulk density, ρ_b , in a consistent set of units (e.g., ρ_b in g per cm^3 of bulk volume, ρ_w in g per cm^3 of pore volume, ρ_m in g per cm^3 of solid-phase volume, ϕ in cm^3 of pore volume per cm^3 of bulk volume, $1 - \phi$ in cm^3 of solid-phase volume per cm^3 of bulk volume) is

$$\rho_b = (1 - \phi) \rho_m + \phi \rho_w \quad (7.4-11)$$

The "dry" bulk density, ρ_{bd} , i.e., the density when $S_w = 0$, is defined as

$$\rho_{bd} = \rho_b - \phi \rho_w = (1 - \phi) \rho_m \quad (7.4-12)$$

Thus, substituting ρ_{bd} for $\rho_m (1 - \phi)$ in Equation 7.4-10 gives

$$\left[1 + \frac{\rho_{bd}}{\phi S_w} K_d\right] \frac{\partial c_i}{\partial t} + \frac{u_w}{\phi S_w} \frac{\partial c_i}{\partial x} = 0 \quad (7.4-13)$$

With regard to consistency of units, this substitution between Equations 7.4-10 and 7.4-12 is valid because ϕ is just a fraction. Thus, although in Equation 7.4-13, ρ_{bd} takes on the numerical value of dry bulk density in units of g/cm^3 , it actually has units of

$$\frac{\text{g of solid phase}}{\text{cm}^3 \text{ of solid phase volume}} \times \frac{\text{liters of solid phase volume}}{\text{liter of bulk volume}} \quad (7.4-14)$$

It can now be seen that the apparent velocity of radionuclide A_i is given by the interstitial velocity in the water phase, $v_w = u_w/\phi S_w$, divided by the retardation coefficient, R_d , where

$$R_d = 1 + \frac{\rho_{bd} K_d}{\phi S_w} \quad (7.4-15)$$

In TSPA-1995, the Schenker et al. (1995) distributions were used for both ρ_{bd} and ϕ in the rock matrix of the various hydrogeologic units. Schenker's stochastic distributions for bulk density are based on measurements of both ρ_b and ρ_{bd} , and values in between where $0 < S_w < 1$. For S_w in Equation 7.4-15, the process-level results for matrix water saturation were used (S_w in Tables 7.2-3 and 7.2-4).

Distribution coefficients represent many possible processes, including ion-exchange, sorption, surface complexation, and precipitation/dissolution. Because K_d s are used to model such a wide range of basic phenomenological processes, they must necessarily be modeled as stochastic parameters with a high degree of uncertainty when used in abstracted TSPA models (and even in process-level models). The distributions used for TSPA-1995 are based in part on an expert elicitation workshop conducted for TSPA-1993 (Andrews et. al., 1994), and represent conservative estimates. However, in part because of recent experiments at LANL (Triay et al., 1995c; 1995d; and 1995e), which determined K_d s for Np, U, Pu, and Se for whole-rock tuff samples, the K_d s from TSPA-1993 have been updated (Meijer, 1990; 1992; and 1995). K_d s for three different rock types were measured: devitrified tuff, vitric tuff, and zeolitic tuff. Distribution coefficients for these rock types are different in the unsaturated zone compared to the saturated zone, mainly because of ionic strength. For TSPA-1995, the saturated zone was modeled as devitrified; therefore, besides the three types of K_d distributions in the unsaturated zone, there is one additional set of distributions for the saturated zone. All K_d distributions are shown in Tables 7.4-2 and 7.4-3.

7.5. TRANSPORT OF GASEOUS-PHASE RADIONUCLIDES

For TSPA-1995, geosphere transport of radionuclides in the gaseous phase of the unsaturated zone is not considered. The primary radionuclide to be transported in the gas (air) phase would be ^{14}C . However, given the recent recommendations of the NAS (National Research Council, 1995) on protection of the global population, it is clear that the risk from gaseous release of ^{14}C is negligible. However, TSPA-1995 does assume that the ^{14}C released from the inventory is dissolved in the aqueous phase once it reaches the geosphere (i.e., the top of the TSw), and is then transported by the aqueous phase to the accessible environment. Since this is a very

conservative assumption with respect to computing dose at the accessible environment, Chapter 9 has a sensitivity analysis that computes dose at the accessible environment when ^{14}C is directly released to the atmosphere, i.e., if it never enters the aqueous phase and therefore does not contribute to dose exposure in a water well at the accessible environment.

The other two radionuclides that may be gaseous in the WP/EBS are ^{129}I and ^{36}Cl (Golder, 1993). It is assumed that they leave the waste packages in gaseous form, transport immediately through the EBS, and then dissolve in the aqueous phase in the TSw. Then they are transported through the geosphere as aqueous-phase solutes. Assuming that ^{129}I and ^{36}Cl are released in gaseous form from the inventory is a conservative assumption, and it implies that their transport through the EBS is unaffected by dripping fractures or by a diffusion barrier around the packages. Thus, in the capillary-barrier scenario, ^{129}I controls the peak dose at the accessible environment (see Chapter 9). However, it is debatable whether highly reactive species such as I_2 and Cl_2 would make it through the WP/EBS environment in the gaseous phase, or whether they would instead be dissolved into the aqueous phase. Thus, we have included a sensitivity case (Chapter 9) that considers aqueous-phase transport of ^{129}I and ^{36}Cl through the EBS.

7.6 SATURATED-ZONE TRANSPORT

7.6.1 Saturated-Zone Flux Distribution

The saturated-zone flux affects the arrival time of radionuclides at the accessible-environment boundary as well as the degree of mixing and dilution in the ground water of the tuff aquifer prior to its extraction and use. Since process-level modeling of saturated-zone flow and transport has not changed appreciably since the completion of TSPA-1993, the same abstraction and basis thereof used in the previous TSPA iteration is also used in the current analyses. The saturated-zone fluxes (q_{sz}) come from simulations by Barr (1993), but are based on limited borehole data. The 2-D simulations of Barr were based on a composite or bulk permeability/flux model, which used a conductivity distribution that represents an average of matrix and fracture permeabilities (similar to an equivalent continuum model). The saturated-zone flux distribution used in TSPA-1993 and TSPA-1995 used the entire 2-D distribution of nodal fluxes to represent the possible range of spatially averaged 1-D flux in the saturated zone. Remember that since RIP only considers 1-D transport, that the 2-D flux distribution from the Barr process-level model would have to be averaged to 1-D. Rather than trying to match the breakthrough curve of a 1-D model to some spatially averaged 2-D breakthrough distribution from the composite permeability process-level model, we just used the entire 2-D distribution of steady-state nodal velocities (or fluxes), and sampled from this distribution to determine the 1-D q_{sz} for any given realization.

The actual distribution for q_{sz} (Darcy velocity in the saturated zone) used in TSPA-1995 is a log-normal distribution with a mean of 2.0 m/yr, a median of 1.0696 m/yr, and a standard deviation of 0.4859. Based on this distribution, both TSPA-1993 and TSPA-1995 indicate that the saturated zone is not a significant geosphere barrier compared to the unsaturated zone, as far as time delay of the breakthrough to the accessible environment. The saturated zone's greatest importance lies in its dilution effect. For TSPA-1995, aqueous transport through the saturated zone also assumes longitudinal dispersion, with a dispersivity equal to 10% of the path length from the base of the repository to the accessible environment (i.e., equal to 500 m). Because RIP considers only one-dimensional transport, no lateral dispersion is possible.

7.6.2 Dilution and Dose at the Accessible Environment

After exiting the base of the unsaturated zone, transported contaminants undergo longitudinal dispersion within the saturated zone before reaching the accessible environment at 5 km from the repository footprint. In order to compute doses at the accessible environment, the radionuclides are assumed to be mixed (diluted) into a volume of groundwater equal to the width of the repository times an arbitrary 50-m mixing depth (or screened interval of a well penetrating the saturated-zone tuff aquifer) times the mean aquifer flux. In particular, dose exposure is computed from mass release rate by the following equation:

$$D_i = \frac{M_i}{Q_m} DCF_i \quad (7.6-1)$$

where

D_i = dose for radionuclide i (rem/yr),
 M_i = mass rate of release for radionuclide i (g/yr),
 Q_m = mixing volumetric flow rate (m^3/yr), and
 DCF_i = dose conversion factor for radionuclide i (rem- m^3/g -yr).

Note that M_i/Q_m is the mass concentration of the given nuclide in the media of interest, e.g., the drinking water. M_i is just the mass rate of release into the saturated zone, as computed by RIP. The mixing volumetric flow rate, Q_m , is based on the Darcy velocity in the saturated zone and the screened interval of a water well that penetrates the saturated zone. Here we define the screened interval as the depth, h , in meters from the top of the saturated zone to the total depth of the well. We make the conservative assumption that the vertical dispersion in the saturated zone between the repository boundary and the water well is such that none of the nuclide mass is dispersed beyond the screened interval. Thus, the mixing volumetric flow rate for the purposes of computing mass concentration is given by

$$Q_m = hW_{rep}q_{SZ} \quad (7.6-2)$$

where

W_{rep} = approximate width (m) of repository, perpendicular to the direction of flow in the SZ
 q_{SZ} = saturated-zone Darcy velocity (m/yr).

We assumed a repository width of 4 km and a screened-interval depth of 50 m. If q_{SZ} is 2.0 m/yr (the mean of the q_{SZ} distribution—see above), this gives a Q_m equal to 400,000 m^3/yr .

The dose conversion factors in Equation 7.6-1 were selected from the EPA dose conversion factors (EPA, 1988) for ingestion only. These EPA dose conversion factors were converted to an assumed drinking-water exposure scenario. The receptor was assumed to drink 2 liters of water per day. The dose conversion factors are presented in Table 7.6-1. The dose exposure generated over the time period of interest is the maximally-exposed-individual, whole-body dose for a person that obtains all of their drinking water from the contaminated saturated zone. For simplicity and ease of comparison with other dose analyses, this assumption is different than the

TSPA-1993 evaluation which considered both drinking water and crop irrigation. A comparison of the TSPA-1995 and TSPA-1993 dose conversion factors is included in Table 7.6-1. Generally, the dose conversion factors used in TSPA-1995 are smaller than those used in TSPA-1993. A more detailed analysis of the exposure scenarios will be conducted after the NAS recommendations are evaluated and the regulation for dose has been promulgated.

7.6.3 Dilution in the Regional Aquifer

Based on the recent NAS study (National Research Council, 1995), additional dilution of the concentration at the accessible environment (dose reduction) would be expected to occur between the accessible environment and the location where the critical group is assumed to withdraw ground water, based on two processes. These processes are mixing of ground water from two sub-basins in the vicinity of water use (see Figures 2.5-1 and 2.5-2), and by lateral and vertical dispersion over the longer path length. The dilution of the concentration from mixing of groundwater from the two sub-basins in the vicinity of groundwater withdrawal is 3.5. This was determined by dividing the sum of northwestward flow from the Amargosa Desert (20,000 acre-ft/yr) plus southward flow from Yucca Mountain (8,000 acre-ft/yr) by the southward flow from Yucca Mountain (see Table 2.5-1).

The amount of dispersion over the longer path length is largely a function of the regional flow system and the heterogeneity along the migration paths within the flow system. The reduction in concentration of radionuclides over a path length L in an infinite homogeneous aquifer with a steady-state pore velocity (v_x) may be approximated using an advection-diffusion model:

$$\frac{\partial C}{\partial t} + v_x \frac{\partial C}{\partial x} = D_x \frac{\partial^2 C}{\partial x^2} + D_y \frac{\partial^2 C}{\partial y^2} + D_z \frac{\partial^2 C}{\partial z^2} \quad (7.6-3)$$

where C is the radionuclide concentration, v_x is the average linear velocity in the x direction and D_x , D_y , and D_z are the dispersion coefficients in the x, y, and z directions, respectively. For steady-state transport, the concentration becomes independent of time, and for large time ($t \gg 2D_x/v_x^2$), the longitudinal dispersion term may be neglected. Under these conditions, Equation 7.6-3 reduces to the following form:

$$v_x \frac{\partial C}{\partial x} = D_y \frac{\partial^2 C}{\partial y^2} + D_z \frac{\partial^2 C}{\partial z^2} \quad (7.6-4)$$

This is just the two-dimensional diffusion equation, with an equivalent "time" represented by x/v_x , the downstream travel time. The general solution of Equation 7.6-4 for an instantaneous point source is:

$$C(x,y,z) = \frac{(2\dot{M}/v_x)}{4\pi\phi\sqrt{D_y D_z}(x/v_x)} \exp\left\{-\frac{y^2}{4D_y(x/v_x)} - \frac{z^2}{4D_z(x/v_x)}\right\} \quad (7.6-5)$$

where ϕ is the porosity and \dot{M} is the mass flux (mass input per unit time). The factor of 2 is included because radionuclides cannot disperse into the upper half-plane above the water table.

This effect is incorporated through symmetry about the water table by including an extra image source of the same strength at the same position as the original source, resulting in a concentration that is doubled.

Instead of a point source, if we represent the mass flux into the saturated zone as a line source of length l oriented orthogonal to the saturated zone flow direction, then the downstream concentration may be represented by the superposition of Equation 7.6-5 over a series of infinitesimal point sources between (x,y,z) coordinates $(0, -l/2, 0)$ and $(0, l/2, 0)$. Therefore,

$$C(x,y,z) = (l/l) \int_{-l/2}^{l/2} \frac{(\dot{M}/v_x)}{2\pi\phi\sqrt{D_y D_z}(x/v_x)} \exp\left\{-\frac{(y-\eta)^2}{4D_y(x/v_x)} - \frac{z^2}{4D_z(x/v_x)}\right\} d\eta \quad (7.6-6)$$

Integrating Equation 7.6-6 and letting

$$D_y = \alpha_y v_x = \beta_y x v_x \quad (7.6-7)$$

$$D_z = \alpha_z v_x = \beta_z x v_x$$

gives the concentration:

$$C(x,y,z) = \frac{(\dot{M}/l)}{2\phi v_x x \sqrt{\pi\beta_z}} \exp\left\{-\frac{z^2}{4\beta_z x^2}\right\} \left\{ \operatorname{erf}\left[\frac{l/2+y}{2x\sqrt{\beta_y}}\right] + \operatorname{erf}\left[\frac{l/2-y}{2x\sqrt{\beta_y}}\right] \right\} \quad (7.6-8)$$

The dispersivity model for α_y and α_z assumed in Equations 7.6-7 is based on the observation in field-scale dispersive transport processes that the effective dispersion coefficients are proportional to the distance traveled and the flow velocity.

The concentrations are at a maximum at the centerline, i.e. $y = 0$ and $z = 0$. At the centerline, Equation 7.6-8 reduces to

$$C(x,0,0) = \frac{(\dot{M}/l)}{q_{sz} x \sqrt{\pi\beta_z}} \operatorname{erf}\left\{\frac{l}{4x\sqrt{\beta_y}}\right\} \quad (7.6-9)$$

where $q_{sz} = \phi v_x$ is the saturated-zone Darcy velocity. To obtain a dilution factor, note that

$$\dot{M} = C_{uz} q_{uz} A_{rep} \quad (7.6-10)$$

and

$$S = \frac{C_{uz}}{C}$$

where S is the dilution factor, C_{uz} is the radionuclide concentration in the unsaturated-zone flow entering the saturated zone, q_{uz} is the unsaturated-zone Darcy velocity, and A_{rep} is the "repository" area (actually, the contaminated-flow cross-sectional area entering the saturated zone, assumed to be equal to the waste-package catchment area of 41 m^2 —see Section 7.3—times 10,000 waste packages, which equals approximately $4 \times 10^5 \text{ m}^2$).

Rearranging Equation 7.6-9 and using the definitions in Equation 7.6-10 to solve for the centerline dilution factor gives:

$$S = \frac{q_{sz} l x \sqrt{\pi \beta_z}}{q_{uz} A_{rep} \operatorname{erf} \left\{ \frac{l}{4x \sqrt{\beta_y}} \right\}} \quad (7.6-11)$$

Estimates of the effects of dispersion on peak (centerline) concentration between the repository and points downstream can be made using Equation 7.6-11 by assuming values for the transverse "dispersivity-scale coefficients", β_y and β_z . The distances from the repository to the accessible environment and the potential point-of-use at Amargosa Farms are 5 km and 30 km, respectively. A longitudinal dispersivity-scale coefficient, β_x , of 0.1 was assumed for TSPA-1993 (Andrews et al., 1994). Transverse dispersivity-scale coefficients, β_y and β_z , are generally a factor of 1.5 to 10 smaller than β_x . Using β_x equal to 0.1, the longitudinal dispersivity, α_x , at Amargosa Farms would be 3 kilometers, which seems perhaps too large compared with observed values. Therefore, we conservatively assume that β_x is 0.01, resulting in a minimum value for β_y and β_z of 0.001 (i.e., assuming they are 10 times smaller than β_x). q_{sz} is assumed to be about 2 m/yr (see above), the line source length, l , is given a value of 4 km (see Section 7.6-2), and the "repository" (contaminated-flow) area is about $4 \times 10^5 \text{ m}^2$. A table of dilution values are computed for downstream distances of 5 km and 30 km and for UZ Darcy velocities of $1.25 \times 10^{-3} \text{ m/yr}$ and $3.0 \times 10^{-5} \text{ m/yr}$. (These are the expected values for the high and low q_{inf} ranges discussed earlier in this chapter. Note that $q_{uz} = q_{inf}$.)

Centerline (Minimum) Dilution Factors

q_{uz} (m/yr)	$S = C_{uz}/C$	
	5 km	30 km
1.25×10^{-3}	4.5×10^3	3.1×10^4
3.0×10^{-5}	1.9×10^5	1.3×10^6

The "stirred tank" mixing model discussed in section 7.6.2 for dilution in the saturated zone between the repository and the accessible environment (5 km) gives dilution factors ($= q_{sz} W_{rep} h / q_{uz} A_{rep}$) of about 800 and 3.3×10^4 for the high and low q_{uz} cases, respectively. Therefore, the advection-diffusion *centerline* (minimum) dilution values are larger than the mixing-model dilution values by a factor of about 6 at the 5-km AE boundary. However,

average dilution values for the advection-diffusion model, found by integrating over a 4-kilometer-wide, 50-meter-deep cross-section, are larger by a factor of about 12.

The increased dilution in the advection-diffusion model is largely due to the increased mixing depth (see below) compared with the assumed 50-m depth used in the "stirred tank" mixing model. Although concentrations computed with the advection-diffusion model are sensitive to the choice of dispersion coefficients, the values chosen here are believed to be conservative.

The dilution due to dispersive mixing between the accessible environment ($x = 5$ km) and the potential point of use at Amargosa Farms ($x = 30$ km) may be computed from the ratio of the dilution factors for a given value of q_{0z} , and is found to be about a factor of 7. Total dilution between the accessible environment and the potential point of use is the product of dilution due to dispersive mixing during transit from the accessible environment to the point of use (Amargosa Farms) ($S = 7$) and the subbasin mixing expected due to inflow from the Amargosa Desert aquifer ($S = 3.5$). Therefore a dilution factor (dose reduction factor) of at least 25 can be applied to calculated concentrations at the accessible environment to approximate the doses at Amargosa Valley.

The advection-diffusion model assumes that the line source is in an infinite half-space. This assumption is only valid if the dispersive width and depth of the concentration field are small in comparison with the boundaries of the regional aquifer system. The horizontal width of the dispersive plume may be estimated from the ratio of Equation 7.6-8 at $z = 0$ to Equation 7.6-9. The value of y for which this ratio is 0.1 may be used as an approximate plume width (roughly equivalent to two standard deviations from the centerline). This ratio is:

$$\frac{C(x,y,0)}{C(x,0,0)} = \frac{\operatorname{erf}\left\{\frac{l/2 + y}{2x\sqrt{\beta_y}}\right\} + \operatorname{erf}\left\{\frac{l/2 - y}{2x\sqrt{\beta_y}}\right\}}{2 \operatorname{erf}\left\{\frac{l}{4x\sqrt{\beta_y}}\right\}} \quad (7.6-12)$$

Similarly, for the mixing depth, we have

$$\frac{C(x,0,z)}{C(x,0,0)} = \exp\left\{\frac{-z^2}{4\beta_z x^2}\right\} \quad (7.6-13)$$

Values for the mixing widths and depths at $x = 5$ km and $x = 30$ km using a concentration ratio of 0.1 are:

x (km)	mixing width (km)	mixing depth (km)
5	4.6	0.48
30	7.7	2.9

In order to justify these mixing dimensions, and justify the preceding estimates of dilution from mixing and dispersion, a regional flow and transport model should be constructed based on the hydrostratigraphy of the region, and sensitivity analyses should be conducted to determine the sensitivity of dilution factors to the conceptual flow model, heterogeneity along the flow paths, and parameter uncertainty.

7.7 CLIMATE CHANGE

As discussed in Chapter 2, for the initial value of infiltration flux (Darcy velocity at the surface), q_{inf} , we use a bimodal distribution to represent two possible transport scenarios in the unsaturated zone beneath the repository: a low infiltration case (0.01 to 0.05 mm/yr) and a high infiltration case (0.5 to 2.0 mm/yr). Both of these distributions are sampled uniformly. (0.5 mm/yr was the mean value of q_{inf} in TSPA-1993.)

Climatic Variation of Infiltration Rate

Superimposed on the initial distribution of q_{inf} is the climate change model, given by

$$q_{inf}(t) = q_{inf}(t_0)(1+f) \quad (7.7-1)$$

where

$$f = U(0,4)g_{in}(t)$$

Here, $U(0,4)$ is a random number uniformly sampled between 0 and 4, and $g_{in}(t)$ is a periodic triangular wave with a period of 100,000 years and a peak amplitude of 1 (i.e., $g_{in}(t)$ varies from 0 at 0 years to 1 at 50,000 years and back to 0 at 100,000 years, and continues like this out to 1,000,000 years). This model of climate change is consistent with Long and Childs (1993) model which expects a 2.5 times increase in q_{inf} under full glacial conditions, sometime between 50,000 to 100,000 years from the present. In Equation 7.7-1, $U(0,4)$ has a mean value of 2, so the sample mean of $q_{inf}(t)$ at 50,000 years is 3 times $q_{inf}(t_0)$. Thus, this is slightly conservative with respect to Long and Childs model. Figure 7.7-1 shows the variation in $q_{inf}(t)$ over 1,000,000 years, with $q_{inf}(t_0)$ equal to 0.5 mm/yr.

Climatic Variation of Water-Table Elevation

Not only did we assume q_{inf} to vary with climate, but for some sensitivity cases we also assumed a similar model for a simultaneous rise in the water table, up to a maximum of 80 m. If $h_{wt}(t_0)$ is the initial water-table height, then the time dependent water table height is given by

$$h_{wr}(t) = h_{wr}(t_0) + \Delta h_{wr} \quad (7.7-2)$$

where

$$\Delta h_{wr} = U(0,4) h_{m}(t)$$

Here, $U(0,4)$ is the random number from Equation 7.7-1, and $h_m(t)$ is a periodic triangular wave with a period of 100,000 years and a peak amplitude of 20 m. Thus, if $U(0,4) = 4$, then a maximum water table rise of 80 m would occur at 50,000 years, whereas if $U(0,4) = 0$, there would be no water-table rise. This is illustrated in Figure 7.7-2 for five values of $U(0,4)$.

Effect of Climate on Dripping Flow in EBS

Climate change is also applied to the rate of dripping through fractures in the repository near-field environment. However, rather than change the number of packages that experience fracture dripping, we apply a model similar to Equation 7.7-1, which just increases the amount of fracture flow through the fractures that were dripping initially. In particular, the average flux (Darcy velocity) through dripping fractures changes with climate as follows:

$$q_{drip}(t) = q_{drip}(t_0)(1+f) \quad (7.7-3)$$

where

$$f = U(0,4) g_m(t)$$

as defined above in Equation 7.7-1.

Table 7-2.1 TOUGH2 Results Used in the Testing of the Abstraction Methodology

Unit	q_{inf} (mm/yr)	v_{mat} (min) (m/s)	v_{mat} (max) (m/s)	f_{frac} (min)	f_{frac} (max)
TSw	0.1	2.640E-11	2.890E-11	0	0
	0.5	8.100E-11	1.170E-10	0	0
	1.0	1.110E-10	1.560E-10	0.197	0.389
TSv	0.1	6.040E-11	—	0	0
	0.5	1.170E-10	—	0	0
	1.0	3.400E-10	—	0.155	0.155
CHnv	0.1	2.630E-11	6.120E-11	0	0
	0.5	9.120E-11	2.090E-10	0	0
	1.0	1.150E-10	3.430E-10	0	0
CHnz	0.1	1.240E-11	1.840E-11	0	0
	0.5	6.150E-11	7.940E-11	0	0
	1.0	6.150E-11	6.900E-11	0	0

Note:

q_{inf} is applied infiltration rate

v_{mat} (min) and v_{mat} (max) are the minimum and maximum matrix pore velocities

f_{frac} (min) and f_{frac} (max) are the minimum and maximum fraction of fracture flux

Table 7.2-2 Comparison of TOUGH2 and RIP Travel Times

Infiltration (mm/yr)	RIP (min) (yr)	TOUGH2 (yr)	RIP (max) (yr)
0.1	3.62E+05	4.88E+05	5.67E+05
0.5	9.17E+04	1.29E+05	1.43E+05
1.0	5.83E+04	7.91E+04	1.10E+05

Table 7.2-3 TOUGH2 Abstractions for the Low-Infiltration Case

Unit	q_{inf} (mm/yr)	v_{mat} (min) (m/s)	v_{mat} (max) (m/s)	f_{frac} (min)	f_{frac} (max)	S_w
TSw	0.01	4.29E-12	2.12E-11	0	5.59E-02	0.759
	0.02	5.77E-12	2.83E-11	0	8.97E-02	0.781
	0.05	7.59E-12	4.81E-11	0	1.89E-01	0.821
TSv	0.01	4.59E-12	2.27E-11	0	5.59E-02	0.940
	0.02	6.17E-12	3.03E-11	0	8.97E-02	0.944
	0.05	8.12E-12	5.15E-11	0	1.89E-01	0.952
CHnv	0.01	3.95E-12	2.71E-11	0	0.00E+00	0.398
	0.02	5.37E-12	3.56E-11	0	0.00E+00	0.414
	0.05	9.53E-12	5.96E-11	0	0.00E+00	0.446
CHnz	0.01	2.86E-12	8.91E-12	0	2.00E-01	0.712
	0.02	4.18E-12	1.14E-11	0	2.00E-01	0.728
	0.05	7.04E-12	1.83E-11	0	2.00E-01	0.763

Table 7.2-4 TOUGH2 Abstractions for the High-Infiltration Case

Unit	q_{inf} (mm/yr)	v_{mat} (min) (m/s)	v_{mat} (max) (m/s)	f_{frac} (min)	f_{frac} (max)	S_w
TSw	0.5	8.10E-12	2.87E-10	4.32E-02	2.81E-01	0.897
	1	8.10E-12	5.23E-10	1.14E-01	3.98E-01	0.943
	2	7.95E-12	9.96E-10	2.24E-01	5.81E-01	0.979
TSv	0.5	8.67E-12	3.07E-10	4.32E-02	2.81E-01	0.984
	1	8.67E-12	5.59E-10	1.14E-01	3.98E-01	0.985
	2	8.50E-12	1.07E-09	2.24E-01	5.81E-01	0.986
CHnv	0.5	4.95E-11	3.36E-10	0	1.02E-02	0.548
	1	8.79E-11	5.89E-10	0	1.40E-02	0.605
	2	1.71E-10	1.03E-09	0	2.02E-02	0.659
CHnz	0.5	2.86E-11	6.85E-11	0	4.27E-01	0.954
	1	2.74E-11	1.23E-10	1.23E-01	6.24E-01	0.970
	2	2.74E-11	2.01E-10	2.59E-01	7.26E-01	0.981

Table 7.4-1 Stratigraphy for TSPA-1995

Column	Thickness (m)					Total Thickness	% total area, 25 MTU/acre	% total area, 83 MTU/acre
	TSw	TSv	CHnv	CHnz	PPn			
1	105	8	92	24	115	345	7.2	14.8
2	176	8	72	50	38	344	6.1	8.0
3	87	8	105	32	126	358	4.9	16.4
4	147	8	87	57	61	359	3.4	11.1
5	35	7	132	40	158	372	6.3	20.7
6	113	7	102	43	105	370	8.9	29.0
7	151	8	55	68	—	282	9.2	0.0
8	105	15	54	18	48	240	17.7	0.0
9	80	15	63	21	56	235	14.7	0.0
10	85	15	47	16	42	205	21.6	0.0

Table 7.4-2 TSPA-1995 Sorption-Coefficient Distributions (K_d in ml/g) for Unsaturated-Zone units (Meijer, 1995)

ELEMENT	ROCK TYPE	DIST	E[x]	COV ¹	MIN	MAX	COMMENTS
Am	D ²	uniform			100	2000	Same for Ac, Cm, Nb, Sm, Th, and Zr
	V ³	beta	400	0.20	100	1000	
	Z ⁴	uniform			100	1000	
Pu	D	beta	100	0.25	20	200	
	V	beta	100	0.25	50	200	
	Z	beta	100	0.25	30	200	
U	D	beta	2.0	0.3	0	4.0	
	V	beta	1.0	0.3	0	3.0	
	Z	exp	7.0	—	0	30.0	
Np	D	beta	1.0	0.3	0	6.0	
	V	exp	1.0	—	0	15.0	
	Z	beta	0.5	0.25	0	3.0	
Ra	D	uniform			100	500	
	V	uniform			50	100	
	Z	uniform			1000	5000	

7-34

Table 7.4-2 TSPA-1995 Sorption-Coefficient Distributions (K_d in ml/g) for Unsaturated-Zone units (Meijer, 1995). (Continued)

ELEMENT	ROCK TYPE	DIST	E[x]	COV ¹	MIN	MAX	COMMENTS
Cs	D	uniform			20	1000	
	V	uniform			10	100	
	Z	uniform			500	5000	
Sr	D	uniform			10	50	
	V	uniform			0	20	
	Z	uniform			500	2000	
Ni	D	beta	100	0.33	0	500	Same for Pd
	V	beta	50	0.33	0	100	
	Z	beta	100	0.33	0	500	
Pb	D	uniform			100	500	
	V	uniform			100	500	
	Z	uniform			100	500	
Sn	D	uniform			20	200	
	V	uniform			20	200	
	Z	uniform			100	300	

Table 7.4-2 TSPA-1995 Sorption-Coefficient Distributions (K_d in ml/g) for Unsaturated-Zone units (Meijer, 1995). (Continued)

ELEMENT	ROCK TYPE	DIST	E[x]	COV ¹	MIN	MAX	COMMENTS
Pa	D	uniform			0	100	
	V	uniform			0	100	
	Z	uniform			0	100	
Se	D	exp	3		0	30	
	V	exp	3		0	20	
	Z	exp	2		0	15	
Cl, I, Tc, C					0	0	

7-36

- 1 Coefficient of variation: $COV = \sigma[x]/E[x]$
- 2 D = Devitrified tuff
- 3 V = Vitric tuff
- 4 Z = Zeolitic tuff

Table 7.4-3 TSPA-1995 Sorption Coefficient Distributions (K_d in ml/g) for Saturated-Zone units (Meijer, 1995)

ELEMENT	ROCK TYPE	DIST	E[x]	COV ¹	MIN	MAX	COMMENTS
Am	D ²	uniform			100	2000	Same for Ac, Cm, Nb, Sm, Th, and Zr
	V ³	beta	400	0.20	100	1000	
	Z ⁴	uniform			100	1000	
Pu	D	beta	100	0.15	50	300	
	V	beta	100	0.15	50	300	
	Z	beta	100	0.15	30	300	
U	D	beta	2.0	0.30	0	5.0	
	V	beta	1.0	0.30	0	4.0	
	Z	beta	7.0	0.30	5	20.0	
Np	D	beta	3.0	0.3	0	10.0	
	V	exp	1.5	—	0	15.0	
	Z	beta	4.0	0.25	0	12.0	
Ra	D	uniform			100	500	
	V	uniform			100	500	
	Z	uniform			1000	5000	

7-37

Table 7.4-3 TSPA-1995 Sorption Coefficient Distributions (K_d in ml/g) for Saturated-Zone units (Meijer, 1995) (Continued)

ELEMENT	ROCK TYPE	DIST	E[x]	COV ¹	MIN	MAX	COMMENTS
Cs	D	uniform			20	1000	
	V	uniform			10	100	
	Z	uniform			500	5000	
Sr	D	uniform			10	200	
	V	uniform			20	50	
	Z	Log uniform			2000	50000	
Ni	D	beta	100	0.33	0	500	Same for Pd
	V	beta	100	0.33	0	200	
	Z	beta	100	0.33	0	500	
Pb	D	uniform			100	500	
	V	uniform			100	500	
	Z	uniform			100	500	
Sn	D	uniform			20	200	
	V	uniform			20	200	
	Z	uniform			100	300	

Table 7.4-3 TSPA-1995 Sorption Coefficient Distributions (K_d in ml/g) for Saturated-Zone units (Meijer, 1995) (Continued)

ELEMENT	ROCK TYPE	DIST	E[x]	COV ¹	MIN	MAX	COMMENTS
Pa	D	uniform			0	100	
	V	uniform			0	100	
	Z	uniform			0	100	
Se	D	exp	3		0	30	
	V	exp	3		0	20	
	Z	exp	2		0	15	
C1, I, Tc, C					0	0	

7-39

- 1 Coefficient of variation: $COV = \sigma[x]/E[x]$
- 2 D = Devitrified tuff
- 3 V = Vitric tuff
- 4 Z = Zeolitic tuff

Table 7.6-1. Dose Conversion Factors and Specific Activities

Isotope	TSPA 1995 Dose Conversion Factor (rem/yr)/(g/m ³)	TSPA 1993 Dose Conversion Factor (rem/yr)/(g/m ³)	Specific Activity (Ci/g)
²²⁷ Ac	7.34E8	2.28E9	7.23E-1
²⁴¹ Am	9.00E6	2.81E7	3.44E0
^{242m} Am	2.46E7	7.67E7	9.73E0
²⁴³ Am	5.21E5	1.63E6	2.00E-1
¹⁴ C	6.57E3	1.72E6	4.46E0
³⁶ Cl	7.19E1	—	3.30E-2
²⁴⁴ Cm	1.17E8	3.65E8	8.09E1
²⁴⁵ Cm	4.63E5	1.44E6	1.72E-1
²⁴⁶ Cm	8.21E5	2.57E6	3.08E-1
¹³⁵ Cs	5.85E6	1.23E3	1.15E-3
¹²⁹ I	3.52E1	2.05E2	1.77E-4
^{93m} Nb	1.07E5	—	2.83E2
⁹⁴ Nb	9.65E2	2.42E5	1.88E-1
⁵⁹ Ni	1.14E1	—	7.58E-2
⁶³ Ni	2.57E4	—	6.18E1
²³⁷ Np	2.25E3	1.31E5	7.06E-4
²³¹ Pa	3.59E5	1.12E6	4.72E-2
²¹⁰ Pb	2.95E8	2.17E9	7.64E1
¹⁰⁷ Pd	5.54E-2	—	5.15E-4
²³⁸ Pu	3.03E6	3.10E6	1.71E1
²³⁹ Pu	1.58E5	1.24E4	6.22E-2
²⁴⁰ Pu	5.80E5	4.56E4	2.28E-1
²⁴¹ Pu	5.08E6	3.96E5	1.03E2
²⁴² Pu	9.22E3	7.25E2	3.82E-3

Table 7.6-1. Dose Conversion Factors (Continued)

Isotope	TSPA 1995 Dose Conversion Factor (rem/yr)/(g/m ³)	TSPA 1993 Dose Conversion Factor (rem/yr)/(g/m ³)	Specific Activity (Ci/g)
²²⁶ Ra	9.43E5	8.79E6	9.90E-1
²²⁸ Ra	2.82E8	—	2.73E2
⁷⁹ Se	4.37E2	1.10E5	6.98E-2
¹⁵¹ Sm	7.34E3	—	2.63E1
¹²⁶ Sn	3.99E2	6.08E4	2.84E-2
⁹⁹ Tc	1.79E1	7.72E2	1.70E-2
²²⁹ Th	5.41E5	4.38E5	2.13E-1
²³⁰ Th	7.99E3	6.00E3	2.02E-2
²³² Th	2.16E-1	1.62E-1	1.10E-7
²³³ U	2.02E3	1.36E3	9.69E-3
²³⁴ U	1.27E3	4.56E2	6.26E-3
²³⁵ U	4.14E-1	1.48E-1	2.16E-6
²³⁶ U	1.25E1	4.48E0	6.48E-5
²³⁸ U	6.18E-2	3.63E-2	3.37E-7
⁹³ Zr	3.00E0	—	2.51E-3

Source: EPA, 1988 (Ingestion only).

Assumed: Receptor drinks 2 l/day of water.

— = No dose conversion factor for TSPA 1993

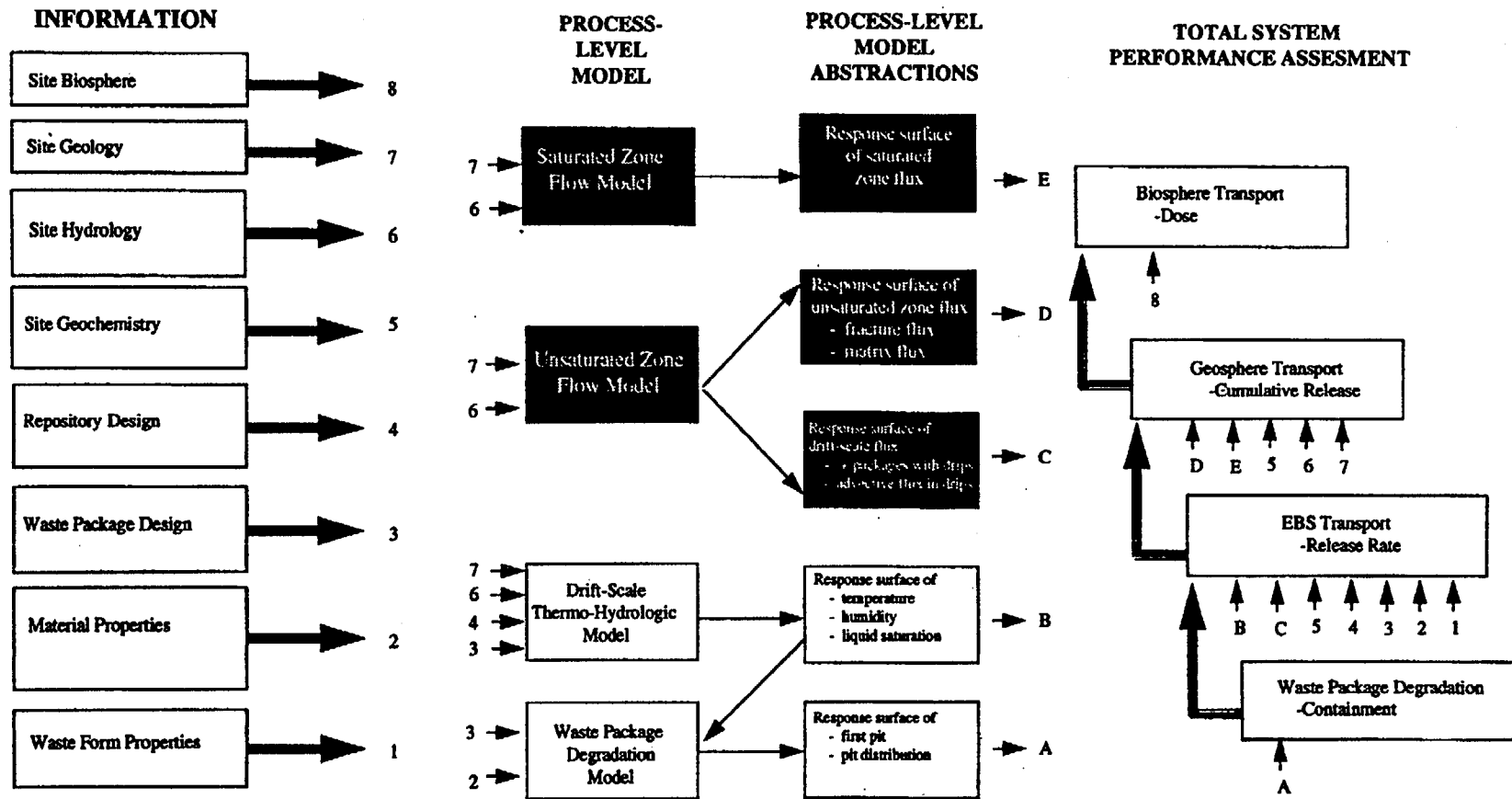


Figure 7.1-1 Information flow schematic for unsaturated zone flow model.

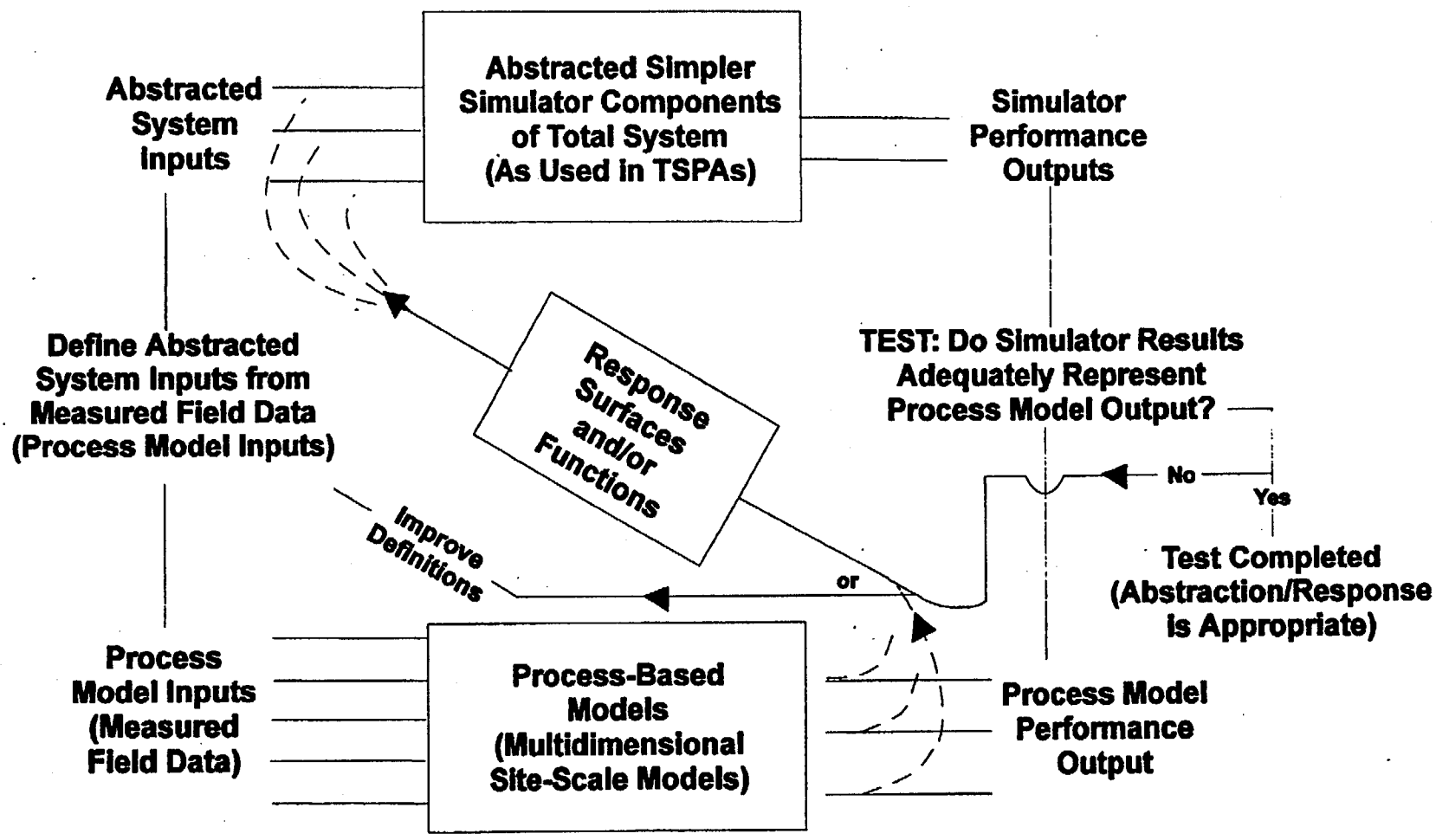


Figure 7.2-1 Illustration of Proposed Testing of Process Model Abstractions/Responses Used in Total System Simulators (after Nelson, 1995).

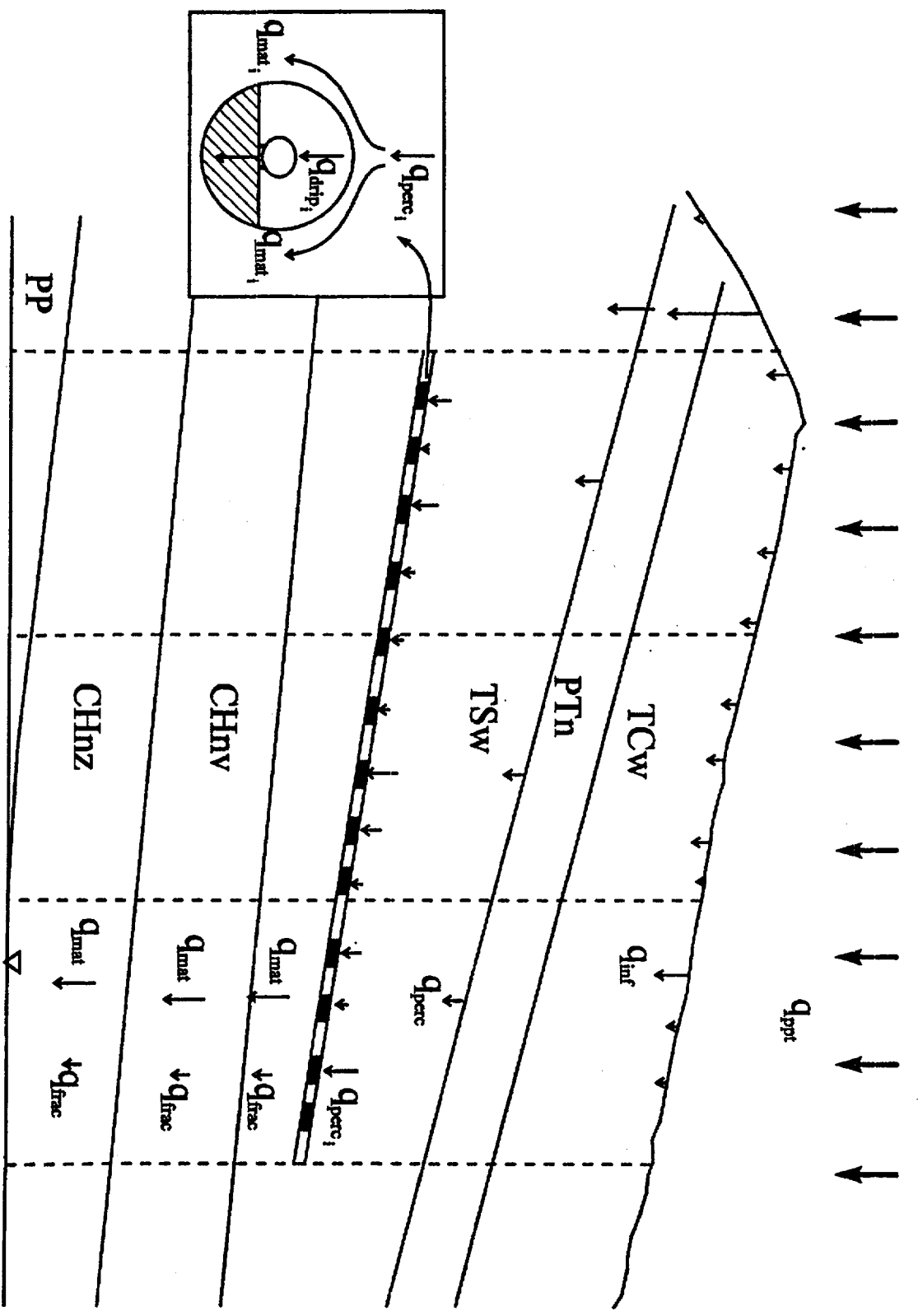
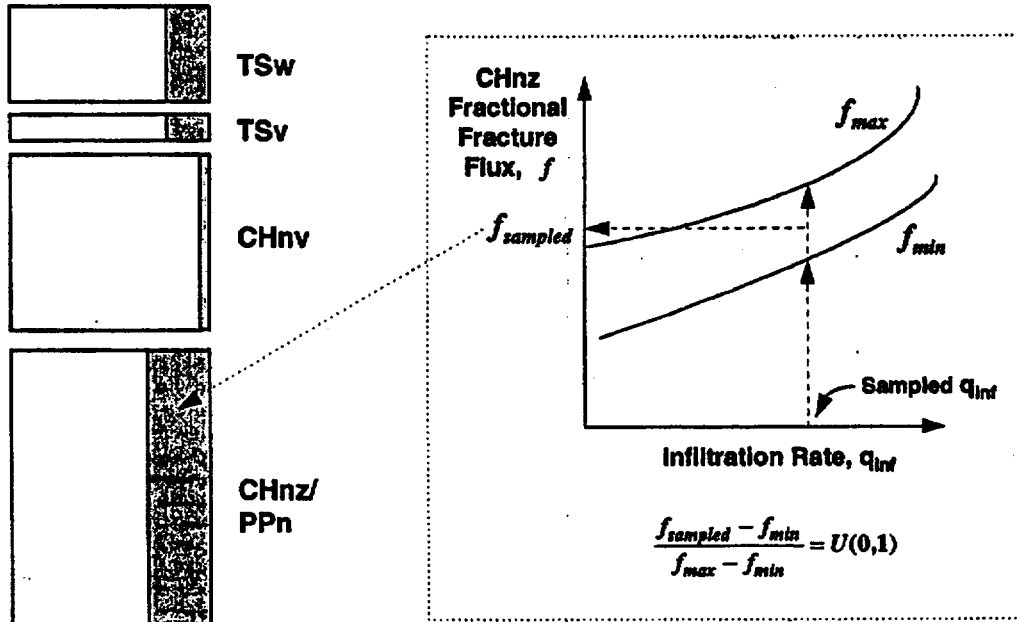


Figure 7.2-2 Schematic Depiction of Distribution of Infiltration into Fracture and Matrix Percolation Flux Components (TSPA-1995).

How Much?

(Fractional-Fracture-Flow Process-Level Abstraction)



How Fast?

(Matrix-Velocity-Field Process-Level Abstraction)

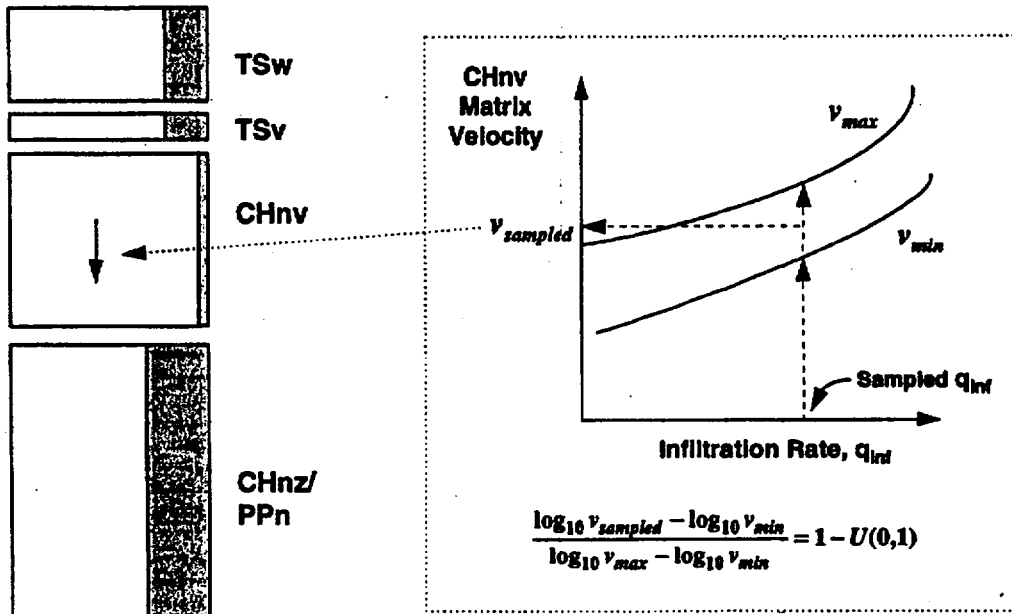


Figure 7.2-3 Schematic of proposed abstraction methodology for determining velocity and fraction of fracture flow as a function of infiltration flux, q_{inf} .

LBL/USGS Site Scale Model, 2D Cross Section

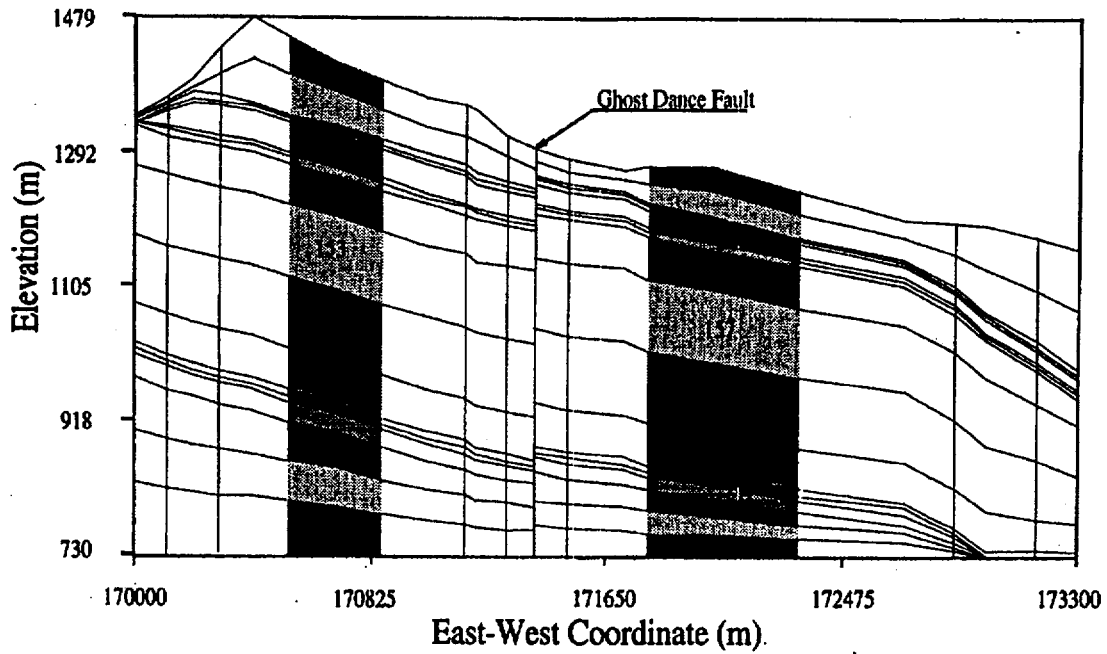


Figure 7.2-4 LBL/USGS Site Scale Model, 2-dimensional cross section.

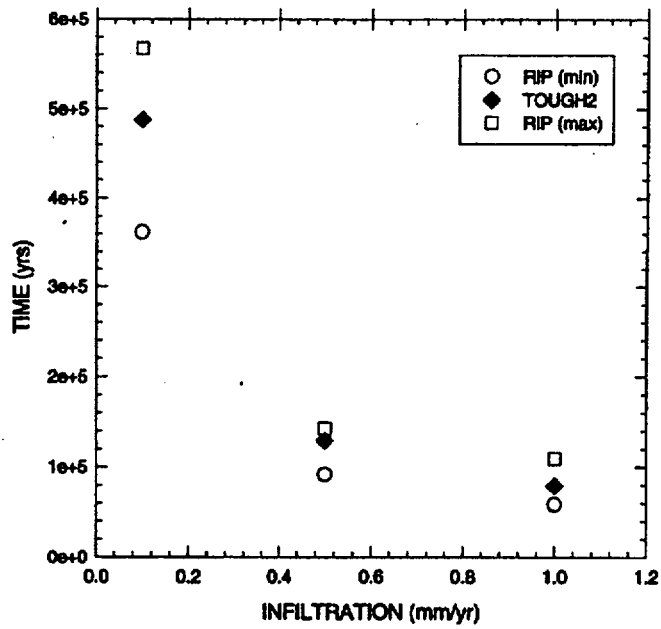


Figure 7.2-5 Comparison of single-point arrival times for TOUGH2 and RIP.

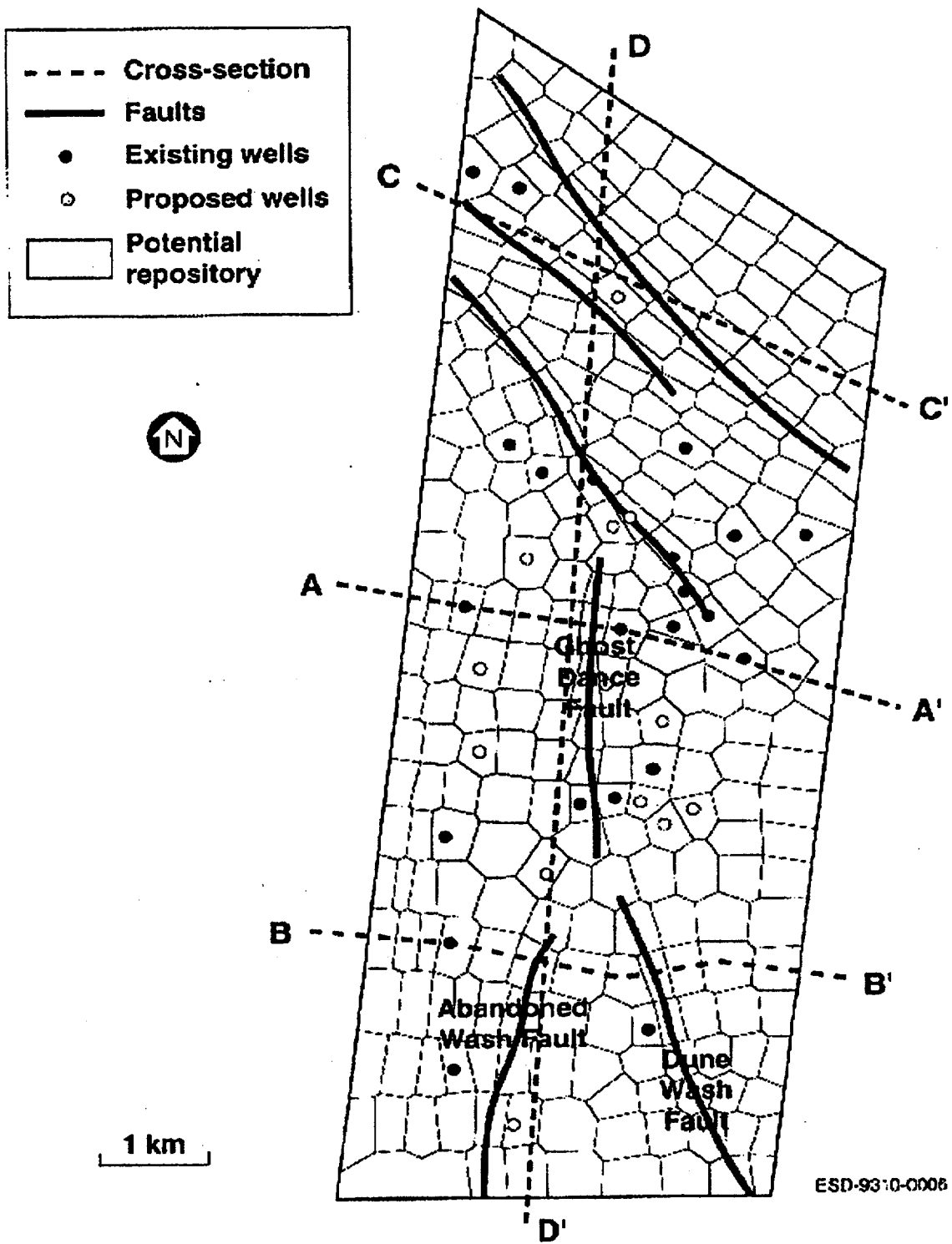


Figure 7.2-6 Plan view of the LBL/USGS Site-Scale Model of the Unsaturated Zone at Yucca Mountain (from Wittwer et al., 1995).

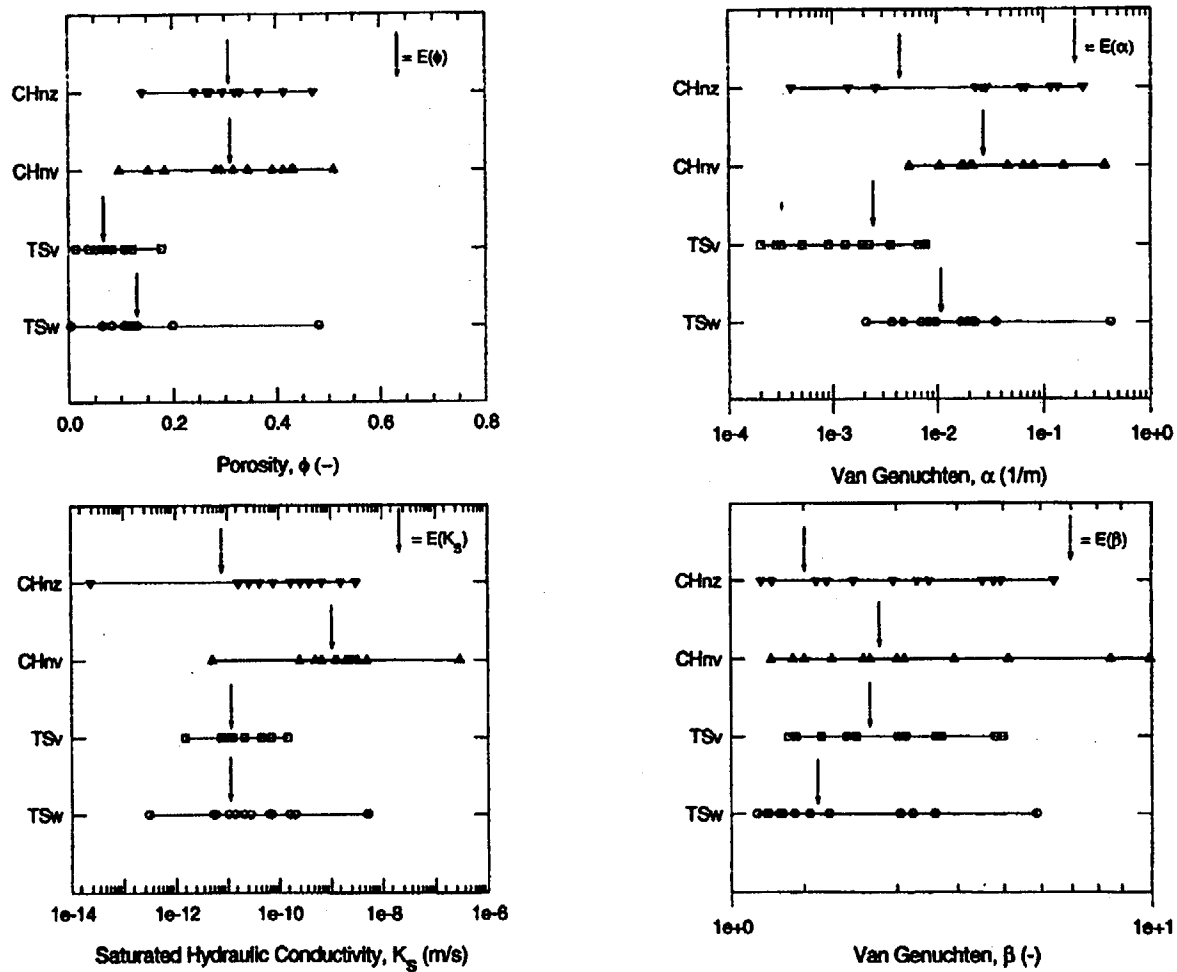


Figure 7.2-7 Range of matrix hydrologic property values sampled randomly from parameter distributions presented in Schenker et al., (1995).

TSw

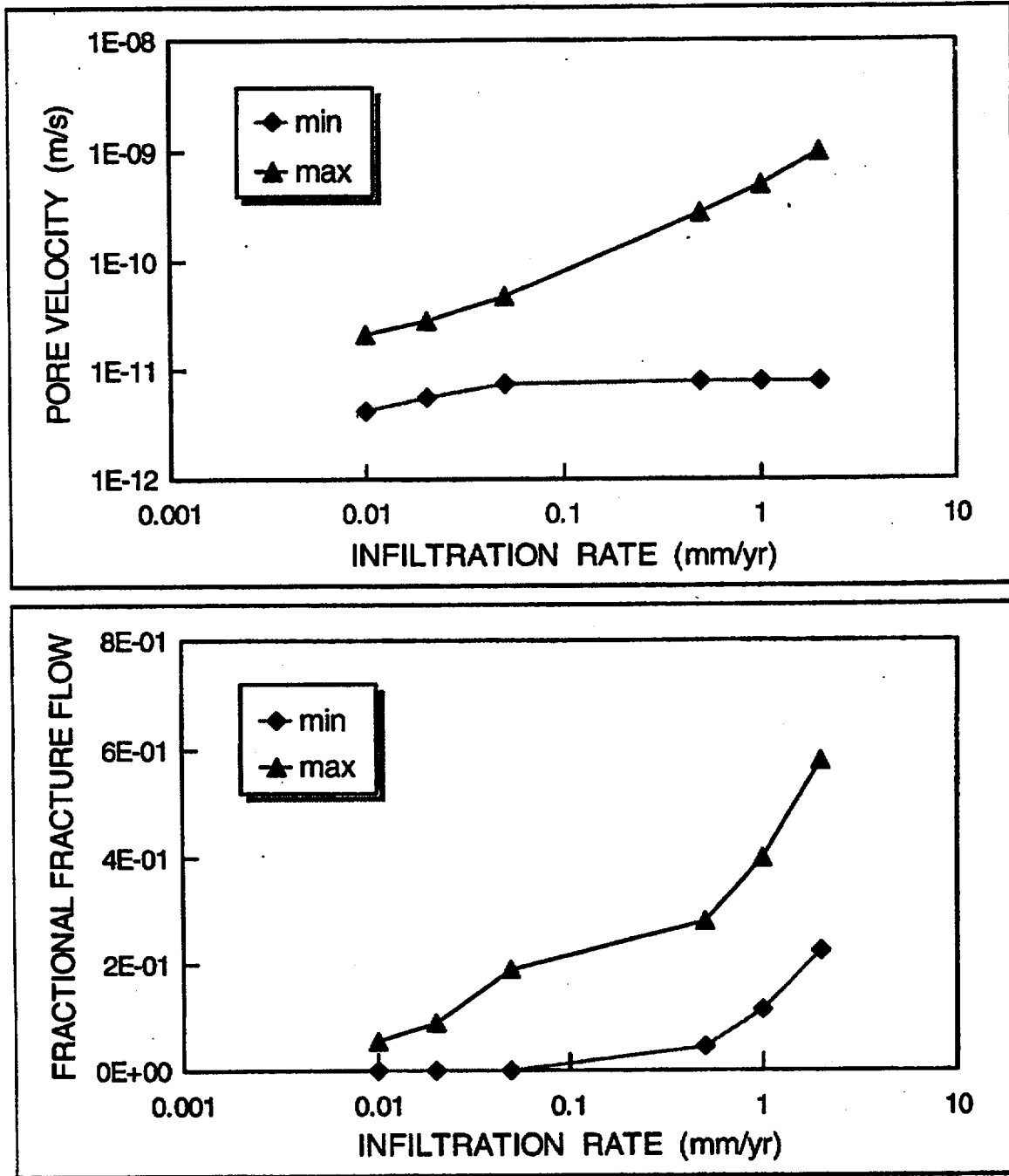


Figure 7.2-8 Ranges of pore velocity and fractional fracture flow for TSw.

TSv

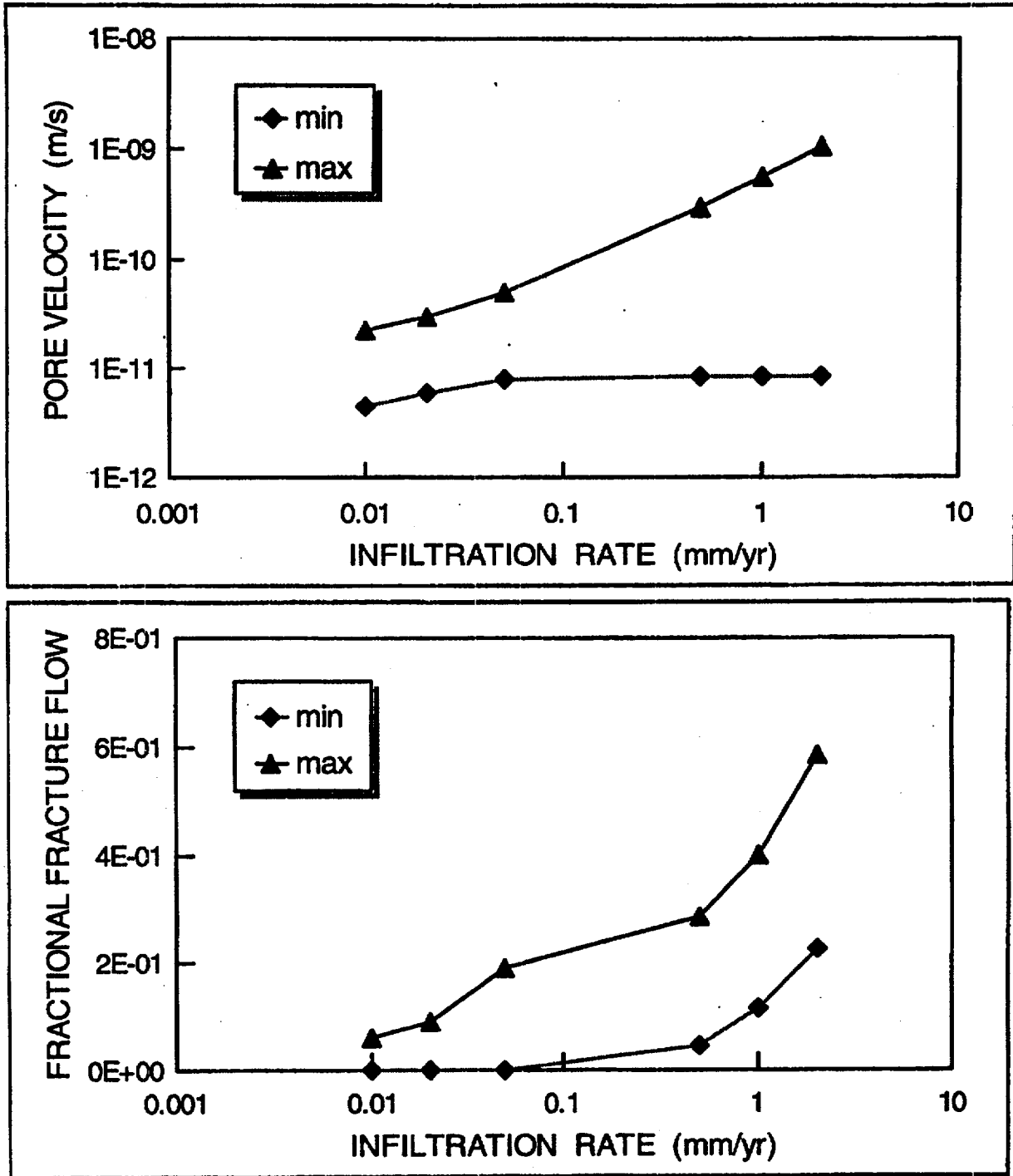


Figure 7.2-9 Ranges of pore velocity and fractional fracture flow for TSv.

CHnv

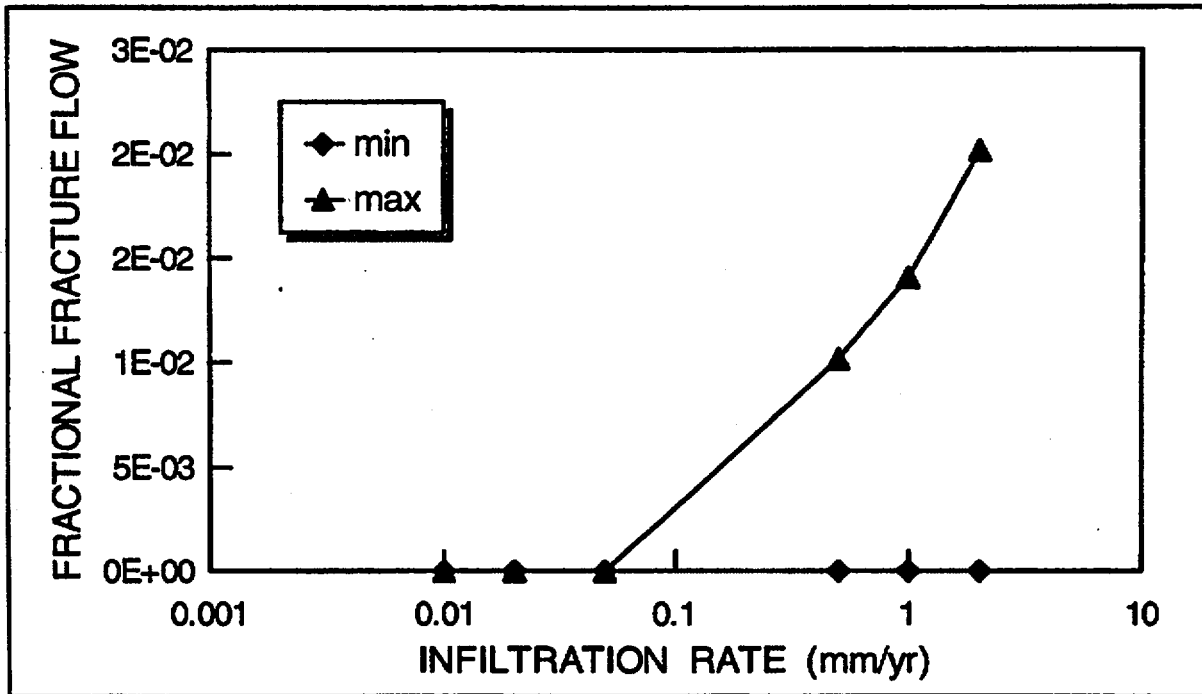
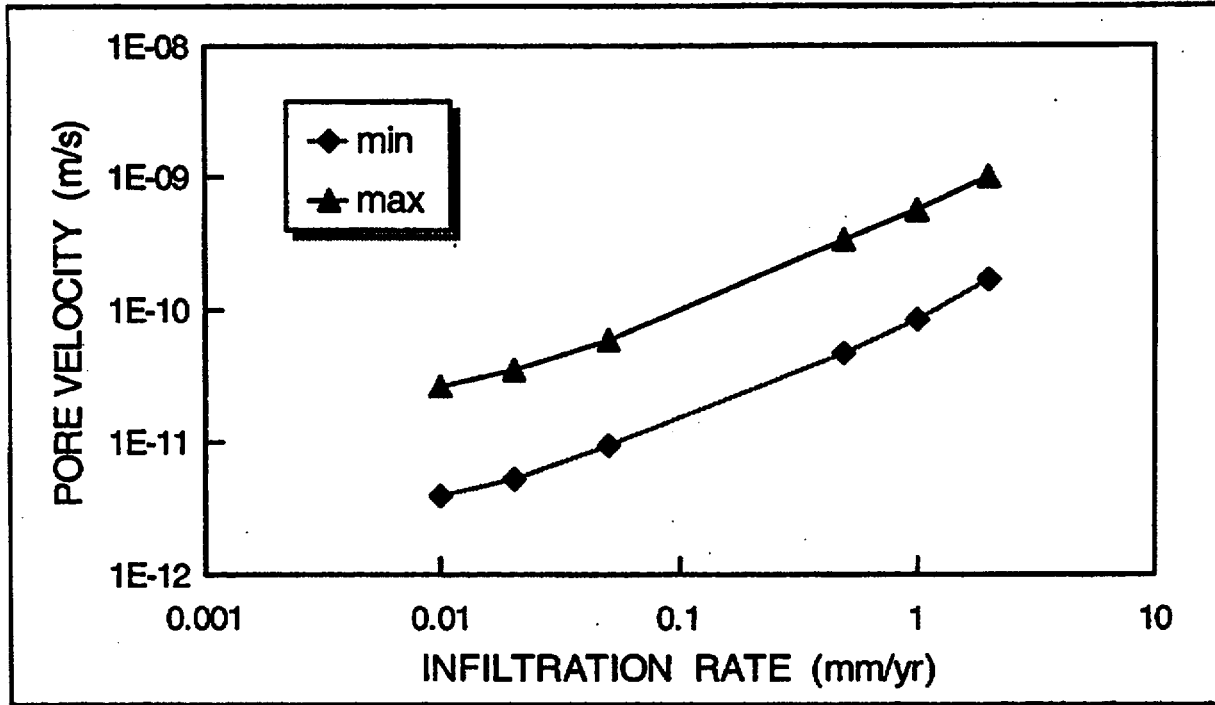


Figure 7.2-10 Ranges of pore velocity and fractional fracture flow for CHnv.

CHnz

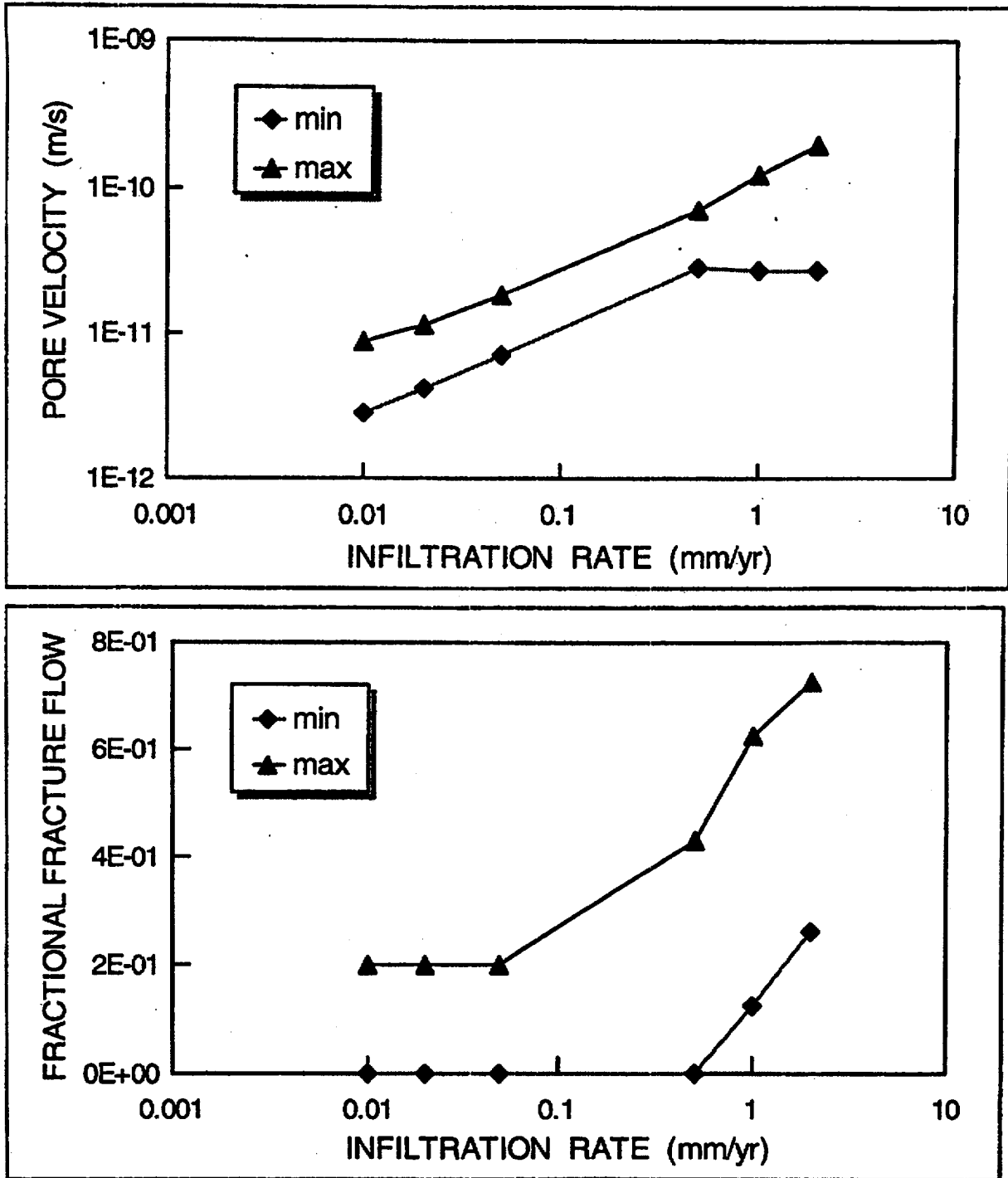
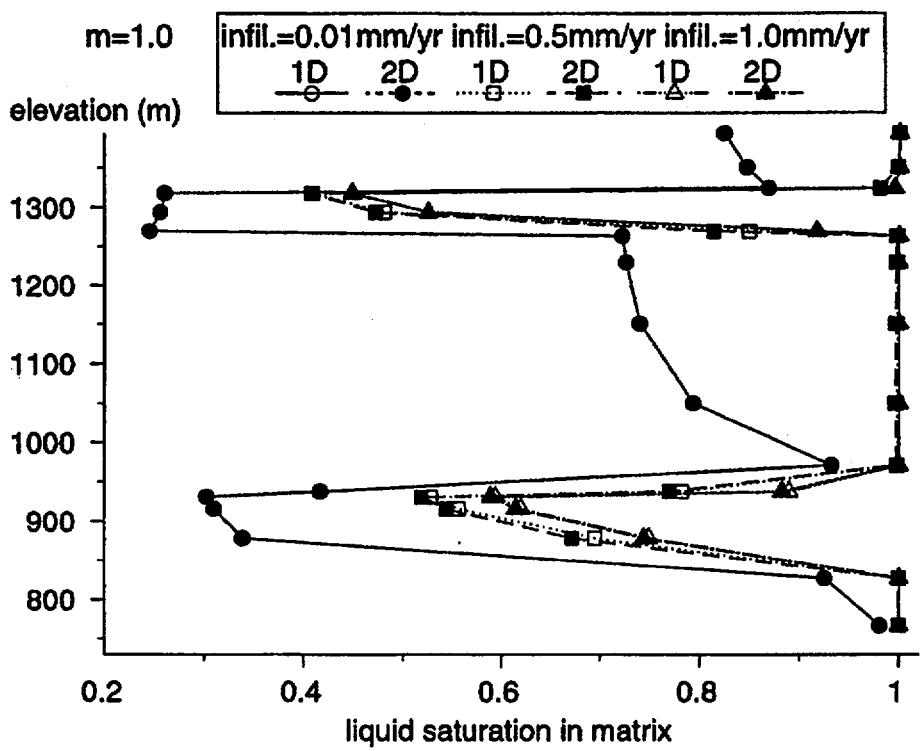


Figure 7.2-11 Ranges of pore velocity and fractional fracture flow for CHnz.

A)



B)

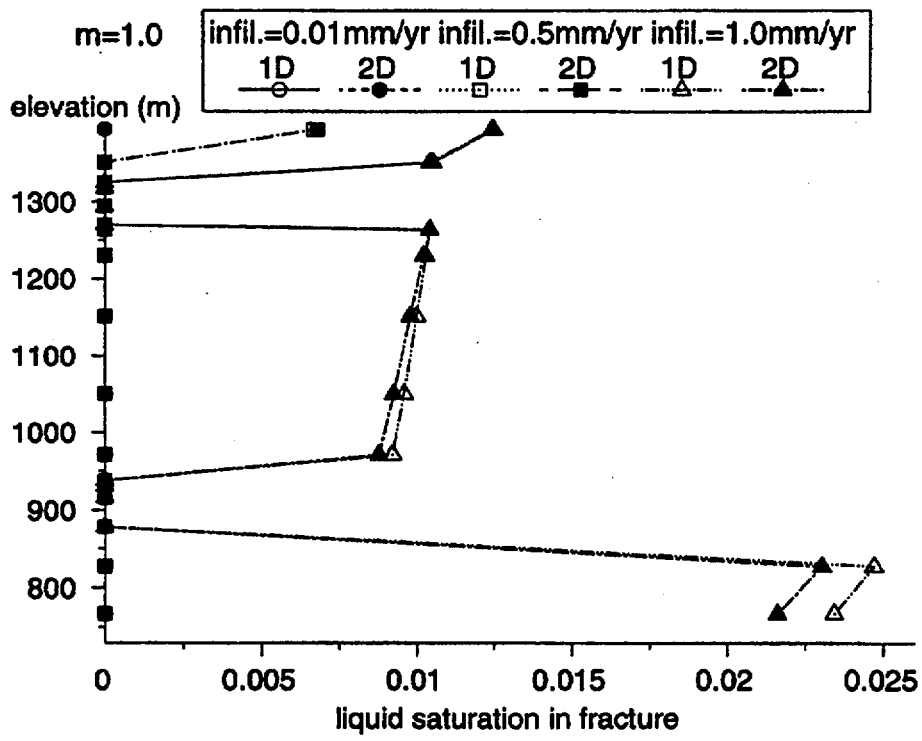


Figure 7.2-12 Liquid saturation distributions along Column 153 of the LBL/USGS site-scale model, for (A) matrix, and (B) fracture.

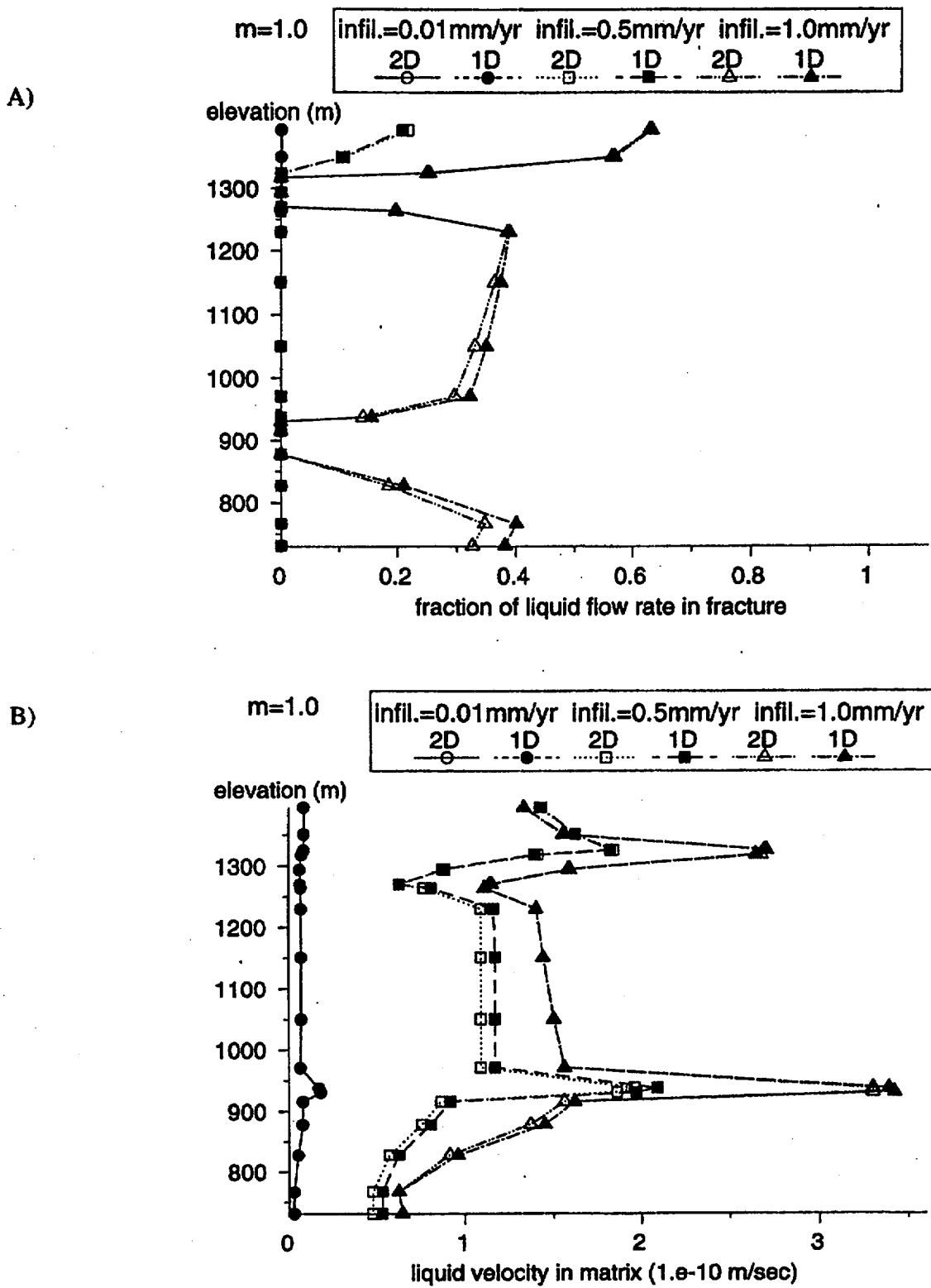


Figure 7.2-13 Liquid flow distribution along Column 153 of the LBL/USGS site-scale model, showing (A) fracture of liquid flow rate in fracture, and (B) pore velocity in matrix.

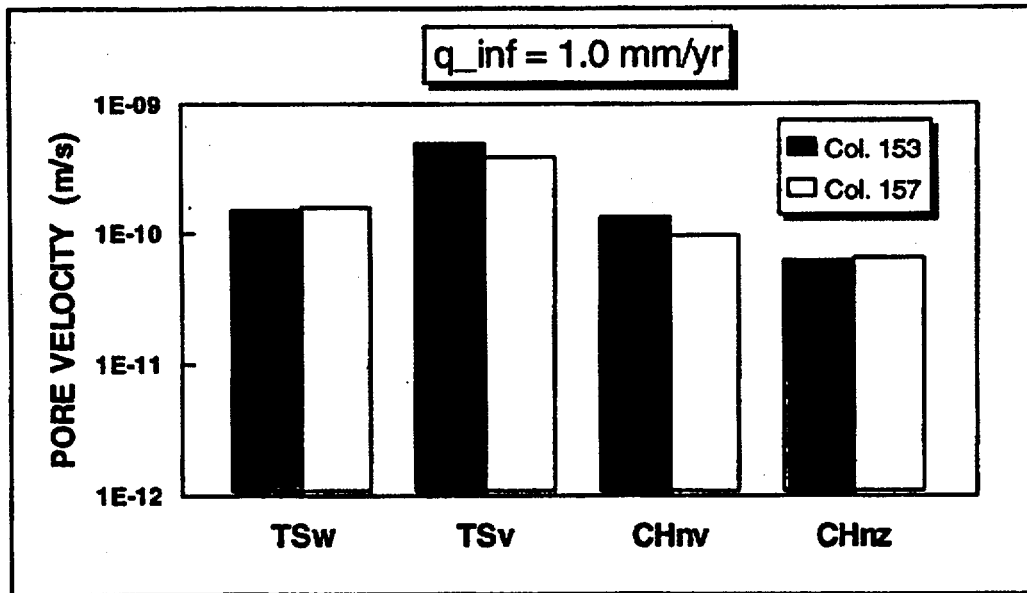
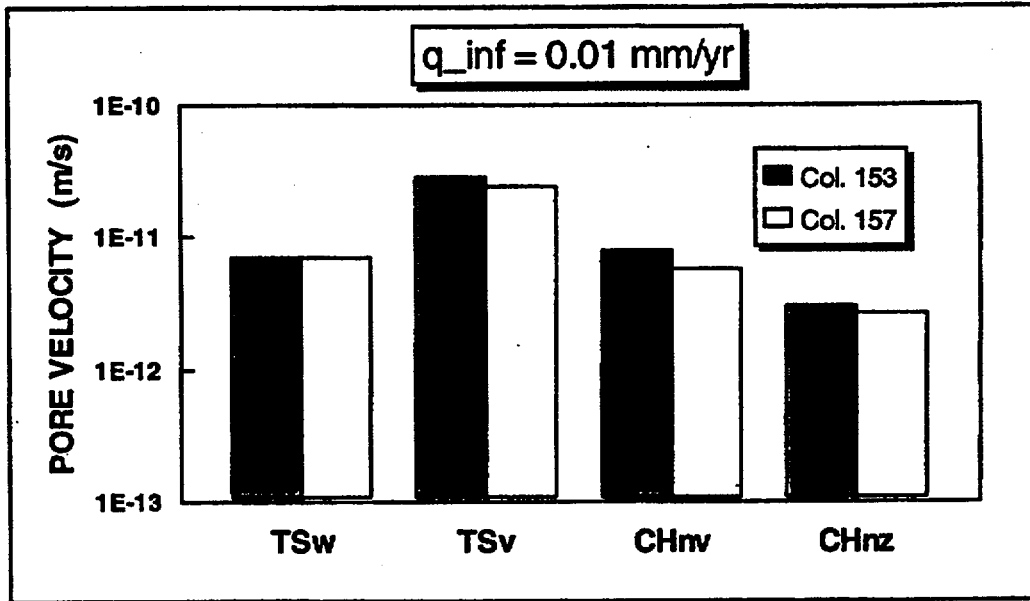


Figure 7.2-14 Comparison of matrix pore velocities for columns 153 and 157 with infiltration of: (i) 0.01 mm/yr and (ii) 1.0 mm/yr.

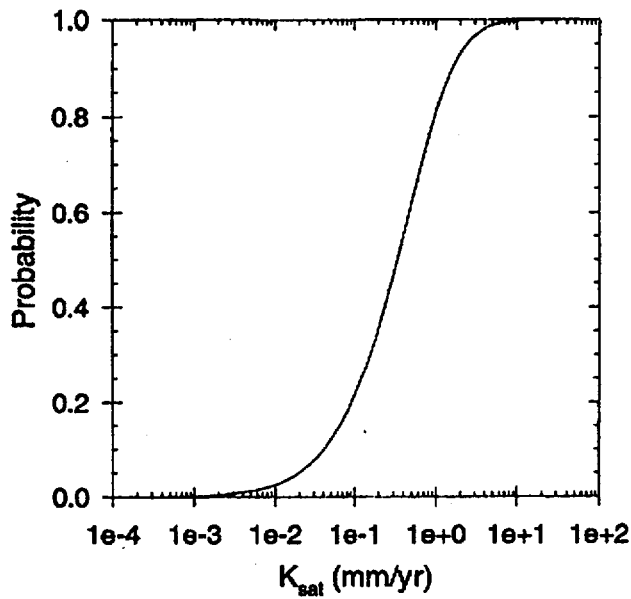


Figure 7.3-1 CDF for K_{sat} (in the TSw) when q_{inf} is 2 mm/yr.

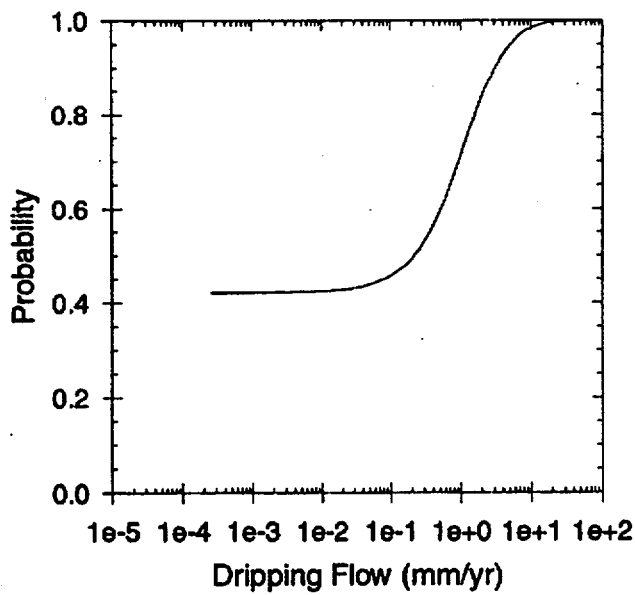


Figure 7.3-2 CDF for dripping flux, q_{drip} , on waste packages when q_{inf} is 2 mm/yr.

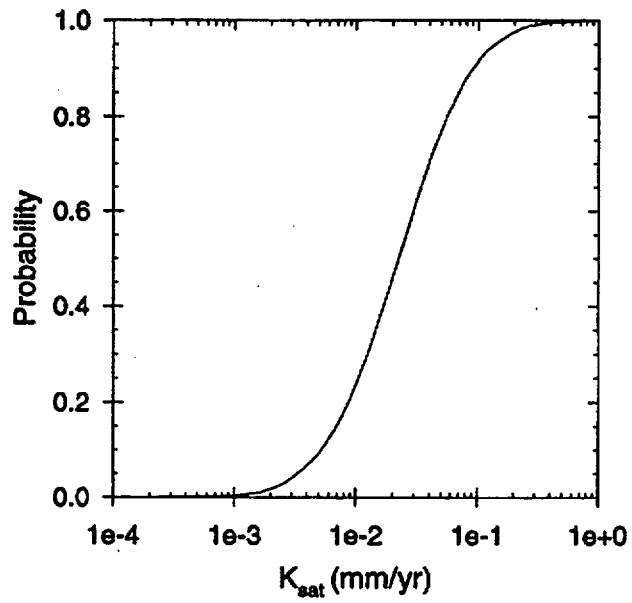


Figure 7.3-3 CDF for K_{sat} (in the TSw) when q_{inf} is 0.05 mm/yr.

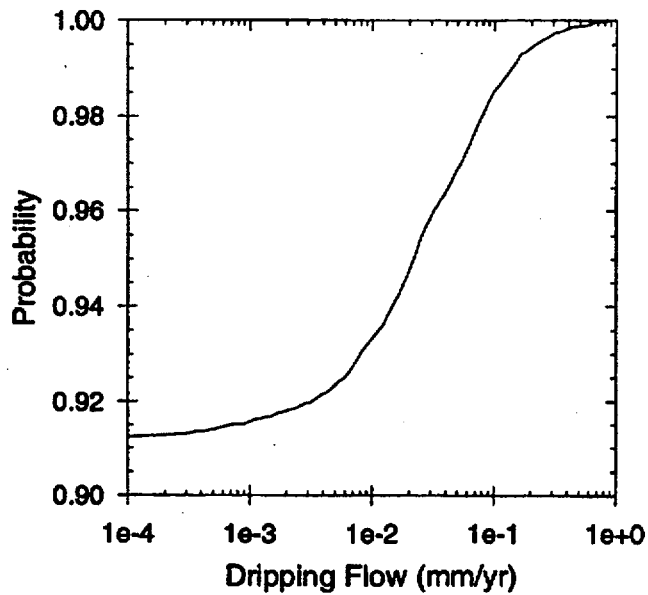


Figure 7.3-4 CDF for dripping flux, q_{drip} , on waste packages when q_{inf} is 0.05mm/yr.

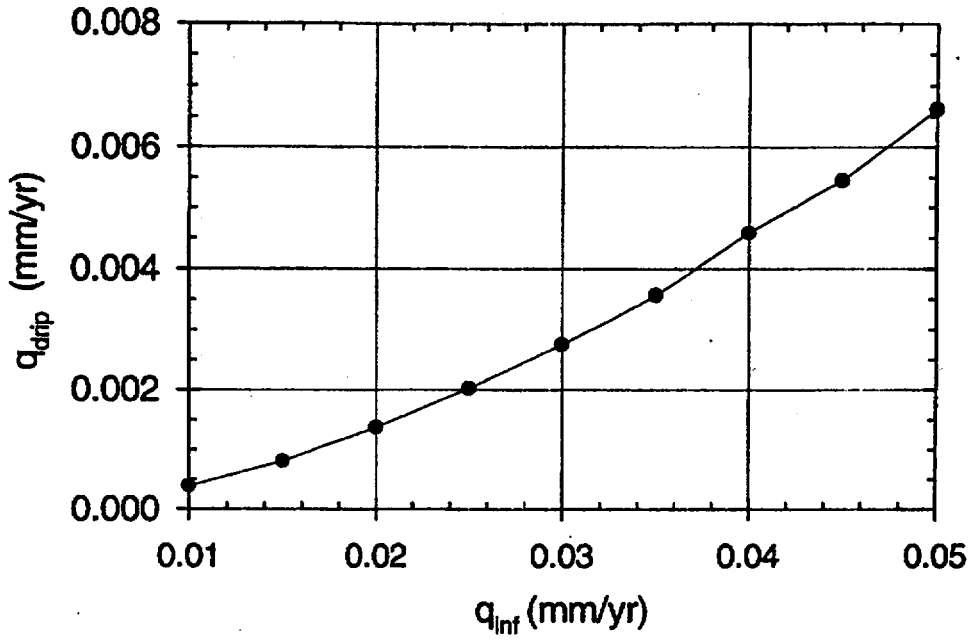


Figure 7.3-5 Average dripping flux (Darcy velocity), q_{drip} , on waste packages for low unsaturated-zone infiltration rates.

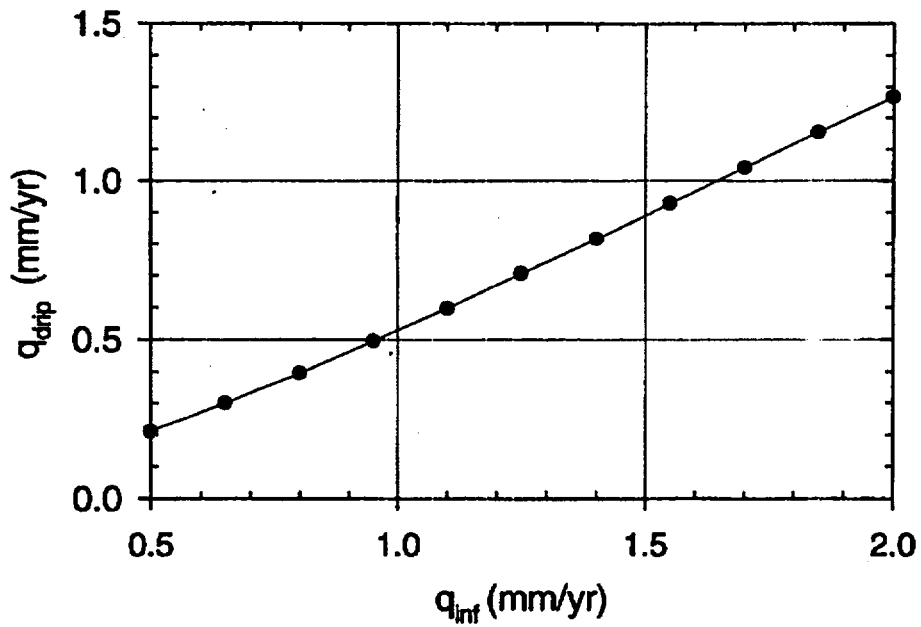


Figure 7.3-6 Average dripping flux (Darcy velocity), q_{drip} , on waste packages for high unsaturated-zone infiltration rates.

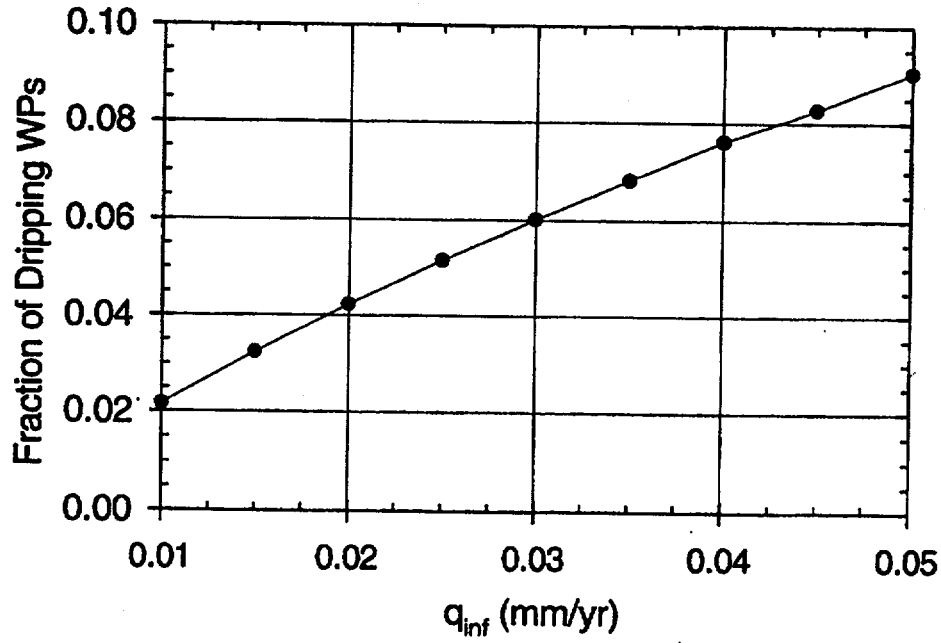


Figure 7.3-7 Average fraction of waste packages with drips, f_{drip} , for low unsaturated-zone infiltration rates.

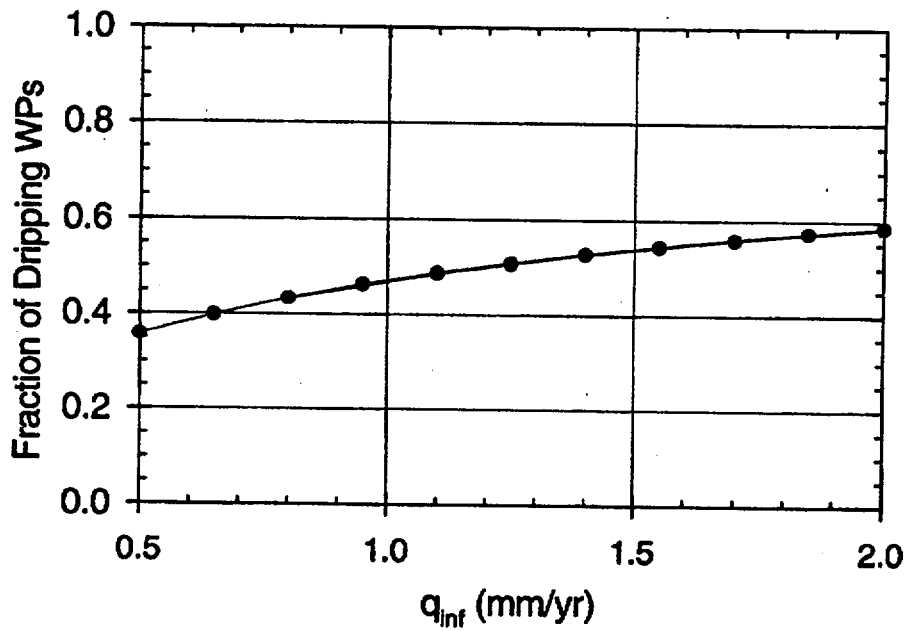


Figure 7.3-8 Average fraction of waste packages with drips, f_{drip} , for high unsaturated-zone infiltration rates.

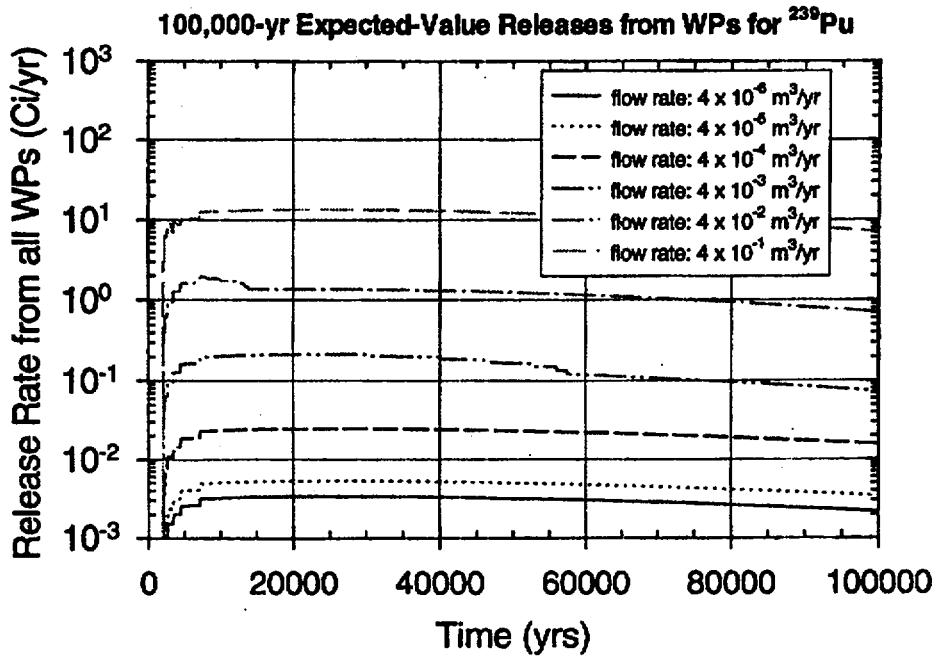


Figure 7.3-9 100,000-yr expected-value releases for ²³⁹Pu from all waste packages, for various values of the dripping flow rate, Q_{drip} .

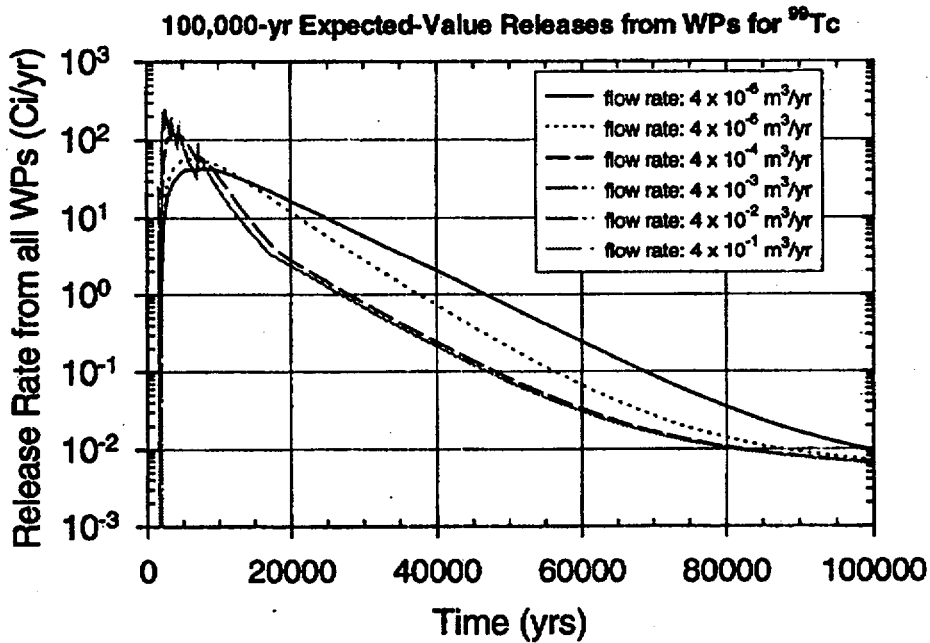
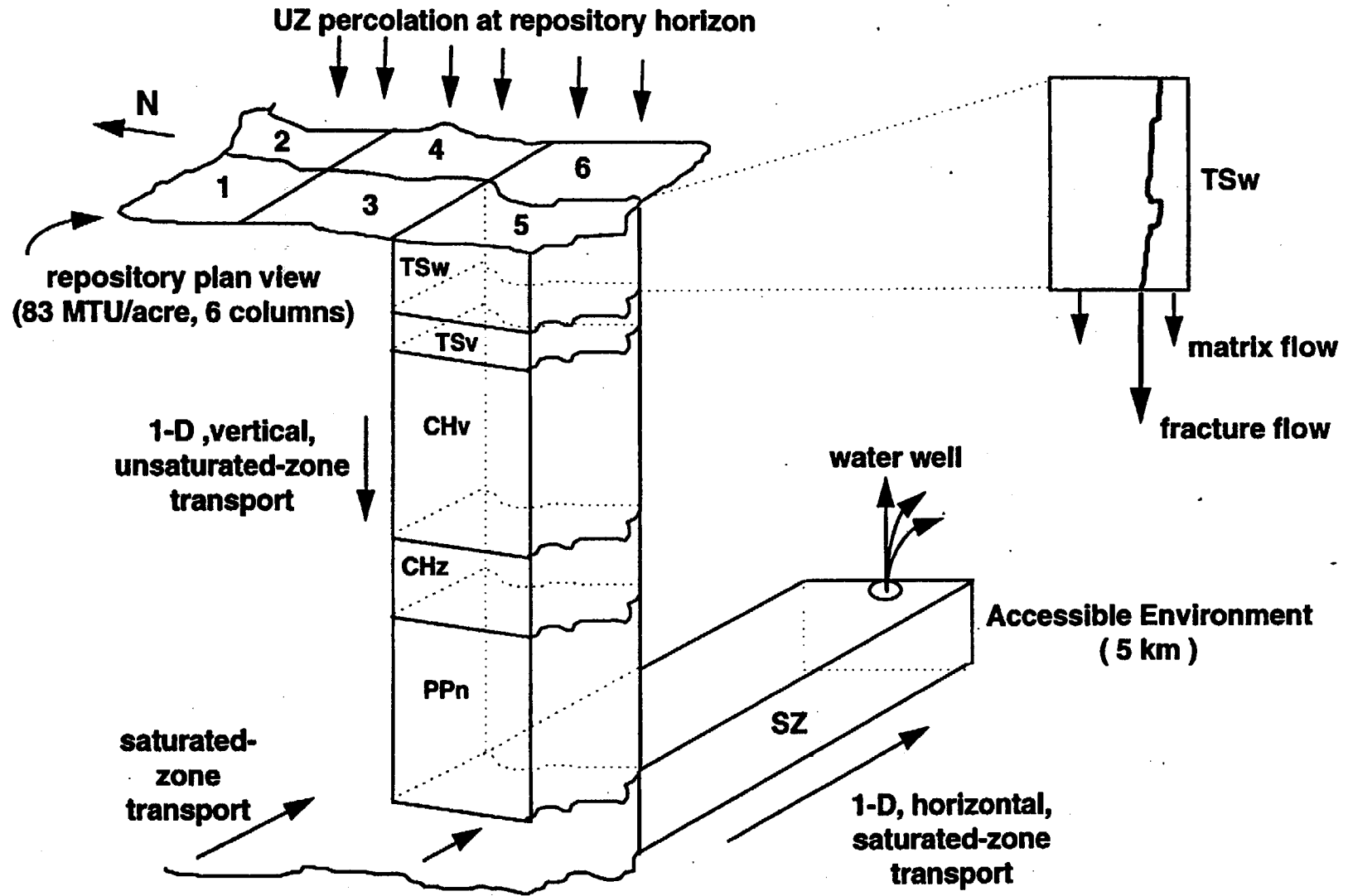


Figure 7.3-10 100,000-yr expected-value releases for ⁹⁹Tc from all waste packages, for various values of the dripping flow rate, Q_{drip} .



7-61

Figure 7.4-1 Schematic of UZ and SZ pathway geometry in RIP TSPA model.

(Intra-unit Fracture Connectivity: TSPA Abstraction)

- Average path length in fracture or in matrix before transitioning is equal $1/\lambda$, where λ is the transition rate:

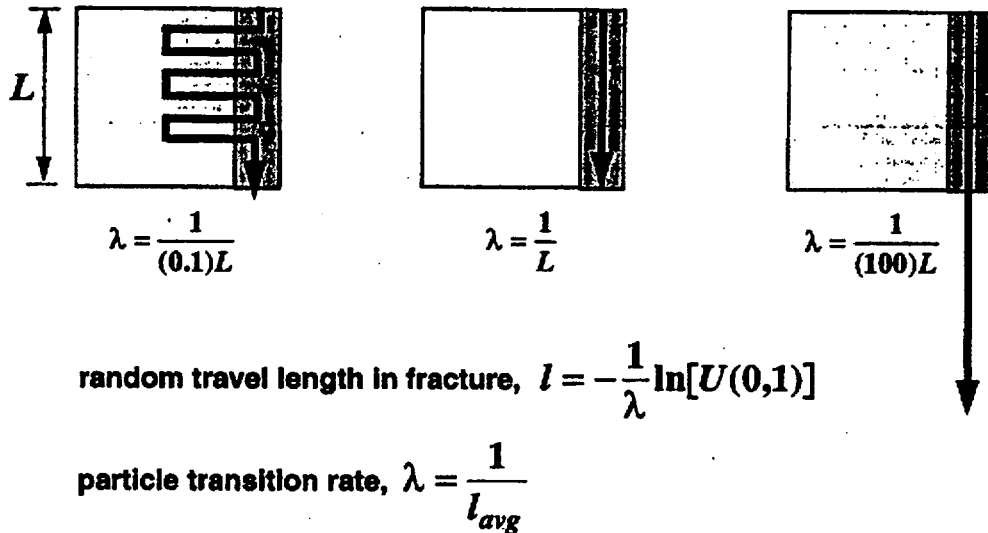


Figure 7.4-2 Schematic of fracture/matrix interaction in RIP: Markovian-particle-transitioning process to represent intra-unit fracture connectivity.

(Inter-unit Fracture Connectivity: TSPA Abstraction)

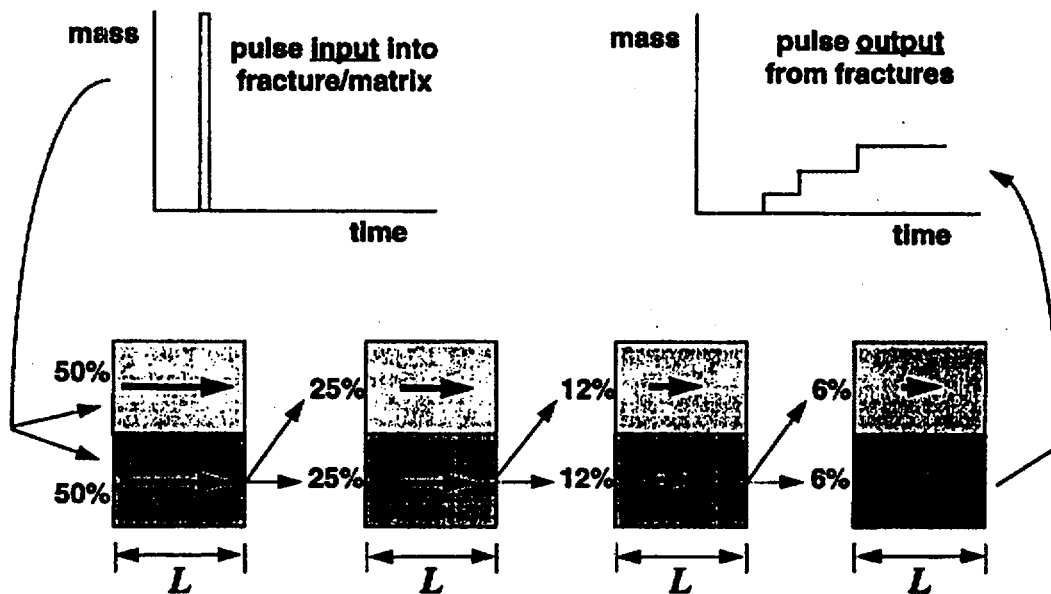


Figure 7.4-3 Schematic of inter-unit fracture and pathway connectivity in RIP.

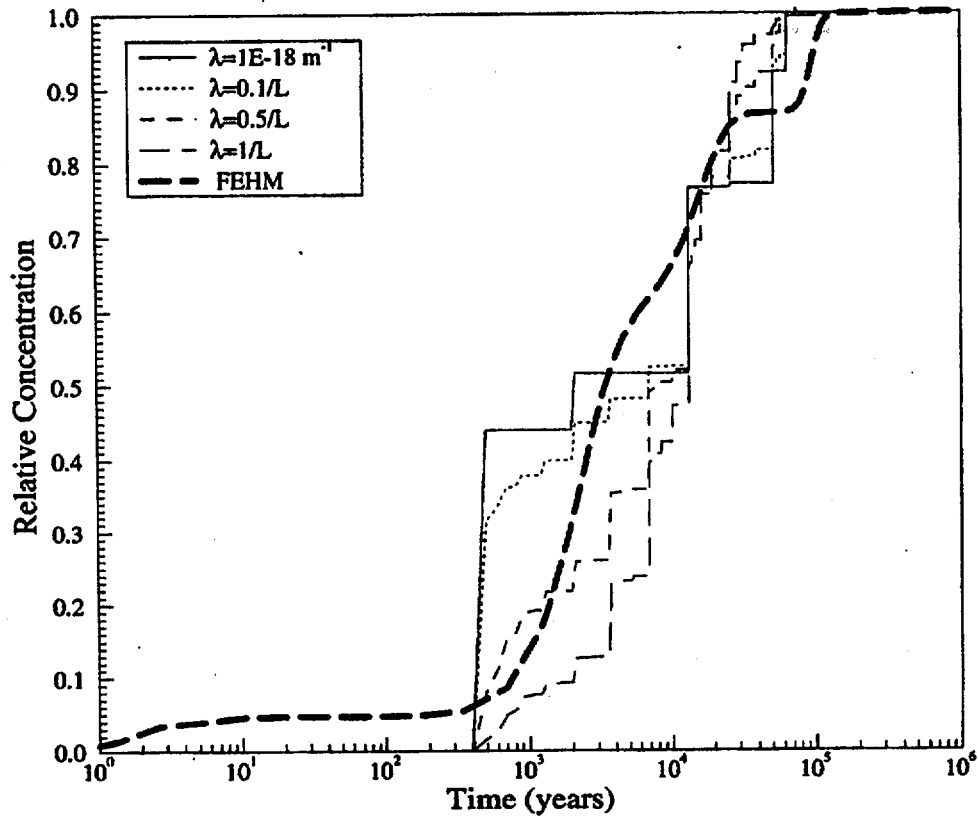


Figure 7.4-4 Comparisons between RIP simulations with different fracture/matrix transition rates and the FEHM simulation for an infiltration rate of 4.0 mm/yr and no matrix diffusion (from Li et al., 1995).

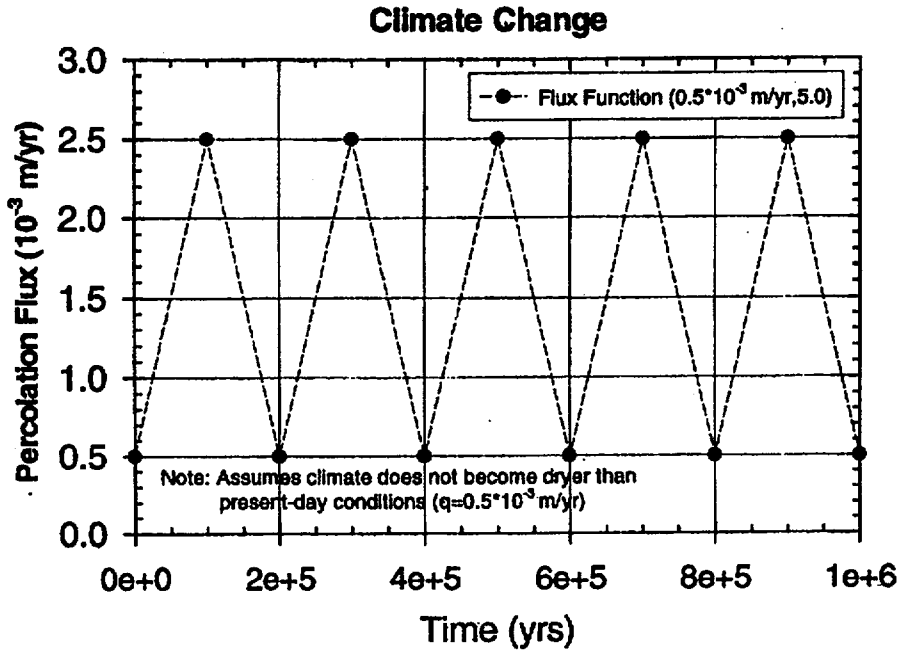


Figure 7.7-1 Effect of climate change on infiltration rate, q_{inf} .

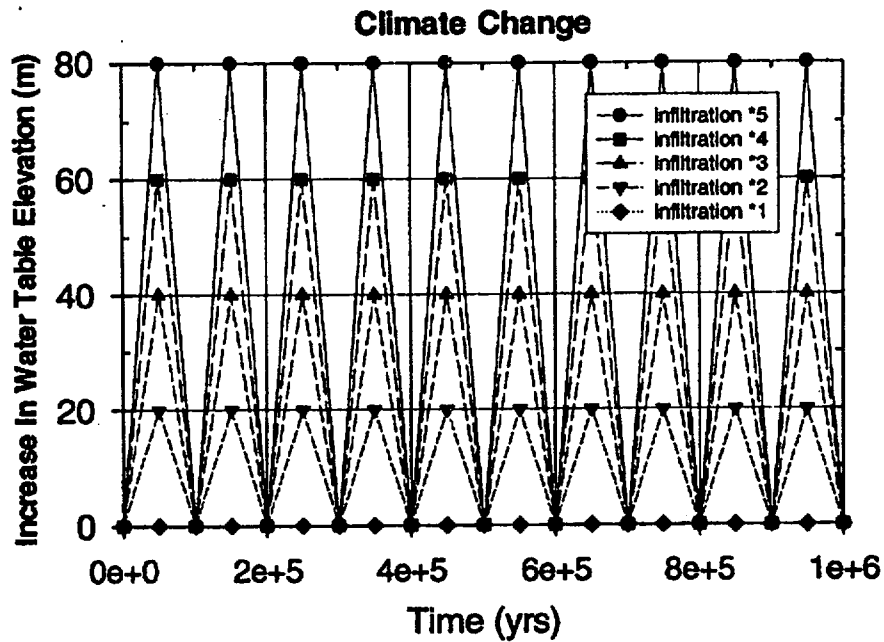


Figure 7.7-2 Effect of climate change on water-table elevation.

8. WASTE PACKAGE/ENGINEERED BARRIER SYSTEM RESULTS

Jerry A. McNeish, Joon H. Lee, Joel E. Atkins, Vinod Vallikat

8.1 INTRODUCTION

Analyses were conducted to evaluate the potential releases from the waste package(WP)/engineered barrier system (EBS). RIP (Golder, 1993), a total system performance assessment code, was used to conduct the performance analyses presented in this chapter. Due to the varying degrees of uncertainties in many of the features of the subsystem components, a sensitivity analysis of the multiple conceptual models was conducted. For example, implementation of the waste package degradation modeling discussed in Chapter 5 led to an evaluation of the impacts of different conceptual models for the initiation of the carbon steel outer barrier corrosion and the cathodic protection of the corrosion resistant (Alloy 825) inner barrier by the outer barrier. This chapter documents and analyzes the sensitivity of the EBS release to the alternate conceptual models. Additional results are also presented to show the effects of using alternate values for various other parameters in the waste package environment. Sensitivity of EBS release to cladding performance and waste form surface area changes were also performed.

As indicated in Figure 8.1-1, the EBS release results are predicated on the abstraction of process model results and laboratory-derived properties, and utilize a range of possible repository and in-drift material design options. The NRC release rate requirements are presented for comparison, though a strict compliance evaluation is not conducted. These EBS release results are directly used as input to the geosphere transport analyses which evaluate the cumulative release and peak dose at the accessible environment boundary (see Chapter 9).

The chapter presents 1) the major assumptions and key parameter values (Section 8.2), 2) sensitivity analyses of the peak release rate from the EBS as affected by variations in the conceptual model of the subsystem, and 3) the cumulative release from the EBS over 10,000 years using multiple realizations for the distribution of the parameters. Note, that the cases considered in this chapter do not include any effects caused by climate change, because the effect of climate change from 0 to 10,000 years is expected to be negligible.

8.2 MAJOR ASSUMPTIONS AND KEY PARAMETER VALUES

This section discusses the major assumptions incorporated into the RIP simulations for the waste package/EBS subsystem performance analyses. The discussion also includes the key parameters used in the simulations.

8.2.1 Major Assumptions in Waste Package/Engineered Barrier System Performance Analyses

The major assumptions for the waste package/EBS subsystem incorporated in the performance analyses conducted for TSPA-1995 are discussed below.

- 1) In TSPA-1995, the waste disposal containers for both spent fuel and vitrified defense high-level waste were assumed to have a two-layer container design with a 100 mm thick carbon steel outer layer and a 20 mm thick Alloy 825 inner layer. This assumption was prompted by the lack of information on the performance of the moderately corrosion resistant barrier materials (Monel 400 and 70/30 Cu/Ni alloy). Details of the waste container design were discussed in Section 3.5.
- 2) In the analyses, the entire waste form surface was assumed to be covered with a "thin" water film (i.e., uniform thickness of 1.0 mm) when the waste container had at least one pit penetration and the surface temperature was less than 100 °C. Alteration of the waste form is assumed to initiate after the first pit penetration. The water film thickness was used in the calculation of the radionuclide concentration at the waste form surface.
- 3) If a waste container has at least one pit penetration and the waste package surface temperature cools to less than 100 °C, then the waste packages that are dripped on are assumed to release radionuclides both by advection and diffusion. In this EBS release model, the diffusion coefficient in the diffusive release model discussed in Section 6.5 was set to 10^{-7} cm²/sec. This diffusion coefficient value was obtained from the data developed by Conca and coworkers (Conca, 1990; Conca and Wright, 1992). In the absence of water drips, a diffusive release was assumed, and the diffusion coefficient was calculated using the empirical functional form described in Section 6.5.
- 4) The releases of ¹⁴C, ³⁶Cl, and ¹²⁹I from the EBS were assumed to be gaseous. As discussed in detail in Chapters 7 and 9, the gaseous elements are assumed to escape unimpeded from the EBS, and then be dissolved and transported into the geosphere in the aqueous phase. However, there is some uncertainty in the dominant release behavior of ¹²⁹I from the waste package and EBS. Because of the abundance of Cs (about 10 to 1 in the molar ratio), it has been suggested that all the iodine released from the spent fuel UO₂ matrix and grains would form CsI salt which is believed to be the most thermodynamically stable form and is readily soluble in water (Van Konynenburg, 1995; Malinauskas, 1995). This argument supports the contention that aqueous, not gaseous release is the dominant EBS release mechanism for ¹²⁹I. It has also been pointed out that, in some conditions, iodine can escape from the aqueous solution into the air (Gray, 1995b). While the nominal EBS case assumed gaseous release, the ¹²⁹I release mode is uncertain and a sensitivity study of the ¹²⁹I release rate to its release mode from the EBS was conducted. The results are discussed in Section 8.3.
- 5) In all TSPA-1995 simulations, an invert composed of gravel was assumed to underlie the waste packages.

8.2.2 Key Parameter Values

The key parameter values used in the RIP simulations of the EBS release rate are presented in Tables 8.2-1 to 8.2-5 along with the TSPA-1993 (Andrews, et al., 1994) parameter values for comparison. The waste package parameters used for the RIP implementation are given in Table 8.2-1. Generally, the parameters used in TSPA-1995 are similar to those in TSPA-1993 (Andrews, et al., 1994). The waste burnup values are slightly lower in TSPA-1995

(36,666 megawatt days/metric ton heavy metal (MWd/MTHM) combined) than for TSPA-1993 (39,075 MWd/MTHM combined) (Andrews, et al., 1994). The TSPA-1995 inventory is compared with the TSPA-1993 (Andrews, et al., 1994) inventory in Table 8.2-2. The gap fraction inventory used in TSPA-1995 is the same as in TSPA-1993 (Andrews, et al., 1994) (Table 8.2-3).

The summary of the exposure parameters used in the RIP implementation for TSPA-1995 are presented in Table 8.2-4 and compared with those in TSPA-1993 (Andrews, et al., 1994). The nominal surface area for the spent fuel used in TSPA-1995 is about 5 times larger than the value used in TSPA-1993 (Andrews, et al., 1994). Discussions of the spent fuel surface area are given in Section 6.2. Comparison of the transport parameter values used in TSPA-1993 (Andrews, et al., 1994) and TSPA-1995 are summarized in Table 8.2-5. In both TSPA-1993 and TSPA-1995, the diffusion coefficient in unsaturated geologic media was derived from the data developed by Conca (Engel, 1995) for a wide variety of geologic materials with varying degrees of water saturation. Details of the data and diffusion coefficient model were discussed in Section 6.5. The repository infiltration rate used in TSPA-1995 was selected from two distributions: 1) 0.01-0.05 mm/yr (uniformly distributed); and 2) 0.5-2.0 mm/yr (uniformly distributed). The geometric factor for diffusion in TSPA-1995 was embedded in the diffusive release model discussed in Section 6.5.

8.3 EBS PEAK RELEASE RATE

8.3.1 Introduction

Currently, a potential repository for the permanent disposal of the nation's high-level radioactive wastes including spent nuclear fuel (SF) and vitrified defense high-level waste (DHLW) is subject to the post-closure subsystem regulatory requirements of the U.S. Nuclear Regulatory Commission (NRC). The NRC sub-system performance measures that are relevant to the evaluation of the engineered barrier system (EBS) of the Yucca Mountain site are specified in 10 CFR Part 60. These include the substantially complete containment requirement (10 CFR 60.113(a)(1)(ii)(A)) and the EBS controlled release rate requirement (10 CFR 60.113(a)(1)(ii)(B)). Waste package performance analyses relevant to the substantially complete containment requirement were presented in Chapter 5. To facilitate discussions in the following section of the analyses of the EBS release rates, the NRC regulatory requirements for the EBS controlled release rate are restated below:

The release rate of any radionuclide from the engineered barrier system following the containment period shall not exceed one part in 10,000 per year of the inventory of that radionuclide calculated to be present at 1,000 years following permanent closure, or such other fraction of the inventory as may be approved by the Commission: provided, that this requirement does not apply to any radionuclide which is released at a rate less than 0.1 % of the calculated total release rate limit. The calculated total release rate limit shall be taken to be one part in 100,000 per year of the inventory of radioactive waste, originally emplaced in the underground facility, that remains after 1,000 years of radioactive decay.
[10 CFR 60 (a)(1)(ii)(B)]

Calculated NRC release rate limits of each radionuclide for the spent fuel are tabulated in Table 8.3-1. The 1,000-year inventory of the spent fuel in the table was determined using the ORIGEN2 code (Croff, 1983) based on the fuel characteristics discussed in Section 3.7. Taking the 1,000-year inventory of a radionuclide and multiplying by 10^{-5} yields the NRC maximum EBS release rate limit for that radionuclide. Any radionuclide with a calculated maximum release rate of less than 0.1 % of the total release rate limit of 1.24×10^3 Ci/yr (i.e. 1.24 Ci/yr) need not be considered.

A sensitivity analysis was conducted using a suite of different conceptual models relevant to waste package and EBS parameters and designs to evaluate the corresponding EBS release rates. The analysis included the effect of: 1) different corrosion initiation thresholds for the waste disposal container; 2) alternative thermal loading; 3) repository level percolation rate; 4) cathodic protection of the inner barrier (Alloy 825) by the carbon steel outer barrier; 5) EBS release models; 6) cladding failure; 7) ^{129}I release mode; and 8) alternative thermal-hydrologic models. The EBS release rates for the cases listed above were simulated with the "expected" values of the input parameters, i.e. the simulations were for a single realization.

Table 8.3-2 summarizes the nominal cases studied in the EBS release sensitivity analyses for TSPA-1995. Presented in Table 8.3-3 is the summary of the major cases in terms of the time for the first pit penetration and the number of waste packages with their first pit penetration which were obtained from waste package performance analyses discussed in Chapter 5. The table shows that the case for 83 MTU/acre, with no backfill, high infiltration rate and using the RH switch for corrosion initiation of the carbon steel outer barrier (labelled as "83/N/H") is most conservative (i.e., has earliest first pit penetration and most waste packages with at least one pit penetration) among those listed in the table. In the following sections, results of the sensitivity analyses for the EBS peak release rates are presented.

8.3.2 Selection of Radionuclides of Concern

As discussed in the previous section, those radionuclides with the calculated maximum release rate greater than 0.1 % of the total NRC release limit need to be considered. Radionuclides with a calculated maximum release rate smaller than the NRC limit for the radionuclide are excluded. To select radionuclides to be considered in this study, the EBS release rates of all 39 radionuclides in the TSPA 1995 inventory were calculated for a period of 10,000 years for the most conservative case with the largest release rates, which is also the case with the highest waste package degradation (83 MTU/acre, no backfill, high infiltration rate, and RH switch for corrosion initiation of the outer barrier (see Section 5.7.6 and Table 8.3-3)). For the radionuclides which did not have any release in 10,000 years, the calculations were conducted for up to 100,000 years. The results are presented in Table 8.3-4. As shown in column 3 of the table, the radionuclides which have a maximum release rate exceeding 0.1 % of the NRC total release rate limit (i.e., 1.24 Ci/yr) are ^{241}Am , ^{243}Am , ^{14}C , ^{135}Cs , ^{59}Ni , ^{237}Np , ^{210}Pb , ^{107}Pd , ^{226}Ra , ^{79}Se , and ^{99}Tc . Among them, the maximum release rates of ^{241}Am and ^{243}Am are less than the NRC limit (column 2), thus they were excluded from further analyses. These radionuclides were also not included in the recent EBS release sensitivity study (M&O, 1994a).

The radionuclides considered for further analysis are given in Table 8.3-5. As shown in Table 8.3-5, the maximum release rates of the radionuclides in TSPA-1995 are 3 to 6 times higher than

those in the additional sensitivity study to TSPA-1993 (M&O, 1994a) that is due mainly to the release by advective transport incorporated in this year's iteration. Assuming no areal infiltration, TSPA-1993 (Andrews, et al., 1994) and the additional EBS release sensitivity study (M&O, 1994a) found that diffusive transport through the gravel backfill from "failed" waste packages dominated the advective transport component. Although the dominant transport modes considered are different in TSPA-1995 due to the presence of areal infiltration, the radionuclides to be included in TSPA-1995 are the same as those considered in TSPA-1993 (Andrews, et al., 1994) and the additional EBS study (M&O, 1994a), except ^{107}Pd . The higher release rate of ^{107}Pd in TSPA-1995 may be the result of a high water dripping rate assumed in the high infiltration rate case, and may need further consideration to be included in future sensitivity studies, but is not evaluated further at this time. Additionally, the times for the maximum release rate for the radionuclides with a substantial gap fraction (^{14}C , ^{135}Cs , ^{79}Se and ^{99}Tc) and high solubility in water (also the gap fraction radionuclides and ^{59}Ni) are close to those for the same nuclides in the TSPA-1993 additional sensitivity study (M&O, 1994a). The time for the maximum release rate of ^{237}Np (16,600 years) is much later than the previous study (7,000 years), and the release rates of ^{210}Pb and ^{226}Ra which are the principal daughters of the uranium decay chain still increase at 100,000 years, whereas in the previous study, they had maximum release rates at 60,000 and 20,000 years respectively.

In the following sections, a short-hand notation is employed to designate the cases to be simulated and help to facilitate the discussions of the results and their analyses. For example, in the notation of "83/no/loq/RH", the first group ("83") designates the thermal load, i.e., 83 MTU/acre, and the second group designates the backfill presence, i.e., "no" indicates the no backfill case and "yes" indicates the with backfill case. The third group ("loq") designates the infiltration rate used in the analysis, either from the low infiltration range ("loq") or from the high infiltration range ("hiq"). The fourth group ("RH") indicates the criteria used for corrosion initiation of the carbon steel outer barrier, either relative humidity only criteria ("RH") or relative humidity and temperature criteria ("RH&T").

8.3.3 Effects of Alternative Waste Container Corrosion Initiation Conceptual Models

As discussed in Chapter 5, there is uncertainty in the initiation threshold for the corrosion of the carbon steel outer barrier on the waste packages in the potential repository. The outer barrier corrosion may initiate if relative humidity is above a threshold level, or if both relative humidity and temperature reach threshold levels. The relative humidity level at which corrosion occurs is also uncertain. The impacts of the different switches (RH only or RH and temperature) for the initiation of the carbon steel outer barrier corrosion on the waste container corrosion degradation were discussed in Sections 5.7.5 and 5.7.6. Another major uncertainty associated with the waste package performance is the extent of cathodic protection of the corrosion resistant (Alloy 825) inner barrier by the carbon steel outer barrier. Using the measure for the cathodic protection provided from expert elicitation, the impacts on the waste container performance were also addressed in Section 5.7.8.

In this section, the sensitivities of the EBS release rates to the alternative waste container corrosion initiation conceptual models are presented for each radionuclide discussed in the previous section. The first sensitivity case evaluates the impact of the model for initiation of the outer barrier corrosion. The analysis assumes either 1) the outer barrier initiates corrosion only

after both the temperature has dropped below 100 °C and the relative humidity has reached a threshold level between 65 and 75 percent (RH&T) or 2) the outer barrier initiates corrosion as soon as relative humidity reaches the threshold level regardless of the temperature at that time (RH only). The results for the release rate histories of the eight radionuclides (^{14}C , ^{99}Tc , ^{79}Se , ^{135}Cs , ^{59}Ni , ^{237}Np , ^{210}Pb , and ^{226}Ra), are presented respectively in Figures 8.3-1a to 8.3-1h for the case of 83 MTU/acre thermal load without backfill and with the high or low infiltration rates. The NRC limit for each radionuclide is also indicated in the figure caption. As shown in the figures, using RH and T as the criteria for corrosion initiation simply delays the initial releases about 400 years and does not significantly affect the release behavior of the radionuclides. A fraction of the ^{14}C is present in the gap, and the release of ^{14}C from the EBS is assumed to be gaseous. In Figure 8.3-1a, the initial spikes are due to the gap fraction release. The other release spikes in Figure 8.3-1a are indicative of when waste package groups fail. The release rates are not significantly affected by the corrosion initiation assumptions or the infiltration rates. However, the infiltration rate is the major parameter affecting the release rates of other radionuclides.

The results for the sensitivity of the EBS release rates to the cathodic protection of the corrosion resistant inner barrier by the carbon steel outer barrier are shown in Figures 8.3-2a to 8.3-2h for the eight radionuclides for the case of 83 MTU/acre thermal loading without backfill and with a high infiltration rate. The cathodic protection was implemented for the case with both RH and T criteria for the outer barrier corrosion initiation. As discussed in Chapter 5, the cathodic protection model assumed that 75 percent of the initial outer barrier thickness had to be degraded before the inner barrier pitting could begin. Because most of the waste packages for the cathodic protection case did not have pit penetrations until after 10,000 years (see Section 5.7.8), the release rate calculations were extended to 100,000 years. For the case evaluated, the cathodic protection significantly delayed the initiation of EBS release beyond 10,000 years, to a starting time of approximately 15,000 years. However, all the radionuclides, except ^{14}C , exceed their NRC limit at this time. For ^{14}C , although it is released as a gas from the EBS, the release rate is lower than the NRC limit. This is due to its (relatively) short half-life (5,730 years) and the lower near-field temperature at that time which produces lower waste form alteration rates.

8.3.4 Effects of Alternative Thermal Loading and Repository Level Percolation Rate

The sensitivity of the EBS release rate to thermal load was evaluated by comparing the results from the 25 MTU/acre cases with the corresponding 83 MTU/acre cases. The details of the alternative thermal loading cases are described in Chapter 4. The results are presented in Figures 8.3-3a to 8.3-3h. The figures also present the effects from using different infiltration rates.

In general, the releases for the 83 MTU/acre cases begin earlier than those from the corresponding 25 MTU/acre cases regardless of the infiltration rates. This is as expected based on the waste package degradation histories for the cases discussed in Section 5.7.7. The release rates for the 83 MTU/acre cases are also generally higher than the corresponding 25 MTU/acre cases. The higher release rate is primarily due to the higher near-field temperature conditions in the 83 MTU/acre cases which leads to greater waste form alteration rates. Again, except for ^{14}C , the infiltration rate has a more significant impact on the release rate than does thermal load. In the case of ^{14}C , because of its relatively short half-life, the time for the waste package degradation is also a major parameter affecting its EBS release rate. All the radionuclides, except

²³⁷Np, exceed their NRC limit in the high infiltration rate case regardless of the thermal loading. In the 25 MTU/acre case with the high infiltration rate, the release rate of ²³⁷Np which is a solubility limited species is below the NRC limit.

8.3.5 Alternative EBS Release Conceptual Models: Effects of Backfill and Capillary Barrier

This section combines an evaluation of the sensitivity of the EBS release rate to the presence of a backfill and the sensitivity of the EBS release rate to the EBS release conceptual models. The effects of a backfill were considered by comparing the alternative no-backfill and backfill cases: 1) the no-backfill case assumes an air-filled drift and a gravel invert underneath the waste package; and 2) the backfill case assumes gravel is placed around the waste package.

Three EBS release conceptual models were considered: 1) advection-dominant transport from a "failed" waste package under dripping fractures; 2) advective transport controlled by diffusion through a "failed" waste package under dripping fractures; and 3) diffusion dominant transport from a "failed" waste package in the presence of a capillary barrier. A brief description of each EBS release conceptual model is given below (see also Section 6.5).

As discussed in Section 8.2, when a waste container has at least one pit penetration, and the surface temperature is below 100 °C, the entire surface of the waste form inside the "failed" waste package is assumed to be covered with a "thin" film of water, followed by alteration of the waste form, and mobilization of the radionuclides contained in the waste form. In addition, the number of waste packages under dripping fractures are estimated as a function of the distribution of the percolation flux and the saturated matrix conductivity of the near-field rock surrounding the repository drifts (discussed in Section 7.3).

In the first EBS release conceptual model, if a "failed" waste package is predicted to be under dripping fractures, the entire waste form is conservatively assumed to be exposed to the (dripping) advective flux, and the radionuclides are released by advection. The diffusive release from the "failed" waste package under dripping fractures is also calculated with the model (and the diffusion coefficient set to 10^{-7} cm²/sec) presented in Section 6.5. In this case, the total release from the "failed" waste package is the sum of advective and diffusive release, and the advective release component is always dominant. For a "failed" waste package that is not subjected to dripping water, the radionuclides are assumed to be released by diffusion only, and the diffusion coefficient is determined as a function of the liquid saturation level of the gravel invert underneath the waste package.

The second EBS release conceptual model considers an alternative approach to advective release from a "failed" waste package under dripping fractures and takes into account the performance of the "failed" waste container as a potentially important barrier to radionuclide release. Because the pits (or holes) of the "failed" waste container are filled with fine, "gel"-like corrosion products, it is assumed the pits filled with corrosion products prevent the dripping water from flowing directly into the waste package and contacting the waste form inside. Instead, the dripping water is diverted around the waste container. Thus, in this conceptual model, radionuclides are transported through the corrosion product-filled holes by diffusion, and once outside the waste container, they are released by advection. This alternative model incorporates

more realism into EBS release because it assumes any advective release from a waste container failed by pitting corrosion depends on the number of pit penetrations at that time. As in the first EBS release conceptual model, for a "failed" waste package that is not subjected to dripping fractures, radionuclides are released by diffusion only, and the diffusion coefficient is calculated from the liquid saturation level of the gravel invert.

The third EBS release conceptual model is similar to the presence of a Richard's (or capillary) barrier wherein, if it performs with 100 % efficiency in diverting any dripping water away from the waste package, no advective flow or dripping are allowed to occur through the waste packages. In this case, the dominant radionuclide release mechanism is diffusion which is strongly dependent upon the liquid saturation level in the gravel invert.

The effects of backfill for the eight radionuclides were calculated using the 83 MTU/acre thermal load case, with the high or low infiltration rate, and using the RH switch for the corrosion initiation of the carbon steel outer barrier. The results are shown in Figures 8.3-4a to 8.3-4h, in which the effects of backfill are compared for the cases with and without backfill. For all eight radionuclides, there is not a significant difference in the EBS release rates. This is consistent with the results for the waste package degradation discussed in Chapter 5, in which no significant difference was observed in the presence or absence of backfill.

The results using the alternative advective release model (EBS release conceptual model 2) are presented in Figures 8.3-5a to 8.3-5h. The results shown in the figures are for the cases of the 83 MTU/acre thermal loading, with no backfill, with the low or high infiltration rate, and using the RH switch or the RH and temperature switch for the initiation of the carbon steel outer barrier corrosion. The case for the 83 MTU/acre thermal loading, with no backfill, with the high infiltration rate, and using the RH switch for the corrosion initiation yielded the highest EBS peak release rates for all eight radionuclides. These results can be compared with Figures 8.3-4a to 8.3-4h to evaluate the sensitivity of EBS release rate to the two different EBS release models.

When calculated with the conservative advective release model (EBS release conceptual model 1), the case labelled as "83/no/hq/RH" as shown in Figures 8.3-4a to 8.3-4h in the figures yielded the most conservative release rates from the EBS for all eight radionuclides. For the same case (83/no/hq/RH) but with the alternative advective release model (Figures 8.3-5a to 8.3-5h), the release rates of all the radionuclides, except for ^{14}C which is released in gas and ^{210}Pb which is the principal decay daughter of uranium, are below (^{135}Cs , ^{59}Ni and ^{237}Np) or slightly above (^{99}Tc and ^{79}Se) their NRC limit. The shapes of the release rate curves mimic the pitting time histories (see Section 5.7).

Sensitivity of the EBS peak release rate to the presence of the capillary barrier is presented in Figures 8.3-6a to 8.3-6h. The calculations were made for the case of the 83 MTU/acre thermal loading, with the high infiltration rate, with backfill, and using the RH for the initiation of the outer barrier corrosion. The results for the no backfill cases with the 83 MTU/acre and 25 MTU/acre thermal loading are also presented for comparison.

As expected, the release of ^{14}C is not affected by the presence of the capillary barrier. In general, the release rates of all the radionuclides (except ^{14}C) are about 5 to 7 orders of magnitude lower in the presence of the capillary barrier compared to the release rates for the corresponding cases

Accn #: MOL.19981207.0290

Batch #: MOY-981207-15

QA Record: N

LSS Record: Y

Status Code: E

Access Code: PUB

Retention Code: TL

Document Type:

CORRESPONDENCE

Document Date: 19981125

Document Version: (No Entry)

Document #:

(No Entry)

Trace ID:

WBS

Trace #:

1.2.5.3.5

Comment:

THIS IS A VIABILITY ASSESSMENT (VA) RELATED DOCUMENT - DO NOT DELETE; ITEM 4 IS A SURROGATE RECORD SHOWING ONE DISKETTE, THIS ITEM WAS SENT TO PHILL JONES OF THE M+O PER PHYLLIS BURNHAM OF USGS

Author Name:

MCKINLEY PW

Organization:

USGS

Title:

GEOGRAPHIC NODAL INFORMATION STUDY AND EVALUATION SYSTEM (GENISES) DATA TRANSMITTAL - BOREHOLE SATURATIONS, BY LE FLINT - SECTION 4.2.1.2 IN THE REPORT "HYDROGEOLOGY OF THE UNSATURATED ZONE, NORTH RAMP AREA OF THE EXPLORATORY STUDIES FACILITY, YUCCA MOUNTAIN, NEVADA", EDITED BY JP ROUSSEAU, EM KWICKLIS AND DC GILLIES; DTN: GS960908312231.007 TDIF: 305682

Identifiers:

(No Entry)

Package ID:

(No Entry)

Related Record Code:

ATT

Related Record Accn #:

MOL.19981207.0291

Receiver Name:

JONES P

Organization:

M+O

Special Class:

(No Entry)

ENTERED DATE: 12/08/98

ENTERED BY: COLLINS

MODIFIED DATE: 12/08/98

MODIFIED BY: COLLINS

Accn #: MOL.19981207.0291

Batch #: MOY-981207-15

QA Record: N

LSS Record: Y

Status Code: E

Access Code: PUB

Retention Code: TL

Document Type:

DATA

Document Date: 19981125

Document Version: (No Entry)

Document #:

(No Entry)

Trace ID:

(No Entry)

Trace #:

(No Entry)

Comment:

(No Entry)

Author Name:

N/A

Organization:

USGS

Title:

HARD COPY OF DATA ANNOTATED WITH PARAMETERS AND ATTRIBUTES FOR HYDROGEOLOGY OF THE UNSATURATED ZONE, NORTH RAMP, ESF (C)

Identifiers:

(No Entry)

Package ID:

(No Entry)
Related Record Code: (No Entry) Related Record Accn #: (No Entry)
Receiver Name: (No Entry) Organization: (No Entry)
Special Class: (No Entry)
ENTERED DATE: 12/08/98
ENTERED BY: COLLINS
MODIFIED DATE: 12/08/98
MODIFIED BY: COLLINS

Accn #: MOL.19981207.0292

Batch #: MOY-981207-15

QA Record: N

Document Type:

DATA

Document Date: 19981130

Document Version: (No Entry)

Document #:

(No Entry)

Trace ID:

(No Entry)

LSS Record: Y

Trace #:

(No Entry)

Comment:

THIS SPECIAL PROCESS DISKETTE CAN BE LOCATED THROUGH THE RECORDS PROCESSING CENTER

Author Name:

ANNA LO

Organization:

USGS

Title:

MODEL DATA FILE FOR PRELIMINARY THREE-DIMENSIONAL DISCRETE FRACTURE MODEL, TIVA CANYON TUFF, YUCCA MOUNTAIN AREA, NYE COUNTY, NEVADA, BY LO ANNA (C)

Identifiers:

(No Entry)

Package ID:

(No Entry)

Related Record Code:

(No Entry)

Related Record Accn #:

(No Entry)

Receiver Name:

(No Entry)

Organization:

(No Entry)

Special Class:

(No Entry)

ENTERED DATE: 12/08/98

ENTERED BY: COLLINS

MODIFIED DATE: 12/08/98

MODIFIED BY: COLLINS

Accn #: MOL.19981207.0293

Batch #: MOY-981207-15

QA Record: N

Document Type:

CORRESPONDENCE

Document Date: 19981130

Document Version: (No Entry)

Document #:

(No Entry)

Trace ID:

WBS

LSS Record: Y

Trace #:

1.2.5.3.5

Comment:

Status Code: E
Access Code: PUB
Retention Code: TL

Status Code: E
Access Code: PUB
Retention Code: TL

THIS IS A VIABILITY ASSESSMENT (VA) RELATED DOCUMENT - DO NOT DELETE

Author Name: MCKINLEY PW
Organization: USGS

le:
GEOGRAPHIC NODAL INFORMATION STUDY AND EVALUATION SYSTEM (GENISES) DATA
TRANSMITTAL - PRELIMINARY 3-DIMENSIONAL DISCRETE FRACTURE MODEL OF THE
TOPOPAH SPRING TUFF IN THE EXPLORATORY STUDIES FACILITY, YUCCA MOUNTAIN
AREA, NYE COUNTY, NEVADA (USGS OFR 97-834) BY LO ANNA; DTN:
GS970208312281.001 TDIF: 306014

Identifiers:

(No Entry)

Package ID:

(No Entry)

Related Record Code:

Related Record Accn #:

ATT	MOL.19981207.0294
ATT	MOL.19981207.0295
ATT	MOL.19981207.0296
ATT	MOL.19981207.0297

Receiver Name:

Organization:

JONES P
M+O

Special Class:

(No Entry)

ENTERED DATE: 12/08/98

ENTERED BY: COLLINS

MODIFIED DATE: 12/08/98

MODIFIED BY: COLLINS

cn #: MOL.19981207.0294

ch #: MOY-981207-15

VA Record: N

LSS Record: Y

Document Type:

DATA

Status Code: E
Access Code: PUB
Retention Code: TL

Document Date: 19981130

Document Version: (No Entry)

Document #:

(No Entry)

Trace ID:

Trace #:

(No Entry)

(No Entry)

Comment:

(No Entry)

Author Name:

Organization:

ANNA LO
USGS

Title:

DATA SUMMARY SHEET FOR PRELIMINARY THREE-DIMENSIONAL DISCRETE FRACTURE
MODEL OF THE TOPOPAH SPRING TUFF IN THE EXPLORATORY STUDIES FACILITY, YUCCA
MOUNTAIN, NYE COUNTY, NEVADA, (USGS OFR 97-834) BY LO ANNA (C)

Identifiers:

(No Entry)

Package ID:

(No Entry)

Related Record Code:

Related Record Accn #:

(No Entry)

(No Entry)

Receiver Name:

Organization:

(No Entry)

(No Entry)

Special Class:

(No Entry)

ENTERED DATE: 12/08/98

ENTERED BY: COLLINS

MODIFIED DATE: 12/08/98

MODIFIED BY: COLLINS D

Accn #: MOL.19981207.0295
Batch #: MOY-981207-15

QA Record: N

LSS Record: Y

Status Code: E
Access Code: PUB
Retention Code: TL

Document Type:
DATA

Document Date: 19981130
Document Version: (No Entry)

Document #:
(No Entry)

Trace ID: Trace #:
(No Entry) (No Entry)

Comment:
(No Entry)

Author Name: Organization:
ANNA LO USGS

Title:
HARD COPY OF README FILE EXPLAINING THE MODEL INPUT AND OUTPUT FILES FOR
PRELIMINARY THREE-DIMENSIONAL DISCRETE FRACTURE MODEL OF THE TOPOPAH SPRING
TUFF IN THE EXPLORATORY STUDIES FACILITY, YUCCA MOUNTAIN, NYE COUNTY,
NEVADA, (USGS OFR 97-834) BY LO ANNA (C)

Identifiers:
(No Entry)

Package ID:
(No Entry)

Related Record Code: Related Record Accn #:
(No Entry) (No Entry)

Receiver Name: Organization:
(No Entry) (No Entry)

Special Class:
(No Entry)

ENTERED DATE: 12/08/98
ENTERED BY: COLLINS D
MODIFIED DATE: 12/08/98
MODIFIED BY: COLLINS D

Accn #: MOL.19981207.0296
Batch #: MOY-981207-15

QA Record: N

LSS Record: Y

Status Code: E
Access Code: PUB
Retention Code: TL

Document Type:
DATA

Document Date: 19981130
Document Version: (No Entry)

Document #:
(No Entry)

Trace ID: Trace #:
(No Entry) (No Entry)

Comment:
(No Entry)

Author Name: Organization:
ANNA LO USGS

Title:
HARD COPY OF INPUT FILES FOR PRELIMINARY THREE-DIMENSIONAL DISCRETE
FRACTURE MODEL OF THE TOPOPAH SPRING TUFF IN THE EXPLORATORY STUDIES
FACILITY, YUCCA MOUNTAIN, NYE COUNTY, NEVADA, (USGS OFR 97-834) BY LO ANNA
(C)

Identifiers:

Trace ID:

WBS

Trace #:

1.2.5.3.5

Comment:

THIS IS A VIABILITY ASSESSMENT (VA) RELATED DOCUMENT - DO NOT DELETE

Author Name:

MCKINLEY PW

Organization:

USGS

Title:

GEOGRAPHIC NODAL INFORMATION STUDY AND EVALUATION SYSTEM (GENISES) DATA TRANSMITTAL - PRELIMINARY THREE-DIMENSIONAL DISCRETE FRACTURE MODEL, TIVA CANYON TUFF, YUCCA MOUNTAIN AREA, NYE COUNTY, NEVADA (USGS OFR 97-833) BY LO ANNA

Identifiers:

(No Entry)

Package ID:

(No Entry)

Related Record Code:

ATT

ATT

ATT

ATT

ATT

Related Record Accn #:

MOL.19981207.0299

MOL.19981207.0300

MOL.19981207.0301

MOL.19981207.0297

MOL.19981207.0292

Receiver Name:

JONES P

Organization:

M+O

Special Class:

(No Entry)

ENTERED DATE: 12/08/98

ENTERED BY: COLLINS

MODIFIED DATE: 12/08/98

MODIFIED BY: COLLINS

Accn #: MOL.19981207.0299

Batch #: MOY-981207-15

QA Record: N

Document Type:

DATA

Document Date: 19981130

Document Version: (No Entry)

Document #:

(No Entry)

Trace ID:

(No Entry)

Trace #:

(No Entry)

Comment:

(No Entry)

Author Name:

ANNA LO

Organization:

USGS

Title:

DATA SUMMARY SHEET FOR PRELIMINARY THREE-DIMENSIONAL DISCRETE FRACTURE MODEL OF THE TIVA CANYON TUFF IN THE EXPLORATORY STUDIES FACILITY, YUCCA MOUNTAIN, NYE COUNTY, NEVADA, (USGS OFR 97-833) BY LO ANNA (C)

Identifiers:

(No Entry)

Package ID:

(No Entry)

Related Record Code:

(No Entry)

Related Record Accn #:

(No Entry)

Receiver Name:

(No Entry)

Organization:

(No Entry)

Special Class:

(No Entry)

Status Code: E
Access Code: PUB
Retention Code: TL

LSS Record: Y

ENTERED DATE: 12/08/98
ENTERED BY: COLLINS
MODIFIED DATE: 12/08/98
MODIFIED BY: COLLINS

Accn #: MOL.19981207.0300

Batch #: MOY-981207-15

QA Record: N

LSS Record: Y

Status Code: E

Access Code: PUB

Retention Code: TL

Document Type:

DATA

Document Date: 19981130

Document Version: (No Entry)

Document #:

(No Entry)

Trace ID:

(No Entry)

Trace #:

(No Entry)

Comment:

(No Entry)

Author Name:

ANNA LO

Organization:

USGS

Title:

HARD COPY OF THE README FILE EXPLAINING THE MODEL INPUT AND OUTPUT FILES AND INPUT DATA FOR PRELIMINARY THREE-DIMENSIONAL DISCRETE FRACTURE MODEL OF THE TIVA CANYON TUFF IN THE EXPLORATORY STUDIES FACILITY, YUCCA MOUNTAIN, NYE COUNTY, NEVADA, (USGS OFR 97-833) BY LO ANNA (C)

Identifiers:

(No Entry)

Package ID:

(No Entry)

Related Record Code:

(No Entry)

Related Record Accn #:

(No Entry)

Receiver Name:

(No Entry)

Organization:

(No Entry)

Special Class:

(No Entry)

ENTERED DATE: 12/08/98

ENTERED BY: COLLINS

MODIFIED DATE: 12/08/98

MODIFIED BY: COLLINS

Accn #: MOL.19981207.0301

Batch #: MOY-981207-15

QA Record: N

LSS Record: Y

Status Code: E

Access Code: PUB

Retention Code: TL

Document Type:

CORRESPONDENCE

Document Date: 19981201

Document Version: (No Entry)

Document #:

(No Entry)

Trace ID:

(No Entry)

Trace #:

(No Entry)

Comment:

(No Entry)

Author Name:

RICHARDSON GA

Organization:

USGS

Title:

LOCATION OF ORIGINAL DISKETTES PROVIDED BY THE PI (LARRY ANNA) FOR PRELIMINARY THREE-DIMENSIONAL DISCRETE FRACTURE MODEL OF THE TIVA CANYON

TUFF IN THE EXPLORATORY STUDIES FACILITY, YUCCA MOUNTAIN, NYE COUNTY,
NEVADA, (USGS OFR 97-833) BY LO ANNA (C)

Identifiers:

No Entry)

Package ID:

(No Entry)

Related Record Code:

ATT

Related Record Accn #:

MOL.19981207.0292

Receiver Name:

(No Entry)

Organization:

(No Entry)

Special Class:

(No Entry)

ENTERED DATE: 12/08/98

ENTERED BY: COLLINS

MODIFIED DATE: 12/08/98

MODIFIED BY: COLLINS

without a capillary barrier as shown in Figures 8.3-3a to 8.3-3h and 8.3-4a to 8.3-4h. Unlike the other sensitivity results discussed, the releases from the lower thermal load case for all the radionuclides (except ^{14}C) begin about 5,000 years earlier than for the higher thermal loading case, but the release rates are still lower than the higher thermal loading. The results are in contrast to the waste package degradation histories for the corresponding thermal loading cases, in which the waste package degradation for the high thermal load case was more severe and started earlier than for the low thermal load case. This difference in the release rate result is caused by the higher saturation of the gravel invert underneath the waste package in the lower thermal load case, which gives higher values for the diffusion coefficient in the invert and thus higher diffusive releases. The breakthrough curves for the release rates in the higher thermal load case are very sharp, and the release rates are higher than for the lower thermal load case. This is probably due mostly to a buildup of the radionuclides inside the waste package as the waste form alters at a greater rate because of the higher near-field temperature in the high thermal load case, providing for a high concentration gradient across the gravel invert.

8.3.6 Effects of Cladding Failure

The sensitivity of the EBS release rate to the spent fuel cladding failure was evaluated by varying the fraction of the waste form available for release. This was a simplified approach to simulate cladding failure and was implemented in RIP by only allowing failure of the cladding for a selected percentage of the waste packages. Simulations were conducted with 1, 10, and 100 % availability of the spent fuel waste form. Another set of simulations were performed with the same percentages of the spent fuel waste form availability, but with the surface area of the spent fuel within the failed cladding increased by a factor of 100. The multiplication factor used reflects the volume increases of the oxidized spent fuel in the failed cladding and was conservatively estimated from a recent report by Gray and Wilson (1995) and information provided by Gray (1995a). A detailed discussion of the spent fuel surface area is given Section 6.2.

The EBS release results for the cases with the different cladding failure fraction, but without the surface area increase are given in Figures 8.3-7a to 8.3-7h. The calculations are for the case of the 83 MTU/acre thermal loading, with no backfill, with the high infiltration rate, and using the RH switch for the initiation of the outer barrier corrosion. All the radionuclides including ^{14}C showed the decreased release rates with the reduction in the cladding failure from 100% to 1%, i.e. the reduction of the fraction of spent fuel available for release. This was expected because the decrease in the cladding failure was achieved in the simulations by reducing the inventory available for release. However, all the radionuclides, except ^{59}Ni and ^{237}Np , exceed their NRC limit even with only 1 percent cladding failure, using the conservative advective release model (EBS release conceptual model 1).

Additional sensitivity analyses assumed that all the spent fuel inside the failed cladding (1% and 10% failure) is oxidized completely to U_3O_8 , causing an increase in the surface area by a factor of 100. Comparison of the results to the 100% cladding failure without the surface area increase is given in Figures 8.3-8a to 8.3-8h. The simulations were run for the case of the 83 MTU/acre thermal loading, with no backfill, with the high infiltration rate, and using the RH switch for the initiation of the outer barrier corrosion. The surface area increase was expected to lead to an increase in the peak release rates for the radionuclides. However, as shown in the figures, the effect was not significant. The fact that the radionuclides considered (except ^{59}Ni , ^{237}Np and ^{210}Pb)

are highly soluble and have a significant gap fraction inventory may have lessened the effects. For ^{237}Np the release rates are the same for all three cases.

8.3.7 Effects of Alternative Thermal-Hydrologic Model

The effect of the alternative thermal-hydrologic model (LLNL model) (Buscheck, 1995; Buscheck, Nitao and Ramspott, 1995), on the release rate from the EBS was evaluated by comparing the results from a corresponding, but not identical, case. Details of the alternate thermal-hydrologic model were given in Section 4.2. As discussed in Section 5.7.10, with the temperature and humidity profiles calculated with the alternate thermal-hydrologic model, the waste package simulation results showed that there was insignificant waste package degradation for the LLNL model cases with the 80 MTU/acre case with or without backfill and the 24 MTU/acre case with backfill. Only the 24 MTU/acre case with no backfill and no infiltration had significant waste package degradation. Thus, the sensitivity analyses for the alternate thermal-hydrologic model were only conducted for the LLNL model case of the 24 MTU/acre thermal loading, with no backfill, and with no infiltration, and a roughly equivalent case, i.e. the case with 25 MTU/acre thermal loading, no backfill, and the presence of a capillary barrier effect. The comparisons are made in Figures 8.3-9a to 8.3-9h. The results for the alternate thermal-hydrologic model (LLNL model) are indicated in the figures with the designation "LLNL-24/no/no/cap. barrier."

Except for ^{14}C , diffusion in the aqueous phase is the dominant release mechanism for the radionuclides for these two cases. As shown in the figures, the release rates of all the radionuclides are two orders of magnitude higher in the current thermal-hydrologic model than in the LLNL model results. The predictions for the temperature and the liquid saturation level in the gravel invert by the alternate LLNL model are lower than the current model, which leads to lower diffusive flux.

8.3.8 Sensitivity of ^{129}I Release Rate to Its Release Mode

Although the peak release rate (0.96 Ci/yr) of ^{129}I from the EBS (given in Table 8.3-4) is less than the total NRC release limit (1.24 Ci/yr) in Table 8.3-1, its release mode (gaseous or aqueous) from the EBS has a significant impact on the release rate at the accessible environment, which is discussed in detail in Chapter 9. In addition, as discussed in Section 8.2.1, its dominant release mode is uncertain. Because of the impact to the accessible environment release rate and the uncertainty in its release mode, simulations were run for the sensitivity of the ^{129}I release mode to its release rate from the EBS. The results shown in Figure 8.3-10 are for the case of 83 MTU/acre, with no backfill, high infiltration rate, and using the RH switch for the corrosion initiation. The initial release spikes in the figure are due to the release of the ^{129}I gap fraction. The other peaks in the release history occur as each waste package group fails. While, in the high infiltration rate case, the release rate of ^{129}I from the EBS in the aqueous phase is not much different from the gaseous release rate, the aqueous phase peak release rate in the low infiltration rate case is about two orders of magnitude lower than the gas phase release cases. The impact of ^{129}I release mode on the release to the accessible environment is further discussed in Chapter 9.

8.3.9 Most Important Model Parameters

Additional analyses were conducted to identify key model parameters which have a large impact on important performance measures such as peak release rate from the EBS. Using Latin Hypercube Sampling to sample the parameter values, one hundred realizations were simulated with RIP for two cases. These cases were the 25 MTU/acre and 83 MTU/acre thermal loads, both with no backfill and high infiltration. Once the realizations were simulated, stepwise linear regression was used to determine which parameters could be used to explain the EBS peak release rate. In Tables 8.3-6 and 8.3-7, the parameters are listed in order of importance along with the percent of the variability which the parameters explain up to that point.

Since the structure of the relationship between the model parameters and the EBS peak release is not known, the stepwise linear regression was done on three transformations of the data. The first transformation was rank regression. The peak release rates were assigned integer values from 1 through 100, corresponding to their rank among the simulations. Each of the model parameters was also assigned an integer value for each realization corresponding to the rank of the value of the parameter at that observation. The ranks of the model parameters are then used to explain the ranks of the peak release rate. Rank regression was used because it is a robust method which is useful when the underlying relationship is not understood.

There are intuitive reasons to believe that the EBS peak release rate should be explained well by a multiplicative model. Thus, for both the second and the third transformation, the natural log of the peak EBS release rate was treated as the dependent variable. For the second transformation, the model parameters were used to explain the natural log of the EBS peak release rate. For the third transformation, the natural logs of the model parameters were used to explain the natural log of the EBS peak release rate. The results for all three of these transformations are shown in Tables 8.3-6 and 8.3-7.

For both the rank regression and log-log transformation, a small number of parameters explain most of the variability. This supports the idea that the log-log transformations might be appropriate. For both of these transformations, and for both thermal loads, ⁹⁹Tc solubility, the infiltration rate, and the spent fuel dissolution rate are the three most important parameters. This is consistent with the current understanding of EBS processes. Spent fuel dissolution rate is important, because the spent fuel has to dissolve before it may be transported out of the EBS. ⁹⁹Tc solubility in particular is important because ⁹⁹Tc is a highly soluble, abundant radionuclide. Thus, once mobilized from the spent fuel waste form, its solubility determines the amount of ⁹⁹Tc available for transport. The two cases analyzed in this section both assumed the advection dominant EBS release model (EBS release conceptual model 1), thus, infiltration rate is also important for determining the EBS peak release rates.

8.4 CUMULATIVE EBS RELEASE AT 10,000 YEARS

8.4.1 Introduction

Cumulative releases of radionuclides from the EBS provide for an additional comparison of EBS performance, as a supplement to the analysis of peak EBS release rates discussed in the previous section. In this section, cumulative releases of some of the radionuclides considered for the EBS

release rate were calculated, and the results were normalized to the EPA release limits to the accessible environment (AE) specified in 40 CFR Part 191. Although the EPA normalized cumulative release limits are not directly applicable to the releases from the waste package and EBS, the normalized release calculation provides another useful approach to compare the EBS release behavior of radionuclides.

The cumulative releases from the EBS at 10,000 years are presented in this section only to evaluate the effect of alternative thermal loading and infiltration rates on the release. Alternative waste package degradation conceptual models, backfill, and cladding failure have been sufficiently discussed in previous sections. 100 realizations were simulated for each case. The cumulative normalized releases are presented only for release from the EBS in this section.

8.4.2 Effects of Alternative Thermal Load

The complementary cumulative distribution function (CCDF) results from the 83 MTU/acre case without backfill and with high infiltration are presented in Figure 8.4-1 for the total release as well as for ^{14}C , ^{129}I , ^{99}Tc , ^{237}Np , and ^{59}Ni . The total release from the EBS is contributed primarily by ^{14}C and ^{237}Np . The uniform release of two gases, ^{14}C , and ^{129}I , independent of the other uncertainty in the subsystem is demonstrated by the nearly vertical normalized release curves. The ^{59}Ni release also shows little variability over the 100 realizations. The alteration-limited radionuclide, ^{99}Tc , has approximately 3 orders of magnitude variability in the release due to significant variability in dissolution of the waste form, whereas the solubility-limited radionuclide, ^{237}Np , has less variability.

As a comparison with Figure 8.4-1, the CCDF results from the 25 MTU/acre case without backfill and with high infiltration are presented in Figure 8.4-2 for the total release as well as for selected radionuclides, ^{14}C , ^{129}I , ^{99}Tc , ^{237}Np , and ^{59}Ni . As in the high thermal loading case, the total release from the EBS is contributed primarily by ^{14}C and ^{237}Np . However, the total releases are over a half of an order of magnitude lower than for the 83 MTU/acre case. The difference in the releases between the two thermal loading cases is attributable to the previously described differences in waste container degradation and waste form alteration/dissolution rates. The higher thermal load case has higher dissolution rates of the waste form and generally greater degradation of the waste container, leading to earlier and higher releases.

8.4.3 Effects of Infiltration on EBS Release

As an evaluation of the effect of infiltration on the cumulative release from the EBS at 10,000 years, the two thermal load cases (83 MTU/acre and 25 MTU/acre) with no backfill were simulated with both the high and low infiltration rates. The CCDF results for total normalized release from the EBS at 10,000 years are presented in Figure 8.4-3, in which both the high and low infiltration cases for the 83 MTU/acre case are shown to produce greater release than the 25 MTU/acre cases. Also, the releases are greater from the high infiltration cases for a given thermal load than from the low infiltration case. These trends were observed in the waste container degradation analyses presented in Chapter 5, where the 83 MTU/acre case had earlier waste container failure and greater waste container degradation, and can be further explained by the higher dissolution rate of the waste form at higher temperatures in the high thermal load case.

CCDF results for individual radionuclides (^{14}C , ^{99}Tc , ^{129}I , ^{237}Np , and ^{59}Ni) for the same cases as in Figure 8.4-3, are presented in Figures 8.4-4 to 8.4-8. For the radionuclides with gaseous release (^{14}C and ^{129}I), the results presented in 8.4-4 and 8.4-6 are similar to the total release, but the variability between the high and low infiltration case for a given thermal load is not as great. ^{99}Tc release behavior is more variable than was the gaseous radionuclide release perhaps due to more variable diffusive release rate for ^{99}Tc (Figure 8.4-5). Also, an important difference in the release behavior related to infiltration is observed in the results presented in Figure 8.4-5. The high infiltration cases (both 83 MTU/acre and 25 MTU/acre) produce the highest normalized releases because ^{99}Tc release is strongly dependent on the dissolution rate of the waste form and the infiltration rate. The low infiltration cases have a greater variability. The release results for ^{237}Np as seen in Figure 8.4-7 are similar to ^{99}Tc , except there is a greater overall range of normalized releases, from approximately 10^{-4} to 5×10^{-1} at the 50th percentile probability. For the cases evaluated in this section, the greatest normalized releases are produced by ^{237}Np . For the cumulative normalized release of ^{59}Ni presented in Figure 8.4-8, the releases for a particular thermal load with high infiltration are higher and have less variability than for the low infiltration case. Again, both of the high infiltration cases have higher releases than the lower infiltration cases, showing the importance of the percolation flux through the repository.

8.5 SUMMARY AND CONCLUSIONS FROM EBS PERFORMANCE ANALYSES

The analyses of the waste package/EBS performance presented in Chapter 8 evaluated the release of radionuclides from the EBS in relation to the NRC peak release rate standard. The analyses considered the effects on the EBS peak release rate of alternative corrosion initiation models, two alternative thermal loads, two different infiltration rate ranges, backfill conditions, cladding performance, alternative thermal-hydrologic models, and alternative EBS release models. Eight radionuclides were selected for the analysis based on the maximum release rate that exceeded 0.1% of the NRC total release rate limit. These radionuclides, ^{14}C , ^{135}Cs , ^{59}Ni , ^{237}Np , ^{210}Pb , ^{226}Ra , ^{79}Se , and ^{99}Tc , were included in the evaluations which attempted to demonstrate the importance of the various parameters and conceptual models listed above.

The evaluations, which were based on thermo-hydrologic modeling results presented in Chapter 4, demonstrated the significance of the rate of percolation or dripping on the waste containers. Generally, the influence of infiltration was more significant than the alternate waste degradation conceptual models (i.e., Temperature and RH vs. RH only) in terms of causing radionuclides to exceed their NRC release rate limit.

The higher thermal load cases produced higher releases than the corresponding lower thermal load case. This is consistent with earlier waste container failure and higher degradation in the higher thermal load case. In the case when a capillary barrier was assumed, the releases for the low thermal load case began earlier, but the peak release rate remained lower than the peak release rate for the high thermal load case.

Also demonstrated in the analyses are the effects of the alternative advective release model controlled by diffusion through the waste container on the EBS release rate, i.e., diffusive release through the perforations in "failed" waste container and advective release from the outside contacting the dripping water. Compared to the case with the conservative advective release model that yielded the highest release rate (83 MTU/acre, no backfill and high infiltration), the alternative

advective model yielded the release rates for most nuclides within their NRC limit, except for ^{14}C and ^{210}Pb . The implication is that the "partially failed" waste containers by pitting corrosion should still be able to perform as a potentially important barrier to radionuclide release, and EBS transport models that incorporate more realism should be considered in future EBS performance analyses.

Multiple realization simulations to analyze the effects of thermal loading and infiltration produced similar results to the peak release rate analyses. Generally, the higher thermal load produces greater release, and higher infiltration produced significantly higher release than the low infiltration cases. The strong influence of repository percolation rate points to the high importance of the repository flux as it relates to the radionuclide release.

Table 8.2-1.. Comparison of TSPA-1995 Container Parameters with TSPA-1993 Container Parameters

RIP Package Information	TSPA-1993 ¹⁾	TSPA-1995
Number of packages	Spent Fuel: 6468 DHLW: 3829	Spent Fuel: 6468 DHLW: 3829
Waste burnup (MWd/MTHM) ²⁾	42,300 - PWR 32,250 - BWR 39,075 - combined	39,651 - PWR 31,186 - BWR 36,666 - combined
Mass waste/pkg = MTHM in repository/# of waste containers	9.74 MTHM/pkg for PWR/BWR 1.828 MTHM/pkg-DHLW	9.74 MTHM/pkg for PWR/BWR 1.828 MTHM/pkg-DHLW

¹⁾ Andrews, et al. (1994)

²⁾ MWd/MTHM = megawatt days/metric tons of heavy metal

Table 8.2-2.. Comparison of Selected Radionuclide Inventory in TSPA-1995 with TSPA-1993 Inventory

INVENTORY	TSPA-1993 ^{1), 2)} (Ci/container)	TSPA-1995 ³⁾ (Ci/container)
²⁴³ Am	2.74E+02	2.48E+02
¹⁴ C	1.44E+01	1.38E+01
¹³⁵ Cs	5.52E+00	5.13E+00
¹²⁹ I	3.62E+00	3.43E-01
²³⁷ Np	4.74E+00	4.35E+00
²³⁹ Pu	3.65E+00	3.56E+03
⁷⁹ Se	4.67E+00	4.41E+00
¹²⁶ Sn	9.01E+00	8.50E+00
⁹⁹ Tc	1.47E+00	1.40E+02
²³⁴ U	1.39E+00	1.34E+01

1) Andrews, et al. (1994)

2) TSPA-1993 inventory is for 30-year-old fuel. Ci/container = Ci/MTHM x 9.2 MTHM/container.

3) TSPA-1995 inventory is for 30-year-old fuel. Ci/container = Ci/MTHM x 7.94 MTHM/container.

Table 8.2-3.. Comparison of TSPA-1995 Gap Fraction with TSPA-1993 Gap Fraction

INVENTORY	TSPA-1993 ¹⁾ Gap Fraction	TSPA-1995 Gap Fraction
²⁴³ Am	0.0	0.0
¹⁴ C	0.0125 →0.0575: Uniform	0.0125 →0.0575: Uniform
¹³⁵ Cs	0.02	0.02
¹²⁹ I	0.02	0.02
²³⁷ Np	0.0	0.0
²³⁹ Pu	0.0	0.0
⁷⁹ Se	0.02	0.02
¹²⁶ Sn	0.0	0.0
⁹⁹ Tc	0.02	0.02
²³⁴ U	0.0	0.0

¹⁾ Andrews, et al. (1994)

Table 8.2-4. Comparison of TSPA-1995 Exposure Parameters with TSPA-1993 Exposure Parameters

RIP Model Parameter	TSPA-1993 RIP Base Case ¹⁾	TSPA-1995 RIP Nominal Case
(1) Fraction of containers with moist continuous conditions (2) Fraction of waste wetted (3) ECA ²⁾ (4) Diffusion coefficient	(1) Dependent on flux, temperature, saturation (2) 1.0 (3) 8.5-46.5 m ² (4) Conca curve	(1) Dependent on flux, temperature, saturation (2) If temperature is <100 degrees C, fraction is 1.0. Otherwise, it's 0.0. (3) 40.94 m ² (4) Conca curve
(1) Fraction of containers with dripping fractures (2) Fraction of waste wetted (3) ECA (4) EDC	N/A	(1) Dependent on flux, and saturated hydraulic conductivity (2) If temperature is <100 degrees C, fraction is 1.0. Otherwise, it's 0.0. (3) 40.94 m ² (4) 3.15e-4 m ² /yr
Air alteration rate	0	0
Matrix dissolution rate (g/m ² /yr)	Temperature dependent	Temperature dependent
Surface area of matrix (m ² /g) (combined with matrix dissolution rate)	1. Surface Area of Spent Fuel (ASF)/(1.10062E7) m ² /g where Spent fuel surface area = 78-107 m ² (uniform) 2. Surface Area of DHLW (AHL)/(7.012E6) m ² /g where AHL = 200-600 m ²	1. Surface Area of Spent Fuel (ASF)/(1.10062E7) m ² /g where Spent fuel surface area = 500 m ² 2. Surface Area of DHLW (AHL)/(7.012E6) m ² /g where AHL = 200-600 m ²

Table 8.2-4.. Comparison of TSPA-1995 Exposure Parameters with TSPA-1993 Exposure Parameters (Continued)

RIP Model Parameter	TSPA-1993 RIP Base Case ¹⁾	TSPA-1995 RIP Nominal Case
Water volume contacting matrix (m ³)	Water volume contacting matrix: ASF*DWATER : DWATER = 0.001 m (thickness of water film contacting waste form matrix)	Water volume contacting matrix: ASF*DWATER : DWATER = 0.001 m (thickness of water film contacting waste form matrix)

¹⁾ Andrews, et al. (1994)

²⁾ ECA = effective catchment area

Table 8.2-5. Comparison of TSPA-1995 Transport Parameters with TSPA-1993 Transport Parameters

RIP Model Parameter	TSPA-1993 RIP Base Case ¹⁾	TSPA-1995 RIP Nominal Case
Diffusion coefficient (m ² /yr)	Curve fit to Conca data	Curve fit to Conca data (see Section 6.5)
Repository infiltration rate (m/yr)	VTOUGH results	Selected from two ranges: 0.01-0.05 mm/yr and 0.5 -2.0 mm/yr
Geometric factor for diffusion (m)	28.05*N*(f _s): N = porosity of backfill = 0.1-0.3; f _s = 1, if liquid saturation > 0.08	See Section 6.5
Delay pathway (only in moist continuous)	In-drift emplacement: 0.5 m crushed tuff zone	Implemented in diffusive release component of geometric factor for diffusion (see Section 6.5)

¹⁾ Andrews, et al. (1994)

Table 8.3-1.. Calculation of the NRC Release Limit

Radionuclide	1,000-Year Inventory (Ci/MTU)	1,000-Year Inventory for 63,000 MTU (Ci)	NRC Limit (Ci/yr)
²²⁷ Ac	3.88E-04	2.45E+01	2.45E-04
²⁴¹ Am	1.06E+03	6.69E+07	6.69E+02
^{242M} Am	2.66E-01	1.68E+04	1.68E-01
²⁴³ Am	2.33E+01	1.47E+06	1.47E+01
¹⁴ C	1.26E+00	7.96E+04	7.96E-01
³⁶ Cl	1.13E-02	7.13E+02	7.13E-03
²⁴⁴ Cm	6.65E-11	4.19E-06	4.19E-11
²⁴⁵ Cm	3.19E-01	2.01E+04	2.01E-01
²⁴⁶ Cm	6.19E-02	3.90E+03	3.90E-02
¹³⁵ Cs	5.26E-01	3.31E+04	3.31E-01
¹²⁹ I	3.52E-02	2.22E+03	2.22E-02
^{93M} Nb	2.32E+00	1.46E+05	1.46E+00
⁹⁴ Nb	8.19E-01	5.16E+04	5.16E-01
⁵⁹ Ni	2.40E+00	1.51E+05	1.51E+00
⁶³ Ni	2.13E-01	1.34E+04	1.34E-01
²³⁷ Np	1.24E+00	7.82E+04	7.82E-01
²³¹ Pa	3.88E-04	2.44E+01	2.44E-04
²¹⁰ Pb	3.75E-03	2.36E+02	2.36E-03
¹⁰⁷ Pd	1.29E-01	8.12E+03	8.12E-02
²³⁸ Pu	1.97E+00	1.24E+05	1.24E+00
²³⁹ Pu	3.56E+02	2.24E+07	2.24E+02
²⁴⁰ Pu	4.90E+02	3.09E+07	3.09E+02
²⁴¹ Pu	3.19E-01	2.01E+04	2.01E-01
²⁴² Pu	2.06E+00	1.30E+05	1.30E+00
²²⁶ Ra	3.76E-03	2.37E+02	2.37E-03

Table 8.3-1. Calculation of the NRC Release Limit (Continued)

Radionuclide	1,000-Year Inventory (Ci/MTU)	1,000-Year Inventory for 63,000 MTU (Ci)	NRC Limit (Ci/yr)
²²⁸ Ra	1.42E-08	8.93E-04	8.93E-09
⁷⁹ Se	4.48E-01	2.82E+04	2.82E-01
¹⁵¹ Sm	2.06E-01	1.30E+04	1.30E-01
¹²⁶ Sn	8.66E-01	5.46E+04	5.46E-01
⁹⁹ Tc	1.43E+01	9.03E+05	9.03E+00
²²⁹ Th	1.60E-04	1.01E+01	1.01E-04
²³⁰ Th	2.10E-02	1.32E+03	1.32E-02
²³² Th	1.42E-08	8.93E-04	8.93E-09
²³³ U	4.05E-03	2.55E+02	2.55E-03
²³⁴ U	2.52E+00	1.58E+05	1.58E+00
²³⁵ U	1.76E-02	1.11E+03	1.11E-02
²³⁶ U	2.94E-01	1.85E+04	1.85E-01
²³⁸ U	3.16E-01	1.99E+04	1.99E-01
⁹³ Zr	2.44E+00	1.54E+05	1.54E+00
Total	1.97E+03	1.24E+08	1.24E+03

Table 8.3-2.. Summary of Analysis Variations for Major Cases Evaluated in TSPA-1995

Thermo-hydrologic Modeling	Areal Power Loading (MTU/acre)	Backfill Configuration	Infiltration ³⁾
FEHM ¹⁾	25	No	Low
			High
		Yes	Low
			High
	83	No	Low
			High
		Yes	Low
			High
TOUGH ²⁾	24	No	0
		Yes	0
	80	No	0
		Yes	0

¹⁾ FEHM modeling by S. Lingineni (see Chapter 4).

²⁾ TOUGH modeling by T. Buscheck provided for comparison purposes (Buscheck, et al., 1995).

³⁾ Low infiltration range: 0.01 to 0.05 mm/yr; High infiltration range: 0.5 to 2.0 mm/yr

Table 8.3-3. Waste Package Degradation Information for Major Cases as Implemented in RIP Simulations

Case	# of Packages with at Least 1 Pit Penetration in 100,000 years ¹⁾		Time to First Pit Penetration for Each Waste Package Group (years)					
			1	2	3	4	5	6
	Spent Fuel ²⁾	DHLW ³⁾	mean	mean	mean	mean	mean	mean
25/N/L	1116	564	1797	2434	3247	3961	7741	47119
25/N/H	2184	1098	2813	4130	5330	10266	29182	69958
25/Y/L	840	420	2831	4276	6694	17600	45275	79242
25/Y/H	2088	1050	2353	3853	5383	7551	15613	59021
83/N/L	5658	2850	1435	1978	2362	2797	3954	11844
83/N/H	6000	3030	1348	1845	2179	2848	4408	16517
83/Y/L	5064	2556	1790	2476	2906	3459	4560	11611
83/Y/H	5358	2700	1651	2217	2695	3481	4406	7178

8-24

- 1) Packages which pitted after 100,000 years and before 1,000,000 years were assumed to fail log-uniformly over that period of time.
- 2) Total number of spent fuel packages = 6468.
- 3) Total number of DHLW packages = 3829.

Table 8.3-4.. Comparison of NRC Release Rate Limit with an Expected Value Case for up to 100,000 years (83 MTU/acre, no backfill, and high infiltration rate. RH criteria for corrosion initiation¹⁾)

Radio-nuclide	NRC Limit (Ci/yr)	83 MTU/acre, No Backfill and High Infiltration Rate Case		
		Max. Release Rate (Ci/yr)	Time for Max. Release Rate (years)	Max. Release Rate/ NRC Limit
²²⁷ Ac	2.45E-04	1.54E-02	16,600	6.28E+01
²⁴¹ Am	6.69E+02	8.92E+00	2,200	1.33E-02
^{242M} Am	1.68E-01	5.38E-05	2,200	3.20E-04
²⁴³ Am	1.47E+01	2.11E+00	16,600	1.43E-01
¹⁴ C	7.96E-01	3.11E+01	2,200	3.91E+01
³⁶ Cl	7.13E-03	2.93E-01	2,200	4.11E+01
²⁴⁴ Cm	4.19E-11	-- ²⁾	--	--
²⁴⁵ Cm	2.01E-01	4.09E-08	7,100	2.03E-07
²⁴⁶ Cm	3.90E-02	3.56E-05	7,200	9.13E-04
¹³⁵ Cs	3.31E-01	7.39E+00	2,200	2.23E+01
¹²⁹ I	2.22E-02	9.60E-01	2,200	4.32E+01
^{93M} Nb	1.46E+00	--	--	--
⁹⁴ Nb	5.16E-01	3.31E-02	16,600	6.41E-02
⁵⁹ Ni	1.51E+00	3.12E+01	2,200	2.07E+01
⁶³ Ni	1.34E-01	8.96E-04	2,100	6.69E-03
²³⁷ Np	7.82E-01	2.10E+00	16,600	2.68E+00
²³¹ Pa	2.44E-04	1.86E-02	16,600	7.62E+01
²¹⁰ Pb	2.36E-03	1.26E+01	100,000+ ³⁾	5.34E+03
¹⁰⁷ Pd	8.12E-02	1.69E+00	2,200	2.08E+01
²³⁸ Pu	1.24E+00	4.05E-06	2,100	3.27E-07
²³⁹ Pu	2.24E+02	7.19E-01	16,700	3.21E-03
²⁴⁰ Pu	3.09E+02	5.39E-01	4,500	1.74E-03
²⁴¹ Pu	2.01E-01	--	--	--

Table 8.3-4. Comparison of NRC Release Rate Limit with an Expected Value case for up to 100,000 years (83 MTU/acre, no backfill, and high infiltration rate, RH switch for corrosion initiation. ¹⁾) (Continued)

Radio-nuclide	NRC Limit (Ci/yr)	83 MTU/acre, No Backfill and High Infiltration Rate Case		
		Max. Release Rate (Ci/yr)	Time for Max. Release Rate (years)	Max. Release Rate/ NRC Limit
²⁴² Pu	1.30E+00	2.32E-02	100,000+	1.78E-02
²²⁶ Ra	2.37E-03	1.69E+01	100,000+	7.13E+03
²²⁸ Ra	8.93E-09	1.51E-03	100,000+	1.68E+05
⁷⁹ Se	2.82E-01	6.21E+00	2,200	2.20E+01
¹⁵¹ Sm	1.30E-01	7.32E-04	2,100	5.63E-03
¹²⁶ Sn	5.46E-01	1.62E-02	16,600	2.97E-02
⁹⁹ Tc	9.03E+00	2.00E+02	2,200	2.21E+01
²²⁹ Th	1.01E-04	1.62E-03	100,000+	1.60E+01
²³⁰ Th	1.32E-02	5.05E-03	166,600	3.82E+01
²³² Th	8.93E-09	2.32E-08	100,000+	2.60E+00
²³³ U	2.55E-03	3.82E-04	100,000+	1.50E-01
²³⁴ U	1.58E+00	7.29E-03	16,600	4.61E-03
²³⁵ U	1.11E-02	2.22E-05	35,100	2.00E-03
²³⁶ U	1.85E-01	3.35E-04	28,000	1.81E-03
²³⁸ U	1.99E-01	3.33E-04	16,600	1.67E-03
⁹³ Zr	1.54E+00	2.63E-04	16,600	1.71E-04

- ¹⁾ This case yielded the most conservative results (the largest release rates).
- ²⁾ -- Indicates that the maximum release rate was very small and is not reported.
- ³⁾ 100,000+ indicates that the release rate was increasing at the end of the simulation.

Table 8.3-5. Radionuclides Considered for the Comparison with the NRC EBS Release Rate Limit in TSPA-1995¹⁾ and TSPA-1993²⁾

Radio-Nuclide	TSPA-1995		TSPA-1993	
	Maximum Release Rate (Ci/yr)	Time for Max. Release Rate (years)	Maximum Release Rate (Ci/yr)	Time for Max. Release Rate (years)
¹⁴ C	3.11E+01	2,200	6.20E+00	1,000
¹³⁵ Cs	7.39E+00	2,200	1.90E+00	1,500
⁵⁹ Ni	3.12E+01	2,200	6.30E+00	2,000
²³⁷ Np	2.10E+00	16,600	3.90E+00	7,000
²¹⁰ Pb	1.26E+01	100,000+ ³⁾	1.90E+00	60,000
¹⁰⁷ Pd	1.69E+00	2,200	--- ⁴⁾	--- ⁴⁾
²²⁶ Ra	1.69E+01	100,000+ ³⁾	1.30E+00	20,000
⁷⁹ Se	6.21E+00	2,200	1.60E+00	2,000
⁹⁹ Tc	2.00E+02	2,200	6.00E+01	1,500

- 1) Nuclides were selected based on the case that yielded the most conservative results: 83 MTU/acre with no backfill, high infiltration rate, and using the RH criteria for corrosion initiation of the outer barrier. The waste container design assumed a 10-cm thick carbon steel outer barrier and a 2-cm thick Alloy 825 inner barrier.
- 2) Nuclides were selected based on the "reference" design that yielded the most conservative results: 57 kW/acre, a 10-cm thick (carbon steel) outer barrier, a 0.95-cm (Alloy 825) inner barrier, using water saturation as the corrosion initiation for aqueous corrosion, and using Westinghouse model for aqueous corrosion rate (Andrews, et al., 1994).
- 3) 100,000+ indicates that the release rate was increasing at the end of the simulation.
- 4) Not included.

Table 8.3-6. Regression Statistics for 10,000 Year EBS Peak Release Rate for the Case of 25 MTU/acre, no Backfill, High Infiltration Rate

Parameter	Rank(P.M.) ¹⁾ vs Rank(x)		ln(P.M.) vs x		ln(P.M.) vs ln(x)	
	Rank Importance	% of Variance Explained ²⁾	Rank Importance	% of Variance Explained ²⁾	Rank Importance	% of Variance Explained ²⁾
Solubility Cs	4	73				
Solubility Ni			3	32		
Solubility Np	5	74	4	34	4	80
Solubility Pb					5	80
Solubility Se						
Solubility Tc	1	51			1	51
Waste Package f_{drip} ³⁾						
q_{drip} ⁴⁾						
$q_{inf}(UZ)$ ⁵⁾	2	62	2	28	3	79
Surface Area of DHLW						
Eff. Diff. Coeff.			5	37		
Glass Diss. Rate						
SF Diss. Rate	3	73	1	18	2	65

- 1) P.M. = the performance measure (in this case EBS peak release rate)
- 2) % of variance explained by parameters ranked less than or equal to the given parameter, e.g., for parameter with rank 3, the number listed is the % variance explained by the parameters ranked 1, 2, and 3, together.
- 3) Fraction of waste packages with drips.
- 4) q_{drip} = flux of dripping fractures
- 5) $q_{inf}(UZ)$ = percolation rate in unsaturated zone

Table 8.3-7.: Regression Statistics for 10,000 Year EBS Peak Release Rate for the Case of 83MTU/acre, no Backfill, High Infiltration Rate

Parameter	Rank(P.M.) ¹⁾ vs Rank(x)		ln(P.M.) vs x		ln(P.M.) vs ln(x)	
	Rank Importance	% of Variance Explained ²⁾	Rank Importance	% of Variance Explained ²⁾	Rank Importance	% of Variance Explained ²⁾
Solubility Cs			5	46		
Solubility Ni	5	91			5	89
Solubility Np						
Solubility Pb						
Solubility Se						
Solubility Tc	1	60	3	41	1	51
Waste Package f_{drip} ³⁾						
q_{drip} ⁴⁾						
$q_{inf}(UZ)$ ⁵⁾	3	91	2	33	3	87
Surf. Area of DHLW	4	91	4	45	4	88
Eff. Diff. Coef.						
Glass Diss. Rate						
SF Diss. Rate	2	80	1	25	2	76

- 1) P.M. = the performance measure (in this case EBS peak release rate)
- 2) % of variance explained by parameters ranked less than or equal to the given parameter, e.g., for parameter with rank 3, the number listed is the % variance explained by the parameters ranked 1, 2, and 3, together.
- 3) fraction of waste packages with drips.
- 4) q_{drip} = flux of dripping fractures
- 5) $q_{inf}(UZ)$ = percolation rate in unsaturated zone

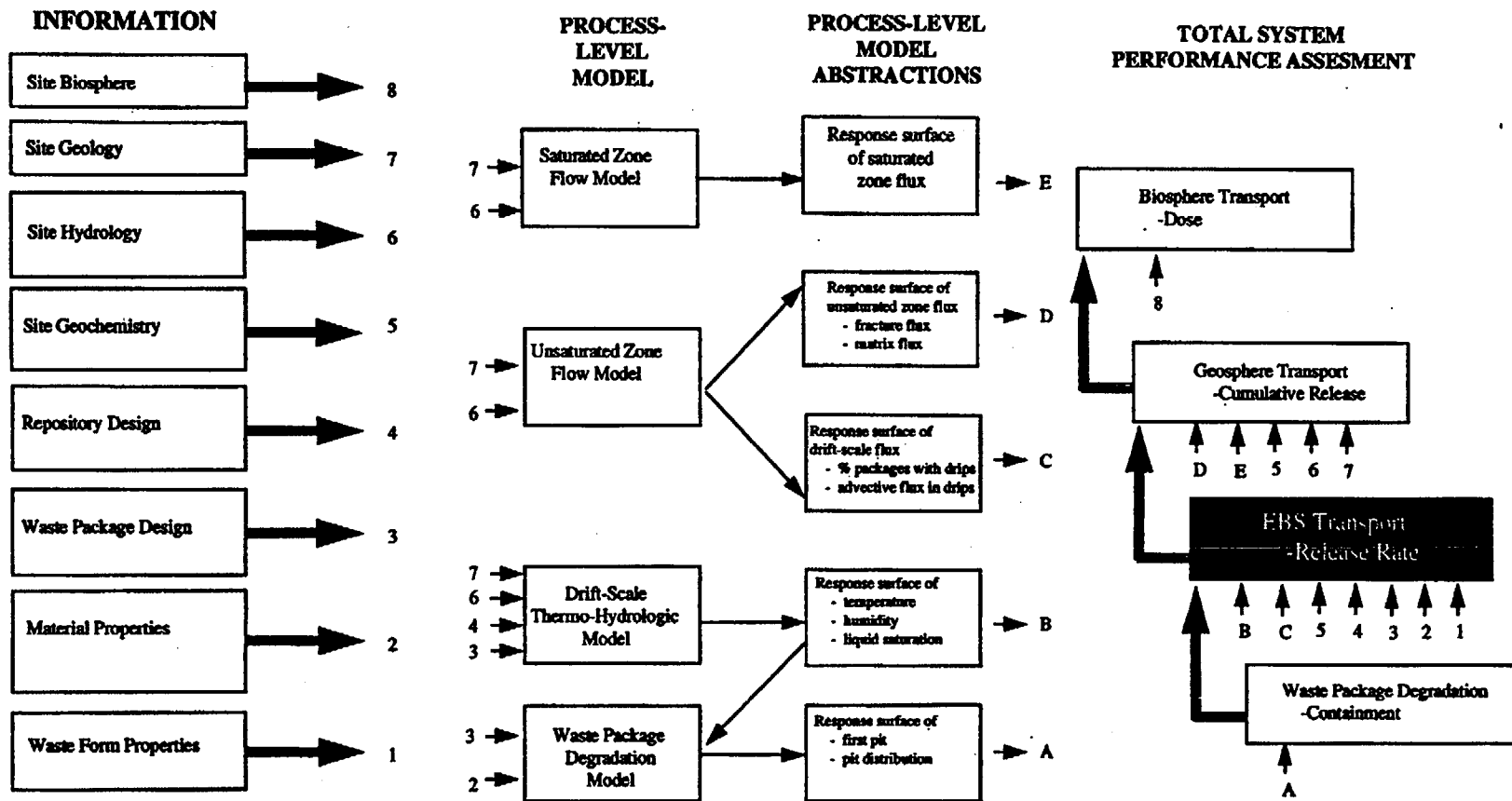


Figure 8.1-1 Relationship of Chapter 8 to the Overall Information Flow Diagram for TSPA 1995 (Figure 1.4-6)

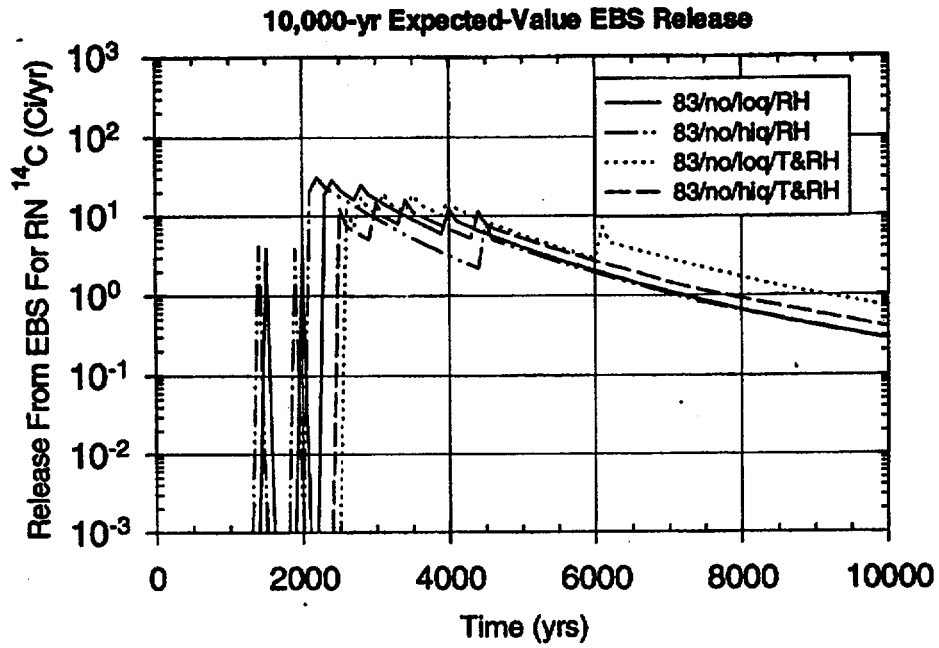


Figure 8.3-1a Sensitivity of the EBS release rate for ^{14}C to the initiation of the carbon steel outer barrier corrosion (NRC limit = 0.796 Ci/yr).

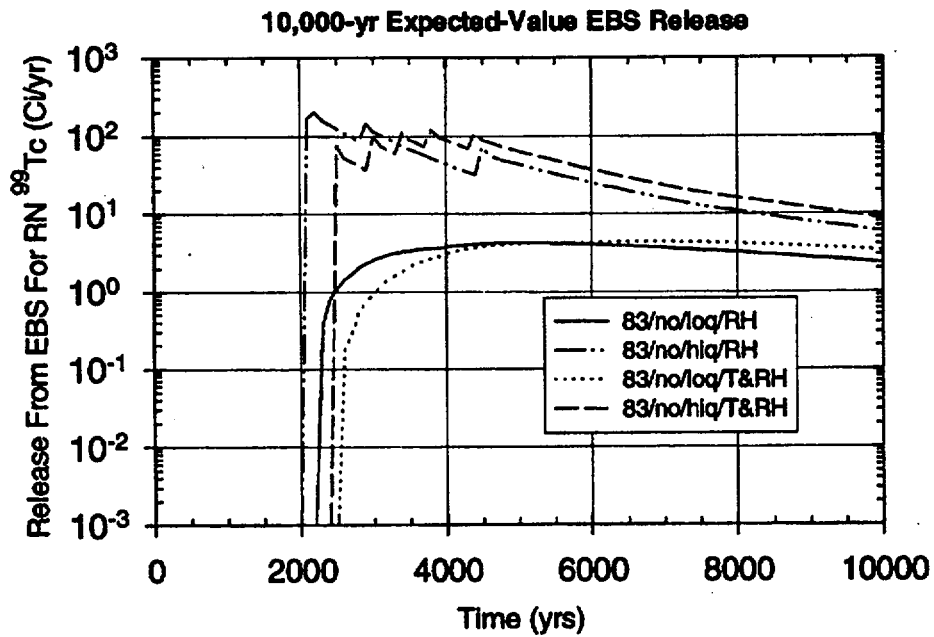


Figure 8.3-1b Sensitivity of the EBS release rate for ^{99}Tc to the initiation of the carbon steel outer barrier corrosion (NRC limit = 9.03 Ci/yr).

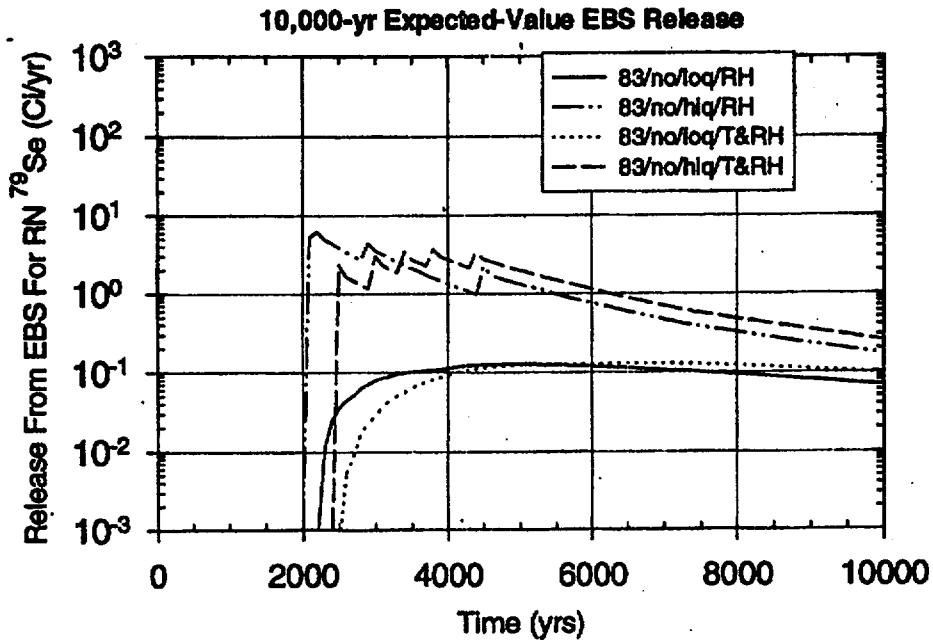


Figure 8.3-1c Sensitivity of the EBS release rate for ^{79}Se to the initiation of the carbon steel outer barrier corrosion (NRC limit = 0.282 Ci/yr).

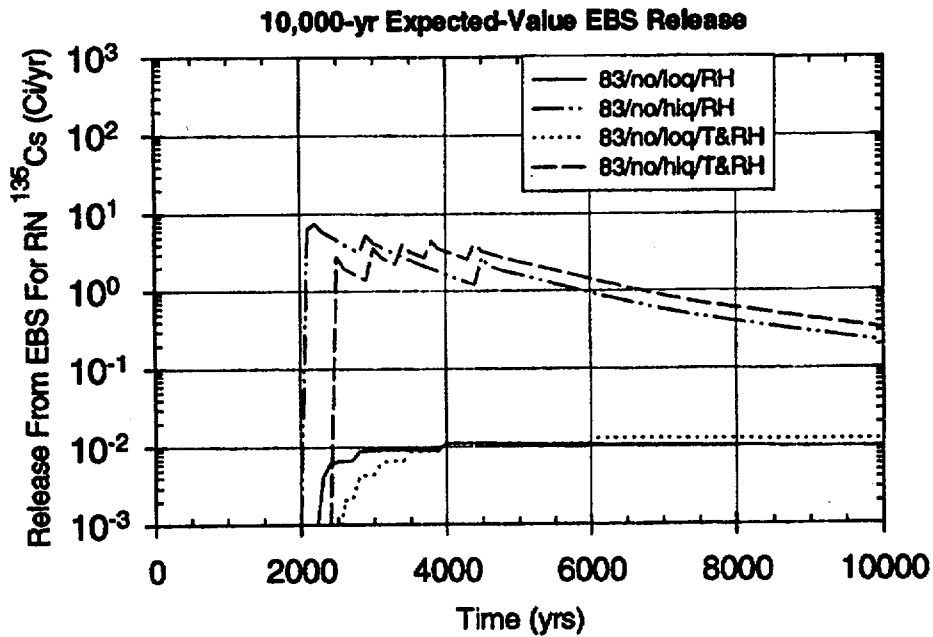


Figure 8.3-1d Sensitivity of the EBS release rate for ^{135}Cs to the initiation of the carbon steel outer barrier corrosion (NRC limit = 0.331 Ci/yr).

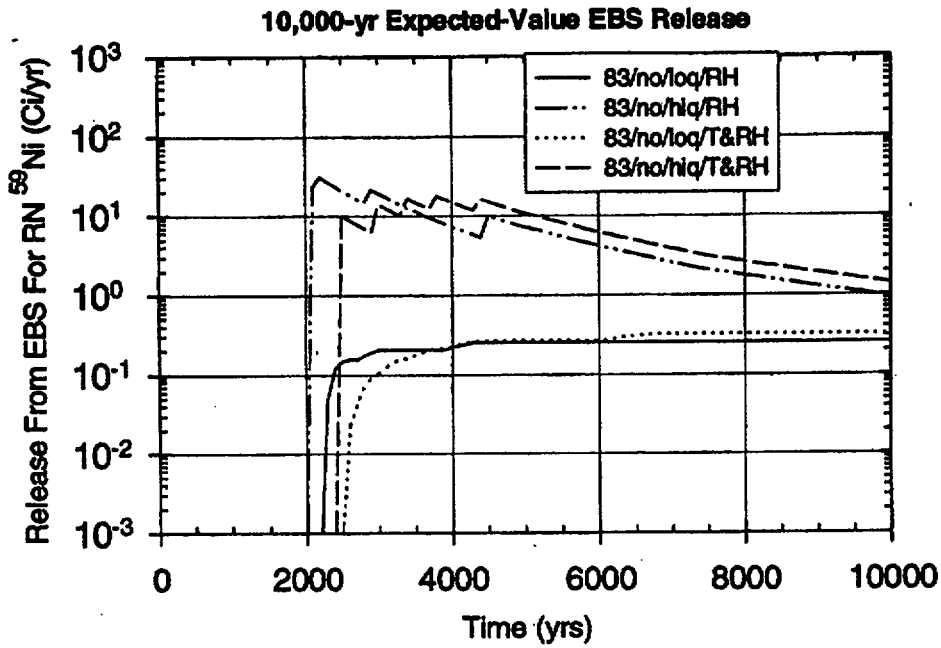


Figure 8.3-1e Sensitivity of the EBS release rate for ⁵⁹Ni to the initiation of the carbon steel outer barrier corrosion (NRC limit = 1.51 Ci/yr).

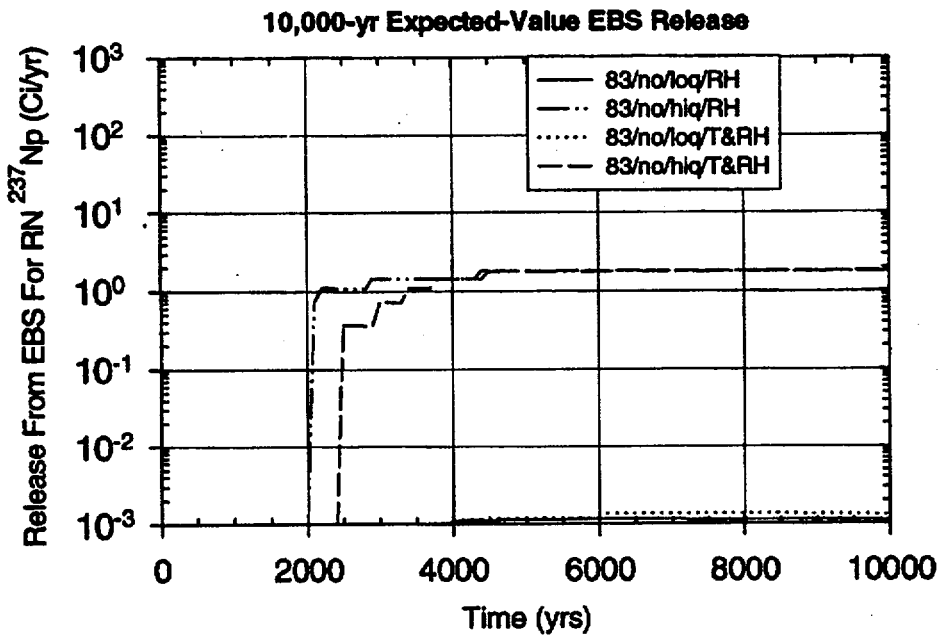


Figure 8.3-1f Sensitivity of the EBS release rate for ²³⁷Np to the initiation of the carbon steel outer barrier corrosion (NRC limit = 0.782 Ci/yr).

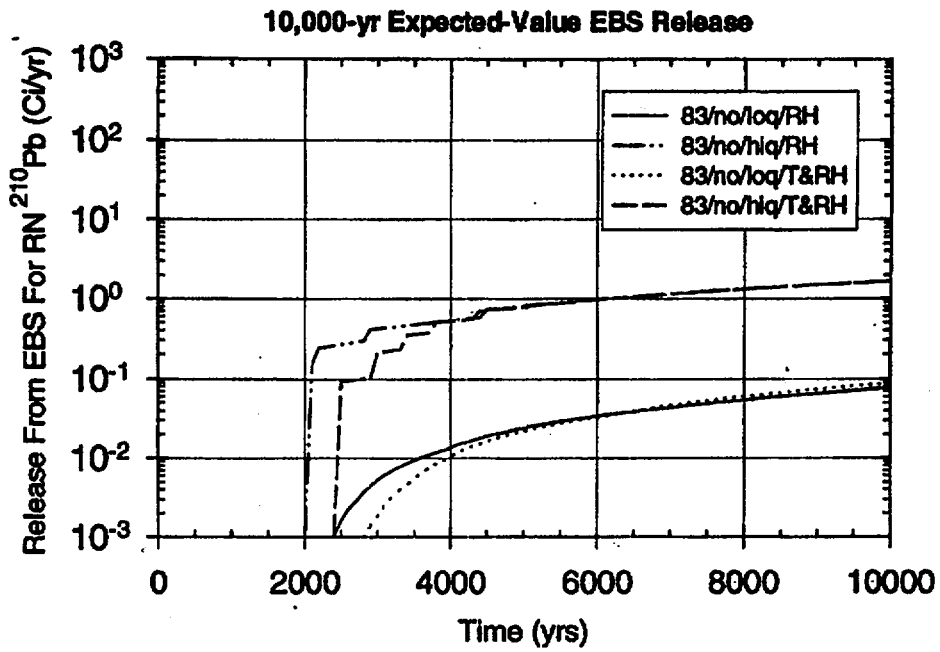


Figure 8.3-1g Sensitivity of the EBS release rate for ^{210}Pb to the initiation of the carbon steel outer barrier corrosion (NRC limit = 0.00236 Ci/yr).

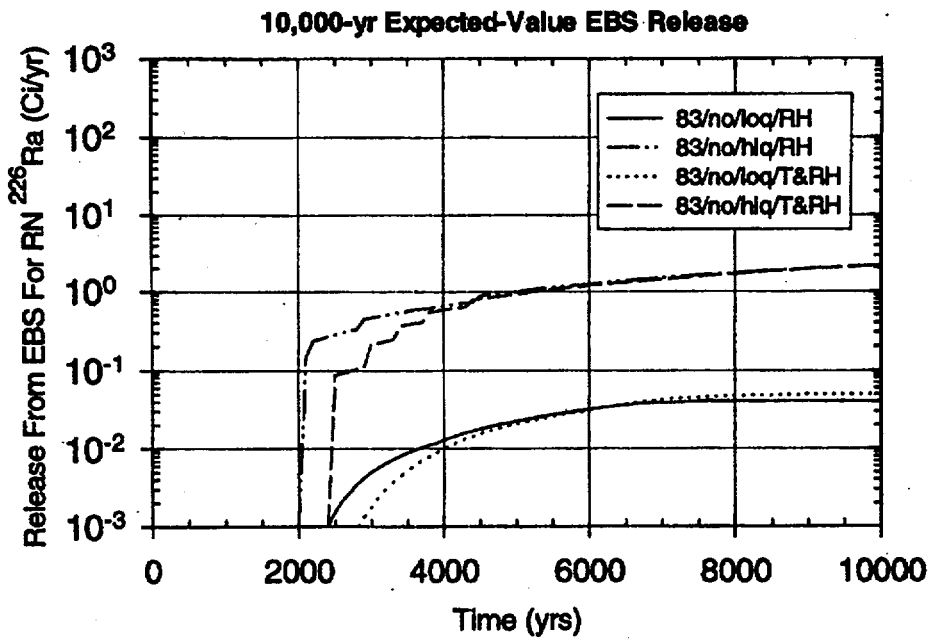


Figure 8.3-1h Sensitivity of the EBS release rate for ^{226}Ra to the initiation of the carbon steel outer barrier corrosion (NRC limit = 0.00237 Ci/yr).

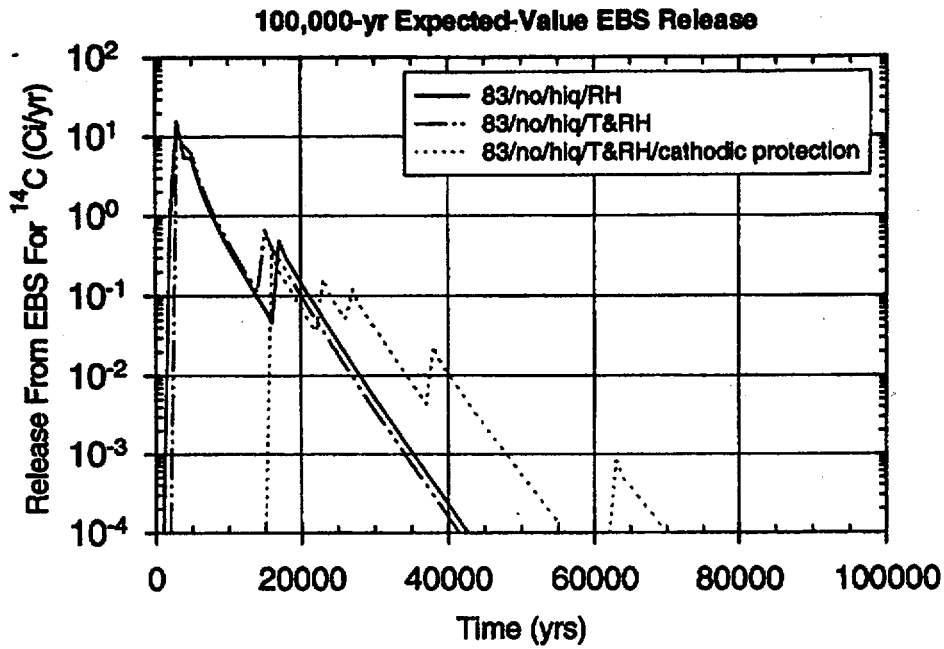


Figure 8.3-2a Sensitivity of the EBS release rate for ^{14}C to cathodic protection (NRC limit = 0.796 Ci/yr).

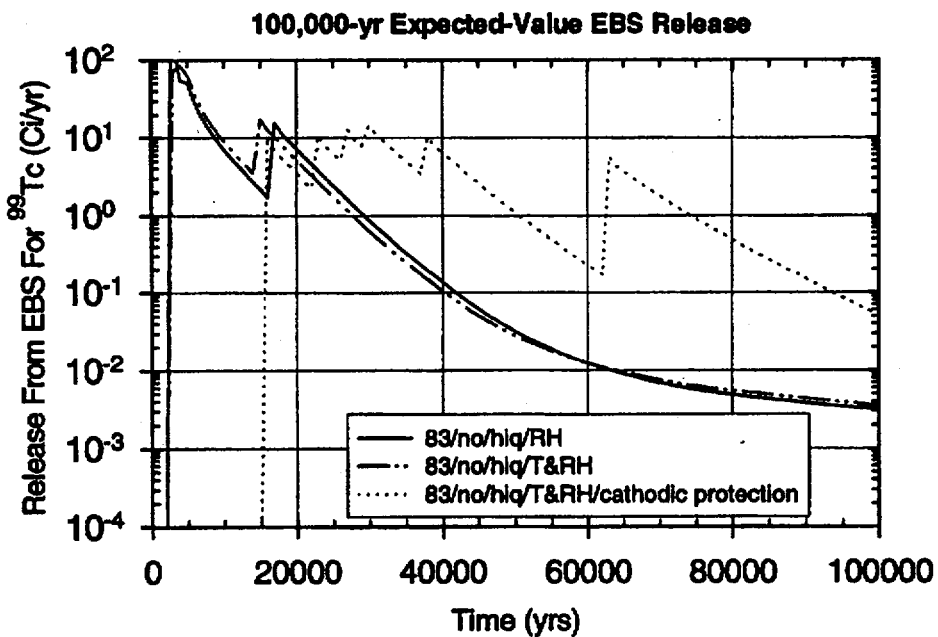


Figure 8.3-2b Sensitivity of the EBS release rate for ^{99}Tc to cathodic protection (NRC limit = 9.03 Ci/yr).

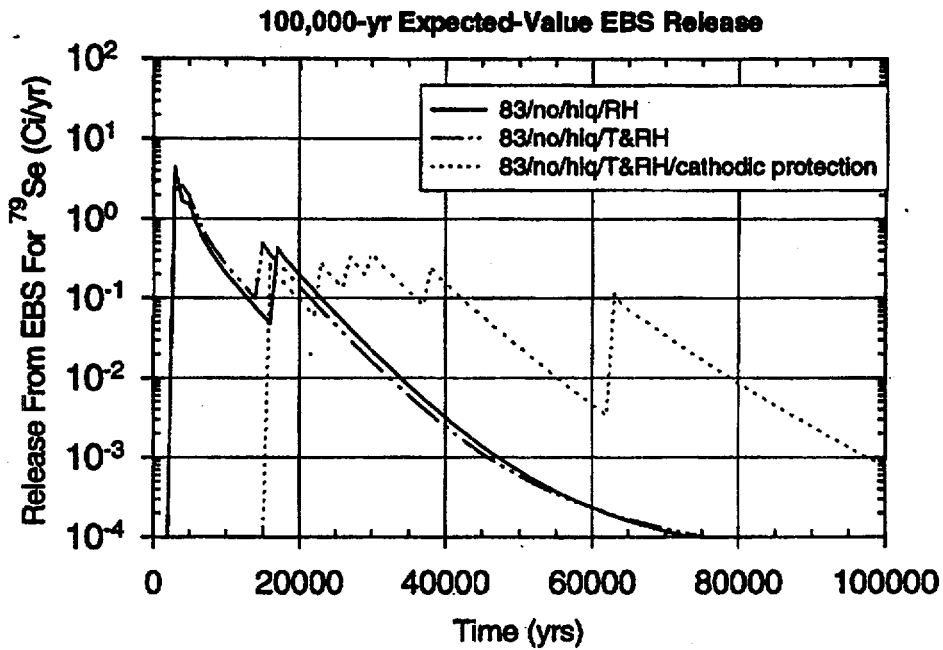


Figure 8.3-2c Sensitivity of the EBS release rate for ⁷⁹Se to cathodic protection (NRC limit = 0.282 Ci/yr).

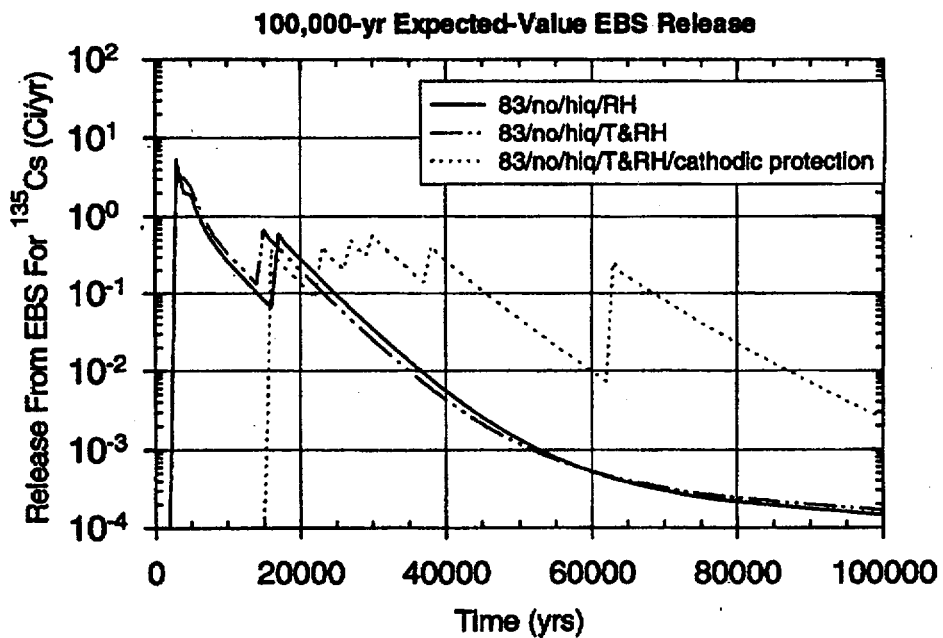


Figure 8.3-2d Sensitivity of the EBS release rate for ¹³⁵Cs to cathodic protection (NRC limit = 0.331 Ci/yr).

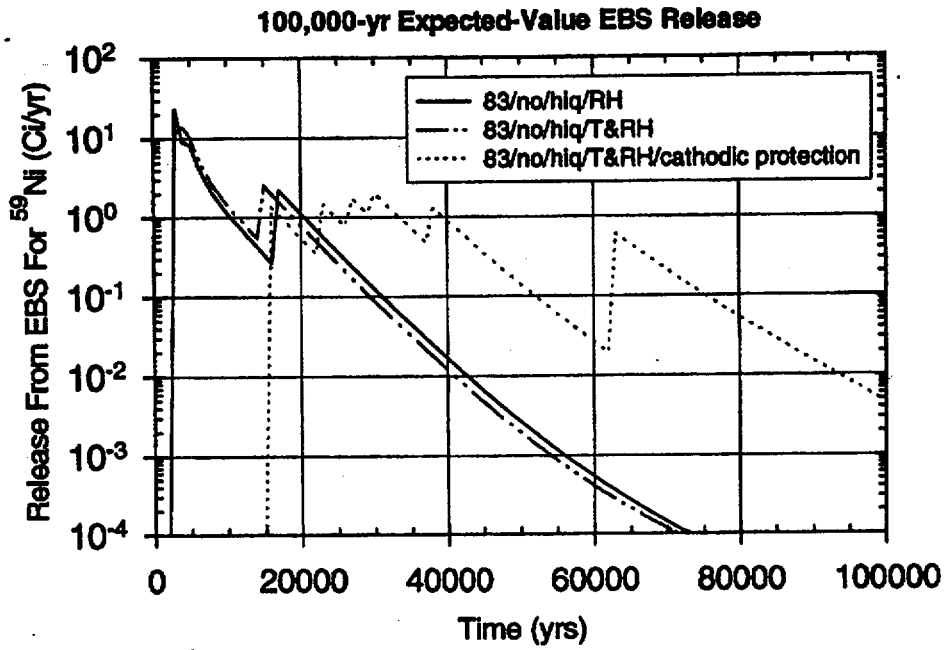


Figure 8.3-2e Sensitivity of the EBS release rate for ^{59}Ni to cathodic protection (NRC limit = 1.51 Ci/yr).

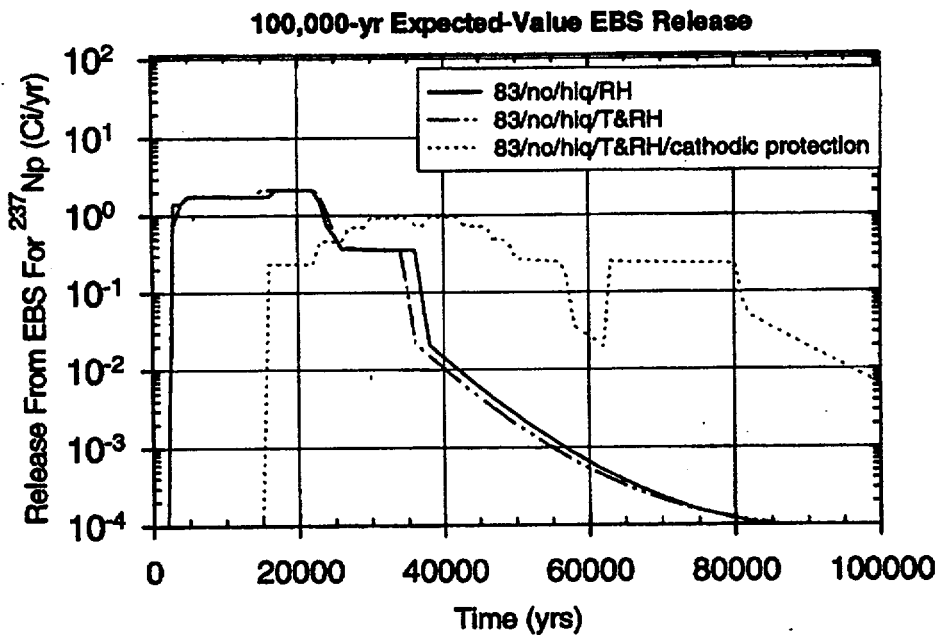


Figure 8.3-2f Sensitivity of the EBS release rate for ^{237}Np to cathodic protection (NRC limit = 0.782 Ci/yr).

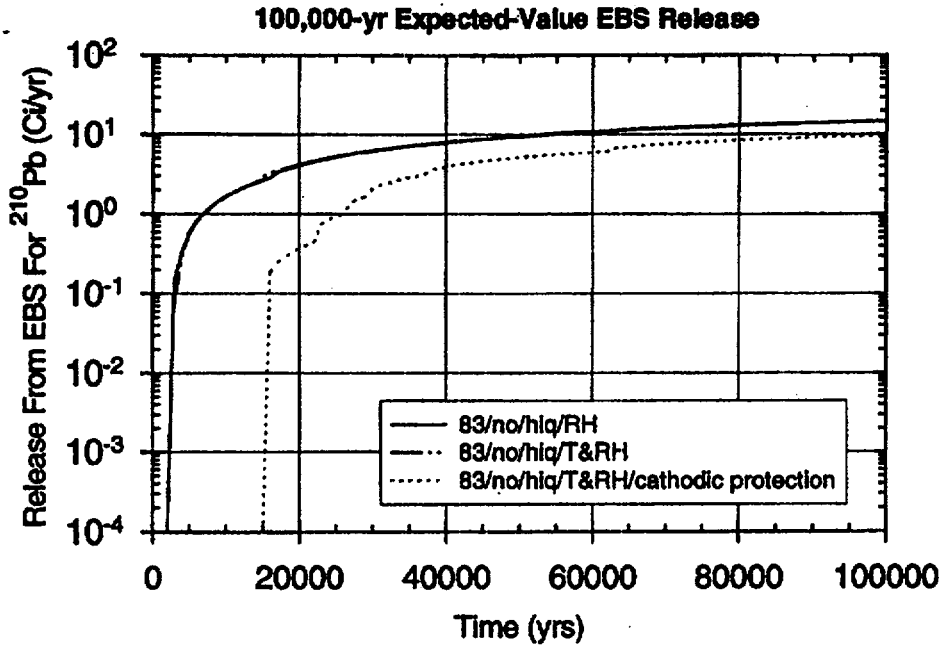


Figure 8.3-2g Sensitivity of the EBS release rate for ^{210}Pb to cathodic protection (NRC limit = 0.00236 Ci/yr).

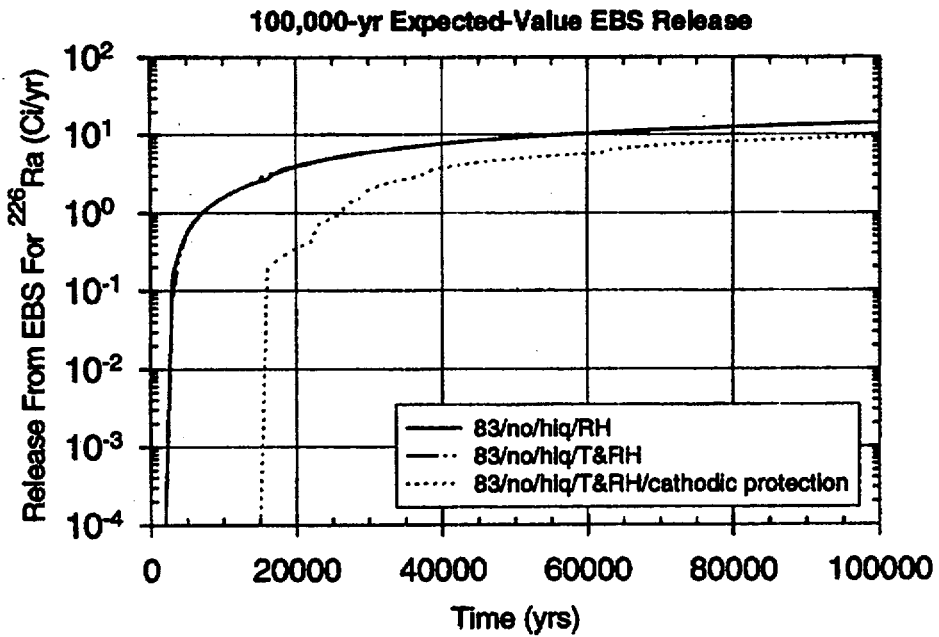


Figure 8.3-2h Sensitivity of the EBS release rate for ^{226}Ra to cathodic protection (NRC limit = 0.00237 Ci/yr).

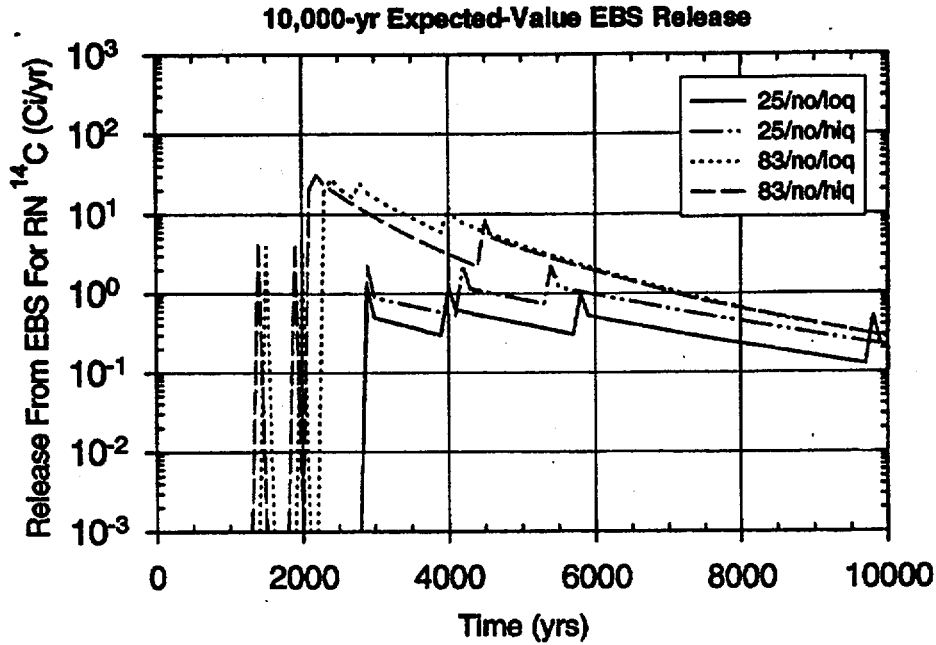


Figure 8.3-3a Sensitivity of the EBS release rate for ¹⁴C to thermal loading and infiltration rate (NRC limit = 0.796 Ci/yr).

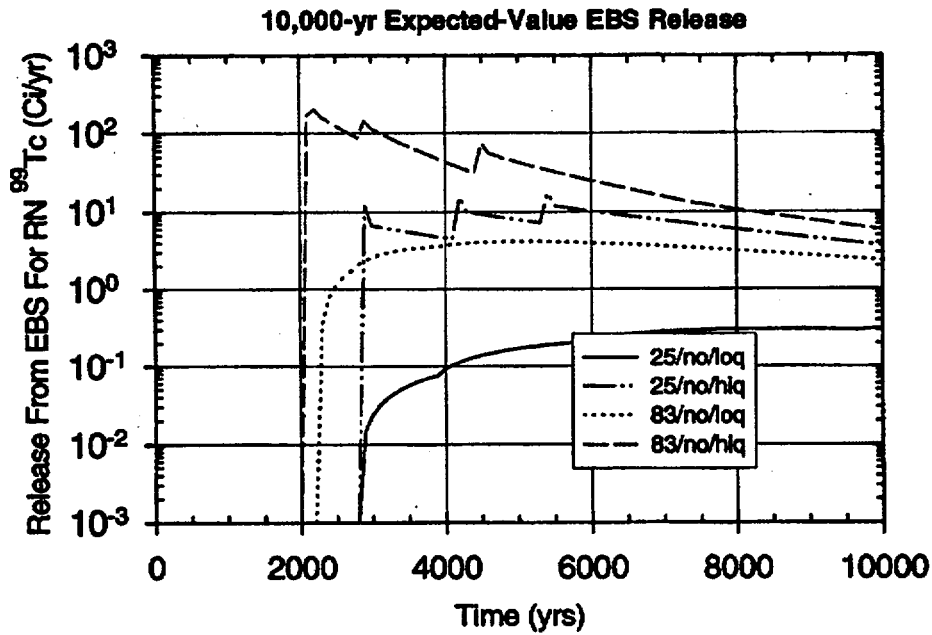


Figure 8.3-3b Sensitivity of the EBS release rate for ⁹⁹Tc to thermal loading and infiltration rate (NRC limit = 9.03 Ci/yr).

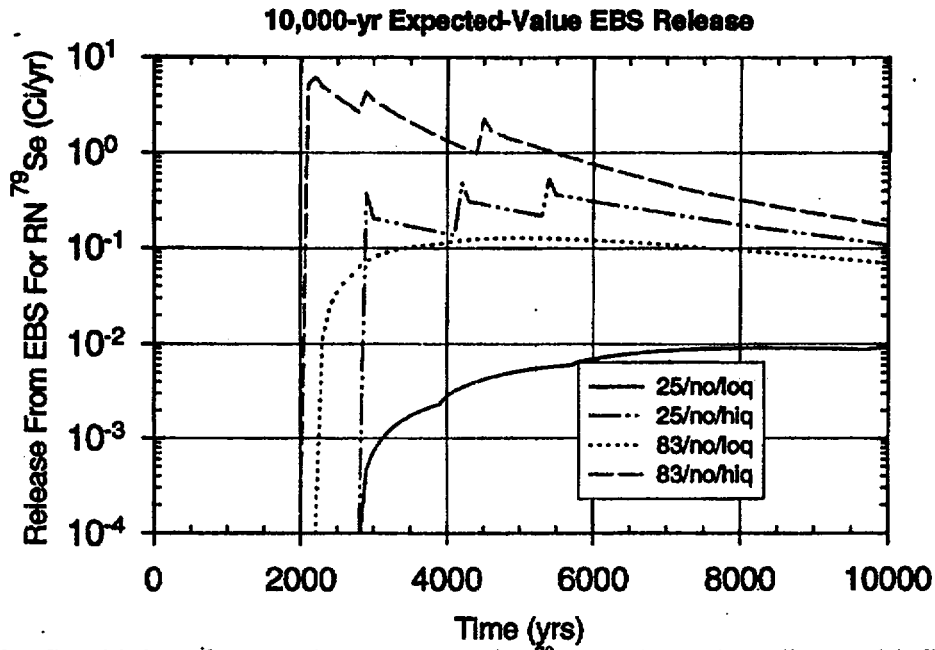


Figure 8.3-3c Sensitivity of the EBS release rate for ^{79}Se to thermal loading and infiltration rate (NRC limit = 0.282 Ci/yr).

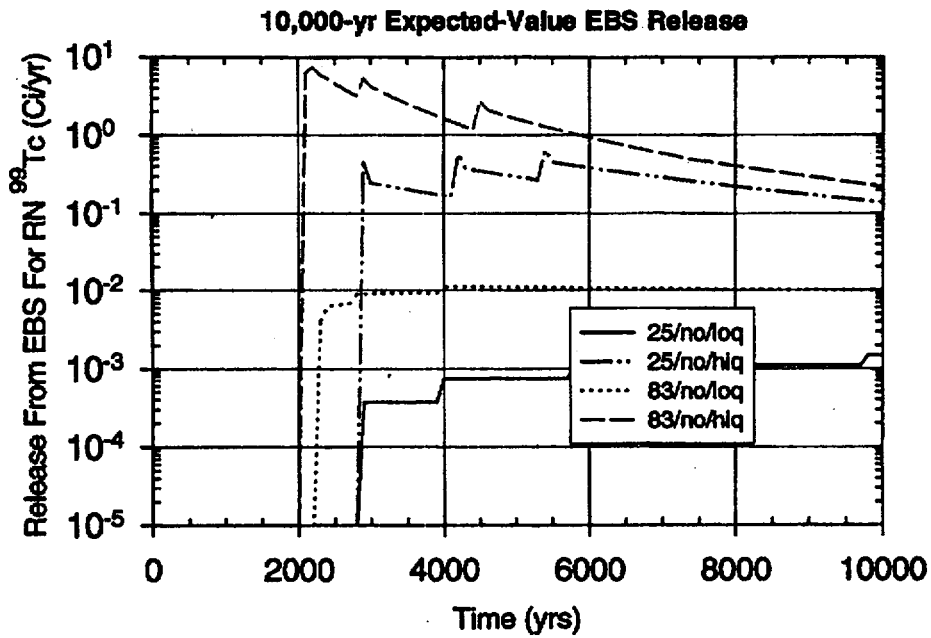


Figure 8.3-3d Sensitivity of the EBS release rate for ^{135}Cs to thermal loading and infiltration rate (NRC limit = 0.331 Ci/yr).

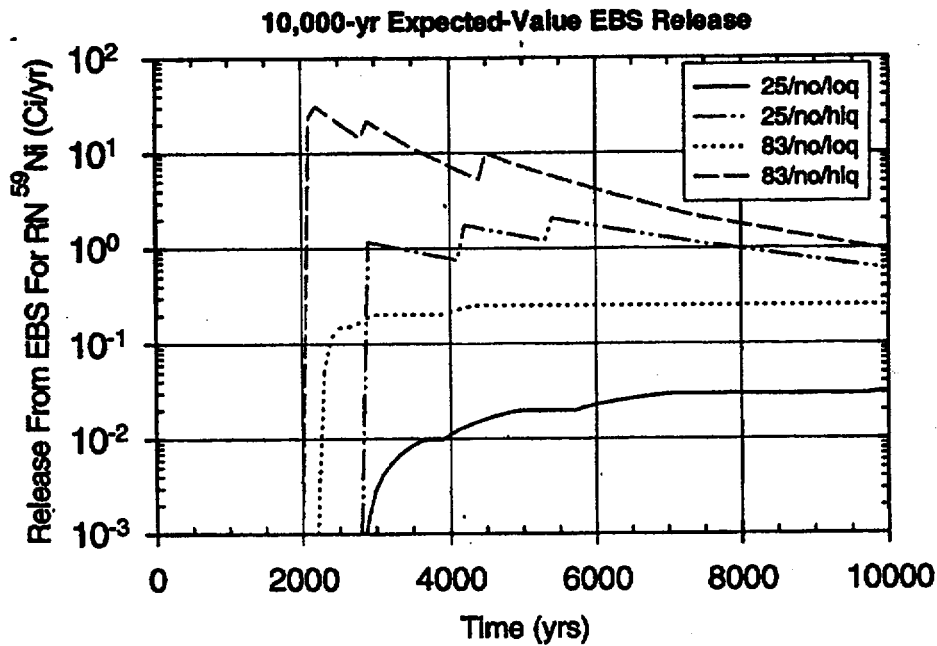


Figure 8.3-3e Sensitivity of the EBS release rate for ^{59}Ni to thermal loading and infiltration rate (NRC limit = 1.51 Ci/yr).

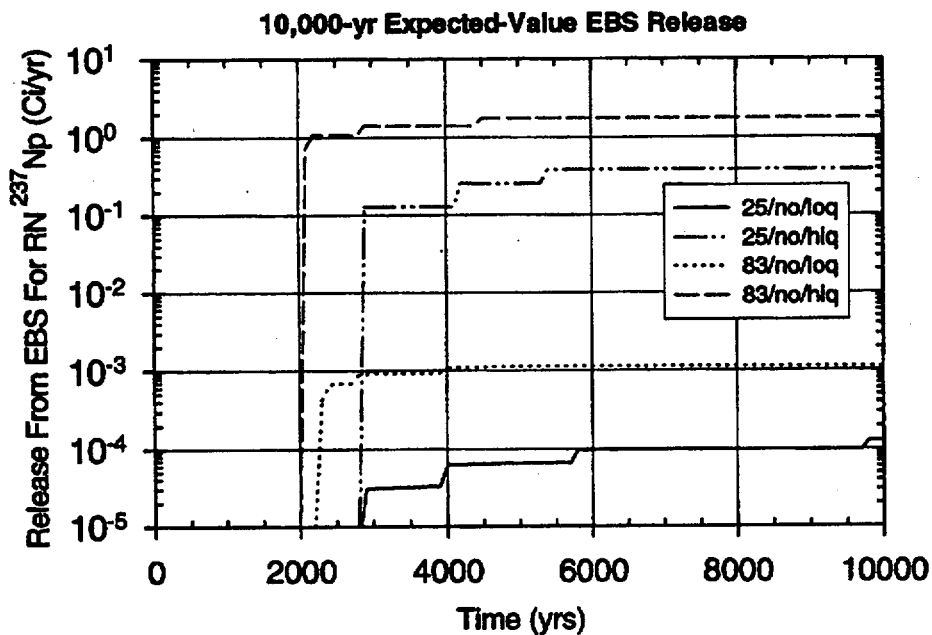


Figure 8.3-3f Sensitivity of the EBS release rate for ^{237}Np to thermal loading and infiltration rate (NRC limit = 0.782 Ci/yr).

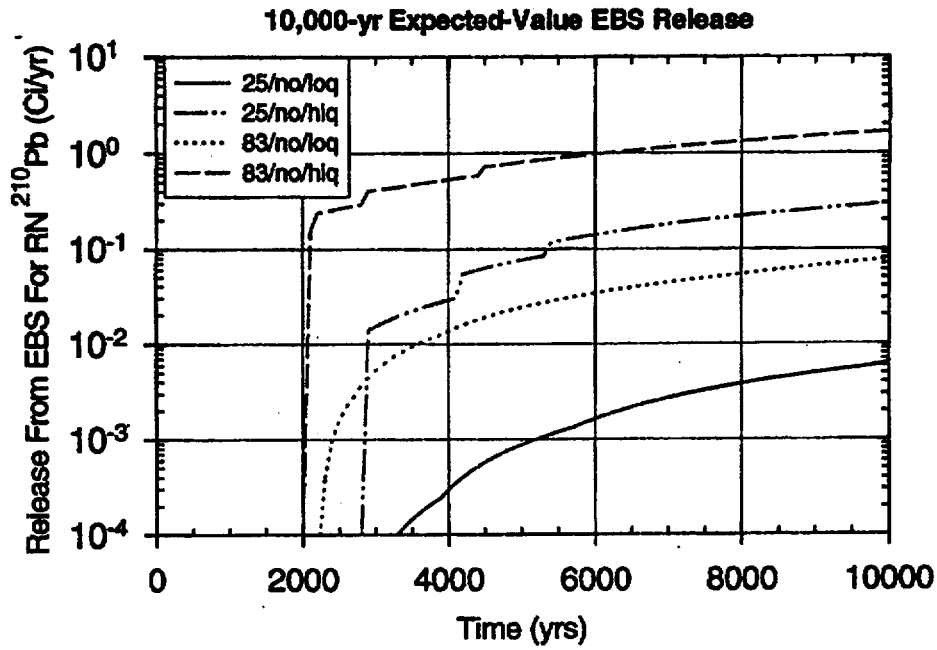


Figure 8.3-3g Sensitivity of the EBS release rate for ²¹⁰Pb to thermal loading and infiltration rate (NRC limit = 0.00236 Ci/yr).

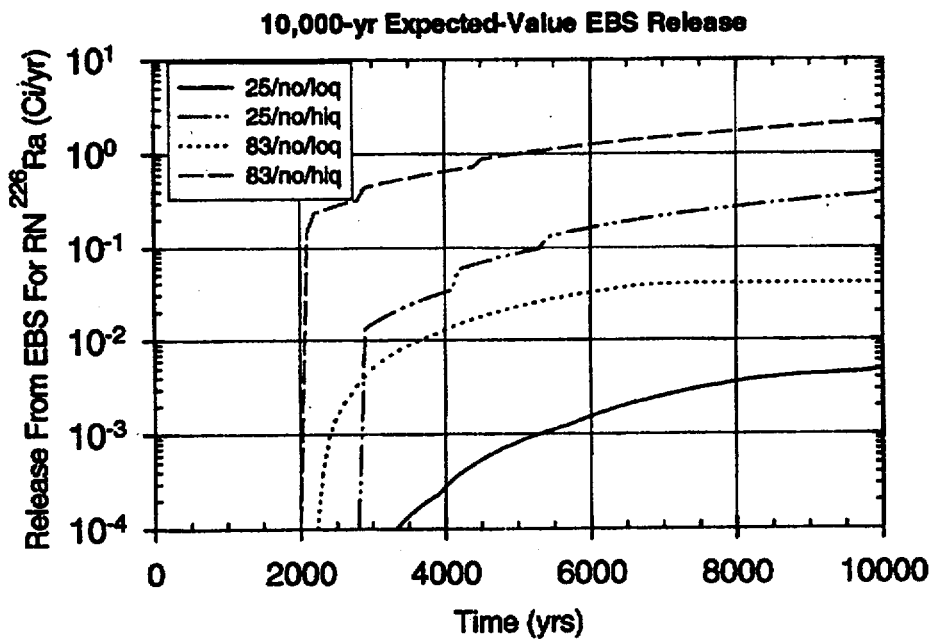


Figure 8.3-3h Sensitivity of the EBS release rate for ²²⁶Ra to thermal loading and infiltration rate (NRC limit = 0.00237 Ci/yr).

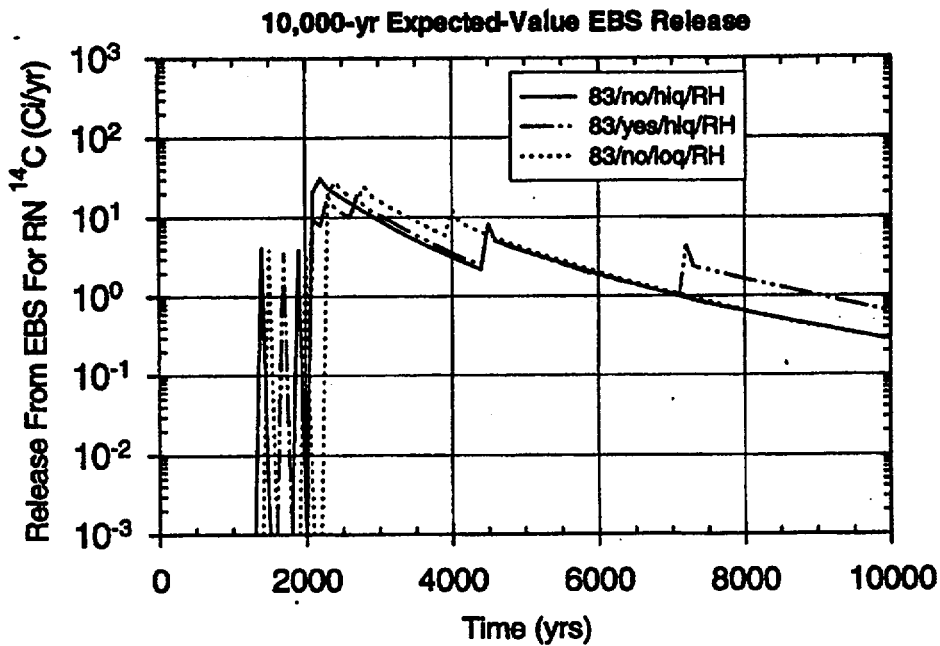


Figure 8.3-4a Sensitivity of the EBS release rate for ^{14}C to the presence of backfill (NRC limit = 0.796 Ci/yr).

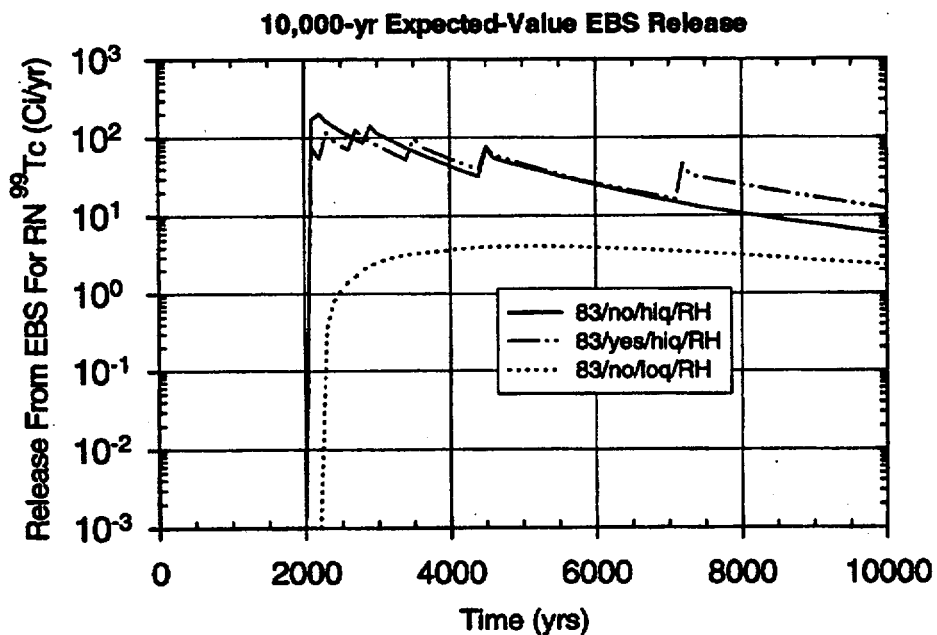


Figure 8.3-4b Sensitivity of the EBS release rate for ^{99}Tc to the presence of backfill (NRC limit = 9.03 Ci/yr).

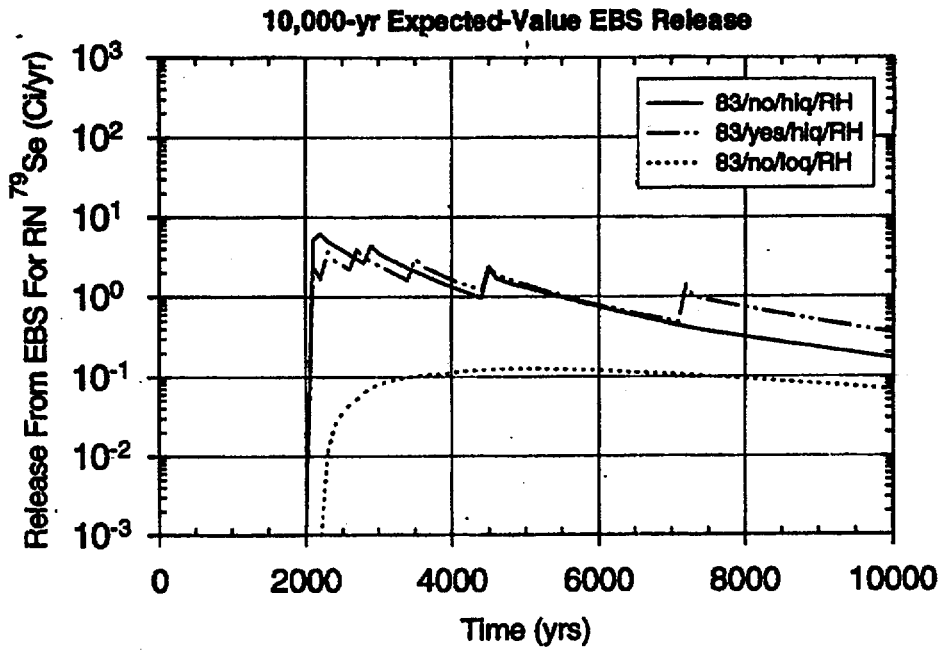


Figure 8.3-4c Sensitivity of the EBS release rate for ^{79}Se to the presence of backfill (NRC limit = 0.282 Ci/yr).

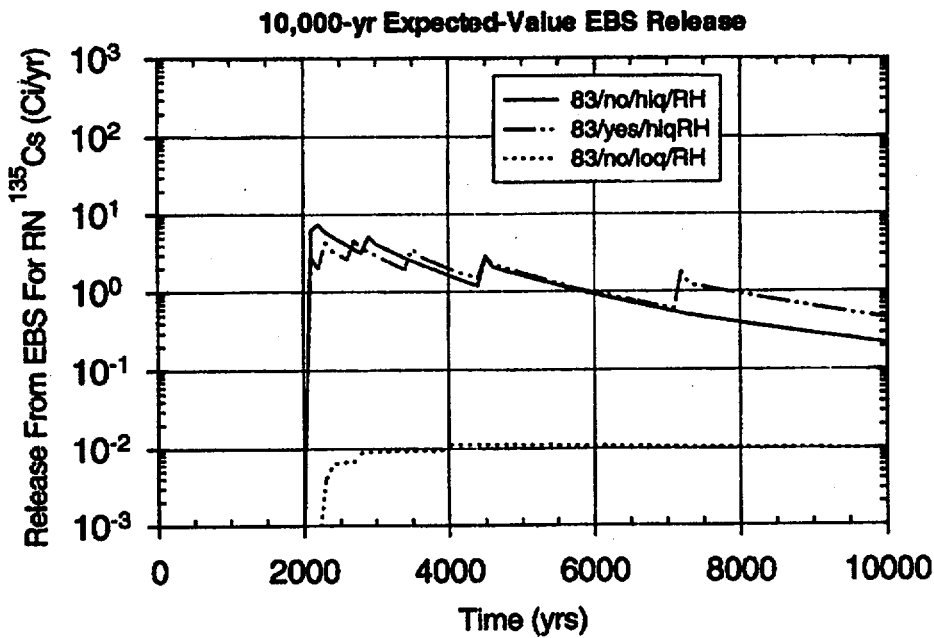


Figure 8.3-4d Sensitivity of the EBS release rate for ^{135}Cs to the presence of backfill (NRC limit = 0.331 Ci/yr).

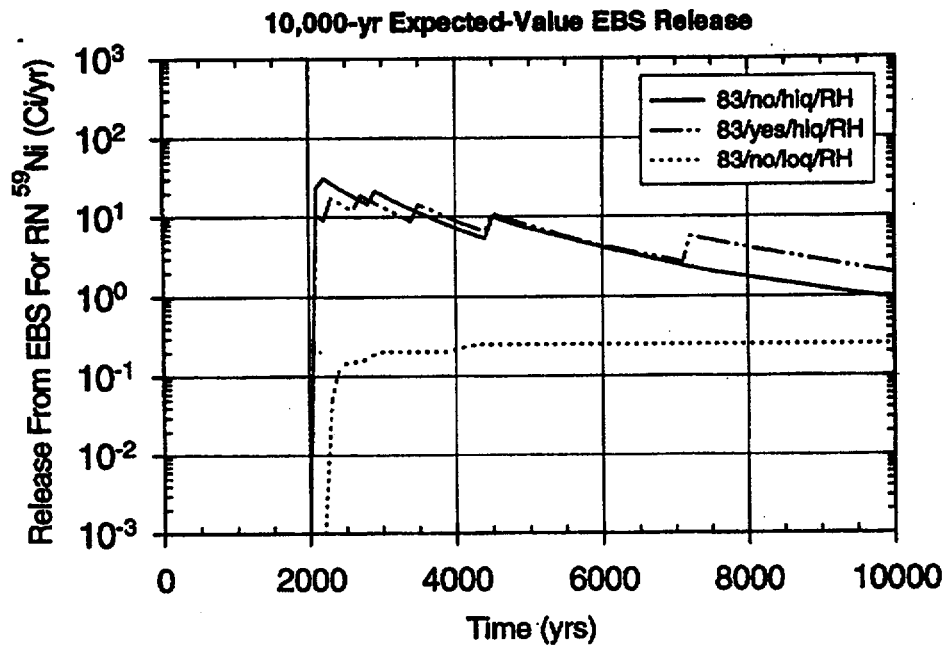


Figure 8.3-4e Sensitivity of the EBS release rate for ^{59}Ni to the presence of backfill (NRC limit = 1.51 Ci/yr).

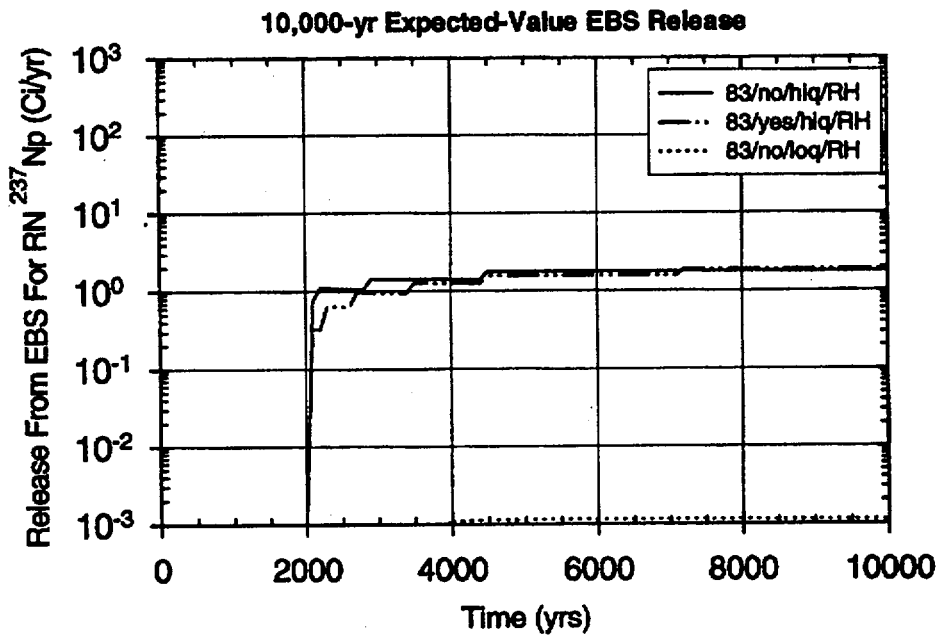


Figure 8.3-4f Sensitivity of the EBS release rate for ^{237}Np to the presence of backfill (NRC limit = 0.782 Ci/yr).

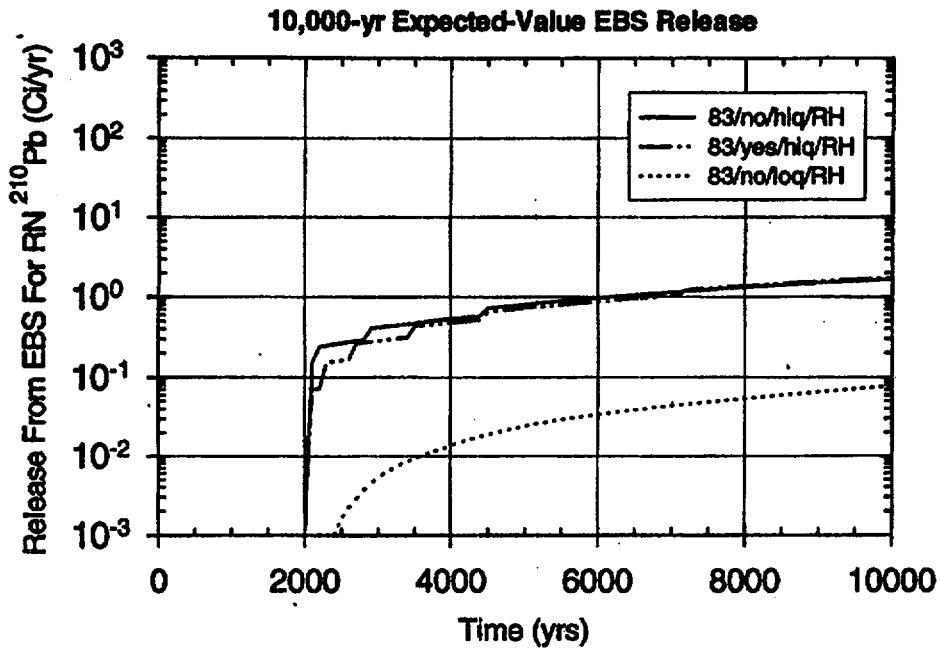


Figure 8.3-4g Sensitivity of the EBS release rate for ^{210}Pb to the presence of backfill (NRC limit = 0.00236 Ci/yr).

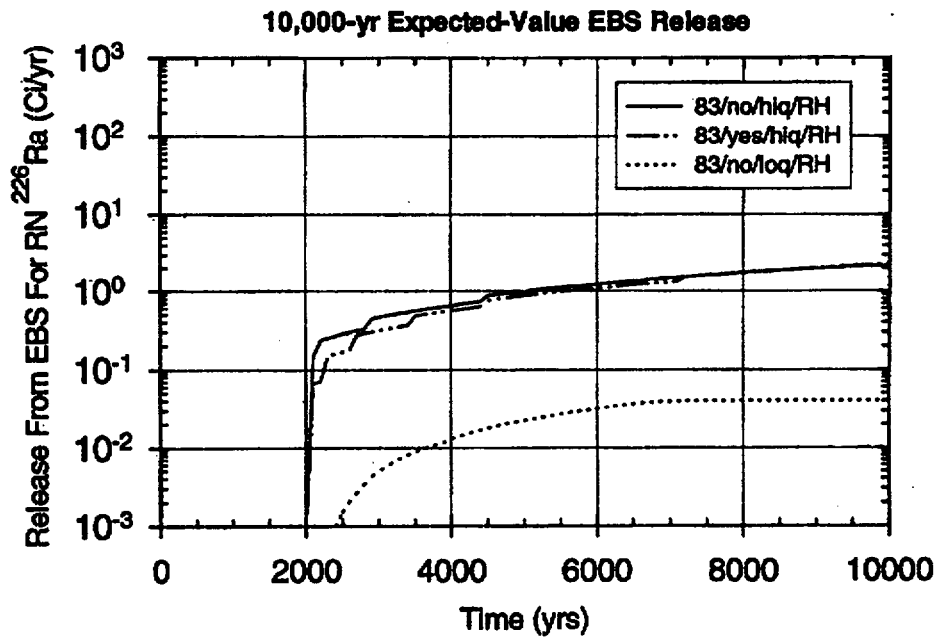


Figure 8.3-4h Sensitivity of the EBS release rate for ^{226}Ra to the presence of backfill (NRC limit = 0.00237 Ci/yr).

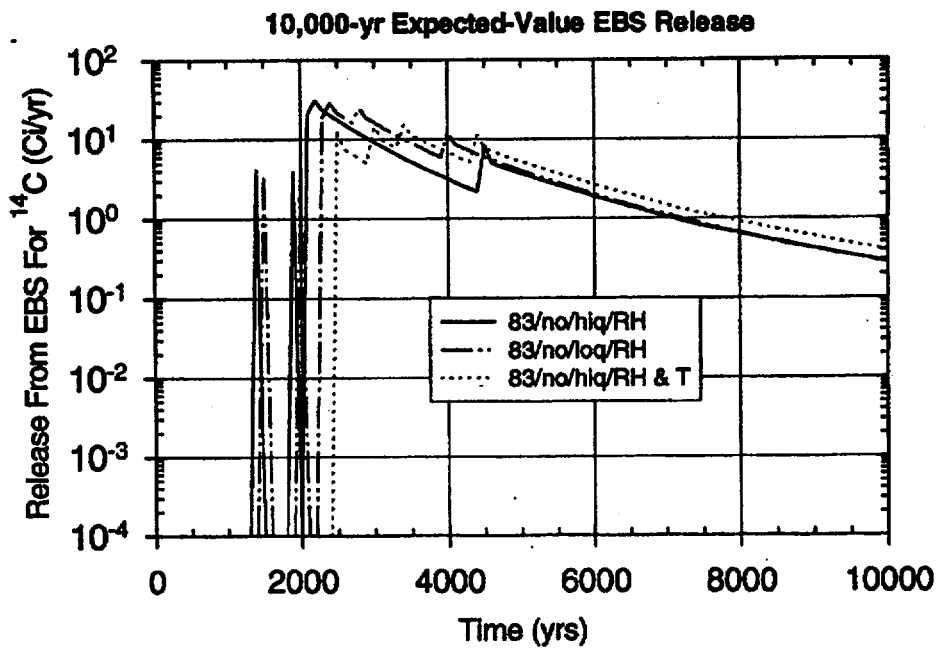


Figure 8.3-5a Sensitivity of the EBS release rate for ^{14}C to the alternative advective release model (NRC limit = 0.796 Ci/yr).

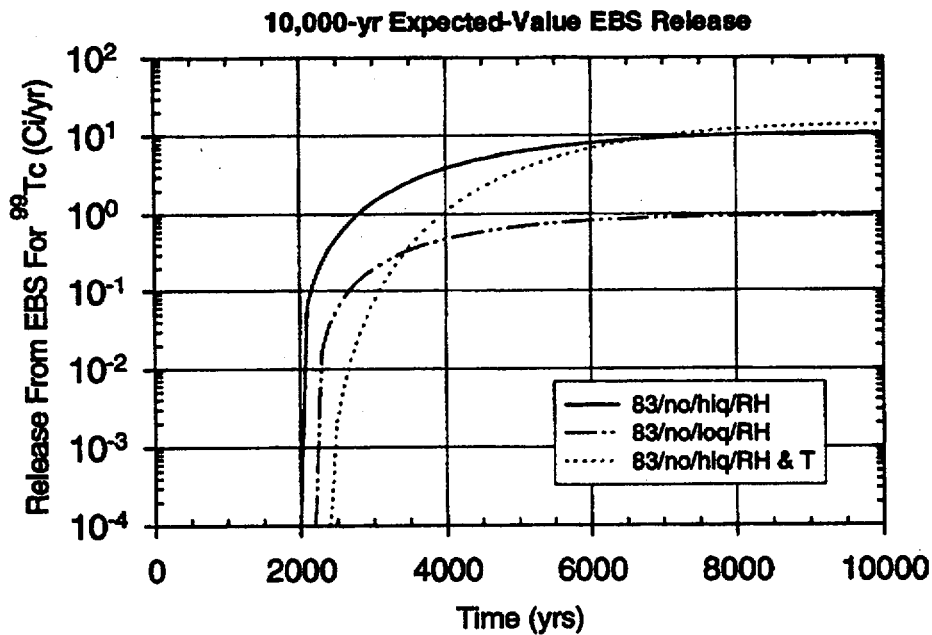


Figure 8.3-5b Sensitivity of the EBS release rate for ^{99}Tc to the alternative advective release model (NRC limit = 9.03 Ci/yr).

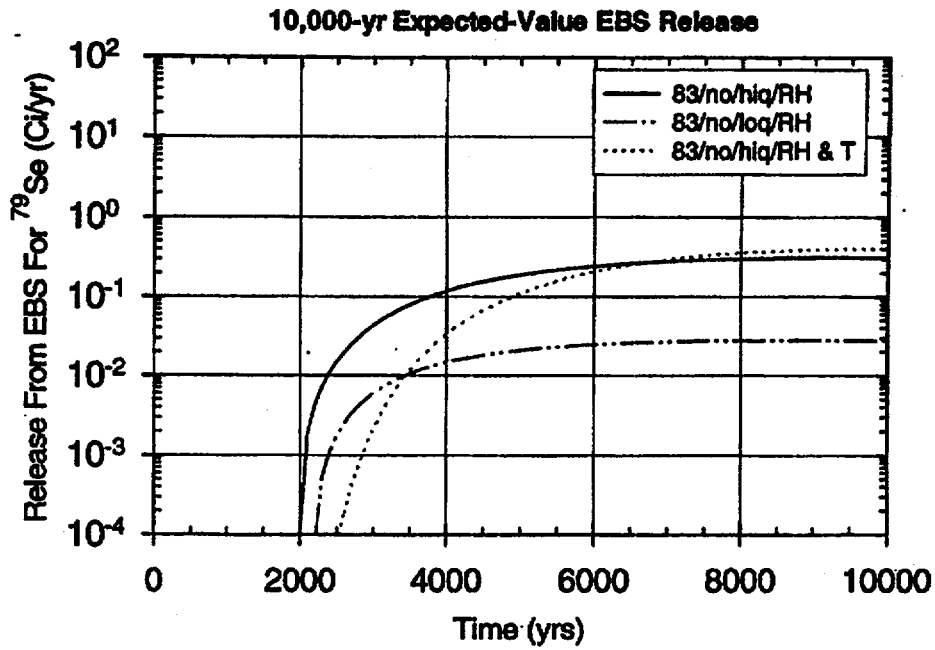


Figure 8.3-5c Sensitivity of the EBS release rate for ^{79}Se to the alternative advective release model (NRC limit = 0.282 Ci/yr).

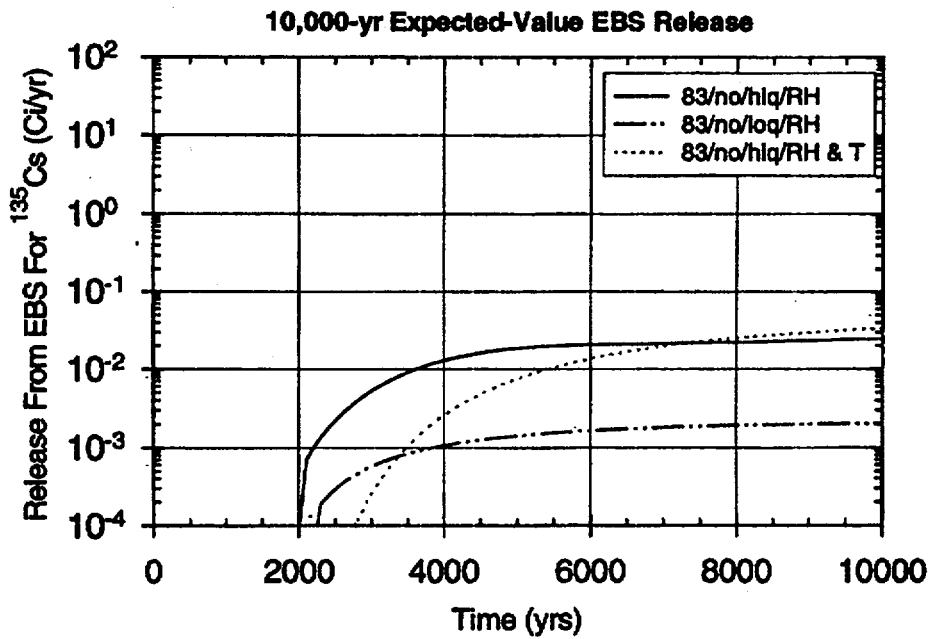


Figure 8.3-5d Sensitivity of the EBS release rate for ^{135}Cs to the alternative advective release model (NRC limit = 0.331 Ci/yr).

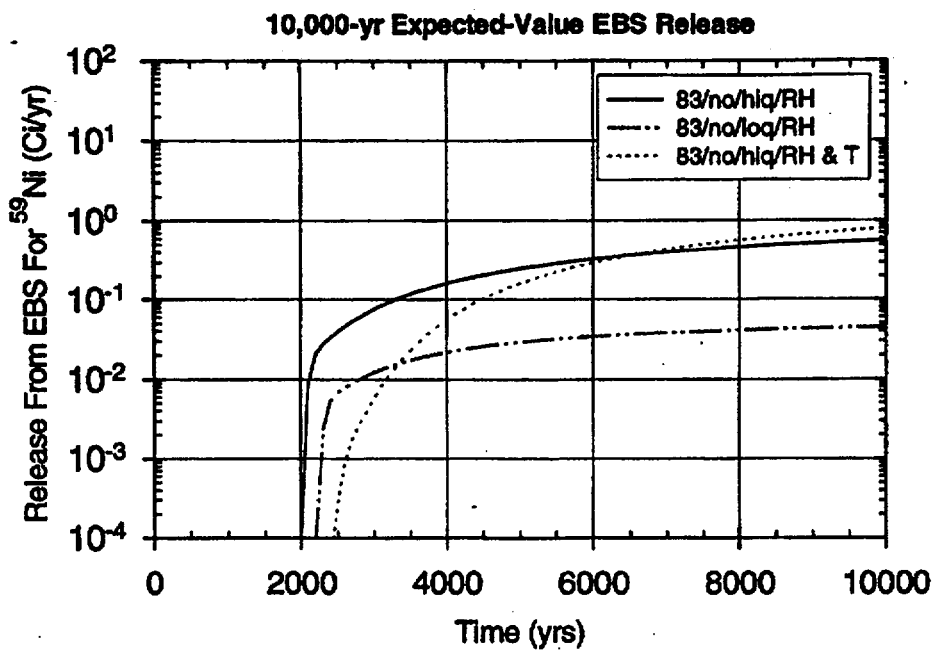


Figure 8.3-5e Sensitivity of the EBS release rate for ^{59}Ni to the alternative advective release model (NRC limit = 1.51 Ci/yr).

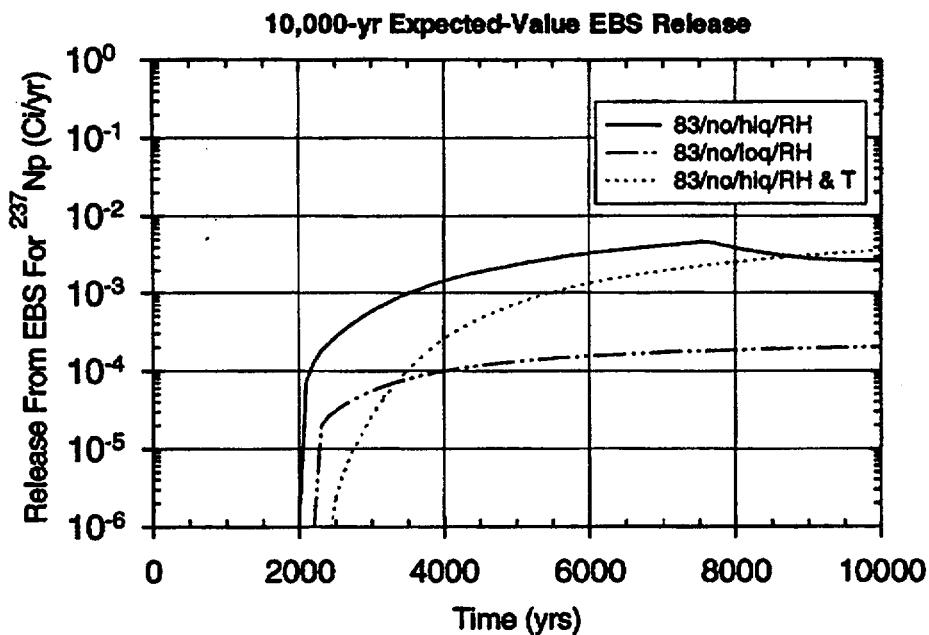


Figure 8.3-5f Sensitivity of the EBS release rate for ^{237}Np to the alternative advective release model (NRC limit = 0.782 Ci/yr).

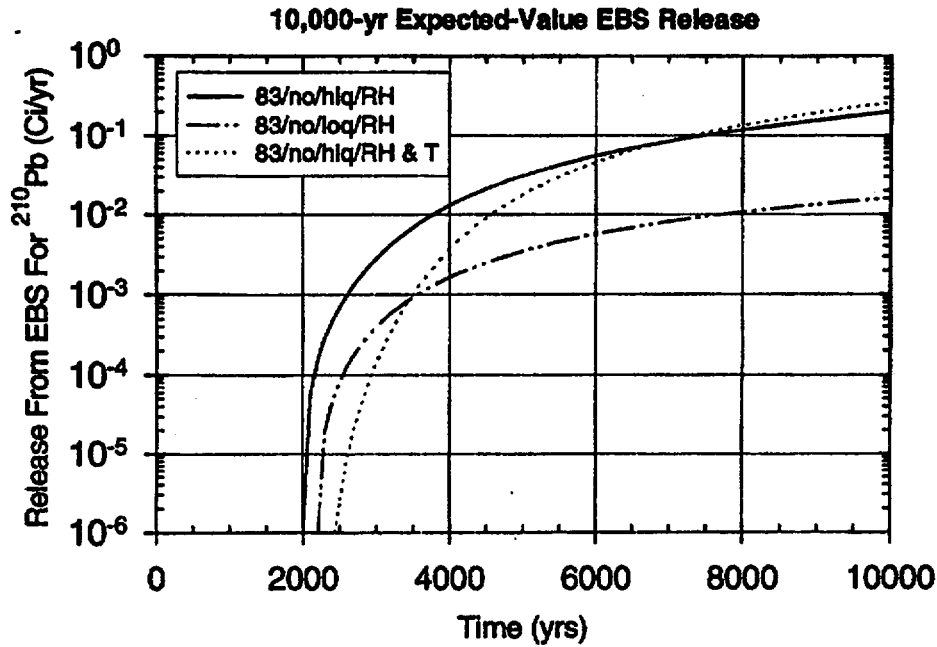


Figure 8.3-5g Sensitivity of the EBS release rate for ²¹⁰Pb to the alternative advective release model (NRC limit = 0.00236 Ci/yr).

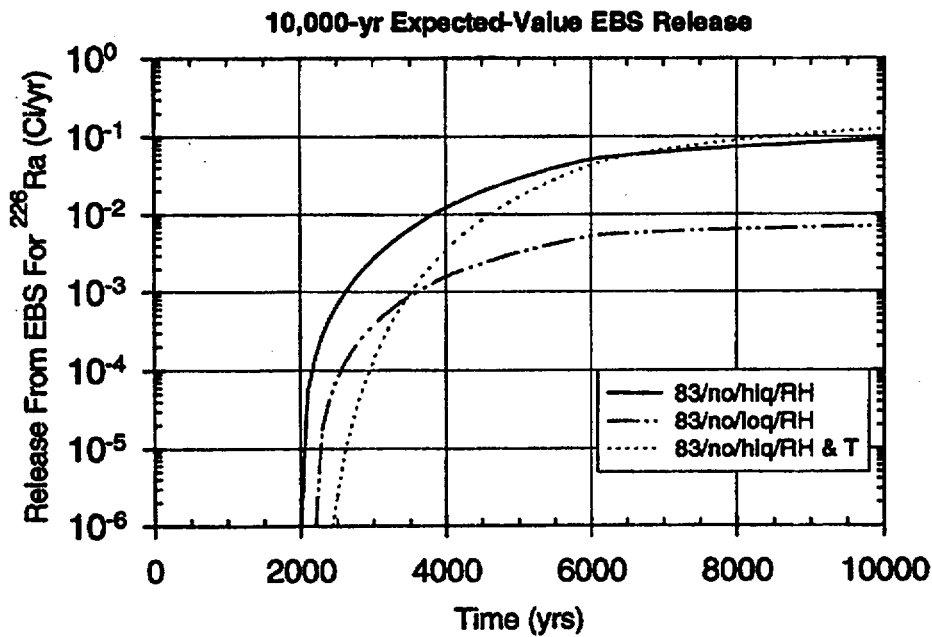


Figure 8.3-5h Sensitivity of the EBS release rate for ²²⁶Ra to the alternative advective release model (NRC limit = 0.00237 Ci/yr).

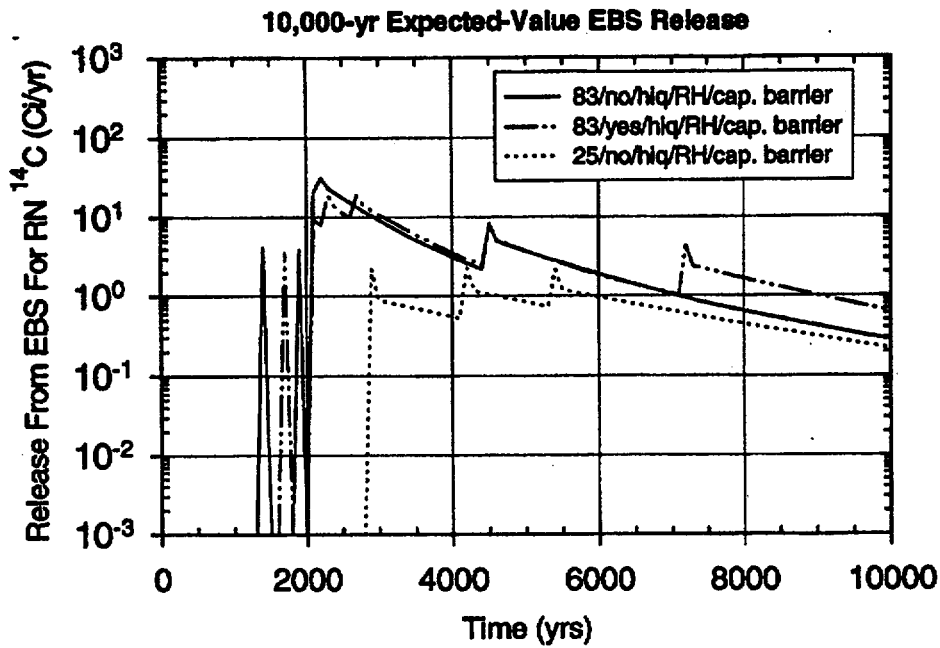


Figure 8.3-6a Sensitivity of the EBS release rate for ^{14}C to the presence of a capillary barrier (NRC limit = 0.796 Ci/yr).

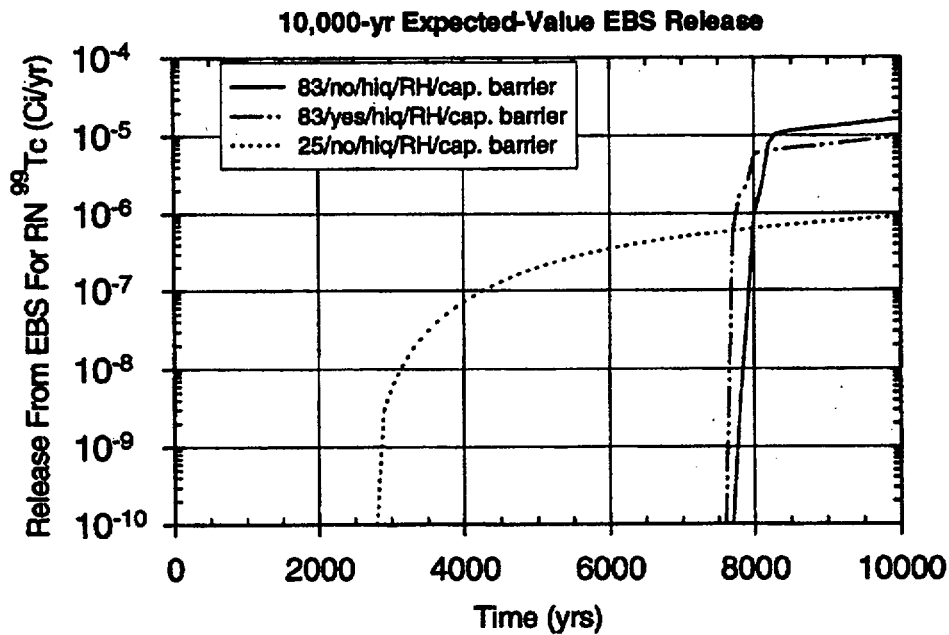


Figure 8.3-6b Sensitivity of the EBS release rate for ^{99}Tc to the presence of a capillary barrier (NRC limit = 9.03 Ci/yr).

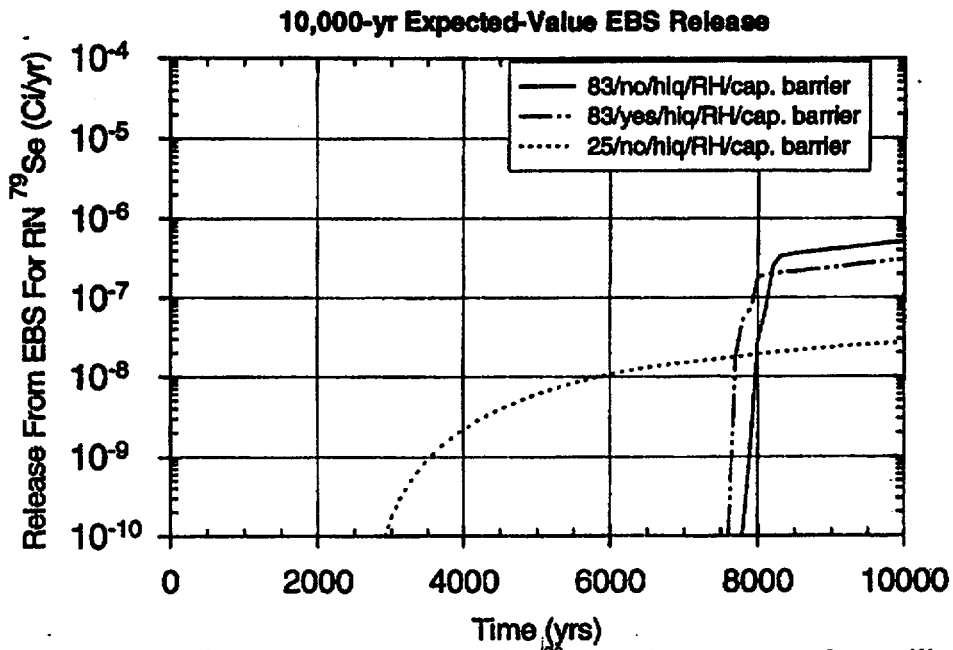


Figure 8.3-6c Sensitivity of the EBS release rate for ⁷⁹Se to the presence of a capillary barrier (NRC limit = 0.282 Ci/yr).

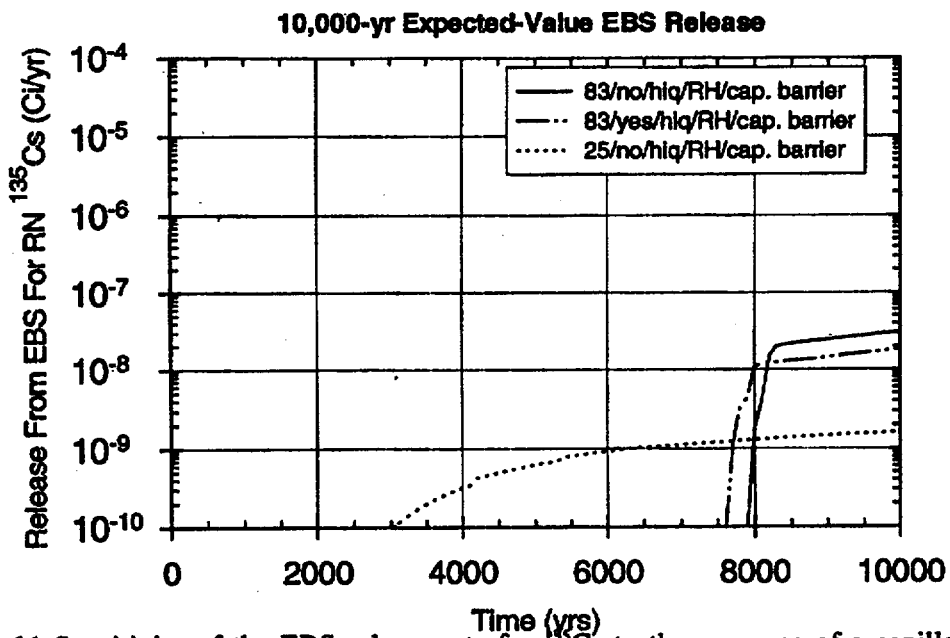


Figure 8.3-6d Sensitivity of the EBS release rate for ¹³⁵Cs to the presence of a capillary barrier (NRC limit = 0.331 Ci/yr).

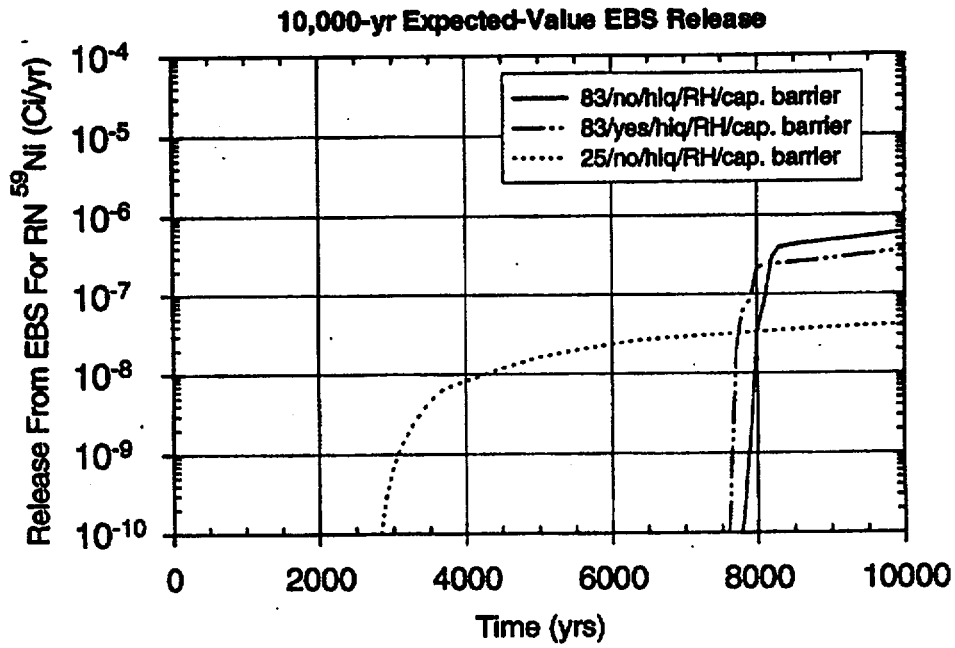


Figure 8.3-6e Sensitivity of the EBS release rate for ^{59}Ni to the presence of a capillary barrier (NRC limit = 1.51 Ci/yr).

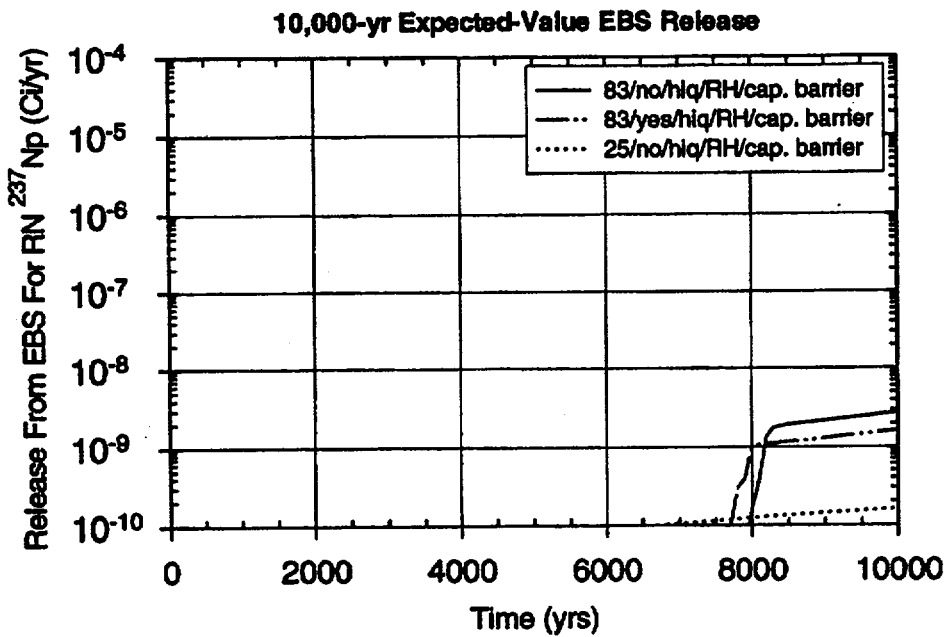


Figure 8.3-6f Sensitivity of the EBS release rate for ^{237}Np to the presence of capillary barrier (NRC limit = 0.782 Ci/yr).

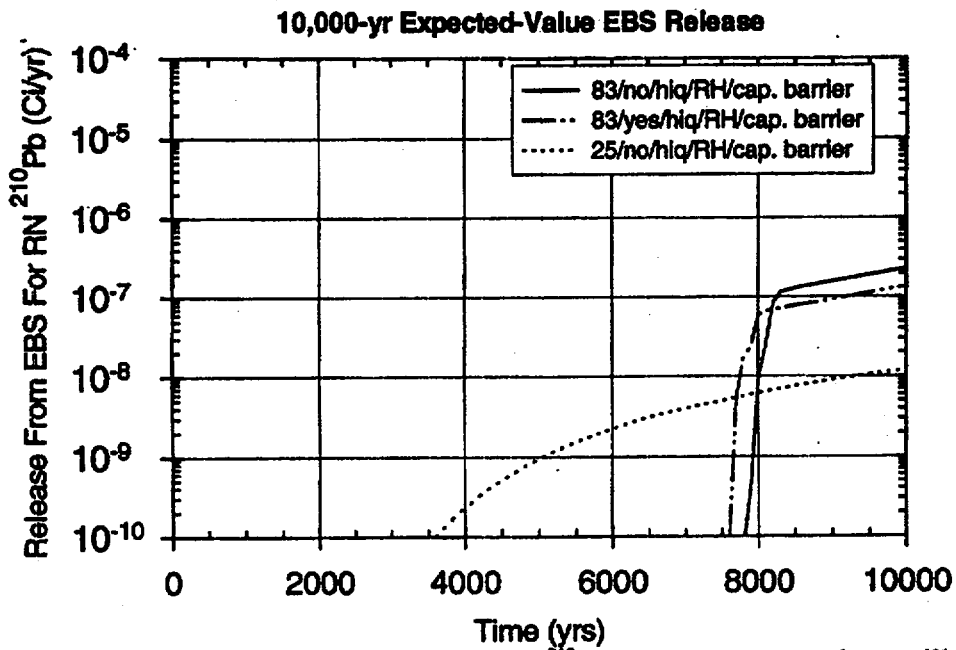


Figure 8.3-6g Sensitivity of the EBS release rate for ^{210}Pb to the presence of a capillary barrier (NRC limit = 0.00236 Ci/yr).

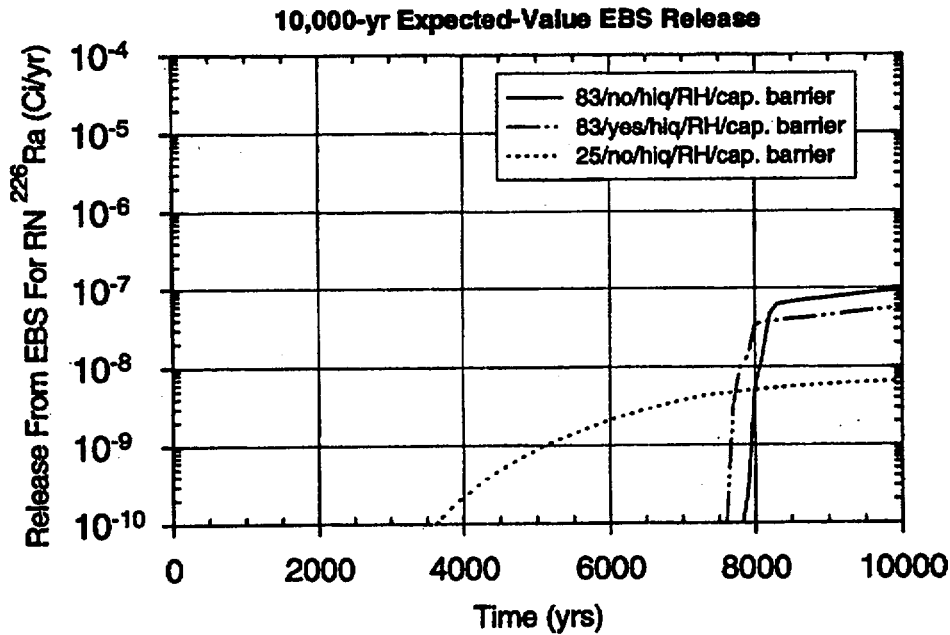


Figure 8.3-6h Sensitivity of the EBS release rate for ^{226}Ra to the presence of a capillary barrier (NRC limit = 0.00237 Ci/yr).

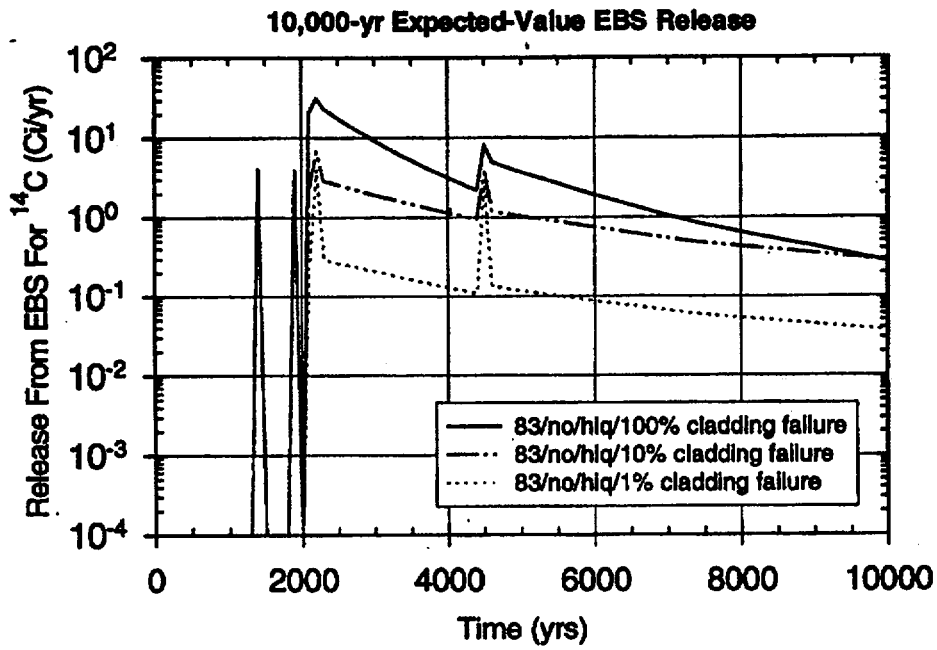


Figure 8.3-7a Sensitivity of the EBS release rate for ^{14}C to cladding failure (NRC limit = 0.796 Ci/yr).

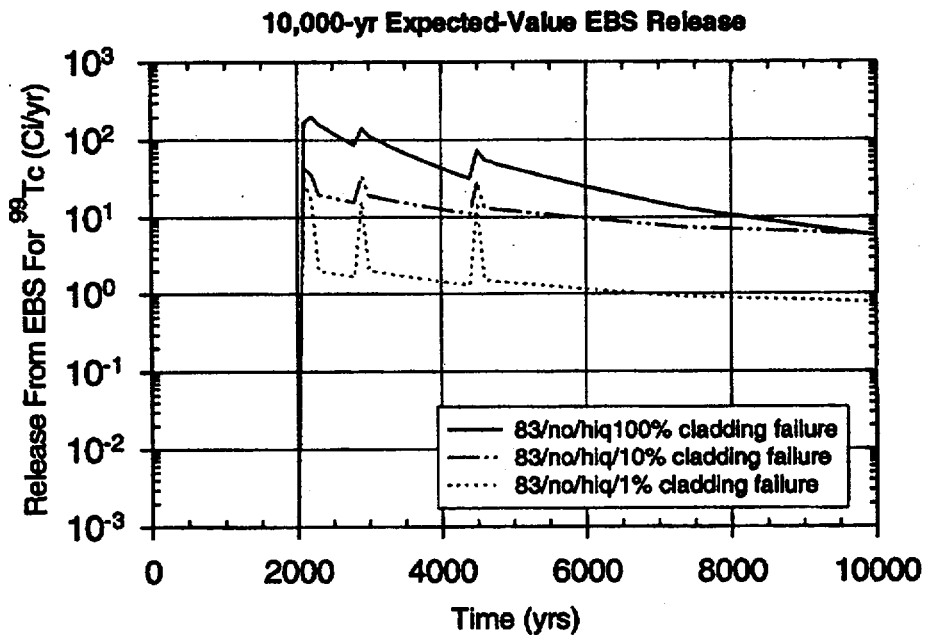


Figure 8.3-7b Sensitivity of the EBS release rate for ^{99}Tc to cladding failure (NRC limit = 9.03 Ci/yr).

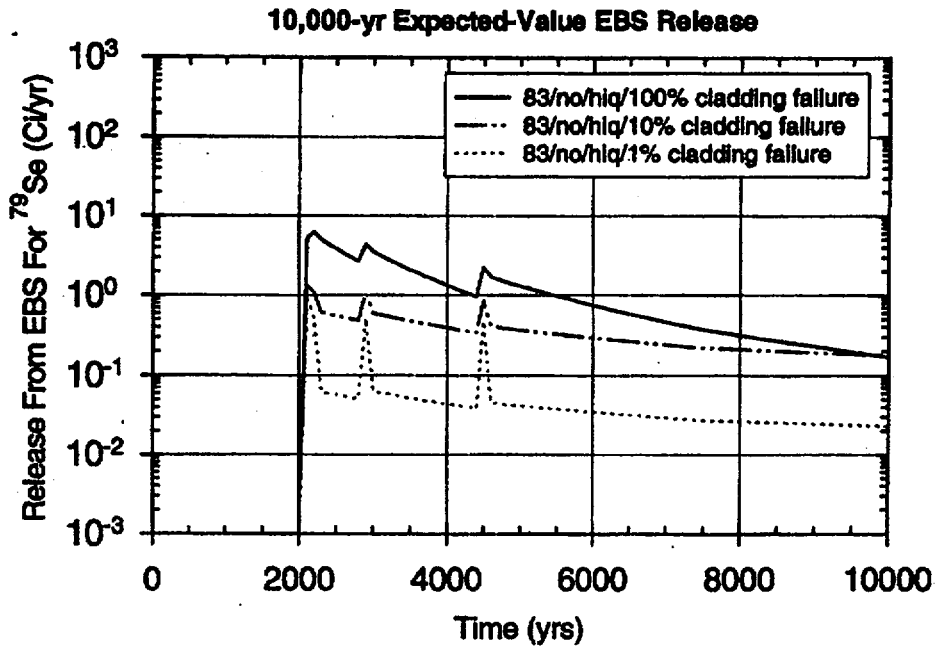


Figure 8.3-7c Sensitivity of the EBS release rate for ^{79}Se to cladding failure (NRC limit = 0.282 Ci/yr).

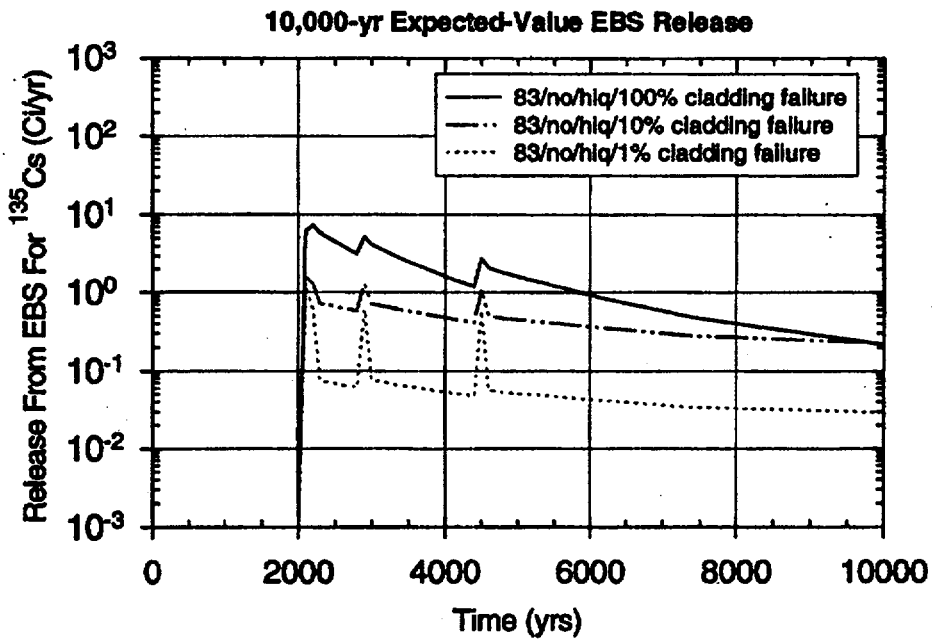


Figure 8.3-7d Sensitivity of the EBS release rate for ^{135}Cs to cladding failure (NRC limit = 0.331 Ci/yr).

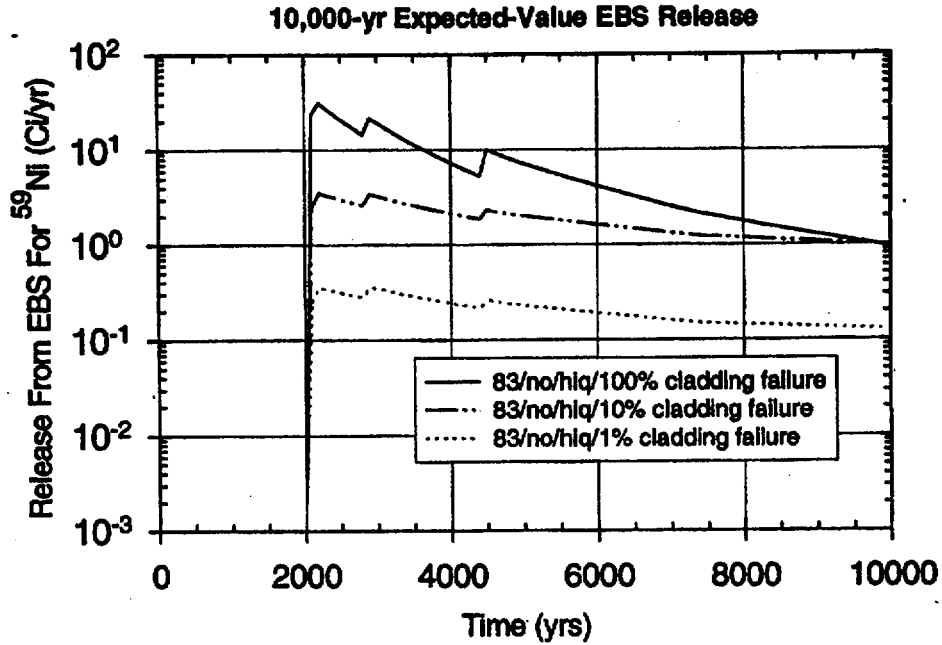


Figure 8.3-7e Sensitivity of the EBS release rate for ^{59}Ni to cladding failure (NRC limit = 1.51 Ci/yr).

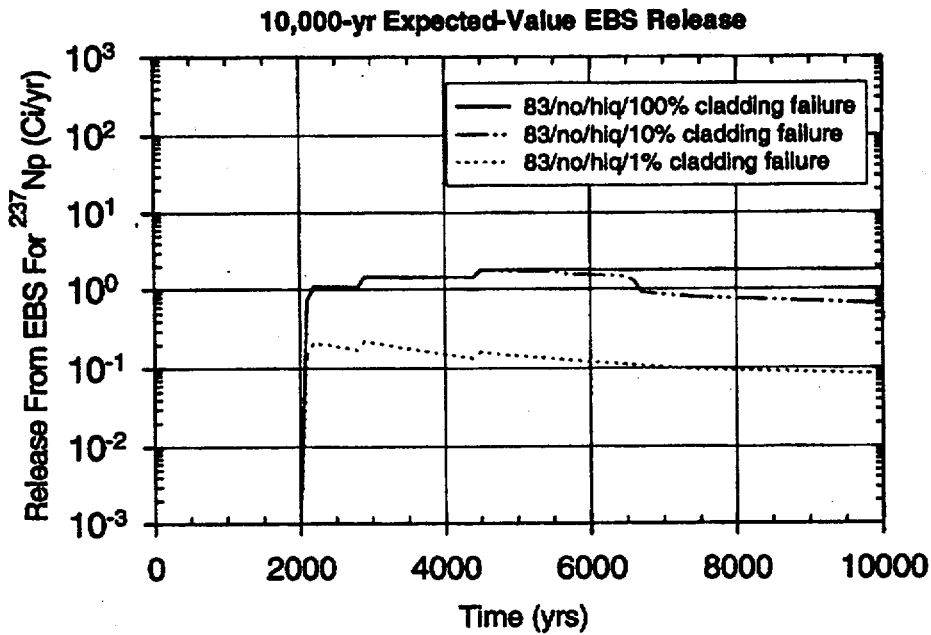


Figure 8.3-7f Sensitivity of the EBS release rate for ^{237}Np to cladding failure (NRC limit = 0.782 Ci/yr).

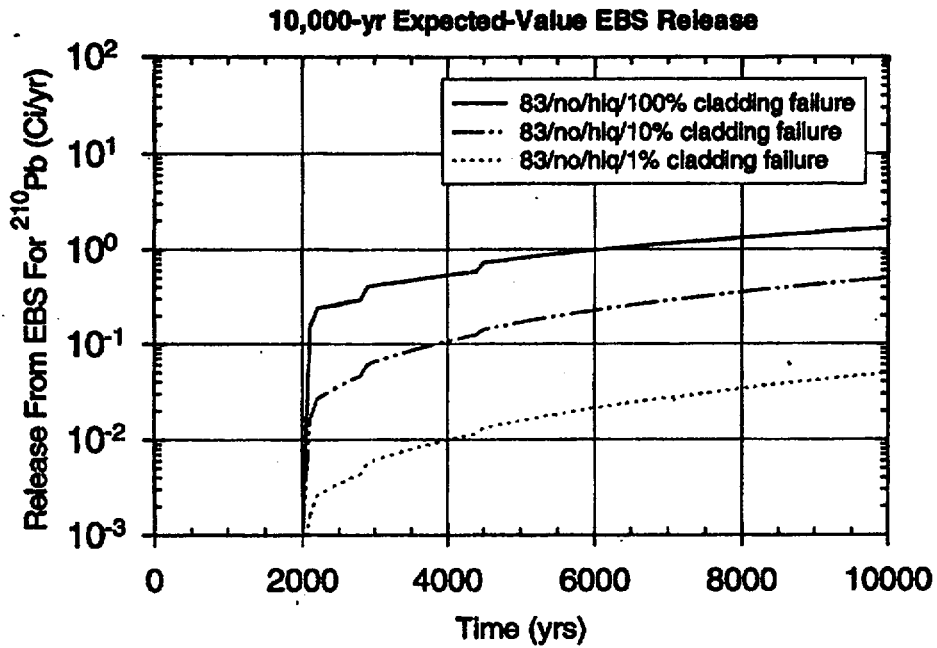


Figure 8.3-7g Sensitivity of the EBS release rate for ^{210}Pb to cladding failure (NRC limit = 0.00236 Ci/yr).

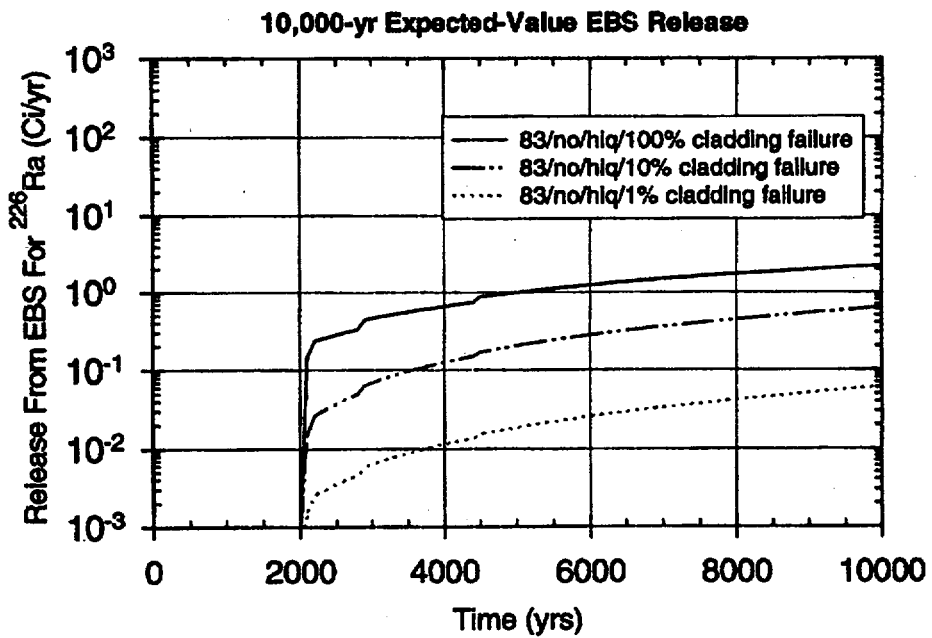


Figure 8.3-7h Sensitivity of the EBS release rate for ^{226}Ra to cladding failure (NRC limit = 0.00237 Ci/yr).

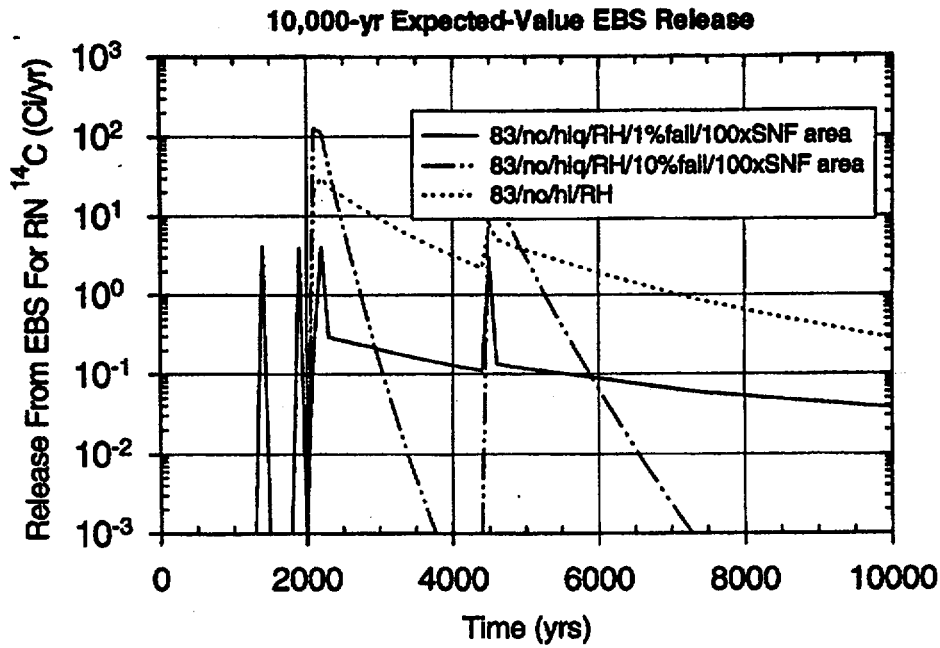


Figure 8.3-8a Sensitivity of the EBS release rate for ^{14}C to cladding failure with the spent fuel surface area increased by a factor of 100 (NRC limit = 0.796 Ci/yr).

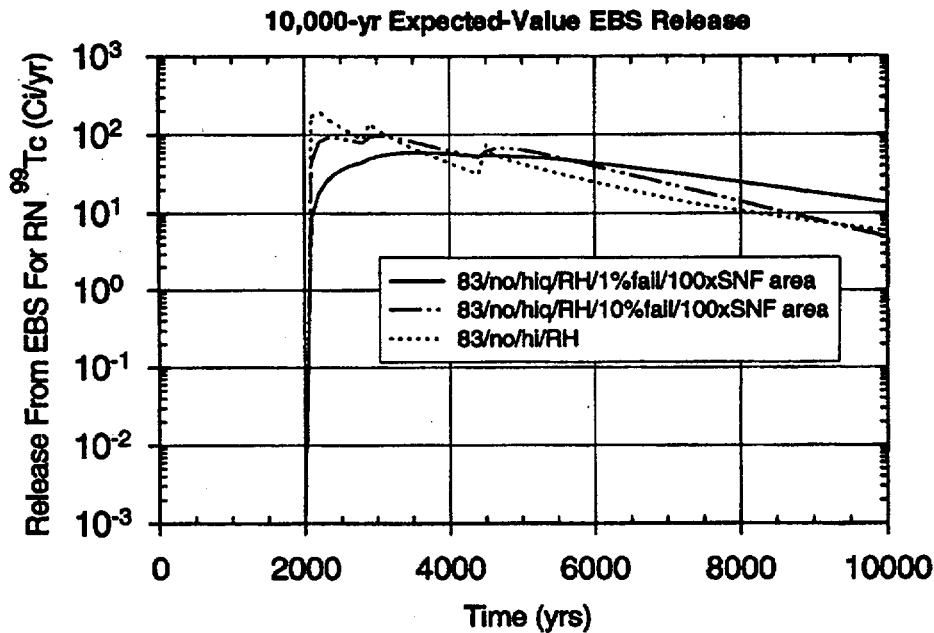


Figure 8.3-8b Sensitivity of the EBS release rate for ^{99}Tc to cladding failure with the spent fuel surface area increased by a factor of 100 (NRC limit = 9.03 Ci/yr).

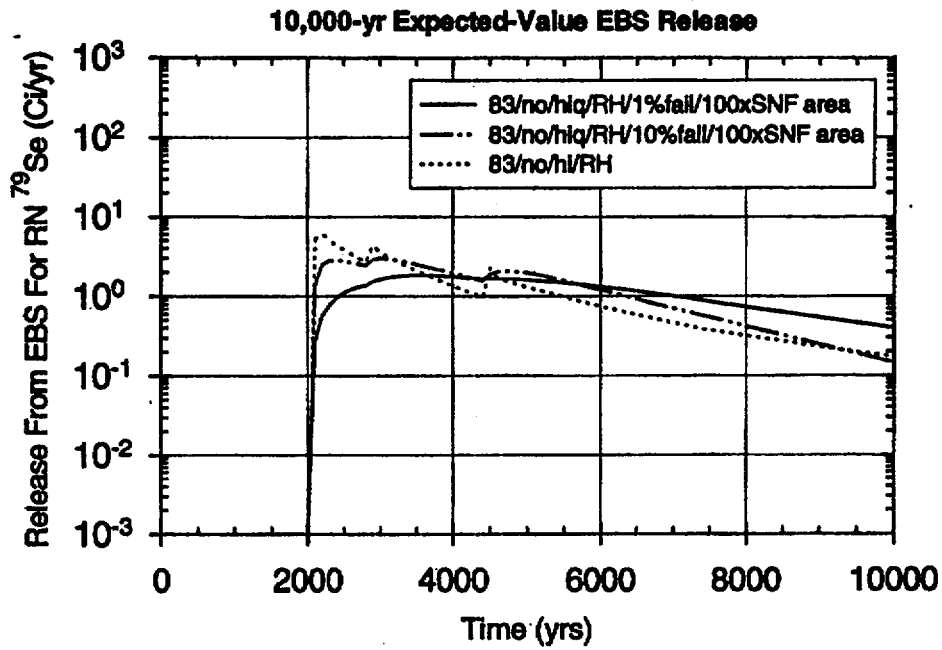


Figure 8.3-8c Sensitivity of the EBS release rate for ^{79}Se to cladding failure with the spent fuel surface area increased by a factor of 100 (NRC limit = 0.282 Ci/yr).

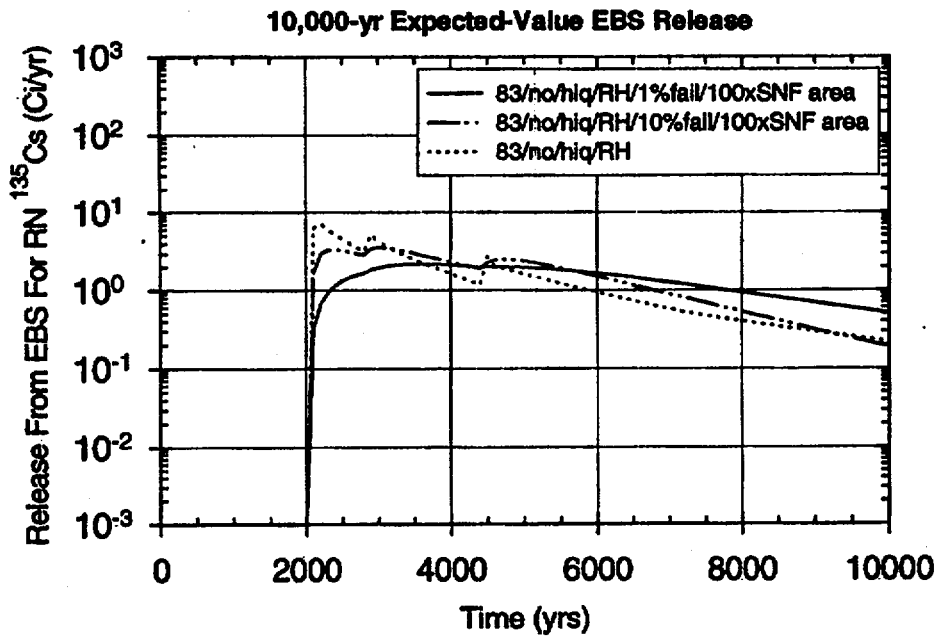


Figure 8.3-8d Sensitivity of the EBS release rate for ^{135}Cs to cladding failure with the spent fuel surface area increased by a factor of 100 (NRC limit = 0.331 Ci/yr).

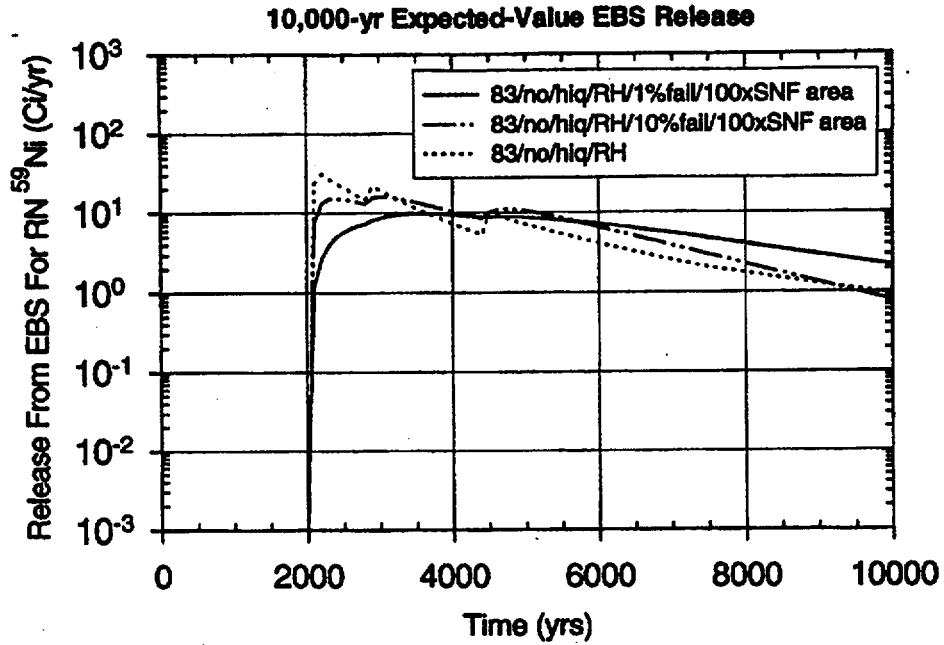


Figure 8.3-8e Sensitivity of the EBS release rate for ⁵⁹Ni to cladding failure with the spent fuel surface area increased by a factor of 100 (NRC limit = 1.51 Ci/yr).

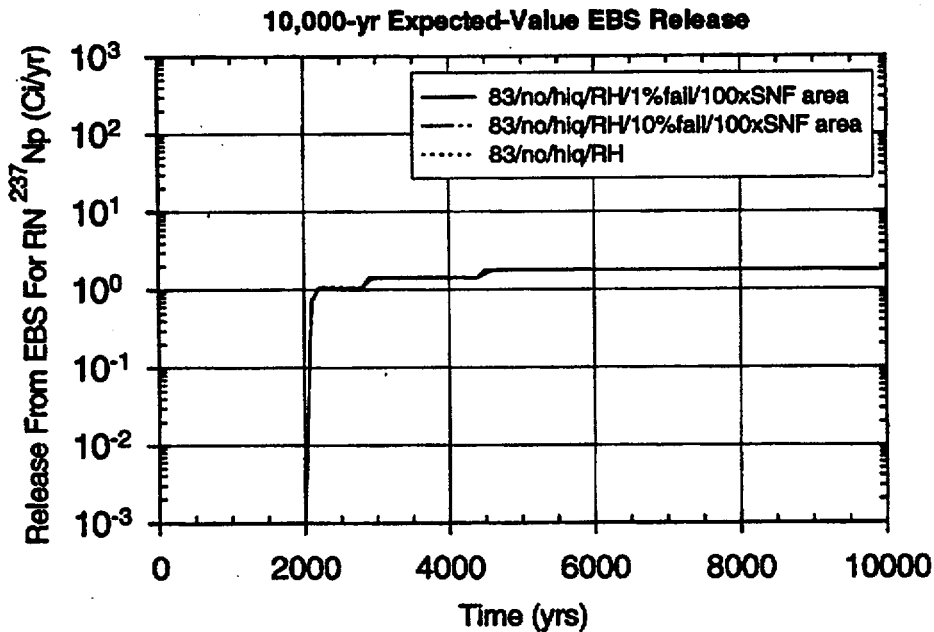


Figure 8.3-8f Sensitivity of the EBS release rate for ²³⁷Np to cladding failure with the spent fuel surface area increased by a factor of 100 (NRC limit = 0.782 Ci/yr).

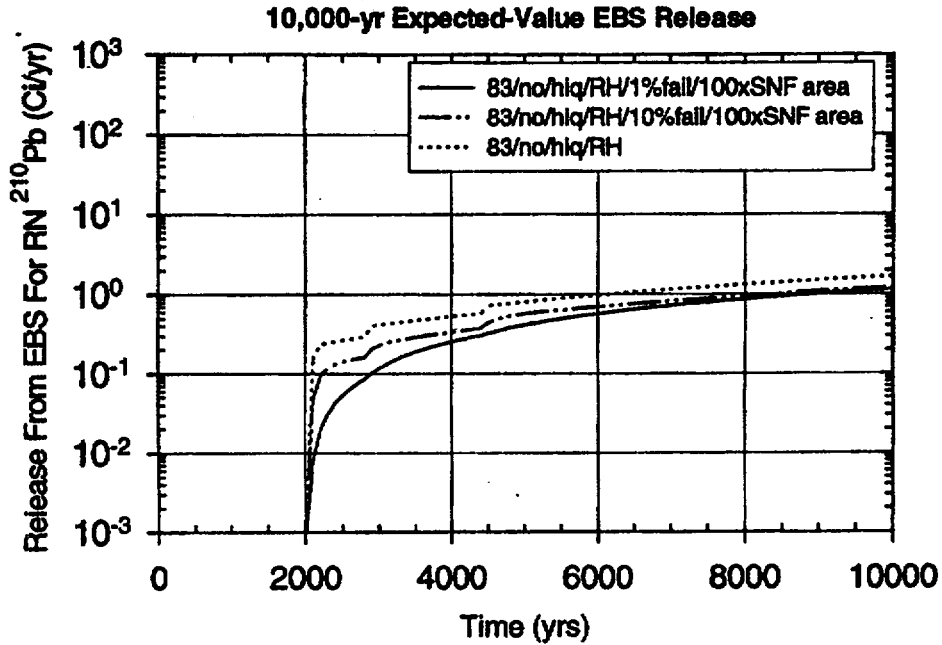


Figure 8.3-8g Sensitivity of the EBS release rate for ^{210}Pb to cladding failure with the spent fuel surface area increased by a factor of 100 (NRC limit = 0.00236 Ci/yr).

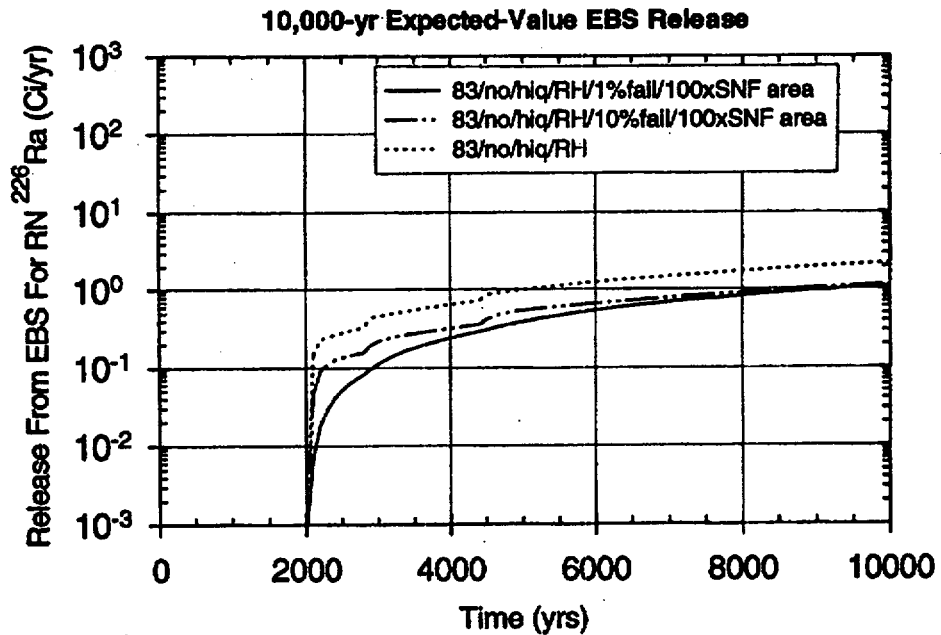


Figure 8.3-8h Sensitivity of the EBS release rate for ^{226}Ra to cladding failure with the spent fuel surface area increased by a factor of 100 (NRC limit = 0.00237 Ci/yr).

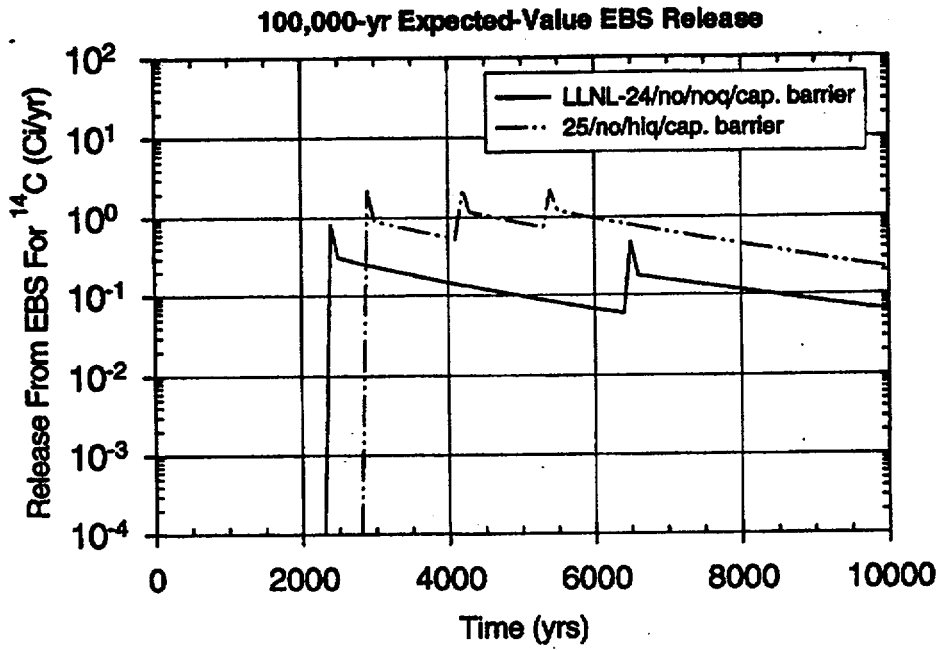


Figure 8.3-9a Sensitivity of the EBS release rate for ^{14}C to the thermal-hydrologic model (NRC limit = 0.796 Ci/yr).

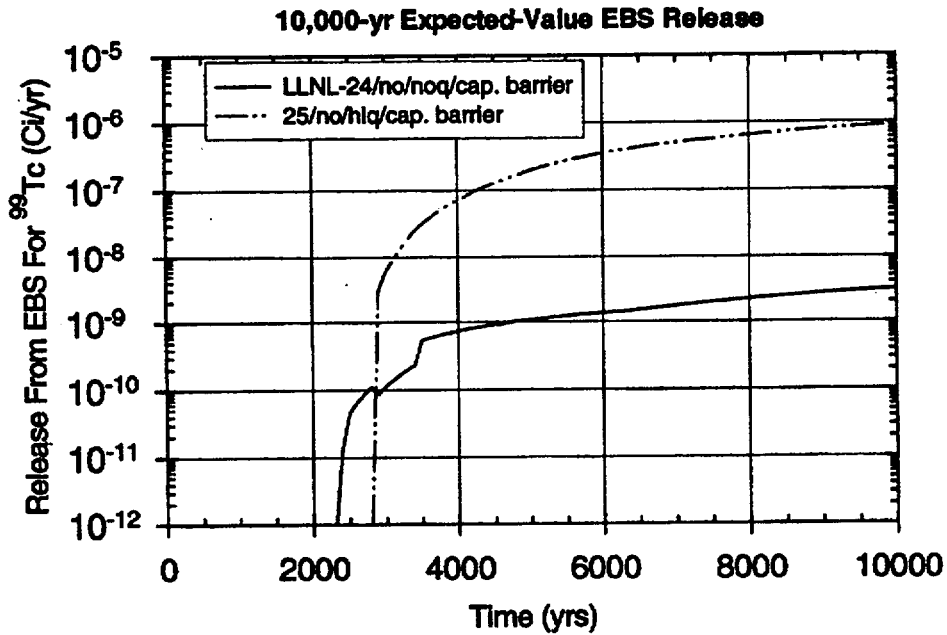


Figure 8.3-9b Sensitivity of the EBS release rate for ^{99}Tc to the thermal-hydrologic model (NRC limit = 9.03 Ci/yr).

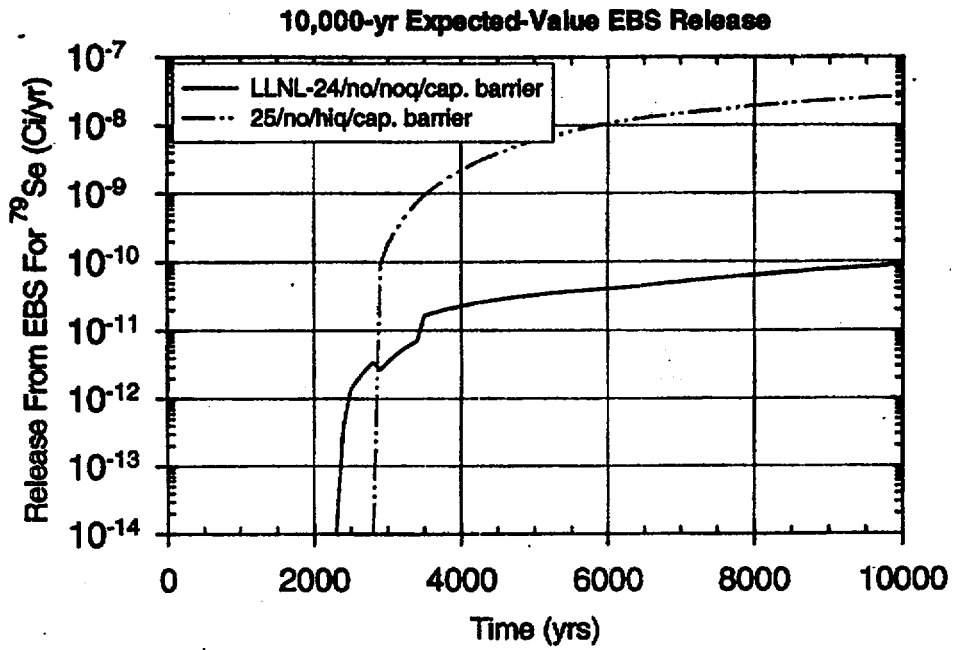


Figure 8.3-9c Sensitivity of the EBS release rate for ^{79}Se to the thermal-hydrologic model (NRC limit = 0.282 Ci/yr).

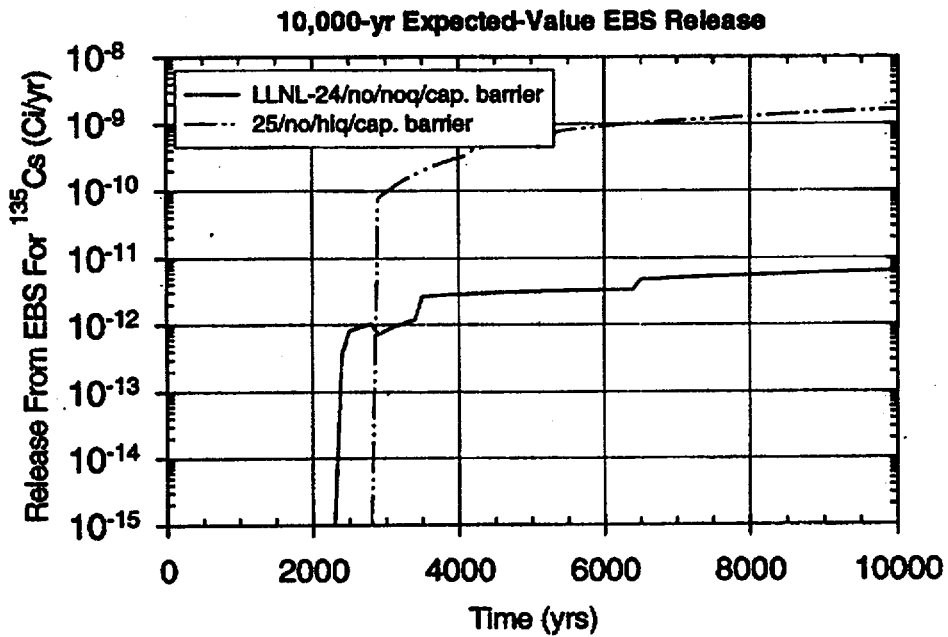


Figure 8.3-9d Sensitivity of the EBS release rate for ^{135}Cs to the thermal-hydrologic model (NRC limit = 0.331 Ci/yr).

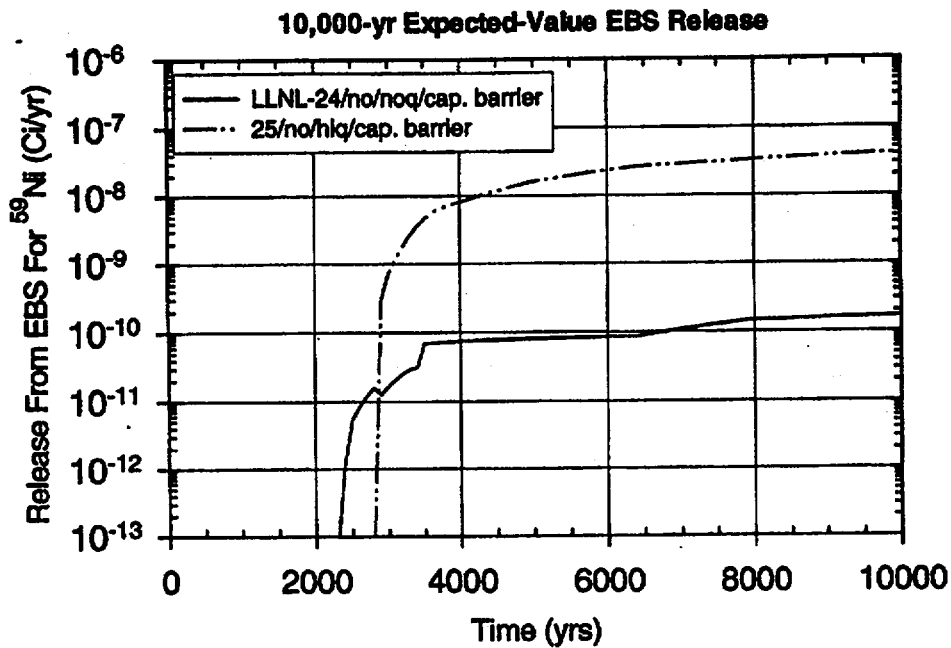


Figure 8.3-9e Sensitivity of the EBS release rate for ⁵⁹Ni to the thermal-hydrologic model (NRC limit = 1.51 Ci/yr).

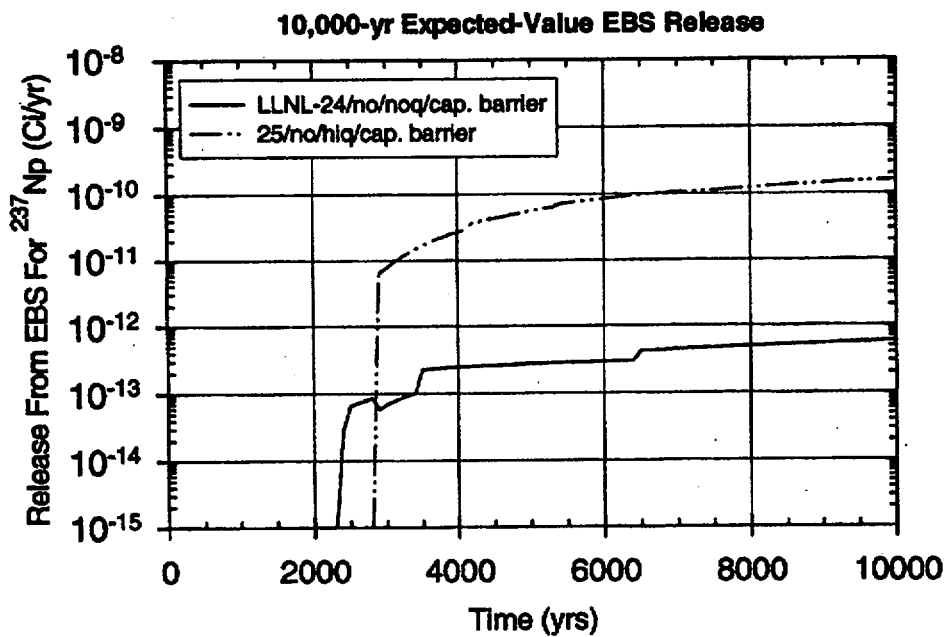


Figure 8.3-9f Sensitivity of the EBS release rate for ²³⁷Np to the thermal-hydrologic model (NRC limit = 0.782 Ci/yr).

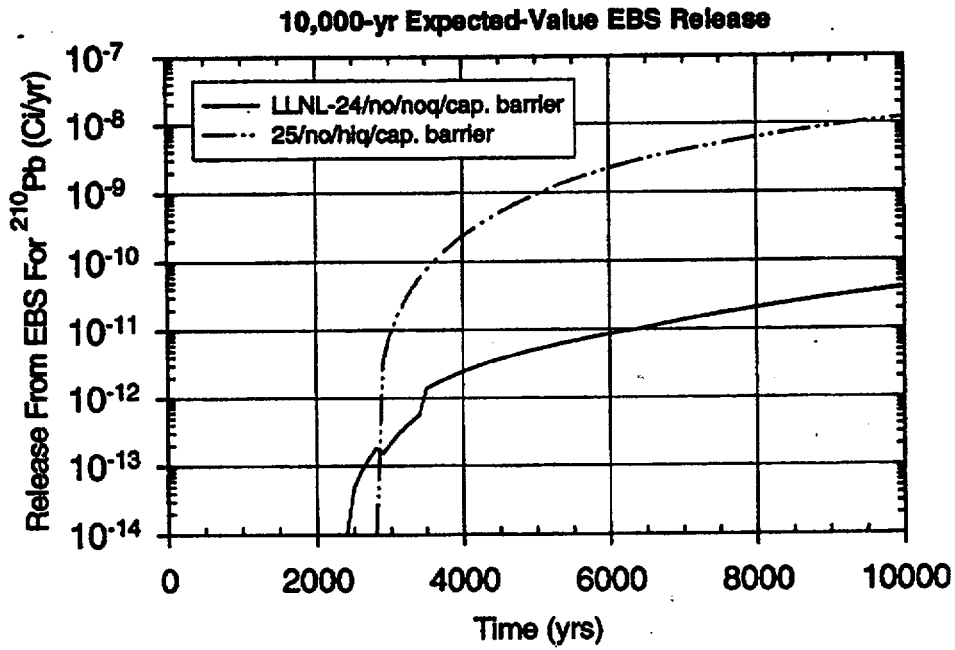


Figure 8.3-9g Sensitivity of the EBS release rate for ²¹⁰Pb to the thermal-hydrologic model (NRC limit = 0.00236 Ci/yr).

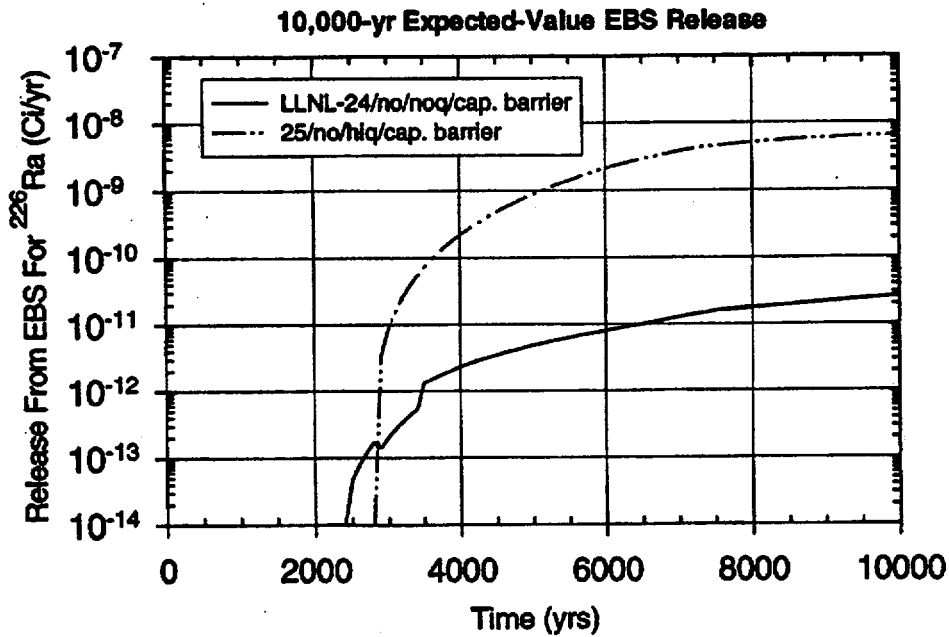


Figure 8.3-9h Sensitivity of the EBS release rate for ²²⁶Ra to the thermal-hydrologic model (NRC limit = 0.00237 Ci/yr).

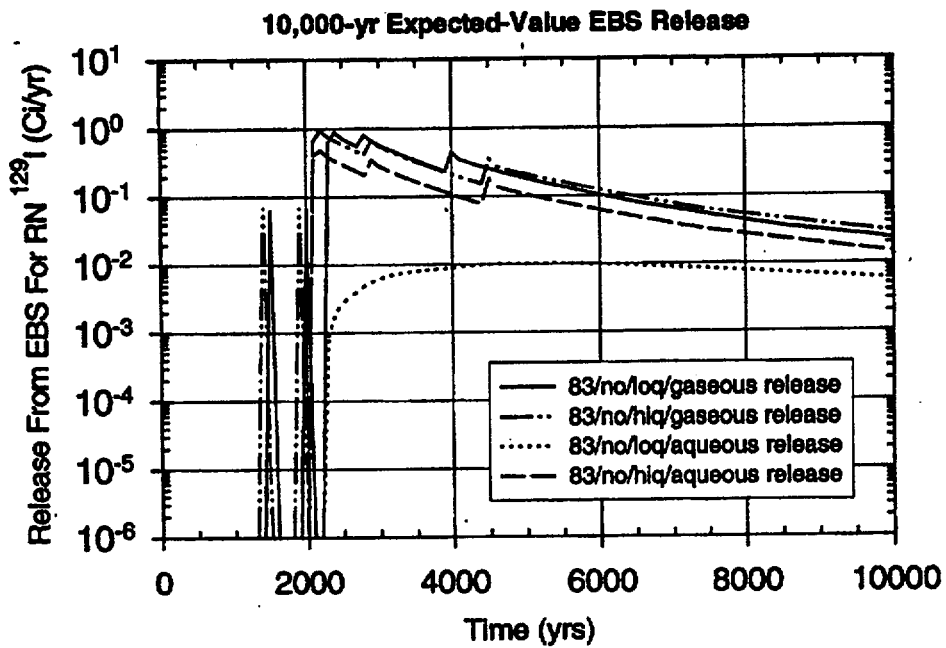


Figure 8.3-10 Sensitivity of the EBS release rate for ^{129}I to its release mode from the EBS (NRC limit = 0.022 Ci/yr).

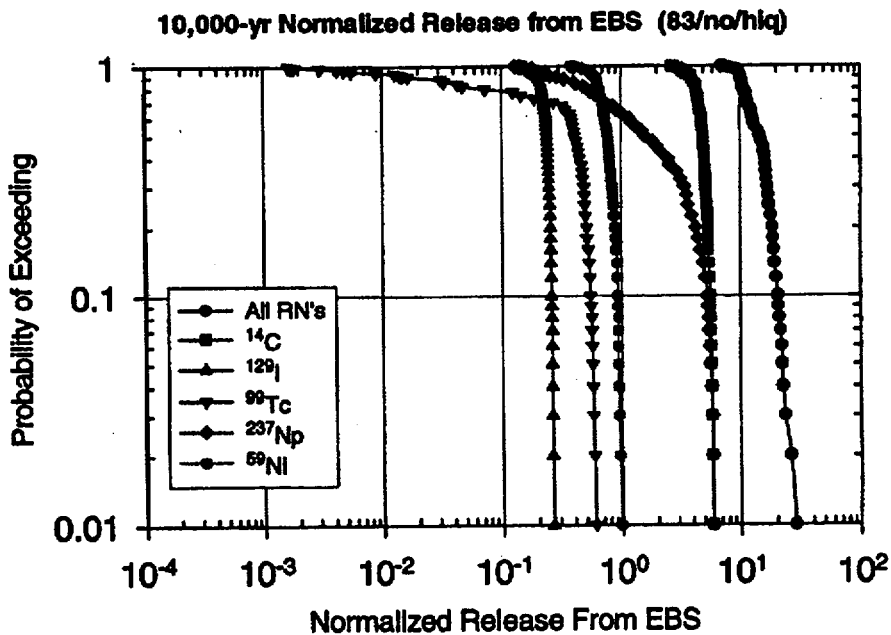


Figure 8.4-1 CCDF's of normalized cumulative release from the EBS (normalized to the 10 CFR 191.13 limit): 83 MTU/acre, no backfill, high infiltration rate, R.H. switch for the corrosion initiation.

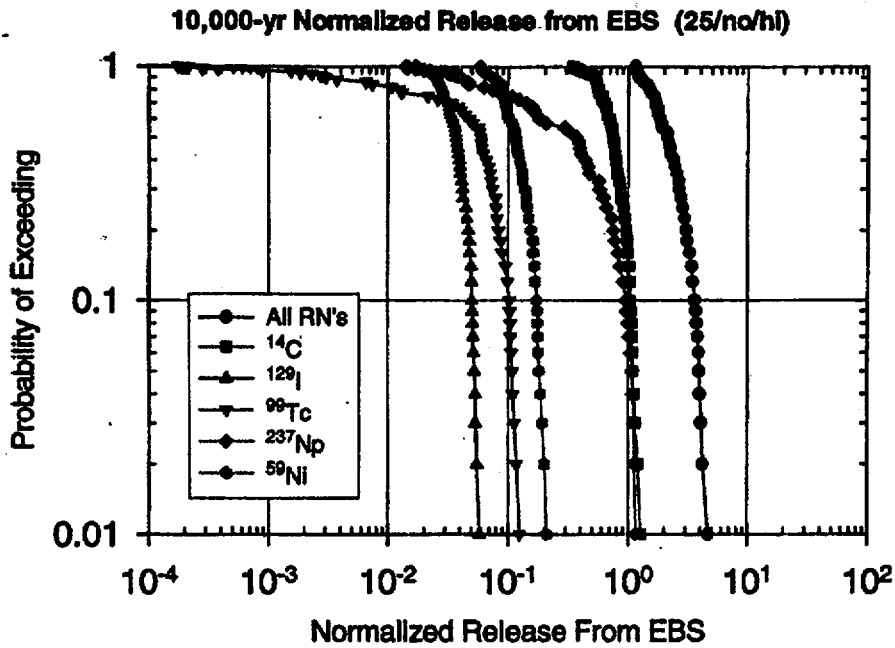


Figure 8.4-2 CCDF's of normalized cumulative release from the EBS (normalized to the 10 CFR 191.13 limit): 25 MTU/acre, no backfill, high infiltration rate, R.H. switch for the corrosion initiation.

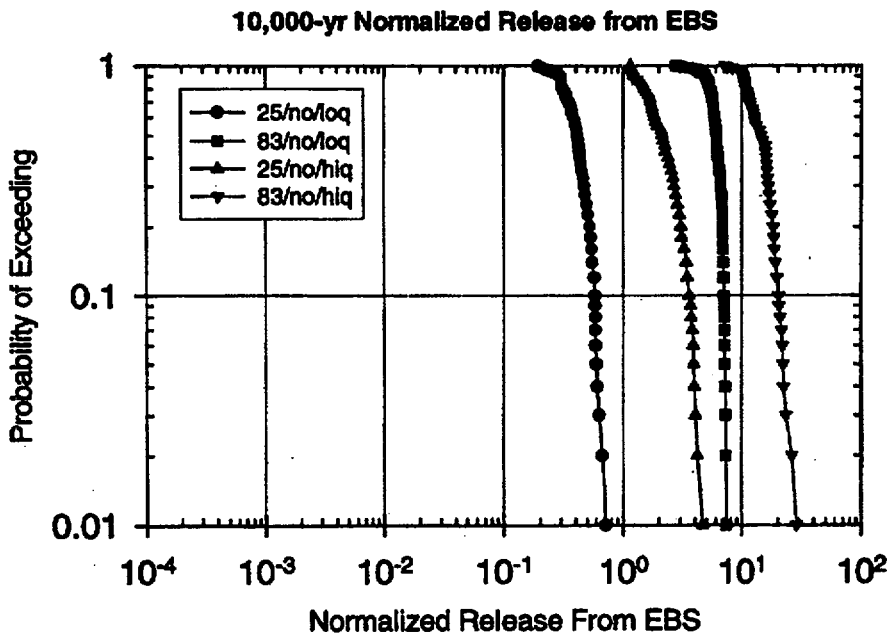


Figure 8.4-3 CCDF's of normalized cumulative release for all the radionuclides from the EBS (normalized to the 10 CFR 191.13 limit): 25 or 83 MTU/acre, no backfill, high or low infiltration rate, R.H. switch for corrosion initiation.

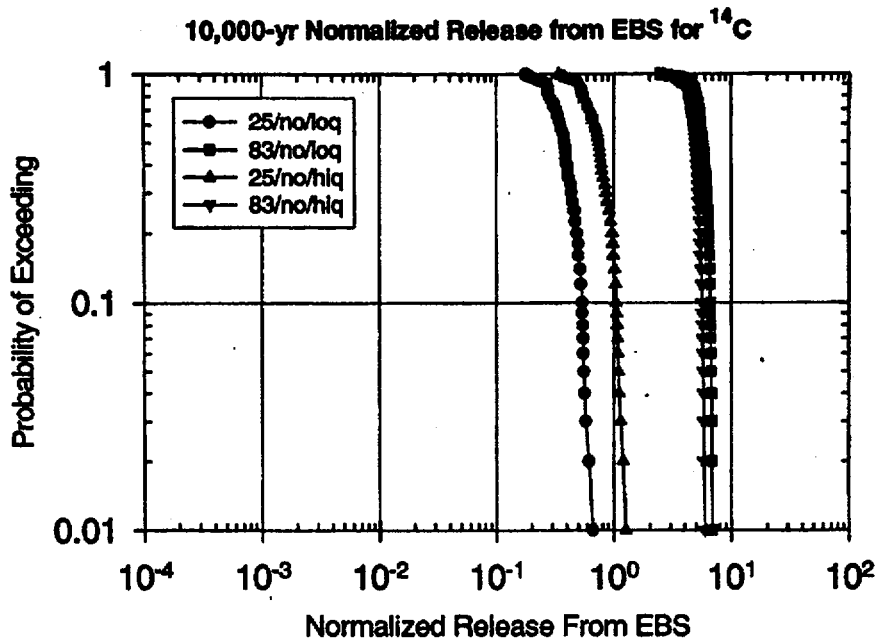


Figure 8.4-4 CCDF's of normalized cumulative release for ¹⁴C from the EBS (normalized to the 10 CFR 191.13 limit): 25 or 83 MTU/acre, no backfill, high or low infiltration rate, R.H. switch for the corrosion initiation.

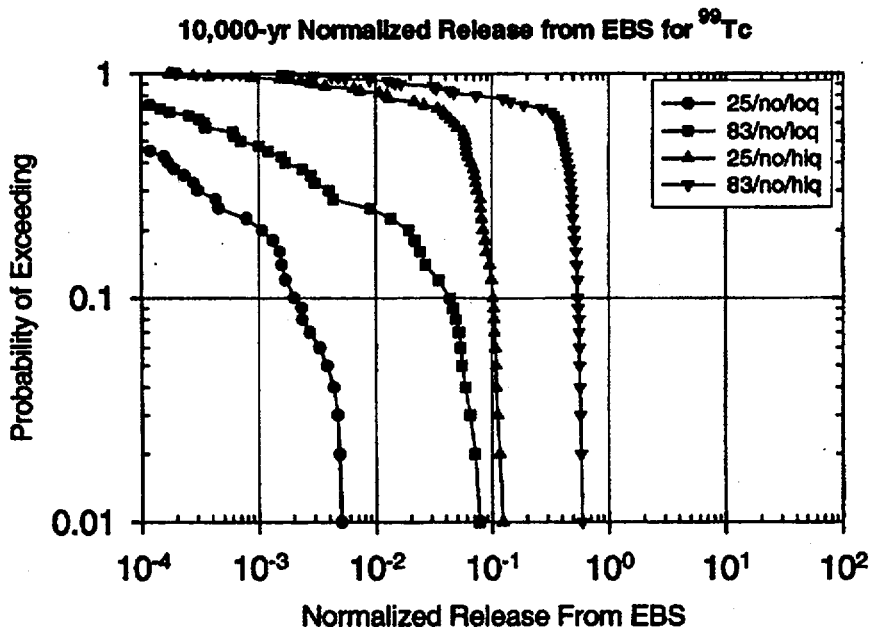


Figure 8.4-5 CCDF's of normalized cumulative release for ⁹⁹Tc from the EBS (normalized to the 10 CFR 191.13 limit): 25 MTU/acre or 83 MTU/acre, no backfill, high or low infiltration rate, R.H. switch for the corrosion initiation.

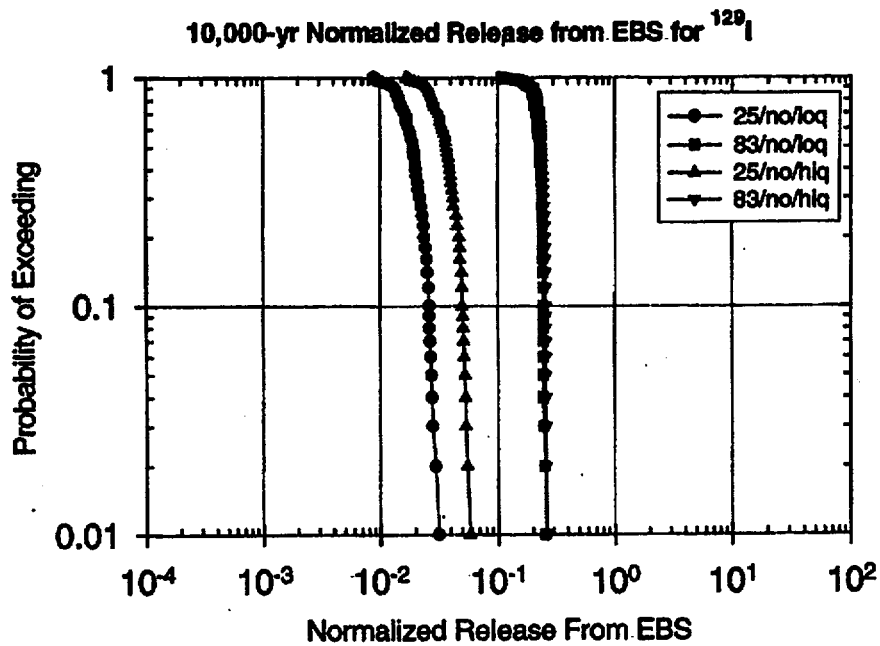


Figure 8.4-6 CCDF's of normalized cumulative release for ^{129}I from the EBS (normalized to the 10 CFR 191.13 limit): 25 or 83 MTU/acre, no backfill, high or low infiltration rate, R.H. switch for the corrosion initiation.

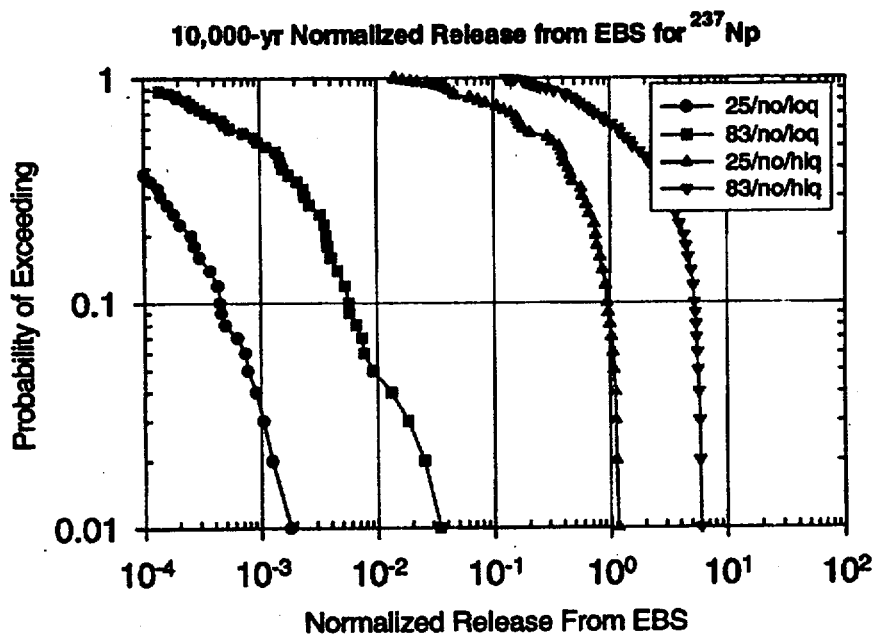


Figure 8.4-7 CCDF's of normalized cumulative release for ^{237}Np from the EBS (normalized to the 10 CFR 191.13 limit): 25 or 83 MTU/acre, no backfill, high or low infiltration rate, R.H. switch for the corrosion initiation.

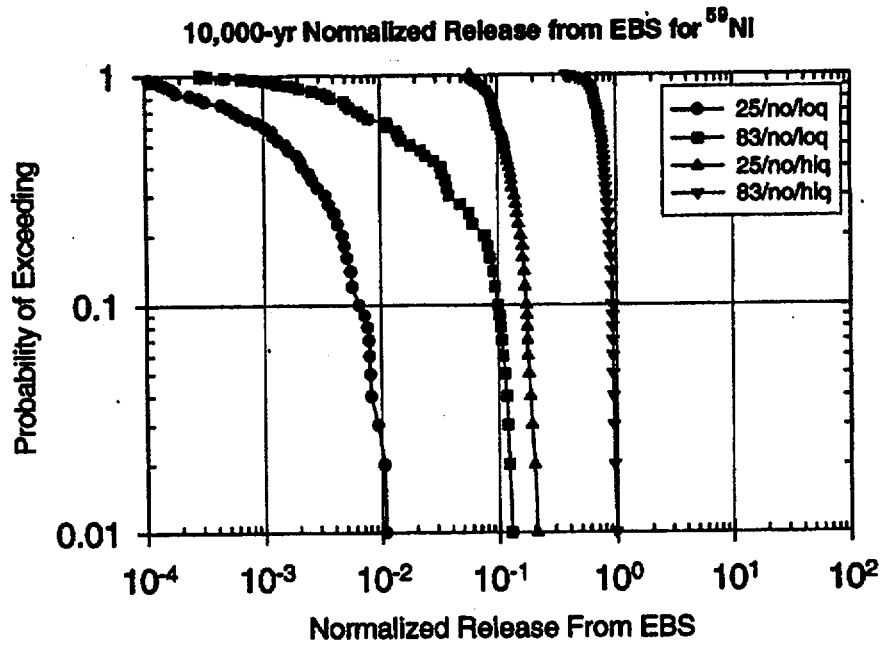


Figure 8.4-8 CCDF's of normalized cumulative release for ⁵⁹Ni from the EBS (normalized to the 10 CFR 191.13 limit): 25 MTU/acre or 83 MTU/acre, no backfill, high or low infiltration rate, R.H. switch for the corrosion initiation.

9. NATURAL-BARRIER RELEASE AND DOSE

S. David Sevougian, Jerry A. McNeish, Q. Laura Wang, Joel E. Atkins, Vinod Vallikat

9.1 INTRODUCTION

This chapter presents the predicted radionuclide release and radiation dose at the accessible-environment boundary, 5 km from the repository footprint boundary. As shown in Figure 9.1-1, these results represent the culmination of the TSPA-1995 Information Flow Diagram.

Inherent in the analyses in this chapter is the uncertain or stochastic nature of the predictions. This statistical behavior is captured by plots of the complementary cumulative distribution function (CCDF) of a particular performance measure over the time period of interest, either 10,000 or 1,000,000 years. (Note: $CCDF = 1 - CDF$, where CDF is the cumulative distribution function.) The performance measure for radionuclide release (in Curies) is the total (i.e., the sum of all radionuclides) cumulative release over 10,000 years, normalized to the Table 1 values in 40 CFR Part 191. The performance measure for radiation dose (in rem/yr) is the total (i.e., the sum of all radionuclides) peak dose to a person at the accessible environment using the tuff aquifer for his or her drinking water (2 liters/day), calculated over both 10,000 years and 1,000,000 years. (The treatment and effect of radionuclides that are transported in the gaseous phase, i.e., ^{14}C , rather than the aqueous phase, is discussed in Section 7.5.) The 1,000,000-year time frame for peak dose is the one suggested in the recent report by the National Research Council (1995). [Note: *the peak doses calculated in this chapter should not be compared to the average dose a member of the "critical" population may be exposed to over the time period of interest. As discussed in Chapter 10, the average dose is expected to be some orders of magnitude less than the peak dose to the maximally-exposed individual.*]

The expected value of a statistical distribution is one of the most important parameters used to characterize the behavior of the distribution. Thus, besides showing CCDFs that represent the entire range of the various parameter distributions, expected-value time histories ("breakthrough curves") are also given in this chapter for the five or six radionuclides with the highest release rates or doses at the accessible environment. An expected-value release-rate history is the breakthrough curve for rate-of-release of radioactivity (Ci/yr) at the accessible environment for a single realization that uses the expected values for all stochastic parameters. Similarly, an expected-value dose history is the breakthrough curve for dose exposure (rem/yr) at the accessible environment for a single realization that uses the expected values for all stochastic parameters. For the 10,000-year time period, expected-value time histories for both release rate and dose are evaluated, whereas for 1,000,000 years primarily only dose time histories are evaluated.

The effect of model and parameter uncertainty on predicted results is evaluated by a number of sensitivity analyses. Alternative repository designs and alternative scenarios for natural-system behavior are considered, including (1) low and high water-infiltration rates through the unsaturated zone (0.01-0.05 mm/yr and 0.5-2.0 mm/yr); (2) low and high thermal load (25 MTU/acre and 83 MTU/acre); (3) alternative thermohydrologic models for the near-field environment (the model discussed in Chapter 4 vs. the Buscheck et al. model); (4) three waste-package-degradation (corrosion-initiation) models (relative-humidity controlled, temperature and

relative-humidity controlled, and temperature and relative-humidity controlled with cathodic protection); (5) five conceptual models of EBS transport and water movement (drips directly on waste form, drips on waste package but not on waste form, no drips or capillary-barrier effect, no drips and aqueous EBS transport of ^{129}I and ^{36}Cl , and no drips and aqueous EBS transport of ^{129}I and ^{36}Cl plus ^{14}C transport directly to atmosphere—the "diffusion-only" model); (6) fracture/matrix interaction in the geosphere (the effect of intra-unit fracture connectivity within a given hydrogeologic unit); and (7) climate change (with and without water table rise).

In addition to CCDFs and expected-value time histories, evaluation of repository performance using linear regression analysis provides an explanation for the degree of the variance in the performance measures (total peak dose or cumulative release) that can be explained by one or more of the model parameters. Thus, in this chapter, stepwise linear regression is used to determine the sensitivity of the performance measures (either cumulative release or peak dose) to the uncertain model parameters for the two time periods of interest, 10,000 and 1,000,000 years.

This chapter is organized according to the time period of interest, and then by the sensitivity analyses discussed above. Section 9.2 discusses 10,000-year repository performance, while Section 9.3 discusses 1,000,000-year repository performance. Section 9.4 deals with subsystem performance, e.g., 1,000,000-year releases from the EBS compared to 1,000,000-year releases from the various natural barriers. All results in Chapter 9 are generated using the RIP TSPA model (Golder, 1994).

9.2 10,000-YEAR REPOSITORY PERFORMANCE

This section presents expected-value release-rate and radiation dose histories for various radionuclides over 10,000 years. Total cumulative release CCDFs over all nuclides and total-peak-dose CCDFs over all nuclides for the 10,000-year time frame are also presented. Each point on the total cumulative release CCDF is the integrated release of radioactivity (integral over 10,000 years and over all nuclides) for a particular realization of the stochastic parameters, normalized by the Table-1 release limits in 40 CFR Part 191. Thus, the cumulative release CCDFs originally had units of Curies, but have been nondimensionalized by the Table-1 release limits. Each point on the total-*peak*-dose CCDF represents the maximum dose exposure (rem/yr) over the entire time of the simulation for that particular realization. This peak dose may occur at any time during the 10,000-year time span, and represents a sum over all nuclides at that particular time. Unless otherwise noted, all CCDFs represent the result of 100 realizations of the stochastic parameters.

9.2.1 Alternative Thermal Loads, Thermohydrologic Models, and Infiltration Scenarios

As discussed in Chapter 4 (Linginini et al.), process-level simulations for the near-field repository environment included two alternative thermal loads (25 MTU/acre or 83 MTU/acre), combined with two backfill scenarios (no backfill, i.e., air surrounding the waste packages, or gravel backfill) and two infiltration rate scenarios ("high" = 0.3 mm/yr or "low" = 0.05 mm/yr). Thus, the process-level thermohydrologic simulations produced 2^3 scenarios for near-field repository performance, which are abstracted into the RIP TSPA model. These scenarios are

designated in the figures for this chapter as: 83/yes/hiq, 83/yes/loq, 83/no/hiq, 83/no/loq, 25/yes/hiq, 25/yes/loq, 25/no/hiq, and 25/no/loq, where

83 = 83 MTU/acre,

25 = 25 MTU/acre,

yes = gravel backfill,

no = no backfill,

hiq = infiltration rate (q_{inf}) uniformly sampled in the range 0.5 to 2.0 mm/yr, and

loq = infiltration rate (q_{inf}) uniformly sampled in the range 0.01 to 0.05 mm/yr.

For all eight of these cases, the near-field performance was combined with the geosphere TSPA model to produce 10,000-year simulations of the performance of the combined EBS and natural barrier system. *Because the four scenarios with low infiltration rate do not produce any releases to the accessible environment over 10,000 years, there are no plots for these in Section 9.2.* (All eight scenarios are applicable for the 1,000,000-year performance discussed in Section 9.3.)

The figures in this section also include the designation "clime", which means that they were generated with the model for infiltration-rate variation introduced in Section 7.7. However, the results in Section 9.2 do *not* include the model for changes in water-table elevation, also described in Section 7.7. (Climate change has little effect over 10,000 years.)

Besides the process-level simulations presented in Chapter 4, near-field thermohydrologic simulations by Buscheck et al. (1995) were also evaluated for their effect on releases/doses at the accessible environment. The Buscheck et al. thermal modeling results for 80 MTU/acre did *not* produce significant waste package failure in 100,000 years. For example, the 80 MTU/acre, no-backfill case resulted in over 99 percent of the packages being intact (i.e., no pits completely through the package) up to 100,000 years, while the 80 MTU/acre, backfill case had 100 percent intact packages up to 100,000 years (see Chapter 5). For the Buscheck et al. low thermal load (24 MTU/acre), the no-backfill case had over 99 percent of the packages intact at 100,000 years, while the backfill case had 90 percent of the packages intact. *Over the shorter time-frame of 10,000 years, there were no package failures (see Chapter 5), and therefore no releases to the accessible environment, for the following three cases: (1) Buscheck et al. 80 MTU/acre with backfill; (2) Buscheck et al. 24 MTU/acre with backfill; and (3) Buscheck et al. 80 MTU/acre without backfill.* Thus, in Section 9.2.1, for the Buscheck et al. thermohydrologic model, the only case for which 10,000-year releases and doses to the geosphere are presented is 24 MTU/acre without backfill. These results are discussed at the end of this section.

Release to Accessible Environment (AE)

The 10,000-year, expected-value, release-rate histories for alternative thermal loads, assuming the high-infiltration range, varying infiltration due to climate change, and the thermohydrologic model of Chapter 4 (Linginini et al.), are presented in Figures 9.2-1 to 9.2-4 for the most important radionuclides during the 10,000-year time frame—⁹⁹Tc, ¹⁴C, ¹²⁹I, and ³⁶Cl. All of these are nonsorbing nuclides, i.e., $K_d = 0$ in the geosphere, and they dominate both the release-rate history curves and the normalized-release CCDFs over 10,000 years (as well as doses—see below). (The most important sorbing radionuclide, ²³⁷Np, is also shown on these plots, for

comparison, and has much lower releases and doses than the sorbing nuclides during the first 10,000 years.)

The 83 MTU/acre, no-backfill case (Figure 9.2-1) compared to the 25 MTU/acre no-backfill case (Figure 9.2-2) shows the 83 MTU/acre releases begin approximately 1000 years earlier and reach release-rate peaks about 5 times greater than the 25 MTU/acre case. The step-like nature of the release-rate curves for the 83 MTU/acre case is probably a result of time and spatial discretization within the RIP model. In particular, the column with the fastest travel time breaks through first with its release dispersed over the length of the time step, followed by the second fastest column, etc. The earlier initial breakthrough for the 83 MTU/acre case is due to earlier and greater waste-package failures because of its higher temperature history compared to the 25 MTU/acre case. (Higher temperature causes a higher pit-growth rate, and this is the main controlling factor for waste-package failure—cf. Figures 4.2-8, 4.2-12, and 5.5-1.)

The release-rate history curves for the cases with gravel backfill (Figures 9.2-3 and 9.2-4) have a similar shape to those without backfill. However, for the gravel backfill cases, the difference in initial breakthrough time between the 83 MTU/acre case (Figure 9.2-3) and the 25 MTU/acre case (Figure 9.2-4) is not significant. The no-backfill cases were simulated in the process-level, thermohydrologic analyses (Chapter 4) using a drift filled only with air, and an invert under the waste packages. The backfill case was simulated with gravel in the drift around the waste packages. The temperature, relative humidity, and saturation histories from these process-level results were then incorporated in the TSPA model, where they affect waste-package degradation (corrosion) and diffusion through the EBS. An important conclusion in comparing the predicted releases from the backfill versus no backfill scenarios is that there is very little difference in the release rate curves between the two cases, e.g., compare Figure 9.2-1 with Figure 9.2-3. The difference is even smaller over long time frames (see Section 9.3). This is because the thermohydrologic modeling in Chapter 4 resulted in very similar temperature and relative-humidity histories for the no-backfill and backfill scenarios.

The 10,000-year total cumulative release CCDFs for 100 realizations, normalized to the 40-CFR-Part-191 Table-1 release limits are shown in Figures 9.2-5 to 9.2-8. (The release limits are indicated by the shaded area in the figures.) Figure 9.2-5 compares the two thermal loading scenarios assuming no backfill, while Figure 9.2-6 compares the two thermal loading scenarios assuming a gravel backfill. (Again, these cases use results from the thermohydrologic model described in Chapter 4.) Although the expected-value release-rate history curves for the 83 MTU/acre cases showed higher release-rate *peaks* than the 25 MTU/acre cases, the *integrated release* from the two cases is approximately the same at most values of the sampled parameter distributions. (At the high end of the cumulative release CCDFs, the 83 MTU/acre load produces slightly higher normalized releases.) One thing to be realized when integrating the release-rate history curves is that, although ^{99}Tc has the greatest releases to the accessible environment in Ci/yr on the expected-value plots, ^{14}C dominates the *normalized* cumulative release CCDFs because it has a much lower release-limit factor than ^{99}Tc (100 for ^{14}C vs. 10,000 for ^{99}Tc) in the 40-CFR-Part-191 Table 1. That is, since ^{99}Tc release rates are only about 10 times *higher* than those of the ^{14}C , when they are each divided by their respective release-limit factor, ^{99}Tc will be 10 times *lower* than ^{14}C . The other nuclides on the history curves, ^{129}I and ^{36}Cl , have release-limit factors equal to ^{14}C , so their integrated releases are unimportant.

Figure 9.2-7 shows the difference between backfill and no backfill CCDFs for the 83 MTU/acre case, while Figure 9.2-8 shows the same comparison for the 25 MTU/acre case. As can be seen from these two figures, gravel backfill makes very little difference in the cumulative releases over a 10,000-year time span, at least according to the process-level thermohydrologic model of Chapter 4. However, it is important to note that we have used the same conceptual model for advective transport through the EBS for both the backfill and no-backfill thermohydrologic models, i.e., both of these two cases (backfill and no-backfill) had the same number of dripping fractures on the waste packages in the TSPA model according to the value of the infiltration rate (see Chapter 7). If EBS transport were assumed to be different in these two cases (e.g., if drips on the waste-package were assumed for the no-backfill scenario, but not assumed for the backfill scenario), then the results could be very different, as discussed in Section 9.2.3.

Peak Dose at Accessible Environment

The 10,000-year expected-value dose histories for the alternative thermal loads, assuming a climate change model (but no water table rise) and the thermohydrologic model of Chapter 4, are presented in Figures 9.2-9 to 9.2-12. Most of the conclusions regarding release rate, discussed above, are applicable to dose also. In particular, for no backfill the 83 MTU/acre cases show an earlier initial breakthrough and greater peak dose for individual radionuclides compared to the 25 MTU/acre case. One important difference between release rate histories and dose histories is that ^{129}I is just as important as ^{99}Tc on the dose histories, whereas for release rate ^{99}Tc was the predominant nuclide. This is because ^{129}I has a higher dose-conversion-factor-to-specific-activity ratio than ^{99}Tc . In particular, from Table 7.6-1, the dose conversion factor (DCF) for ^{129}I is $35.2 \text{ (rem/yr)/(g/m}^3\text{)}$ and for ^{99}Tc it is $17.9 \text{ (rem/yr)/(g/m}^3\text{)}$. The specific activity of ^{129}I is $1.77 \times 10^{-4} \text{ Ci/g}$ and for ^{99}Tc it is 0.017 Ci/g . Taking the ratio of DCF to specific activity gives the dose conversion factor in units of $\text{(rem/yr)/(Ci/m}^3\text{)}$. This conversion factor is $1.99 \times 10^5 \text{ (rem/yr)/(Ci/m}^3\text{)}$ for ^{129}I and $1.05 \times 10^3 \text{ (rem/yr)/(Ci/m}^3\text{)}$ for ^{99}Tc . This is a ratio of 189, which explains why the $^{99}\text{Tc}/^{129}\text{I}$ dose ratio is about 1 while the release-rate ratio is about 200 (cf. Figures 9.2-1 and 9.2-9). (To get actual dose in rem/yr from release rate in Ci/yr also requires the volumetric fluid-flow rate in m^3/yr .)

The 10,000-year total-peak-dose CCDFs are shown in Figures 9.2-13 to 9.2-16. Figure 9.2-13 compares the two thermal loading scenarios when there is no backfill, while Figure 9.2-14 compares the two thermal loading scenarios when there is a gravel backfill. For both backfill scenarios, the 25 MTU/acre peak doses are slightly lower than the 83 MTU/acre peak doses because of the high peak for ^{99}Tc and ^{129}I between 9,000 and 10,000 years in the 83 MTU/acre cases, as indicated on the expected-value history plots. As with releases, there is very little difference on the total-peak-dose CCDFs between backfill and no-backfill scenarios (Figures 9.2-15 and 9.2-16), but again this conclusion is dependent on using the same model for EBS advective transport for both backfill and no-backfill.

Buscheck's Thermohydrologic Model

The last sensitivity case in this section examines 10,000-year predicted releases and doses at the accessible environment that result from coupling the RIP TSPA model to near-field simulations from the Buscheck et al. (1995) thermohydrologic model.

Figure 9.2-17 compares the CCDF of total release for the Buscheck et al. 24 MTU/acre model (without backfill) with the CCDF of total release for the Lingineni et al. 25 MTU/acre model (without backfill) that was described in Chapter 4. Figure 9.2-18 compares the comparable peak dose CCDFs. Overall, as expected from the temperature history (Figure 4.2-21), the use of the Buscheck et al. model results in lower releases and lower doses at the accessible environment because the slightly higher temperature for the Lingineni model results in higher corrosion and dissolution rates. The expected-value history curves for releases and doses (Figures 9.2-19 and 9.2-20) show the same behavior. For example, if we compare Figure 9.2-20 with Figure 9.2-10, it is clear that the total peak dose at the accessible environment over the 10,000-year time span (which results mainly from ^{99}Tc and ^{129}I) is about 2 times higher for the Lingineni et al. 25 MTU/acre model, which is confirmed on the CCDF plot (Figure 9.2-18) by comparing the two CCDF curves at a probability of 0.5. Similar differences are found on the release-rate histories (Figure 9.2-19 vs. Figure 9.2-2). (As noted previously, ^{14}C dominates the normalized cumulative release CCDFs because it has a much lower 40-CFR-Part-191 release-limit factor than ^{99}Tc .)

9.2.2 Alternative Waste-Package Degradation Models

Because of the considerable uncertainty about corrosion-initiation processes and corrosion rates, several conceptual models of waste-package degradation have been examined in previous chapters of this report (Chapters 5 and 8). The impact of these various conceptualizations on total peak dose and cumulative release at the accessible environment is presented in this section.

All other results in Section 9.2 have used the corrosion-initiation model that begins corrosion when the relative humidity (R.H.) rises above 65%. In this section, we look at two other corrosion initiation models and their effect on doses at the accessible environment. The first model assumes that two criteria must be met to initiate corrosion: the relative humidity must be above 65% and the temperature must be below 100°C. The other sensitivity case is for a model that includes *cathodic protection* plus initiation of corrosion when both R.H. > 65% and T < 100°C.

For the 25 MTU/acre thermal load (with the Lingineni et al. thermohydrologic model), the temperature is always below 100°C by the time the R.H. rises above 65%. Therefore, the 25 MTU/acre case is not useful for checking the sensitivity of doses at the accessible environment to the corrosion-initiation models. Instead, we look at the 83 MTU/acre thermal load (without backfill and with high q_{inf}), for which the relative humidity reaches 65 percent before the temperature drops below 100°C. Thus, if corrosion initiation is delayed until both the temperature and relative humidity conditions are satisfied, it is suspected that the releases will be less than if the corrosion is initiated immediately upon reaching R.H. = 65%, i.e., the dose at the accessible environment should be less than for the cases previously discussed in this chapter.

100-realization, total peak dose and cumulative release CCDFs are shown for the R.H.-only corrosion-initiation model and the combined R.H. & T initiation model in Figures 9.2-21 and 9.2-22, respectively. *No releases are shown for the cathodic protection model because no nuclides reached the accessible environment in 10,000 years when using this model.* The two models that are shown do not exhibit major differences in releases or doses, with the R.H.&T model only showing a reduction in release and dose by about a factor of 2 to 5 compared the R.H.-only model during the 10,000-year time span. Clearly, however, the cathodic-protection

scenario offers dramatic dose reduction if the time frame of interest is 10,000 years. This should be compared to the minimal reduction exhibited during a 1,000,000-year time frame (Section 9.3.2).

9.2.3 Alternative Conceptual Models for EBS Transport

This section compares 10,000-year performance for five different conceptual models of water movement and radionuclide transport in the repository drifts: (1) fractures dripping directly onto the waste-form, i.e., directly on the spent fuel and DHLW glass; (2) fractures dripping on the corroding metal waste containers, but not directly on the waste form; (3) no dripping fractures (the so-called capillary-barrier effect); (4) no dripping fractures and also aqueous (rather than gaseous) transport of ^{129}I and ^{36}Cl ; and (5) no dripping fractures and also aqueous transport of ^{129}I and ^{36}Cl plus direct shunting of ^{14}C to the atmosphere (i.e., ^{14}C does not travel to the accessible environment in the aqueous phase, so it has no effect on dose). The first four of these models have been discussed in more detail in Chapter 6, and EBS releases for these four models were presented in Chapter 8.

The first model, or "drips-on-waste-form" model is the most conservative, i.e., the most pessimistic about repository performance. This model is used for all the simulations in Chapter 9, with the exception of a few discussed in this section. In the "drips-on-waste-form" model, as soon as the first pit completely penetrates the inner waste container, it is assumed that the advective flow from drift-scale dripping fractures goes through the pit, interacts with the waste form, and then advectively transports the radionuclides away from the waste form, through the EBS, and into the geosphere at the same volumetric flow rate as the dripping flow onto the waste form. This model also allows diffusive mass-transfer through the aqueous phase occupying the invert and backfill, but this mode of transport is insignificant compared to the advective transport.

In the second, or "drips-on-waste-container" model, the pits in the waste containers are assumed to always be filled with corrosion products, so that drips cannot directly contact the waste form, but can only contact the outer surface of the waste container. These corrosion-filled pits act as a mass-transfer barrier, such that mass-transfer occurs only by diffusion through the pits. This effectively lowers the radionuclide concentration encountered by drips at the *waste-container* surface, compared to the concentration the drips would have encountered at the *waste-form* surface if the corrosion products did not act as a barrier to advection. Once the radionuclides diffuse through the pits, they are swept away in the dripping water by advection, and they also diffuse through the invert and backfill, although the diffusive transport is again insignificant compared to the advection.

The third EBS transport model is the "no-drip", or capillary-barrier-effect model. This model assumes that the dripping fractures never interact with the waste form, waste package, or EBS, so that the aqueous-phase radionuclides (but *not* gas-phase nuclides) can only enter the geosphere by diffusion through the corroded waste container and then through the invert and/or backfill. Thus there is no advective release of aqueous-phase radionuclides through the EBS. This transport model could result from placing a Richard's (or capillary) barrier above the waste containers, consisting of two materials of disparate capillary properties, which "soaks up" drips from fractures and redistributes the dripping flow as slow matrix flow through the upper layer (the layer with greater capillary suction). The no-drip model might also result from ordinary

single-layer, coarse-gravel backfill. In this conceptualization, the dripping water is slow enough that when it contacts the gravel surface, it spreads out and equilibrates with the vapor phase, and is no longer concentrated enough to continue as advective flow.

In the previous three models, and in all other sections of this chapter, it was assumed that all radionuclides moved through the EBS by aqueous-phase transport except ^{129}I , ^{36}Cl , and ^{14}C , which are assumed to be gas-phase species. Thus, the capillary-barrier model is ineffective in retarding the movement of these three gas-phase radionuclides, and they become the biggest contributors to dose for the no-drip or capillary-barrier EBS transport model (see figures below). However, because of the high reactivity of gaseous I_2 and Cl_2 , it seems quite possible that they may easily be dissolved and reduced in the aqueous phase before they are able to traverse the entire EBS. In that case, their only mode of transport across the EBS would be diffusion through the aqueous phase, just like all the other aqueous-phase radionuclides whose advective EBS transport is stopped by the capillary barrier. Thus, the capillary-barrier effect combined with aqueous EBS transport of ^{129}I and ^{36}Cl is the fourth conceptual model of EBS transport to be examined. In this model, only ^{14}C is transported across the EBS in the gas phase.

The fifth and final EBS transport model is called the "diffusion-only" model. In the previous models, ^{14}C was assumed to transport across the EBS in the gas phase and then enter the aqueous phase in the geosphere (i.e., in the TSw formation), from whence it transports through the unsaturated and saturated zones to a water well at the accessible environment. In reality, most of the ^{14}C may be rapidly transported directly to the atmosphere by movement through the gas phase in the unsaturated zone. This phenomenon has the effect of eliminating the dose exposure to ^{14}C at the accessible environment, i.e., by water ingestion at the accessible environment. As described here, this is not really a new model of EBS transport, but a different model of geosphere transport. However, it is convenient to include it as a comparison case in this section. It is called the "diffusion-only" model, since all radionuclides that reach the accessible environment (i.e., the water well) can only traverse the EBS by diffusion through the aqueous phase.

The 83 MTU/acre case with high infiltration was used as the nominal case for the analyses in this section. We only considered the high-infiltration scenario ($q_{\text{inf}} = 0.5\text{--}2.0$ mm/yr) because, as discussed in the previous section, the low-infiltration scenario ($q_{\text{inf}} = 0.01\text{--}0.05$ mm/yr) does not produce any releases at the accessible environment in 10,000 years.

The 10,000-year expected-value dose histories for the most conservative EBS-transport model (used in all other sections of this chapter), the "drips-on-waste-form" model, have already been shown in Figure 9.2-11. For the second, or "drips-on-waste-container" model, the expected-value dose histories are presented in Figure 9.2-23. As expected, the only major difference between these two figures is in the doses for the aqueous-phase radionuclides, ^{99}Tc and ^{237}Np . ^{99}Tc dose at the accessible environment at 10,000 years is reduced by about a factor of 10 for the "drips-on-waste-container" model compared to the "drips-on-waste-form" model. This will imply that the 10,000-year *total* peak dose will be reduced by about a factor of 2, since ^{129}I and ^{99}Tc contributed equally to the total peak dose on Figure 9.2-11. ^{237}Np for the "drips-on-waste-container" model is lowered to values less than 10^{-8} rem/yr.

Figures 9.2-11 and 9.2-23 may be compared to Figure 9.2-24, which shows the radionuclides with the greatest dose at the accessible environment in the capillary-barrier ("no-drip") scenario. It is apparent that no nuclides that are transported through the EBS via the aqueous phase (e.g., ^{99}Tc) are able to reach the accessible environment during the 10,000-year time frame (at least at doses above 10^{-8} rem/yr) for the capillary-barrier scenario. This is because, without dripping fractures (which are intercepted by the capillary barrier), the only mechanism for release from the EBS is diffusion, which has a very low transport rate. The only nuclides able to escape the EBS are those nuclides (^{129}I , ^{36}Cl , and ^{14}C) that are transported as gas-phase nuclides through the EBS.

As mentioned above, because of the high reactivity of I_2 gas and Cl_2 gas, it seems possible that they may dissolve into the aqueous phase before they traverse the entire EBS. Figure 9.2-25 shows this scenario (i.e., a capillary barrier and aqueous EBS transport of ^{129}I and ^{36}Cl), and demonstrates that only ^{14}C is able to reach the accessible environment in significant quantities over 10,000 years.

The final EBS transport model is the "diffusion-only" model. In this model ^{14}C is assumed to go directly to the atmosphere, and therefore does not contribute to peak dose in a water well at the accessible environment. This case is not accompanied by a figure because the dose at the accessible environment is not measurable after 10,000 years, i.e., diffusive transport of all other radionuclides across the EBS is too slow for them to appear at the accessible environment within 10,000 years.

100-realization, total-peak-dose CCDFs for the first four transport models are presented in Figure 9.2-26. As seen in the expected-value dose histories, the total peak dose is reduced by about 50% for the "drips-on-waste-container" and "capillary-barrier" EBS transport models, compared to the "drips-on-waste-form" model, because of the reduction in ^{99}Tc . It is not reduced anymore than this because of the contribution from gaseous ^{129}I . The fourth model, which combines the "capillary barrier" with aqueous EBS transport of ^{129}I and ^{36}Cl , reduces the peak doses by about an additional factor of 10 for the entire range of the CCDF. The reason for this is evident in Figure 9.2-11, which shows that the peak doses due to ^{99}Tc and ^{129}I are both about 10 times greater than the ^{14}C peak dose. Thus, the "drips-on-waste-container" and "capillary-barrier" scenarios both remove the ^{99}Tc peak dose, which halves the CCDF value, while the $^{129}\text{I}/^{36}\text{Cl}$ capillary barrier removes both ^{99}Tc and ^{129}I , leaving only ^{14}C —at a dose exposure 10 times less than ^{129}I . The final model, which eliminates ^{14}C as a contributor to peak dose at the accessible environment, has no releases at the accessible environment in 10,000 years.

In contrast to the dose CCDFs, the cumulative release CCDFs almost overlay one another (Figure 9.2-27). The reason for this is related to the 40-CFR-Part-191 release-limit factors, and can be seen by examining Figure 9.2-3. First of all, ^{99}Tc , even though it has the highest Ci/yr of all nuclides, is unimportant on the CCDF because its Table-1 release-limit factor is 100 times the factor for ^{129}I and ^{14}C . Secondly, ^{129}I is released at a 10-times lower rate than ^{14}C , so the values in the normalized release CCDFs in the first four EBS transport scenarios are due almost entirely to ^{14}C release—which remains the same in these four scenarios. [Note: Although ^{129}I release-rate is a factor of 10 lower than ^{14}C release rate, its dose is factor of 10 higher because the ratio of its dose conversion factor (DCF) to its specific activity is much greater than ^{14}C . From Table 7.6-1, the DCF for ^{129}I is 35.2 (rem/yr)/(g/m³) and for ^{14}C it is 6570 (rem/yr)/(g/m³). The specific

activity of ^{129}I is 1.77×10^{-4} Ci/g and for ^{14}C it is 4.46 Ci/g. Taking the ratio of DCF to specific activity gives the dose conversion factor in units of (rem/yr)/(Ci/m³). This conversion factor is 1.99×10^5 (rem/yr)/(Ci/m³) for ^{129}I and 1.47×10^3 (rem/yr)/(Ci/m³) for ^{14}C . This is a ratio of 135, which explains the reversal in the $^{129}\text{I}/^{14}\text{C}$ dose ratio compared to the release-rate ratio. (To get actual dose in rem/yr from release rate in Ci/yr also requires the volumetric fluid-flow rate in m³/yr.)]

9.2.4 Fracture/Matrix Interaction in the Geosphere

Intra-unit Fracture Connectivity

The effect of modifying the RIP fracture/matrix interaction term (λ) in the unsaturated zone is evaluated in this section. This term is also called the Poisson transition ratio (Golder, 1994) and represents the inverse of the average (and random) travel length for a particle in one of the two flow modes, fracture or matrix (see Section 7.4.4). Thus, it may be thought of as representing intra-unit fracture connectivity, i.e., average fracture length within a particular hydrogeologic unit. This parameter describes the rate of a Markov process that randomly transitions radionuclides between fracture and matrix flow modes within a RIP pathway, and results in a dispersion of the bimodal behavior of the fracture/matrix breakthrough curve. For all other sensitivity cases in Section 9.2, except those in this section, we used a value of λ equal to $1/h$, where h is the pathway length. This value of λ implies that on average a particle will travel the thickness of the particular hydrogeologic unit before transitioning from fracture to matrix. This is a conservative assumption that favors flow in fractures. (The saturated-zone pathway was modeled with one flow mode that had the average or bulk properties of the fractures and matrix in the saturated zone, so λ is not a parameter for saturated-zone transport.)

For the λ sensitivity analysis, the nominal case is taken to be 83 MTU/acre, with backfill, and high infiltration rate (0.5 - 2.0 mm/yr). As mentioned, the nominal case used $\lambda = 1/h$, where h is the formation (hydrogeologic unit) thickness. The two sensitivity cases are for $\lambda = 1/(0.1h)$, i.e., particles only travel 10% of the formation thickness on average before switching from fracture to matrix within the given formation, and $\lambda = 1/(100h)$, i.e., particles travel 100 times the formation thickness on average before transitioning from fracture to matrix (or, equivalently, if 100 particles are released into the fractures at the top of a unit, 99 of them are expected to remain in the fractures for the entire distance of travel through the unit). The former case [$\lambda = 1/(0.1h)$] represents short fracture lengths within a unit with disconnects between them, while the latter [$\lambda = 1/(100h)$] represents faults traversing an entire formation. One should keep in mind the discussion in Section 7.4.4 about the fact that even though there may be fracture flow within a unit, connected fractures or faults that transect multiple units are not considered. Thus, fracture flow from one unit is divided up into fracture and matrix flow when it reaches the next lowest unit, according to the value of f_{frac} .

The 100-realization total-peak-dose CCDFs and cumulative release CCDFs for the three cases are shown in Figures 9.2-28 and 9.2-29, respectively. Both peak doses and cumulative releases are about 10 times higher for the $\lambda = 1/(100h)$ case compared to the $\lambda = 1/h$ case, because of the larger amount of mass travelling through the highly connected fracture system within each unit. In contrast, both peak doses and cumulative releases are very low for the $\lambda = 1/(0.1h)$ case, being at least a factor of 10^3 lower than the $\lambda = 1/h$ case. This is to be expected, because in this λ

= 1/(0.1h) scenario, the fractures are highly disconnected and much of the nuclide mass travels within the slow matrix-flow regime.

Matrix Flow (Zero Fracture Flow)

The upper bounding case for the λ parameter is when there is only matrix flow in the unsaturated zone, i.e., zero fracture flow ($f_{\text{frac}} = 0$, see Chapter 7). *When the matrix-flow-only model was examined for 10,000-year performance, there were zero releases at the accessible environment for all realizations of the stochastic variables.*

9.2.5 Most Important Model Parameters

The objective in this section is to identify the parameters in the TSPA model that are most important to repository performance. This information can help focus field and laboratory experiments on reducing uncertainty in these parameters. Two complimentary methods are used to define the most important parameters. First, scatter plots of both 10,000-year cumulative normalized release and 10,000-year total peak dose, as a function of various stochastic parameters, are shown for 100 realizations. The scatter plots give a quick visual check of the data to easily spot linear trends (i.e., clear dependencies of the results on given parameters), in either normal space or log space.

A more sophisticated analysis is stepwise linear regression, which fits the results (release or dose) to subsets of model parameters. From this analysis, we extract sensitivity coefficients to define the dependence of the results on the parameters, and then we rank the parameters according to their order of importance. The sensitivity coefficient used is the percent of the variance of the result which can be explained by, or attributed to, a particular parameter (or group of parameters). By "result", we mean "performance measure", such as 10,000-year total peak dose.

Each RIP simulation was based upon approximately 260 stochastic variables. Because only 100 realizations were run for each case, it was not possible to regress on all of these variables. Thus, based on expert judgement, 25 parameters were selected as potentially the most important. Stepwise linear regression was then used to select the five most important parameters for two different performance measures: 10,000-year normalized cumulative release and 10,000-year total peak dose. The scenario tested was 83 MTU/acre thermal load, high q_{inf} range, with backfill, and climate change.

Stepwise linear regression was performed for three transformations of the data. First, rank regression was tried, since it is a robust method when the underlying model is unknown or complex. (Rank regression is where the rank of the dependent variable is fitted with the ranks of the independent variables. For example, the 100 peak doses from the 100 realizations are assigned a rank based on their numerical value, with 1 being assigned to the lowest result and 100 being assigned to the highest result. Then the values of each independent parameter are ranked 1 to 100. These ranks are then used for the regression.) Since many of the model dependencies are known to be multiplicative, we used the natural log of the performance measurement (P.M.) as the dependent variable for two additional regressions (other than the rank regression). These are: (1) $\ln(\text{P.M.})$ vs. $\ln(x)$ and (2) $\ln(\text{P.M.})$ vs. x , where x is a subset of the 25 stochastic parameters that were expected to be the most important. For each transformation,

the five most important independent variables were recorded in Tables 9.2-1 and 9.2-2, as well as the amount of the variability they explain. The regression analysis was accomplished with S-Plus (Statistical Sciences, 1993), an interactive statistical language developed at AT&T Bell Laboratories.

One point to note is that for TSPA-1995 some of the stochastic distributions for parameters have been eliminated and replaced with sensitivity analyses which are conducted for only three or four values of the given parameter. Thus, the analysis in this section will not include such parameters in the importance rankings, even though they could be more important than the ranked parameters. An example is the fracture/matrix particle transition parameter, λ .

The regression analysis will focus on the $\ln(\text{P.M.})$ vs. $\ln(x)$ and $\ln(\text{P.M.})$ vs. x regressions, which are more physically meaningful than the rank regression. The two performance measures, 10,000-year cumulative release (Table 9.2-1) and 10,000-year total peak dose (Table 9.2-2), show exactly the same rankings for the top three variables for each type of regression. In particular, the top three variables for the $\ln(\text{P.M.})$ vs. $\ln(x)$ regression are the matrix velocity in the CHnv ($v_{\text{mat}}-\text{CHnv}$), the unsaturated zone Darcy flux or infiltration flux (q_{inf}), and the climate change modifier ($U_{\text{cli}}(1,3)$); for the $\ln(\text{P.M.})$ vs. x regression they are the infiltration flux (q_{inf}), the fraction of fracture flow in the CHnv ($f_{\text{frac}}-\text{CHnv}$), and the climate change modifier ($U_{\text{cli}}(1,3)$). [$U_{\text{cli}}(1,3) = 1 + U_{\text{cli}}(0,4)/2$, where $U_{\text{cli}}(0,4)$ was defined in Section 7.7.] In general, the $\ln(\text{P.M.})$ vs. $\ln(x)$ regression provides a slightly better fit than the $\ln(\text{P.M.})$ vs. x regression, as indicated by the fact that the top 1, 2, 3, etc. parameters explain more of the variance. For example, ranked parameter #2 in the $\ln(\text{P.M.})$ vs. $\ln(x)$ regression is q_{inf} , which in combination with $v_{\text{mat}}-\text{CHnv}$ explains 68% of the variance of the 10,000-year releases, whereas, ranked parameter #2 in the $\ln(\text{P.M.})$ vs. x regression is $f_{\text{frac}}-\text{CHnv}$, which together with q_{inf} only explains 63% of the variance. Here we should note that many of the variables are collinear in either log space or linear space, due to the abstractions used in the geosphere (see Chapter 7). For example, f_{frac} is proportional to $\log_{10}q_{\text{inf}}$, and $\log_{10}v_{\text{mat}}$ is proportional to $\log_{10}q_{\text{inf}}$. This explains why different variables show up using the two different transformations.

A confirmation of the linear regression analysis for the two performance measures can be seen in the scatter plots in Figures 9.2-30 to 9.2-36 (for the 10,000-year release P.M.) and Figures 9.2-37 to 9.2-43 (for the 10,000-year peak dose P.M.). These figures represent scatter plots of all the parameters that showed up with rank 5 or less in any of the three different regressions. The strongest linear trend is for the top 2 parameters, $v_{\text{mat}}-\text{CHnv}$ and q_{inf} , with a less obvious linear trend for $f_{\text{frac}}-\text{CHnv}$. Any parameters with a ranking lower than 2 do not show an obvious trend. This is because their relationship is masked by collinearity in the model. However, if the remaining residual (i.e., the difference in the fitted value and the observed value) is plotted for each parameter and subset of parameters against the next lower ranked parameter, a linear trend is visible. For example, if the residual left after fitting ranked parameters 1 and 2 is plotted versus ranked parameter 3, a clear linear trend will be visible.

The rankings of the two most important variables in Tables 9.2-1 and 9.2-2 were not unexpected. In TSPA-1993 (Andrews et al., 1994) it was found that the UZ infiltration flux (q_{inf}) had a very strong influence on doses and releases over 10,000 years. This is again true in TSPA-1995. In particular, the peak concentrations of the radionuclides never reach the accessible environment during 10,000 years and variability in q_{inf} simply translates to a shifting in time of the initial

portion of the breakthrough curve. However, since this is the steeply rising portion of the breakthrough curve(s) regardless of the value of q_{inf} (for $q_{inf} = 0.5-2.0$ mm/yr), there is a very strong dependence on q_{inf} . The strong dependence on either v_{mat} -CHnv or f_{frac} -CHnv is also not unexpected because the CHnv is the formation with the highest value of saturated matrix conductivity, K_{mat} , and therefore the lowest value of f_{frac} . Therefore, it tends to control connected fracture flow throughout the mountain, as noted in the Calico Hills System Study (M&O, 1995d); and without fracture flow, no releases can reach the accessible environment in 10,000 years.

9.2.6 Summary of 10,000-year Performance

The following are general conclusions concerning 10,000-year repository performance, based on the sensitivity analyses in Section 9.2:

- (1) 10,000-year total peak dose, due mainly to ^{99}Tc and ^{129}I , is most sensitive to the following model parameters: matrix velocity in the CHnv and percolation flux in the unsaturated zone;
- (2) Over 10,000 years there are zero releases to the accessible environment for the following cases: (i) low infiltration range (0.01 - 0.05 mm/yr), (ii) cathodic protection of the waste package, (iii) Buscheck et al. 80 MTU/acre thermal load with and without backfill and 24 MTU/acre thermal load with backfill, and (iv) matrix-flow-only (zero fracture flow) in the unsaturated zone;
- (3) Depending on the conceptual model of intra-unit fracture connectivity, fracture/matrix interaction can significantly affect peak dose and cumulative release;
- (4) Depending on the conceptual model for radionuclide transport across the EBS (viz., if ^{129}I and ^{36}Cl are assumed to be in the aqueous phase and/or ^{14}C is supposed not to contribute to peak dose since it is dispersed in the atmosphere), a "capillary barrier" that prevents drips (i.e., advective flow) from contacting the waste packages can reduce 10,000-year peak doses at the accessible environment by at least a factor of 20 or more (and up to many orders-of-magnitude if only diffusive releases are possible through the EBS).

9.3 1,000,000-YEAR REPOSITORY PERFORMANCE

In their recent report to Congress, the National Research Council (1995) has concluded that "...there is no scientific basis for limiting the time period of the individual-risk standard to 10,000 years... (and) that compliance assessment be conducted for the time when the greatest risk occurs, within the limits imposed by long-term predictability of both the geologic environment and the distribution of local and global populations." Based on geologic considerations, they also state that "the ultimate restriction on time scale ... is on the order of 1,000,000 years at Yucca Mountain." For these reasons, we have conducted performance assessments of dose and peak dose over a 1,000,000-year time frame, which are presented in this section as a number of sensitivity cases (see Section 9.1) that examine the effect of various system parameters and various repository designs.

9.3.1 Alternative Thermal Loads, Thermohydrologic Models, and Infiltration Scenarios

The effect of alternative thermal loads (25 MTU/acre vs. 83 MTU/acre) and alternative thermohydrologic conceptual models (Linginini et al. vs. Buscheck et al.) are presented in this section. Chapter 4 discusses the differences between the two thermohydrologic conceptualizations. They are also discussed in Section 9.2.1 regarding their incorporation into the RIP TSPA simulations.

Peak Dose at Accessible Environment

The expected-value dose histories (for the radionuclides with the highest doses) for the two different thermal loads, using the Linginini et al. thermohydrologic model, are presented in Figures 9.3-1 to 9.3-4. The "part a" figures are for 1,000,000 years, and the "part b" figures are a blow-up of the "part a" figures over 100,000 years. These four figures are for the high infiltration case ($q_{inf} = 0.5 - 2.0$ mm/yr). ^{237}Np and ^{229}Th at late times, and ^{99}Tc and ^{129}I at early times, produce the highest dose exposure at the accessible environment for both the 83 MTU/acre case and the 25 MTU/acre case. For identical backfill, infiltration, and climate conditions, the 83 MTU/acre case results in slightly higher dose exposure than the 25 MTU cases at times beyond 80,000 years for the highest-releasing sorbing radionuclides, ^{237}Np , ^{229}Th , and ^{233}U . At times earlier than 80,000 years, these retarded ions (^{237}Np , ^{229}Th , and ^{233}U) have generally lower doses for the 83 MTU/acre case compared to the 25 MTU/acre case. However, the time before 80,000 years can be considered just an inconsequential "leading edge" of the breakthrough curve, and when the main peak of radionuclides comes out (beginning at about 200,000 years), the higher thermal load gives slightly higher doses.

The 25 MTU/acre case is affected more by climate change than the 83 MTU/acre case, with the 100,000-year periodic variation of q_{inf} clearly visible for ^{237}Np , ^{229}Th , and ^{233}U . The apparent reason for these differences can be found in Table 8.3-3, which shows the waste-package failure history for the various cases. For the 83 MTU/acre thermal load, most of the packages fail very early during the 1,000,000-year time span, whereas for the 25 MTU/acre thermal load, the failures are much more spread out in time. For sorbing nuclides, this allows the climate effect (due to cyclical variations in the drip rate) to be visible for the low thermal load, but not for the high thermal load (where the nuclides come out essentially as a pulse). Although the cyclic peaks on the 25 MTU/acre ^{237}Np curve are approximately the same magnitude as the values of the 83 MTU/acre ^{237}Np curve at the corresponding times, the average of the 25 MTU/acre ^{237}Np curve (or the integral) is slightly lower. The explanation for the lower average ^{237}Np dose for 25 MTU/acre is the higher temperature history for the 83 MTU/acre case, as discussed below.

For the unretarded nuclides, ^{99}Tc and ^{129}I , the situation is similar, namely, the 83 MTU/acre case yields higher peak doses when the peak of the breakthrough curve reaches the accessible environment. At this time (~ 100,000 years), the higher thermal load gives approximately 3 times higher ^{99}Tc and ^{129}I peaks than the 25 MTU/acre case. Overall, the total dose (summation of all the nuclides, sorbing and nonsorbing) is greater for the high thermal load case at most times, as illustrated by Figure 9.3-5.

The difference in peak doses for ^{99}Tc and ^{129}I at early times for the two different thermal loads is caused by differences in waste package degradation. Both of these nuclides are parent nuclides

(part of the original inventory) that are released directly from the waste package and are dissolution rate-limited. In particular, as fast as the waste-form can produce them (by dissolution), these two ions are transported immediately across the EBS. For ^{99}Tc this is a result of rapid release due to advective (dripping) flow, while for ^{129}I it is a result of rapid release by gaseous transport through the EBS. The 83 MTU/acre case has about 3 times the number of failed packages (first pit breakthrough) at any given time compared to the 25 MTU/acre case, primarily because of the different temperature history (see Chapter 6). The higher temperature history in the 83 MTU/acre case also results in a higher dissolution rate for the waste-form and a higher solubility for some of the nuclides. This combination of factors results in higher doses to the accessible environment for the nonretarded nuclides for the 83 MTU/acre case, and is also the likely cause of the higher doses for the retarded nuclides, ^{237}Np , ^{229}Th , and ^{233}U .

For the low infiltration cases ($q_{\text{inf}} = 0.01 - 0.05$ mm/yr), the expected-value dose histories for the unretarded nuclides ^{129}I , ^{99}Tc , and ^{36}Cl are about 2-3 times greater for the 83 MTU/acre case than for the 25 MTU/acre case (Figures 9.3-6 to 9.3-9). As with the high infiltration scenario, this difference can be attributed to differences in waste package degradation. On the other hand, for the sorbing nuclides ^{237}Np , ^{229}Th , and ^{233}U , the expected-value dose history for the 83 MTU/acre case is lower than for the 25 MTU/acre case. The reason for this is unclear, but is likely related to the differences in the waste-package-failure histories for the two thermal loads (see Table 8.3-3). Regardless, for both thermal loads, these sorbing nuclides are released at such low concentrations (maximum of 0.01 mrem/yr for the 25 MTU/acre case) that they are of little interest.

One interesting comparison is to examine the differences between the high and low infiltration scenarios, i.e., Figures 9.3-1 to 9.3-4 vs. Figures 9.3-6 to 9.3-9. Direct comparisons for the 83 MTU/acre case with backfill are shown in Figures 9.3-10, 9.3-11, and 9.3-12. First of all, the long-lived, sorbing nuclides, such as ^{237}Np and ^{229}Th , do not have significant releases for low UZ infiltration fluxes over the 1,000,000-year time frame. Second, the periods of highest releases (and doses) for nonsorbing nuclides, such as ^{129}I and ^{99}Tc , are spread out over a much broader time interval for the low- q_{inf} case compared to the high- q_{inf} case, and have a much lower peak. For example, consider ^{99}Tc , the highest-dose nonsorbing nuclide that both travels through the geosphere in the aqueous phase and is released from the WP/EBS in the aqueous phase. The primary portion of its breakthrough curve in the high- q_{inf} case (Figures 9.3-3a and 9.3-10) is much narrower (spanning only about 100,000 years), and has a much higher peak (about 20 mrem/yr), than for the low- q_{inf} case (Figures 9.3-8 and 9.3-10), where it reaches an approximate peak of only about 0.1 mrem/yr or less over a broad time frame of about 600,000 years. Doses this low (0.1 mrem/yr) are expected to be well within any regulatory bounds that may be set for a high-level nuclear waste repository. The other nonsorbing nuclide of interest, ^{129}I , travels through the geosphere in the aqueous phase, but is released from the WP/EBS in the gas phase. Similarly to ^{99}Tc , it sustains doses near the peak dose for much longer time in the low- q_{inf} case compared to the high- q_{inf} case (Figure 9.3-11), but its peak is not reduced as much as ^{99}Tc . Specifically, it has a peak dose exposure of about 2 mrem/yr for the low- q_{inf} case compared to 20 mrem/yr for the high- q_{inf} case. This is a reduction by a factor of 10, compared to a reduction of a factor of 200 for ^{99}Tc . As discussed below, the reason ^{129}I is reduced much less than ^{99}Tc is related to dripping water in the drift and to the longer half-life of ^{129}I compared to ^{99}Tc .

The cause of higher, narrower dose histories in the high- q_{inf} scenario (i.e., doses *not* sustained at peak levels for a very long time), compared to the broad, low dose histories in the low- q_{inf} scenario (i.e., doses sustained near peak levels for a long time), is due to the interaction of the mass source term with the UZ flux, q_{inf} . The best way to explain this is to look at the release of ^{129}I , which has a long half-life and is unaffected by dripping fractures on the waste packages, i.e., since ^{129}I crosses the EBS in the gas phase, the ^{129}I release into the geosphere is only a function of the dissolution rate and not a function of the number of packages with dripping flow. Thus, the total release of ^{129}I from the waste packages is almost the same for the low and high infiltration cases. The slight differences in waste-package releases between high and low infiltration (see Figure 8.3-10) are due to slightly different waste-package degradation histories caused by somewhat different temperature and relative-humidity histories derived from the thermohydrologic analyses (Chapter 4). (Once the ^{129}I passes across the EBS, it is assumed to dissolve from the gas phase into the aqueous phase.)

In the high-infiltration case, fluid flow in the unsaturated zone is able to transport ^{129}I mass about as rapidly as it comes out of the waste packages. However, in the low-infiltration case, the fluid cannot transport mass rapidly enough and it begins to accumulate at the beginning of the first pathway, i.e., at the top of the TSw unit. This results in a longer, slower release that is spread out in time compared to the high-infiltration case. For aqueous-phase, high-solubility nuclides like ^{99}Tc , the same phenomenon occurs but, in addition, the low-infiltration ^{99}Tc total releases and peak doses are reduced much more than ^{129}I or ^{36}Cl because the fraction of packages with drips is much lower for the low- q_{inf} case than the high- q_{inf} case (Figures 7.3-7 and 7.3-8). (It is primarily the number of packages with drips rather than the dripping flow rate, Q_{drip} , that is the cause of the reduction in release because, as shown by Figure 7.3.10, the dripping flow rate for both the high- q_{inf} case and the low- q_{inf} case is high enough to transport nearly all of the high-solubility radionuclide mass out of the waste packages. For q_{inf} equal to 1.25 mm/yr, Q_{drip} equals 0.03 m³/yr, and for q_{inf} equal to 0.03 mm/yr, Q_{drip} equals 1.23×10^{-4} m³/yr—see Figures 7.3-5 and 7.3-6—where Q_{drip} is discussed in Chapter 7 and is the volumetric flow rate per package, equal to the catchment area times q_{drip} .) In comparing ^{99}Tc and ^{129}I doses for the two infiltration ranges, there is also a greater reduction of ^{99}Tc because of its shorter half-life compared to ^{129}I .

As discussed in the RIP Theory Manual (Golder, 1994), it would be more physically realistic if mass flow through the pathways influenced the mass transfer out of the waste packages. However, they are decoupled in RIP Version 3.21c. Thus, for the low- q_{inf} case, the rate of mass transfer out of the packages is overestimated. "Nevertheless, accumulating mass at the beginning of the first pathway (as opposed to at the waste package itself) produces similar results in terms of mass transport *through the entire system*." (Golder, 1994.)

The expected-value for low q_{inf} equals 0.03 mm/yr, while the expected value for high q_{inf} equals 1.25 mm/yr. This q_{inf} ratio of 40 seems to appear in the first arrival of ^{237}Np , which first reaches the accessible environment at about 15,000 years in the high- q_{inf} case (Figure 9.3-3b) and at about 550,000 years in the low- q_{inf} case (Figure 9.3-8)—a ratio of 36. The fact that these two ratios are nearly identical is rather fortuitous because the first arrival is not a strict linear function of q_{inf} but is related to the amount of fracture flow determined through process-level modeling abstractions. The arrival-time ratio for the nonsorbing nuclide ^{129}I appears to be about 10. Numerical dispersion in RIP can also mask exact travel times that would be computed with a process-level model. One thing to be noted here is the effect of timestep size, Δt , in RIP. For

example, if we compare Figures 9.2-11 ($\Delta t = 100$ yr) and 9.3-3b ($\Delta t = 1000$ yr), we see that the first arrivals occur earlier for $\Delta t = 100$ yr, which is the more accurate prediction. For example, the first breakthrough of ^{129}I for $\Delta t = 100$ yr is at 6100 years, whereas, it is at 12,000 years for $\Delta t = 1000$ yr.

100-realization CCDFs of the 1,000,000-year total peak dose for the alternative thermal load cases are presented in Figures 9.3-13 to 9.3-15. Figure 9.3-13 shows the 83 MTU/acre case, with and without backfill, at the high and low infiltration ranges, while Figure 9.3-14 shows the 25 MTU/acre case, with and without backfill, at the high and low infiltration ranges. These two figures demonstrate that backfill (as included in the Lingineni et al. process-level, thermohydrologic model and the resulting near-field temperature, relative humidity, and water saturation histories) has little effect on the results. These figures also illustrate that if the low- q_{inf} scenario is operable over the 1,000,000 years postclosure, then the corresponding peak doses will be about 250 times less than the high- q_{inf} scenario for the 83 MTU/acre thermal load and about 500 times less for the 25 MTU/acre thermal load. The much higher doses over the high- q_{inf} range points to the importance of defining and perhaps controlling advective flux through the repository. This issue is discussed in Section 9.3.3, which analyzes the effect of various models of radionuclide transport in the EBS. As a last comparison, Figure 9.3-15 compares the two thermal loading scenarios for the case with backfill, for high and low q_{inf} . For both infiltration ranges there is little difference between the thermal loading scenarios, with the high thermal load yielding at most only about twice the peak dose.

One final difference to notice is that the total-peak-dose CCDFs for the high- q_{inf} case are primarily a result of the ^{237}Np peak, whereas for low q_{inf} , they are primarily due to ^{129}I . This was illustrated by the expected-value dose histories in Figures 9.3-1 and 9.3-6.

Release at Accessible Environment

Figure 9.3-16 shows normalized cumulative release CCDFs at the accessible environment for the different thermal loading scenarios with backfill, at low and high q_{inf} . It may be compared to the corresponding peak dose CCDFs in Figure 9.3-15. In contrast to the peak dose CCDFs, which have a rather large coefficient of variation ($C.V. = S.D.[x]/E[x]$) arising from the distribution of saturated-zone fluid flux and its effect on dilution (see Chapter 7), the cumulative release CCDFs have a C.V. nearly equal to 0 because they are unaffected by dilution or almost any other parameter over the long time frame of 1,000,000 years. For both infiltration ranges, the 83 MTU/acre thermal load results in normalized cumulative releases about 1.5 times higher than the 25 MTU/acre load. This behavior is substantiated by the expected-value release histories for high q_{inf} (Figures 9.3-17 and 9.3-18) and for low q_{inf} (Figures 9.3-19 and 9.3-20). One interesting difference between the release histories and the dose histories is that although ^{99}Tc dominates the release rate (but not the normalized release because of its high release-limit factor) at low q_{inf} , it is ^{129}I that is more important for the doses (Figures 9.3-8 and 9.3-9) because of its higher dose conversion factor to specific activity ratio (see Section 9.2.1). Also, for the high- q_{inf} scenario, ^{237}Np peak dose is about 30 times higher than ^{99}Tc peak dose (Figure 9.3-3a), whereas for release rate the reverse is true (Figure 9.3-17): ^{237}Np peak release rate is about 100 times lower than ^{99}Tc peak release rate.

Buscheck's Thermal Hydrologic Model

As discussed in Section 9.2.1, the only Buscheck thermohydrologic model that showed releases and doses to the geosphere over 10,000 years was the 24 MTU/acre without backfill. However, over 1,000,000 years, all of the Buscheck cases mentioned in Section 9.2.1 have significant releases to the accessible environment.

Figures 9.3-21 to 9.3-24 show the 1,000,000-year expected-value dose histories for high infiltration (1.25 mm/yr) for the two Buscheck thermal loads (80 and 24 MTU/acre) with and without backfill, and Figures 9.3-25 to 9.3-28 show the 1,000,000-year expected-value dose histories for low infiltration (0.03 mm/yr) for the two thermal loads (80 and 24 MTU/acre) with and without backfill. These various cases may be compared to the previously presented Lingineni cases (Figures 9.3-1 to 9.3-4 and 9.3-6 to 9.3-9). Although Buscheck's process-level thermohydrologic simulations assumed zero infiltration, while Lingineni's simulations assumed either $q_{inf} = 0.05$ mm/yr ("low") or 0.3 mm/yr ("high"), the following analyses couple the Buscheck near-field results to the dripping-fracture model in RIP, and to the different infiltration ranges in the far-field. Of course, it would be better to have had dripping fractures in the process-level model simulations, but one could argue that including dripping fractures in the near-field simulations is less important than including them in the transport model for EBS releases. This is demonstrated by comparing total-peak-dose CCDFs in this section with those of Section 9.3.4. This comparison will show that large changes in relative humidity and temperature in the near field (as evident in the Buscheck versus Lingineni thermohydrologic models—see Chapter 4) has much less of an effect on repository performance (i.e., on peak dose at the accessible environment) than the radionuclide transport model in the EBS, i.e., advective transport caused by dripping fractures (see Section 9.3.4). Furthermore, once the temperature and saturation fields return to ambient conditions, both near-field models are the same, and this occurs well before 1,000,000 years.

Our initial comparison of peak doses from the Buscheck model versus the Lingineni model considers the four high-infiltration scenarios:

(1) High thermal load (83 vs. 80 MTU/acre), high infiltration (1.25 mm/yr), no backfill. The Buscheck model (Figure 9.3-21) shows later initial breakthrough times (70,000 – 90,000 years) for sorbing and nonsorbing nuclides compared to the breakthrough times (15,000 – 20,000) for the Lingineni model (Figure 9.3-1a). The Lingineni model has about 3 times higher ^{237}Np peak dose and about a 10 times higher ^{129}I dose (see Figures 9.3-29 and 9.3-30). The ^{129}I peak is much narrower and earlier in the Lingineni model. All of these effects result from the much later and more spread-out package failure times for the Buscheck model (see Chapter 5), which are a result of lower relative humidity compared to the Lingineni model. This conclusion also applies to all of the comparisons discussed below.

(2) Low thermal load (25 vs. 24 MTU/acre), high infiltration (1.25 mm/yr), no backfill. This was the only Buscheck case that produced releases over 10,000 years. Thus, the 1,000,000-year Buscheck dose histories (Figure 9.3-22) are quite similar to the Lingineni dose histories (Figure 9.3-2a). The ^{237}Np peak for the Lingineni thermohydrologic model is only about 1.5 times higher than for the Buscheck model and the ^{129}I and ^{99}Tc peaks are only about 3 times higher. Similarly to the Lingineni model, the low-thermal load Buscheck model shows the cyclical climate

variation to a greater degree than the Buscheck high thermal-loading scenario, which, as mentioned earlier, probably results from the more spread out (in time) waste-package failures for the low thermal load.

(3) High thermal load (83 vs. 80 MTU/acre), high infiltration (1.25 mm/yr), with backfill. This comparison is about the same as case (1), which had no backfill. About the only difference is that the Buscheck model (Figure 9.3-23) with backfill has initial breakthrough times about 50,000 years later than Buscheck without backfill (Figure 9.3-23). The comparable Lingineni results are in Figure 9.3-3a.

(4) Low thermal load (25 vs. 24 MTU/acre), high infiltration (1.25 mm/yr), with backfill. Here we compare Figure 9.3-24 for the Buscheck thermohydrologic model with Figure 9.3-4a for the Lingineni model. The comparison is very similar to the cases with high thermal load without backfill.

For the four low infiltration scenarios, the main differences between the Lingineni et al. and Buscheck et al. models is that for high thermal load (83 or 80 MTU/acre), the Lingineni et al. model (see Figures 9.3-6 and 9.3-8 compared to 9.3-25 and 9.3-27) gives about 3 times higher ^{129}I peak dose (see Figure 9.3-31), whereas for the low thermal load (see Figures 9.3-7a and 9.3-9a compared to 9.3-26 and 9.3-28) the Lingineni et al. model only gives slightly higher ^{129}I peak dose. As with the high- q_{inf} cases, the low- q_{inf} Buscheck cases show considerably retarded initial breakthrough times compared to the low- q_{inf} Lingineni cases, except again for the low-thermal-load/no-backfill scenario.

Finally, Figures 9.3-32 to 9.3-35 illustrate the 100-realization, total-peak-dose CCDFs that compare the Buscheck and Lingineni thermohydrologic models for low and high q_{inf} . Figures 9.3-32 and 9.3-33 are for high thermal load, without and with backfill, respectively; and Figures 9.3-34 and 9.3-35 are for low thermal load, without and with backfill, respectively. Two general conclusions can be drawn. First, the high thermal load shows a greater difference between the two models over the 1,000,000-year time frame, but the difference is not very significant. In particular, the high-thermal-load Lingineni model only gives about 2 to 3 times greater peak doses over the entire sampled range of stochastic variables than the Buscheck model. So, although the Buscheck model delayed the appearance of the peak dose at the accessible environment by tens- to hundreds-of-thousands of years, it did not reduce the peak very much over the long time span of 1,000,000 years. Second, as with the Lingineni thermohydrologic model, backfill makes very little difference in the total peak dose for the Buscheck thermohydrologic model.

Broader Infiltration Range

A final sensitivity analysis was conducted to merge the high (0.5–2.0 mm/yr) and low (0.01–0.05 mm/yr) infiltration range into one range (0.01–2.0 mm/yr) and to show the shape of the CCDF for 1,000,000-year total peak dose over this entire range, and more importantly, to determine the most important model parameters for this case (see Section 9.3.7). Over the broader range, we use log-uniform sampling, whereas over the separate low and high ranges we used uniform sampling. Without log-uniform sampling, the low infiltrations would rarely be sampled in a 100-realization simulation.

Figure 9.3-36 shows the expected-value dose history for the broader infiltration range, for the 83 MTU/acre loading case with backfill. If we compare Figure 9.3-36a to Figures 9.3-3a (high range) and 9.3-8 (low range), Figure 9.3-36a shows behavior intermediate between these two extremes, however, it is more similar to the low-range in the sense that the peak dose over the 1,000,000-year time frame is due to ^{129}I rather than ^{237}Np .

The 100-realization total-peak-dose CCDF over the broader infiltration (q_{inf}) range is shown in Figure 9.3-37, along with the CCDFs for the high and low q_{inf} ranges. The curves show behavior similar to the expected-value dose histories, i.e., the broader-range curve is intermediate between the other two. From the high probability end of the broad-range CCDF (i.e., at the lower end of the q_{inf} range) to the low probability end of the broad-range CCDF (i.e., at the higher end of the q_{inf} range) there is a transitioning from ^{129}I as the peak dose contributor to ^{237}Np as the peak dose contributor.

9.3.2 Alternative Waste Package Degradation Models

As discussed in Section 9.2.4, because of the uncertainty about corrosion-initiation processes and corrosion rates, several alternative conceptual models have been implemented in the RIP TSPA model to examine their effect on releases and doses at the accessible environment. All other results in Section 9.3 use the corrosion-initiation model that assumes corrosion initiates when the relative humidity (R.H.) rises above 65%. In this section, we also look at the 1,000,000-year peak doses that result from other two corrosion models discussed in Section 9.2.4.

100-realization, total-peak-dose CCDFs for 1,000,000 years are shown in Figure 9.3-38 for the three alternative waste-package-degradation models. The peak dose for the R.H. and R.H.&T corrosion-initiation models are nearly identical, when using the Lingineni thermohydrologic model and corresponding temperature and relative humidities for the 83 MTU/acre load without backfill at the high q_{inf} range. This is similar to the 10,000-year peak doses, which were also nearly the same for the two models. In contrast, the effect of cathodic protection over 1,000,000 years is quite different than for 10,000 years. Over 10,000 years, cathodic protection prevented any releases at the accessible environment, but over 1,000,000 years the cathodic protection CCDF is almost the same as the two CCDFs without cathodic protection. The expected-value dose histories for cathodic protection (Figure 9.3-39), show only a slight delay in the initial breakthrough of the various radionuclides compared to the case without cathodic protection (Figure 9.3-1a). However, it is enough of a delay to eliminate any releases over the initial 10,000 years.

9.3.3 Alternative Conceptual Models for EBS Transport

This section compares 1,000,000-year performance for five different conceptual models of water movement and radionuclide transport in the repository drifts: (1) fractures dripping directly onto the waste-form, i.e., directly on the spent fuel and DHLW glass; (2) fractures dripping on the corroding metal waste containers, but not directly on the waste form; (3) no dripping fractures (the so-called capillary-barrier effect); (4) no dripping fractures and aqueous (rather than gaseous) transport of ^{129}I and ^{36}Cl ; and (5) no dripping fractures and aqueous transport of ^{129}I and ^{36}Cl plus direct shunting of ^{14}C to the atmosphere (i.e., ^{14}C does not travel to the accessible environment

in the aqueous phase, and so has no effect on dose). A detailed explanation of the five EBS-transport models was presented in Section 9.2.3.

The 83 MTU/acre case with high infiltration, backfill, and climate change (cyclical q_{inf} , but no water-table rise) was used as the nominal case for the analyses. We only consider the high infiltration scenario ($q_{inf} = 0.5-2.0$ mm/yr) because according to Figures 9.3-13 and 9.3-14, the total peak doses for the low infiltration scenario ($q_{inf} = 0.01-0.05$ mm/yr) are probably below any level of concern.

The 1,000,000-year expected-value dose histories for the most conservative EBS-transport model (used in all other parts of Section 9.3), the "drips-on-waste-form" model, have previously been shown in Figure 9.3-3a. For the second, or "drips-on-waste-container" model, the expected-value dose histories are presented in Figure 9.3-40. Except for ^{129}I , which is released through the gas phase, all other nuclides show a significant dose reduction at the accessible environment for the "drips-on-waste-container" model. The sorbing radionuclides (in particular, ^{237}Np) are reduced much more than the nonsorbing aqueous-phase nuclides, such as ^{99}Tc . For ^{237}Np , the peak dose is reduced by about a factor of 25 over the 1,000,000-year time span, whereas for ^{99}Tc the reduction is only about a factor of 2. However, an important change in the 1,000,000-year behavior for the "drips-on-waste-container" model compared to the "drips-on-waste-form" model is that the nonsorbing nuclides ^{129}I and ^{99}Tc are now the most important dose contributors over the 1,000,000 years, rather than ^{237}Np .

Figures 9.3-3a and 9.3-40 should be compared to Figure 9.3-41, which shows the most important radionuclides to reach the accessible environment in the "no-drip" (capillary-barrier-effect) scenario. Nuclides that are transported through the EBS via the aqueous phase are unable to reach the accessible environment during the 1,000,000-year time frame at doses above 10^{-7} rem/yr, because without dripping fractures (which are intercepted by the capillary barrier), the only mechanism for release from the EBS is by diffusion, which has a very low transport rate (see Figure 9.3-43). The only nuclides able to escape the EBS are those nuclides (^{129}I , ^{36}Cl , and ^{14}C) that are transported as gas-phase nuclides through the EBS. Thus, the peak dose over 1,000,000 years for the capillary-barrier scenario is due almost entirely to ^{129}I .

As discussed in Section 9.2.3, because of the high reactivity of I_2 gas and Cl_2 gas, it seems quite possible that they may dissolve into the aqueous phase before they are able to traverse the entire EBS. Figure 9.3-42 shows this scenario (i.e., a capillary barrier and aqueous EBS transport of ^{129}I and ^{36}Cl), and demonstrates that peak dose over the 1,000,000 years will occur at an early time and be strictly due to ^{14}C dissolved in the aqueous phase. However, as also discussed in Section 9.2.3, it is quite likely that ^{14}C will not dissolve in the aqueous phase after transport across the EBS, but will travel upward, directly to the atmosphere. This case is shown in Figure 9.3-43, and represents the case where the releases and doses at the accessible environment (i.e., from a water well 5 km downgradient from the repository) result entirely from aqueous-phase radionuclides that were transported across the WP/EBS strictly by aqueous diffusion. The doses are extremely low, on the order of 10^{-9} rem/yr.

Figures 9.3-44 and 9.3-45 demonstrate the low mass-transfer rate across a capillary barrier for aqueous-phase nuclides. These figures compare ^{237}Np and ^{99}Tc doses at the accessible

environment over 1,000,000 years for three scenarios: drips-on-waste-form, drips-on-waste-container, and capillary barrier.

100-realization, total-peak-dose CCDFs for the five EBS transport models are presented in Figure 9.3-46, on two different x -axis scales. (The x -axis scale in Figure 9.3-46a is the one used for all other CCDFs in this section, while the extended scale in Figure 9.3-46b is necessary to show the very low doses for the fifth EBS transport model.) As seen in the expected-value dose histories, the total peak dose is reduced by about a factor of about 25 for the "drips-on-waste-container" compared to the "drips-on-waste-form" model, because of the significant reduction in ^{237}Np dose. It is not reduced much more than this for the no-drip (or capillary-barrier-effect) model because of the contribution from gaseous ^{129}I . The fourth model, which combines the "capillary barrier" with aqueous EBS transport of ^{129}I and ^{36}Cl , reduces the peak doses by about an additional factor of about 200 for the entire range of the CCDF. The final model, which eliminates ^{14}C as a contributor to peak dose at the accessible environment, leaving only diffusively transported aqueous-phase nuclides across the EBS, results in an additional reduction by a factor of more than 10^4 in peak dose over the million-year time frame, compared to the fourth model.

9.3.4 Fracture/Matrix Interaction in the Geosphere

Intra-unit Fracture Connectivity

The fracture/matrix interaction term (λ), or intra-unit fracture connectivity, has been discussed in detail in Sections 7.4.4 and 9.2.4. As with 10,000-year repository performance, for 1,000,000-year performance we likewise examine three possible scenarios: (1) the nominal case, $\lambda = 1/h$, which has been used for all other plots in Section 9.3, except the sensitivity cases discussed here; (2) the low-connectivity case, $\lambda = 1/(0.1h)$, for which particles only travel 10% of the formation thickness on average before switching from fracture to matrix within the given formation; and (3) the high-connectivity case, $\lambda = 1/(100h)$, for which particles travel 100 times the formation thickness on average before transitioning from fracture to matrix (i.e., 99 particles out of 100 will traverse the entire formation within a given flow mode, both fracture and matrix flow modes).

In comparing the expected-value dose histories for the $\lambda = 1/100h$ case (Figure 9.3-47) to the $\lambda = 1/h$ case (Figure 9.3-3), there is little difference between the doses for the nonsorbing ions ^{99}Tc and ^{129}I , although they do reach their approximate peaks at slightly earlier times for the $\lambda = 1/100h$ case (at about 20,000 years versus 30,000 years). For the sorbing ions, e.g., ^{237}Np , there seems to be a little more of an effect, whereby at any given time up to 200,000 years, the ^{237}Np peak dose is higher in the $\lambda = 1/100h$ case. After that, it is slightly lower, since the source term has been more rapidly depleted. The $\lambda = 1/0.1h$ case (Figure 9.3-48), for which matrix flow is much more important, shows a more dramatic effect than the $\lambda = 1/100h$ case, when compared to the $1/h$ case. In particular, although the peak dose over a 1,000,000-year time span is still about the same as the other two cases, it takes much longer to reach this peak dose, i.e., there is a significant delay in the breakthrough curve due to the particles spending more time within the slow flowing matrix water. For example, for the $\lambda = 1/0.1h$ case it takes about 275,000 years for the ^{237}Np peak dose to rise about 100 mrem/yr, compared to 85,000 years for the $\lambda = 1/h$ case, and 53,000 years for the $\lambda = 1/100h$ case.

Zero Fracture Flow and Matrix Diffusion

At one extreme of fracture/matrix interaction in the unsaturated zone is the case of zero flow in fractures ("matrix-flow-only"). Figure 9.3-49 shows expected-value dose histories for this matrix-flow-only case, which was the only model used in TSPA-1993 (Andrews et al., 1994). It indicates a further delay in initial breakthrough times for all radionuclides compared to the $\lambda = 1/0.1\text{h}$ case, but much more so for the sorbing nuclides than the nonsorbing nuclides. Also, for this case ^{237}Np peak dose does not reach the 100 mrem/yr level until 525,000 years, compared to 275,000 years for the $\lambda = 1/0.1\text{h}$ case. Furthermore, the matrix-only case shows a slight reduction in peak dose for ^{237}Np , ^{129}I , and ^{99}Tc —by about a factor of 3 over the 1,000,000-year time frame—compared to the three fracture-flow scenarios discussed above. A comparison of the three different λ scenarios to the matrix-only scenario is shown in Figure 9.3-50 for ^{99}Tc and 9.3-51 for ^{237}Np .

Finally, the 100-realization total-peak-dose CCDFs for the three different values of λ compared to matrix-flow-only are shown in Figure 9.3-52. As already seen for the expected-value cases, there is little difference in the total-peak-dose CCDF during the 1,000,000-year time span amongst the three values of λ , although the highly fractured case ($\lambda = 1/100\text{h}$) does show about 2 times the peak dose over a probability range from about 0.2 to 0.7. Also, as pointed out above, but which is not apparent in the CCDFs, the peak dose for the $\lambda = 1/0.1\text{h}$ case occurs much later in time than the other two cases.

Matrix diffusion refers to the diffusion of solutes from fluid-filled fractures into the surrounding rock matrix because of the concentration gradient that exists between the fracture and matrix when high concentrations of nuclides are rapidly transported through fractures. This phenomenon manifests as a retardation of the travel time of the diffusing solutes compared to the case of nondiffusing solutes (e.g., impenetrable fracture coatings). In the extreme case of equilibrium matrix diffusion (Golder, 1993), the solutes in fractures would travel at the same velocity as solutes in the matrix, and the effect would be the same as having matrix-flow-only, i.e., zero fracture flow. Thus, although we have not modeled matrix diffusion, per se, in TSPA-1995, Figures 9.3-49 and 9.3-52 show its maximum effect on the model.

9.3.5 Climate Change

The effect of climate change was evaluated by comparing a case with no climate change to two possible climate-change models. The first climate-change scenario involved a change in infiltration rate only. The periodic time-variation in q_{inf} for this model has been described in detail in Section 7.7, and is based on a 100,000-year cycle. The second climate-change scenario included both the infiltration-rate modifier and a rising and falling water table. The effect of the changing water-table height was to shorten the path length from the repository to the water table during the rising water table, and to gradually return the path length to its original length during the falling water-table condition (i.e., during the second half of the climate-change cycle). The periods of infiltration-rate increase and water-table rise are assumed to be synchronous, when in reality one might expect some delay in the water-table rise.

To demonstrate the effect of climate change, the 83 MTU/acre case with backfill and high infiltration is analyzed. The expected-value dose history for 1,000,000 years with no climate

change ($q_{inf} = 1.25$ mm/yr) is presented in Figures 9.3-53a and b. The case with periodically increasing q_{inf} but no water-table rise has already been presented in Figures 9.3-3a and b, and the case with both periodically increasing q_{inf} and water-table rise is presented in Figures 9.3-54a and b. The scenario of cyclical increase in q_{inf} but no water-table rise (Figure 9.3-3a), when compared to the no climate-change scenario (Figure 9.3-53a), results in a slightly increased peak dose from ^{129}I and ^{99}Tc and slightly narrows the shape of their history curves because of the higher transport rate away from the WP/EBS (cf. the discussion of source term vs. flow rate in Section 9.3.1). The tail of the ^{99}Tc dose history curve in the cyclical- q_{inf} scenario also has a cyclical nature in response to the increasing and decreasing infiltration. The sorbing ions, ^{237}Np , ^{229}Th , and ^{233}U , also reach an earlier, higher, peak dose for the cyclical- q_{inf} scenario than for the no climate-change scenario, which results in a slightly decreased peak dose at late times compared to the no climate-change scenario. Again, this indicates that the source term for the cyclical- q_{inf} scenario may be more depleted by the increases in infiltration which occur every 50,000 years. In contrast to the nonsorbing nuclide, ^{99}Tc , the dose histories of the sorbing nuclides do not exhibit cyclical release for the 83 MTU/acre case, although as pointed in Section 9.3.1, they do have a cyclical nature for low thermal load. The difference is related to the different waste-package-degradation histories for the two thermal loads.

A cyclical water-table-rise plus cyclical- q_{inf} scenario (Figure 9.3-54) results in quite jagged dose peaks compared to the changing- q_{inf} -only scenario, especially for the sorbing nuclides. The 100,000-year period of the peaks corresponds to the 100,000-year period for the maximum increase in q_{inf} and simultaneous maximum rise in the water table. Due to the pathway length shortening which occurs during the period of increasing infiltration (i.e., first 50,000 years of the climate cycle), there is a rapid discharge of mass from the PPn into the saturated zone which is quickly transported to the accessible environment. This leads to the positive spike in the dose history curve. As the infiltration decreases, water-table level drops and pathway length increases, and the amount of mass being discharged to the saturated zone is decreased, leading to a negative spike in the dose history—below the level of the infiltration-change-only scenario.

A comparison of the three different climate scenarios for ^{99}Tc and ^{237}Np is shown in Figures 9.3-55 and 9.3-56, respectively, for the expected-value high-infiltration case. As discussed above, for ^{99}Tc the higher the infiltration rate is, the narrower and higher the history curve is, so the climate change with water table rise produces the highest peaks with the bulk of the ^{99}Tc coming out of the system slightly earlier than for the other two scenarios. For ^{237}Np , the effect is similar but is just spread out over a much longer time frame.

For the low-infiltration case, expected-value dose histories at 1,000,000 years are presented for the three cases in Figures 9.3-57, 9.3-6, and 9.3-58. We again used the 83 MTU/acre thermal load, but this time without backfill. The results are similar to the high-infiltration cases previously presented. The peak dose is higher and arrives earlier for the two climate-change cases. The dose curve is again quite jagged for the case which includes water table change. The decrease at late times for the two climate-change scenarios is again more pronounced than for the no climate-change scenario because of the depletion of the source term. A comparison of the three different climate-change scenarios for ^{99}Tc and ^{237}Np at low infiltration is shown in Figures 9.3-59 and 9.3-60. The behavior shown on these figures is similar to the behavior in Figures 9.3-55a and 9.3-56a. One point of interest is that no ^{237}Np reaches the accessible

environment for the no climate-change scenario; however, the other two cases have such low ^{237}Np peak doses that they would likely be inconsequential compared to any regulatory limits.

As a final evaluation of the effect of climate change on dose, the 100-realization, total-peak-dose CCDFs are presented in Figure 9.3-61 for the 83 MTU/acre case for the low and high infiltration cases. These figures confirm the results which were seen for the expected-value cases, for example, the climate-change scenario with both increasing q_{inf} and rising water table has higher peak doses than the other two cases.

9.3.6 Alternative Solubility Models for Np, Pu, and Am

In this section, results calculated using the distributions of solubility-limited aqueous radionuclide concentrations for Np, Pu, and Am (Section 6.3.2) are compared with results calculated using the temperature- and pH-dependent functions for Np, Pu, and Am solubility controls in J-13-like water, derived in Section 6.3.3. For both of these cases, the pH has been set to a value of 7. Although the derived functions incorporate pH-dependence explicitly, the near-field pH evolution is uncertain to the extent that adequate constraints do not exist for making a pH choice other than a random selection from a distribution. As such, this comparison emphasizes differences between using implicit temperature effects (i.e., the random selections from the elicited distribution) versus explicit incorporation of time-dependent thermal effects on the aqueous concentrations of Np, Pu, and Am in J-13-like water. (Direct comparisons are shown in Figures 6.3-21, 6.3-22, and 6.3-23 for the derived functions for Np, Pu, and Am solubility limits, respectively, versus the concentration ranges of their corresponding elicited distributions.)

100-realization, total-peak-dose CCDFs for 1,000,000 years are shown for the two solubility models in Figure 9.3-62. The different solubility models produce nearly identical peak doses (^{237}Np) at the accessible environment over the 1,000,000-year time frame. This is not unexpected if we review the linear regression analysis in Section 9.3.7, which shows very little dependency of the results on Np solubility, at least for the range of Np solubility in the elicited distribution (see Chapter 6). (The contribution to total peak dose from Am and Pu is negligible.)

9.3.7 Most Important Model Parameters

The objective in this section is to find the most important model parameters in the TSPA model over a 1,000,000-year time frame, using 1,000,000-year total peak dose as a performance measure. Thus, scatter plots of 1,000,000-year total peak dose versus given model parameters are presented to demonstrate visually any linear trends in the results. Also, three stepwise linear-regression analyses are performed, as described in Section 9.2.5. These analyses determine the percent of variability of the results which can be explained by sets of one or more model parameters. In the present section we two different scenarios are analyzed: 83 MTU/acre thermal load, backfill, and climate change (cyclical q_{inf} only) over the *high* q_{inf} range and 83 MTU/acre thermal load, backfill, and climate change (cyclical q_{inf} only) over the *low* q_{inf} range. Similarly to Section 9.2.5, for each type of regression the five most important independent parameters were recorded (Tables 9.3-1 and 9.3-2), as well as the amount of the variability they explain.

For both the low- q_{inf} and high- q_{inf} scenarios, the $\ln(P.M.)$ vs. $\ln(x)$ fit is much better than the $\ln(P.M.)$ vs. x fit. For example, for low q_{inf} , the $\ln(P.M.)$ vs. $\ln(x)$ fit explains 89% of the variance using ranked parameter #1, while the $\ln(P.M.)$ vs. x fit only explains 49% of the variance (Table 9.3-2). Also, both fits are much better for the low- q_{inf} case than the high- q_{inf} case, e.g., the $\ln(P.M.)$ vs. $\ln(x)$ fit explains 97% of the variance using ranked parameters #1 and #2 for low q_{inf} (Table 9.3-2), but only 85% of the variance for high q_{inf} when using ranked parameters #1 through #5 (Table 9.3-1).

The most important difference between the analysis in Section 9.2.5 for 10,000-year performance and the analysis in this section for 1,000,000-year performance is that over the 1,000,000-year time frame, dilution in the saturated zone (i.e., q_{SZ}) is the most important parameter, whereas over the 10,000-year time span a UZ parameter ($v_{mat}-CHnv$) was the most important. An explanation of this difference is that the breakthrough of the dose peak has generally occurred within the 1,000,000-year time period (i.e., the engineered and natural barriers are not predicted to isolate the bulk of the waste from the accessible environment over that time period), so that the only model parameter of importance is how much the waste mass has been diluted (or how much it has decayed); whereas, for 10,000 years only the leading edge of the breakthrough curve has arrived at the accessible environment, so a change in an important UZ parameter can significantly shift this steeply rising portion of the breakthrough curve (see Section 9.2.5).

Over 1,000,000 years for the low- q_{inf} scenario, q_{SZ} is the overwhelming parameter of importance, explaining 89% of the variance by itself (in the $\ln(P.M.)$ vs. $\ln(x)$ regression). For the high q_{inf} scenario, q_{SZ} is also the most important, but explains only about 48% of the variability (in the $\ln(P.M.)$ vs. $\ln(x)$ regression). q_{SZ} explains more of the variance in the low- q_{inf} case because of its greater effect on dilution at low values of the UZ flux. The strong effect of q_{SZ} is clearly visible on the scatter plots for both q_{inf} scenarios, Figures 9.3-63 and 9.3-70.

As with 10,000-year performance, the UZ flux (q_{inf}) also influences the results, although much less so in the low- q_{inf} case, where a linear trend on the scatter plot (Figure 9.3-75) is not really discernible. Thus, beyond the first ranked variable (q_{SZ}), no visual linear trends are discernible on the scatter plots for the low- q_{inf} case (Figures 9.3-75 to 9.3-80). However, for the high- q_{inf} case (Figures 9.3-63 to 9.3-69), a visual linear trend is also apparent for ranked parameter #2 (q_{inf} in Figure 9.3-64). Beyond that, one would have to fit the residuals to the parameters in order to discern a linear trend, as described in Section 9.2.5.

As discussed in Section 9.2.5, for TSPA-1995 some of the stochastic distributions for parameters have been eliminated and replaced by sensitivity analyses, which are conducted for only three or four values of the given parameter. Thus, the analyses in Sections 9.2.5 and 9.3.7 do not include such parameters in the importance rankings, even though they could be more important than the ranked parameters. An example of this is the fracture/matrix particle transition parameter, λ . A more important example is q_{inf} , which is equivalent in TSPA-1995 to the mean UZ percolation flux at repository depth. In particular, q_{inf} has been separated into two ranges, or sensitivity cases. Within each range, we have included q_{inf} in the stepwise linear regression, but its importance has been much reduced compared to if we had constructed 100-realization CCDFs over the entire q_{inf} range from 0.01-2.0 mm/yr, as shown in Figure 9.3-37. Thus, q_{SZ} is the #1 ranked parameter. However, if stepwise linear regression is performed on the results represented by the middle curve in Figure 9.3-37, then q_{inf} becomes the #1 ranked parameter and

q_{sz} becomes the #2 ranked parameter. This is shown in Table 9.3-3, and demonstrates the clear importance of defining the percolation flux in the unsaturated zone. Of course, it is actually the ratio of q_{inf} (i.e., q_{UZ}) to q_{sz} that determines dilution in the saturated zone, so this again points out that over the 1,000,000-year time frame, it is primarily dilution that controls peak dose at the accessible environment.

9.3.8 Summary of 1,000,000-year Performance

The following general conclusions can be drawn about 1,000,000-year repository performance from the sensitivity analyses in Section 9.3:

(1) 1,000,000-year total peak dose, due mainly to ^{129}I over the low infiltration range ($q_{inf} = 0.01 - 0.05$ mm/yr) and to ^{237}Np over the high infiltration range ($q_{inf} = 0.5 - 2.0$ mm/yr), is most sensitive to the following model parameters: (i) dilution in the saturated zone (or equivalently, the saturated-zone bulk Darcy flux, q_{sz}), and (ii) percolation flux in the unsaturated zone (where the mean UZ percolation flux equals the infiltration flux, q_{inf});

(2) 1,000,000-year total peak dose may be greatly reduced by a barrier that intercepts dripping water on the waste packages (the capillary-barrier effect), i.e., diffusion-only (no advection) through the WP/EBS produce extremely low doses at the accessible environment;

(3) Low intra-unit fracture connectivity in the unsaturated zone (i.e., high Poisson transition rate in the RIP model) can delay peak doses significantly, but can only slightly reduce the peak dose that occurs during the 1,000,000-year time frame after repository closure (a similar conclusion applies to matrix diffusion);

(4) Alternative thermal loads, alternative thermohydrologic models for the near-field, and alternative corrosion-initiation models (including cathodic protection) do not have a very large effect on the peak dose that occurs during the 1,000,000-year time span (a factor of three is about the largest effect);

(5) Over 1,000,000 years, climate change with water table rise can increase peak dose at the accessible environment by a factor of about 2 to 10 compared to no change in climate; climate change without water table rise (varying infiltration rate only) falls in between these two extremes.

9.4 SUBSYSTEM PERFORMANCE

Another important aspect of the TSPA analysis is to determine the ability of various *parts* of the system, both engineered and natural, to contain or retard the transport of the waste. To evaluate the containment capability of these various subsystems, cumulative (but not normalized) expected-value releases were calculated for a particular case (83 MTU/acre, with backfill, "high" $q_{inf} = 1.25$ mm/yr initially, and cyclical q_{inf} due to climate change) at various times (10,000, 100,000, and 1,000,000 years) at the following locations:

1. From the engineered barrier system (EBS),
2. From the base of the repository-level formation (TSw),

3. From the base of the unsaturated zone (PPn), and
4. At the accessible environment (AE).

Results are presented in Table 9.4-1 and in Figures 9.4-1 to 9.4-5 for total release, ^{99}Tc release, ^{129}I release, ^{237}Np release, and ^{229}Th release (assuming radionuclide decay throughout the simulations). Generally, the saturated zone does not act as a significant containment barrier as evidenced by the releases at the base of the unsaturated zone and at the accessible environment being nearly identical. For the total release (Figure 9.4-1), the TSw barrier provides nearly an order-of-magnitude reduction in the radioactivity released from the EBS at 10^6 years. An additional 7 times decrease in radioactivity released at 10^6 years is provided by the combination of the other natural barriers (TSv, CHnv, and CHnz).

For the cumulative release of the nonsorbing nuclides ^{99}Tc and ^{129}I (Figures 9.4-2 and 9.4-3), the containment provided by the various subsystems, and combinations thereof, is about the same at times greater than approximately 100,000 years. This is because the nonsorbing nuclides have a relatively rapid travel time, so most of their mass has already passed through the entire system (i.e., all subsystems) after 100,000 years have transpired, whereas between 10,000 and 100,000 years much of their mass is still travelling within the UZ.

For ^{237}Np release (Figure 9.4-4), the individual natural barriers, and combinations thereof (primarily the UZ), provide additional reduction of radioactivity compared to the EBS, up to and slightly beyond 1,000,000 years. This is supported by Figure 9.3-17, which shows that there is still a significant amount of ^{237}Np in the system at 1,000,000 years. ^{229}Th releases (Figure 9.4-5) provide a look at the impact of radioactive in-growth of a sorbing species, where the number of curies released from the EBS is actually less than the release at the other three locations (TSw, PPn, and AE) after 1,000,000 years because there is a source of ^{229}Th production within the unsaturated zone (i.e., decay of ^{237}Np). This is proven by Figure 9.4-6, which is the same as Figure 9.4-5, except with decay turned off. In this no-decay case, each of the successive barriers acts to reduce ^{229}Th releases further.

Table 9.2-1 - Regression statistics for 10,000-year normalized cumulative release, 83 MTU/acre, high- q_{inf} range (0.5-2.0 mm/year), with backfill and climate change (no water-table rise)

Parameter	rank (P.M.) ¹ vs. rank (x)		ln (P.M.) vs. x		ln (P.M.) vs. ln (x)	
	Rank Importance	% of variance explained ²	Rank Importance	% of variance explained ²	Rank Importance	% of variance explained ²
$U_{dl}(1,3)$	4	87	3	68	3	72
Np K_d (TSw, PPn)						
Np K_d (SZ)						
Np K_d (TSv, CHnv)			5	70	5	76
Np K_d (CHnz)						
ϕ_{TSw}						
ϕ_{TSv}						
ϕ_{CHnv}						
ϕ_{CHnz}						
Q_{SZ}	3	84	4	69	4	75
Sol Np						
Sol Tc						
Sol Th						
WP f_{drip} ³						
Q_{drip}						
f_{fnc} CHnv	2	80	2	63		
v_{max} CHnv	1	60			1	50
f_{fnc} CHnz	5	89				
v_{max} CHnz						
Q_{inf} (UZ)			1	45	2	68
A_{wp} (DHLW)						
f_{fnc} TSv						
v_{max} TSv						
f_{fnc} TSw						
v_{max} TSw						

¹ P.M. = performance measure

² % of variance explained by parameters ranked less than or equal to the given parameter, e.g., for parameter with rank 3, the % variance listed is for parameters ranked 1, 2, and 3.

³ fraction of waste packages with drips

Table 9.2-2 . Regression statistics for 10,000-year total peak dose, 83 MTU/acre, high- q_{inf} range (0.5-2.0 mm/year), with backfill and climate change (no water-table rise)

Parameter	rank (P.M.) ¹ vs. rank (x)		ln (P.M.) vs. x		ln (P.M.) vs. ln (x)	
	Rank Importance	% of variance explained ²	Rank Importance	% of variance explained ²	Rank Importance	% of variance explained ²
$U_{d,1,3}$	3	81	3	67	3	71
Np K_d (TSw, PPn)						
Np K_d (SZ)						
Np K_d (TSv, CHnv)					4	72
Np K_d (CHnz)						
ϕ_{TSw}						
ϕ_{TSv}						
ϕ_{CHnv}						
ϕ_{CHnz}						
Q_{sz}						
Sol Np						
Sol Tc						
Sol Th						
WP f_{drip} ³						
Q_{drip}						
f_{frc} CHnv	2	78	2	62		
v_{mat} CHnv	1	58			1	48
f_{frc} CHnz	4	84	4	69		
v_{mat} CHnz						
Q_{inf} (UZ)			1	45	2	67
A_{wp} (DHLW)						
f_{frc} TSv			5	71		
v_{mat} TSv	5	87				
f_{frc} TSw					5	73
v_{mat} TSw						

¹ P.M. = performance measure

² % of variance explained by parameters ranked less than or equal to the given parameter, e.g., for parameter with rank 3, the % variance listed is for parameters ranked 1, 2, and 3.

³ fraction of waste packages with drips

Table 9.3-1.. Regression statistics for 1,000,000-year total peak dose, 83 MTU/acre, high- q_{inf} range (0.5 - 2.0 mm/yr), with backfill and climate change (no water-table rise)

Parameter	rank (P.M.) ¹ vs. rank (x)		ln (P.M.) vs. x		ln (P.M.) vs. ln (x)	
	Rank Importance	% of variance explained ²	Rank Importance	% of variance explained ²	Rank Importance	% of variance explained ²
$U_{crit}(1,3)$	4	82	3	53	4	81
$N_p K_d$ (TSw, PPn)						
$N_p K_d$ (SZ)						
$N_p K_d$ (TSv, CHnv)						
$N_p K_d$ (CHnz)						
ϕ_{TSw}						
ϕ_{TSv}						
ϕ_{CHnv}						
ϕ_{CHnz}						
q_{sz}	1	55	1	23	1	48
Sol N_p						
Sol T_c						
Sol T_h						
WP f_{drip} ³						
q_{drip}						
f_{enc} CHnv						
v_{enc} CHnv						
f_{enc} CHnz						
v_{enc} CHnz						
q_{inf} (UZ)	2	70	2	45	2	65
A_{wp} (DHLW)						
f_{enc} TSv	5	84	5	62		
v_{enc} TSv					5	85
f_{enc} TSw					3	75
v_{enc} TSw	3	78	4	60		

¹ P.M. = performance measure

² % of variance explained by parameters ranked less than or equal to the given parameter, e.g., for parameter with rank 3, the % variance listed is for parameters ranked 1, 2, and 3.

³ fraction of waste packages with drips

Table 9.3-2 . Regression statistics for 1,000,000-year total peak dose, 83 MTU/acre, low- q_{inf} range (0.01–0.05 mm/yr), with backfill and climate change (no water-table rise)

Parameter	rank (P.M.) ¹ vs. rank (x)		ln (P.M.) vs. x		ln (P.M.) vs. ln (x)	
	Rank Importance	% of variance explained ²	Rank Importance	% of variance explained ²	Rank Importance	% of variance explained ²
$U_{d1}(1,3)$			3	57		
Np K_d (TSw, PPn)						
Np K_d (SZ)						
Np K_d (TSv, CHnv)			4	60		
Np K_d (CHnz)						
ϕ_{TSw}						
ϕ_{TSv}						
ϕ_{CHnv}						
ϕ_{CHnz}						
q_{sz}	1	89	1	49	1	89
Sol Np						
Sol Tc						
Sol Th						
WP f_{drip} ³						
q_{drip}						
f_{frac} CHnv						
v_{max} CHnv						
f_{frac} CHnz			5	62		
v_{max} CHnz	2	95			2	97
q_{inf} (UZ)			2	55		
A_{wp} (DHLW)						
f_{frac} TSv						
v_{max} TSv						
f_{frac} TSw						
v_{max} TSw	3	97			3	98

¹ P.M. = performance measure

² % of variance explained by parameters ranked less than or equal to the given parameter, e.g., for parameter with rank 3, the % variance listed is for parameters ranked 1, 2, and 3.

³ fraction of waste packages with drips

Table 9.3-3. Regression statistics for 1,000,000-year total peak dose, 83 MTU/acre, entire- q_{inf} range (0.01-2.0 mm/yr), with backfill and climate change (no water-table rise)

Parameter	rank (P.M.) ¹ vs. rank (x)		ln (P.M.) vs. x		ln (P.M.) vs. ln (x)	
	Rank Importance	% of variance explained ²	Rank Importance	% of variance explained ²	Rank Importance	% of variance explained ²
$U_{ch}(1,3)$	4	86	3	78	5	88
$N_p K_d$ (TSw, PPn)						
$N_p K_d$ (SZ)						
$N_p K_d$ (TSv, CHnv)			4	80		
$N_p K_d$ (CHnz)						
ϕ_{TSw}						
ϕ_{TSv}						
ϕ_{CHnv}						
ϕ_{CHnz}						
q_{sz}	2	81	2	75	2	74
Sol N_p	5	87				
Sol Tc						
Sol Th						
WP f_{drip} ³					3	83
q_{drip}						
f_{frac} CHnv						
v_{min} CHnv						
f_{frac} CHnz						
v_{min} CHnz						
q_{inf} (UZ)	1	46	1	64	1	50
A_{wp} (DHLW)						
f_{frac} TSv						
v_{min} TSv						
f_{frac} TSw			5	81		
v_{min} TSw	3	85			4	86

¹ P.M. = performance measure

² % of variance explained by parameters ranked less than or equal to the given parameter, e.g., for parameter with rank 3, the % variance listed is for parameters ranked 1, 2, and 3.

³ fraction of waste packages with drips

Table 9.4-1. Cumulative releases from various subsystems: Expected-value releases at various times for 83 MTU/acre thermal load, with backfill, $q_{\text{inf}} = 1.25$ mm/yr, and climate change (no water-table rise)

Year of Release (yrs)	RN	Release from EBS (Ci)	Release from TSw (Ci)	Release to SZ (Ci)	Release to AE (Ci)
10,000	Total	5.00×10^5	8.38×10^4	2.47×10^2	1.20×10^2
	^{129}I	1.59×10^3	2.97×10^2	1.15	5.62×10^{-1}
	^{237}Np	1.52×10^4	1.94×10^3	4.74×10^{-4}	7.86×10^{-5}
	^{99}Tc	3.26×10^5	6.09×10^4	2.34×10^2	1.14×10^2
	^{229}Th	2.51	3.68×10^{-1}	1.29×10^{-5}	3.59×10^{-7}
100,000	Total	2.32×10^6	6.94×10^5	3.07×10^5	3.07×10^5
	^{129}I	1.84×10^3	1.82×10^3	1.72×10^3	1.72×10^3
	^{237}Np	3.89×10^4	7.67×10^3	4.66×10^2	3.89×10^2
	^{99}Tc	3.76×10^5	3.44×10^5	3.04×10^5	3.03×10^5
	^{229}Th	2.13×10^2	3.41×10^2	4.06×10^1	1.90×10^1
1,000,000	Total	1.99×10^7	2.54×10^6	3.75×10^5	3.65×10^5
	^{129}I	1.84×10^3	1.84×10^3	1.84×10^3	1.84×10^3
	^{237}Np	3.89×10^4	3.23×10^4	2.60×10^4	2.58×10^4
	^{99}Tc	3.77×10^5	3.46×10^5	3.17×10^5	3.15×10^5
	^{229}Th	1.54×10^3	2.14×10^4	1.39×10^4	6.57×10^3

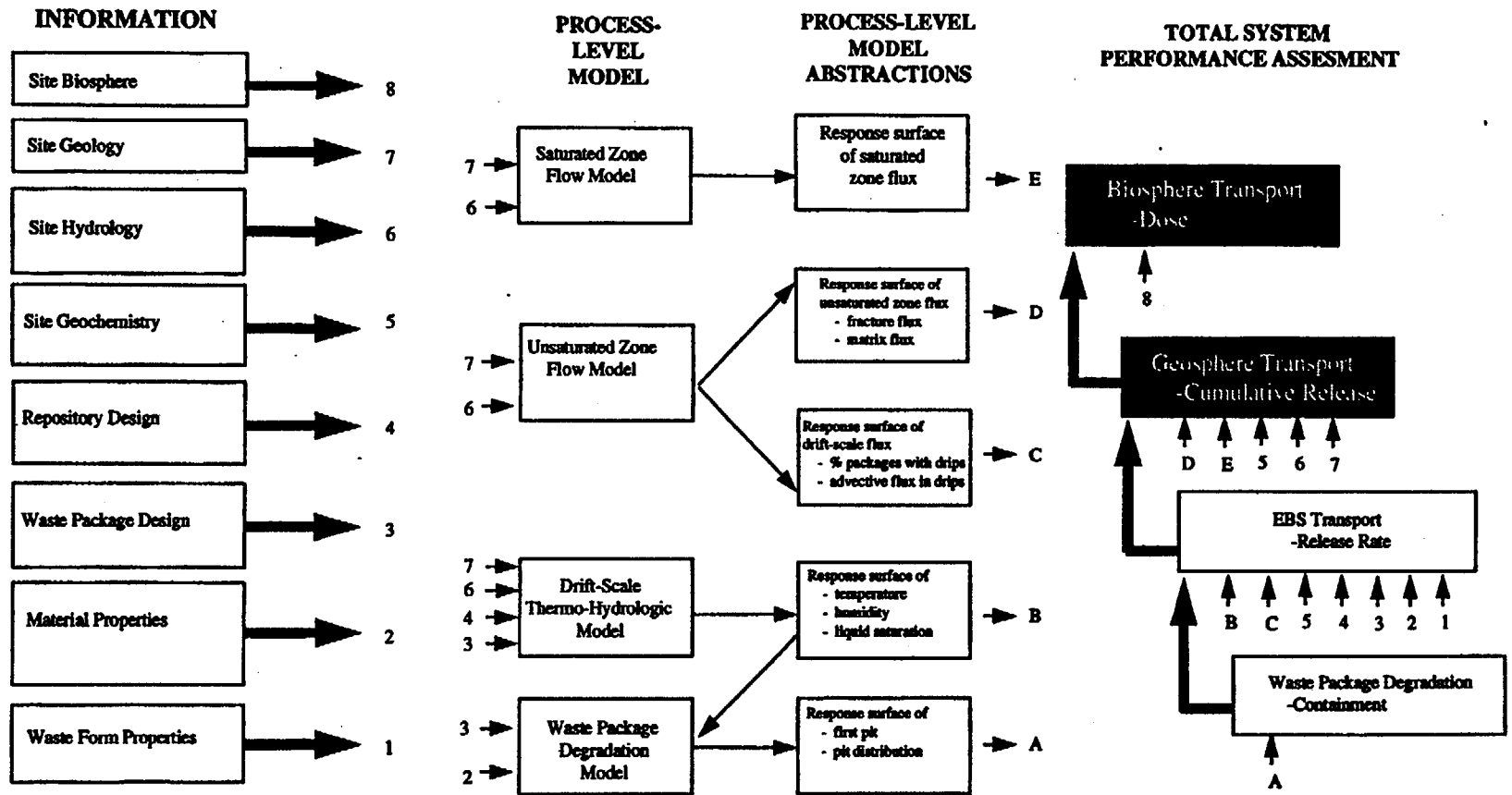


Figure 9.1-1 Relationship of Chapter 9 to the Overall Information Flow Diagram for TSPA 1995 (Figure 1.4-6).

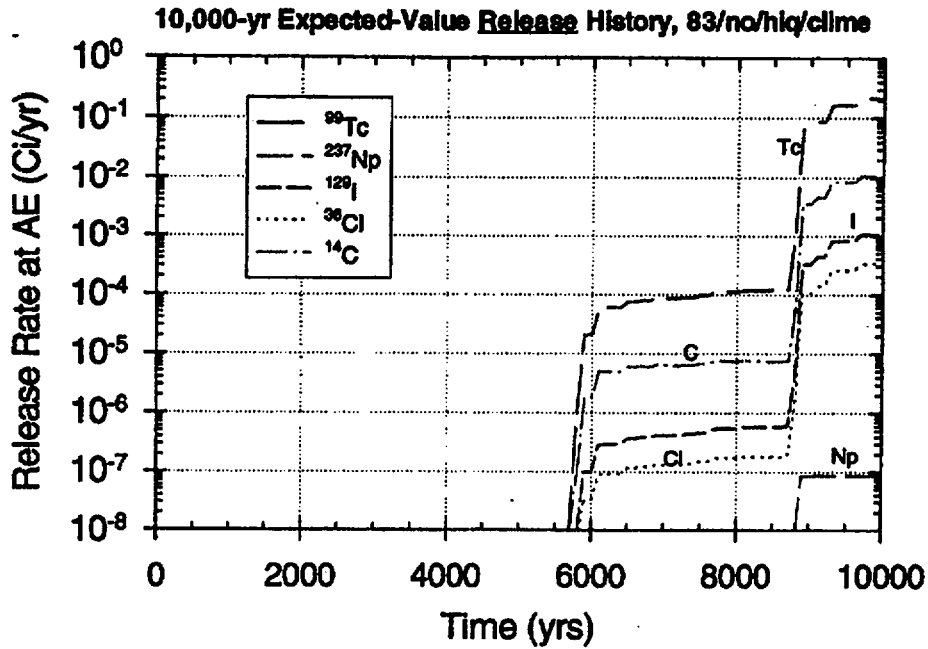


Figure 9.2-1 Expected-value release-rate history: 10,000 years, 83 MTU/acre, no backfill, high infiltration ($q_{\text{inf}} = 1.25$ mm/yr).

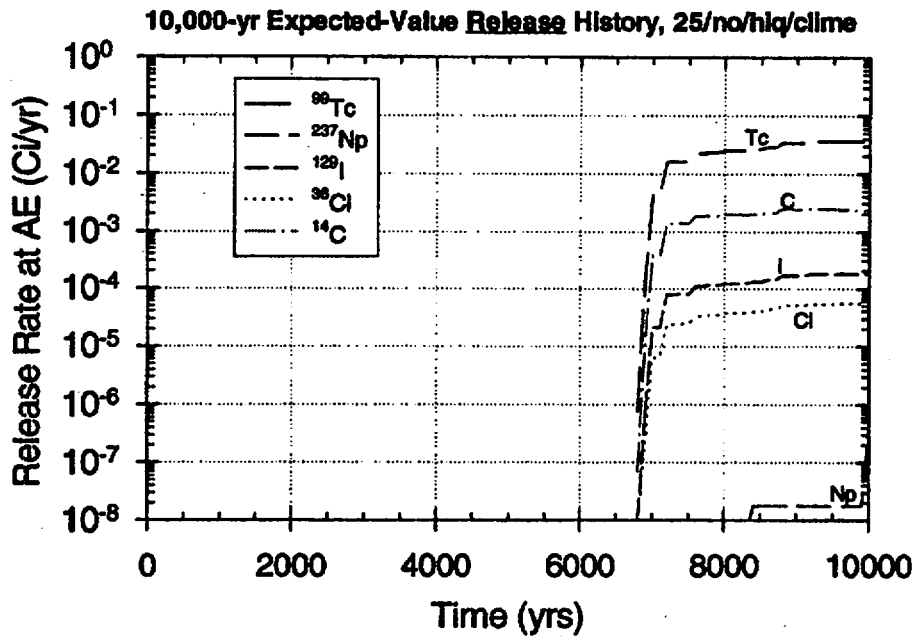


Figure 9.2-2 Expected-value release-rate history: 10,000 years, 25 MTU/acre, no backfill, high infiltration ($q_{\text{inf}} = 1.25$ mm/yr).

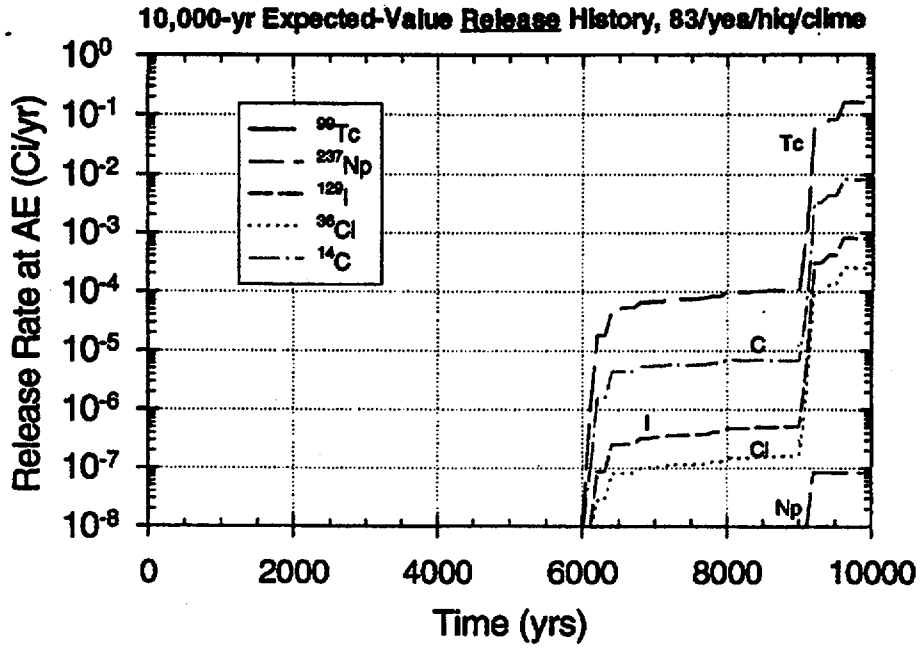


Figure 9.2-3 Expected-value release-rate history: 10,000 years, 83 MTU/acre, backfill ("yes"), high infiltration ($q_{inf} = 1.25$ mm/yr).

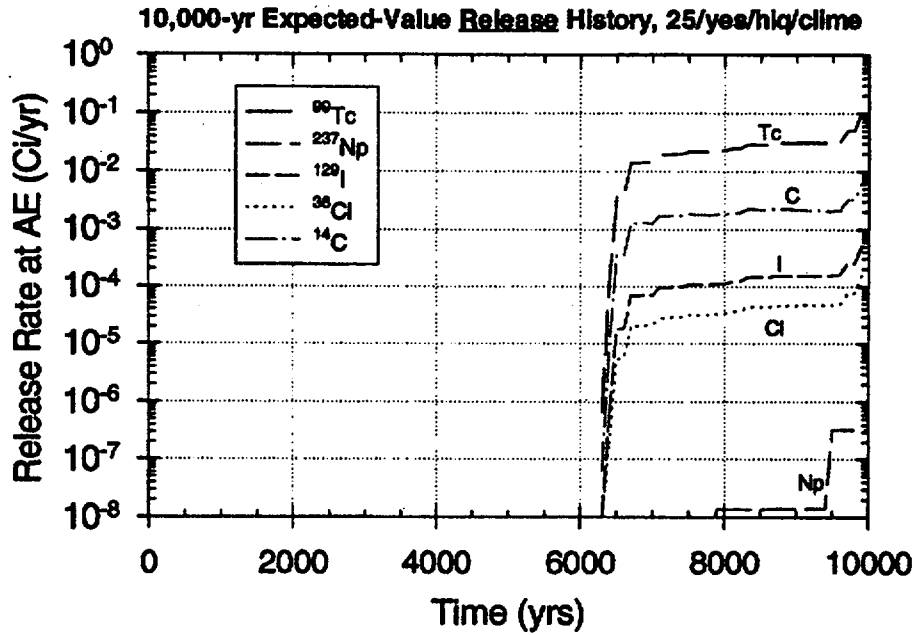


Figure 9.2-4 Expected-value release-rate history: 10,000 years, 25 MTU/acre, backfill ("yes"), high infiltration ($q_{inf} = 1.25$ mm/yr).

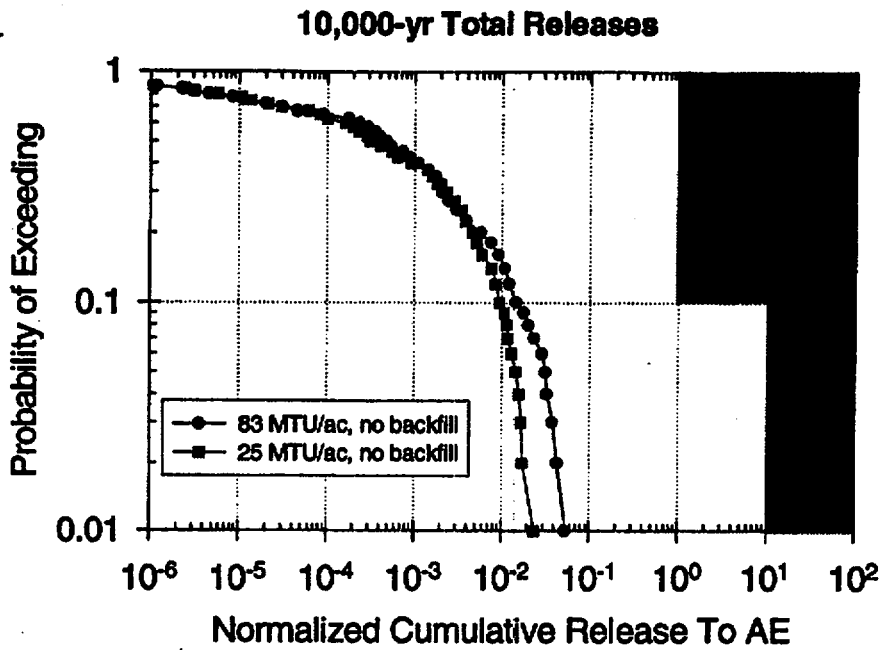


Figure 9.2-5 CCDF of Total Normalized Cumulative Release: 10,000 years, 83 MTU/acre and 25 MTU/acre, no backfill, high infiltration range.

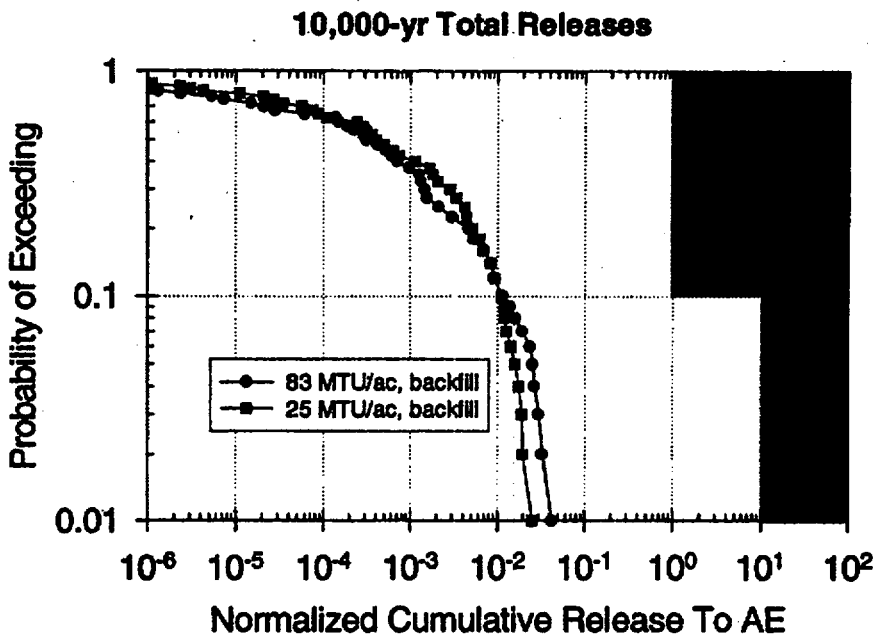


Figure 9.2-6 CCDF of Total Normalized Cumulative Release: 10,000 years, 83 MTU/acre and 25 MTU/acre, backfill, high infiltration range.

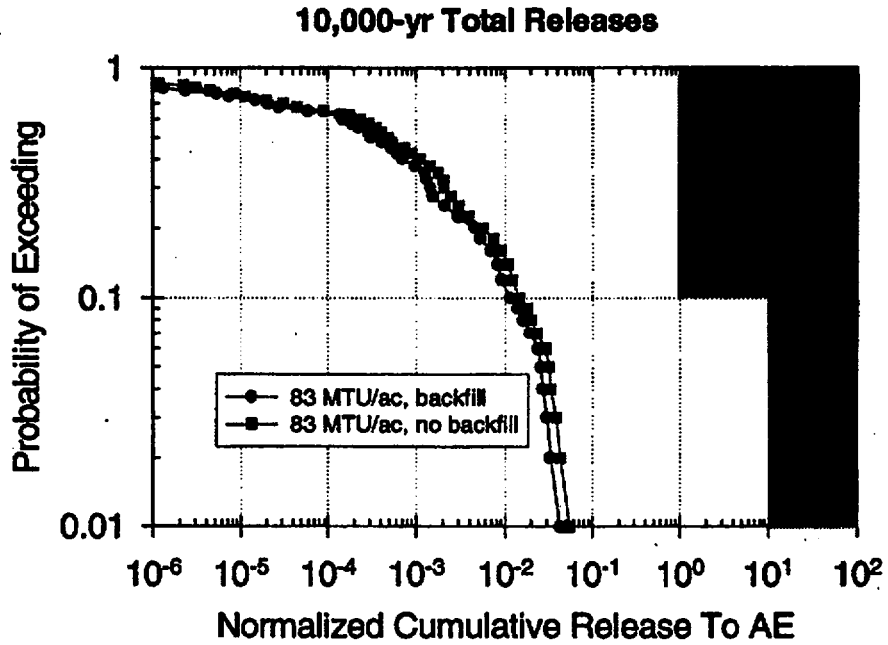


Figure 9.2-7 CCDF of Total Normalized Cumulative Release: 10,000 years, 83 MTU/acre, with and without backfill, high infiltration range.

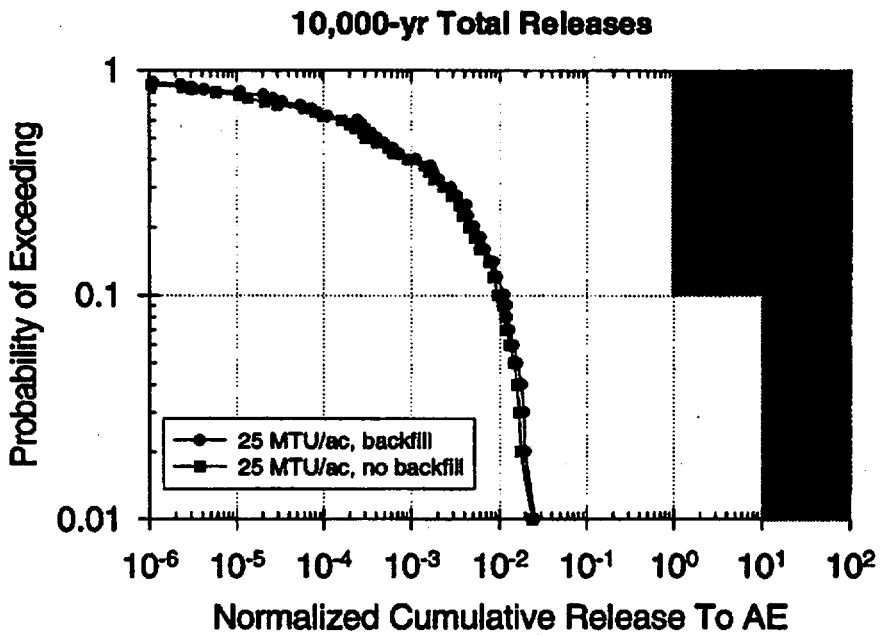


Figure 9.2-8 CCDF of Total Normalized Cumulative Release: 10,000 years, 25 MTU/acre, with and without backfill, high infiltration range.

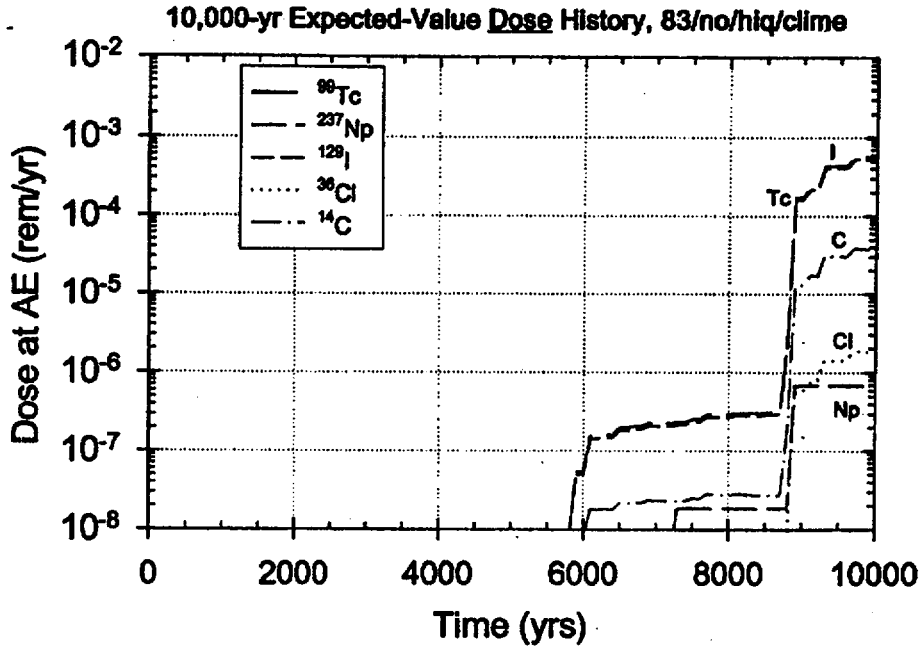


Figure 9.2-9 Expected-value dose history: 10,000 years, 83 MTU/acre, no backfill, high infiltration ($q_{\text{inf}} = 1.25$ mm/yr).

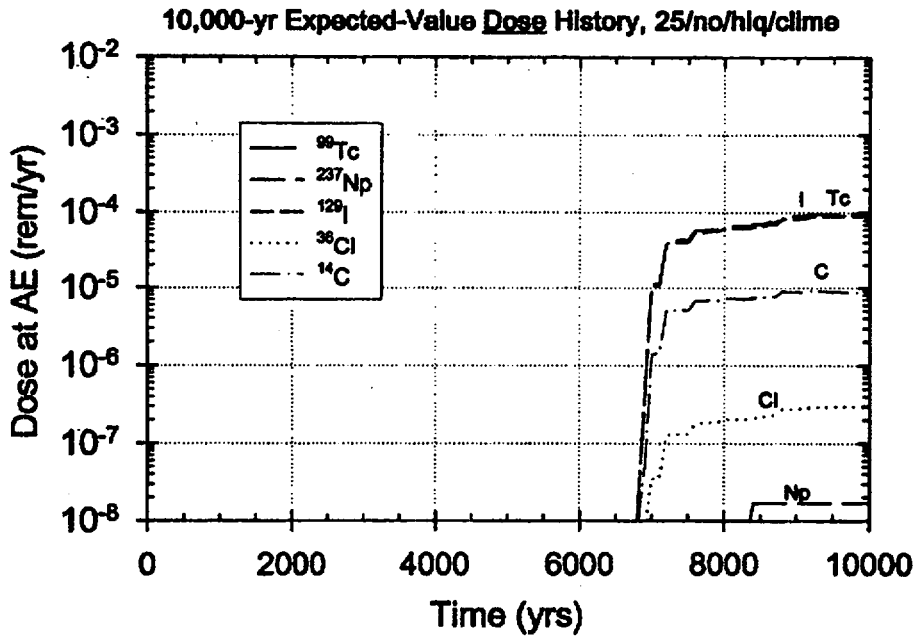


Figure 9.2-10 Expected-value dose history: 10,000 years, 25 MTU/acre, no backfill, high infiltration ($q_{\text{inf}} = 1.25$ mm/yr).

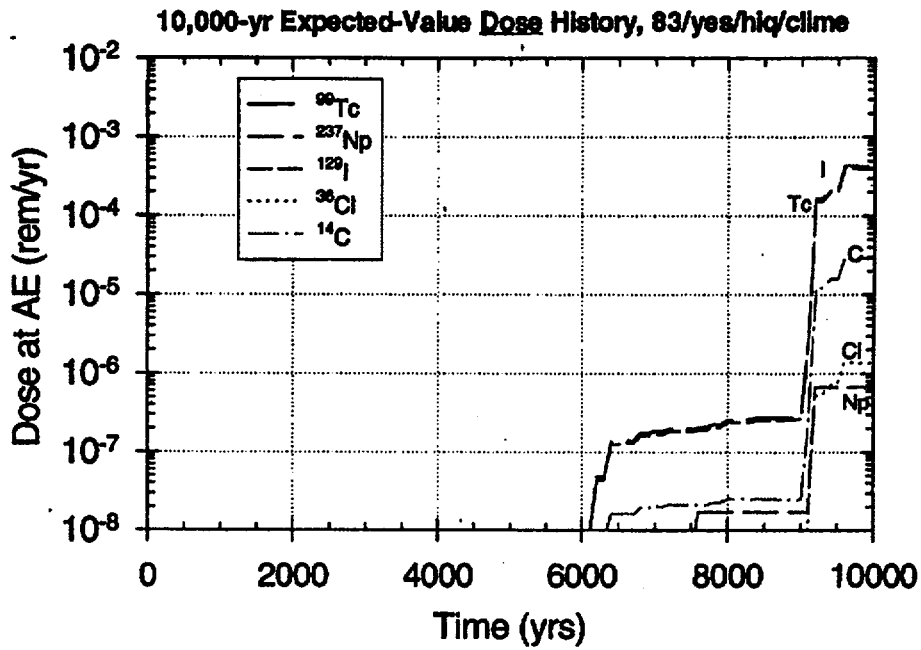


Figure 9.2-11 Expected-value dose history: 10,000 years, 83 MTU/acre, backfill ("yes"), high infiltration ($q_{inf} = 1.25$ mm/yr).

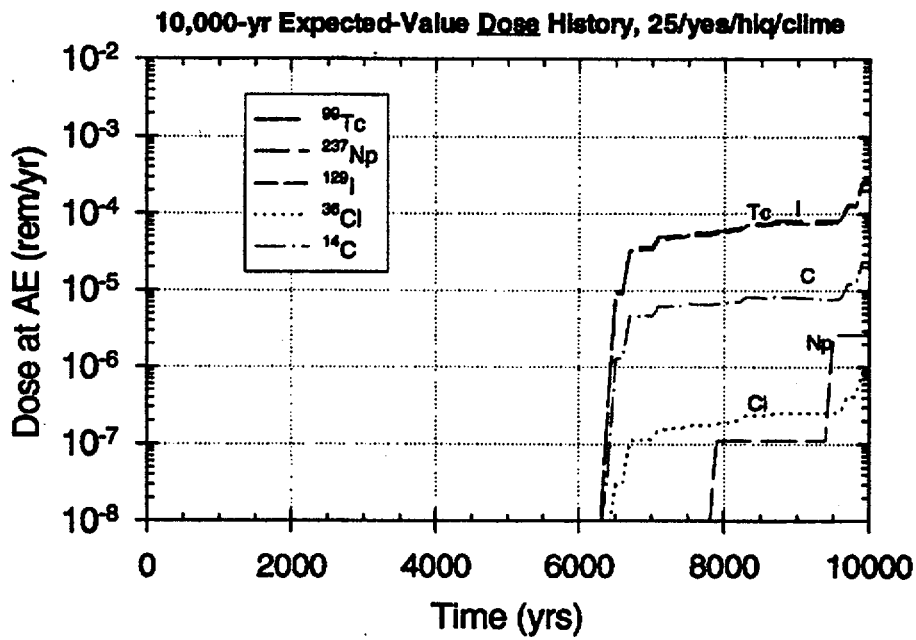


Figure 9.2-12 Expected-value dose history: 10,000 years, 25 MTU/acre, backfill ("yes"), high infiltration ($q_{inf} = 1.25$ mm/yr).

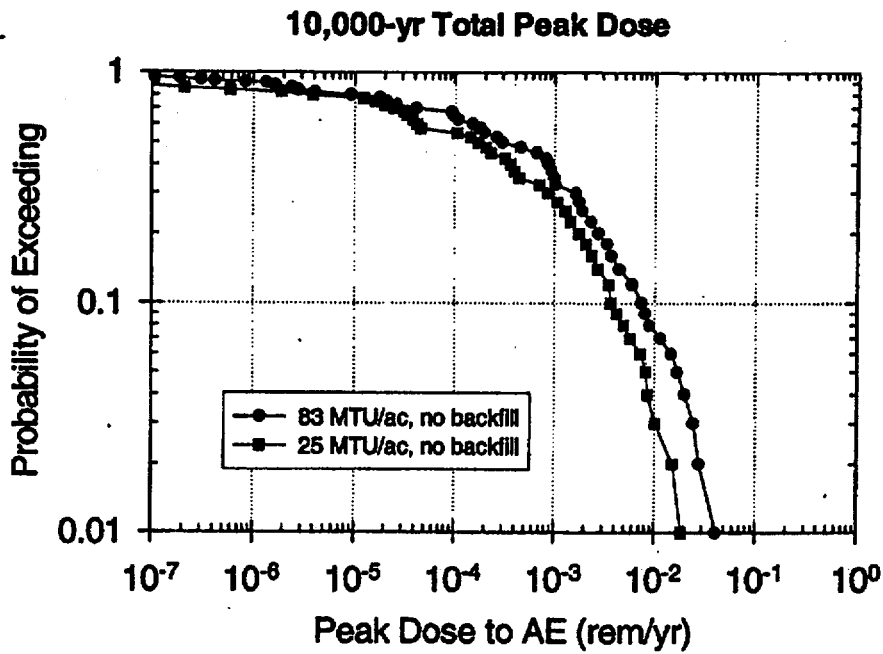


Figure 9.2-13 CCDF of Total Peak Dose: 10,000 years, 83 MTU/acre and 25 MTU/acre, no backfill, high infiltration range.

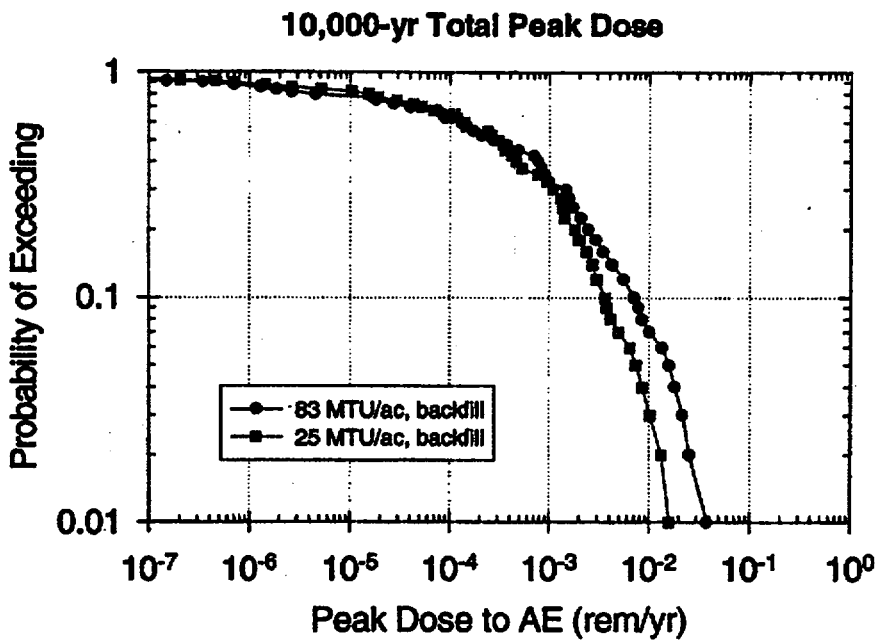


Figure 9.2-14 CCDF of Total Peak Dose: 10,000 years, 83 MTU/acre and 25 MTU/acre, backfill, high infiltration range.

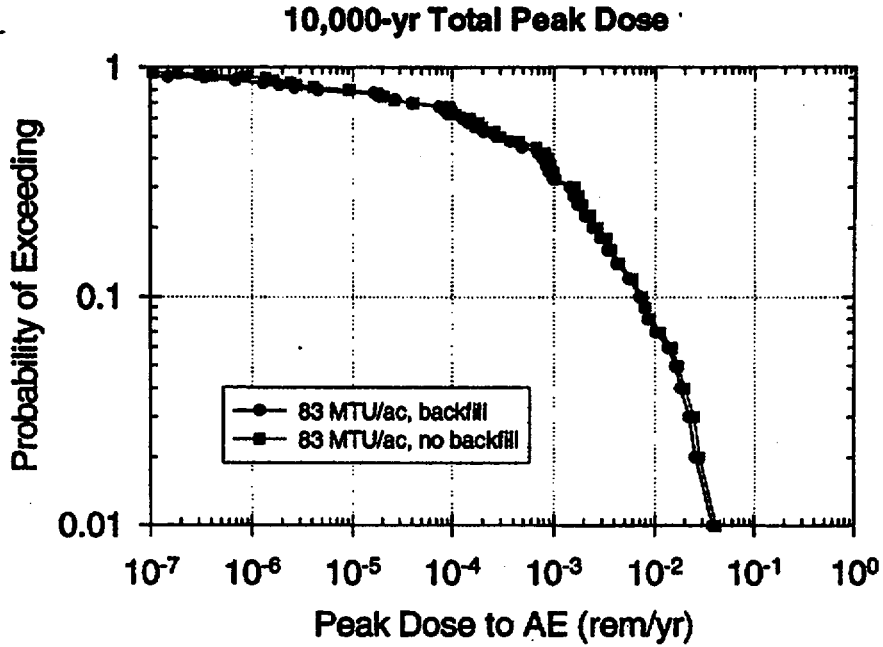


Figure 9.2-15 CCDF of Total Peak Dose: 10,000 years, 83 MTU/acre, with and without backfill, high infiltration range.

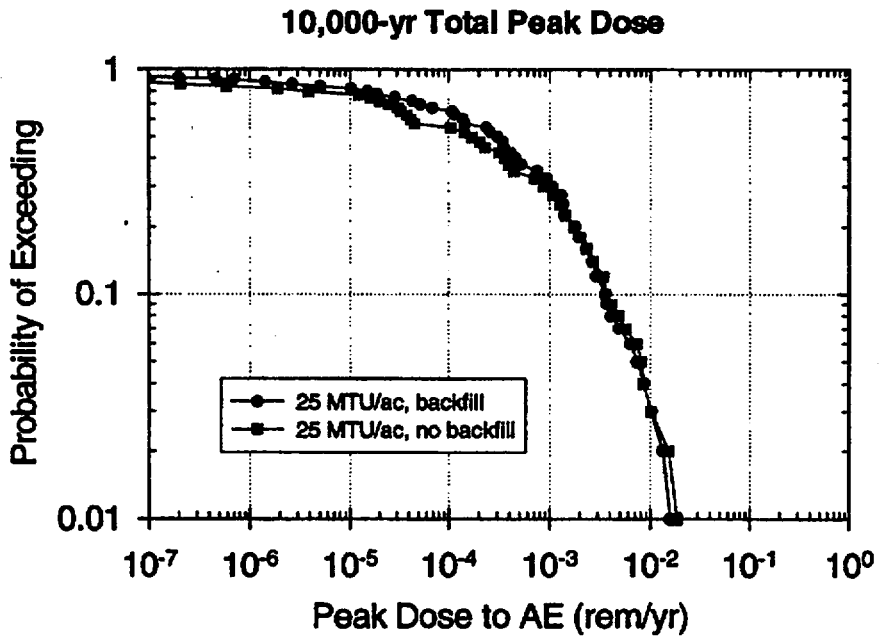


Figure 9.2-16 CCDF of Total Peak Dose: 10,000 years, 25 MTU/acre, with and without backfill, high infiltration range.

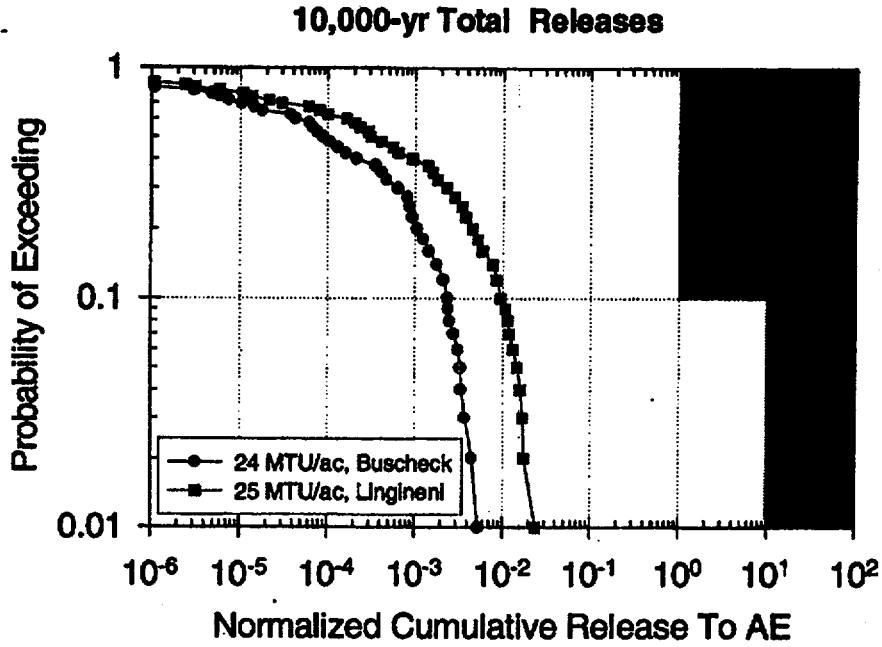


Figure 9.2-17 CCDF of Total Normalized Cumulative Release: 10,000 years, Buscheck 24 MTU/acre and Lingineni 25 MTU/acre, no backfill, high infiltration range.

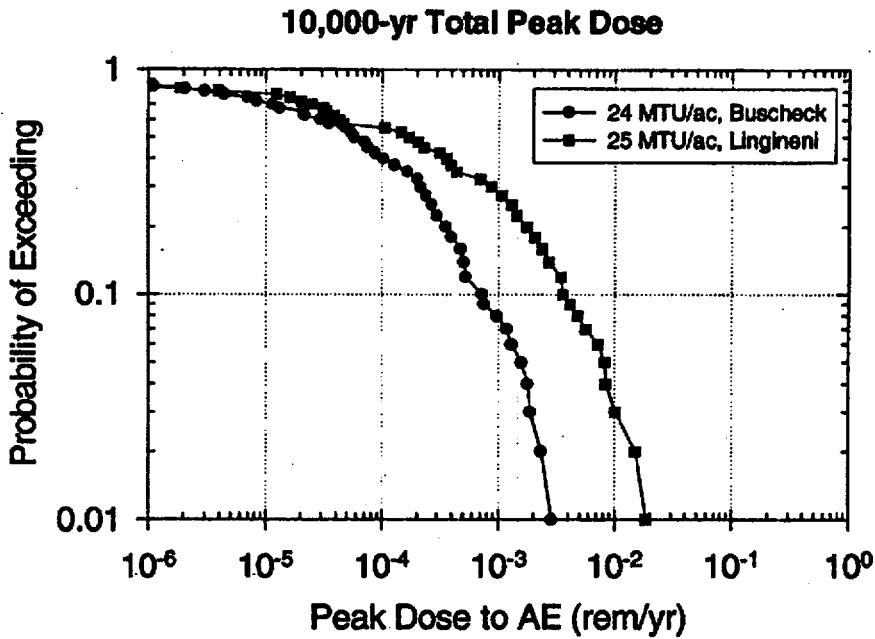


Figure 9.2-18 CCDF of Total Peak Dose: 10,000 years, Buscheck 24 MTU/acre and Lingineni 25 MTU/acre, no backfill, high infiltration range.

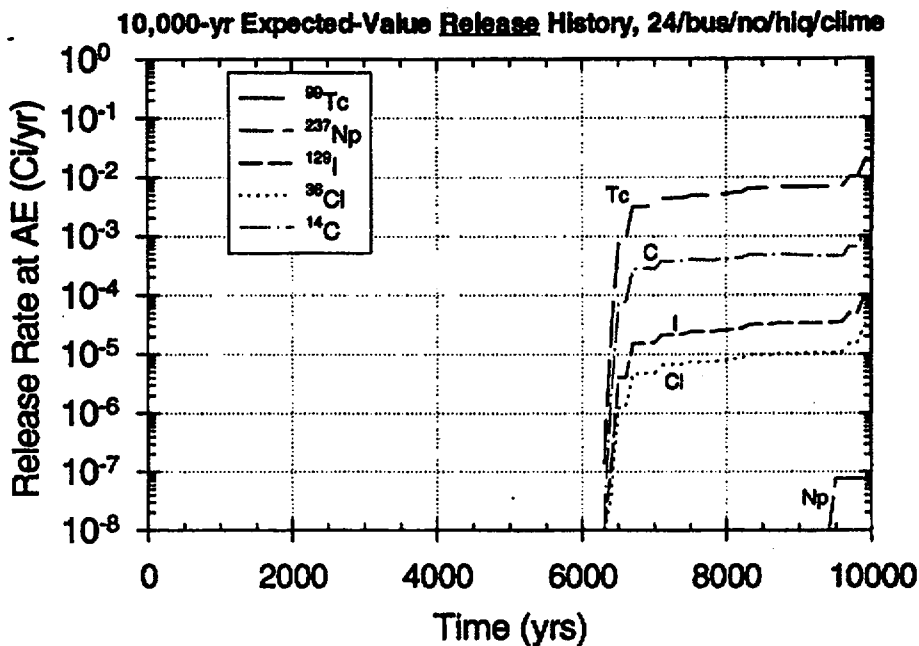


Figure 9.2-19 Expected-value release-rate history: 10,000 years, Buscheck 24 MTU/acre, no backfill, high infiltration ($q_{inf} = 1.25$ mm/yr).

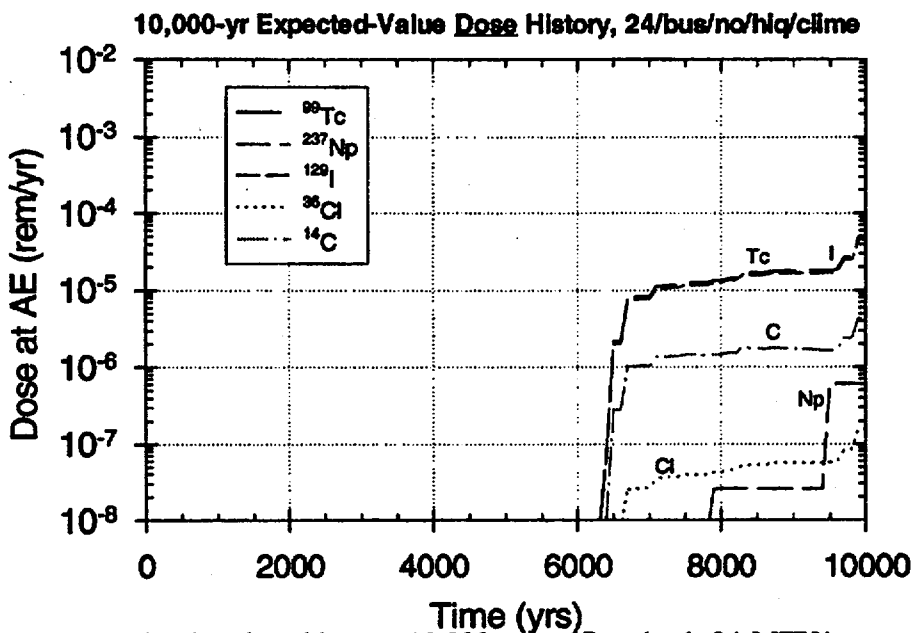


Figure 9.2-20 Expected-value dose history: 10,000 years, Buscheck 24 MTU/acre, no backfill, high infiltration ($q_{inf} = 1.25$ mm/yr).

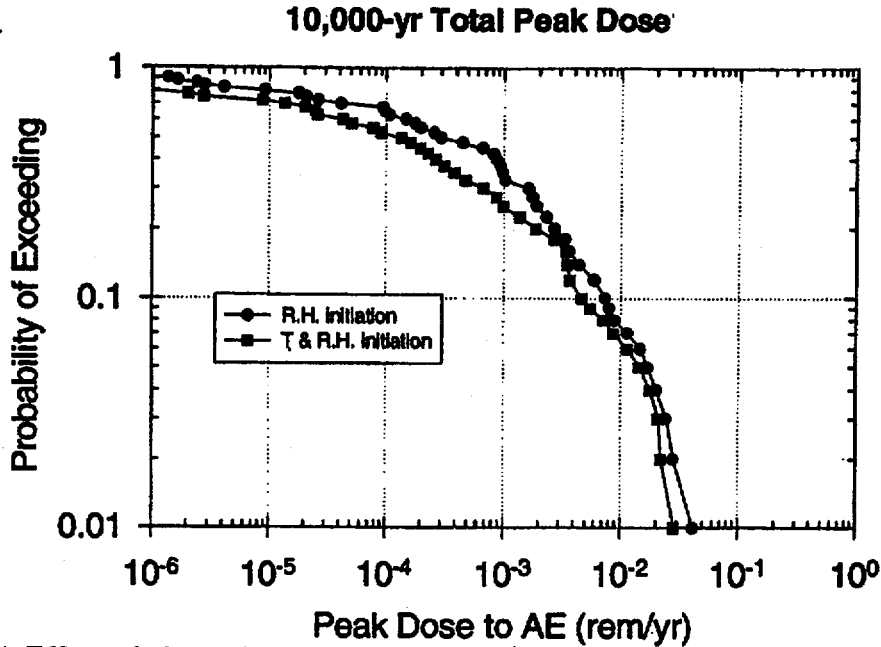


Figure 9.2-21 Effect of alternative corrosion initiation models: Relative humidity only vs. temperature and relative humidity. CCDF of Total Peak Dose: 10,000 years, 83 MTU/acre, no backfill, high infiltration range.

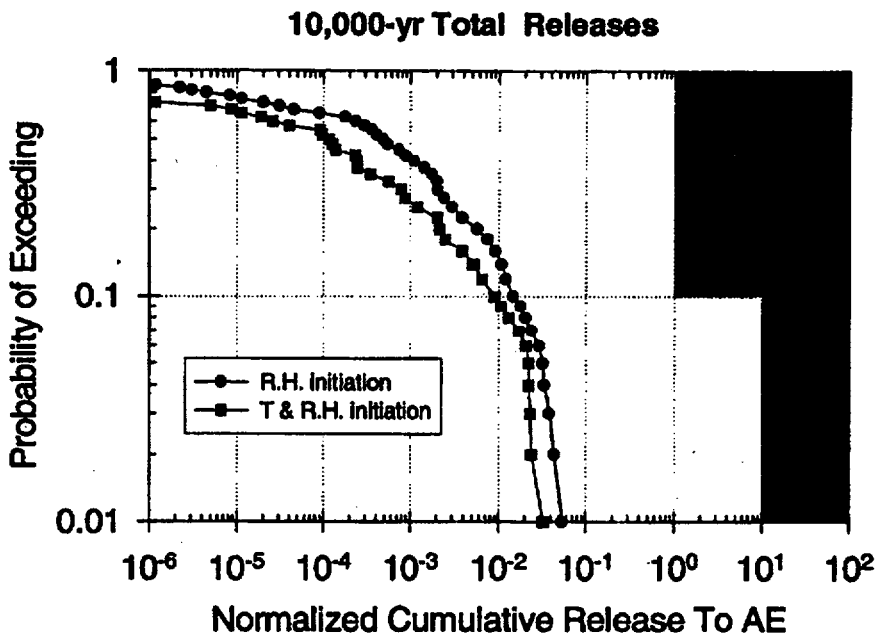


Figure 9.2-22 Effect of alternative corrosion initiation models: Relative humidity only vs. temperature and relative humidity. CCDF of Total Normalized Cumulative Release: 10,000 years, 83 MTU/acre, no backfill, high infiltration range.

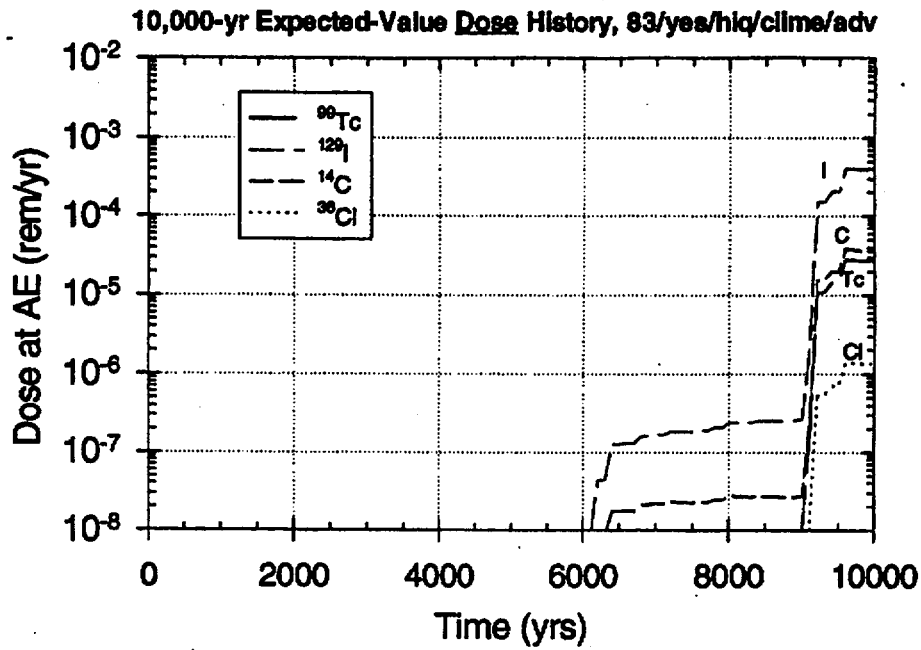


Figure 9.2-23 Expected-value dose history: 10,000 years, "drips-on-waste-container" EBS transport model, 83 MTU/acre, backfill, high infiltration ($q_{inf} = 1.25$ mm/yr).

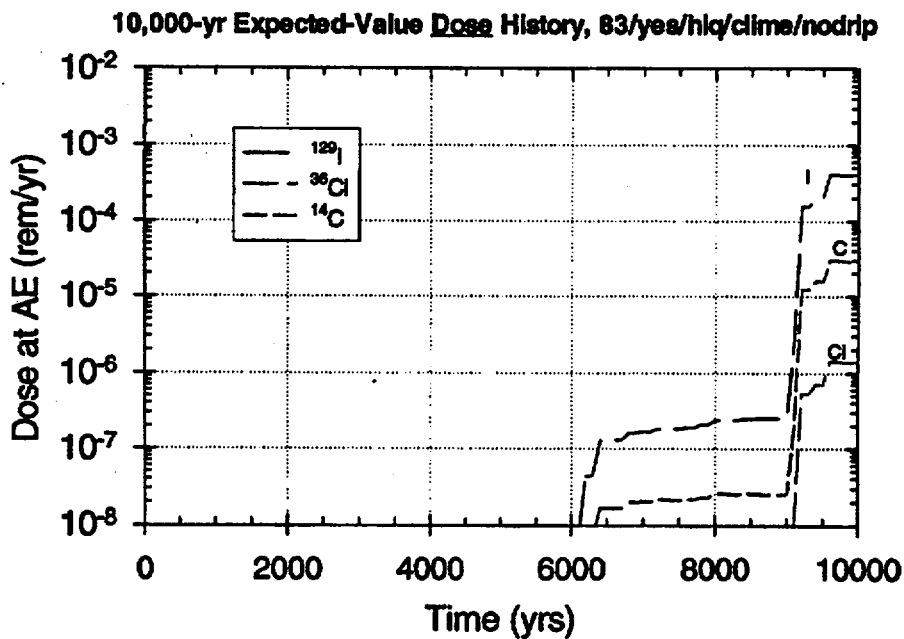


Figure 9.2-24 Expected-value dose history: 10,000 years, capillary-barrier-effect ("no drips") EBS transport model, 83 MTU/acre, backfill, high infiltration ($q_{inf} = 1.25$ mm/yr).

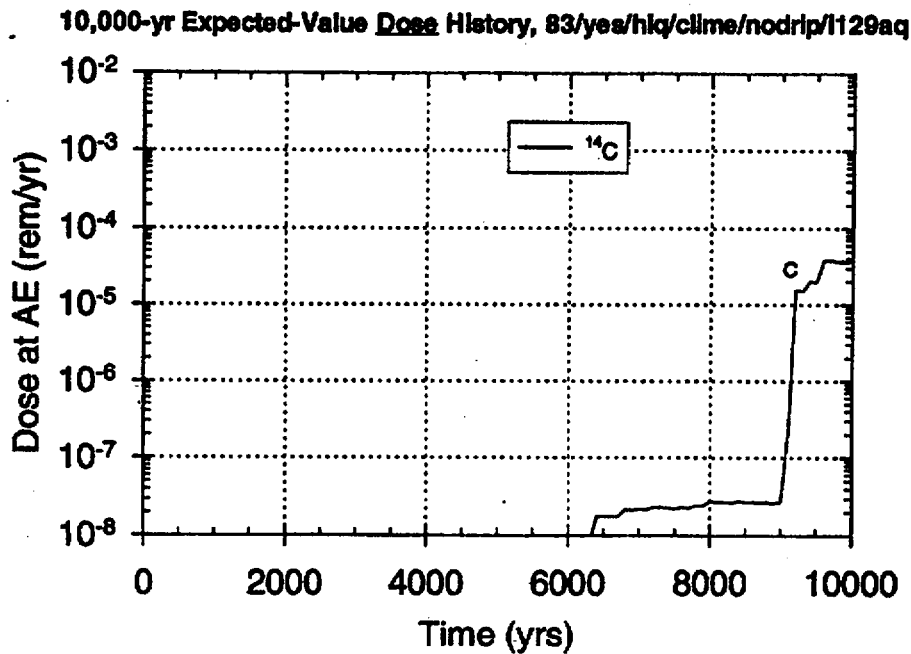


Figure 9.2-25 Expected-value dose history: 10,000 years, capillary-barrier-effect ("no drips") EBS transport model with ^{129}I and ^{36}Cl transported through EBS in the aqueous phase, 83 MTU/acre, backfill, high infiltration ($q_{\text{inf}} = 1.25 \text{ mm/yr}$).

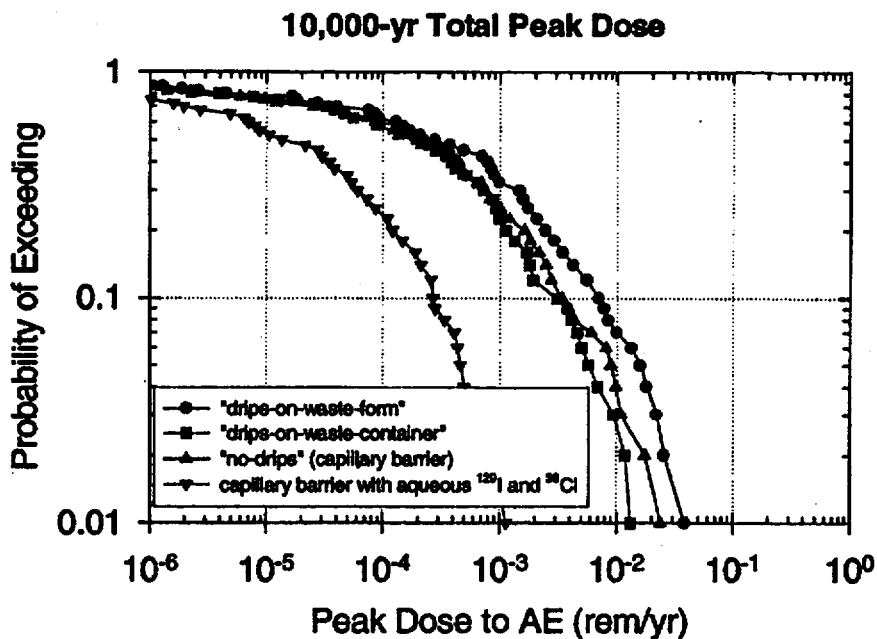


Figure 9.2-26 Comparison of EBS transport models. CCDF of Total Peak Dose: 10,000 years, 83 MTU/acre, backfill, high infiltration range.

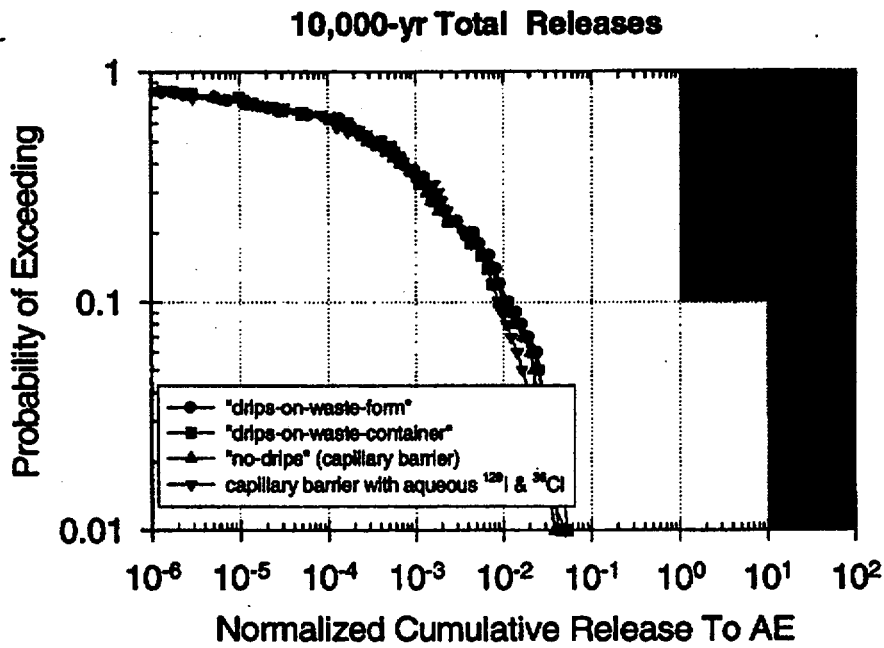


Figure 9.2-27 Comparison of EBS transport models. CCDF of Total Normalized Cumulative Release: 10,000 years, 83 MTU/acre, backfill, high infiltration range.

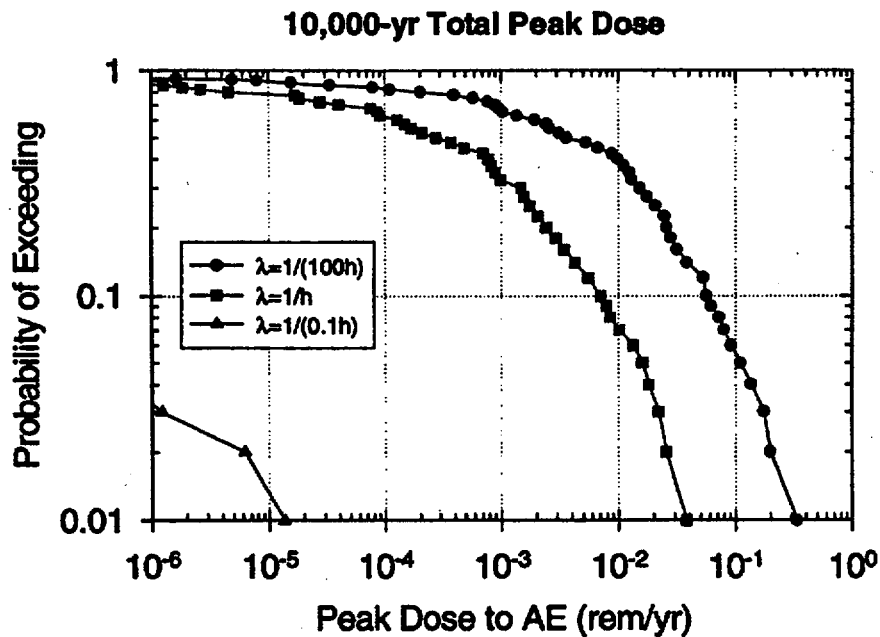


Figure 9.2-28 Comparison of intra-unit fracture connectivity parameter: $\lambda=1/(0.1 \text{ h})$ vs. $\lambda=1/h$ vs. $\lambda=1/(100 \text{ h})$, where h = pathway length in each unit. CCDF of Total Peak Dose: 10,000 years, 83 MTU/acre, backfill, high infiltration range.

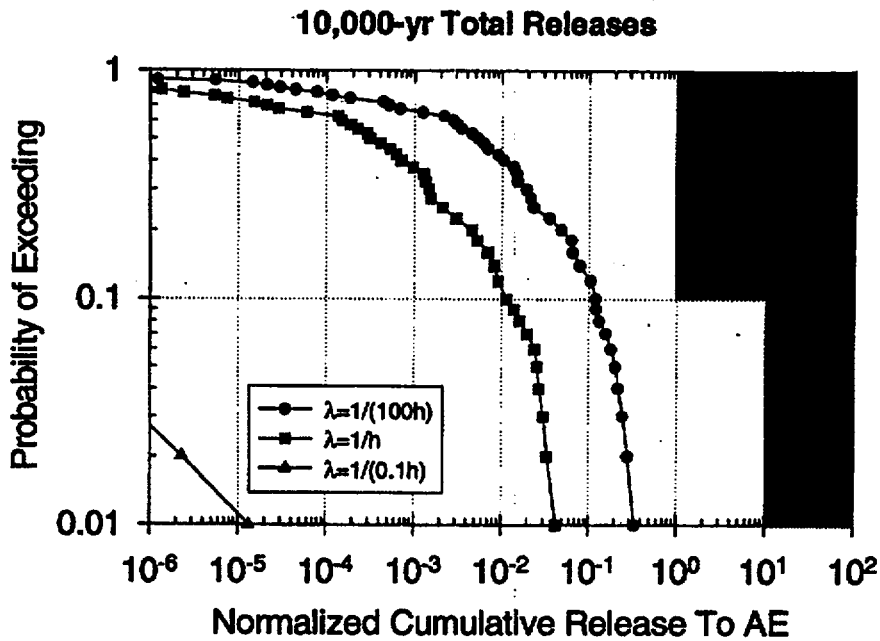


Figure 9.2-29 Comparison of intra-unit fracture connectivity parameter: $\lambda=1/(0.1 h)$ vs. $\lambda=1/h$ vs. $\lambda=1/(100 h)$, where h = pathway length in each unit. CCDF of Total Normalized Cumulative Release: 10,000 years, 83 MTU/acre, backfill, high infiltration range.

Figure 9.2-31 Scatter plot of 10,000-year total normalized cumulative release versus UZ percolation flux (mm/yr) for 83 MTU/acre, backfill, high infiltration ($q_{inf} = 1.25$ mm/yr).

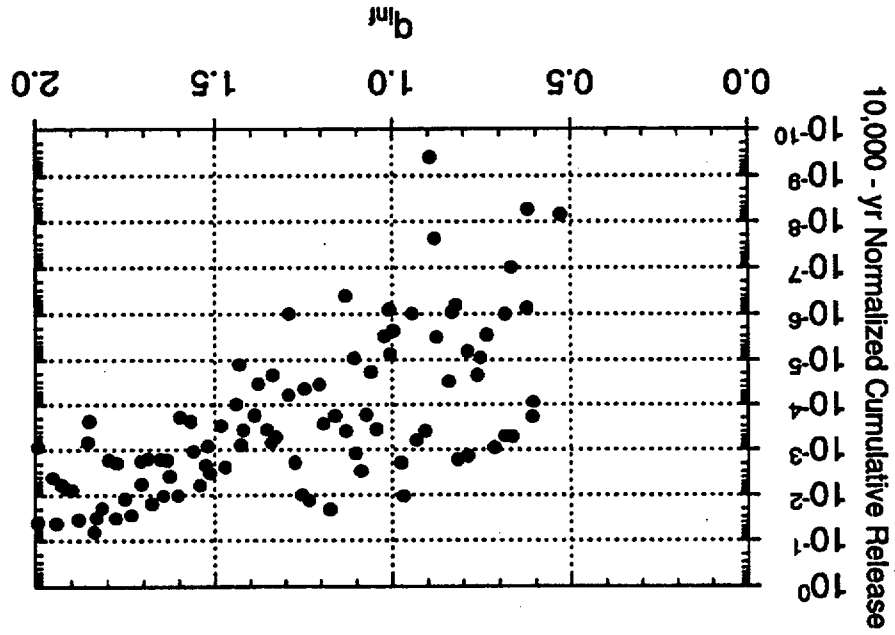


Figure 9.2-30 Scatter plot of 10,000-year total normalized cumulative release versus matrix velocity (m/yr) in the CHnv for 83 MTU/acre, backfill, high infiltration ($q_{inf} = 1.25$ mm/yr).

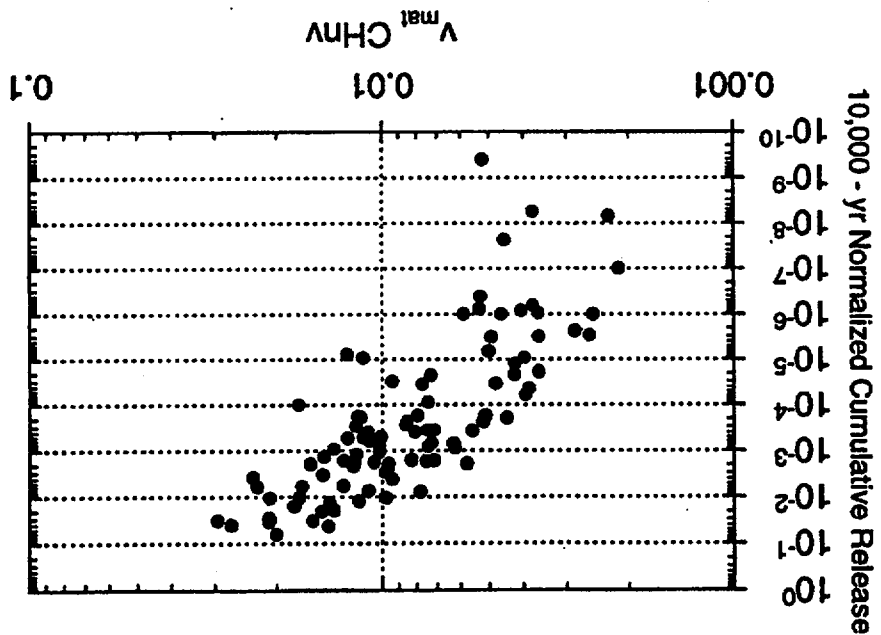


Figure 9.2-33 Scatter plot of 10,000-year total normalized cumulative release versus climate change modifier for 83 MTU/acre, backfill, high infiltration ($q_{inf} = 1.25$ mm/yr).

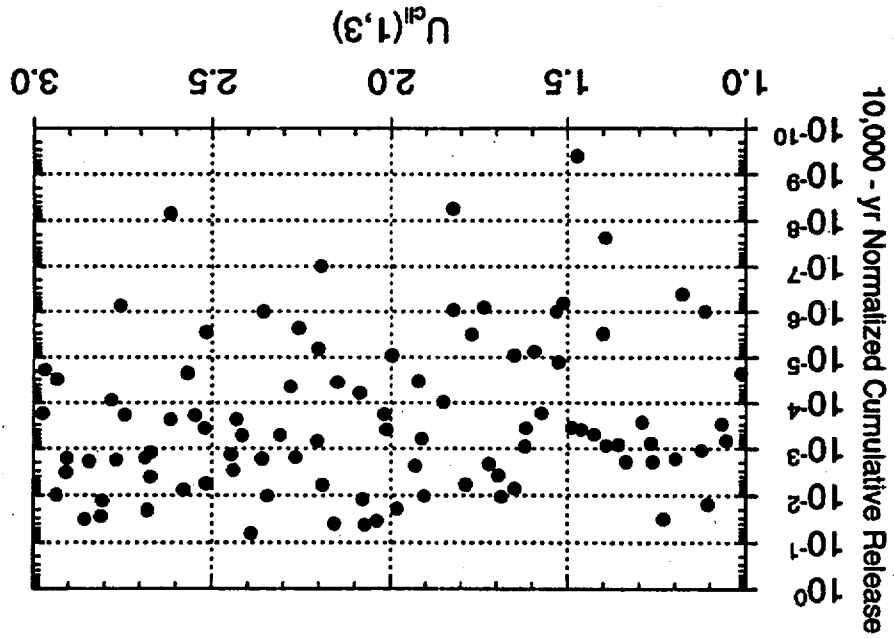
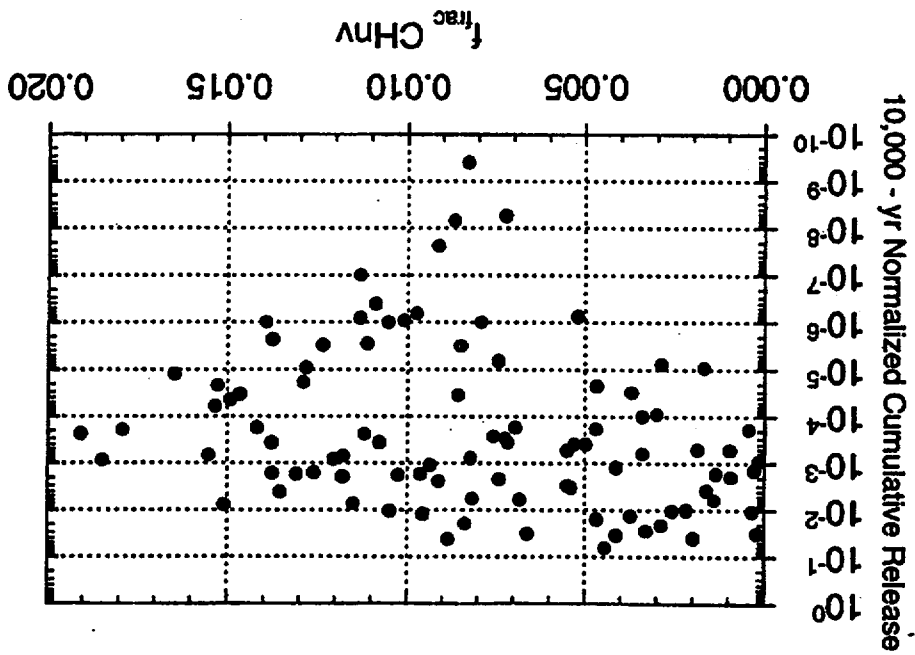


Figure 9.2-32 Scatter plot of 10,000-year total normalized cumulative release versus fraction of fracture flow in the CHN for 83 MTU/acre, backfill, high infiltration ($q_{inf} = 1.25$ mm/yr).



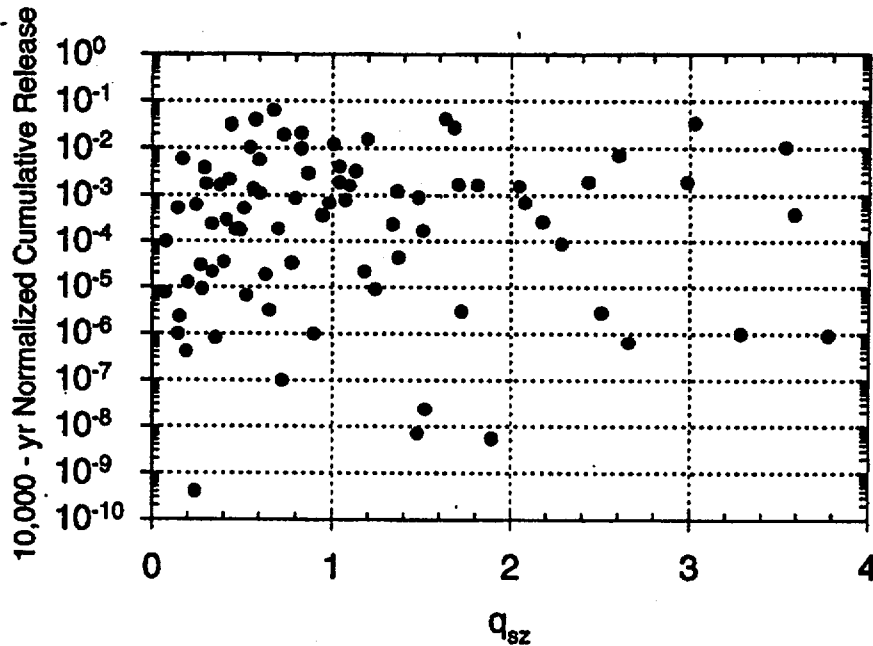


Figure 9.2-34 Scatter plot of 10,000-year total normalized cumulative release versus saturated-zone Darcy velocity (m/yr) for 83 MTU/acre, backfill, high infiltration ($q_{inf} = 1.25$ mm/yr).

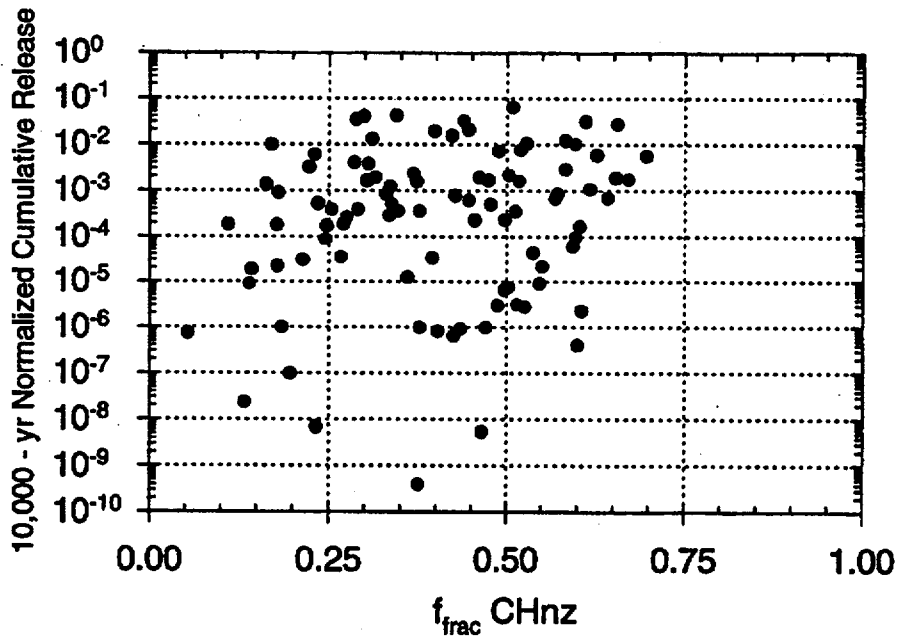


Figure 9.2-35 Scatter plot of 10,000-year total normalized cumulative release versus fraction of fracture flow in the CHnz for 83 MTU/acre, backfill, high infiltration ($q_{inf} = 1.25$ mm/yr).

Figure 9.2-37 Scatter plot of 10,000-year total peak dose versus matrix velocity (m/yr) in the CHNv for 83 MTU/acre, backfill, high infiltration ($q_{inf} = 1.25$ mm/yr).

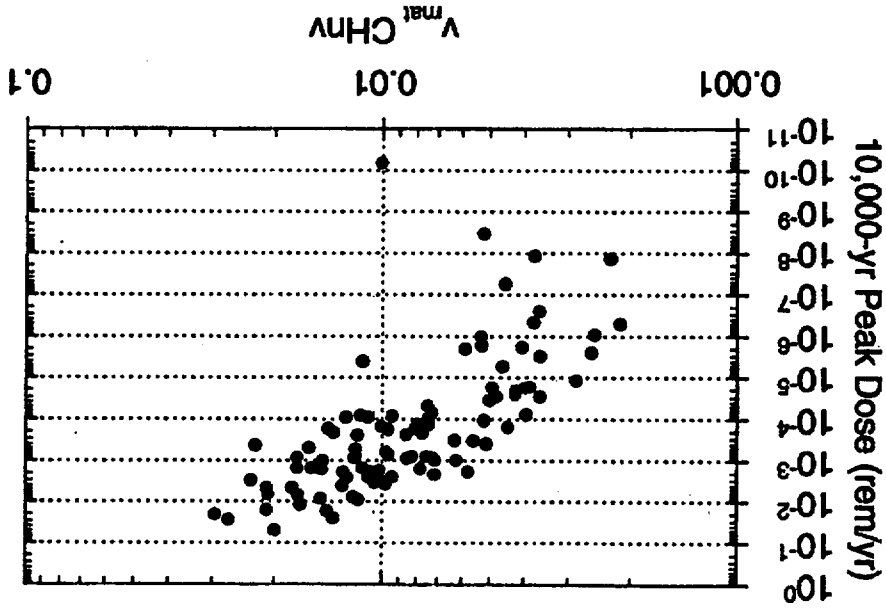


Figure 9.2-36 Scatter plot of 10,000-year total normalized cumulative release versus $Np K_d$ (TSv, CHNv) sorption coefficient in the vitric tuff for 83 MTU/acre, backfill, high infiltration ($q_{inf} = 1.25$ mm/yr).

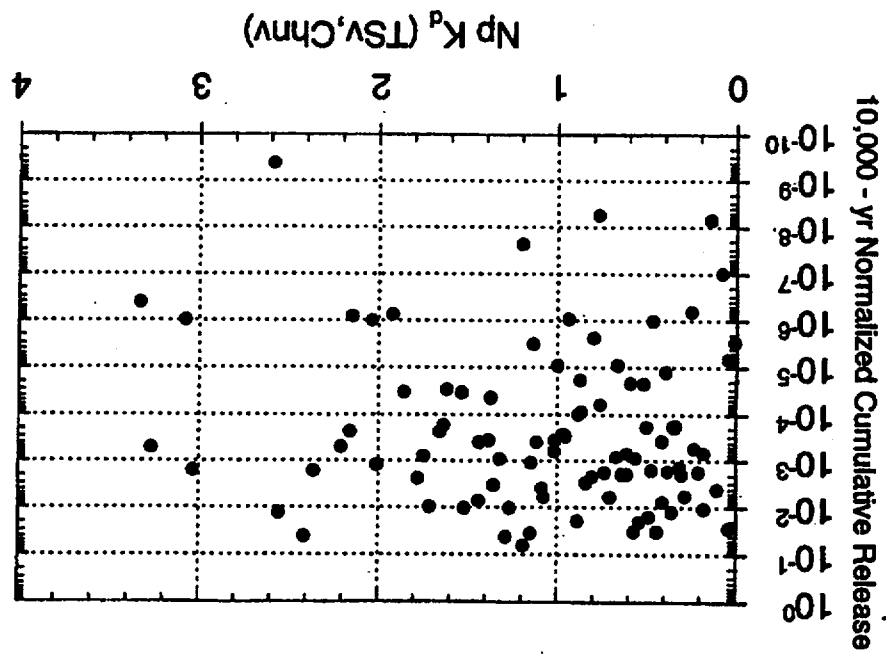


Figure 9.2-39 Scatter plot of 10,000-year total peak dose versus fraction of fracture flow in the CHNv for 83 MTU/acre, backfill, high infiltration ($q_{int} = 1.25$ mm/yr).

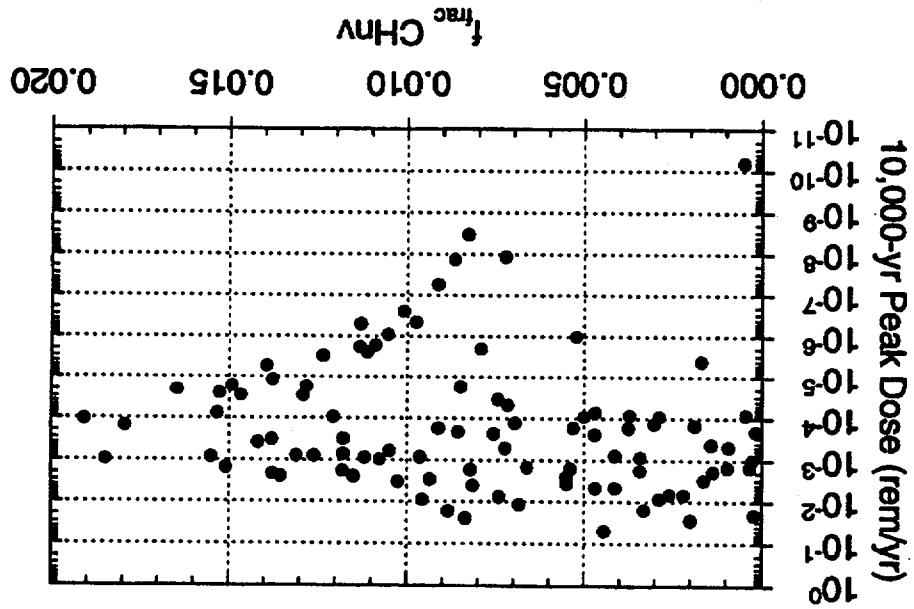


Figure 9.2-38 Scatter plot of 10,000-year total peak dose versus UZ percolation flux (mm/yr) for 83 MTU/acre, backfill, high infiltration ($q_{int} = 1.25$ mm/yr).

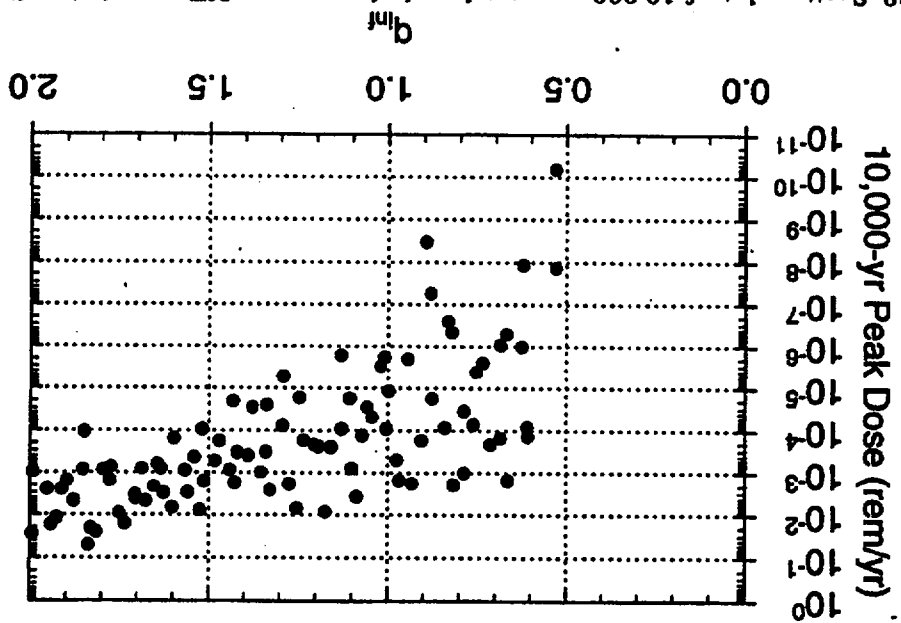


Figure 9.2-41 Scatter plot of 10,000-year total peak dose versus fraction of fracture flow in the CHZ for 83 MTU/acre, backfill, high infiltration ($q_{inf} = 1.25$ mm/yr).

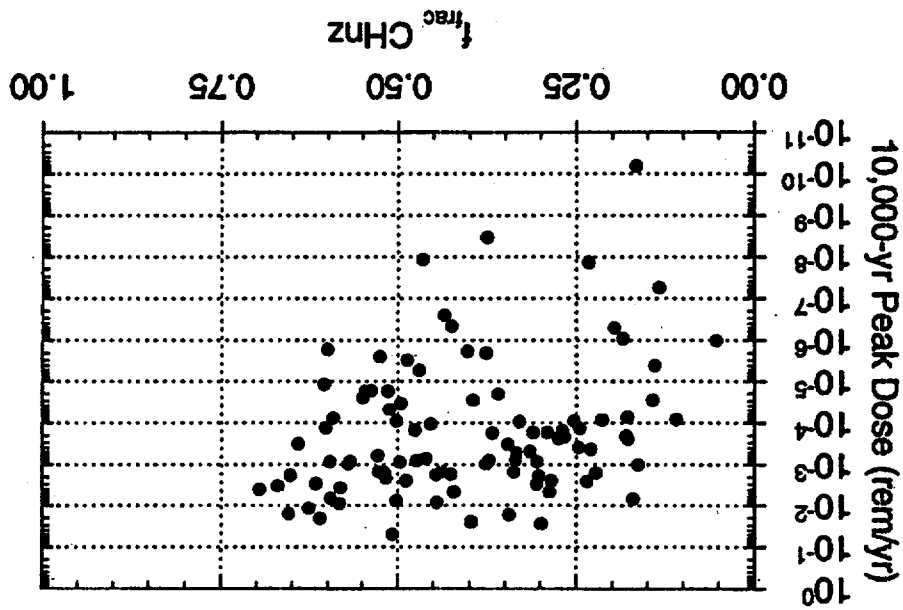
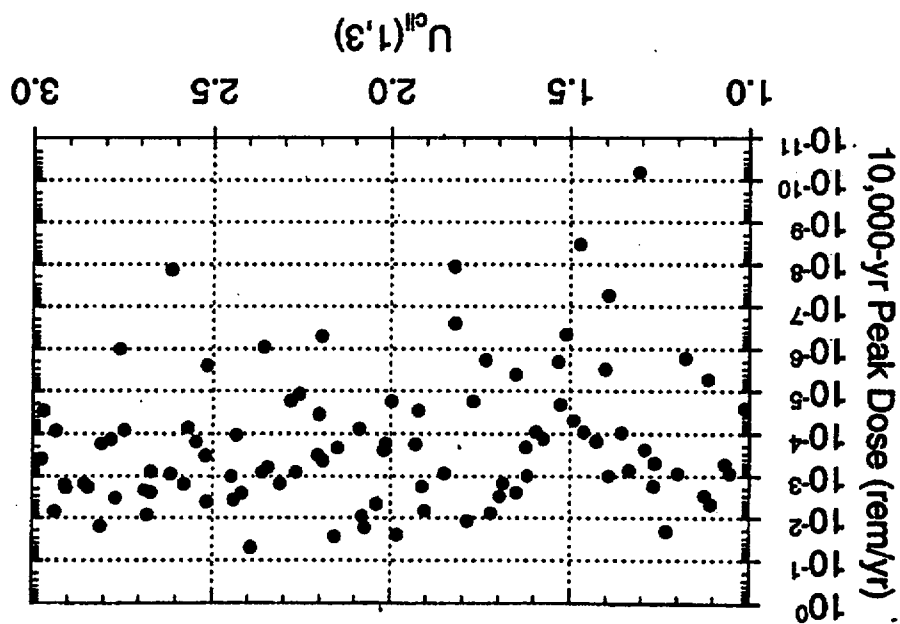


Figure 9.2-40 Scatter plot of 10,000-year total peak dose versus climate-change modifier for 83 MTU/acre, backfill, high infiltration ($q_{inf} = 1.25$ mm/yr).



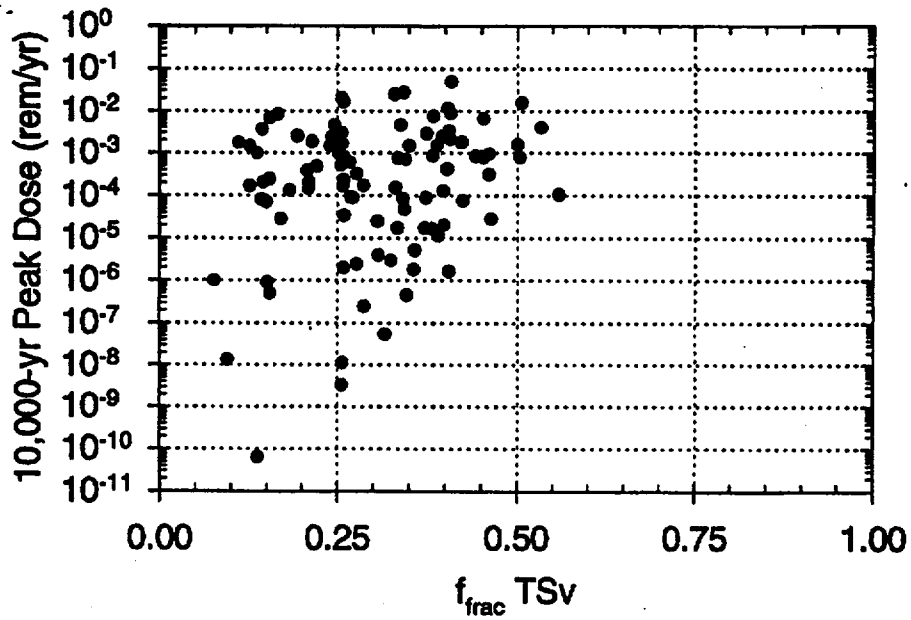


Figure 9.2-42 Scatter plot of 10,000-year total peak dose versus fraction of fracture flow in the TSv for 83 MTU/acre, backfill, high infiltration ($q_{\text{inf}} = 1.25$ mm/yr).

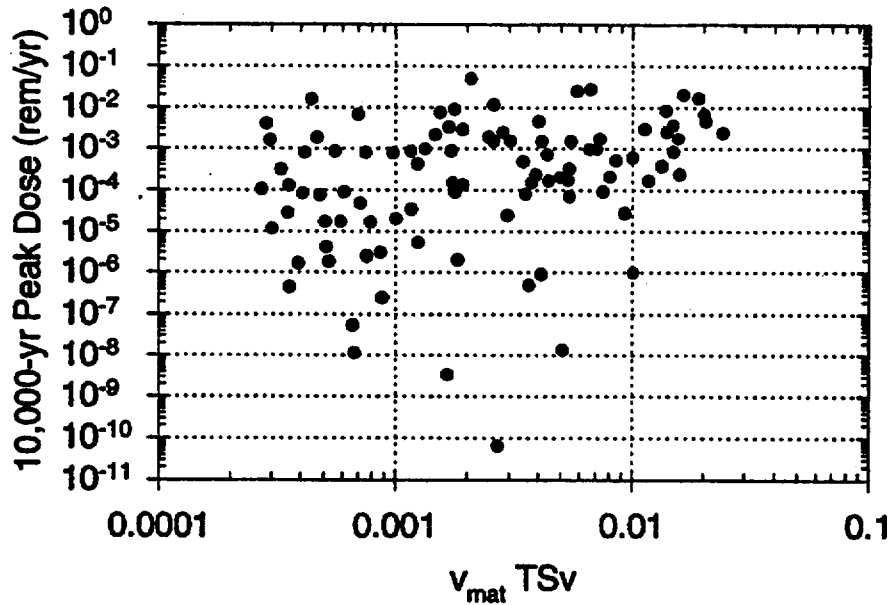


Figure 9.2-43 Scatter plot of 10,000-year total peak dose versus matrix velocity (m/yr) in the TSv for 83 MTU/acre, backfill, high infiltration ($q_{\text{inf}} = 1.25$ mm/yr).

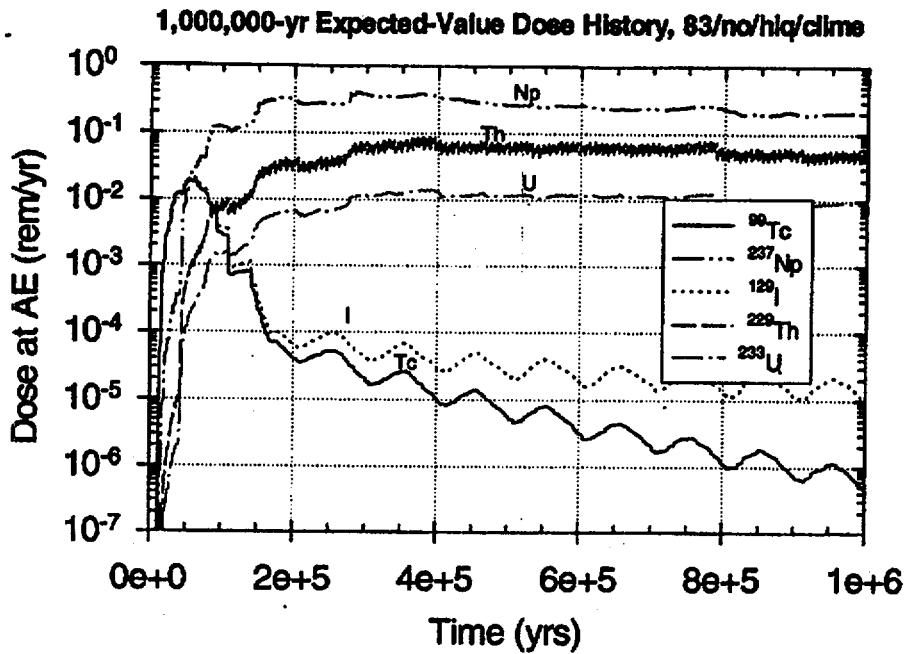


Figure 9.3-1a Expected-value dose history: 1,000,000 years, 83 MTU/acre, no backfill, high infiltration (initial $q_{inf} = 1.25$ mm/yr), cyclical- q_{inf} climate model.

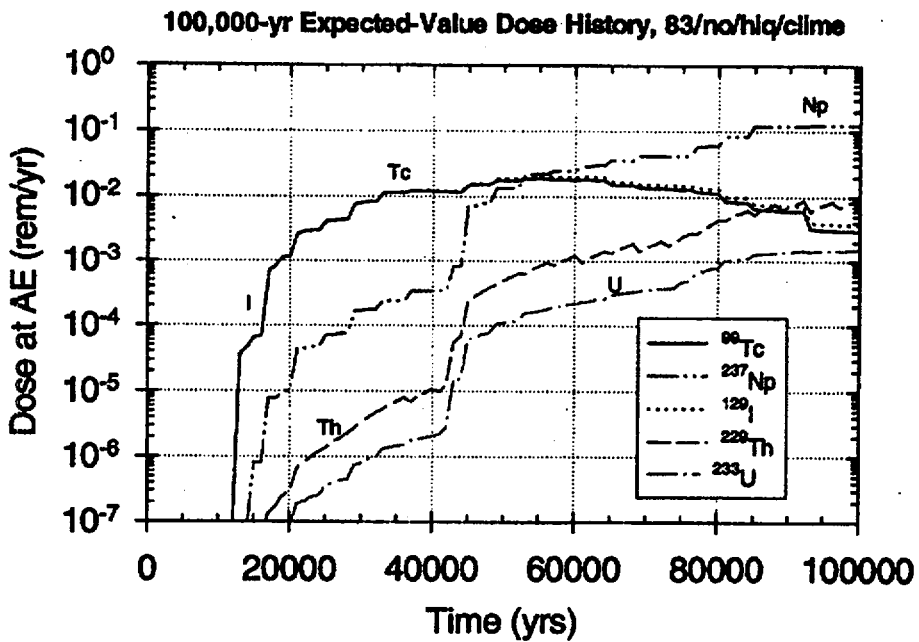


Figure 9.3-1b Expected-value dose history: 100,000 years, 83 MTU/acre, no backfill, high infiltration (initial $q_{inf} = 1.25$ mm/yr), cyclical- q_{inf} climate model.

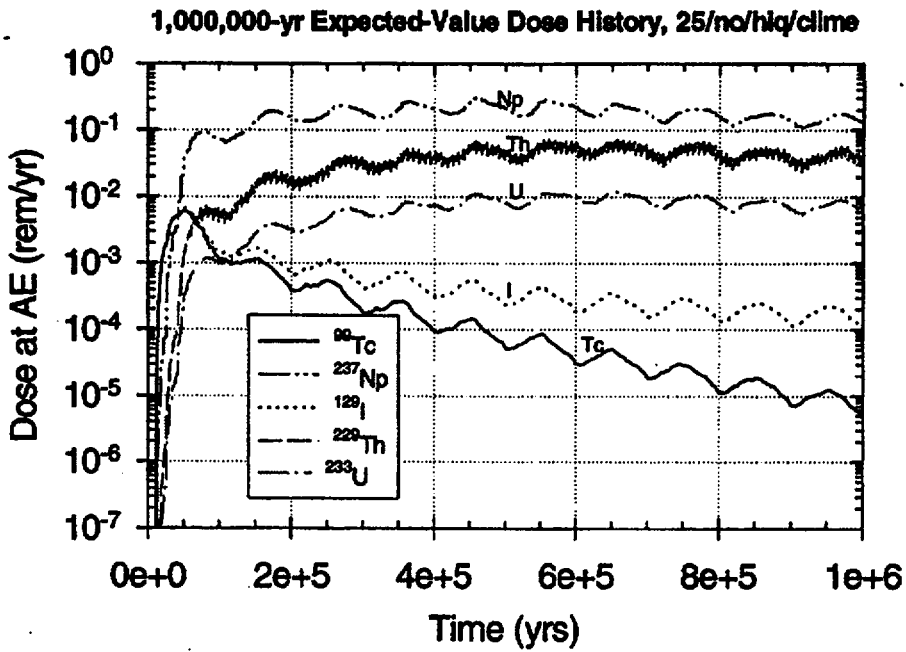


Figure 9.3-2a Expected-value dose history: 1,000,000 years, 25 MTU/acre, no backfill, high infiltration (initial $q_{inf} = 1.25$ mm/yr), cyclical- q_{inf} climate model.

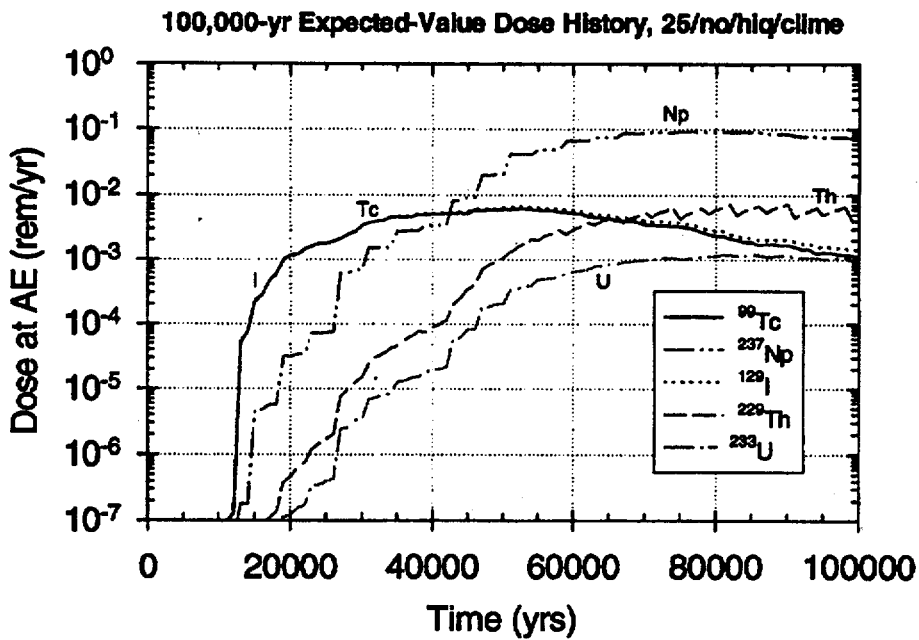


Figure 9.3-2b Expected-value dose history: 100,000 years, 25 MTU/acre, no backfill, high infiltration (initial $q_{inf} = 1.25$ mm/yr), cyclical- q_{inf} climate model.

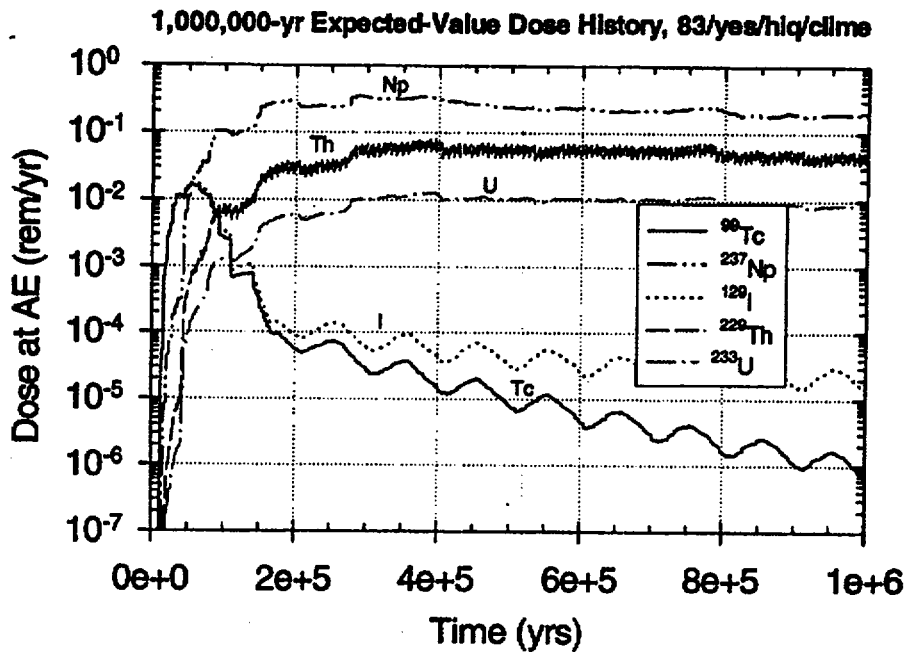


Figure 9.3-3a Expected-value dose history: 1,000,000 years, 83 MTU/acre, backfill, high infiltration (initial $q_{inf} = 1.25$ mm/yr), cyclical- q_{inf} climate model.

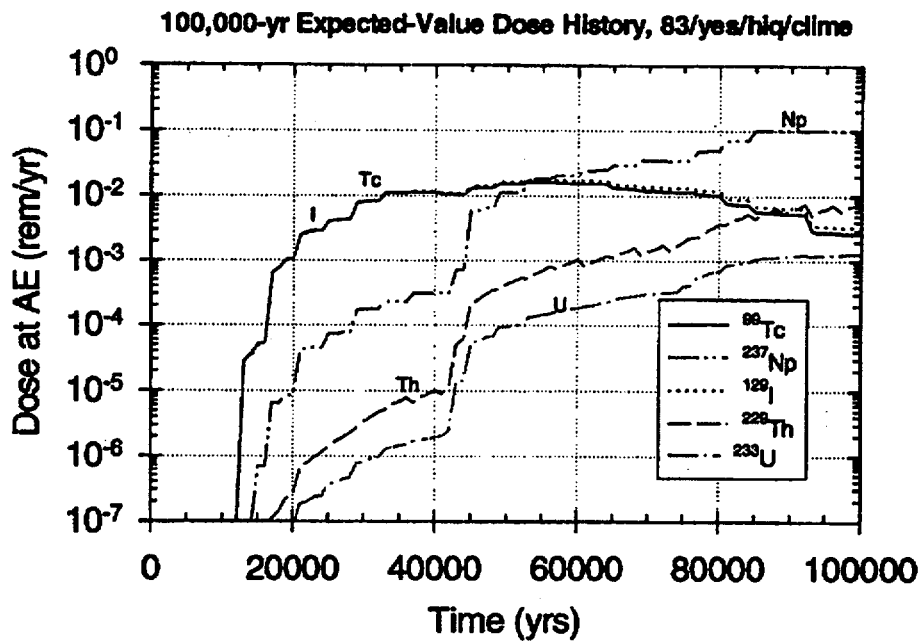


Figure 9.3-3b Expected-value dose history: 100,000 years, 83 MTU/acre, backfill, high infiltration (initial $q_{inf} = 1.25$ mm/yr), cyclical- q_{inf} climate model.

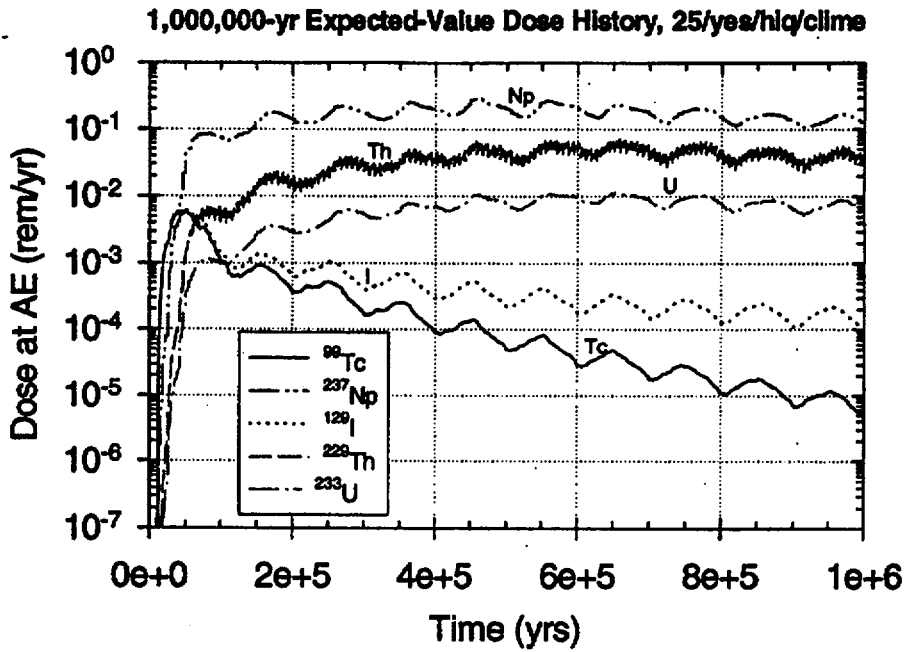


Figure 9.3-4a Expected-value dose history: 1,000,000 years, 25 MTU/acre, backfill, high infiltration (initial $q_{inf} = 1.25$ mm/yr), cyclical- q_{inf} climate model.

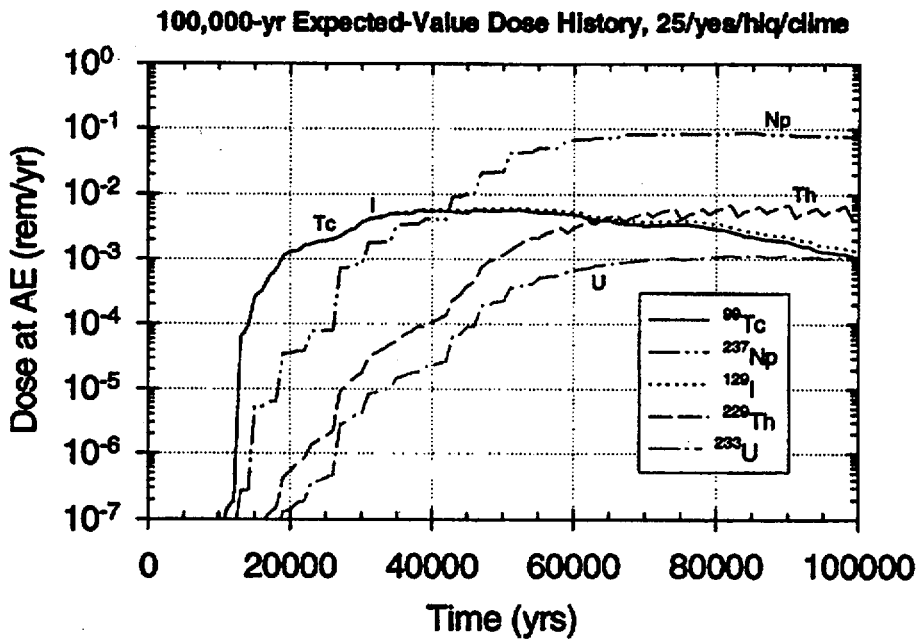


Figure 9.3-4b Expected-value dose history: 100,000 years, 25 MTU/acre, backfill, high infiltration (initial $q_{inf} = 1.25$ mm/yr), cyclical- q_{inf} climate model.

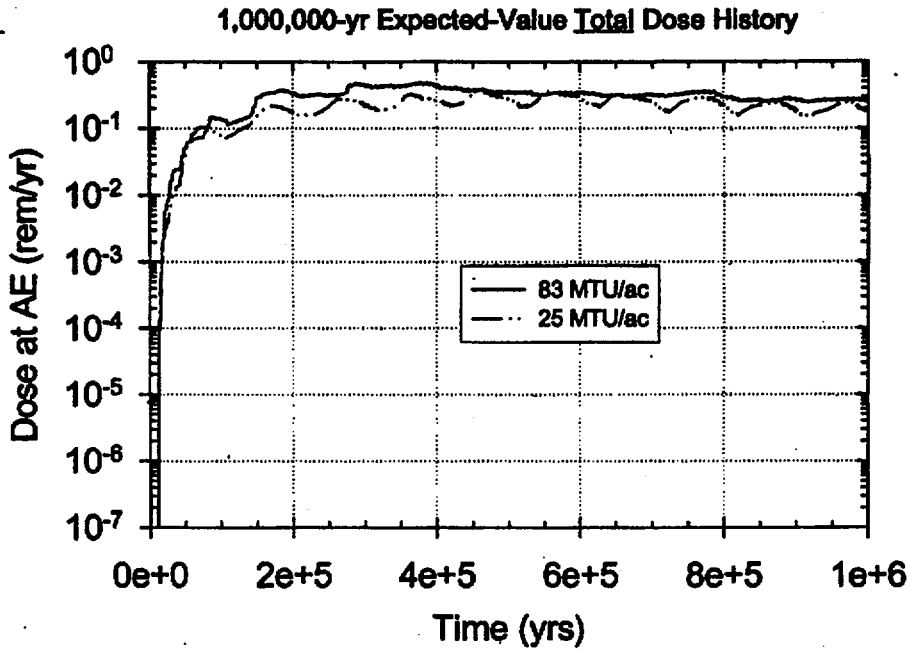


Figure 9.3-5 Expected-value total dose history: 1,000,000 years, 83 MTU/acre versus 25 MTU/acre, no backfill, high infiltration (initial $q_{inf} = 1.25$ mm/yr), cyclical- q_{inf} climate model.

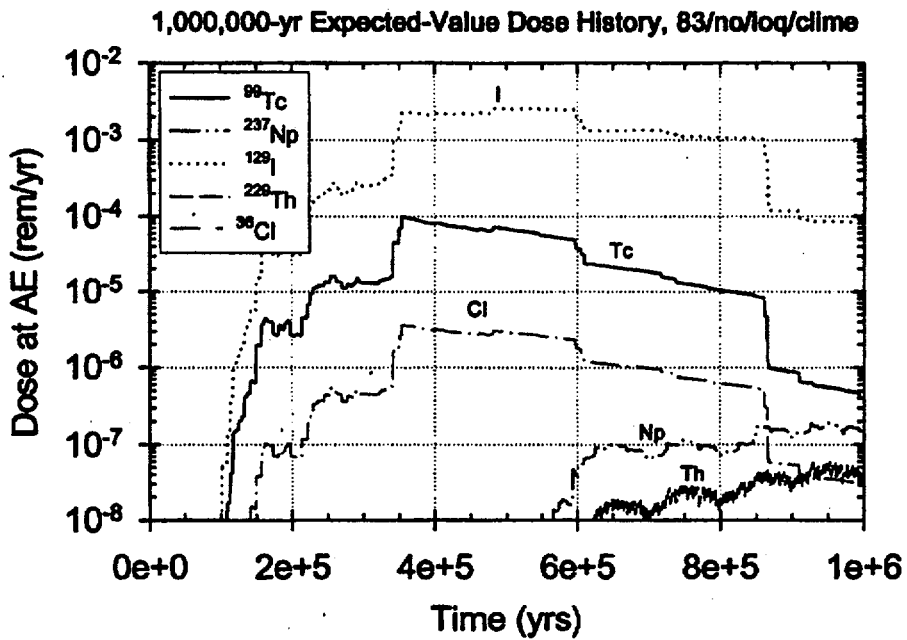


Figure 9.3-6 Expected-value dose history: 1,000,000 years, 83 MTU/acre, no backfill, low infiltration (initial $q_{inf} = 0.03$ mm/yr), cyclical- q_{inf} climate model.

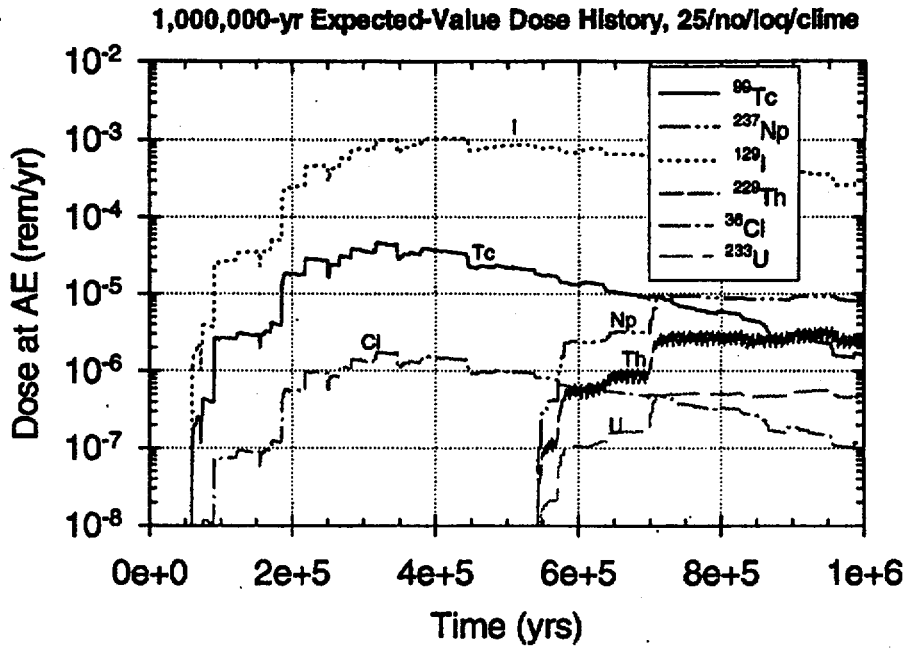


Figure 9.3-7a Expected-value dose history: 1,000,000 years, 25 MTU/acre, no backfill, low infiltration (initial $q_{\text{inf}} = 0.03$ mm/yr), cyclical- q_{inf} climate model.

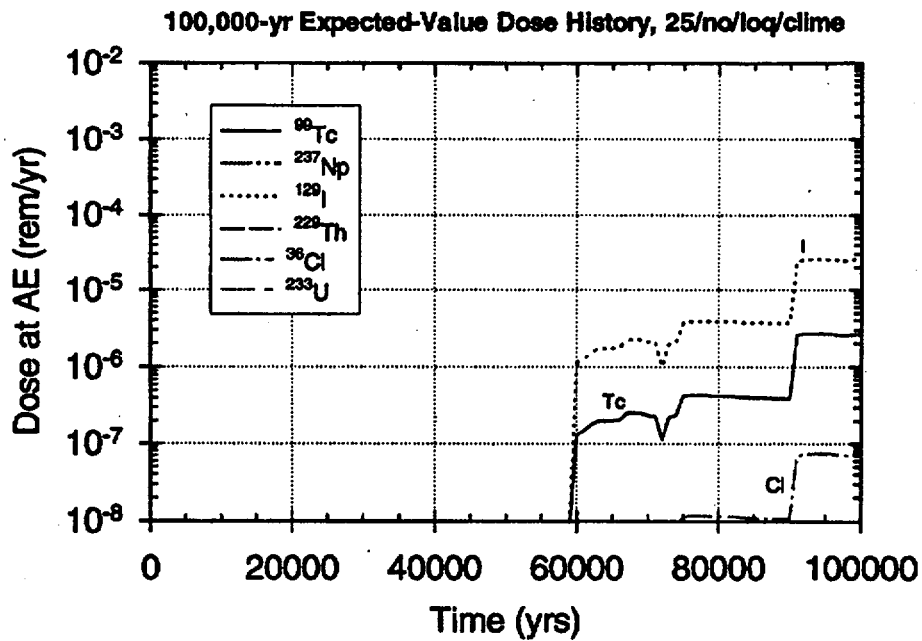


Figure 9.3-7b Expected-value dose history: 100,000 years, 25 MTU/acre, no backfill, low infiltration (initial $q_{\text{inf}} = 0.03$ mm/yr), cyclical- q_{inf} climate model.

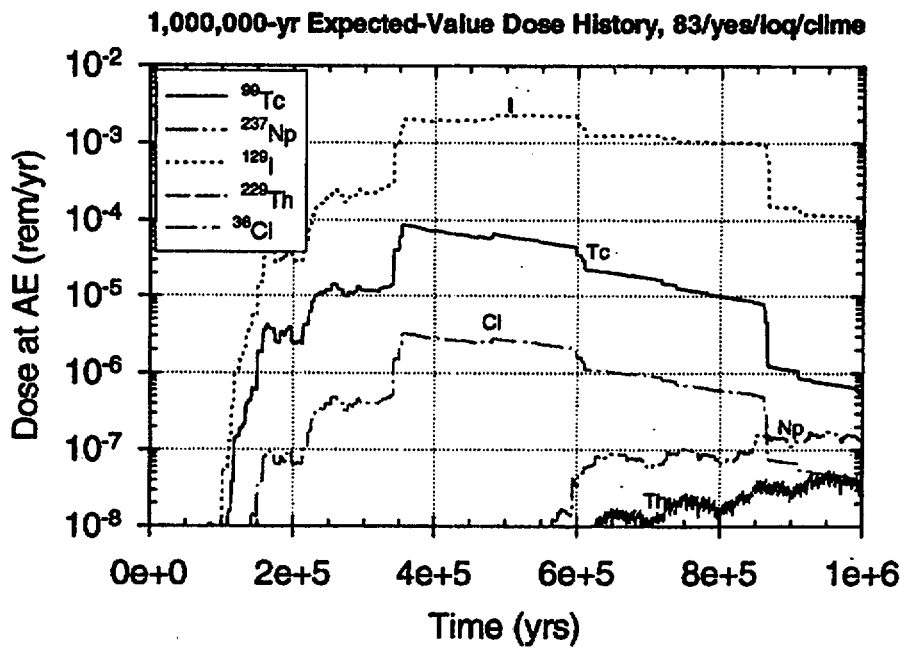


Figure 9.3-8 Expected-value dose history: 1,000,000 years, 83 MTU/acre, backfill, low infiltration (initial $q_{inf} = 0.03$ mm/yr), cyclical- q_{inf} climate model.

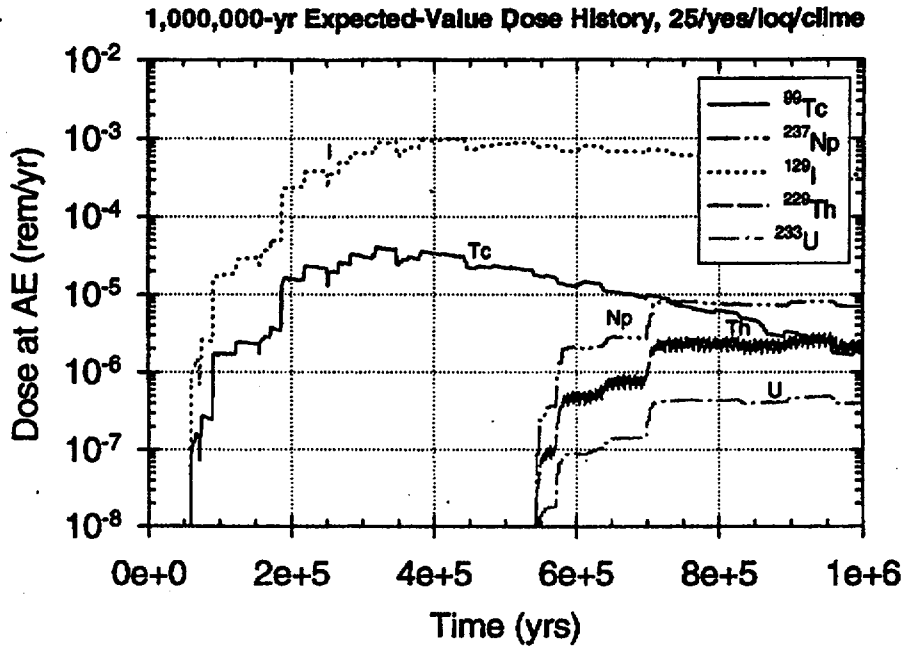


Figure 9.3-9a Expected-value dose history: 1,000,000 years, 25 MTU/acre, backfill, low infiltration (initial $q_{inf} = 0.03$ mm/yr), cyclical- q_{inf} climate model.

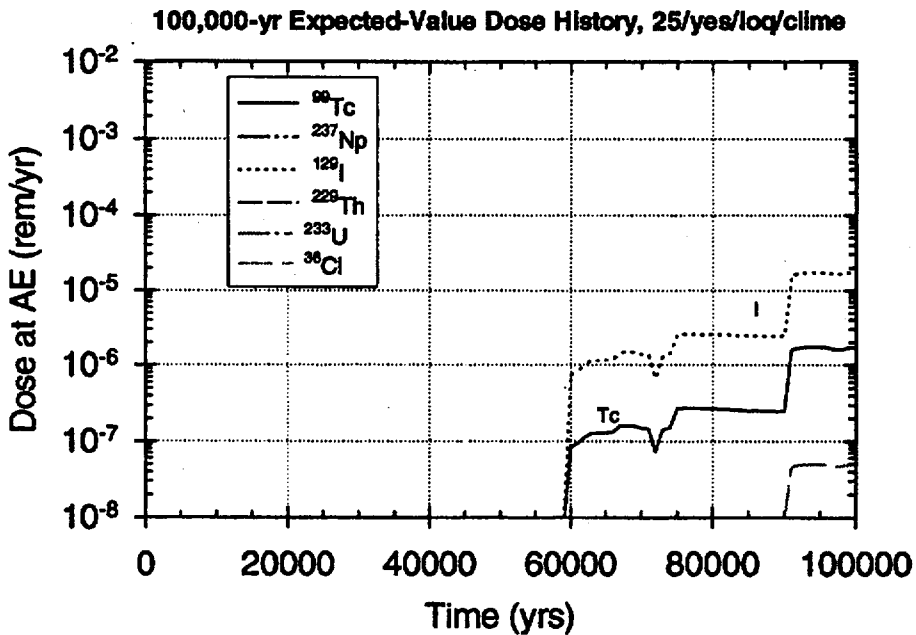


Figure 9.3-9b Expected-value dose history: 100,000 years, 25 MTU/acre, backfill, low infiltration (initial $q_{inf} = 0.03$ mm/yr), cyclical- q_{inf} climate model.

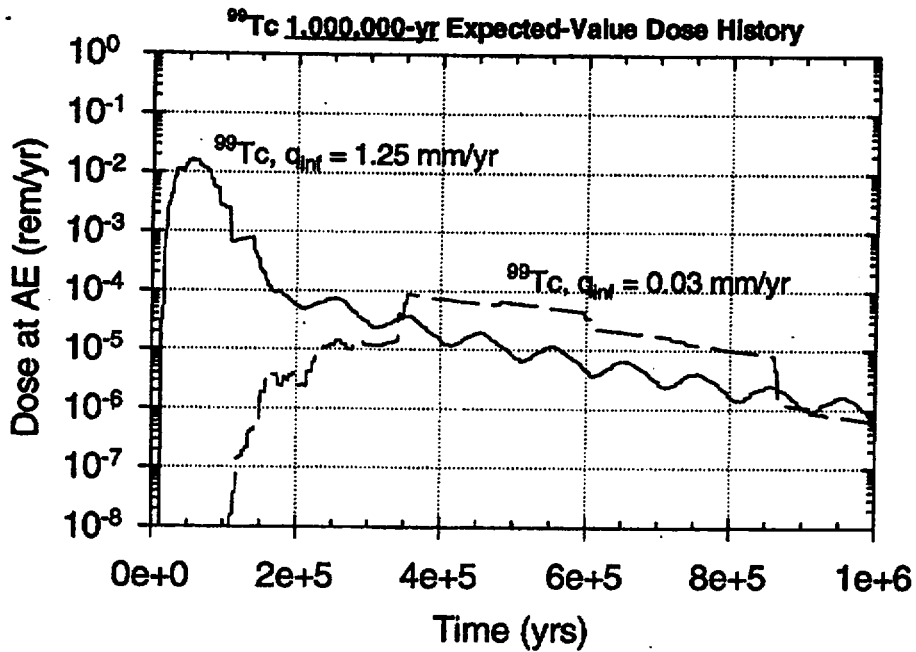


Figure 9.3-10 Expected-value dose history for ^{99}Tc . 1,000,000 years, infiltration rate comparison: "high" ($q_{\text{inf}} = 1.25 \text{ mm/yr}$) versus "low" ($q_{\text{inf}} = 0.03 \text{ mm/yr}$) infiltration, 83 MTU/acre, backfill, cyclical- q_{inf} climate model.

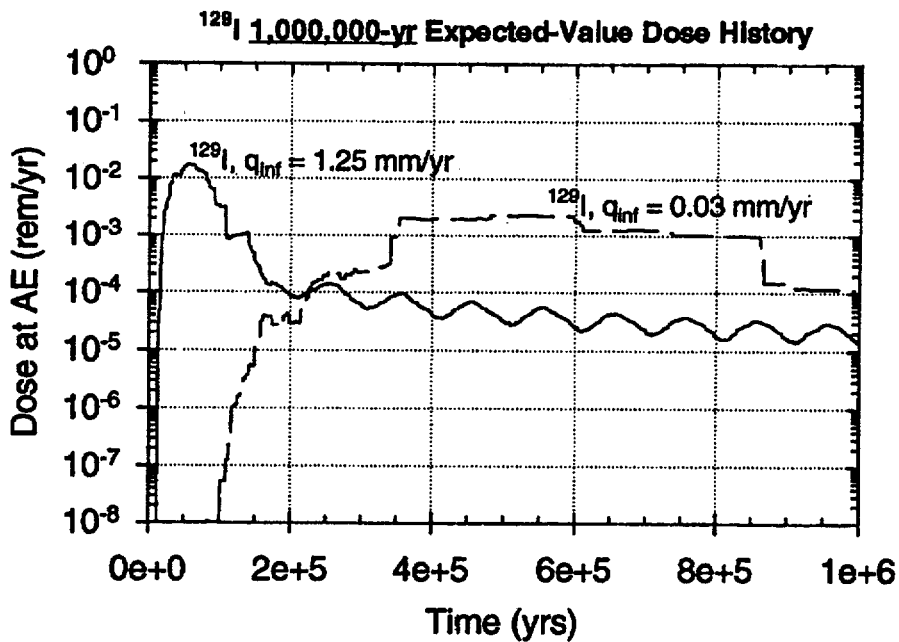


Figure 9.3-11 Expected-value dose history for ^{129}I . 1,000,000 years, infiltration rate comparison: "high" ($q_{\text{inf}} = 1.25 \text{ mm/yr}$) versus "low" ($q_{\text{inf}} = 0.03 \text{ mm/yr}$) infiltration, 83 MTU/acre, backfill, cyclical- q_{inf} climate model.

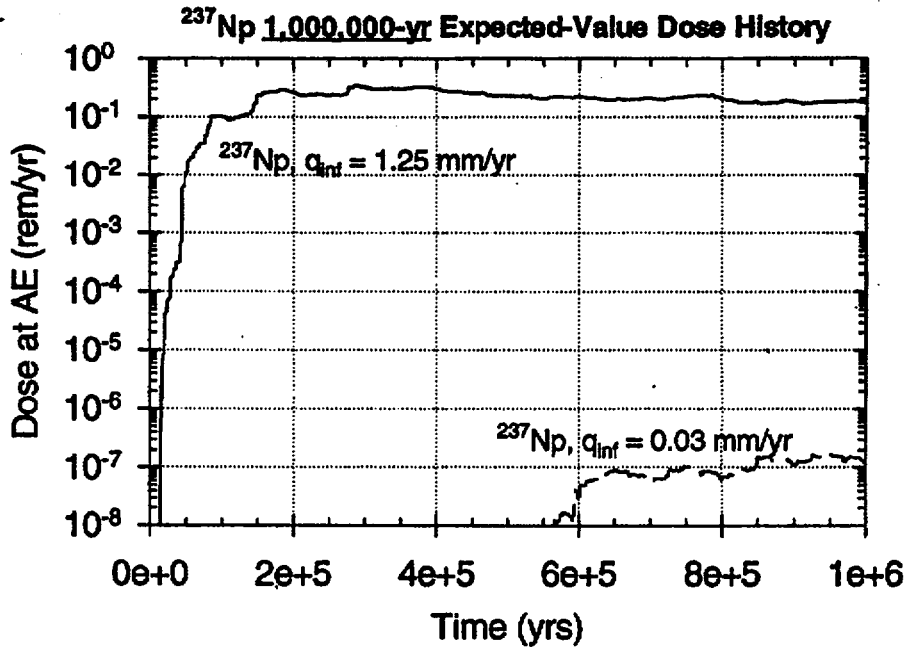


Figure 9.3-12 Expected-value dose history for ²³⁷Np. 1,000,000 years, infiltration rate comparison: "high" ($q_{inf} = 1.25$ mm/yr) versus "low" ($q_{inf} = 0.03$ mm/yr) infiltration, 83 MTU/acre, backfill, cyclical- q_{inf} climate model.

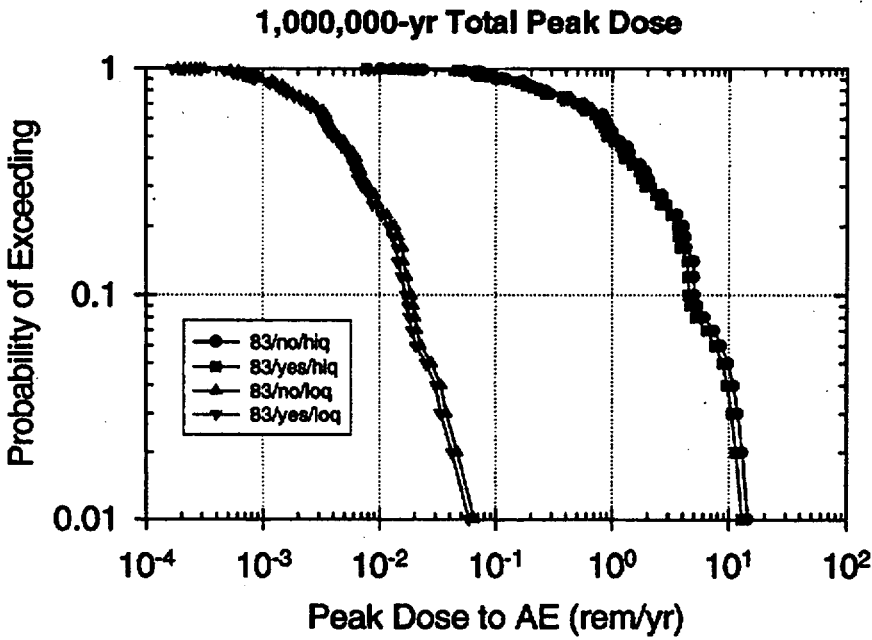


Figure 9.3-13 CCDF of Total Peak Dose: 1,000,000 years, 83 MTU/acre, with ("yes") and without ("no") backfill, high and low infiltration (q_{inf}) ranges, cyclical- q_{inf} climate model.

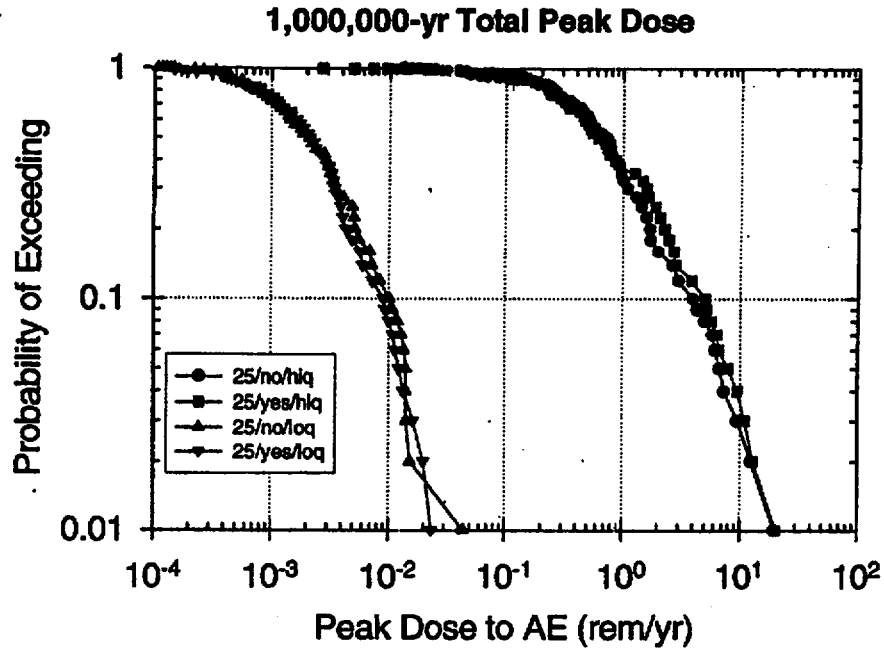


Figure 9.3-14 CCDF of Total Peak Dose: 1,000,000 years, 25 MTU/acre, with ("yes") and without ("no") backfill, high and low infiltration (q_{inf}) ranges, cyclical- q_{inf} climate model.

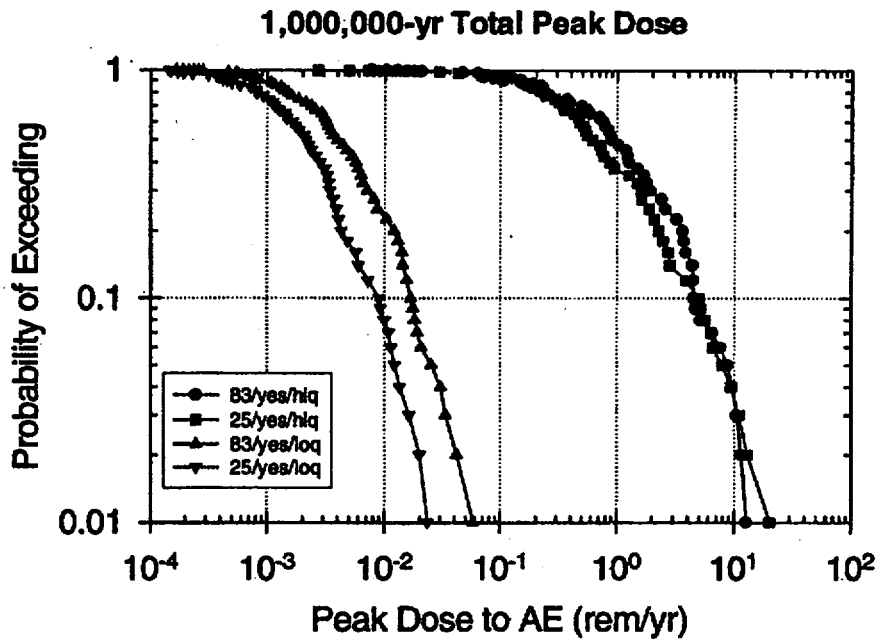


Figure 9.3-15 CCDF of Total Peak Dose: 1,000,000 years, 83 MTU/acre and 25 MTU/acre, with ("yes") backfill, high and low infiltration (q_{inf}) ranges, cyclical- q_{inf} climate model.

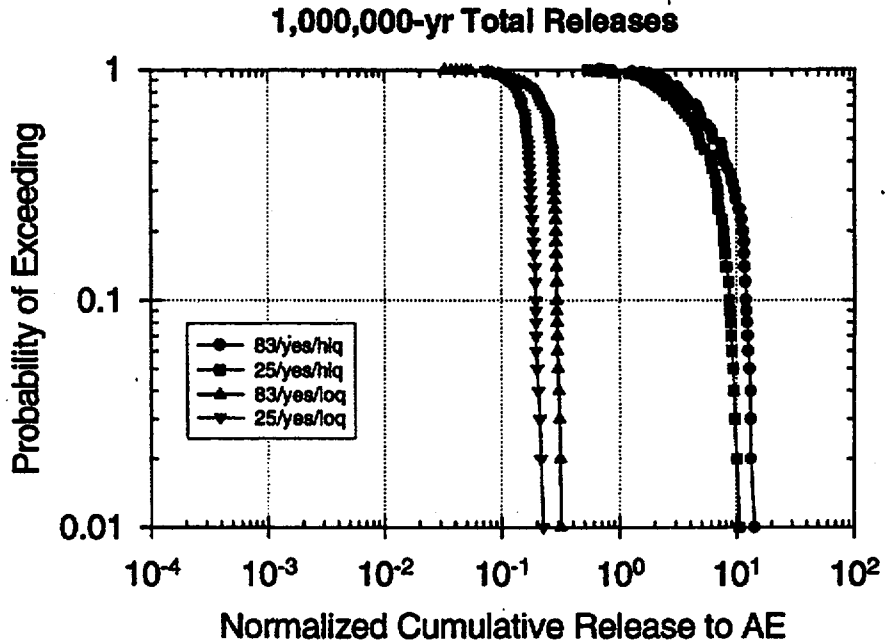


Figure 9.3-16 CCDF of Total Normalized Cumulative Release: 1,000,000 years, 83 MTU/acre and 25 MTU/acre, with ("yes") backfill, high and low infiltration (q_{inf}) ranges, cyclical- q_{inf} climate model.

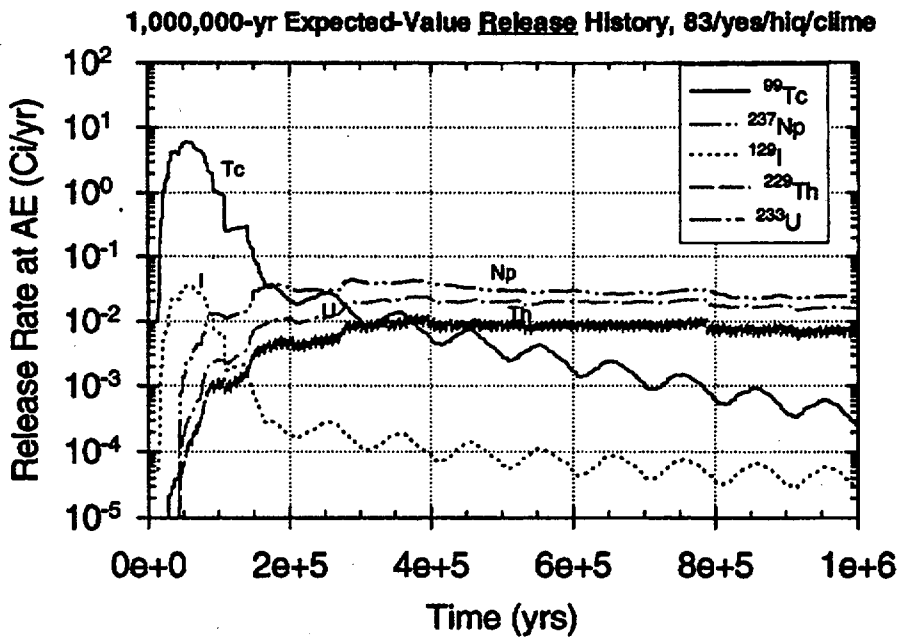


Figure 9.3-17 Expected-value release-rate history: 1,000,000 years, 83 MTU/acre, backfill, high infiltration (initial $q_{inf} = 1.25$ mm/yr), cyclical- q_{inf} climate model.

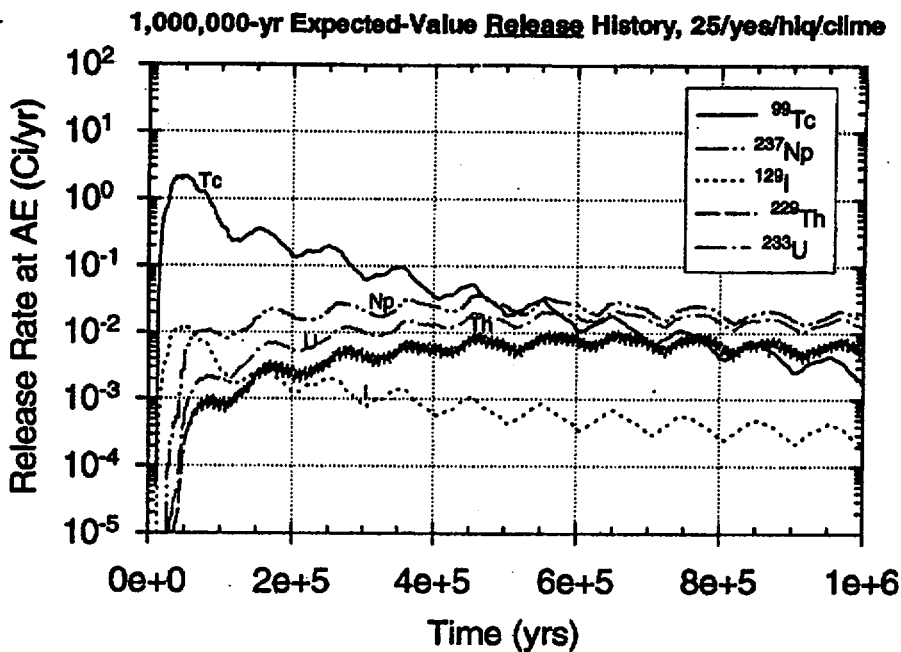


Figure 9.3-18 Expected-value release-rate history: 1,000,000 years, 25 MTU/acre, backfill, high infiltration (initial $q_{inf} = 1.25$ mm/yr), cyclical- q_{inf} climate model.

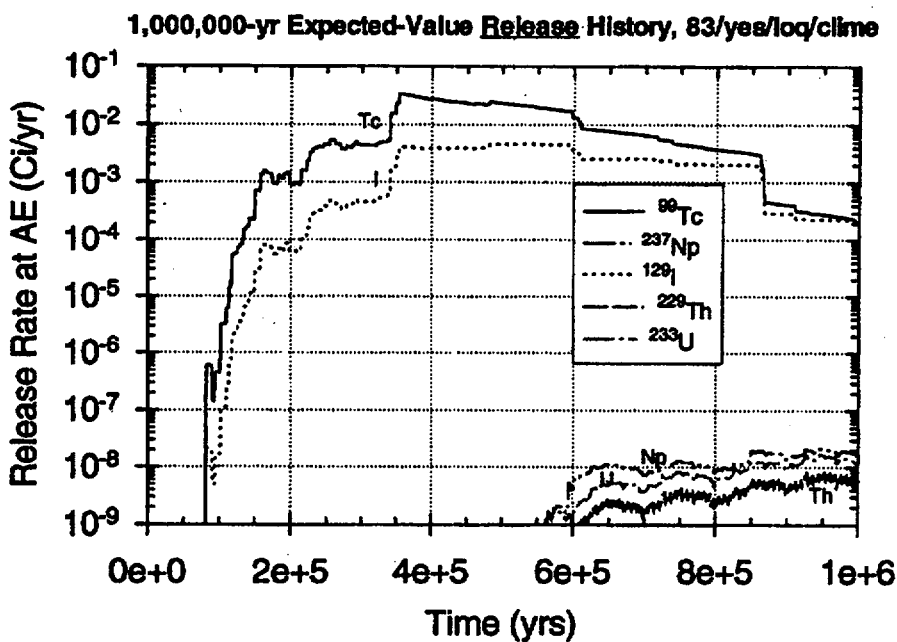


Figure 9.3-19 Expected-value release-rate history: 1,000,000 years, 83 MTU/acre, backfill, low infiltration (initial $q_{inf} = 0.03$ mm/yr), cyclical- q_{inf} climate model.

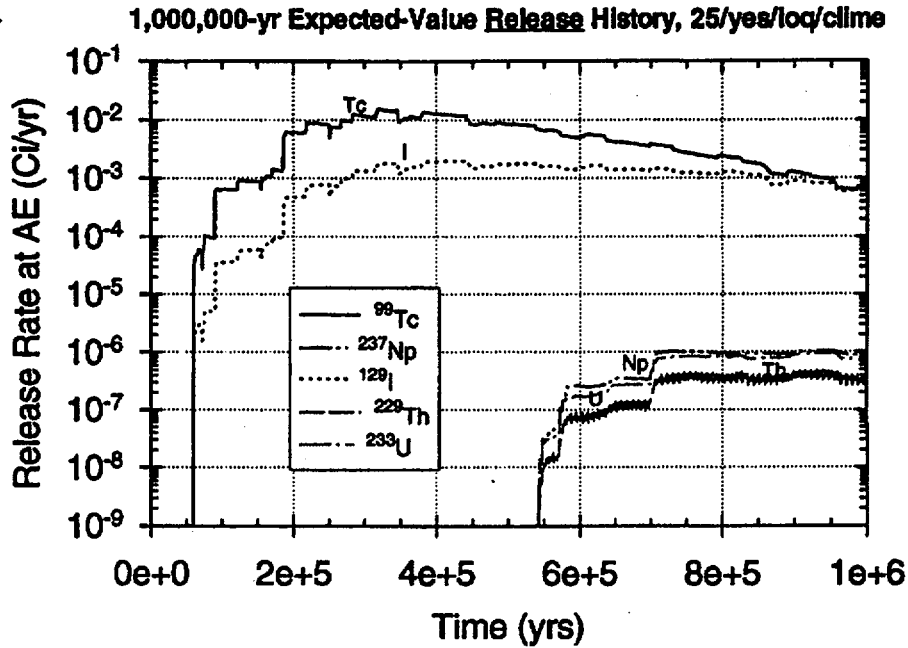


Figure 9.3-20 Expected-value release-rate history: 1,000,000 years, 25 MTU/acre, backfill, low infiltration (initial $q_{\text{inf}} = 0.03$ mm/yr), cyclical- q_{inf} climate model.

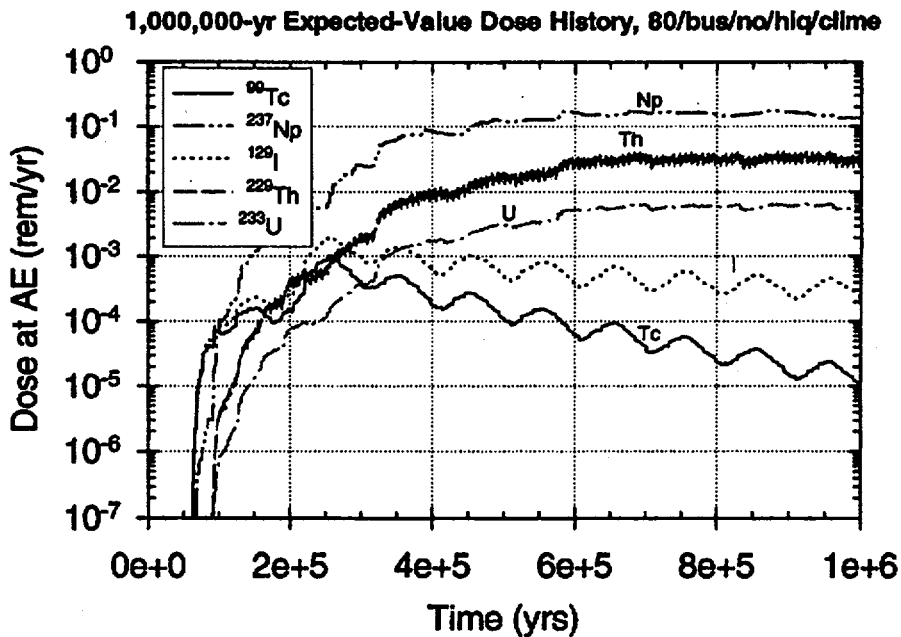


Figure 9.3-21 Expected-value dose history: 1,000,000 years, Buscheck 80 MTU/acre, no backfill, high infiltration (initial $q_{\text{inf}} = 1.25$ mm/yr), cyclical- q_{inf} climate model.

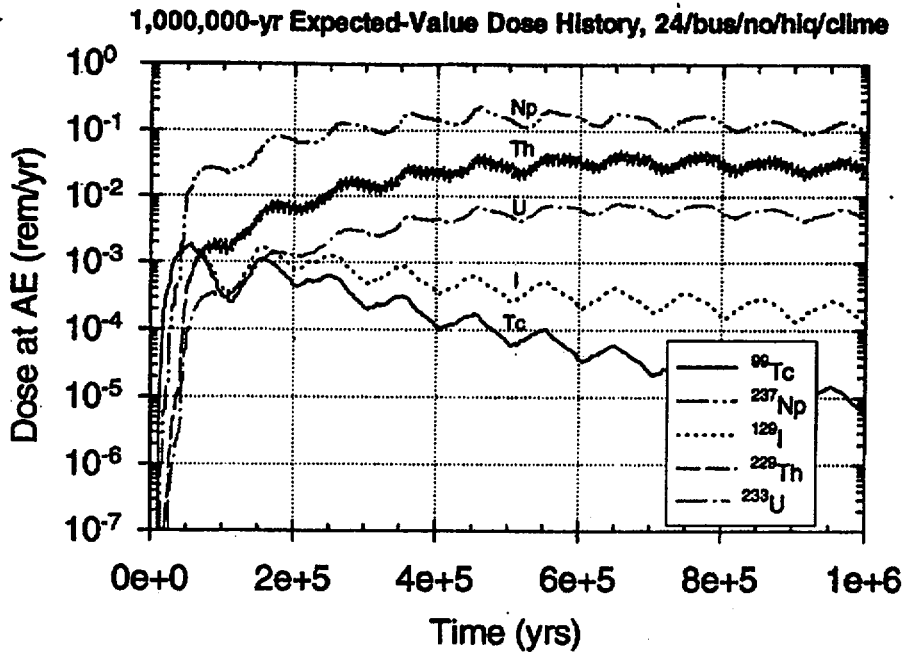


Figure 9.3-22 Expected-value dose history: 1,000,000 years, Buscheck 24 MTU/acre, no backfill, high infiltration (initial $q_{inf} = 1.25$ mm/yr), cyclical- q_{inf} climate model.

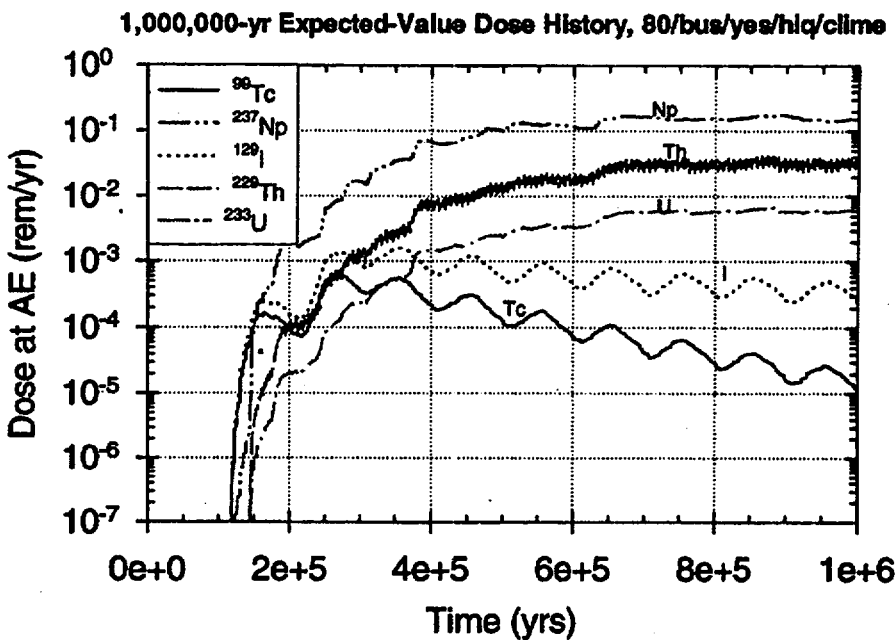


Figure 9.3-23 Expected-value dose history: 1,000,000 years, Buscheck 80 MTU/acre, backfill, high infiltration (initial $q_{inf} = 1.25$ mm/yr), cyclical- q_{inf} climate model.

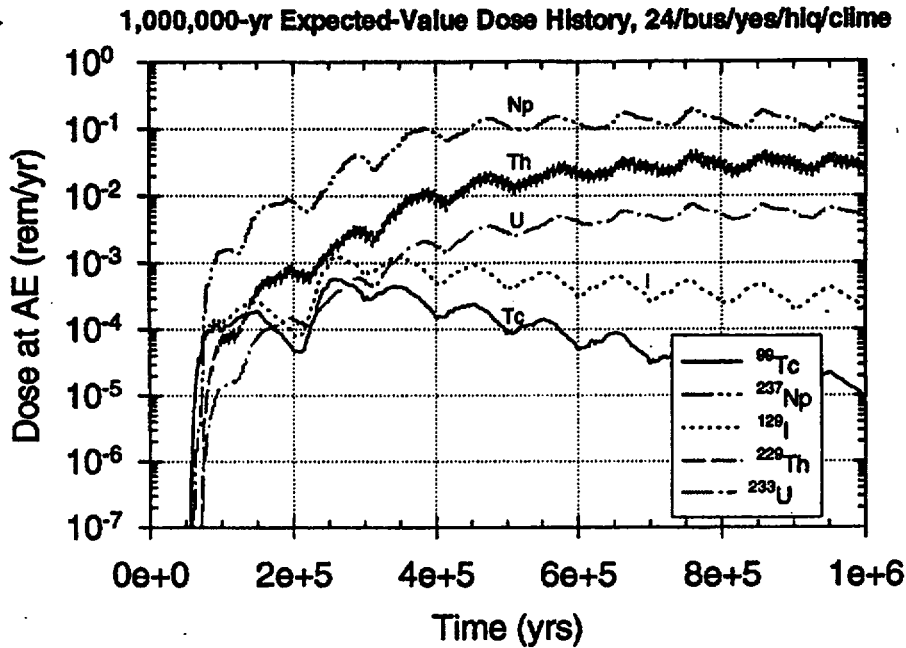


Figure 9.3-24 Expected-value dose history: 1,000,000 years, Buscheck 24 MTU/acre, backfill, high infiltration (initial $q_{inf} = 1.25$ mm/yr), cyclical- q_{inf} climate model.

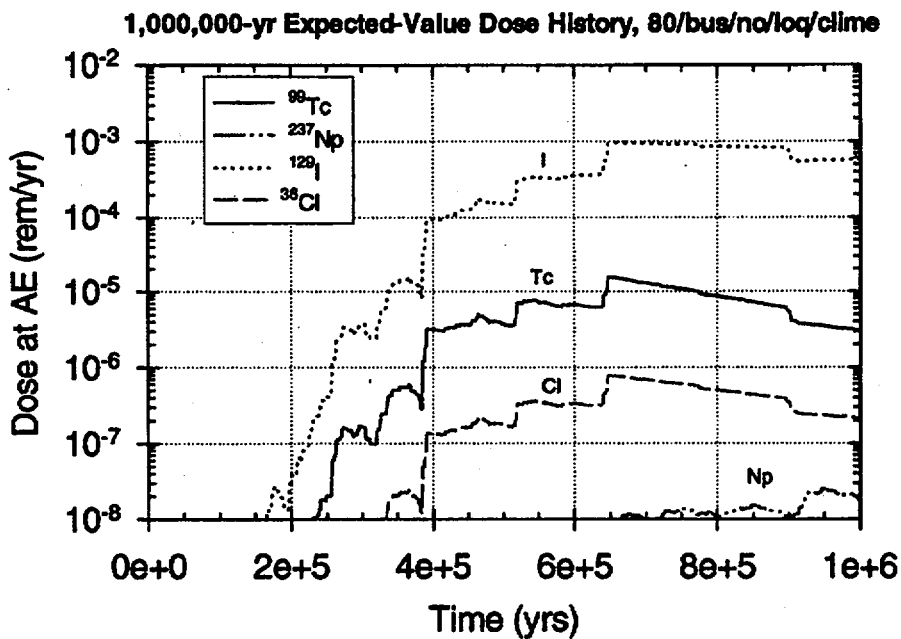


Figure 9.3-25 Expected-value dose history: 1,000,000 years, Buscheck 80 MTU/acre, no backfill, low infiltration (initial $q_{inf} = 0.03$ mm/yr), cyclical- q_{inf} climate model.

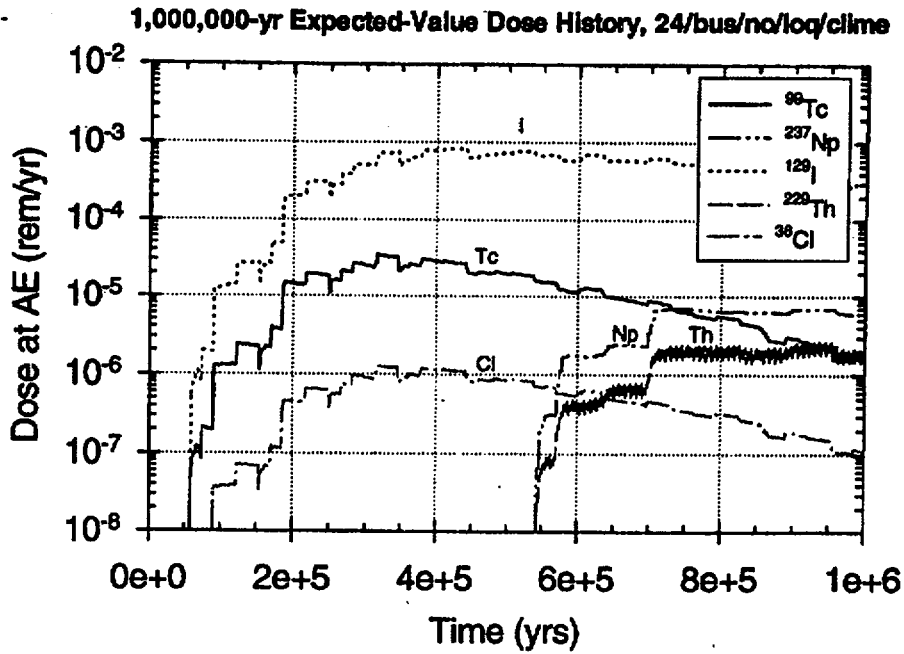


Figure 9.3-26 Expected-value dose history: 1,000,000 years, Buscheck 24 MTU/acre, no backfill, low infiltration (initial $q_{inf} = 0.03$ mm/yr), cyclical- q_{inf} climate model.

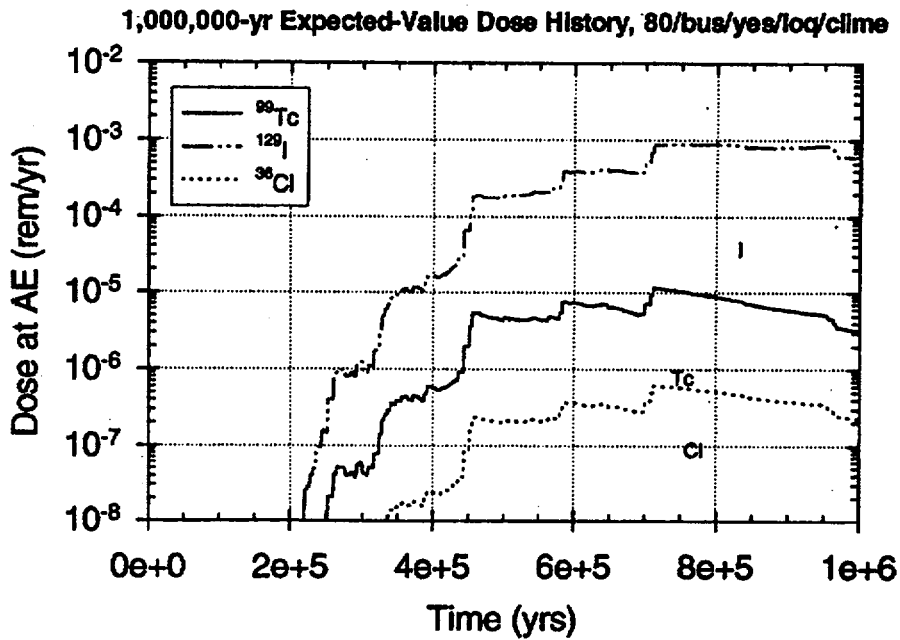


Figure 9.3-27 Expected-value dose history: 1,000,000 years, Buscheck 80 MTU/acre, backfill, low infiltration (initial $q_{inf} = 0.03$ mm/yr), cyclical- q_{inf} climate model.

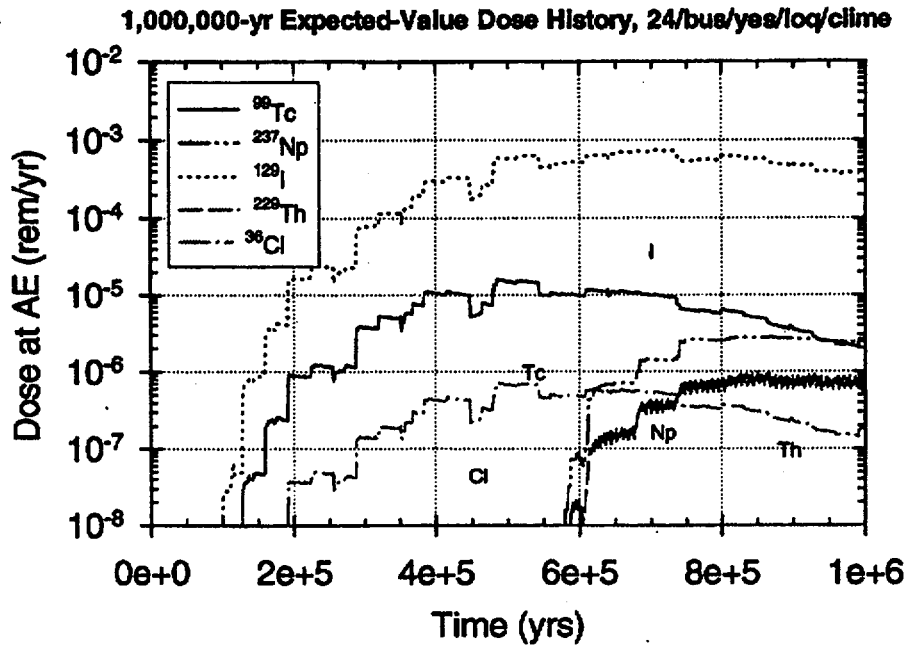


Figure 9.3-28 Expected-value dose history: 1,000,000 years, Buscheck 24 MTU/acre, backfill, low infiltration (initial $q_{inf} = 0.03$ mm/yr), cyclical- q_{inf} climate model.

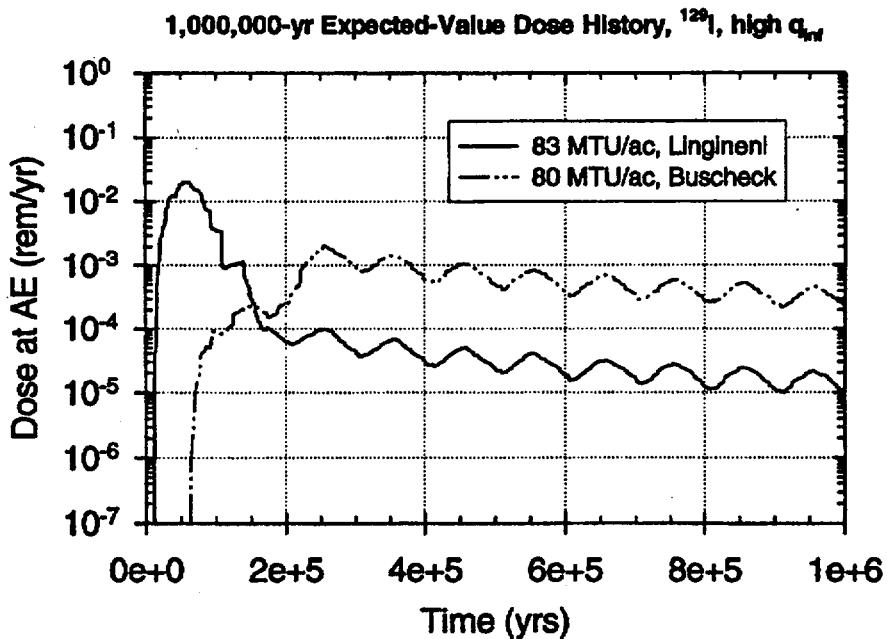


Figure 9.3-29 Expected-value dose history for ¹²⁹I. 1,000,000 years, comparison of thermohydrologic models: Lingineni 83 MTU/acre and Buscheck 80 MTU/acre, high infiltration rate ($q_{inf} = 1.25$ mm/yr), no backfill, cyclical- q_{inf} climate model.

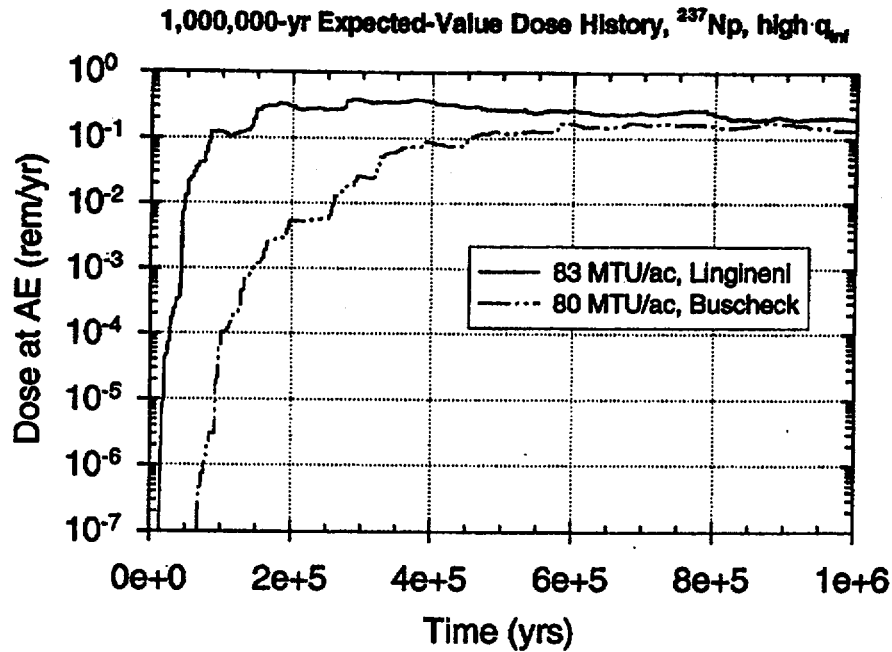


Figure 9.3-30 Expected-value dose history for ^{237}Np . 1,000,000 years, comparison of thermohydrologic models: Lingineni 83 MTU/acre and Buscheck 80 MTU/acre, high infiltration rate ($q_{inf} = 1.25$ mm/yr), no backfill, cyclical- q_{inf} climate model.

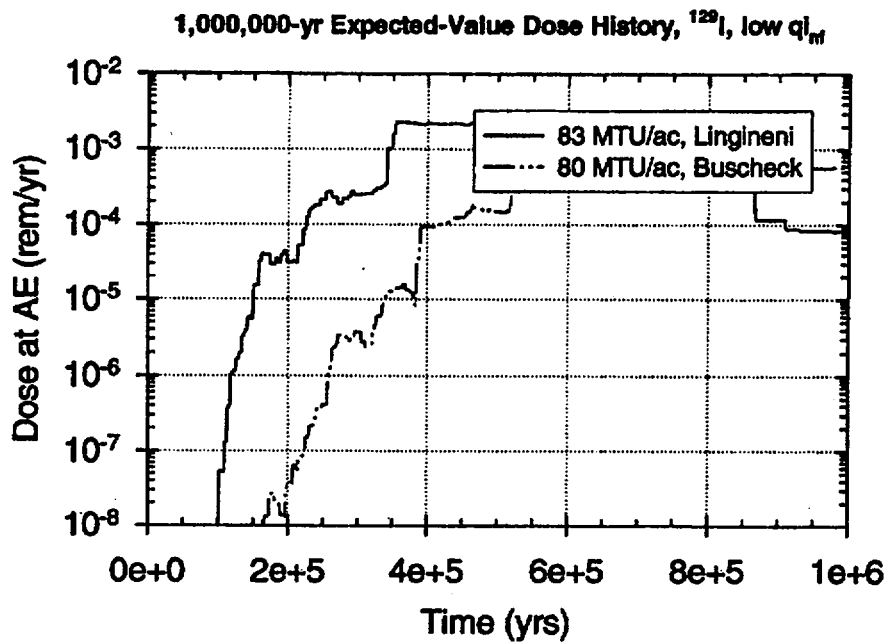


Figure 9.3-31 Expected-value dose history for ^{129}I . 1,000,000 years, comparison of thermohydrologic models: Lingineni 83 MTU/acre and Buscheck 80 MTU/acre, low infiltration rate ($q_{inf} = 0.03$ mm/yr), no backfill, cyclical- q_{inf} climate model.

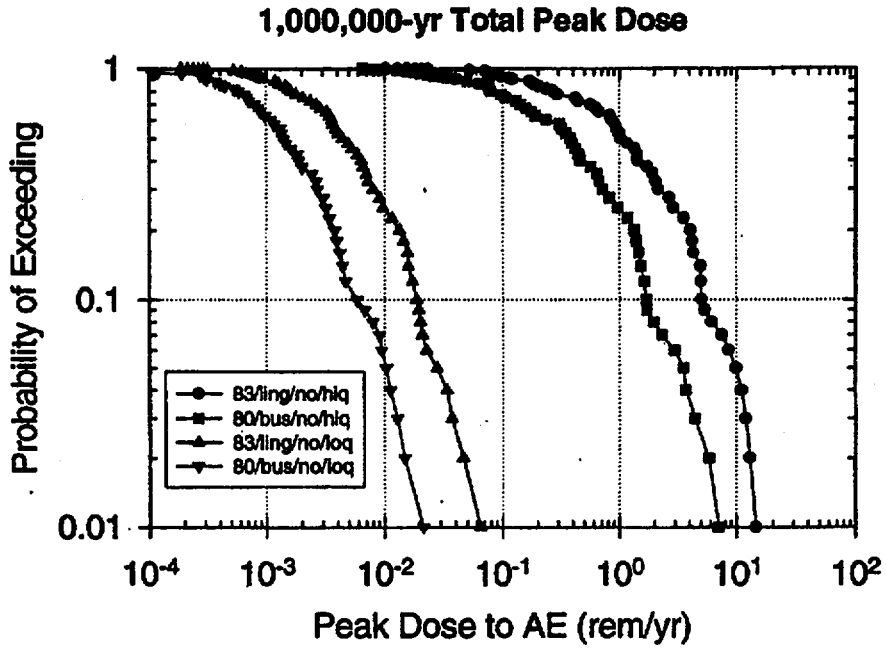


Figure 9.3-32 CCDF of Total Peak Dose: 1,000,000 years, Lingineni 83 MTU/acre and Buscheck 80 MTU/acre, no backfill, high and low infiltration (q_{inf}) ranges, cyclical- q_{inf} climate model.

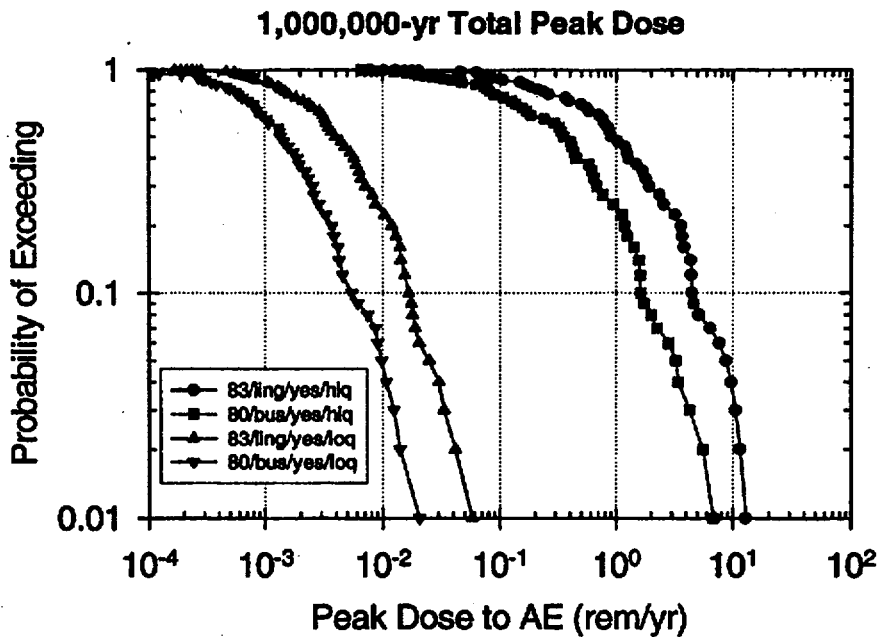


Figure 9.3-33 CCDF of Total Peak Dose: 1,000,000 years, Lingineni 83 MTU/acre and Buscheck 80 MTU/acre, backfill, high and low infiltration (q_{inf}) ranges, cyclical- q_{inf} climate model.

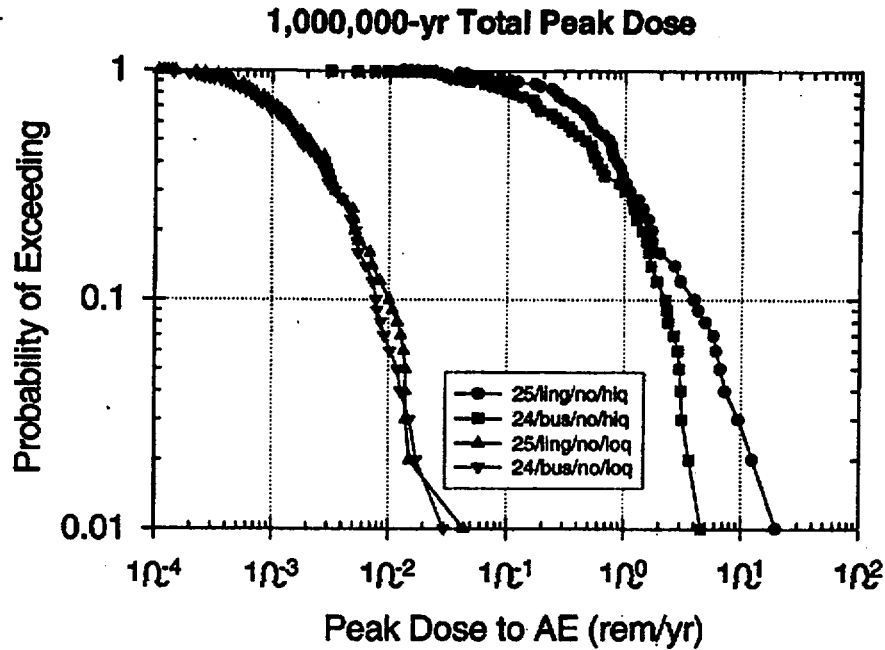


Figure 9.3-34 CCDF of Total Peak Dose: 1,000,000 years, Lingineni 25 MTU/acre and Buscheck 24 MTU/acre, no backfill, high and low infiltration (q_{inf}) ranges, cyclical- q_{inf} climate model.

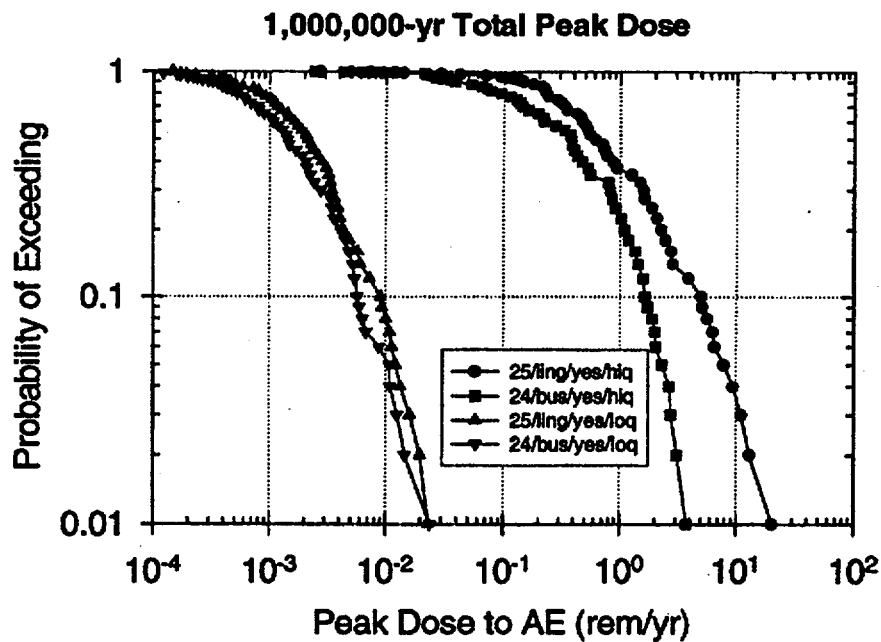


Figure 9.3-35 CCDF of Total Peak Dose: 1,000,000 years, Lingineni 25 MTU/acre and Buscheck 24 MTU/acre, backfill, high and low infiltration (q_{inf}) ranges, cyclical- q_{inf} climate model.

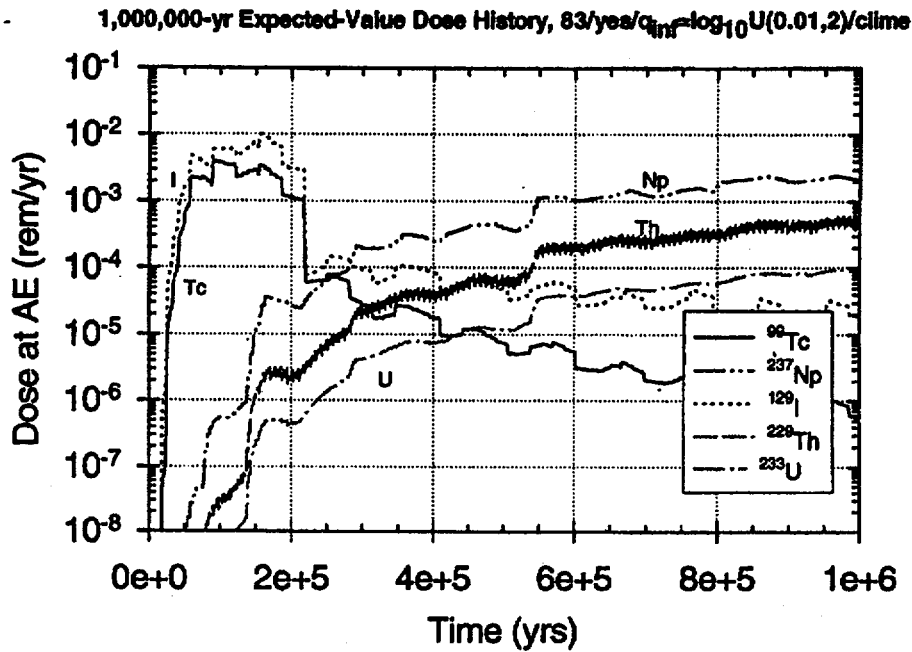


Figure 9.3-36a

Expected-value dose history: 1,000,000 years, 83 MTU/acre, backfill, intermediate infiltration rate (initial $q_{inf} = 0.376$ mm/yr), cyclical- q_{inf} climate model.

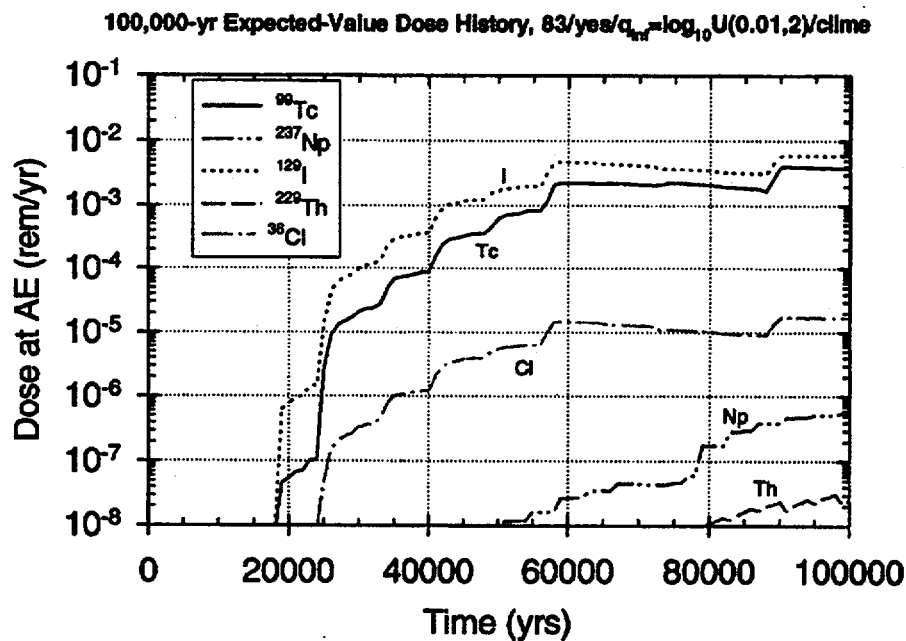


Figure 9.3-36b

Expected-value dose history: 100,000 years, 83 MTU/acre, backfill, intermediate infiltration rate (initial $q_{inf} = 0.376$ mm/yr), cyclical- q_{inf} climate model.

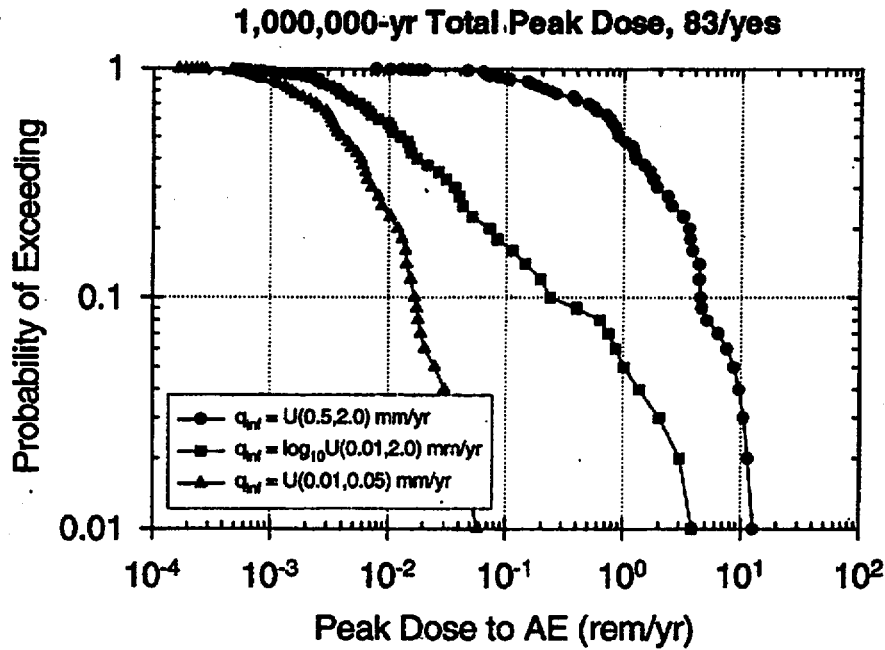


Figure 9.3-37 CCDF of Total Peak Dose: 1,000,000 years, 83 MTU/acre, backfill, high infiltration range ($q_{inf} = 0.5-2.0$ mm/yr), low infiltration range ($q_{inf} = 0.01-0.05$ mm/yr), and entire infiltration range ($q_{inf} = 0.01-2.0$ mm/yr), cyclical- q_{inf}

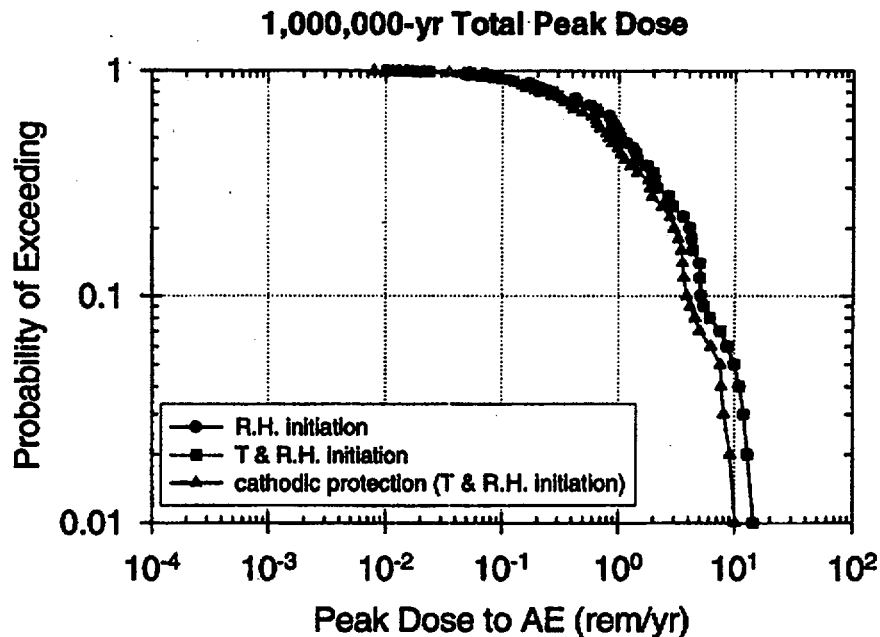


Figure 9.3-38 Effect of alternative corrosion-initiation models: Relative humidity only vs. temperature and relative humidity vs. temperature, relative humidity, and cathodic protection. CCDF of Total Peak Dose: 1,000,000 years, 83 MTU/acre, no backfill, high infiltration range, cyclical- q_{inf} climate model.

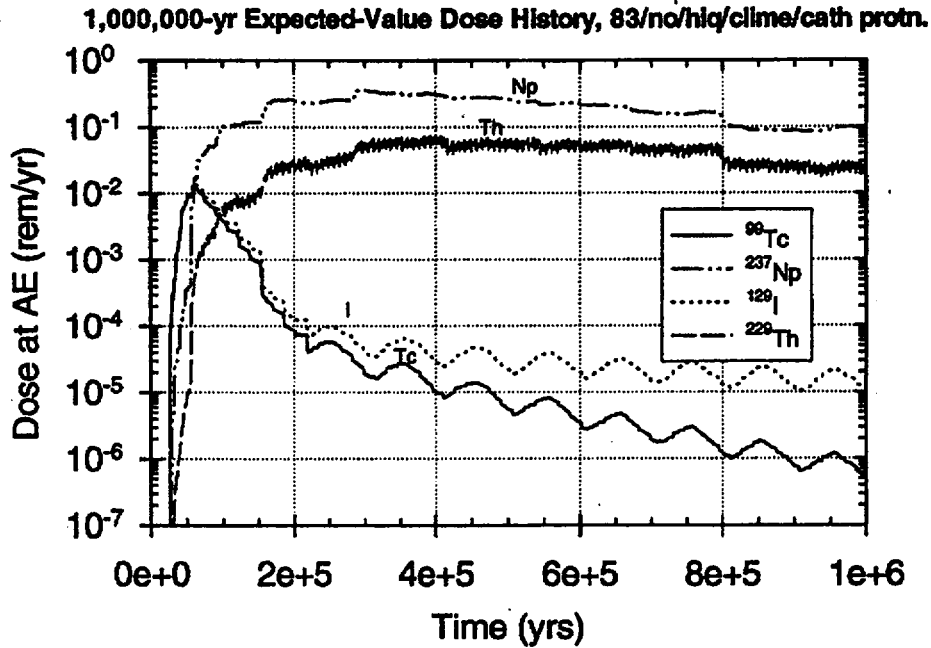


Figure 9.3-39 Expected-value dose history: 1,000,000 years, cathodic protection (with temperature and relative humidity corrosion-initiation), 83 MTU/acre, no backfill, high infiltration (initial $q_{\text{inf}} = 1.25$ mm/yr), cyclical- q_{inf} climate model.

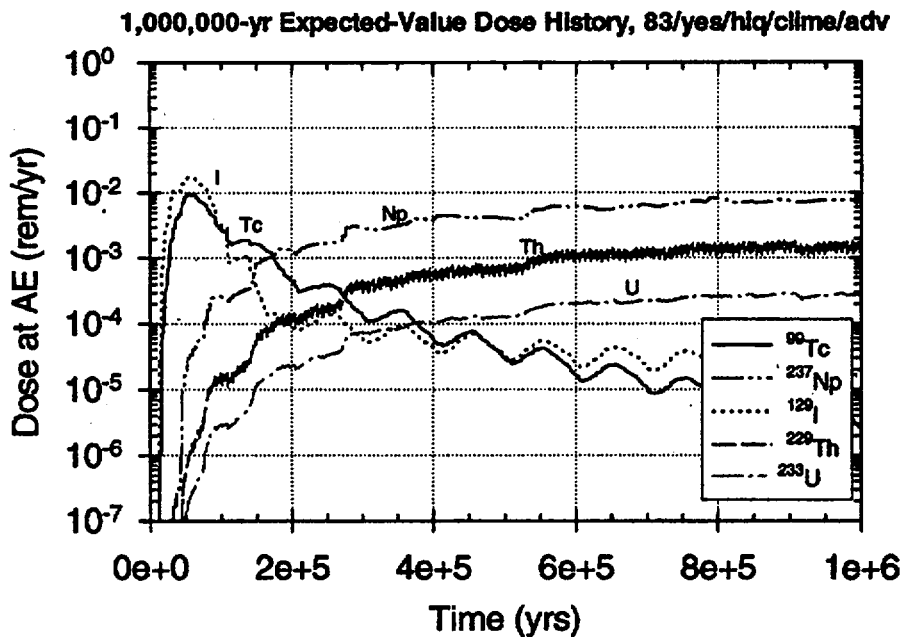


Figure 9.3-40 Expected-value dose history: 1,000,000 years, "drips-on-waste-container" EBS transport model, 83 MTU/acre, backfill, high infiltration (initial $q_{\text{inf}} = 1.25$ mm/yr), cyclical- q_{inf} climate model.

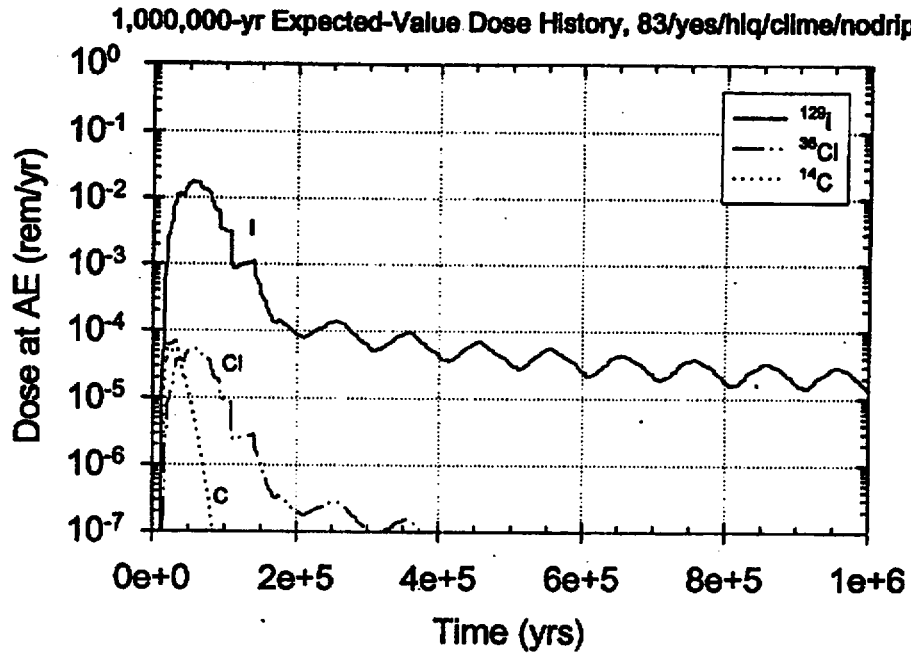


Figure 9.3-41 Expected-value dose history: 1,000,000 years, capillary-barrier-effect ("no drips") EBS transport model, 83 MTU/acre, backfill, high infiltration (initial $q_{inf} = 1.25$ mm/yr), cyclical- q_{inf} climate model.

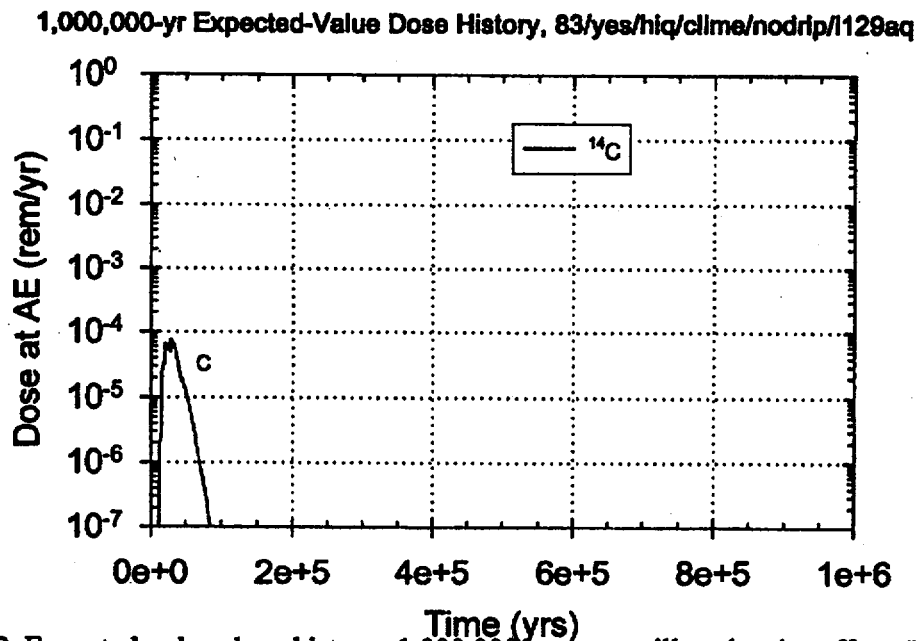


Figure 9.3-42 Expected-value dose history: 1,000,000 years, capillary-barrier-effect ("no drips") EBS transport model with ^{129}I and ^{36}Cl transported through EBS in the aqueous phase, 83 MTU/acre, backfill, high infiltration (initial $q_{inf} = 1.25$ mm/yr), cyclical- q_{inf} climate model.

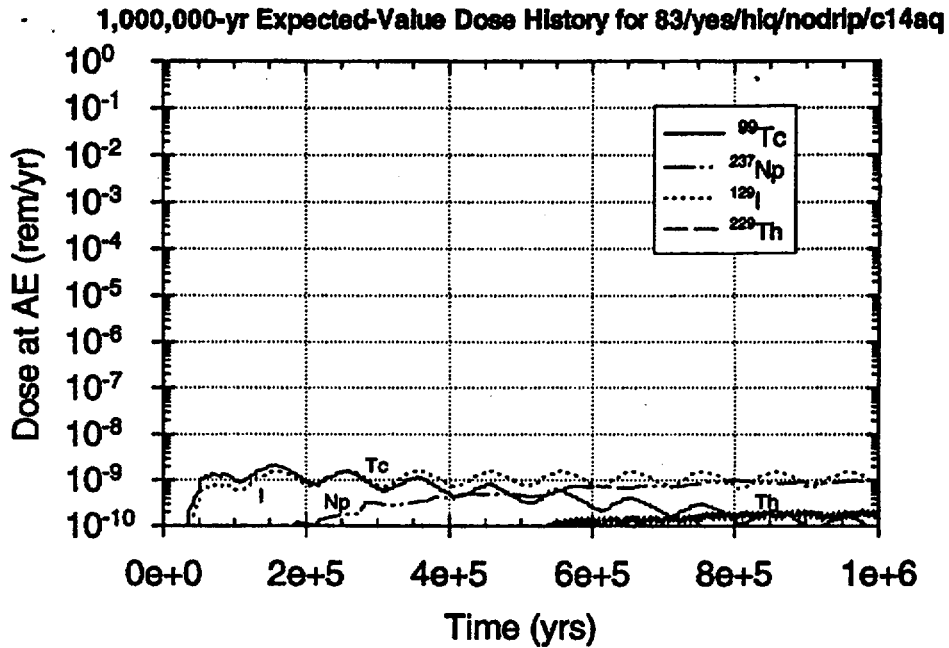


Figure 9.3-43 Expected-value dose history: 1,000,000 years, "diffusion-only" EBS transport model, 83 MTU/acre, backfill, high infiltration (initial $q_{inf} = 1.25$ mm/yr), cyclical- q_{inf} climate model.

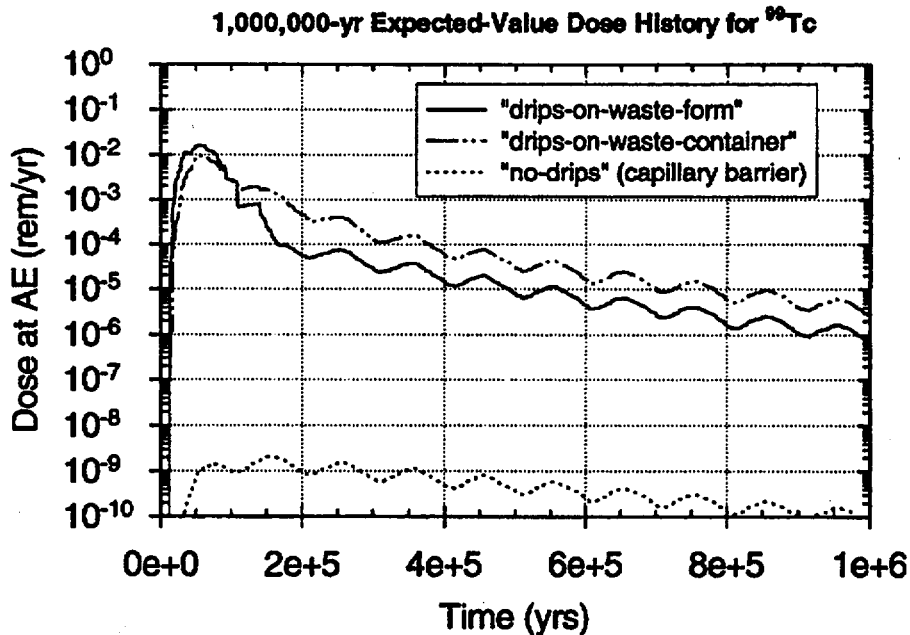


Figure 9.3-44 Comparison of EBS transport models. Expected-value dose history for ⁹⁹Tc: 1,000,000 years, "drips-on-waste-form" model vs. "drips-on-waste-container" model vs. "no-drip" model, 83 MTU/acre, high infiltration (initial $q_{inf} = 1.25$ mm/yr), cyclical- q_{inf} climate model.

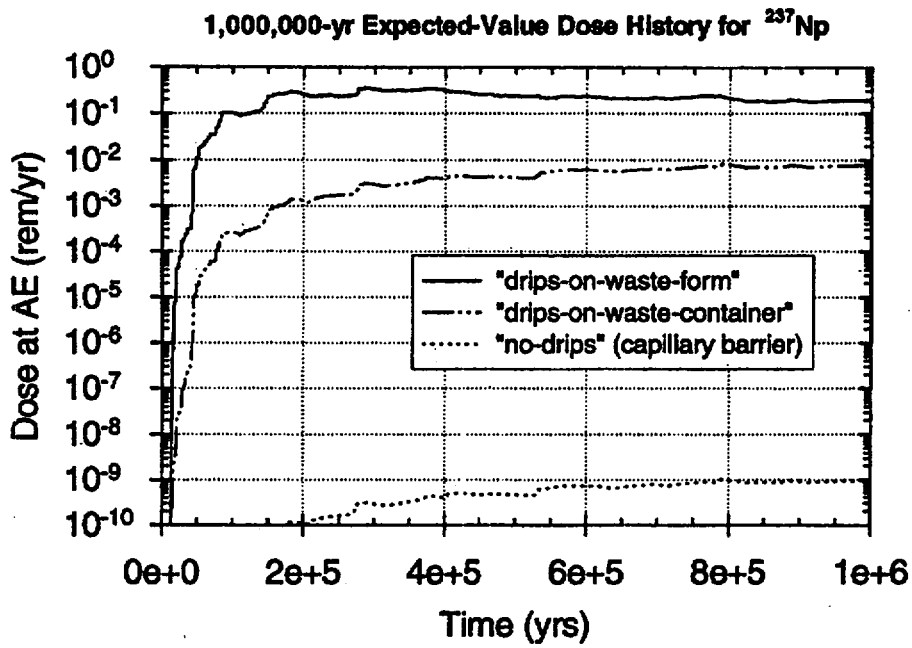


Figure 9.3-45 Comparison of EBS transport models. Expected-value dose history for ^{237}Np : 1,000,000 years, "drips-on-waste-form" model vs. "drips-on-waste-container" model vs. "no-drip" model, 83 MTU/acre, high infiltration (initial $q_{inf} = 1.25$ mm/yr), cyclical- q_{inf} climate model.

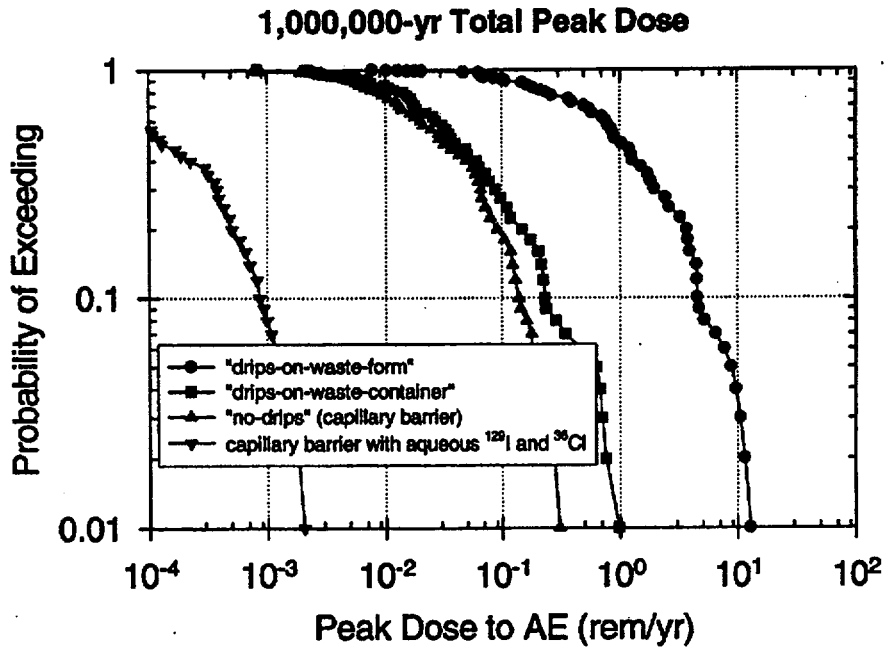


Figure 9.3-46a

Comparison of EBS transport models. CCDF of Total Peak Dose: 1,000,000 years, 83 MTU/acre, high infiltration range, cyclical- q_{inf} climate model.

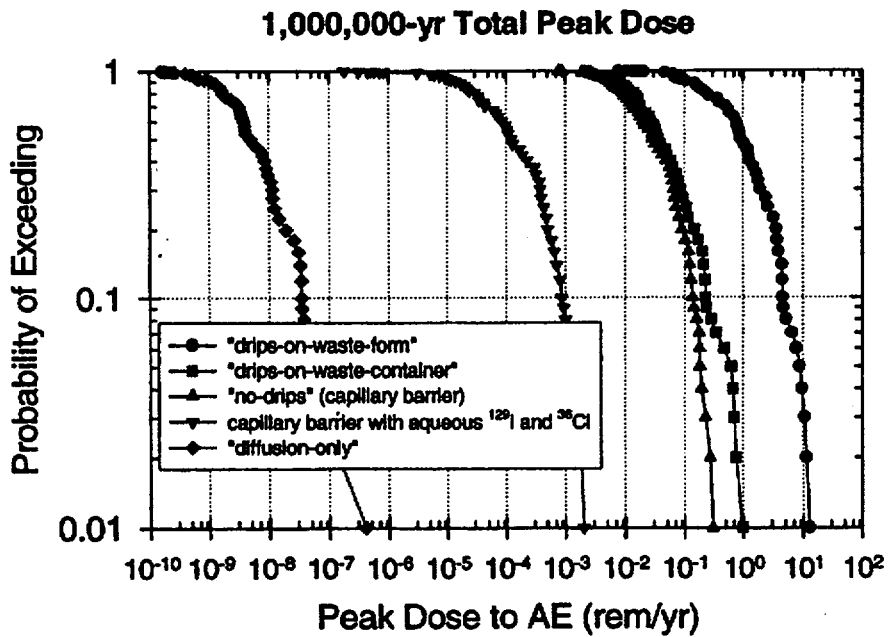


Figure 9.3-46b

Comparison of EBS transport models. CCDF of Total Peak Dose: 1,000,000 years, 83 MTU/acre, high infiltration range, cyclical- q_{inf} climate model.

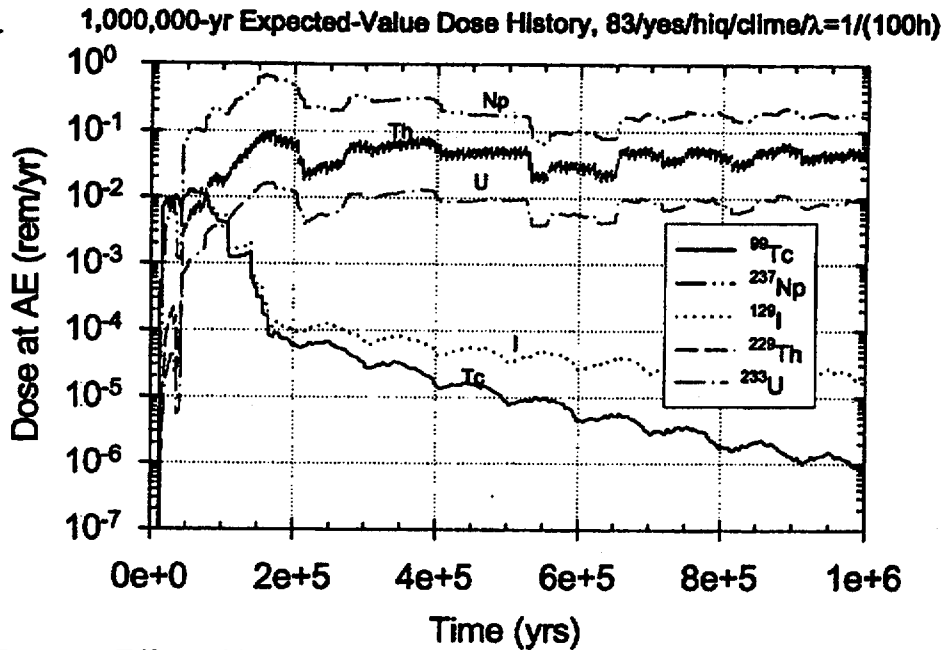


Figure 9.3-47a

Effect of intra-unit fracture connectivity parameter: $\lambda=1/(100 h)$, where h = pathway length in each unit. Expected-value dose history: 1,000,000 years, 83 MTU/acre, backfill, high infiltration (initial $q_{\text{inf}} = 1.25$ mm/yr), cyclical- q_{inf} climate model.

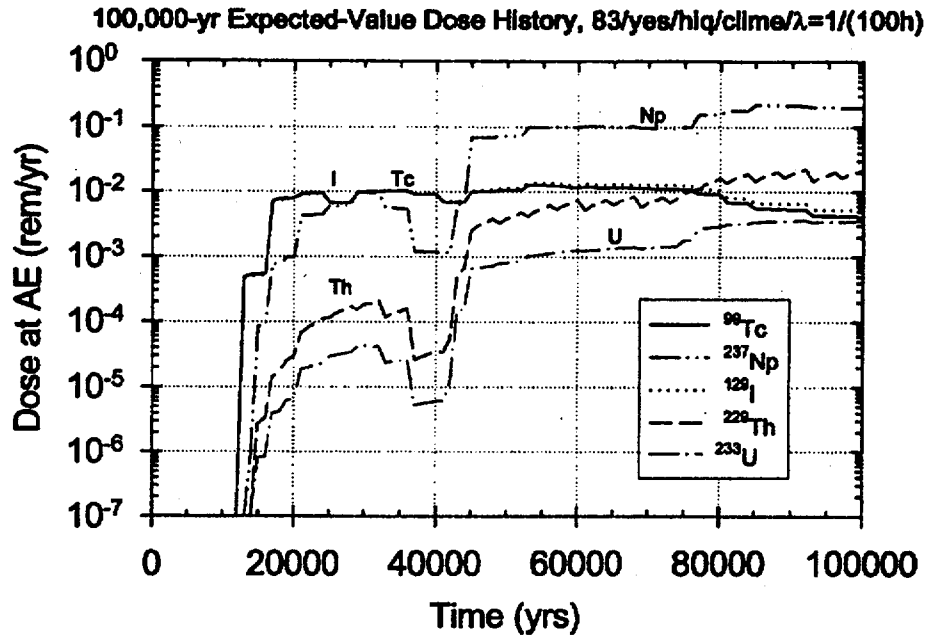


Figure 9.3-47b

Effect of intra-unit fracture connectivity parameter: $\lambda=1/(100 h)$, where h = pathway length in each unit. Expected-value dose history: 100,000 years, 83 MTU/acre, backfill, high infiltration (initial $q_{\text{inf}} = 1.25$ mm/yr), cyclical- q_{inf} climate model.

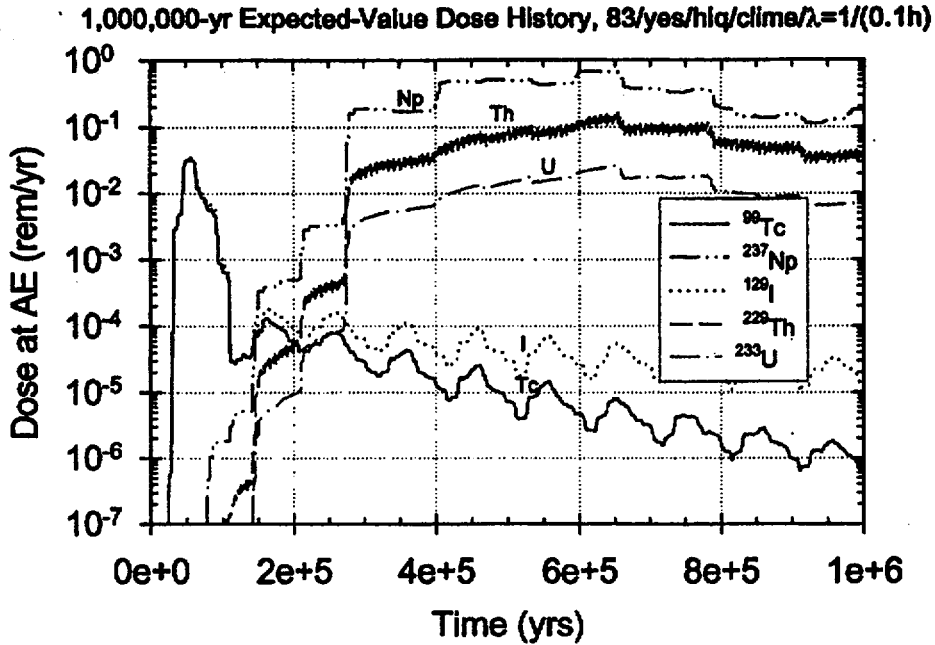


Figure 9.3-48a

Effect of intra-unit fracture connectivity parameter: $\lambda=1/(0.1 h)$, where h = pathway length in each unit. Expected-value dose history: 1,000,000 years, 83 MTU/acre, backfill, high infiltration (initial $q_{\text{inf}} = 1.25$ mm/yr), cyclical- q_{inf} climate model.

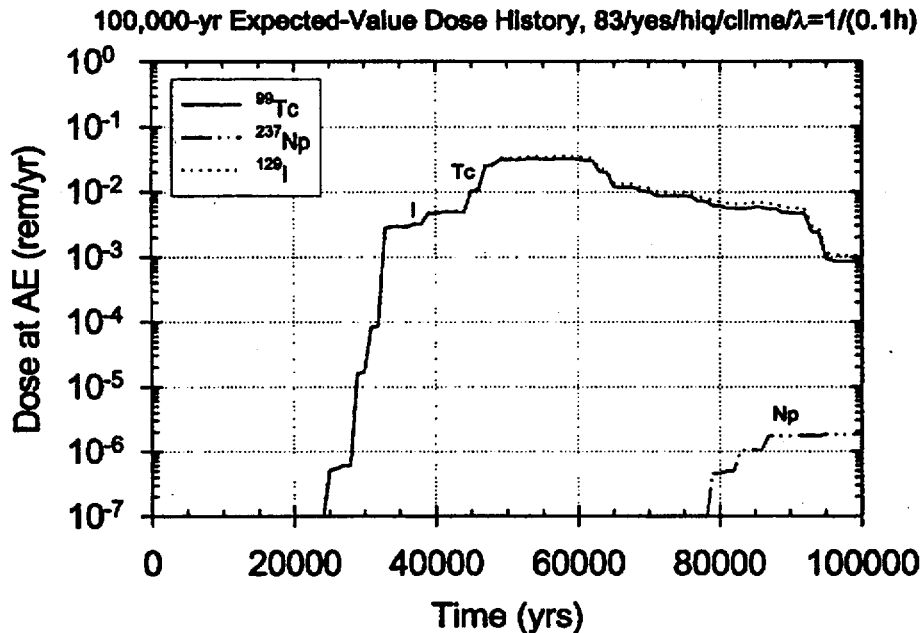


Figure 9.3-48b

Effect of intra-unit fracture connectivity parameter: $\lambda=1/(0.1 h)$, where h = pathway length in each unit. Expected-value dose history: 100,000 years, 83 MTU/acre, backfill, high infiltration (initial $q_{\text{inf}} = 1.25$ mm/yr), cyclical- q_{inf} climate model.

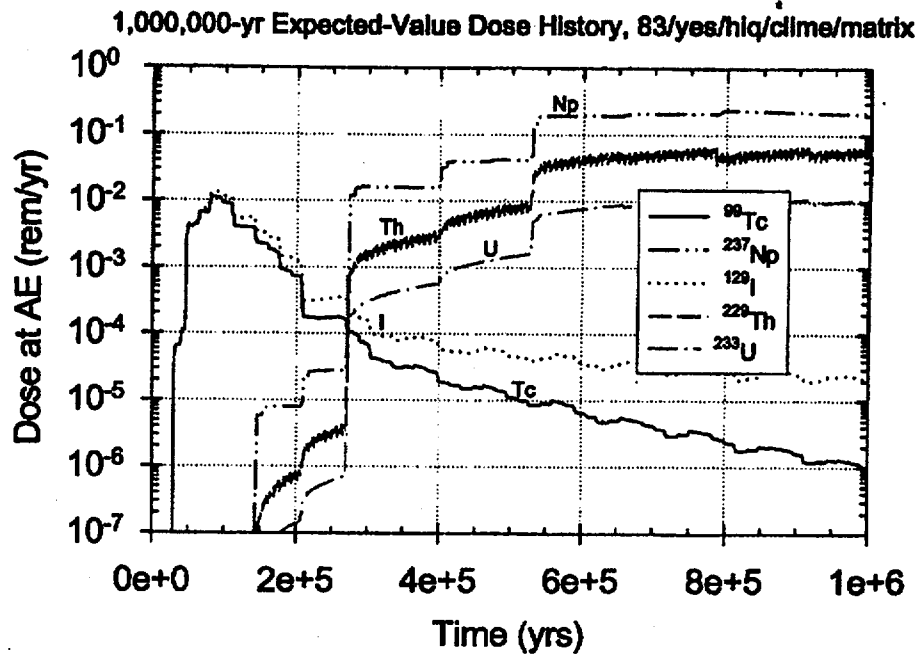


Figure 9.3-49 Effect of matrix-only flow (no fracture flow). Expected-value dose history: 1,000,000 years, 83 MTU/acre, backfill, high infiltration (initial $q_{inf} = 1.25$ mm/yr), cyclical- q_{inf} climate model.

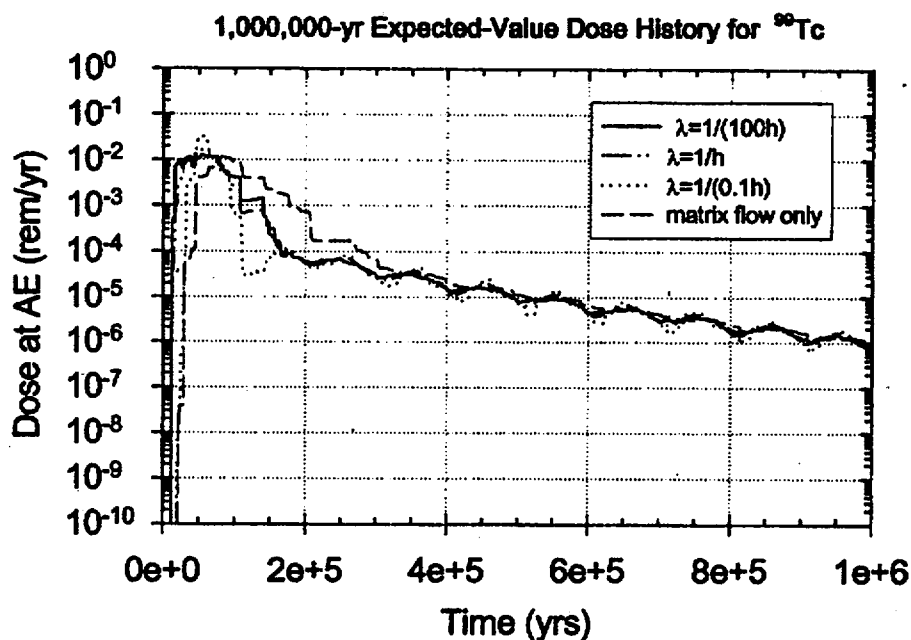


Figure 9.3-50 Comparison of intra-unit fracture connectivity parameter: $\lambda=1/(100 h)$ vs. $\lambda=1/h$ vs. $\lambda=1/(0.1 h)$ vs. matrix-flow-only, where h = pathway length in each unit. Expected-value dose history for ^{99}Tc : 1,000,000 years, 83 MTU/acre, backfill, high infiltration (initial $q_{inf} = 1.25$ mm/yr), cyclical- q_{inf} climate model.

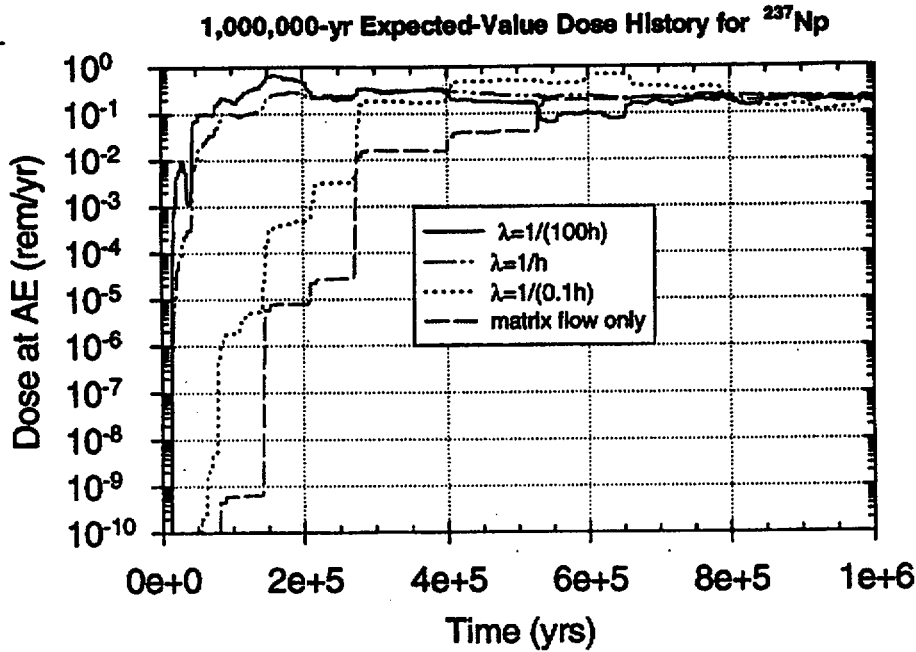


Figure 9.3-51 Comparison of intra-unit fracture connectivity parameter: $\lambda=1/(100 \text{ h})$ vs. $\lambda=1/h$ vs. $\lambda=1/(0.1 \text{ h})$ vs. matrix-flow-only, where h = pathway length in each unit. Expected-value dose history for ^{237}Np : 1,000,000 years, 83 MTU/acre, backfill, high infiltration (initial $q_{\text{inf}} = 1.25 \text{ mm/yr}$), cyclical- q_{inf} climate model.

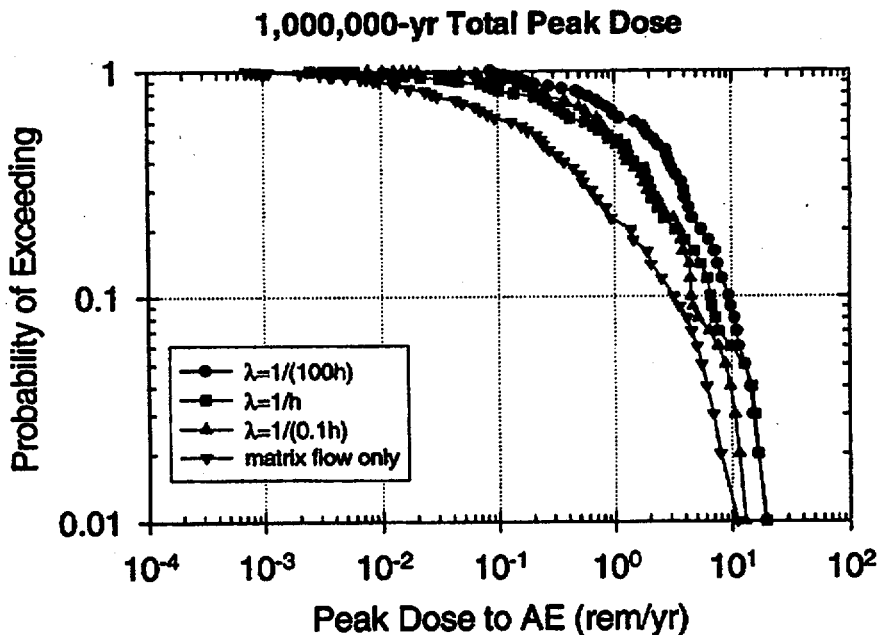


Figure 9.3-52 Comparison of intra-unit fracture connectivity parameter: $\lambda=1/(100 \text{ h})$ vs. $\lambda=1/h$ vs. $\lambda=1/(0.1 \text{ h})$ vs. matrix-flow-only (no fractures), where h = pathway length in each unit. CCDF of Total Peak Dose: 1,000,000 years, 83 MTU/acre, backfill, high infiltration range, cyclical- q_{inf} climate model.

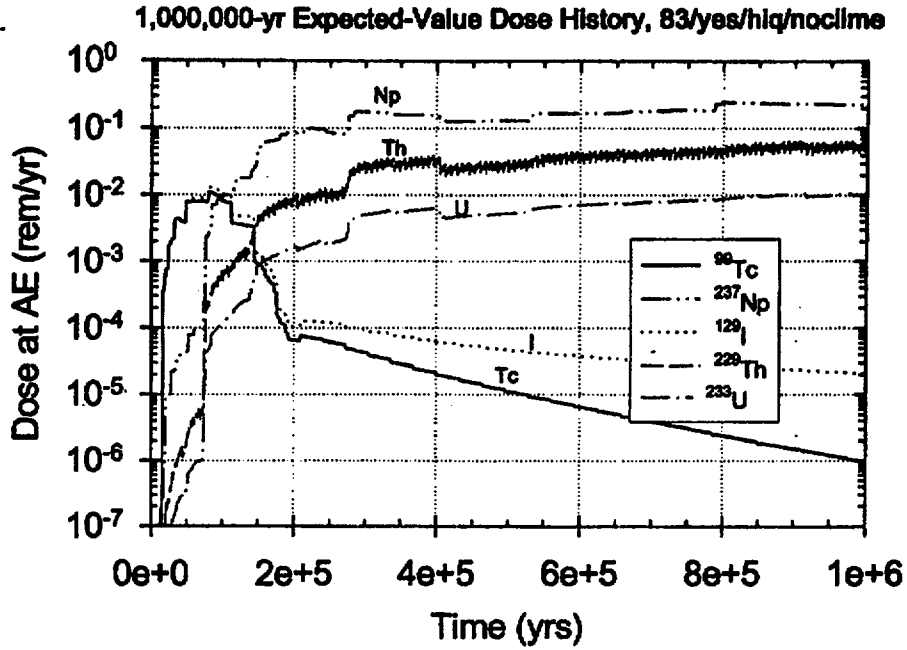


Figure 9.3-53a

No climate-change model. Expected-value dose history: 1,000,000 years, 83 MTU/acre, backfill, high infiltration ($q_{inf} = 1.25$ mm/yr).

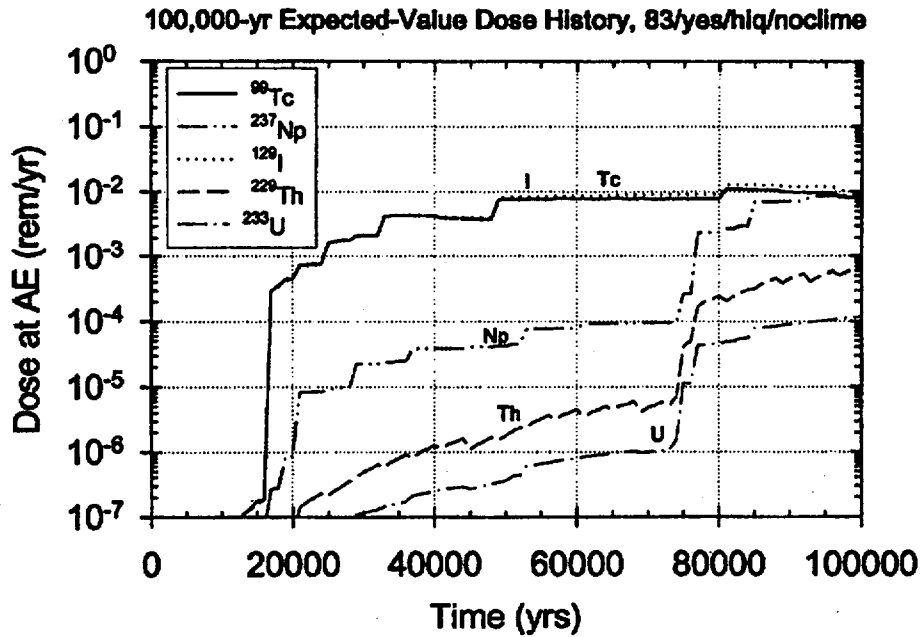


Figure 9.3-53b

No climate-change model. Expected-value dose history: 100,000 years, 83 MTU/acre, backfill, high infiltration ($q_{inf} = 1.25$ mm/yr).

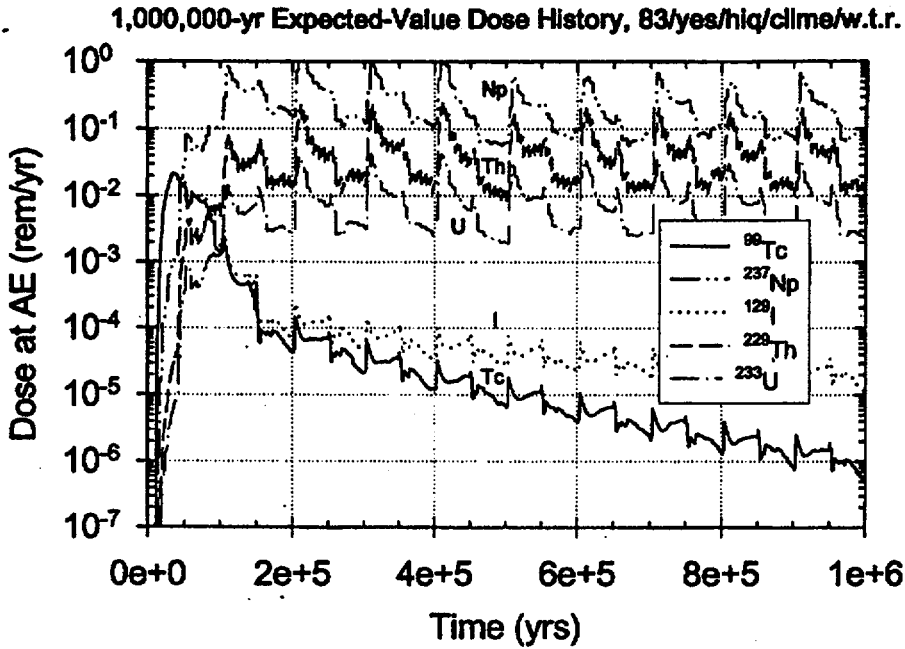


Figure 9.3-54a

Climate-change model with cyclical q_{inf} and cyclical water table rise. Expected-value dose history: 1,000,000 years, 83 MTU/acre, backfill, high infiltration (initial $q_{\text{inf}} = 1.25$ mm/yr).

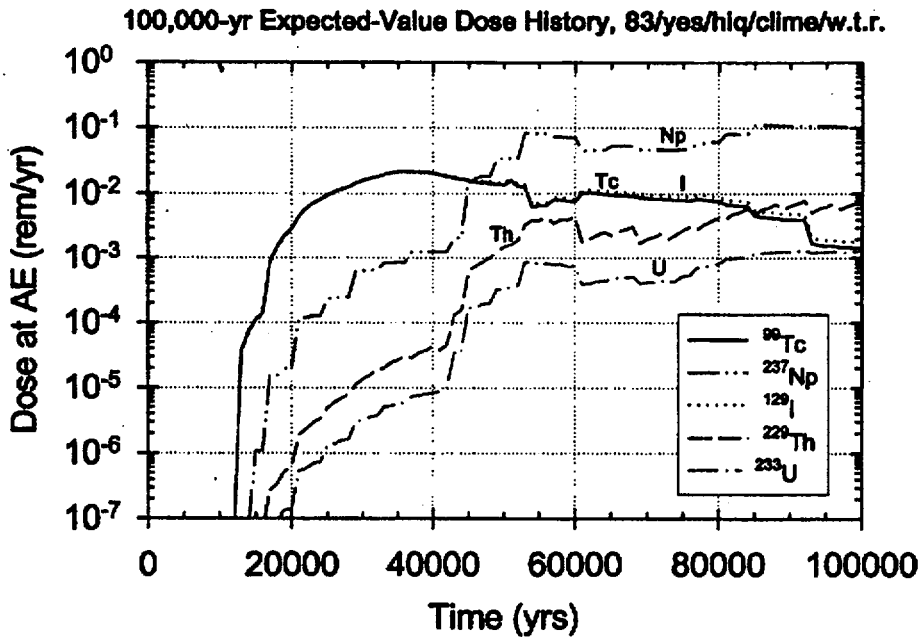


Figure 9.3-54b

Climate-change model with cyclical q_{inf} and cyclical water table rise. Expected-value dose history: 100,000 years, 83 MTU/acre, backfill, high infiltration (initial $q_{\text{inf}} = 1.25$ mm/yr).

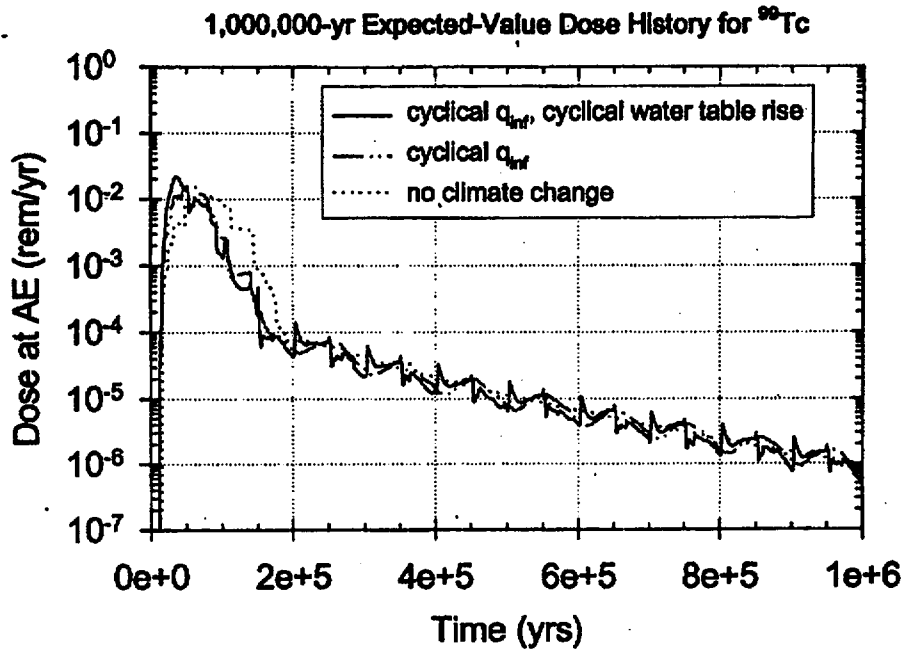


Figure 9.3-55a

Effect of climate on ^{99}Tc dose: Climate change with and without water table rise vs. no climate change. Expected-value dose history: 1,000,000 years, 83 MTU/acre, backfill, high infiltration (initial $q_{\text{inf}} = 1.25 \text{ mm/yr}$).

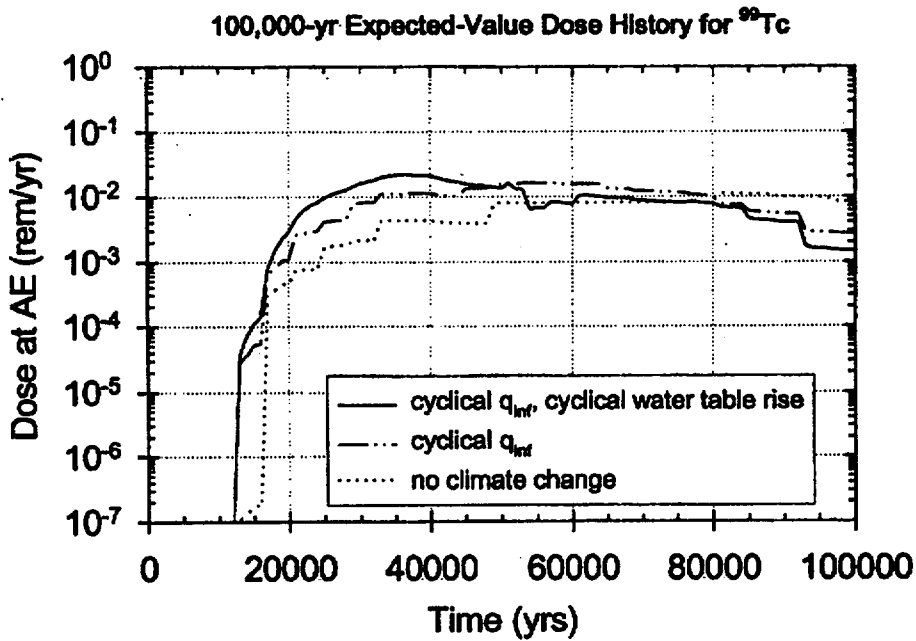


Figure 9.3-55b

Effect of climate on ^{99}Tc dose: Climate change with and without water table rise vs. no climate change. Expected-value dose history: 100,000 years, 83 MTU/acre, backfill, high infiltration (initial $q_{\text{inf}} = 1.25 \text{ mm/yr}$).

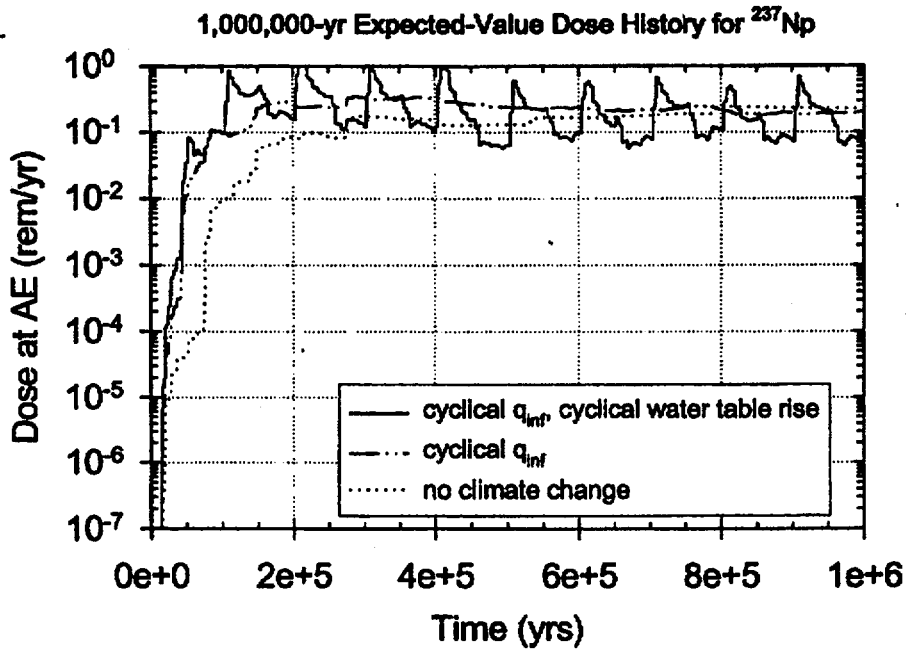


Figure 9.3-56a

Effect of climate on ^{237}Np dose: Climate change with and without water table rise vs. no climate change. Expected-value dose history: 1,000,000 years, 83 MTU/acre, backfill, high infiltration (initial $q_{\text{inf}} = 1.25$ mm/yr).

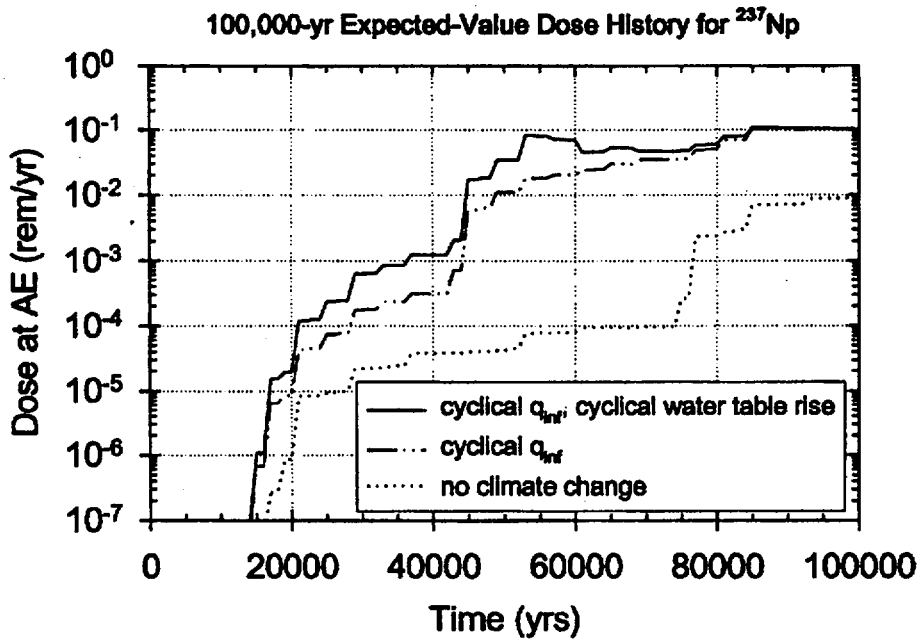


Figure 9.3-56b

Effect of climate on ^{237}Np dose: Climate change with and without water table rise vs. no climate change. Expected-value dose history: 100,000 years, 83 MTU/acre, backfill, high infiltration (initial $q_{\text{inf}} = 1.25$ mm/yr).

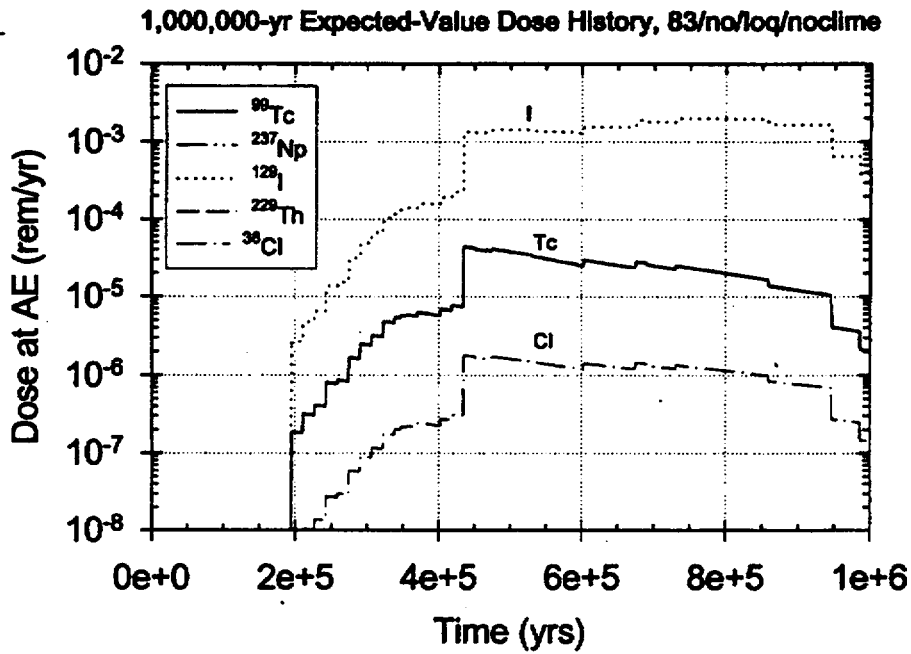


Figure 9.3-57 No climate-change model. Expected-value dose history: 1,000,000 years, 83 MTU/acre, no backfill, low infiltration ($q_{inf} = 0.03$ mm/yr).

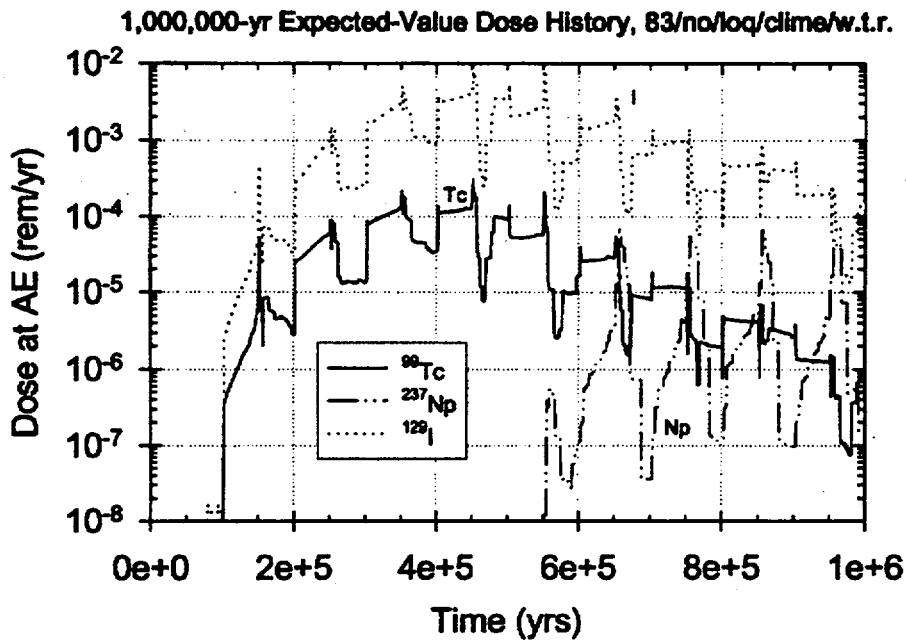


Figure 9.3-58 Climate-change model with cyclical q_{inf} and cyclical water table rise. Expected-value dose history: 1,000,000 years, 83 MTU/acre, no backfill, low infiltration (initial $q_{inf} = 0.03$ mm/yr).

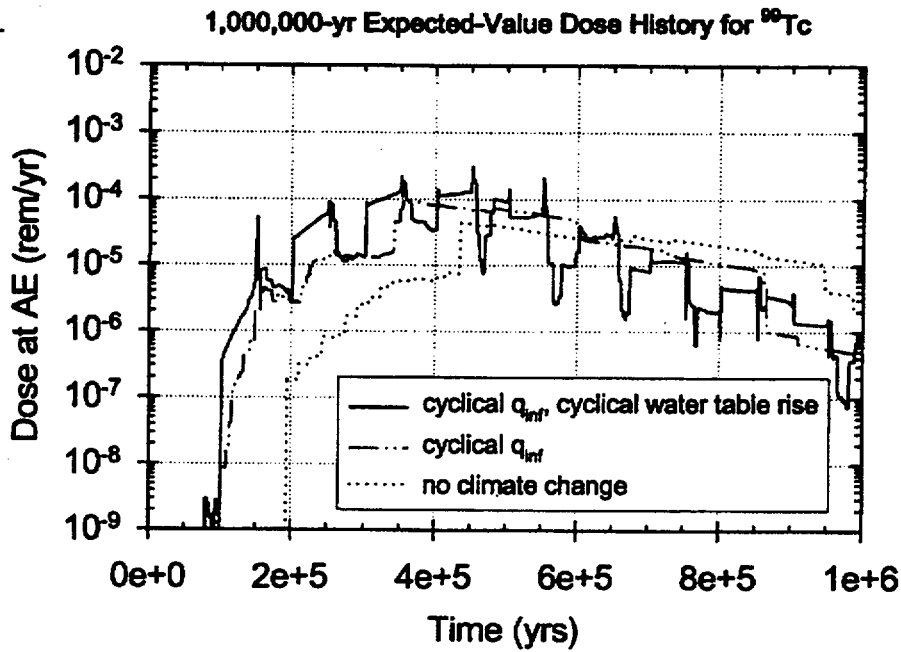


Figure 9.3-59 Effect of climate on ^{99}Tc dose: Climate change with and without water table rise vs. no climate change. Expected-value dose history: 1,000,000 years, 83 MTU/acre, no backfill, low infiltration (initial $q_{\text{inf}} = 0.03$ mm/yr).

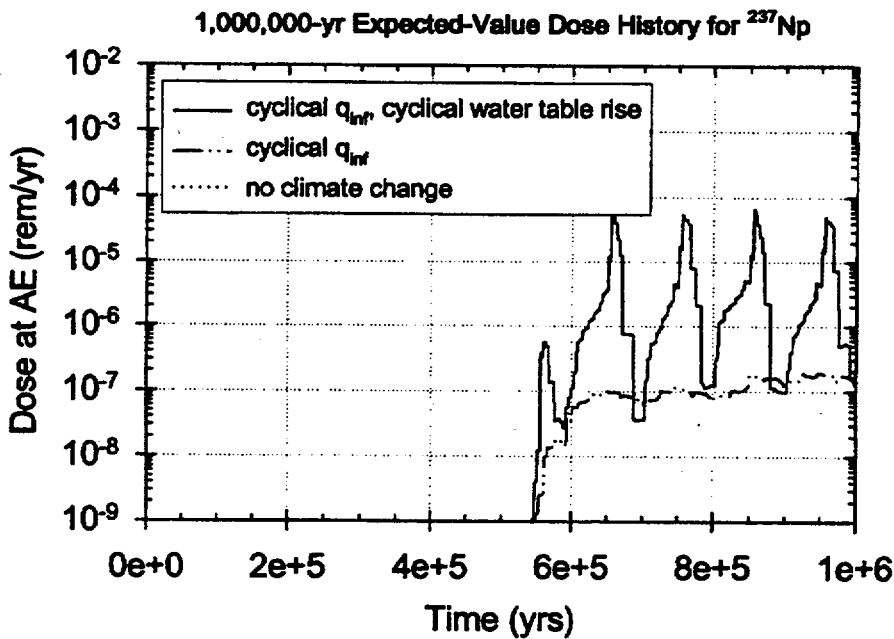


Figure 9.3-60 Effect of climate on ^{237}Np dose: Climate change with and without water table rise vs. no climate change. Expected-value dose history: 1,000,000 years, 83 MTU/acre, no backfill, low infiltration (initial $q_{\text{inf}} = 0.03$ mm/yr).

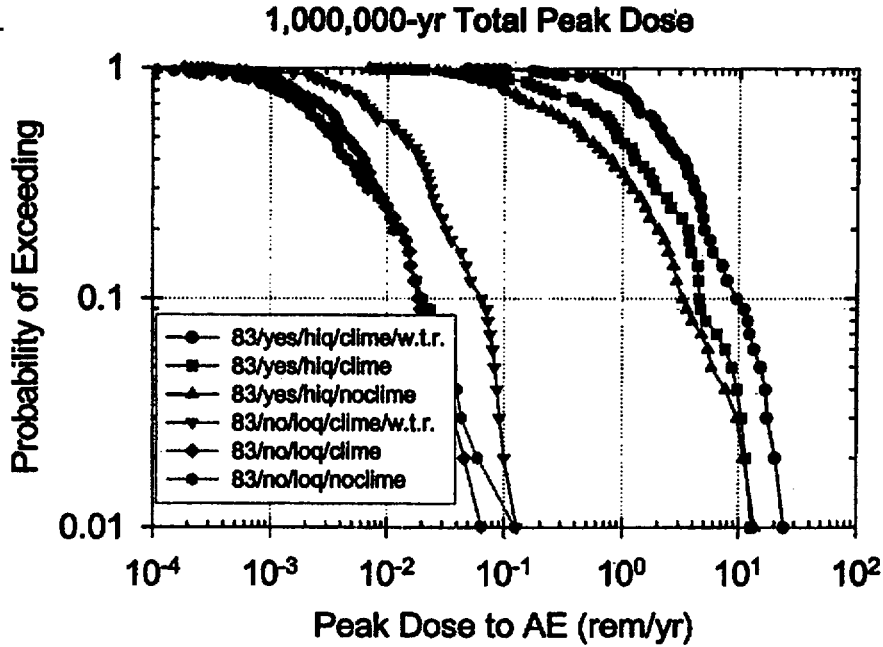


Figure 9.3-61 Effect of climate on total dose: Climate change with and without water table rise ("w.t.r.") vs. no climate change. CCDF of Total Peak Dose: 1,000,000 years, 83 MTU/acre, with and without backfill, high and low infiltration ranges.

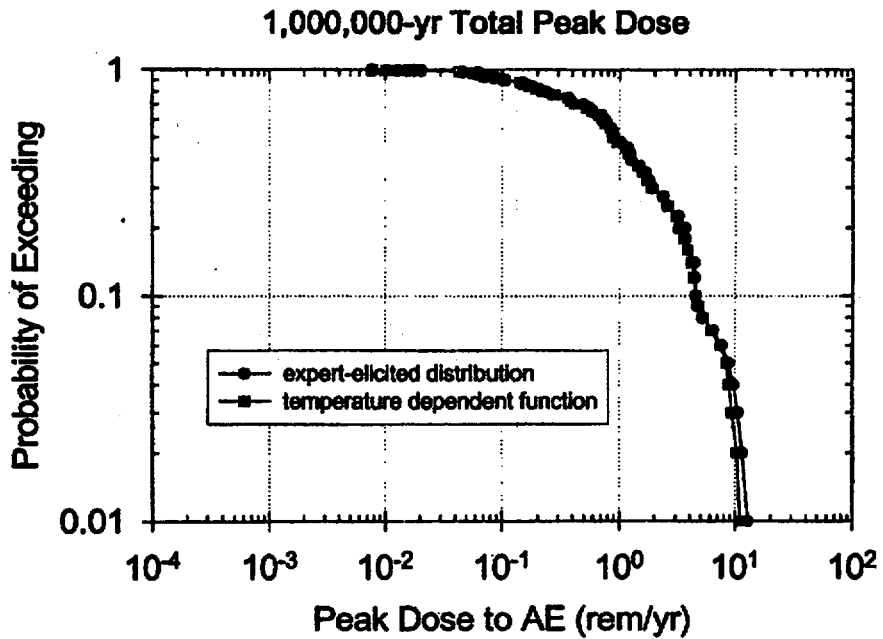


Figure 9.3-62 Effect of alternative models for Np, Pu, and Am solubility: LANL expert-elicited model vs. Sassani temperature-dependent model. CCDF of Total Peak Dose: 1,000,000 years, 83 MTU/acre, backfill, high infiltration range.

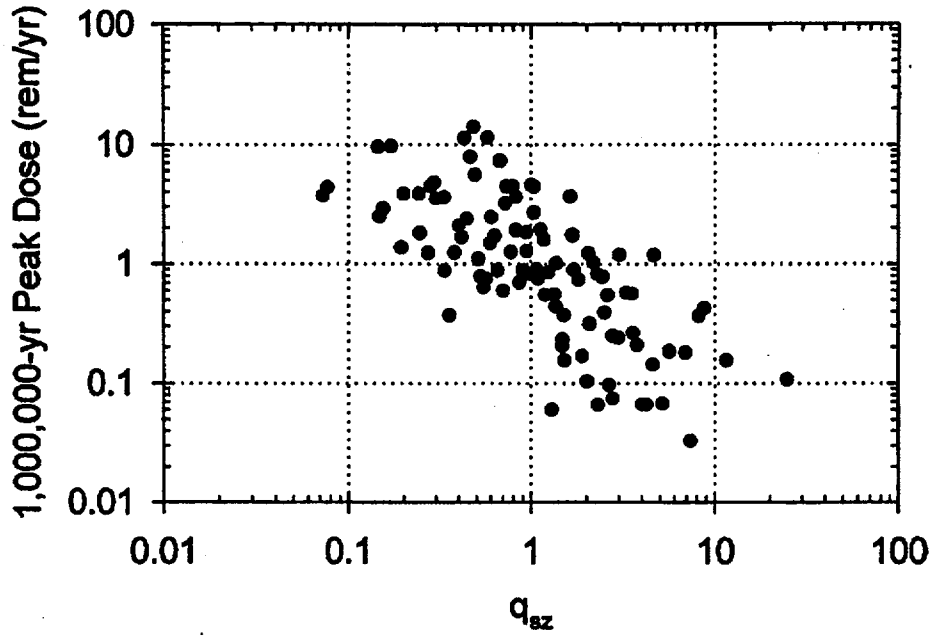


Figure 9.3-63 Scatter plot of 1,000,000-yr total peak dose versus saturated zone Darcy velocity (m/yr) for 83 MTU/acre, backfill, high infiltration (initial $q_{inf} = 1.25$ mm/yr), cyclical- q_{inf} climate model.

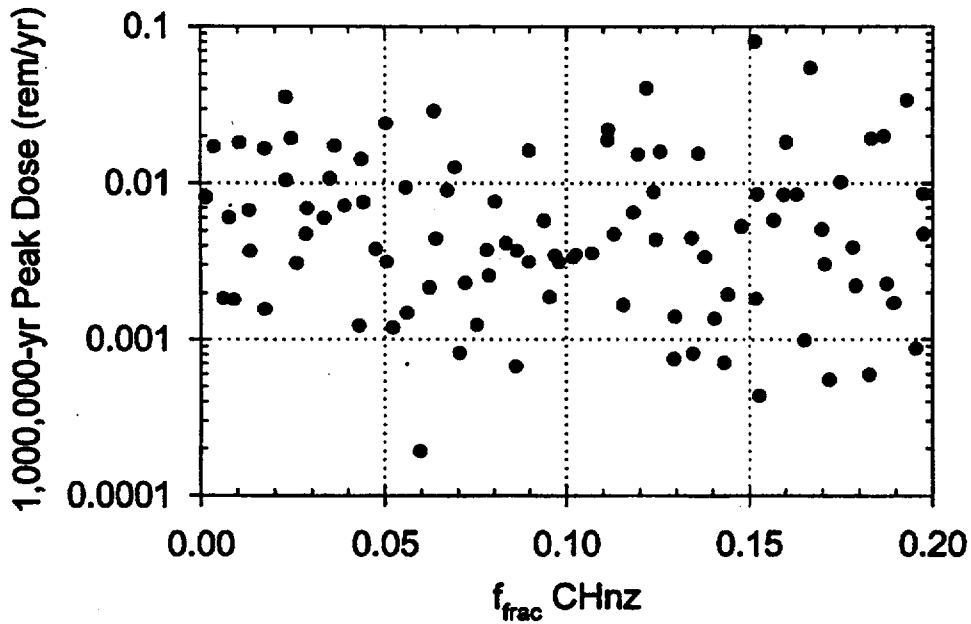


Figure 9.3-64 Scatter plot of 1,000,000-yr total peak dose versus UZ percolation flux (mm/yr) for 83 MTU/acre, backfill, high infiltration (initial $q_{inf} = 1.25$ mm/yr), cyclical- q_{inf} climate model.

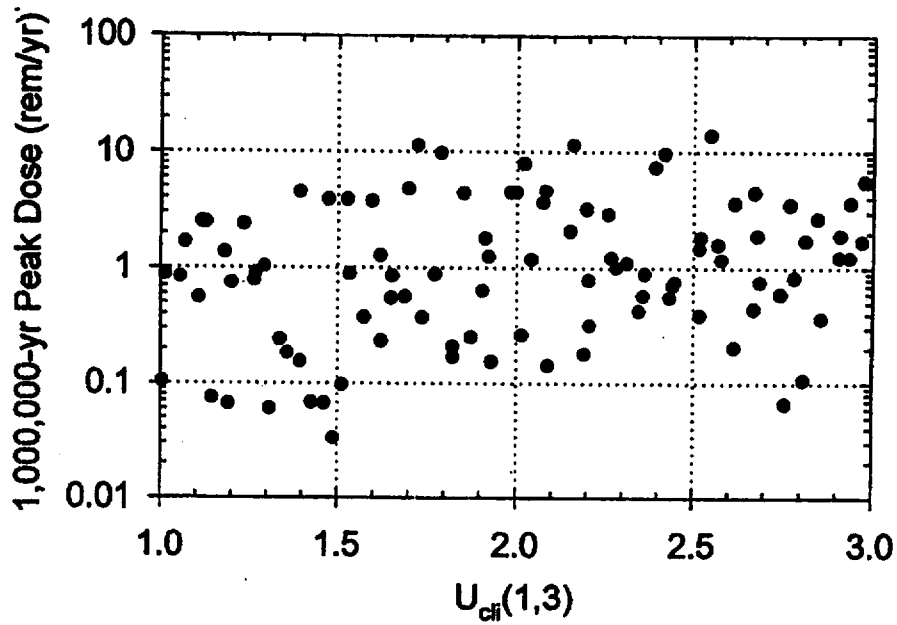


Figure 9.3-65 Scatter plot of 1,000,000-yr total peak dose versus climate change modifier for 83 MTU/acre, backfill, high infiltration (initial $q_{inf} = 1.25$ mm/yr), cyclical- q_{inf} climate model.

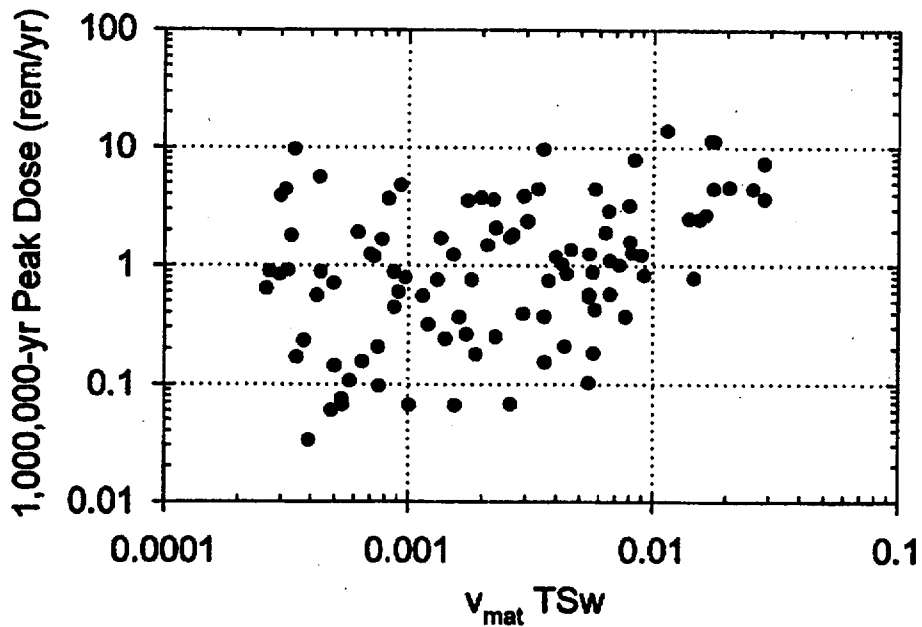


Figure 9.3-66 Scatter plot of 1,000,000-yr total peak dose versus matrix velocity (m/yr) in the TSW for 83 MTU/acre, backfill, high infiltration (initial $q_{inf} = 1.25$ mm/yr), cyclical- q_{inf} climate model.

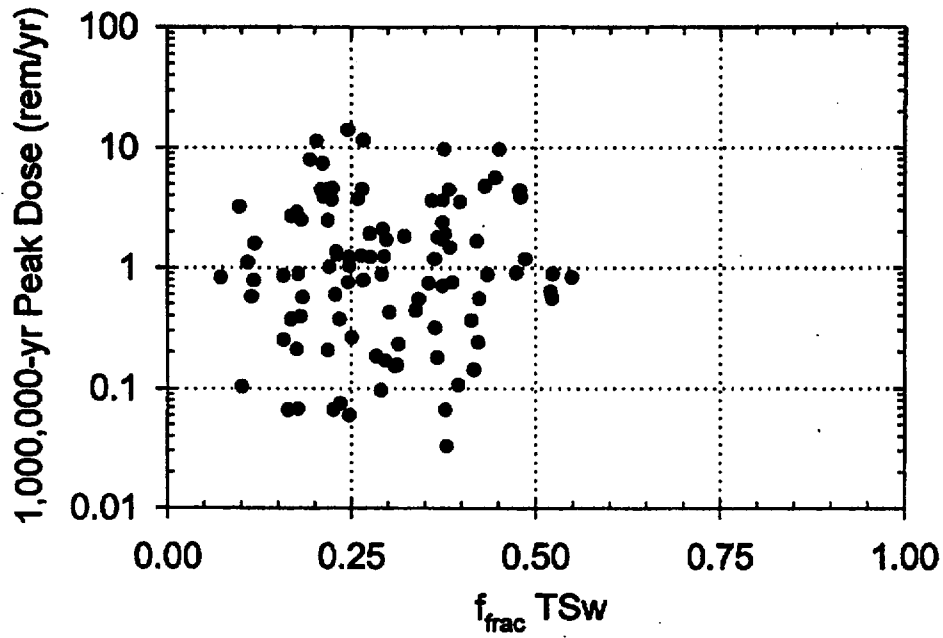


Figure 9.3-67 Scatter plot of 1,000,000-yr total peak dose versus fraction of flow in fractures in the TSw for 83 MTU/acre, backfill, high infiltration (initial $q_{\text{inf}} = 1.25$ mm/yr), cyclical- q_{inf} climate model.

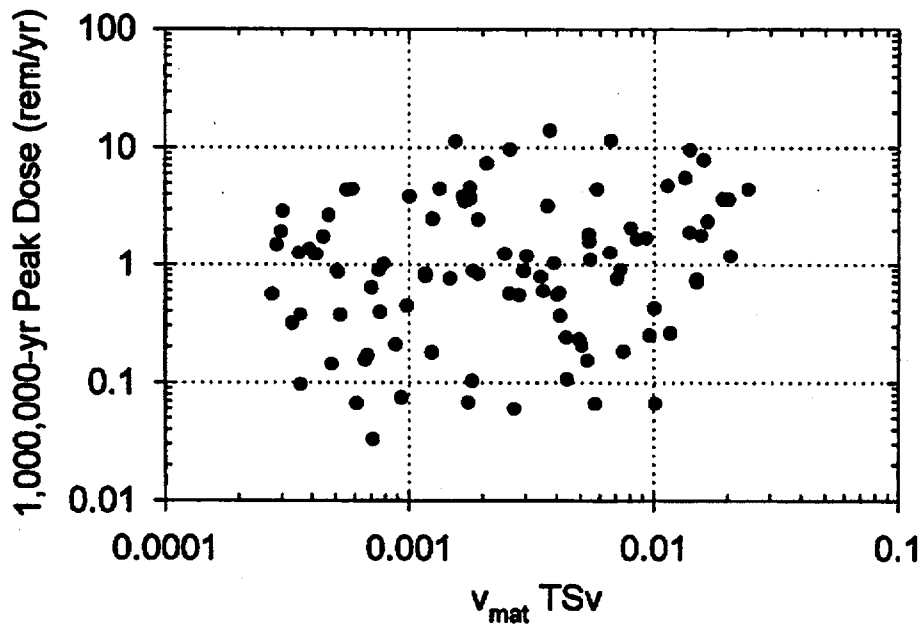


Figure 9.3-68 Scatter plot of 1,000,000-yr total peak dose versus matrix velocity (m/yr) in the TSw for 83 MTU/acre, backfill, high infiltration (initial $q_{\text{inf}} = 1.25$ mm/yr), cyclical- q_{inf} climate model.

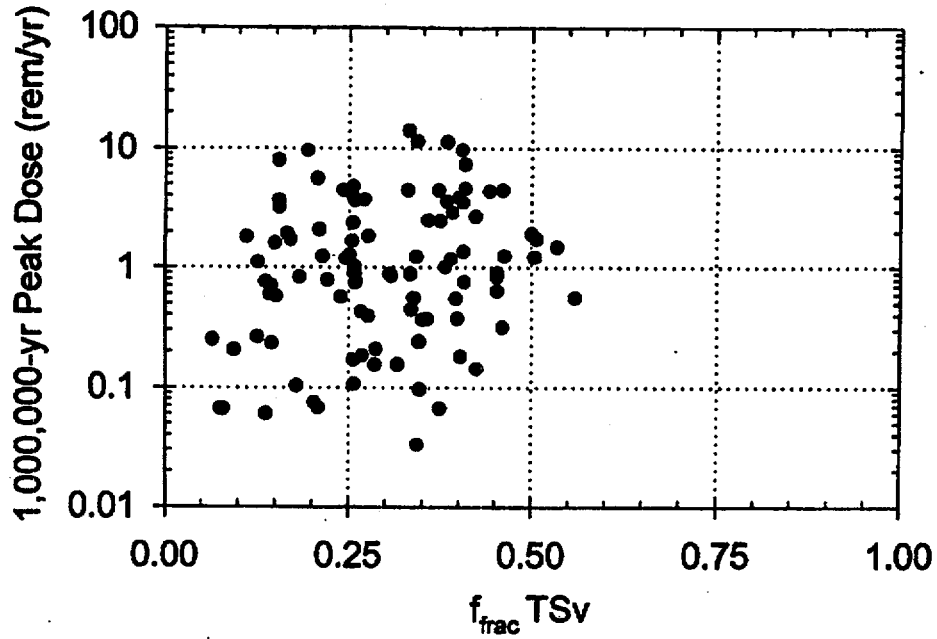


Figure 9.3-69 Scatter plot of 1,000,000-yr total peak dose versus fraction of flow in fractures in the TSv for 83 MTU/acre, backfill, high infiltration (initial $q_{\text{inf}} = 1.25$ mm/yr), cyclical- q_{inf} climate model.

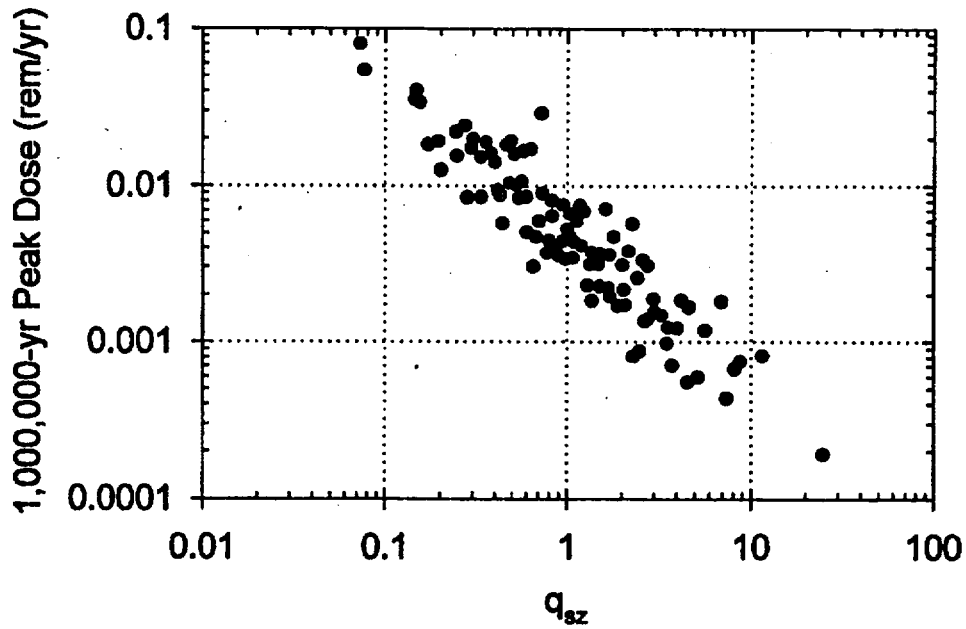


Figure 9.3-70 Scatter plot of 1,000,000-yr total peak dose versus saturated zone Darcy velocity (m/yr) for 83 MTU/acre, backfill, low infiltration (initial $q_{\text{inf}} = 0.03$ mm/yr), cyclical- q_{inf} climate model.

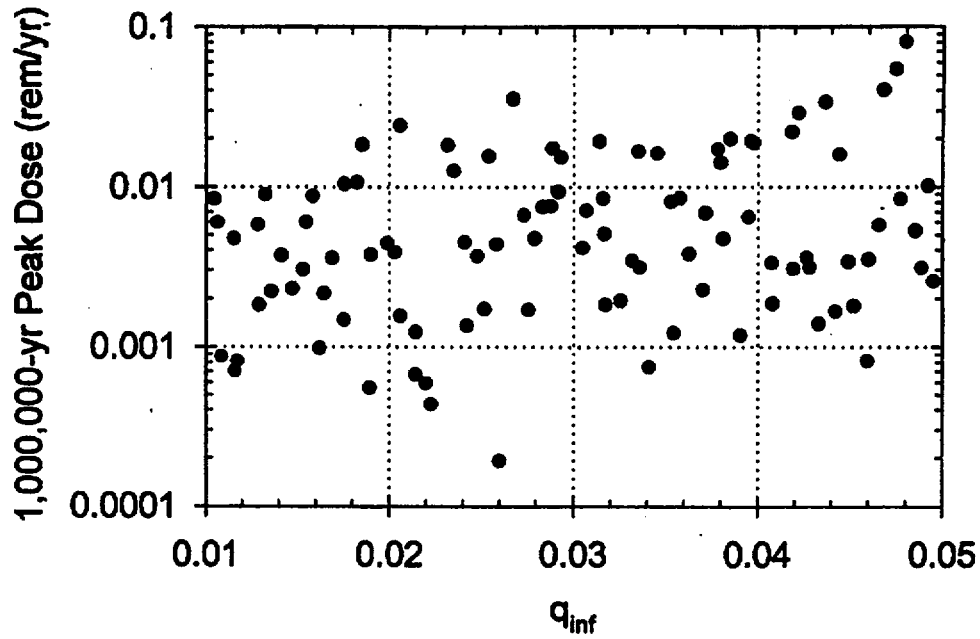


Figure 9.3-71 Scatter plot of 1,000,000-yr total peak dose versus UZ percolation flux (mm/yr) for 83 MTU/acre, backfill, low infiltration (initial $q_{inf} = 0.03$ mm/yr), cyclical- q_{inf} climate model.

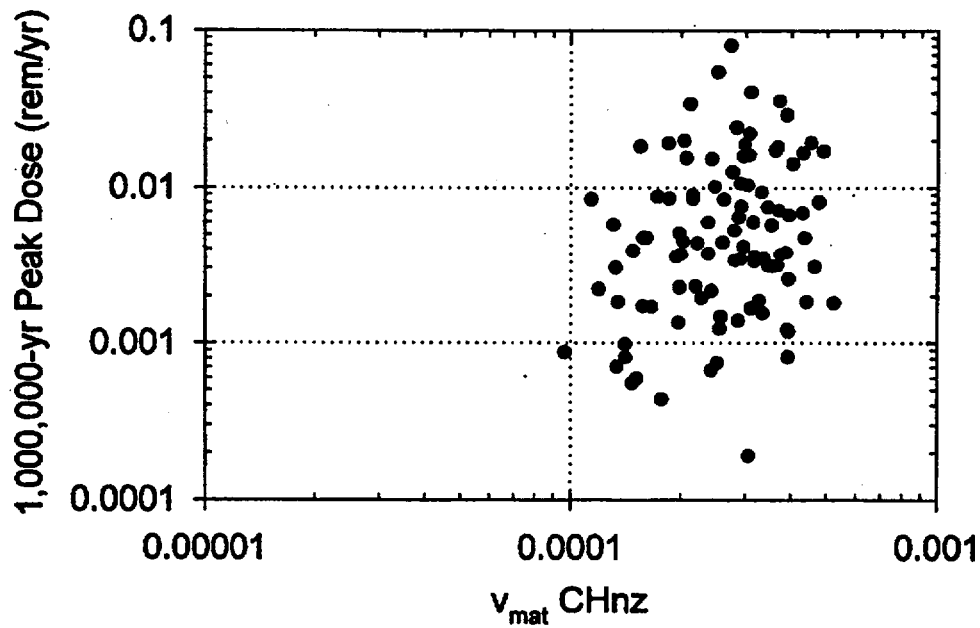


Figure 9.3-72 Scatter plot of 1,000,000-yr total peak dose versus matrix velocity (m/yr) in the CHnz for 83 MTU/acre, backfill, low infiltration (initial $q_{inf} = 0.03$ mm/yr), cyclical- q_{inf} climate model.

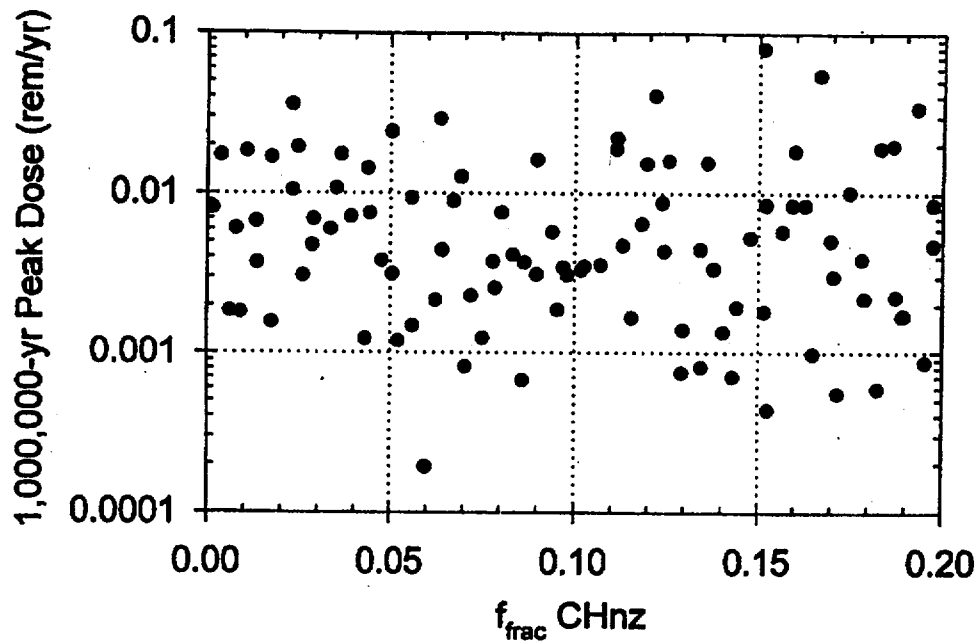


Figure 9.3-73 Scatter plot of 1,000,000-yr total peak dose versus fraction of flow in fractures in the CHnz for 83 MTU/acre, backfill, low infiltration (initial $q_{\text{inf}} = 0.03$ mm/yr), cyclical- q_{inf} climate model.

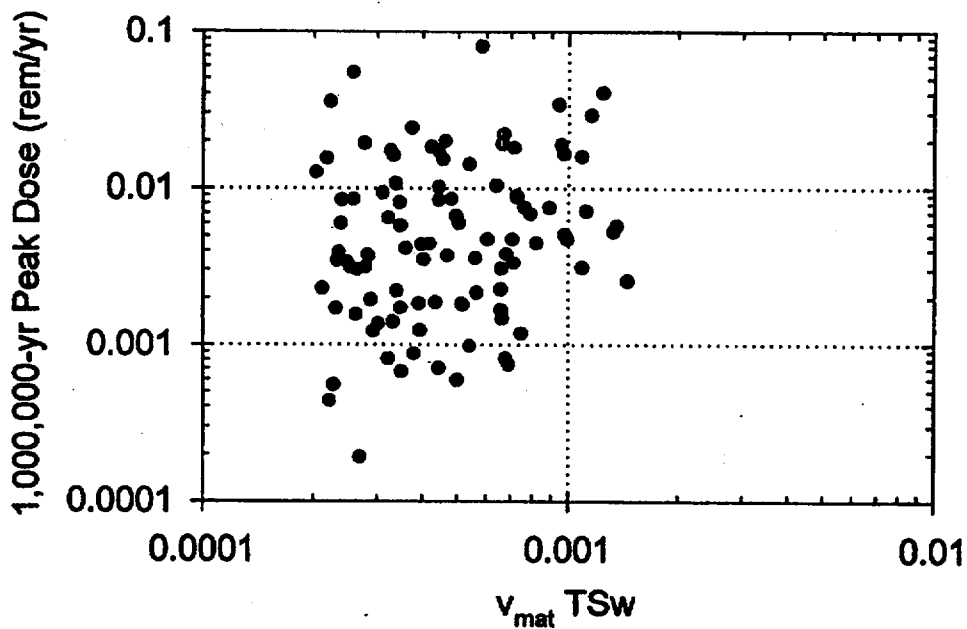


Figure 9.3-74 Scatter plot of 1,000,000-yr total peak dose versus matrix velocity (m/yr) in the TSW for 83 MTU/acre, backfill, low infiltration (initial $q_{\text{inf}} = 0.03$ mm/yr), cyclical- q_{inf} climate model.

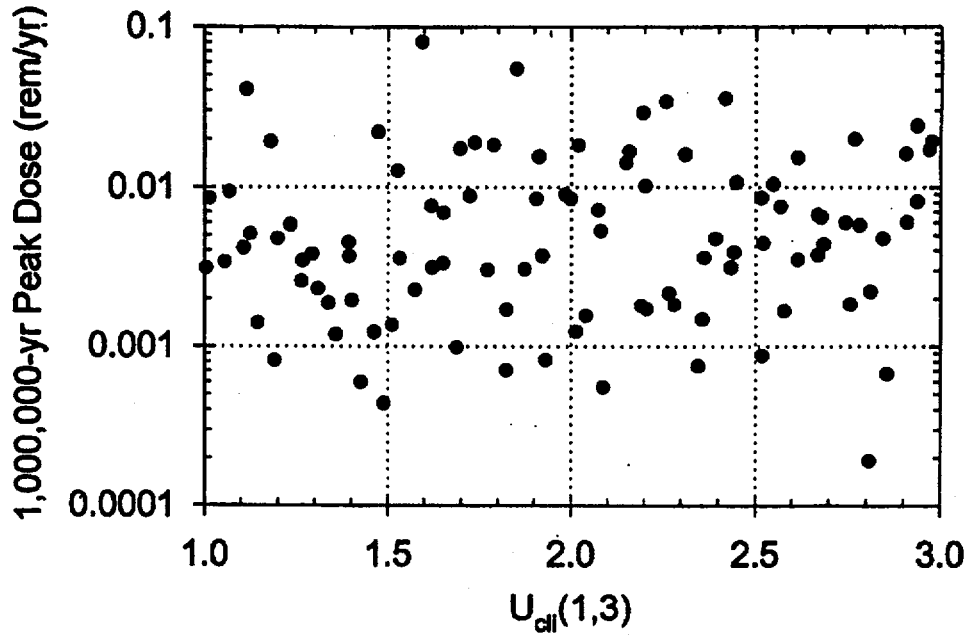


Figure 9.3-75 Scatter plot of 1,000,000-yr total peak dose versus climate change modifier for 83 MTU/acre, backfill, low infiltration (initial $q_{inf} = 0.03$ mm/yr), cyclical- q_{inf} climate model.

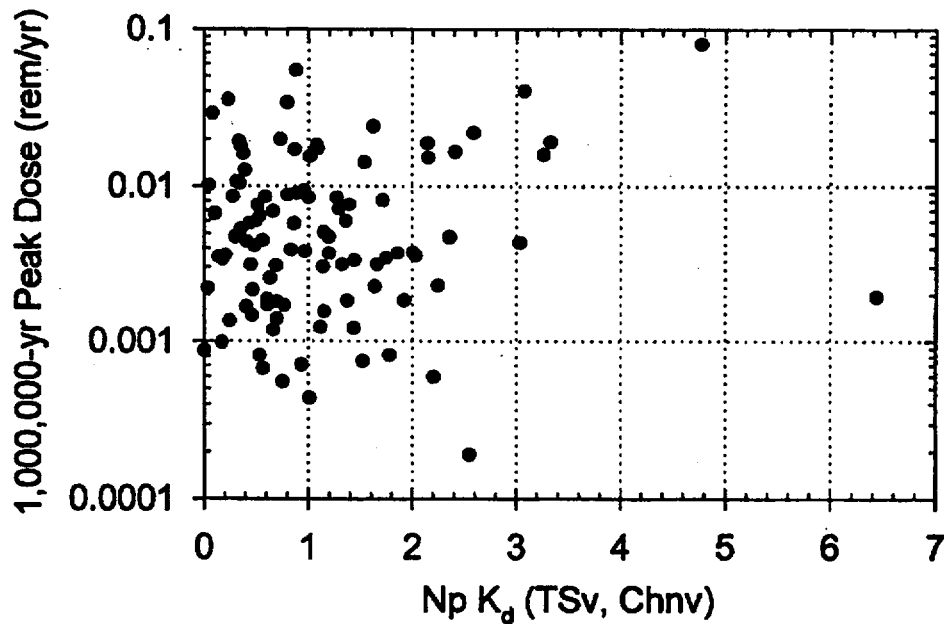


Figure 9.3-76 Scatter plot of 1,000,000-yr total peak dose versus Np sorption coefficient in the vitric tuff for 83 MTU/acre, backfill, low infiltration (initial $q_{inf} = 0.03$ mm/yr), cyclical- q_{inf} climate model.

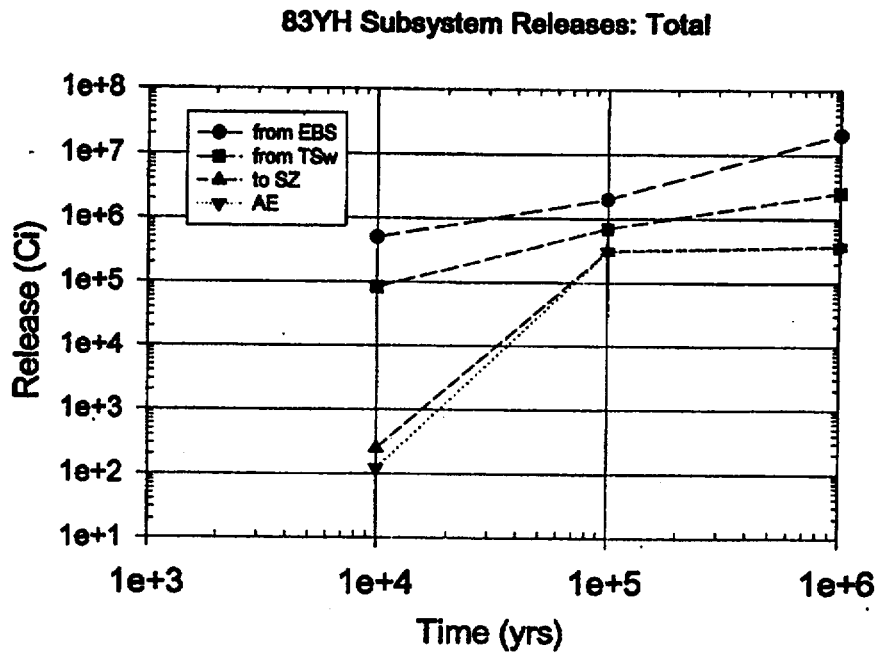


Figure 9.4-1. Subsystem Total Release. Expected-value release at 10,000, 100,000 and 1,000,000 years for 83 MTU/acre, backfill, high infiltration ($q_{inf} = 1.25$ mm/yr), no climate change, with decay.

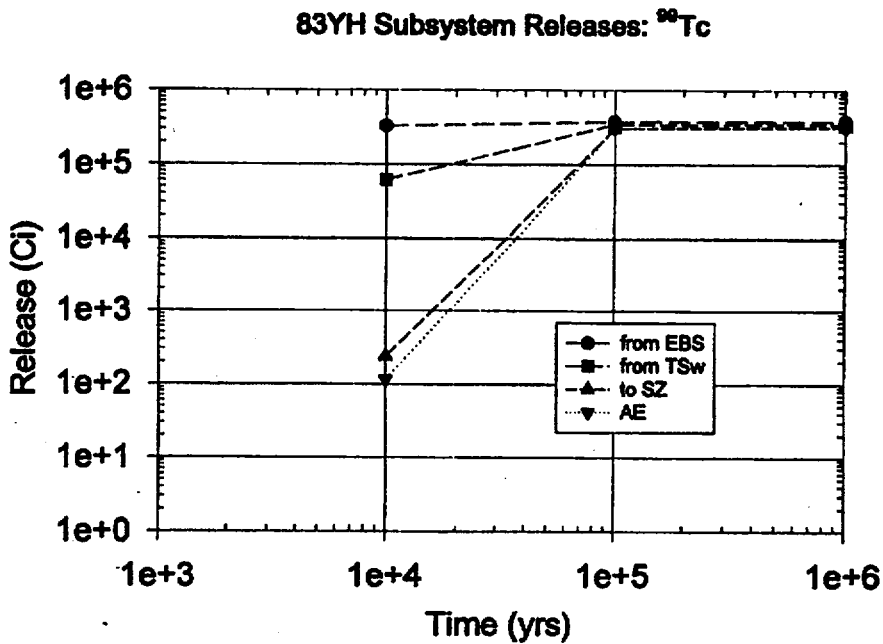


Figure 9.4-2. Subsystem ⁹⁹Tc Release. Expected-value release at 10,000, 100,000 and 1,000,000 years for 83 MTU/acre, backfill, high infiltration ($q_{inf} = 1.25$ mm/yr), no climate change, with decay.

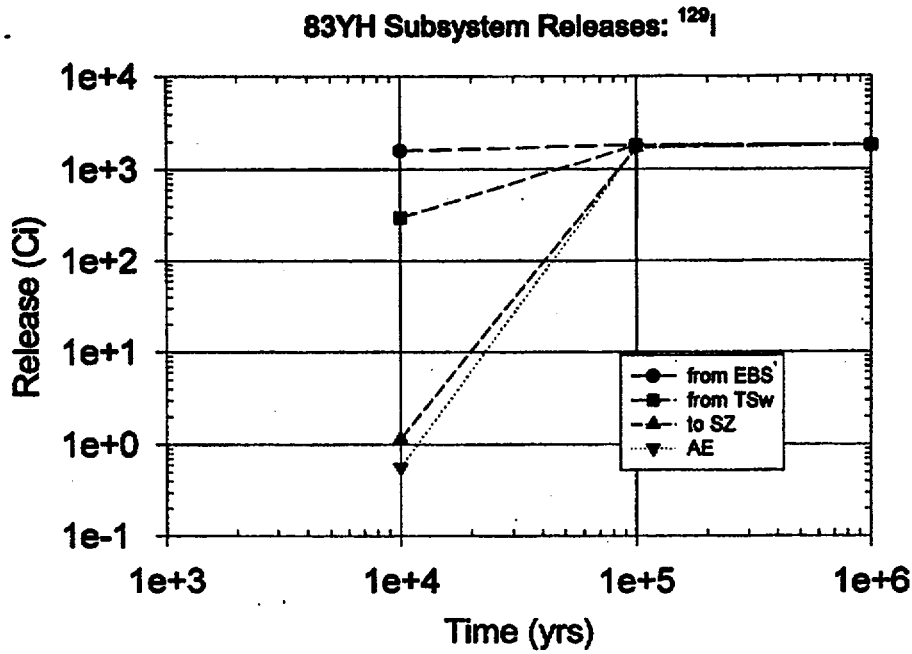


Figure 9.4-3. Subsystem ¹²⁹I. Expected-value release at 10,000, 100,000 and 1,000,000 years for 83 MTU/acre, backfill, high infiltration ($q_{inf} = 1.25$ mm/yr), no climate change, with decay.

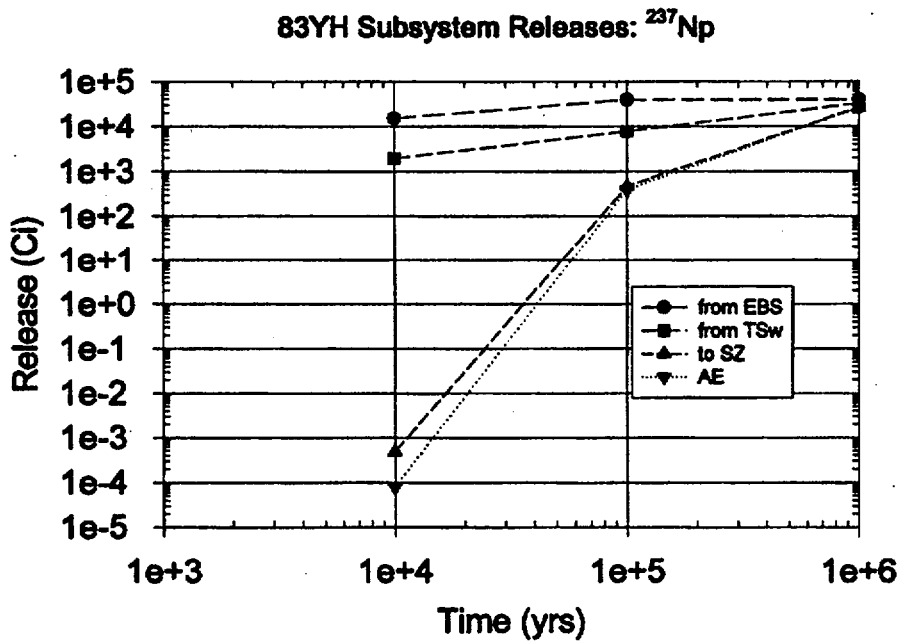


Figure 9.4-4. Subsystem ²³⁷Np. Expected-value release at 10,000, 100,000 and 1,000,000 years for 83 MTU/acre, backfill, high infiltration ($q_{inf} = 1.25$ mm/yr), no climate change, with decay.

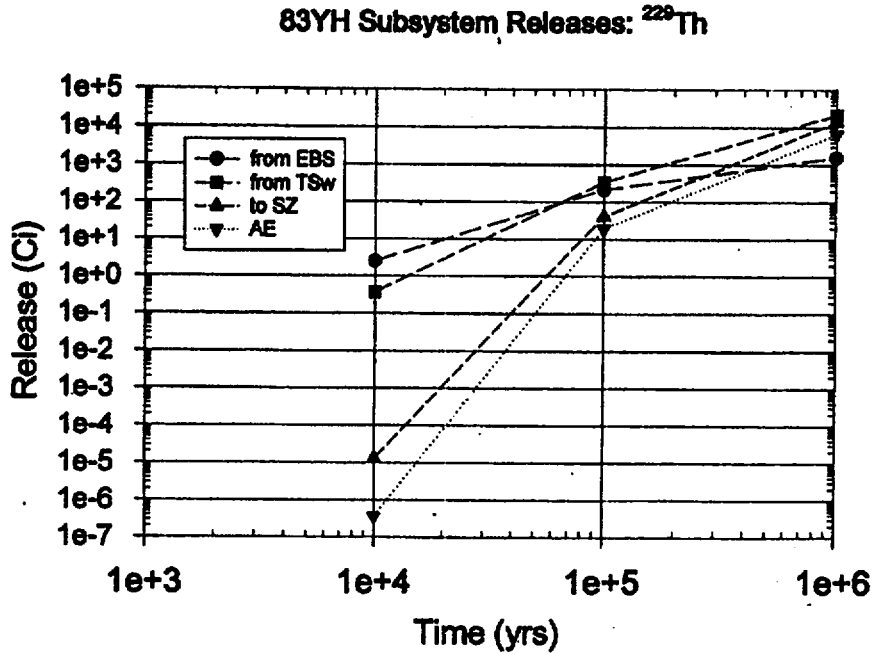


Figure 9.4-5. Subsystem ²²⁹Th. Expected-value release at 10,000, 100,000 and 1,000,000 years for 83 MTU/acre, backfill, high infiltration ($q_{inf} = 1.25$ mm/yr), no climate change, with decay.

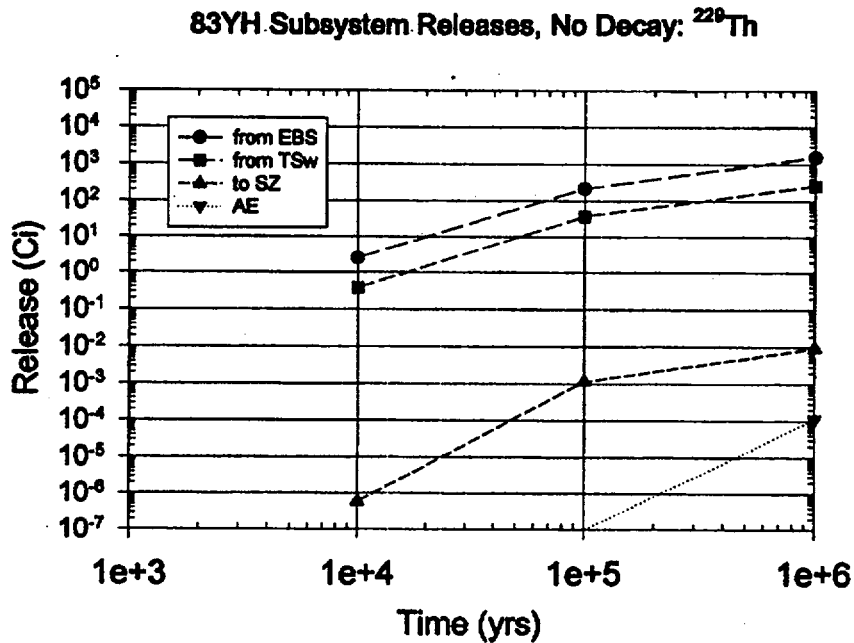


Figure 9.4-6. Subsystem ²²⁹Th. Expected-value release at 10,000, 100,000 and 1,000,000 years for 83 MTU/acre, backfill, high infiltration ($q_{inf} = 1.25$ mm/yr), no climate change, no decay.

10. CONCLUSIONS AND RECOMMENDATIONS

Robert W. Andrews and James O. Duguid

10.1 CAVEATS

This report documents a total system performance assessment of the Yucca Mountain potential repository, including the conceptual and parameter assumptions used. The report describes the results and their significance with respect to predicted postclosure performance, in terms of (1) the waste package lifetime (substantially complete containment); (2) the radionuclide release from the engineered barrier system; (3) the cumulative radionuclide release at the accessible environment over 10,000 years; and (4) the maximum radiation dose in 10,000 and 1,000,000 years to an individual located at the accessible environment boundary. The results and conclusions derived in this study must be tempered by the assumptions that are made in the course of the analyses. It is important to stress that the representativeness of the results, and therefore the robustness of the conclusions, are based on the assumptions used.

In the present discussion, the term *robust* has a very specific connotation to imply that changes in the considered conceptual model or parameter distribution will not significantly change the results or conclusions of the analyses. One can almost always consider "worst-case" scenarios for virtually every model or parameter distribution that would extend the envelope of the considered values to highly unlikely extremes and have significant effects on the predicted performance. That is not the philosophy incorporated in the present document nor will it be the approach taken in subsequent performance assessment iterations leading up to the evaluation of the suitability and licensability of the Yucca Mountain potential repository site. However, the *robustness* of the assumptions incorporated in the analyses are in many instances synergistic, with the effect of one model or parameter on the predicted performance being dependent on assumptions made regarding another totally unrelated component of the system. This is not unexpected, given the complexity of the system being simulated, the dependence of numerous factors on the overall response of the total system, and the range of alternative conceptual models possible at the present stage of scientific investigations. Even given this caution, however, it is possible to make reasonable conclusions and recommendations based on the current analyses, while at the same time acknowledging the need for complete substantiation and documentation of the process-level models ultimately to be used as the basis for abstractions used in performance assessment analyses.

The present analyses focus attention on models and parameters that earlier performance assessment analyses have determined to be significant. In particular, the emphasis is on evaluating the impact of alternative models of the near-field thermohydrologic environment in the vicinity of the waste package, alternative assumptions regarding the initiation and rate of degradation of the waste package materials, alternative assumptions regarding the efficiency of capillary barriers if placed in the drifts, alternative conceptual representations of advective flow in the drifts and percolation flux in the unsaturated zone, and alternative conceptual models of transport in the unsaturated zone.

In addition to the above conceptual assumptions, alternative thermal loading designs and backfill emplacement options are examined. These design options are not exhaustive of the range of designs that have been or are being considered. For example, alternative waste package designs (in terms of both the use of filler materials and alternative waste package materials) have been proposed that are not considered in the present analyses. It is impossible to evaluate every alternative design because each alternative often requires additional information that may not be available. Performance assessment analyses, which strive to be reasonably conservative representations of the range of behavior of the natural and engineered components of the overall system, lag slightly behind the most current scientific and engineering understanding because of the time required for the analyses. However, because performance assessments require evidence (i.e., data) with which to support the development of representative or "valid" conceptual models and parameters, they often point to the need for additional information to properly evaluate the alternative designs being considered.

Performance assessment is an iterative process. The analyses strive to use the most current understanding of the site and designs that can be substantiated, which implies that work in progress cannot be directly incorporated in the current iteration. The process-level models used for the abstraction of results into TSPA are "frozen" some months before the completion of the performance assessment. In the present iteration, this has necessitated using process-level understanding of unsaturated- and saturated-zone flow and transport that is currently undergoing revision. The delay in developing and documenting process-level models was identified as a significant issue in TSPA-1993 (Andrews, et al., 1994) and it remains so with the current iteration. With the exception of a preliminary version of the unsaturated-zone flow model (Wittwer et al., 1995), which does not address many important heterogeneity and scaling issues, there are still no documented models that have been substantiated adequately enough to be used with confidence in performance assessments. It is therefore recommended to (1) focus the data collection program primarily on observations and testing in the Exploratory Studies Facility (and the collection of "perishable" data) and (2) emphasize data interpretation/synthesis and process-level model development, substantiation, testing and review.

Although the models and parameter values used in the current TSPA iteration can be directly traced back to reasonable (and representative) assumptions, they have not all come directly from the process-level models because these models do not exist in all cases. This is not to imply that the process-level models, even when complete, will explain all alternative reasonable explanations for the observations made, nor to imply that the completion of the process-level models is all that performance assessment requires. There will be a number of issues associated with model and parameter variability and heterogeneity and scaling that will not be resolved within the context of the process models as currently envisioned. These issues will have to be "resolved" by sensitivity analyses using simplified TSPA models.

Performance assessment is often expected to "drive" the scientific investigation and design programs. This expectation is inspired by the belief that the priority of each investigation should be driven by the significance of that component of the system to the overall predicted performance. Those processes or parameters that significantly affect the predicted performance should be given increased focus, while those that contribute marginally to the overall performance should be deemphasized. While such an approach makes sense, its application has been limited because the degree to which performance assessment can "drive" the rest of the scientific and

design programs is, with few exceptions, directly related to the conceptual understanding existing at the time the analyses are performed. For different conceptual assumptions, one might reach very different conclusions of the significance, or lack thereof, of particular aspects of the investigation program. That is to say, the conclusions drawn are necessarily predicated on the assumptions included in the analyses. Because a number of assumptions in TSPA-1995 are not directly tied to substantiated conceptual models, care must be taken in "over-interpreting" the results or "over-utilizing" the results in the allocation of priorities. However, it is believed that a performance assessment-based prioritization approach can be used successfully in combination with technical judgment to provide a firm technical basis for the allocation of scientific investigation and engineering design priorities. This prioritization should be iterative and flexible, because priorities may change as understanding advances and performance assessment predictions become more refined and focused.

10.2 SIGNIFICANT CONCLUSIONS

Five different measures of performance were evaluated in TSPA-1995. The waste package failure distribution (if failure is defined by the penetration of the first pit through the corrosion-resistant inner package material) may be considered to represent the substantially complete containment requirement of NRC and is presented in Chapter 5. The peak release rate from the engineered barrier system, which may be compared to the NRC requirement, has been presented in Chapter 8. The total system performance is quantified with respect to three measures, namely, the cumulative release of radionuclides at the accessible environment over 10,000 years normalized to the Table 1 values in the remanded EPA environmental standard (40 CFR Part 191), and the peak radiation dose over both 10,000 and 1,000,000 years incurred by an individual located at the accessible environment boundary who uses water from the tuff aquifer as a sole source of drinking water. Because the conclusions are slightly different for the various scales (in space and time), each performance measure is discussed separately below.

10.2.1 Substantially Complete Containment

Because the initiation and rate of aqueous corrosion (by both humid air and liquid water) are dependent on the thermohydrologic environment, the determination of when the first pit penetrates the corrosion-resistant barrier is dependent on the thermal load. However, this dependency is more complicated than it may appear at first glance. One may initially assume that higher thermal loads would lead to lower humidities for longer times and therefore delay the onset of aqueous corrosion and extend the duration of the containment period. While the first part of this statement is true, the effect on containment is also significantly influenced by the temperature of the waste package surface, with higher temperatures yielding higher corrosion rates (this being especially significant for the assumed pitting corrosion model for the corrosion-resistant material). Therefore, from some of the results presented in Chapter 5, the rate of container degradation does not appear to be directly correlated with the thermal load.

The preceding conclusion must be tempered by the assumed thermohydrologic model and the assumed spacing of waste packages within the repository drifts. For example, the assumptions made in the drift-scale thermohydrologic analyses conducted by Buscheck (1995) (namely the lower thermal conductivity of the backfill, the lack of any applied infiltration rate, and the relative humidity reduction caused by temperature gradients between the waste package and drift

walls) generate significantly lower humidities for significantly longer periods for the higher thermal loads, and result in no waste package failures in the first 10,000 years for the higher thermal load case. Although the validity of each of these assumptions needs to be substantiated, the potential benefits in extending the waste package lifetime are apparent.

In addition to the effect of the thermohydrologic regime affecting waste package lifetimes, the conceptual model for corrosion also impacts the calculated failure distribution. In TSPA-1993 (Andrews, et al., 1994), the apparent benefits of cathodic protection of the Alloy 825 inner corrosion-resistant barrier were mentioned but not evaluated. The need for the development of a defensible model to incorporate this process in future performance assessments was stated as a high priority. Although no model of cathodic protection is currently available, sensitivity analyses incorporating what is believed to be a reasonable first-order approximation have been performed. As expected, incorporating cathodic protection significantly extends the lifetime of the waste packages. The cathodic protection has a two-fold effect. First, it directly extends the package lifetime by delaying the onset of pitting corrosion of the corrosion-resistant material. Second, this primary effect has an important multiplicative effect by causing a lower temperature during pitting of the corrosion-resistant layer, and therefore significantly reducing the pitting corrosion rate of this material. Because of its possibly large effect on containment, the cathodic protection model needs to be confirmed using literature- and laboratory-derived information.

The pitting-corrosion model for the corrosion-resistant layer was identified as being overly conservative in TSPA-1993 (Andrews, et al., 1994). In the absence of any cathodic protection considerations, the corrosion-resistant material did not substantially extend the containment time. Based on the assumptions made in TSPA-1993 (Andrews, et al., 1994), an additional centimeter of corrosion-allowance material would have been better than utilizing the corrosion-resistant material at all. Thus, a more definitive model of pitting of corrosion-resistant materials was identified in TSPA-1993 (Andrews, et al., 1994) as an important information need. Although no experimentally-based improved model for pitting of corrosion-resistant materials is available, sensitivity analyses are performed using an assumed model in which pitting growth rates are time dependent (with a decreasing rate with time). This revised model has a significant effect on the predicted failure distribution, confirming that the validity of this model is an important activity.

While the conceptual representations of drift-scale thermal hydrology and the corrosion degradation models significantly affect the waste package "failure" distribution over the first 10,000 years (and, therefore, also affect 10,000-year total system performance measures, such as the cumulative release at the accessible environment or peak dose at the accessible environment), these models have generally less significance when the performance measure is extended to longer times (i.e., 1,000,000 years). This observation was also made in TSPA-1993 (Andrews et al., 1994 and Wilson et al., 1994) and in the sensitivity analyses conducted to develop the environmental standards for Yucca Mountain (Duguid et al., 1994). However, these models do have some effect at longer times by limiting the total inventory that is accessible for release and transport because some waste packages are predicted to never fail. Also, if diffusive releases dominate or if it is assumed that the advective flux through the EBS is dependent on the percent of package surface penetrated by pits, the corrosion degradation models can have an effect even on long-term doses. However, all conceptualizations of these models for TSPA-1995 generate the bulk of package failures early enough during the 1,000,000 year time span that the results are

fairly insensitive to the particular conceptualization (no more than a factor of 3 difference in peak dose among these various conceptualizations).

10.2.2 Peak Release Rate from the Engineered Barrier System

Once the waste package has been degraded for modeling purposes, to the extent that the initial pit has penetrated the corrosion-resistant material, alteration/dissolution and advective/diffusive release processes can occur resulting in transport of dissolved radionuclides to the geosphere. For the current conceptualization of diffusive release, the diffusion coefficient is a function of the liquid saturation in the drift materials, and the area through which diffusion can occur is dependent on the distribution of pits through the waste package. Both the saturation and the area are functions of time. For this conceptualization of diffusion, diffusive releases are very small. Therefore, the substantiation of the probability and quantity of drift-scale advective flux (i.e., drip rate) becomes an important performance issue. The drift-scale advective flux is a function of the percolation flux distribution as discussed in the conceptual representation presented in Chapter 7. It is not directly evaluated in the site-scale unsaturated zone flow model (Wittwer et al., 1995) because the distribution of flux over a drift-scale of roughly 100 m² is not quantifiable in this model. It is controlled by small-scale heterogeneity and variability, which is not incorporated in the site-scale model, although it may be discernible by unperturbed observations and testing in the ESF.

In those cases where advection dominates the EBS release, the infiltration-rate distribution has a significant effect. The conceptual representation of how dripping water contacts the waste package is also important. In the cases where the dripping water is assumed to be distributed evenly over the package surface (perhaps due to spreading associated with an emplaced backfill), the advective release becomes dependent on the percent of the waste package surface area degraded as a function of time. Therefore, all the uncertainties in the waste package degradation conceptual model described above become significant. In the cases where the dripping water, if it is predicted to be present, is concentrated at a particular spot on the waste package surface, all of the advective flux flows through the waste package and EBS releases are conservatively high. The emplacement of a Richard's (or capillary) barrier, is assumed to perform with 100% efficiency in diverting any dripping water away from the waste package, significantly reduces the advective releases from the EBS.

The above observations point to the continued need to define, with some degree of confidence, the potential existence and distribution of localized flux that might intersect the potential repository drifts. It is important to point out that these flux values are small. Even if an average percolation flux of 1 mm/yr and an interception area of 100 m² is considered, the volumetric flow rate would be only 0.1 m³/yr (100 l/yr or 0.3 l/day or 0.2 ml/min or approximately 1 drip every 15 seconds), which may be difficult to directly measure in the presence of any ventilation.

An additional issue of importance in the evaluation of peak EBS release rates is the form of the radionuclide when the waste form is altered. For many cases presented in Chapter 8, after dissolution from the waste form, some radionuclides (namely, ¹⁴C, ³⁶Cl and ¹²⁹I) are assumed to be immediately transported to the host rock in the gaseous phase, where there is presumed to be sufficient water available into which these radionuclides would dissolve and subsequently be transported in the aqueous phase to the accessible environment. Sensitivity analyses are

performed to evaluate the alternative assumption that these radionuclides are immediately dissolved into whatever water may exist on the waste-form surface and then transported through the EBS by aqueous advective/diffusive processes, rather than by gas-phase transport. These different assumptions not only affect the predicted peak EBS release rates (especially in the cases of low or no advective flux through the EBS), but also the peak doses at the accessible environment.

For the assumptions made regarding the performance of the cladding and the dissolution of the waste form, the dissolution rate itself does not significantly affect the peak EBS release rate. This is probably a result of the observation that the dissolution rate significantly controls the release of the high-solubility radionuclides, but these radionuclides (^{135}Cs , ^{79}Cs , and ^{99}Tc) are also presumed to be present in the gap fraction. Therefore, a certain percentage of the inventory for these radionuclides (assumed to be 2% in the analyses presented in Chapter 8) is available for transport from the waste form surface to the edge of the EBS as soon as the cladding fails.

10.2.3 Cumulative Release of Radionuclides at the Accessible Environment - 10,000 Years

When considering a 10,000-year total system performance measure, there are many EBS and natural barrier system factors that affect the predicted results. The results presented in Chapters 8 and 9 indicate that under certain conceptual assumptions the engineered barriers by themselves can provide complete containment of the radionuclides for the entire 10,000-year time period. Similarly, for cases when the percolation flux distribution is at the lower end of the possible range of likely values, the natural barrier by itself can provide complete isolation of the radionuclides from the accessible environment for the entire 10,000-year time period. This is, of course, the definition of redundant barriers.

For cases when the most conservative estimates of both EBS and natural barrier performance are considered, i.e., those cases which produce some non-zero integrated release to the accessible environment over 10,000 years, several factors are important. The predominant factor is the percolation flux distribution, which not only affects the likelihood of there being advective flux (i.e., dripping) through the EBS, but also affects the magnitude of the advective release from the EBS, the distribution of radionuclide transport between the fractures and matrix in the unsaturated zone, and the average matrix velocity through the unsaturated zone. That is, for conservative assumptions regarding the waste package degradation model, the percolation flux distribution controls the 10,000-year cumulative release. This is the same conclusion reached in TSPA-1991 (Barnard et al., 1992) and TSPA-1993 (Wilson et al., 1994 and Andrews et al., 1994). It is worthwhile to point out that the radionuclides of interest over the 10,000-year time period are highly soluble with little or no sorption, such as ^{99}Tc , ^{129}I , and ^{14}C . Slightly sorbed radionuclides such as ^{237}Np can be released in small quantities over 10,000 years in cases of high percolation flux. For the parameter distributions used in the present analyses (that may be subject to change upon evaluation of the controlling phase of the radionuclide), highly sorbed and low solubility radionuclides such as plutonium, americium and curium, are not transported appreciable distances through the EBS or host rock in 10,000 years.

10.2.4 Peak Radiation Dose to Maximally Exposed Individual at the Accessible Environment - 10,000 Years

Similar conclusions regarding the significance of particular conceptual models and parameters reached for the 10,000-year cumulative release total system performance measure are also germane to the 10,000-year peak radiation dose prediction. If the EBS and/or natural system perform in such a way as to preclude, either individually or collectively, any release of radionuclides to the accessible environment in 10,000 years, then there would clearly not be any dose consequences in the accessible environment over this time frame.

For those cases when radionuclides do arrive at the accessible environment boundary within 10,000 years (as noted above, this is primarily a function of the percolation flux distribution), the factors which delay, disperse or dilute the radionuclides have the greatest effect on the calculated peak dose, for given assumptions about the biosphere. Delaying the arrival of radionuclides at the accessible environment can be an issue over 10,000 years because it affects the arrival time of the leading edge of the breakthrough curve. In addition to the percolation flux, delay can be enhanced by sorption and matrix-diffusion mechanisms in the geosphere. For example, the non-zero retardation of neptunium can be sufficient to delay the arrival of this radionuclide until after the 10,000-year time period. In addition, utilizing an enhanced matrix diffusion or decreasing the mean fracture flow path length can reduce the average radionuclide travel time.

Dispersive effects have two impacts on the arrival of radionuclides at the accessible environment. On one hand, increased dispersion, especially when it occurs in the geosphere, can cause an earlier arrival of the breakthrough curve. Significant dispersion in the unsaturated zone could cause some radionuclides to arrive before 10,000 years, whereas a "plug flow" assumption would result in the initial arrival after this time. On the other hand, increased dispersion tends to lower the magnitude of the peak height. Over a 10,000-year time period, these issues are competing with one another in their combined effect on peak concentrations or peak doses. Because there are very few instances when the actual predicted *peak* arrival time is less than 10,000 years for any radionuclide (it generally occurs in the time frame of tens to hundreds of thousands of years, depending on the nuclide and the flow and transport conceptualization), the dispersive effect on initial arrival time is more significant, i.e., by shifting the initial arrival to an earlier time, increased dispersion leads to an increased peak dose during the 10,000-year time period. As discussed below, the opposite is true for longer time periods of interest.

Dilution of radionuclides in the saturated zone is an important process in the determination of peak concentrations and ultimately peak doses. It is important to note that dilution is not a factor in the evaluation of cumulative release. For all dose calculations presented in Chapter 9, it is assumed that the dilution in the saturated zone occurs within a volumetric flow equal to the cross-sectional width of the repository (taken to be 4000 m and kept the same for both low and high thermal loads for consistency even though the cross-sectional width is greater for lower thermal loads) times an assumed mixing depth of 50 m (which may be considered to be the slotted interval of the individual's well) times the uncertain Darcy flux within the tuff aquifer. Higher Darcy fluxes generate the potential for greater dilution and therefore lower peak doses at the accessible environment. Therefore, as noted in TSPA-1993 (Andrews, et al., 1994 and Wilson, et al., 1994), the local Darcy flux distribution within the saturated zone in the vicinity of the potential Yucca Mountain site is an important parameter for concentration-, dose-, or risk-based performance measures.

10.2.5 Peak Radiation Dose to Maximally Exposed Individual at the Accessible Environment - 1,000,000 Years

While the predicted peak radiation dose over a 10,000-year time period is dependent on numerous factors, in extending the time to 1,000,000 years only a few factors dominate the predicted response. In general, factors which tend to delay the arrival of the peak concentration at the accessible environment are found to be less significant. This is a direct result of the extremely long time period considered and the long half-lives of some of the key radionuclides that always contribute to the predicted peak dose (notably ^{99}Tc with a 200,000-year half-life, ^{237}Np with a 2,000,000-year half-life, and ^{129}I with a 20,000,000-year half-life). Even for the low end of the assumed percolation-flux distribution and even assuming a nonconservative conceptual representation of fracture-matrix flow and transport, the above radionuclides are either not sorbed at all or are only slightly sorbed (^{237}Np) and they break through within 1,000,000 years. In addition, even with the most nonconservative waste package degradation model assumptions, a certain fraction of waste packages would be degraded within the 1,000,000-year period. Thus, although a combination of waste package performance and site performance can contribute to containing and isolating radioactive wastes within the Yucca Mountain area for some tens- to even hundreds-of-thousands of years, it is unlikely that such barriers can be reasonably shown to delay the above radionuclides sufficiently to preclude their release over a 1,000,000-year time period.

While delay itself does not contribute appreciably to the prediction of long-term doses, dispersion and dilution are still significant processes. Dispersion in this case is the result of both geosphere and EBS processes. Dispersion tends to spread out the release of the radionuclides over time and therefore reduce the peak concentration and peak dose. Geosphere dispersion is enhanced by increased matrix diffusion or decreased the mean fracture-flow length (in cases where fracture transport is active) or increased vertical, lateral and/or longitudinal dispersion in the saturated zone. As noted in Chapter 7, the dispersive effects in the saturated zone are enhanced with increasing distance between the repository and the assumed user of the tuff aquifer. This effect has significant ramifications with respect to the definition of where the average member of the critical population proposed in the recent NAS recommendations resides. If the critical group is located in the Amargosa Valley, some 25 km down gradient from the present "accessible environment" as defined in 40 CFR Part 191, the increased geosphere dispersion may be expected to reduce the peak concentration and peak dose by several orders-of-magnitude.]

Besides dispersion in the geosphere, dispersive-type effects within the engineered barrier system are extremely important in reducing the predicted peak concentration and dose at the accessible environment. Spreading of releases from the EBS can occur as a result of either a wide distribution of waste-package failure times, an extremely low alteration/dissolution rate, or diffusion-dominated releases through the package and EBS. The first two factors are generally insufficient to significantly decrease the peak release rate over the range of parameter values considered in this TSPA iteration. However, diffusion-dominated releases from the EBS can significantly reduce the peak release rate. Such diffusion-dominated releases occur when either a very low percolation flux distribution is assumed (in which case only a small percent of the packages experience advective release) or an efficient capillary barrier in the backfill is considered. In both cases, the diffusion through the waste package and other EBS materials is a highly nonlinear function of the in-drift liquid saturation (generally very low for all thermal loads, except when advective flow into the drift

occurs), as well as the effective surface area through which diffusion occurs (which is controlled by the waste package degradation model).

Confidently demonstrating that diffusive release is the dominant transport mechanism in the EBS would be key to reducing the predicted long-term dose to individuals or critical groups. It is not at all coincidental that virtually every other high-level radioactive waste disposal program around the world that has published results of total system performance has incorporated a diffusive barrier in their engineered barrier design (see Neall et al., 1995). In other countries the diffusive barrier is a bentonite or bentonite-sand mixture, because these programs have focussed on crystalline host rocks within the saturated zone. A potential diffusive barrier in the unsaturated zone such as Yucca Mountain is crushed rock with low capillary suction.

Besides the spreading out (in time) of the release of radionuclides from the source term, the predicted peak dose at the accessible environment boundary over the 1,000,000-year time period is also significantly affected by dilution in the saturated zone. This dilution can occur naturally by the mixing of different ground-water sources along the flow path between the repository and the user of the tuff aquifer (or other ground-water sources that are supplied by the tuff aquifer), or anthropogenically by the user tapping alternative sources of water for consumption (i.e., by slotting the well over different isolated aquifers). Although alternative dilution scenarios are discussed in Chapter 7, analyses of the exact effect of these scenarios on repository performance are beyond the scope of the present document. Assuming that the EPA accepts the NAS recommendations for protecting individuals of critical groups as an appropriate environmental standard for Yucca Mountain, additional analyses of regional ground-water flow patterns should be conducted. It is relevant to point out that dilution by saturated-zone mixing is not important for the cumulative release performance measure and is less significant at shorter distances between the potential repository and the defined location of the critical group.

10.3 PRIORITIZATION OF SITE CHARACTERIZATION AND DESIGN ACTIVITIES

As discussed in Sections 10.1 and 10.2, it is difficult to confidently and unambiguously identify the most significant elements of the Yucca Mountain site characterization and design programs that contribute to the predictions of total system performance. This is primarily a result of the lack of definitive process-level models with which to abstract the necessary response surfaces for input to the total system performance assessment. In many instances, the lack of a representative process-level models allows for various reasonable approximations to be made, the results of which are significantly different. That is to say that the conceptual assumption does make a difference on the predicted performance. In this Section, the key conceptual assumptions made in the course of this TSPA iteration are discussed. Identification of the significant assumptions assists in defining the key site characterization and design activities for improving the process-level models. The types of information expected for the various process-level models are discussed in Section 10.6.

In addition to the lack of definitive process-level models, as described in Section 10.2, the importance of particular models or parameters is also a function of the performance measure considered. For the substantially complete containment criterion, definition of the relevant corrosion degradation models as well as the initiation and rate parameters for these models should be considered a high priority information need. For the peak EBS release rate, the existence and magnitude of percolation flux which passes through the EBS is of highest priority (assuming the

gaseous radionuclides are highly soluble where the waste form contacts water). The 10,000-year cumulative release or peak dose predictions are affected principally by the corrosion degradation model and the unsaturated zone aqueous flux model for fracture-matrix transport. The 1,000,000-year peak dose is primarily controlled by the relative magnitude of advective and diffusive releases through the EBS (which in turn is affected by the distribution of percolation flux which intersects the repository drifts), the advective flux in the unsaturated-zone (if this flux is at the low end of the considered distribution), and the degree of dispersion and mixing in the saturated zone aquifer between the repository footprint and the user of the tuff aquifer. These key issues are highlighted in the discussion below.

The predominant site characterization issue remains the distribution of percolation flux in the unsaturated zone. In the conceptualizations embodied in the analyses presented in Chapters 8 and 9, the percolation flux distribution controls (1) the likelihood and magnitude of advective flux through the EBS, (2) the EBS diffusion coefficient in the cases where there are some "drips" into the EBS, (3) the fraction of volumetric flow in fractures and (4) the matrix velocity. It is important to point out that this parameter is not measurable. It is inferred from a number of observations that must be synthesized and explained by the site-scale unsaturated zone flow model. However, it is expected that different conceptual assumptions will be possible to explain the varying observations. Also, the scale of the model does not allow the spatial refinement required to address heterogeneity and scaling issues of importance to define the distribution of flux over each of the 10,000 waste packages. Therefore, it is recommended that an unsaturated-zone flow model at the scale of individual drifts be developed and tested. This testing should consist of both representativeness/reasonableness of the model (perhaps by comparison with the distribution of any advective seeps or the distribution of ground-water residence times observed along the ESF axis) and the significance of alternative models on surrogates of performance (such as the likelihood and magnitude of seepage fluxes intersecting the drifts). It bears noting that the distribution of flux may be affected over some time period by the imposed thermal regime. Therefore, the same alternative conceptualization used to evaluate flow in the vicinity of the drifts should be used in the substantiation of the thermohydrologic response.

The representation of fracture-matrix coupling, while significantly affecting the predicted total system performance over 10,000 and 100,000 years, generally has a less significant effect over the 1,000,000-year time period unless the percolation flux is at the lower end of the expected distribution range. Therefore, the need for detailed characterization of fracture-matrix transport issues in the geosphere is dependent on whether the EPA accepts the NAS recommendation of a peak concentration, dose, or risk performance standard.

The representation of saturated-zone flow and transport is generally insignificant to the predicted performance over a 10,000-year time period, but can be very significant in the prediction of 1,000,000-year peak individual doses, especially if the individual of concern is located in areas of current water consumption such as the Amargosa Valley. Although it is generally recognized that the saturated zone contributes little in the way of delay (unless the potential for modifications in geochemistry is considered which could cause significant changes in the oxidation potential and therefore solubility of some of the key radionuclides), it can significantly affect the dispersive spreading and mixing of any radionuclides released to the saturated zone and therefore reduce the peak concentrations several orders of magnitude. Better understanding of the regional saturated-zone flow system in general and the mixing of different ground-water sources, including recharge

of the alluvial aquifer along the Amargosa Valley in particular, is required to better approximate the degree of dilution expected.

In addition to identifying the key site-related processes affecting post-closure, it is also important to discuss some processes that are generally less significant using current conceptual understanding. Principal among these, as alluded to in Section 10.2, is the role of transport in the unsaturated zone. The key radionuclides reaching the accessible environment and impacting dose calculations over either long or short time periods are not sorbed at all or are only slightly sorbed. While the role of matrix diffusion over short time periods can be significant, it is generally insignificant over the 1,000,000-year time period. These results indicate that the conceptual model of unsaturated zone transport does not warrant significant additional investigation, except as it helps to confirm the understanding of the natural ground-water tracers observed in the unsaturated-zone waters. This is a direct result of the fact that delay in the 1,000,000-year time frame is not possible within the unsaturated zone except under the most nonconservative of expected percolation flux distributions.

Repository and drift designs (in particular the emplacement of backfill materials) impact the predicted performance in two important ways. On one hand, the hydrologic and thermal characteristics of the EBS materials can significantly affect the prediction of relative humidity in the vicinity of the waste packages, as well as the distribution of advective flux in the drift itself in the presence of drips. The former will impact the waste package degradation for long periods of time (although generally not as much as 1,000,000 years). The latter will affect the release of radionuclides from the EBS. In addition to these direct effects, the potential performance benefits of an efficient capillary barrier are apparent over long time periods, in that it forces the EBS releases to occur through diffusion only, which is orders of magnitude less than the advective flux even at the low percolation flux distribution range. The design issue of significance then is the ability to emplace backfill within the drifts (recognizing that this would be emplaced after the presumed 100-year retrieval period) and the ability to engineer the backfill to specifications to enhance the overall system performance (either by reducing the thermal conductivity in order to reduce the humidity or by engineering a capillary barrier). If preliminary scoping analyses indicate that engineering a capillary barrier is not feasible, then even greater emphasis must be placed on confidently predicting the drift-scale hydrologic flow regime and precluding the possible intersection of advective drips with the waste packages.

The focus of the role of the in-drift materials discussed above is in how these materials affect the in-drift thermal hydrology. Although not examined in this TSPA iteration, an additional role of the EBS materials is their effect on the near-field geochemical environment. An important parameter which affects the long term dose calculations is the solubility of neptunium. This parameter is not identified as important in the sensitivity analyses for the simple reason that its values are constrained at the high end of the solubility range representing oxidizing conditions. However, within representative solubility values, the peak dose has been shown to be almost linearly dependent on the solubility of neptunium (see Duguid et al., 1994). Studies described in Chapter 6 indicate the potential that the current estimates of neptunium solubility may be metastable and the stable phase may be some seven to ten orders of magnitude less soluble. This solubility is dependent on the geochemical and thermal alteration of the liquid phase into which the neptunium dissolves. Assuming that long-term doses are the performance measure of interest, delineating the expected neptunium solubility remains an important information need.

One of the elements in the selection of candidate materials and fabrication techniques for application to alternative waste package designs has been the predictability of the material's degradation behavior. In fact this has been noted as one of the advantages associated with the tentative selection of the mild steel corrosion-allowance material (the other being that it may provide significant cathodic protection of the corrosion-resistant material). Some designs have been proposed without considering whether applicable predictive models exist to describe the performance of the material over the range of likely environments. For example, although there is some indication that corrosion-resistant materials should perform very well in delaying the penetration of pits created by corrosion, the models available to substantiate this belief are very uncertain. In addition, there do not appear to exist representative models to allow confident prediction of the potential benefits of cathodic protection. It is recommended that any proposed change in waste package design (which may be for a variety of reasons unrelated to performance, such as cost or fabricability) be accompanied with representative model(s) and their bases for making predictions of material degradation. For example, if a particular material is proposed for guarding against potential microbiologically-influenced corrosion, the basis for the material selection should include the mechanistic model used to support the decision. Analog information should also be used where possible.

The waste package degradation processes, models and parameters could be considered unimportant to the long-term (i.e., 1,000,000 year) performance of the repository system. This assumption, however, must be tempered with the observation that the rate of package degradation over time is an important aspect of the long-term isolation of the wastes, because it allows for the spreading of the release over time. Therefore, the long-term degradation of the waste package can still be a significant issue. However, confidently predicting the long-term (i.e., 1,000,000 year time period) behavior of engineered materials is difficult to validate.

10.4 SUMMARY OF CONCEPTUAL ASSUMPTIONS NOT EVALUATED

Although this TSPA iteration includes a significant amount of sensitivity and uncertainty analyses, it does not test every key assumption or combination of assumptions, because of (1) limitations on the ability of the mathematical models to address certain issues without overly burdening the computational resources (i.e., there is always a trade-off between detail possible and time requirements), (2) limitations on available information (i.e., it is possible to conduct additional sensitivity analyses but the representativeness would be questioned), (3) a belief or expectation that the alternative representations are less likely than those examined and, finally, (4) a lack of time. The tested assumptions are believed to be the most important, although this is not demonstrable without conducting the additional analyses. That is, it is possible that some key issue that is significant to performance is either masked by other assumptions made in the analyses or is not observable because that process or model has not been included in the assessment. This section briefly discusses some of the analyses not performed.

The near-field thermohydrologic environment is based on two alternate models using two-dimensional representations of the drift and emplaced materials. Three-dimensional effects should be examined to determine if they affect the predicted humidities in the vicinity of the waste package. The impact of uncertain hydrologic and thermal properties of the backfill/invert material and potential effects of heterogeneity on the predicted drift-scale response should be evaluated. The possible incorporation of repository edge effects is discussed in Section 4.3. Finally, the linking of

representative drift-scale thermohydrologic analyses with the considered model for the distribution of "drips" into the drifts should be considered.

The primary failure mode considered for waste package material degradation is aqueous corrosion (i.e., by water and humid air). Alternative modes of failure (e.g., defective containers, mechanical container failure due to rock fall) should be examined and demonstrated to be insignificant before confidently using the single failure mode.

The EBS release model considered in the present analyses does not rely on an explicit determination of the flow regime in the drift. It simply assumes that the water intersecting the drifts as "drips" is either evenly distributed over the waste package or is concentrated on the first pits through the waste package. More explicit evaluation of the in-drift hydrology would appear to be useful (albeit adding an additional level of assumptions), especially given the importance of diffusive versus advective releases from the EBS on the long-term dose prediction.

The EBS model at present does not consider any geochemical effects, whether beneficial or deleterious. Such effects are likely to occur due to the presence of introduced materials in the drifts and should be considered in subsequent iterations of TSPA.

The unsaturated zone flow model used in the abstraction of flux distributions, although developed from an early version of the site-scale flow model (Wittwer et al., 1995), was extended to try to account for the potential for non-equilibrium fracture-matrix flow. The results of this model are compared to a dual-permeability formulation, but should also be compared to the unsaturated zone transport model currently under development. In addition, the duration and magnitude of thermal perturbations to the unsaturated zone flow field should be evaluated.

The saturated zone flow model used in the present analyses is a very simple mixing model. As alternative biosphere locations are considered, conducting more representative regional- and or site-scale saturated-zone flow and transport models (with the transport aimed at addressing mixing and dispersion effects) should be considered.

The biosphere transport model used in the present analyses is simply based on dose conversion factors published by EPA. Although it would be desirable to have the regulatory agency define the appropriate biosphere for analyses, it would be useful to construct alternative biospheres to evaluate the sensitivity of the predicted long-term dose to various biosphere assumptions.

10.5 POTENTIAL IMPACTS OF ALTERNATIVE ENVIRONMENTAL STANDARDS

The Energy Policy Act of 1992 mandated that the Environmental Protection Agency (EPA) standard (40 CFR Part 191) no longer apply to a repository at Yucca Mountain, and that the National Academy of Sciences (NAS) make recommendations for the development of a new Yucca Mountain specific standard. The NAS formed the Committee on Technical Bases for Yucca Mountain Standards in the spring of 1993 and released their recommendations in August of 1995. The recommendations of the NAS that affect the total system performance assessment (TSPA) calculations and the effects of these recommendations on the presentation of dose calculations in TSPA-1995 are summarized below.

The Committee on Technical Bases for Yucca Mountain Standards recommended that the environmental standards for a repository be based on the risk of fatal cancer to an average member of a critical group (NAS, 1995). They stated that compliance assessment of this risk should be at the time when the greatest risk occurs within the limits of the long-term stability of the geologic environment. They suggested that a risk limit in the range of 10^{-6} to 10^{-5} excess cancer fatalities per year would be appropriate and that the geologic environment in the vicinity of Yucca Mountain would be expected to remain stable for at least 1,000,000 years. In terms of radiation dose, this risk limit range translates to a range of 2 to 20 mrem/yr to the average member of the critical group, using accepted dose conversion factors.

The critical group is defined according to the International Commission on Radiological Protection (ICRP) as a relatively homogeneous group of people whose location and habits are such that they receive the highest dose from the expected repository releases (ICRP, 1985a and ICRP, 1985b). The dose within the entire population is a distribution of which the critical group represents the extreme (i.e., those members of the population expected to receive the highest dose). "In the case of Yucca Mountain, these individuals presumably would live in the near vicinity of the site and would potentially be exposed to radiation through the use of contaminated ground water" (NAS, 1995). The critical group under this assumption would be using ground water and be located down gradient from the repository site. The critical-group dose is defined as the dose received by an average member of the critical group.

The ICRP definition of the critical group requires that:

- The persons calculated to receive the highest dose based on cautious, but reasonable, assumptions be included in the group.
- The group be homogeneous in dose; there should be a relatively small difference between those individuals receiving the highest and lowest doses (ICRP, 1991). The ICRP Publication 46 (ICRP, 1985b) suggests that if the ratio of calculated average dose to the regulatory limit is less than 0.1, then the group should be considered homogeneous if the distribution of individual doses lies substantially within a range of a factor of ten, or a factor of three on either side of the average. For ratios greater than 0.1 a smaller range is required for homogeneity.
- The size of the group is recommended by the ICRP to be a few tens of persons. The group should not be a single person and homogeneity requires that the group not be too large.

Based on the ICRP guidance the NAS recommended that the critical group be:

"Representative of those individuals in the population who, based on cautious, but reasonable, assumptions, have the highest risk resulting from repository releases. The group should be small enough to be relatively homogeneous with respect to diet and other aspects of behavior that affect risks. The critical group includes the individuals at maximum risk and is homogeneous with respect to risk. A group be considered homogeneous if the distribution of individual risk within the group lies within a total range of a factor of ten and the ratio of the mean of the individual risks in the group to the standard is less than or equal to one-tenth. If the ratio of the mean group risk to the standard is greater than or equal to

one, the range of the risk within the group must be within a factor of 3 for the group to be considered homogeneous. For groups with ratios of mean group risk to standard between one-tenth and one, homogeneity requires a range of risk interpolated between these limits."

In the present and near future, these persons are presumed to live in the vicinity of the repository in the direction that migration of the ground-water plume of radionuclides would take in the far future (NAS, 1995). In order to develop an exposure scenario, assumptions about lifestyle, location, eating habits, and other factors will have to be made. The ICRP recommends use of the present knowledge with cautious, but reasonable, assumptions in making projections into the future. These assumptions are part of the exposure scenario that would be used as the basis to determine whether the repository would meet a performance standard based on risk to an average member of the critical group. In developing this scenario the NAS states that there is no scientific basis to make projections of the nature of future human societies to within reasonable limits of certainty. The NAS also states that there are scenarios that include the use of contaminated ground water that are likely to lead to exposure, and that if the ground water either is not used or is treated, exposure is not likely to occur. This implies that there are natural factors and physical processes such as topography, hydrogeology, soil type, climate, and location that should be included in developing scenarios for determination of the critical group and exposure to an average member of that group. The scenarios and/or the method of constructing them is a policy decision and is expected to be a major part of the rule-making process if the EPA decides to accept the NAS recommendations to develop a risk based standard for Yucca Mountain.

The NAS considered two approaches to illustrate the development of exposure scenarios that the EPA might use to initiate the rule making process (NAS, 1995). The majority of the NAS Committee believed that a probabilistic approach based on physical characteristics of the site and their influence on population distribution could be used to develop the exposure scenario. The second, and more widely used method of scenario development, is to assume that a subsistence farmer is present at the time of peak concentration and that this person/family represents the most exposed member of the critical group. This latter approach appears to be simpler to explain to the public and is more consistent with the recommendations of the IAEA (NAS, 1995, Appendix D).

Prior to the release of the NAS recommendations, the dose calculations performed in TSPA-1995 were based on dose to the maximally exposed individual at the accessible environment. These results were based on the assumption of a subsistence farmer located 5,000 meters down gradient from the repository. The NAS recommendations alter these assumptions in two important ways.

First, the artificial boundary at 5,000 meters is no longer assumed. The approach of using present conditions to develop an exposure scenario would likely lead to consideration of locations farther from the repository (i.e., at farming communities in the Amargosa Valley). The increased distance to the assumed location(s) of the future exposure or future well locations would allow for significantly more radionuclide dilution and dispersion and the potential mixing of different ground-water sources (see Chapter 7). Retardation over the longer transport path and radioactive decay over the longer transport time would be expected, but would not significantly change the concentration because of the long half-lives of the radionuclides involved (i.e., only the time of the assumed exposure would change). Consequently the only reduction in dose would be from the dispersion (which decreases radionuclide concentration in the ground water that is being used in the exposure scenario).

The second dose reduction factor is caused by considering the average member of a critical group instead of the maximally exposed individual. The reduction in dose between the maximally exposed individual and an average member of the critical group would be no more than one order of magnitude if the maximally exposed individual is assumed to be a member of the critical group (i.e., the range of dose within the critical group should be no more than one order of magnitude as recommended by ICRP). The assumptions made to define the maximally exposed individual, i.e., the definition of the subsistence farmer, could change based on studies of the life styles of the current population of the Amargosa Valley. These changes would have to be defined during the EPA rule making and would further reduce the dose to an average member of the critical group.

10.6 RECOMMENDED DEVELOPMENT, SUBSTANTIATION, DOCUMENTATION AND TESTING OF PROCESS LEVEL MODELS TO BE USED IN FUTURE TOTAL SYSTEM PERFORMANCE ASSESSMENTS

The following discussion summarizes the initial expectations for the level of detail required in the process level models being developed and tested by different organizations that will be used as the foundation for future Total System Performance Assessments.

Performance assessments attempt to predict, with reasonable levels of conservatism, the long-term behavior of the repository system and all potentially significant features, events and processes that may impact the ability of the site and engineered barriers to contain and isolate the radioactive wastes. Because long-term predictions are required in these assessments, models are used. These models attempt to incorporate all the relevant processes affecting the containment and isolation of the waste. The goal is to have the models be as realistic as possible, but failing that, to ensure that they conservatively capture the important characteristics in order to bound the prediction of the performance.

The basis of the process level models as the foundation of performance assessment predictions must be demonstrated. Developing the confidence required in these process models relies on the testing, and data acquisition, data interpretation, data synthesis and conceptual model development conducted by the site, design, and research organizations. The model documents to be prepared by the site, design, and research organizations should summarize this understanding and the level of confidence in using the developed models for making predictions.

It warrants noting that the performance assessment analyses may not use a process model explicitly, but some abstracted representation based on the detailed process model. This abstracted/simplified model has to be compared with the more detailed process model and the results have to be shown to be reasonable or conservative. Therefore, the detailed process models are required as the justification for the abstractions used in the performance assessment models. As a result, both the developing organizations (i.e., the suppliers) and the implementing organizations (i.e., the customers) have distinct roles and responsibilities that must be performed to successfully develop defensible site suitability and ultimately licensing documents.

The primary models of importance to performance assessment have been tentatively prioritized with respect to their significance to overall system performance as shown in Table 10.6-1. The primary focus (Priority 1 models) is on the conceptual understanding of the hydrologic regime in the vicinity of the waste packages as it significantly impacts the initiation and rate of corrosion degradation, the

mobilization of the radionuclides from the waste form, and the release of radionuclides from the waste package and EBS, i.e., the source term for geosphere transport. Of subsequent importance (Priority 2 models) are issues related to the mobilization and release of radionuclides from the EBS. Priority 3 models generally relate to the understanding of transport in the geosphere as well as the key externally initiated scenarios. Dissolution is included here because it is believed to be reasonably, albeit very conservatively bounded at present. Priority 4 model refers to models which will either be conservatively bounded in future TSPAs or for which direct testing and substantiation are not possible (i.e., assumptions will always be required, the technical basis for which might be always extremely limited).

It is important to point out that the fundamental justification of the process level models is the responsibility of the appropriate developing organization. These models should be supported by available information that independently corroborates the model predictions of the observed processes being considered. Alternative models and parameters that could be invoked to reproduce the observations equally well should be clearly discussed and evaluated by the developing organization. That is, it is the responsibility of the developing organization to place reasonable bounds on the model and the corresponding parameters included in the model. Some examples of relevant observations for the higher priority process models are presented in Table 10.6-2.

It is the responsibility of performance assessment to evaluate the significance of the inherent uncertainty in both the models and parameters and of the effects of this uncertainty on predicted performance. Performance assessment should take the best-estimate models and parameter values and conduct sensitivity analyses with respect to various measures of performance and/or surrogate measures of performance. An example surrogate might be the transport of an unretarded or partially retarded dissolved species from the repository horizon to the water table, assuming the release occurs instantly (i.e., time = 0) and at a constant rate or an instantaneous pulse. In other cases, the sensitivity of the uncertainty with respect to overall system performance should be evaluated. The following list (Table 10.6-3) details the performance measures or surrogate performance measures which might be the outcome of the sensitivity analyses performed by performance assessment using the process models and the inherent uncertainty and variability in these models and the corresponding parameters.

The inherent complexity of probabilistic total system performance assessments, as well as current computational constraints, precludes a direct incorporation of most of the underlying process models into the performance assessment process. The approach taken in this and related studies is to first perform detailed calculations using the process models, and then abstract/simplify the results for input into TSPA codes. Because of limitations on computer and time resources, only a limited number of detailed process model evaluations are typically carried out - thus preventing the consideration of all alternate conceptual models and sources of parameter uncertainty/variability.

For each of the detailed process models, it is expected that there will be a corresponding model report. Each of the model documents is expected to contain the following basic elements¹:

¹These elements apply whether considering physical-chemical processes occurring in the natural geologic setting or physical-chemical processes occurring in the engineered portions of the system.

1. Goals and objectives of model.
2. Processes considered in the model and processes excluded (and technical basis).
3. Conceptual representation and alternatives of the processes considered in the model.
4. Software employed in the analysis of the model (if applicable) and numerical solution technique.
5. Temporal and spatial scale considered in the model (and technical basis).
6. Boundary conditions applied to the model domain (and technical basis).
7. Initial conditions applied to the model domain (and technical basis).
8. Physical-chemical properties within the model domain (and technical basis).
9. Effect of scale on the physical-chemical properties within the model domain.
10. Independent physical-chemical observations which will be used in model testing/calibration.
11. Comparison of model predictions with independent physical-chemical observations.
12. Sensitivity analyses of comparison of model predictions with independent observations
13. Uncertainty analyses of comparison of model predictions with independent observations
14. Alternative models that could explain observations
15. Applicability of model and alternatives to making long-term predictions (i.e., outside the spatial and temporal scales of the independent observations)
16. Relevant natural analogs to support long-term model predictions of the processes included in the model
17. Possible effect of other processes not included in the model (qualitative)
18. Summary and Conclusions

The following discussions focus on some of the higher priority models:

Site-scale UZ Hydrologic Model. The model should include a description of hydrogeologic units and an explanation of the observed hydrologic property differences. Once the hydrogeologic units have been specified, the geometry must be defined, including a comparison of the "observed" and "as modeled" structural contours and isopachs. All relevant hydrogeologic properties for each hydrogeologic unit should be specified. The actual distribution of the values should be shown in order to define the "representativeness" of the values assumed in the analyses. The spatial variability of the "observed" values should be presented. The development of equivalent "block-average" properties from measurements made at the core scale should be discussed. Alternate representations of fracture-matrix coupling should be "tested" with the model. All boundary conditions (both location and type) must be justified or their significance evaluated by sensitivity analyses. In particular, justification of the infiltration rates assumed in the model is required. For each assumed conceptual model and parameter distribution, comparisons should be made between the simulated/predicted flow system (i.e., the results of the model) and relevant direct observations of the flow system. Finally, the uncertainty associated with the model and the derived results should be discussed.

Drift-scale thermohydrologic model. This model should be based on the general hydrogeologic conceptual description and associated parameters (including a discussion of the uncertainty/variability in the model and associated parameters and the effects of scaling of small-scale measurements to the larger-scale discretization) used in the site-scale UZ model. This model

description should include the conceptual design(s) being analyzed. This model should discuss the representativeness of laboratory or literature derived thermohydrologic parameters to the scale of the model developed. This model description should include the boundary conditions and their uncertainty/variability, in particular the prescribed aqueous flux. This model should be compared with observations made in similar geohydrologic settings (for example, the G-tunnel experiments). This model should be used as a basis for planning *in-situ* experiments conducted from ESF test alcoves, with the calibration measures being defined. This model documentation should discuss the possible effects of thermochemistry and thermomechanics on the thermohydrologic regime. The document should discuss natural analogs which may be used to support the conceptual representation.

Waste Package Degradation Model. This model document should describe the materials selected in the current design options and discuss the general advantages and disadvantages of each material selected. This model should include the environments under which degradation is likely to occur. This model should describe the range of possible degradation modes². This model should describe the fabrication of the different materials to form the waste package and any zones of mechanical/chemical weakness due to the fabrication process. This model should present the physical/chemical phenomenology behind the significant degradation modes. This model should present the parametric relationship between the rates of degradation (assumed to be principally some form of corrosion such as pitting corrosion or stress corrosion cracking) and the environmental parameters such as geochemistry, man-made materials, temperature, and hydrology. This model should also discuss the changes in the environmental parameters caused by the degradation process itself. The data with which the parametric model has been constructed should be described and their representativeness discussed. The ability to extrapolate short-term accelerated tests to the long-term predictions required should be discussed. Comparison of model predictions with analog materials under similar environmental conditions should be presented.

Waste Package-scale Thermochemical Models (including Radionuclide Solubility). The mobility of the radionuclides that have been dissolved from the waste form is dependent on the aqueous solubility of the radionuclides and the ability of the radionuclides to sorb onto colloidal particles. Both of these processes are dependent on the geochemical environment in the vicinity of the waste packages and the changes in that geochemistry due to the degradation of the package and the thermal hydrologic environment and the presence of man-made materials. Models of the very near field (waste package scale) geochemistry are therefore required. These models should describe the fundamental thermodynamic relationships incorporated in the model as well as the potential role of non-equilibrium thermodynamics on the anticipated geochemistry. The uncertainty in the model as well as the basic thermodynamic database used in the model should be presented. Comparisons of the model predictions with direct observations of reaction rates should be presented. Comparisons should also be made with direct observations of radionuclide solubilities from both oversaturation and undersaturation. The stable and metastable phases in any solubility measurements should be presented as well as the role of colloidal or organic enhancement in the total mobile phase of the radionuclides. The uncertainty in the laboratory measurements as well as the model approximation of the laboratory measurements should be presented. Comparisons on model predictions with analog

²Models are required for each potentially significant degradation mode.

solubility and or mobility observations should be presented to enhance the confidence in the predictions based on the model.

Drift-Scale Transport Model. Radionuclides which are mobilized from the dissolution of the waste form may be transported through the waste package and the EBS by either advective or diffusive processes. The magnitudes of both the advective and diffusive components of transport are a function of the drift-scale thermal hydrology described above. In addition to the thermohydrologic regime, the diffusion through the partially saturated materials in the drift needs to be substantiated. This may include both laboratory observations, appropriate *in-situ* tests and, if available, analog observations. Also, the potential for the drift-scale thermochemical regime to affect the retardation potential of the drift materials should be addressed and quantified. The uncertainty in the conceptual representation of drift-scale transport should be discussed qualitatively and, if possible, quantitatively. The variability in advective and diffusive transport should be discussed qualitatively. The effects of colloids on transport enhancement should be addressed.

Site-Scale Unsaturated Zone Transport Model. Radionuclides that are released from the EBS will be transported in the geosphere to the accessible environment, or will be decayed during transport along the flow path given a sufficiently low advective-dispersive velocity. The UZ transport model needs to incorporate all the aspects (and the corresponding uncertainty and variability) of the UZ flow model and, in addition, the transport process models and parameters including dispersion, matrix diffusion, and matrix and fracture sorption. The developed model should discuss the model domain considered and the relevance of the applied boundary conditions for both flow of water and gas and the transport of dissolved species. The uncertainty in the boundary conditions for both flow and transport should be discussed and quantitatively evaluated. The observations used to enhance the confidence in the developed model include the *in-situ* observations of ground-water ages. The representativeness and uncertainty in these observations should be described. The calibration of the model with these observations should be presented and alternative models and parameters that can be reasonable prescribed that also explain the observations should be discussed. If alternative models than those used to represent the hydrologic conditions in the UZ flow model are required to explain the geochemical observations, these should be clearly discussed. The representativeness of laboratory derived batch experiments to *in-situ* conditions should be substantiated. Effects of scale on representative transport properties (in particular for fracture-matrix transport and matrix diffusion) should be defined and substantiated by *in-situ* observations where possible. The effects of colloids on transport enhancement should be addressed.

Repository-Scale Unsaturated Zone Thermo-Hydrology Model. In addition to the drift-scale thermo-hydrology model identified above, the long-term transient thermohydrologic response of the ground-water flow regime in the unsaturated hydrogeologic units must also be defined. It is acknowledged that evaluation of repository-scale (about 10^9 m³) thermo-hydrology will only be possible during the performance confirmation period. Therefore the technical basis for the repository-scale process will be primarily provided by the short-term, limited areal extent testing done from the ESF. This model should start with the unsaturated zone flow model describing the ambient hydrogeologic conditions. Given that a range of possible hydrologic models are anticipated, at least that same number of thermohydrologic models should be described. It may be possible to use natural analogues of thermal hydrologic perturbations (for example, intruded magma bodies into unsaturated fractured tuffs) to bound the possible effects of the thermal source associated with the spent fuel waste. As

in other flow and/or transport processes, the effects of scale, the treatment of heterogeneities, and the technical basis for such approximations should be presented.

Site-Scale Unsaturated Zone Geochemical Model. Similar to describing the ambient hydrology, it is important to define the expected ambient hydrogeochemistry of the unsaturated zone pore waters because it defines the initial condition of any possible perturbation caused by the thermal effects or interactions with repository-induced materials (whether introduced intentionally or unintentionally). The ambient geochemical environment is expected to be spatially variable, due to local heterogeneities in aqueous flow paths as well as the mineralogy along these flow paths. The "observed" ambient geochemistry is expected to be uncertain due to the difficulties in measuring the pore water geochemistry in unsaturated media. Therefore, it is important to qualitatively, and to the extent practical, quantitatively, describe the range in the likely aqueous geochemistry expected at the potential repository depth. This geochemical synthesis should also be used to substantiate the aqueous flow regimes predicted in the unsaturated-zone flow model. The "observed" geochemistry should be compared to the predicted geochemical environments using appropriate geochemical reaction path models.

Drift-Scale Thermo-Chemical Model. The aqueous geochemistry in the vicinity of the waste packages may be significantly altered from the ambient geochemistry as a result of the materials emplaced in the drifts (both intentionally and unintentionally) and the thermal regime imposed due to the emplacement of the waste. The change in the geochemical environment may impact the waste package degradation (i.e., corrosion) and radionuclide transport properties of the in-drift materials. This alteration may extend into the rock itself. Predictions of the drift-scale thermo-chemical environment require an appropriate thermo-chemical model. This model should be substantiated, to the extent practical, using laboratory information and appropriate natural analogs. The representativeness of the model used to make the near-field geochemical environment predictions should be discussed.

Waste Form Dissolution Model. Once water comes into contact with the waste form, the waste form can be altered and the radionuclides can be dissolved. The rate of alteration and subsequent dissolution is dependent on a number of environmental factors (notably the hydrology, geochemistry and temperature) and the nature of the waste form surfaces exposed to these conditions. Laboratory investigations of possible alteration and dissolution rates given a range of environments have been underway for some years. The applicability of these laboratory-determined rates to expected *in-situ* conditions has to be postulated and subsequently substantiated. This substantiation may utilize natural analogs of uranium ore deposits in unsaturated media (such as the Pena Blanca site being investigated by NRC). In addition to the laboratory dissolution rates (commonly normalized to the exposed surface area of the test material), the range in possible spent fuel and glass surface areas as a function of environmental conditions should also be defined. As with any laboratory derived parameter, the applicability of this parameter to actual conditions should be discussed and the uncertainty and possible variability described.

Regional and Site-Scale Saturated Zone Flow Models. The ultimate point of release of the aqueous radionuclides is to the saturated zone. Predicting the ambient flow in the saturated zone is important to define the potential ground-water flow paths to the accessible environment. The ambient saturated-zone hydrology is also important because it defines the initial condition for any subsequent modifications due to future climate changes. As with the unsaturated-zone flow model, the regional

and site-scale saturated-zone flow models should be compared to all relevant potentiometric information during the calibration process as well as geochemical indications of the regional flow directions and rates. Of particular importance is the degree of mixing, including dispersion, of different ground-water flow systems along the likely travel path from the potential repository to the defined location of the critical group. The uncertainty and variability of the developed model should be presented. This may be accomplished by presenting a range of possible flow fields which capture the range of possible hydraulic properties and hydrologic boundary conditions.

Volcanic Direct and Indirect Effects Models. The possibility of future volcanic processes needs to be considered in postclosure performance assessment if the probability of these processes occurring within some reasonable distance of the potential repository is greater than a specified limit (on the order of 10^{-4} over 10^4 years). Direct effects of such volcanic processes imply the direct exhumation of a certain percentage of the waste. The direct effects are controlled by the geometric and physical properties of the extrusive magma body. Indirect effects are related to changes in the ambient properties (thermal, hydrologic, geochemical) caused by an intrusive magma body located in the vicinity of the potential repository. While it may be possible to predict the magnitude of such changes by perturbing the ambient process models, it is likely that other indirect effects will be controlled by the physical/chemical attributes of the intruding body itself. One approach to addressing the indirect effects uses natural analogs of similar intrusive bodies in similar geologic and hydrogeologic settings. The uncertainty in the range of indirect effects should be qualitatively defined and substantiated. Note that the consequences of the indirect effects will be evaluated as part of the total system performance assessment.

Climate Change Indirect Effects Model. If the past is any indication of the future, then the climate in the Yucca Mountain area will change over the time period of concern (up to 1,000,000 years). Although climate change does not directly affect repository performance, the indirect effects of climate change may be significant. These indirect effects may include a change in infiltration rate (with a corresponding change in percolation flux at depth) and a change in the water table elevation. Although it is possible to predict the transient effects associated with given climate changes, it is important to also provide a basis for such predictions. Therefore, it is useful to compare possible past climates with indications of past fluxes or water table elevations in the Yucca Mountain climate. The uncertainty in the predicted effects should be quantified to the extent practical.

General Observations. As noted earlier, information from site characterization, and design- related and research activities over the next few years is expected to result in significant progress in the development of process models which are representative of the site. The incorporation of this body of knowledge in future total system performance assessments, albeit in an abstracted/simplified fashion, requires: (a) the testing of the abstraction methodology for some baseline case, and (b) the generation of abstractions which cover the expected range of conditions. A paradigm for the testing of abstractions is shown in Figure 7.2-2 and has been demonstrated for the unsaturated hydrologic system in Section 7.2. In what follows, a generic approach for the development of abstractions is presented.

- Based on the appropriate process model (e.g., UZ flow), identify a set of alternate conceptual models (e.g., ECM, nonequilibrium flow) and the corresponding range of spatial variability/parameter uncertainty (e.g., variations in K_{sat}) and driving forces (e.g., infiltration rates).

- For several equally probable representations of the physical system (e.g., unsaturated zone), perform detailed calculations using a multi-dimensional process model.
- Map the performance measures of interest (e.g., pore velocity) into a simplified description of the physical system consistent with that implemented in the TSPA code. Also, develop a response surface of the performance measure (e.g., pore velocity) as a function of the driving force (e.g., infiltration rate) that includes the effects of various conceptual and parameter uncertainties.
- Use these response surfaces as an integral component of the probabilistic performance assessments.

Future iterations of TSPA should thus be based on more representative process models of the natural and engineered systems and should rely on abstractions which cover a broader range of parameter and conceptual uncertainties.

10.7 CONSERVATIVE AND NONCONSERVATIVE FACTORS INFLUENCING THE PREDICTED RESULTS

A large number of sensitivity and uncertainty analyses have been performed during the course of this iteration of total system performance assessment. These analyses are presented and discussed in Chapters 5, 8 and 9 and are summarized in Section 10.2. Such analyses are always an important component of any performance assessment. They provide an important means to gain insights into those components, processes, models and parameters which most significantly affect the predicted waste containment and isolation over the time periods of interest.

While many useful conclusions have been reached on the basis of the sensitivity analyses performed, it is also instructive to step back a little and examine in a more qualitative fashion the implications of some of the assumptions made in the development of the total system performance assessment. The implications may be in the direction of improving the predicted performance (when the conservative assumptions are relaxed) or in the direction of degrading the predicted performance (when the nonconservative assumptions are tightened).

The following discussion addresses the entire system, i.e., the contribution of both the engineered and natural components and is irrespective of the time period of regulatory concern. It is important to point out that while the relative importance of a particular component, process, model, or parameter may depend strongly on the time period of interest, the absolute importance is generally independent of the time frame considered. This is probably not as true for externally-initiated features, events or processes (such as volcanism or other tectonic processes) which have an increased probability of occurring, for a constant recurrence interval, as the time period of interest is increased.

10.7.1 Significance of Nonconservative Assumptions

The question of the significance of nonconservative assumptions may be posed as follows: What components, processes, models, or parameters could, with some reasonable likelihood, be sufficiently different from the assumptions made in the current TSPA iteration, such that the

predicted releases or doses could be a factor of 100 to 1000 greater than those presented in Chapter 9?

Percolation Flux. The primary factor which could cause a significant increase in the predicted releases or doses at the accessible environment is the unsaturated-zone percolation flux. Significantly greater percolation flux values (on the order of 10 mm/yr) would be expected to increase the percentage of waste packages experiencing advective release from the EBS and the magnitude of that advective release if no hydraulically-engineered barrier (such as a capillary barrier or drip shield) were emplaced in the drifts. At some percolation flux, the limiting factor on the predicted release from the EBS would be the dissolution rate of the waste form itself, which in the present analyses is quite conservative. While increasing the percolation flux also decreases the advective travel time in the unsaturated zone and therefore increases the possible release of key radionuclides to the accessible environment, travel time does not appreciably affect the peak dose because the dominant dose contributor is always ^{237}Np (at the higher percolation flux values), and it is released eventually anyway.

Dose Conversion Factor. An additional factor that may increase the predicted dose above the values presented in Chapter 9 is the dose conversion factor. This factor, which converts concentrations to doses, has been derived from an EPA reference, but it is possible that revised biosphere modeling of ingestion pathways and bioconcentration factors may affect the conversion factor. It is recommended that the EPA delineate this conversion ratio as part of their rulemaking process assuming they accept the notion of dose- or risk-based total system performance.

Radionuclide Solubility. Given that it is neptunium which generally controls the predicted peak dose at the higher percolation flux values (it may be iodine or technetium at lower percolation flux values), the solubility of this radionuclide plays a significant role. The assumed solubility value of this radionuclide is already considered to be at the realistic-conservative end of the expected range. Therefore, increasing this value substantially is not believed reasonable. In addition, even if the value were increased, one would quickly reach a point where the dissolution rate would control the release of this radionuclide (assuming a significant advective release component through the EBS).

Colloidal Radionuclide Transport. Finally, colloidal transport of radionuclides has not been considered in the present TSPA analyses. Although natural- and/or radio-colloids may be formed in the waste package environment, their stability and mobility is uncertain. For those nuclides which may exist as a colloidal phase and which are also stable and mobile, their transport to the accessible environment may be significantly enhanced if the colloidal matter does not sorb onto the rock. In such a scenario, albeit unlikely, the peak concentration of some key dose-producing radionuclides (especially plutonium) may be significantly increased which would also increase the predicted dose.

Combined Effects on Nonconservative Assumptions. In sum, considering all of the above factors, the maximum increase in the predicted long term dose above the values presented in Chapter 9 is expected to be on the order of 1000; with a factor of 10 due to the percolation flux, a factor of 30 due to the dose conversion factor, and a factor of 3 due to colloidal transport.

10.7.2 Significance of Conservative Assumptions

The question of the significance of conservative assumptions may be posed as follows: What components, processes, models, or parameters could, with some reasonable likelihood, be sufficiently different from the assumptions made in the current TSPA iteration, such that the predicted releases or doses could be a factor of 100 to 1000 less than those presented in Chapter 9? In answering this question, virtually every element of the total system is a candidate for discussion. A large number of conservative assumptions have been made that would tend to significantly impact the predicted long term release or dose if the assumptions were relaxed or if the nonconservative end of the parameter space was considered.

Percolation Flux. For example, when considering the lowest percolation fluxes, the peak dose is reduced by about 100 to 1000, even when the release of ^{129}I from the EBS is in the gaseous phase. Releasing ^{129}I in the aqueous phase reduces the peak dose an additional factor of 100 to 1000. Low average percolation fluxes have two very positive effects, namely reducing the EBS release rate (because the advective component of the release is reduced) and increasing the travel time (because the propensity for fracture flow and transport is reduced and the matrix velocities are lower).

Waste Package Failure. Limiting the available inventory by either extending the lifetime of a certain fraction of the waste packages or incorporating the potential contribution of cladding has a positive effect on the predicted performance. Therefore, although the time of waste package failure may not be so important in peak dose calculations (even in the most optimal degradation model, some packages have failed by 100,000 years), the fact that only a small fraction of the packages have failed for certain assumptions is still important. This might contribute a factor of 10 to 100 to reducing the peak release and dose.

Saturated-Zone Dilution and Dispersion. An important conservatism that significantly affects the predicted peak dose is the determination of the amount of mixing due to dilution and dispersion in the saturated zone. For the present analyses, the only dispersive mixing is assumed to occur in the vertical plane to a depth of 50 m below the top of the water table. Transverse dispersion would not be considered significant over the 5-km distance to the accessible environment. Also, longitudinal dispersion has a minimal effect when considering essentially a constant source term. However, if one considers the mixing possible between the repository and the ultimate point of ground-water discharge (whether 30 km down-gradient in the Amargosa Valley or 80 km down-gradient at Franklin Lake Playa), then significant reductions (about a factor of 100) in the peak concentrations and doses would result.

Radionuclide Solubility. In those cases where the neptunium release dominates the peak dose, the neptunium solubility plays a key role. It has been suggested that the neptunium solubilities used in the TSPA analyses are based on experiments that represent metastable equilibrium concentrations and that the actual equilibrium concentration may be several orders of magnitude lower. If this were the case, neptunium would be replaced by either technetium or iodine as the peak dose contributor. This would lower the peak dose by an order of magnitude.

Combined Effects of Conservative Assumptions. Combining the above factors (not all of which are multiplicative because different radionuclides are controlling the peak dose depending on the conceptual model and parameter assumptions incorporated) could yield a reduction in the peak dose

by about a factor of 10^8 . This factor is the product of about a factor of 300 due to the percolation flux, a factor of about 300 for the aqueous release of ^{129}I , a factor of 10 for cladding effects, and a factor of 100 for saturated zone dispersion and dilution. In this case, the principal radionuclide would be either ^{99}Tc or ^{129}I .

It should come as no surprise that the above issues are the key factors in the assessment of the total system performance of the Yucca Mountain potential repository. These are the same factors noted in every other countries' assessment of their potential repository concepts³. A more detailed comparison of these studies with the current analyses is beyond the intent of the present discussion.

10.8 FUTURE TSPA ACTIVITIES

Virtually every scientific or technical report ends with a section on the knowledge gained during the course of the study and the needs for additional investigations to improve/refine the conclusions reached as a result of the study. In many regards, performance assessment documents are a little different. Although the need for additional investigations to substantiate assumptions made in the analyses is identified, other YMP organizations than performance assessment are responsible for conducting these investigations, which include (1) collecting, interpreting and synthesizing the data, (2) developing substantiating, and testing the process-level models, and (3) documenting all of the above. Based on the anticipated improvement in understanding and its corresponding documentation, performance assessment can then evaluate the significance of the uncertainty which is likely to still remain. While there is certainly much more that performance assessment could do in the way of additional sensitivity analyses of alternative conceptual models of the natural and engineered barrier systems, the highest priority performance assessment activity in the coming year is a detailed technical analysis of the robustness of the process models being developed and documented. In addition, considering that the next full iteration of total system performance assessment will occur in the Fiscal Year 1997-1998 time frame, a significant effort is involved in assuring that the developed and substantiated process models can be appropriately abstracted for use at that time. This will require substantial integration of the various technical disciplines to assure the completeness and representativeness of the analyses conducted at that time.

³ See Neall et al., (1995) for a comparison of recent total system performance assessments conducted by the high-level radioactive waste disposal programs in Sweden (SKB 91), Finland (TVO 92), Canada (AECL 94), Japan (H-3) and Switzerland (Kristillin-1).

Table 10.6-1 List of Process Level Models Required by Performance Assessment for Development of Future TSPA Abstractions

Priority	Process Model
1	Site-scale UZ hydrology model(s) (ambient)
3	Repository-scale UZ thermo-hydrology model(s)
3	Site-scale UZ geochemical model(s) (ambient)
1	Drift-scale thermo-hydrology model(s)
3	Drift-scale thermo-chemical model(s)
4	Drift-scale thermo-mechanical model(s) ¹
4	Drift-scale coupled T-H-C-M model(s)
2	Waste package degradation model(s)
4	Cladding degradation model(s)
3	Waste form dissolution model(s)
2	Waste-package-scale thermo-chemical model(s) (solubility)
2	Drift-scale transport model(s)
3	Site scale UZ transport model(s)
3	Regional and site scale SZ flow model(s)
3	Site scale SZ transport model(s)
3	Biosphere transport model(s) ²
4	Tectonics direct and indirect effects model(s)
3	Volcanics direct and indirect effects model(s)
2	Climate change indirect effects model(s)

¹ Potentially higher priority if there is no backfill in the drift.

² It is recommended that this model be prescribed during EPA rulemaking if a dose- or risk- based performance measure is selected.

Table 10.6-2 Example Observations Used to Evaluate Representativeness of Process Models

Priority	Process Model	Example Comparison to Observations
1	UZ Hydrology	<i>In-situ</i> saturations Air phase flow rates and pressures following storm events ESF ventilation humidity and aqueous flux (if observed) Ground-water ages in the UZ
1	Drift-scale thermo-hydrology	G-tunnel experiments Laboratory tests Small-scale (temporal and spatial) tests conducted from the ESF Natural analogs
2	Degradation	Observed pitting corrosion rates in candidate materials
2	Solubility	Corrosion of analog materials Laboratory tests Natural analogs
2	Drift-scale transport	Laboratory diffusion experiments ESF transport experiments P-tunnel transport experiments
3	UZ transport	<i>In-situ</i> saturations Ground-water ages in the UZ Gaseous ages in the UZ <i>In-situ</i> transport experiments Natural analogs
3	Repository-scale thermo-hydrology	Performance confirmation tests
3	UZ geochemical	Ambient observed geochemistry
3	Drift-scale thermo-chemical	Laboratory scale tests
3	Waste form dissolution	Laboratory tests under range of hydrologic and geochemical conditions
3	Volcanic effects	Natural analogs Natural analogs in the site and region
3	Regional-site SZ hydrology	Potentiometric levels Ground-water ages in the SZ
3	Climate	Pleistocene playa lake levels Calcite vein deposits

Table 10.6-3. Example Evaluation Measures Used to Determine Significance of Process Models

Priority	Process Model	Possible Evaluation Measures
1	UZ Hydrology	Percolation flux at repository horizon (variability and uncertainty) Percent of flux through fractured media at repository horizon (variability and uncertainty) Travel path length in UZ from repository to water table (variability and uncertainty) Transient nature of impact of climate change on percolation flux (variability and uncertainty)
1	Drift-scale thermohydrology	Humidity in drift (uncertainty and variability) Temperature in drift (uncertainty and variability) Advective flux in drift (uncertainty and variability) Saturation in drift (uncertainty and variability)
2	Degradation	Criteria for pit initiation (uncertainty) Pitting corrosion rate for corrosion allowance materials, corrosion resistant materials and moderately corrosion resistant materials (uncertainty) Effect of near-field geochemical environment on pitting corrosion rates Effect of near-field thermohydrologic environment on pitting corrosion rates Time for first pit to penetrate a waste package (uncertainty and variability) Time for 1000 th pit to penetrate a waste package(uncertainty and variability)
2	Solubility	Solubility of radionuclides (uncertainty) Effect of near-field geochemical environment on solubilities (uncertainty and variability) Effect of near-field thermohydrologic environment on solubilities (uncertainty and variability) Effect of colloids on solubility (uncertainty and variability)
2	Drift-scale transport	EBS release rate normalized to NRC limits
3	UZ transport	Travel time of unretarded species from repository to water table (uncertainty and variability) Travel time of retarded species from repository to water table (uncertainty and variability)
3	Repository-scale thermo-hyd.	Thermally perturbed travel time of unretarded species from repository to water table (uncertainty and variability) Temperature at specified location (TBD) (uncertainty and variability)

Table 10.6-3. Example Evaluation Measures Used to Determine Significance of Process Models
(Continued)

Priority	Process Model	Possible Evaluation Measures
3	UZ geochemical	Retardation coefficients (uncertainty and variability) Retardation coefficient changes with geochemistry and thermo-hydrology (uncertainty and variability) Travel time of retarded species from repository to water table (uncertainty and variability)
3	Drift-scale thermo-chemical	pH, Eh, DOC in drifts (uncertainty and variability) and function of thermo-hydrology
3	Waste form dissolution	Dissolution rates as functions of T-H-C environments (uncertainty and variability) EBS release rate normalized to NRC limits
3	Volcanic effects	Evaluation of doses

11.0 REFERENCES AND ACRONYM LIST

- Andersson, K., 1988. "SKI Project-90: Chemical Data," SKI TR 91:21, Swedish Nuclear Power Inspectorate, Stockholm, Sweden. (NNA.940303.0040)
- Andrews, R. W., T. F. Dale, and J. A. McNeish, 1994. "Total System Performance Assessment-1993: An Evaluation of the Potential Yucca Mountain Repository," B00000000-01717-2200-00099-Rev. 01, Civilian Radioactive Waste Management System, Management and Operating Contractor, Las Vegas, Nevada.
- Apted, M. J., A. M. Liebetau, and D. W. Engel, 1989. "The Analytical Repository Source-Term (AREST) Model: Analysis of Spent Fuel as a Nuclear Waste Form," Pacific Northwest Laboratory, PNL-6347, Richland, Washington.
- Arnold, B. W., S. J. Altman, T. H. Robey, R. W. Barnard, and T. J. Brown, 1995. "Unsaturated-Zone Fast-Path Flow Calculations for Yucca Mountain Groundwater Travel Time Analyses (GWTT-94), SAND95-0857, UC-814. Sandia National Laboratories, Albuquerque, New Mexico.
- Atkins, A., and Nickerson, A. K., 1984. "The Diffusion of Ions Through Water-Saturated Cement," Journal of Materials Science, Vol. 19, pp. 3068-3078.
- Baes, C. F., Jr., and Mesmer, R. E., 1976. "The Hydrolysis of Cations," John Wiley & Sons Inc., New York, 489 pp.
- Bahney, R. H., 1995. "MPC Internal Temperatures," Interoffice Correspondence to J. H. Lee, IOCLV.WP.RHB.05/95-164, May 5.
- Barnard, R. W., M. L. Wilson, H. A. Dockery, J. H. Gauthier, P. G. Kaplan, R. R. Eaton, F. W. Bingham, and T. H. Robey, 1992. "TSPA 1991: An Initial Total-System Performance Assessment for Yucca Mountain," SAND91-2795, Sandia National Laboratories, Albuquerque, New Mexico, September.
- Barner, J. O., 1985, "Characterization of LWR Spent Fuel MCC-Approved Testing Material - ATM-101", Pacific Northwest Laboratory Report, PNL-5109 Rev. 1, UC-70.
- Barr, G. E., 1993. Personal communication.
- Bates, J. K., J. C. Hoh, J. W. Emery, E.C. Buck, J. A. Fortner, S. F. Wolf, and T. R. Johnson, 1995. "Reactivity of Plutonium-Containing Glasses for the Immobilization of Surplus Fissile Materials," Proceedings of the Sixth Annual International Conference on High Level Radioactive Waste Management, Las Vegas, Nevada, April 30-May 5, 1995, American Nuclear Society, Inc., La Grange Park, IL, and American Society of Civil Engineers, New York, New York, pp. 588-593.

- Bates, J. K., W. L. Ebert, and T. J. Gerding, 1990. "Vapor Hydration and Subsequent Leaching of Transuranic-Containing SRL and WV Glasses," Proceedings of the International Topical Meeting on High-Level Radioactive Waste Management, Las Vegas, Nevada, April 8-12, 1990, American Nuclear Society, La Grange Park, IL, and American Society of Civil Engineers, New York, New York, Vol. 2, pp. 1095-1102.
- Bates, J. K., J. P. Bradley, A. Teetsov, C. R. Bradley, and M. Buchholtzen Brink, 1992. "Colloid Formation During Waste Form Reaction: Implications for Nuclear Waste Disposal," Science, Vol. 256, pp. 649-651. (NNA.920416.0050)
- Beavers, J. A., and C. L. Durr, 1991. "Immersion Studies on Candidate Container Alloys for the Tuff Repository," NUREG/CR-5598, Cortest Columbus Technologies, Columbus, Ohio.
- Beckmann, P., and J. E. O. Mayne, 1960. "Inhibitors of the Corrosion of Iron. I. Effects of the Cation," Journal of Applied Chemistry, Vol. 10, pp. 417-419.
- Bennet, P. C., Siegel, D. E., Baedeker, and Hult, M. F., 1993. "Crude Oil in a Shallow Sand and Gravel Aquifer--I. Hydrogeology and Inorganic Geochemistry," Applied Geochemistry, Vol. 8, pp. 529-550.
- Benson, L. V., Robinson, J. H., Blankennagel, R. K., and Ogard, A. E., 1983. "Chemical Composition of Ground Water and the Locations of Permeable Zones in the Yucca Mountain Area, Nevada," Open File Report 83-854, U. S. Geological Survey.
- Blankennagel, R. K., and J. E. Weir Jr., 1973. "Geohydrology of the Eastern Part of Paiute Mesa, Nevada Test Site, Nye County, Nevada," U.S. Geological Survey Professional Paper 712-B, Washington, D.C., 35 pp.
- Boden, P. J., 1994. "Effect of Concentration, Velocity and Temperature," Corrosion (3rd ed.), L. L. Shreir, R. A. Jarmen and G. T. Burstein (ed.), Vol. 1 - Metal/Environment Reactions, pp. 2:3-2:30.
- Bourcier, W., 1993. "Draft Input for LLNL PA Calculation, Glass Wasteform," A memo to R. Stout, March 17.
- Bourcier, W. L., S. A. Carroll, and B. L. Phillips, 1994. "Constraints on the Affinity Term for Modeling Long-Term Glass Dissolution Rates," Scientific Basis for Nuclear Waste Management XVII. Materials Research Society Symposium Proceedings, Vol. 333, pp. 507-512. A. Barkatt and R. A. Van Konynenburg (eds.), Materials Research Society, Pittsburgh, Pennsylvania.
- Brakel, J. V., and Heertjes, P. M., 1974. "Analysis of Diffusion in Macroporous Media in Terms of a Porosity, a Tortuosity and a Constrictivity Factor," International Journal of Heat and Mass Transfer, Vol. 17, pp. 1093-1103.

- Brasher, D. M., and A. D. Mercer, 1968. "Comparative Study of Factors Influencing the Action of Corrosion Inhibitors for Mild Steel in Neutral Solution. I. Sodium Benzoate," British Corrosion Journal, Vol. 3, pp. 121-129.
- Brunauer, S., 1961. "Solid Surface and the Solid-Gas Interface," Advances in Chemistry Series, Vol. 33, American Chemical Society, Washington, D.C.
- Bruton, C. J., B. L. Phillips, A. Meike, S. Martin, and B. Viani, 1993a. "Cement Minerals at Elevated Temperature: Thermodynamic and Structural Characteristics," Proceedings of the Materials Research Society Meeting, Boston, Massachusetts.
- Bruton, C. J., A. B. Meike, B. Viani, S. Martin, and B. L. Phillips, 1993b. "Thermodynamic and Structural Characteristics of Cement Minerals at Elevated Temperature," Proceedings of the Topical Meeting on Site Characterization and Model Validation. Focus '93, September 26-29, 1993, Las Vegas, Nevada, American Nuclear Society, Inc., La Grange Park, Illinois, pp. 150-156.
- Buddemeier, R. W., and J. R. Hunt, 1988. "Transport of Colloidal Contaminants in Groundwater," Applied Geochemistry, Vol. 3, No. 5, pp. 535-548. (NNA.930701.0051)
- Buesch, D. C., R. W. Spengler, T. C. Moyer, and J. K. Geslin, 1995. "Revised Stratigraphic Nomenclature and Macroscopic Identification of Lithostratigraphic Units of the Paintbrush Group Exposed at Yucca Mountain, Nevada," Open-File Report 94-469, U.S. Geological Survey, Lakewood, Colorado.
- Bullen, D., 1992. "Preliminary Data Set for the Golder Associates Waste Package Model," Consultant Report GAI-91-01-001, Golder Associates, Redmond, Washington.
- Buscheck, T. A., and J. J. Nitao, 1992. "The Impact of Thermal Loading on the Repository Performance at Yucca Mountain," Proceedings of the Third International High Level Radioactive Waste Management Conference, Las Vegas, Nevada, April 12-16.
- Buscheck, T. A., and J. J. Nitao, 1993. "The Analysis of Repository Heat-Driven Hydrothermal Flow at Yucca Mountain," Proceedings of the Fourth International High Level Radioactive Waste Management Conference, Las Vegas, Nevada, April 26-30.
- Buscheck, T. A., and J. J. Nitao, 1994. "The Impact of Buoyant Gas-Phase Flow and Heterogeneity on Thermo-Hydrological Behaviour at Yucca Mountain," Proceedings of the Fifth International High-Level Radioactive Waste Management Conference, Las Vegas, Nevada.
- Buscheck, T. A., J. J. Nitao, and S. F. Saterlie, 1994. "Evaluation of Thermo-Hydrological Performance in Support of Thermal Loading Systems Study," Proceedings of the Fifth International High-Level Radioactive Waste Management Conference, Las Vegas, Nevada.
- Buscheck, T. A., 1995, Personal communication to J. H. Lee, August 16 and 17.

- Buscheck, T. A., J. J. Nitao, and L. Ramspott, 1995. "Localized Dry-out: An Approach for Managing the Thermo-hydrological Effects of Decay Heat at Yucca Mountain," presented at the Materials Research Society Symposium on the Scientific Basis for Nuclear Waste Management XIX, 1995 Fall Meeting, Nov. 27 - Dec. 1, Boston, Massachusetts.
- Carslaw, H. S., and J. C. Jaeger, 1959. "Conduction of Heat in Solids," 2nd Edition, Oxford University Press, London.
- Castet, S., Dandurand, J. L., Schott, J., and Gout, R., 1992. "Experimental Study of Aluminum Hydrolysis and Complexation with Acetate and Sodium Ions in Hydrothermal Solutions," Proceedings of the Seventh International Symposium on Water-Rock Interaction, Vol. 2, Y. K. Kharaka and A. Maest (eds.), U.S. Geological Survey, Menlo Park, pp. 1013-1016.
- Chambre, P. L., W. W-L. Lee, C. L. Kim, and T. H. Pigford, 1986. "Steady-State and Transient Radionuclide Transport Through Penetrations in Nuclear Waste Containers," LBL-21806, Lawrence Berkeley Laboratory, University of California, Berkeley, California.
- Chambre, P.L., 1995. "The Steady State Mass Transfer from Perforated Waste Package Containers," Informal Report UCB-NE 4205, Department of Nuclear Engineering, University of California, Berkeley, California.
- Chin, B. A., and E. R. Gilbert, 1989. "Prediction of Maximum Allowable Temperatures for Dry Storage of Zircaloy-Clad Spent Fuel in Inert Atmosphere," Nuclear Technology, Vol. 85, pp. 57-65.
- Choppin, G. R., 1992. "The Role of Natural Organics in Radionuclide Migration in Natural Aquifer Systems," Radiochimica Acta, Vol. 57, pp. 113-120.
- Claassen, H. C., 1985. "Sources and Mechanisms of Recharge for Ground Water in the West-Central Amargosa Desert, Nevada--A Geochemical Interpretation," Professional Paper 712-F, U.S. Geological Survey.
- Clark, D. L., D.E. Hobart, and M. P. Neu, 1995. "Actinide Carbonate Complexes and Their Importance in Actinide Environment Chemistry," Chemical Reviews, Vol. 1995, pp. 25-48.
- Coache, R., 1986. "Amargosa Valley Basin 230-1985 Groundwater Pumpage Inventory, Tabular Material on Water Use," State of Nevada, Department of Conservation and Natural Resources, Water Resources Division, Las Vegas, Nevada.
- Coburn, S. K., 1978. "Corrosion in Fresh Water," Properties and Selection: Irons and Steels, Metals Handbook, Ninth Edition, American Society for Metals, Metal Parks, Ohio, Vol.1, pp.733-738.

- Codell, R. B., and B. Sagar, 1995. "Approaches to Model Abstraction for Performance Assessment," Proceedings of the Sixth Annual International High Level Radioactive Waste Management Conference, Las Vegas, Nevada, pp. 258-260.
- Conca, J. L., 1990. "Diffusion Barrier Transport Properties of Unsaturated Paintbrush Tuff Rubble Backfill," Proceedings of the International Topical Meeting on High Level Radioactive Waste Management, Las Vegas, Nevada, April 8-12, 1990, American Nuclear Society, Inc., La Grange Park, IL, and American Society of Civil Engineers, New York, New York, Vol. 1, pp. 394-401.
- Conca, J. L., and J. Wright, 1990. "Diffusion Coefficients in Gravel Under Unsaturated Conditions," Water Resources Research, Vol. 26, pp. 1055-1066.
- Conca, J. L., and J. Wright, 1992. "Diffusion and Flow in Gravel, Soil, and Whole Rock," Applied Hydrogeology, Vol. 1, pp. 5-24.
- Craig, B., and S.L. Pohlman, 1987. "Forms of Corrosion: Introduction," Corrosion Metals Handbook, 9th Edition, American Society for Metals International, Metals Park, Ohio, Volume 13, pp. 79.
- Crank, J., 1975. "The Mathematics of Diffusion", 2nd Edition, Oxford University Press, New York, New York.
- Croff, A. G., 1983, "ORIGEN2: A Versatile Computer Code for Calculating the Nuclide Compositions and Characteristics of Nuclear Materials," Nuclear Technology, Vol. 62, pp. 335-352.
- Crowe, B. M., F. Perry, J. Geissman, L. McFadden, S. Wells, M. Murrell, J. Paths, G. A. Valentine, L. Bowner, and K. Finnegan, 1995. "Status of Volcanism Studies for the Yucca Mountain Site Characterization Project", Los Alamos LA-MS report., Los Alamos, New Mexico.
- Czarnecki, J. B., and R. K. Waddel, 1984. "Finite-Element Simulation of Ground-Water Flow in the Vicinity of Yucca Mountain, Nevada-California," USGS-OFR-84-4349. Water Resources Investigations Report, U.S. Geological Survey.
- Czarnecki, J. B., 1989. "Characterization of the Subregional Ground-Water Flow System at Yucca Mountain and Vicinity, Nevada-California," Radioactive Waste Management and the Nuclear Fuel Cycle, Vol. 13, No. 1-4, pp. 51-61.
- Dettinger, M. D., 1992. "Geohydrology of Areas Being Considered for Exploratory Drilling and Development of the Carbonate-Rock Aquifers in Southern Nevada--Preliminary Assessment," USGS-WRI-90-4077, U.S. Geological Survey, 35 p.
- DOE (U.S. Department of Energy), 1995. "Mined Geologic Disposal System License Application Annotated Outline", Revision 0, YMP 94-05, Yucca Mountain Site Characterization Office, Las Vegas, Nevada.

- DOE (U.S. Department of Energy), 1995a. "Engineered Barrier Design Requirements Document," YMP/CM-0024, Rev. 1, Office of Civilian Radioactive Waste Management, Las Vegas, Nevada, October.
- DOE (U.S. Department of Energy), 1995b. "In-Situ Thermal Testing Program Strategy," DOE/TMSCO-003, The Yucca Mountain Site Characterization Office, Las Vegas, Nevada.
- DOE (U.S. Department of Energy), 1990. "Yucca Mountain Project Reference Information Base," YNP/CC-0002 (Version 04.002), Nevada Operations Office, Las Vegas, Nevada.
- DOE (U.S. Department of Energy), 1988. "Site Characterization Plan, Yucca Mountain Site," DOE/RW-0199, Office of Civilian Radioactive Waste Management.
- DOE (U.S. Department of Energy), 1987. "Characteristics of Spent Fuel, High-Level Waste, and Other Radioactive Wastes Which May Require Long-Term Isolation," DOE/RW-0184, OCRWM, Washington, D.C.
- Doering, T. W., 1995. "Dimensions of Waste Package Barriers," CRWMS M&O Interoffice Correspondence, IOC LV.WP.TWD.5/95.182, May 26.
- Dudley, W. W., Jr., and J. D. Larson, 1976. "Effect of Irrigation Pumping on Desert Pupfish Habitats in Ash Meadows, Nye County, Nevada," U.S. Geological Survey Professional Paper 927, U.S. Government Printing Office, Washington, D. C.
- Duguid, J. O., R. W. Andrews, E. Brandstetter, T. F. Dale, and M. Reeves, 1994. "Calculations Supporting Evaluation of Potential Environmental Standards for Yucca Mountain," B00000000-01717-2200-00094, CRWMS Management and Operating Contractor, Vienna, Virginia.
- Duncan, J. R., and D. J. Spedding, 1973. "The Effect of Relative Humidity on Adsorption of Sulphur Dioxide on to Metal Surfaces," Corrosion Science, Vol. 13, pp. 993-1001.
- Dyer, J. R., 1993. "Radionuclide Solubility Working Group (SolWOG) Meeting Report (SCP: N/A)," Department of Energy Letter with Enclosure to LLNL and LANL, August 2.
- Ebert, W. L., and J. K. Bates, 1995. "Performance Testing of West Valley Reference 6 Glass," Proceedings of the Sixth Annual International Conference on High Level Radioactive Waste Management, Las Vegas, Nevada, April 30-May 5, 1995, American Nuclear Society, Inc., La Grange Park, Illinois, and American Society of Civil Engineers, New York, New York, pp. 583-587.
- Eikenberg, J., and Lichtner, P. C., 1992. "Propagation of Hyperalkaline Cement Pore Waters into the Geologic Barrier Surrounding a Radioactive Waste Repository," Proceedings of the Seventh International Symposium on Water-Rock Interaction, Vol. 1, Y. K. Kharaka and A. Maest (eds.), U.S. Geological Survey, Menlo Park, pp. 377-380.

- Eikenberg, J., 1990. "On the Problem of Silica Solubility at High pH," PSI Report 74 and NAGRA Technical Report NTB 90-36, Switzerland.
- Einzig, R. E., 1994. "Preliminary Spent Fuel Oxidation Source Term Model," Proceedings of the Fifth International Conference on High-Level Radioactive Waste Management, Las Vegas, Nevada, May 22-26, 1994, American Nuclear Society, La Grange Park, Illinois, and American Society of Civil Engineers, New York, New York, Vol. 2, pp. 554-559.
- Engel, D., 1995. A memo to J.H. Lee, January 30.
- EPA (Environmental Protection Agency), 1988. "Limiting Values of Radionuclide Intake and Air Concentration and Dose Conversion Factors for Inhalation, Submersion, and Ingestion, EPA-520/1-88-020, Washington, D.C.
- EPRI (Electrical Power Research Institute), 1992. "Source Term in the EPRI Performance Assessment," R. Shaw, presented to Nuclear Waste Technical Review Board, Las Vegas, Nevada, October 15, 1992.
- Ervin, E. M., R. R. Luckey and D. J. Burkhardt, 1994. "Summary of Revised Potentiometric Surface Map for Yucca Mountain and Vicinity, Nevada", Proceedings of the Fifth International High Level Radioactive Waste Management Conference, Las Vegas, Nevada, May 22-26, 1994.
- Fabryka-Martin, J., 1995. "Isotopic Dating of Ground Water at Yucca Mountain", Presentation at Nuclear Waste Technical Review Board on Hydrogeology and Geochemistry, San Francisco, California, June 26-27, 1995.
- Farmer, J. C., and R. D. McCright, 1989. "Localized Corrosion and Stress Corrosion Cracking of Candidate Materials for High-Level Radioactive Waste Disposal Containers in U.S.: A Critical Literature Review," Scientific Basis for Nuclear Waste Management XII, W. Lutze and R. C. Ewing (eds.), Proceedings of the Symposium by the Material Research Society, Pittsburg, Pennsylvania, Vol. 127, pp. 359-371.
- Farmer, J. C., R. A. Van Konynenburg, R. D. McCright, and D. B. Bullen, 1988. "Survey of Degradation Modes of Candidate Materials for High-Level Radioactive-Waste Disposal Containers. Volume 3: Localized Corrosion and Stress Corrosion Cracking of Austenitic Alloys," UCID-21362 Vol. 3, Lawrence Livermore National Laboratory, Livermore, California
- Feng, X., E. C. Buck, C. Mertz, J. K. Bates, and J. C. Cunnane, 1993. "Study on the Colloids Generated from Testing of High-Level Nuclear Waste Glasses," Proceedings of the Symposium on Waste Management, Tucson, Arizona, February 28 - March 4, 1993, Vol. 2, 1015-1021. (NNA.930907.0054)

- Finn, P. A., J. K. Bates, E.C. Buck, D. J. Wronkiewicz, J. C. Hoh, and S. F. Wolf, 1995. "Alteration of Spent Fuel Matrix Under Unsaturated Water Conditions," Proceedings of the Sixth Annual International Conference on High Level Radioactive Waste Management, Las Vegas, Nevada, April 30-May 5, 1995, American Nuclear Society, Inc., La Grange Park, Illinois, and American Society of Civil Engineers, New York, New York, pp. 606-608.
- Flint, A. L., and L. E. Flint, 1994. "Spatial Distribution of Potential Near Surface Moisture Flux at Yucca Mountain," Proceedings of the Fifth Annual International Conference on High Level Radioactive Waste Management, Las Vegas, Nevada, pp. 2352-2358.
- Flint, A. L., 1995. "Shallow Infiltration and the Initiation of Fracture Flow at Yucca Mountain, Nevada," Presented to Nuclear Waste Technical Review Board, San Francisco, California, June.
- Fontana, M. G., 1986. "Corrosion Engineering," 3rd Edition, McGraw-Hill, New York.
- Freeze, R. A., and J. A. Cherry, 1979. "Groundwater," Prentice-Hall, Englewood Cliffs, New Jersey.
- French, R. H., A. Elzeftawy, J. Bird, and B. Elliot, 1984. "Hydrology and Water Resources Overview of the Nevada Nuclear Waste Storage Investigations, Nevada Test Site, Nye County, Nevada," NVO-284, Desert Research Institute, Las Vegas, Nevada.
- Fyfe, D., 1994. "The Atmosphere," Corrosion, Vol. 1-Metal/Environment Reactions, 3rd Edition, L. L. Shreir, R. A. Jarman and G. T. Burstein (eds.), Butterworth-Heinemann, pp. 2:31-2:42.
- Gauthier, J., 1993. "Expert Elicitation of the Solubility Distributions to be Used in TSPA#2 Calculations," Draft Report, June 1, 1993.
- Gauthier, J. H., 1995, "Proposed Models of Colloid-Facilitated Transport for Total-System Performance Assessment," Proceedings of the Sixth Annual International Conference on High-Level Radioactive Waste Management, Las Vegas, Nevada, April 30-May 5, 1995, American Nuclear Society, Inc., La Grange Park, IL, and American Society of Civil Engineers, New York, NY, pp. 448-450.
- Gdowski, G. E., and D. B. Bullen, 1988. "Survey of Degradation Modes of Candidate Materials for High-Level Radioactive-Waste Disposal Containers," UCID-21362 Vol. 2, Lawrence Livermore National Laboratory, Livermore, California.
- Gelhar, L. W., 1993, "Stochastic Subsurface Hydrology," Prentice-Hall, Englewood Cliffs, New Jersey.

- Glassley, W., 1993. "Coupled Hydro-Geochemical Processes and their Significance for Yucca Mountain Site Characterization," Proceedings of the Topical Meeting on Site Characterization and Model Validation, Focus '93, September 26-29, 1993, Las Vegas, Nevada, American Nuclear Society, Inc., La Grange Park, Illinois, pp. 122-126.
- Golder Associates, Inc., 1993. "Application of the RIP (Repository Integration Program) to the Proposed Repository at Yucca Mountain: Conceptual Model and Input Data Set," Golder Associates, Redmond, Washington.
- Golder Associates, Inc., 1994. "RIP Performance Assessment and Strategy Evaluation Model: Theory Manual and User's Guide, Version 3.20", Golder Associates, Redmond, Washington.
- Golder Associates, Inc., 1994a. "Alternative Conceptualizations for WIPP Performance Assessment Modeling," prepared for the WIPP Technical Assistance Contractor (WTAC), U.S. Department of Energy, November, 1995.
- Golder Associates, Inc., 1995a. "Implementation of the SPM-2 Data Set Within RIP," Draft Report prepared for the WIPP Technical Assistance Contractor (WTAC), U.S. Department of Energy, August, 1995.
- Golder Associates, Inc., 1995b. "Long-Term Performance Assessment of New York Low-Level Radioactive Waste Disposal Methods," Draft Report prepared for New York State Low-Level Radioactive Waste Siting Commission, 923-D006.003, June 1995.
- Golder Associates, Inc., 1995c. "Verification Report for the Repository Integration Program (RIP)," prepared for the WIPP Technical Assistance Contractor (WTAC), U.S. Department of Energy, August, 1995.
- Gray, W. J., 1995a. A memo to D. Engel, April 28.
- Gray, W. J., 1995b. A personal communication to J. H. Lee, August 21.
- Gray, W. J., H. R. Leider, and S. A. Steward, 1992. "Parametric Study of LWR Spent Fuel Dissolution Kinetics," UCRL-JC-110160, Lawrence Livermore National Laboratory, Livermore, California.
- Gray, W. J., and C. N. Wilson, 1995. "Spent Fuel Dissolution Studies FY 1991-1994," PNL-10450, Pacific Northwest Laboratory, Richland, Washington.
- Guttman, H., 1968. "Effects of Atmospheric Factors on the Corrosion of Rolled Zinc," Metal Corrosion in the Atmosphere, ASTM STP 435, American Society for Testing and Materials, pp. 223-239.

- Guttman, H. and P. J. Sereda, 1968. "Measurement of Atmospheric Factors Affecting the Corrosion of Metals," Corrosion in Natural Environments, ASTM STP 558, American Society for Testing and Materials, pp. 33-51.
- Halsey, W., 1995. "Recommendations for Modifications of the Waste Package Corrosion Model for TSPA-95," Interoffice Correspondence IOC LV.WP.PG.08/95.261, August 3.
- Harrill, J. R., 1986. "Ground-Water Storage Depletion in Pahrump Valley, Nevada-California, 1962-1975," U.S. Geological Survey, Water-Supply Paper 2279.
- Harrill, J. R., J. S. Gates, and J. M. Thomas, 1988. "Major Ground Water Flow Systems in the Great Basin of Nevada, Utah and Adjacent States," Department of Interior, U. S. Geological Survey, Reston, Virginia.
- Haynie, F. H., J. W. Spence, and J. B. Upham, 1978. "Effects of Air Pollutants on Weathering Steel and Galvanized Steel: A Chamber Study," Atmospheric Factors Affecting the Corrosion of Engineering Metals, ASTM STP 646, S.K. Coburn (ed.), American Society for Testing and Materials, pp. 30-47.
- Haynie, F. H., and J. B. Upham, 1974. "Correlation Between Corrosion Behavior of Steel and Atmospheric Pollution Data," Metal Corrosion in the Atmosphere, ASTM STP 435, American Society for Testing and Materials, pp. 326-359.
- Henshall, G. A., W. L. Clarke, and R. D. McCright, 1993. "Modeling Pitting Corrosion Damage of High-Level Radioactive-Waste Containers, with Emphasis on the Stochastic Approach," UCRL-ID-111624, Lawrence Livermore National Laboratory, Livermore, California, January.
- Hersch, P., J. B. Hare, A. Robertson, and S. M. Sutherland, 1961a. "An Experimental Survey of Rust Preventives in Water: I. Methods of Testing," Journal of Applied Chemistry, Vol. 11, pp. 246-250.
- Hersch, P., J. B. Hare, A. Robertson, and S. M. Sutherland, 1961b. "An Experimental Survey of Rust Preventives in Water: III. Some General Results," Journal of Applied Chemistry, Vol. 11, pp. 265-271.
- Hevesi, J. A., A. L. Flint and J. D. Istok, 1993. "Precipitation Estimates in Mountainous Terrain Using Multivariate Geostatistics, Part II: Isohyetal Maps," Journal of Applied Meteorology, Vol. 31, pp. 677-688.
- Ho, C., 1995. "Assessing Alternative Conceptual Models of Fracture Flow," Proceedings of TOUGH Workshop '95, Lawrence Berkeley Laboratory, Berkeley, California, March 20-22.

- Hobart, D. E., D. E. Morris, P. D. Palmer, and T. W. Newton, 1989. "Formation, Characterization and Stability of Plutonium (IV) Colloid: A Progress Report," Proceeding of Nuclear Waste Isolation in the Unsaturated Zone, FOCUS '89, Las Vegas, Nevada, September 17-21, pp. 118-124. (NNA.890815.0254)
- Hoxie, D. T., 1989. "A Conceptual Model for the Unsaturated Zone Hydrogeologic System, Yucca Mountain, Nevada," Radioactive Waste Management Nuclear Fuel Cycle, Vol. 13, No. 1-4, pp. 63-76.
- ICRP (International Commission on Radiological Protection), 1991. "1990 Recommendations to the International Commission on Radiological Protection," Report ICRP-60. Annals of the ICRP.
- ICRP (International Commission on Radiological Protection), 1985a. "Radiation Protection Principles for the Disposal of Solid Radioactive Waste," Report ICRP-46. Annals of the ICRP.
- ICRP (International Commission on Radiological Protection), 1985b. "Principles of Monitoring for the Radiation Protection of the Population," Report ICRP-43. Annals of the ICRP.
- Janecky, D. R., C. J. Duffy, C. D. Tait, and D. Clark, 1994. "Thermochemical Data on Actinides for Modeling," Letter Report, LANL Milestone 4025.
- Jardine, L. J., 1991. "Submission of Data to the SEPDB, LLNL Letter LLYMP9101029 with Attachments to SNL SEPD Administrator," January 22. (NNA.920617.0023)
- Johnson, J. W., E. H. Oelkers, and H. C. Helgeson, 1992. "SUPCRT92: A Software Package For Calculating the Standard Molal Thermodynamic Properties of Minerals, Gases, Aqueous Species, And Reactions From 1 To 5000 Bar and 0 To 1000°C," Computers and Geosciences, Vol. 18, No. 7, pp. 899-947.
- Jones, D. A., and R. S. Howryla, 1993. "Electrochemical Sensor to Monitor Atmospheric Corrosion in Repository Environments," Presented at the Yucca Mountain Waste Package Workshop, Las Vegas, Nevada, September 21-23.
- Kerrisk, J. F., 1984. "Solubility Limits on Radionuclide Dissolution at a Yucca Mountain Repository," LA-9995-MS, Los Alamos National Laboratory, Los Alamos, New Mexico (NNA.870519.0049)
- Kerrisk, J. F., 1987. "Groundwater Chemistry at Yucca Mountain, Nevada, and Vicinity," LA-10929-MS, Los Alamos National Laboratory, Los Alamos, New Mexico.

- Klavetter, E. A., and R. R. Peters, 1986. "Estimation of Hydrologic Properties of an Unsaturated Fractured Rock Mass," SAND84-2642, Sandia National Laboratories, Albuquerque, New Mexico.
- Knauss, K. G., W. L. Bourcier, K. D. McKeegan, C. I. Merzbacher, S. N. Nguyen, F. J. Ryerson, D. K. Smith, H. C. Weed, and L. Newton, 1990. "Dissolution Kinetics of a Simple Analogue Waste Glass As a Function of pH, Time and Temperature," Scientific Basis for Nuclear Waste Management XIII. Materials Research Society Symposium Proceedings, Vol. 176, pp. 371-381, V.M. Oversby and P.W. Brown (eds.), Materials Research Society, Pittsburgh, Pennsylvania.
- Knotkova, D., P. Holler, and J. Vickova, 1981. "The Evaluation of the Microclimate Effect on the Characteristics of Environment and Corrosion of Metals," Proceedings of the Eighth International Congress on Metallic Corrosion, September 6-11, Mainz, FRG, Vol. 1, pp. 859-864.
- Knotkova-Cermakova, D., J. Vickova, and J. Honzak, 1982. "Atmospheric Corrosion of Weathering Steels," Atmospheric Corrosion of Metals, ASTM STP 767, S. W. Dean, Jr. and E. C. Rhea (eds.), American Society for Testing and Materials, pp. 7-44.
- Komp, M. E., 1987. "Atmospheric Corrosion Ratings of Weathering Steels-Calculation and Significance," Materials Performance, pp. 42-44, July.
- Kucera, V., and E. Mattsson, 1974. "Electrochemical Technique for Determination of the Instantaneous Rate of Atmospheric Corrosion," Corrosion in Natural Environments, ASTM STP 558, American Society for Testing and Materials, pp. 239-260.
- Kwicklis, E., 1994. "High Level Radioactive Waste Management, Gas Migration within Clay," May 22 - 26, pp. 2071 - 2080, Presented to Nuclear Waste Technical Review Board, Las Vegas, Nevada, October.
- LANL (Los Alamos National Laboratory), 1992. "Mountain Site Characterization Project Radionuclide Absorption," Workshop at Los Alamos National Laboratory, (ed.), J. A. Canepa, LA-12325-6, 1992, Los Alamos National Laboratory, Los Alamos, New Mexico.
- Larrabee, C. P., 1953. "Corrosion Resistance of High-Strength Low-Alloy Steels As Influenced by Composition and Environment," Corrosion, Vol. 9, pp. 259-271.
- Lee, J. H., 1995. "Response to IOC LV.WP.PG.08/95.261 from William Halsey," Interoffice Correspondence IOC LV.PA.JHL.08/95.001, August 7.
- Levy, S. S., 1992. "Natural Gels in the Yucca Mountain Area, Nevada, USA," Applied Clay Science, Vol. 7, pp. 79-85.

- Li, C., V. Vallikat, S. Mishra, and S. D. Sevougian, 1995. "Influence of the Poisson Transition Rate and Matrix Diffusion on Solute Transport in Fractured Media," Letter Report, CRWMS Management and Operating Contractor, Las Vegas, Nevada.
- Lingineni, S., M. Reeves, and S. Mishra, 1994. "Hydrothermal Analyses at the Waste Package/ Drift Scale, A Benchmarking Study with FEHM and TOUGH2," BBA000000-01717-0200-00001, Las Vegas Nevada.
- Long, A., and S.W. Childs, 1993. "Rainfall and Net Infiltration Probabilities for Future Climate Conditions at Yucca Mountain," in Proceedings of the Fourth Annual High Level Radioactive Waste Management Conference, Las Vegas Nevada, April 26-30, 1993, American Nuclear Society Inc., La Grange Park, IL, and American Society of Civil Engineers, New York, NY, pp. 112-121.
- Longenbaugh, R., C. A. Rautman, and E. E. Ryder, 1994. "Yucca Mountain Thermal Response: An Evaluation of the Effects of Modeled Geologic Structure and Thermal Property Descriptions". SAND94-2247, Sandia National Laboratories, Albuquerque, New Mexico, September.
- Malinauskas, A., 1995. A personal communication to J.H. Lee, August 21.
- Manaktala, H., Turner, D., Ahn, T., Colten-Bradley, V., and Bonano, E., 1995, "Implications of Colloids on the Performance of a HLW Repository," Proceedings of the Sixth Annual International Conference on High-Level Radioactive Waste Management, Las Vegas, Nevada, April 30-May 5, 1995, American Nuclear Society Inc., La Grange Park, IL, and American Society of Civil Engineers, New York, NY, pp. 445-447.
- Marsh, G. P. and K. J. Taylor, 1988. "An Assessment of Carbon Steel Containers for Radioactive Waste Disposal," Corrosion Science, Vol. 28, pp. 289-320.
- Marsh, G. P., K. J. Taylor, and Z. Sooi, 1988. "The Kinetics of Pitting Corrosion of Carbon Steel," SKB Technical Report 88-09, Stockholm, Sweden, February.
- Masamura, K., and I. Matsushima, 1983. "Corrosion and Electrochemical Behavior of Steel in CO₂ Bearing Water," Transactions of the Iron and Steel Institute of Japan, Vol. 23, No. 8, pp. 676-679.
- McCarthy, J. F., and J. M. Zachara, 1989. "Subsurface Transport of Contaminants," Environmental Science and Technology, Vol. 23, No. 5, pp. 496-502. (NNA 830625.0032)
- McCoy, K., 1994. "Corrosion Model for Corrosion-Allowance Materials: Thermal Loading and Degradation of Corrosion-Allowance Materials in Humid Air," CRWMS M&O Interoffice Correspondence, IOC LV.WP.JKM.8/94.201, August 5.

- McCoy, K., 1995. "Cladding Degradation and Fuel Exposure," Interoffice Correspondence to J. H. Lee, IOC.LV.WPD.JKM.3/95.098, March 21.
- McCright, R. D. and H. Weiss, 1985. "Corrosion Behavior of Carbon Steels under Tuff Repository Environmental Conditions," Scientific Basis for Nuclear Waste Management VIII. Material Research Society Symposium Proceedings, Vol. 44, pp. 287-294, C. M. Jantzen, J. A. Stone and R. C. Ewing (eds.), Materials Research Society, Pittsburg, Pennsylvania.
- McCright, R. D., 1994. "Scientific Investigation Plan: Metallic Barriers Task," W.B.S 1.2.2.5.1, Rev. 2, UCRL-xx-xxxx, Lawrence Livermore National Laboratory, Livermore, California, December.
- McCright, R. D., 1995. "Galvanized Effects in Multi-Barrier Waste Package Containers". Personal Communication to J. H. Lee, July 12.
- McGuire, R. K., D. B. Bullen, N. Cook, K. J. Coppersmith, J. Kemeny, A. Long, F. J. Pearson, Jr., F. Schwartz, M. Sheridan, and R. R. Youngs, 1990. "Demonstration of a Risk-Based Approach to High-Level Waste Repository Evaluation," EPRI NP-7057, Electric Power Research Institute, Palo Alto, California.
- McGuire, R. K., M. J. Apted, D. B. Bullen, S. Childs, N. Cook, K. J. Coppersmith, R. L. Keeney, J. M. Kemeny, A. Long, F. J. Pearson, Jr., B. Ross, F. W. Schwartz, M. F. Sheridan, and R. R. Youngs, 1992. Demonstration of a Risk-Based Approach to High-Level Waste Repository Evaluation: Phase 2, EPRI TR-100384, Electric Power Research Institute, Palo Alto, California.
- Means, J. L., A. S. Maest, and D. A. Crear, 1983. "The Organic Geochemistry of Deep Ground Waters and Radionuclide Partitioning Experiments Under Hydrothermal Conditions," Office of Nuclear Waste Isolation, Battelle Memorial Institute, Technical Report ONWI-448, Distribution Category UC-70, July.
- Meijer, A., 1990. "Yucca Mountain Project Far-Field Sorption Studies and Data Needs," LANL Report LA-11671-MS, UC-510, September, 37 p.
- Meijer, A., 1992. "A Strategy for the Derivation and Use of Sorption Coefficients in Performance Assessment Calculations for the Yucca Mountain Site," Proceedings of the DOE/Yucca Mountain Site Characterization Project Radionuclide Absorption Workshop at Los Alamos National Laboratory, September 11-12, 1990, J. A. Canepa (ed.), LA-12325-C, Los Alamos National Laboratory, Los Alamos, New Mexico.
- Meijer, A., 1995. Memo to S. D. Sevougian, June 7, 1995.
- Meike, A., 1995. "A Discussion of Some Specific Needs for Historical Analogs within the Introduced Materials Task," LLNL Milestone MOL 128 Draft Report, June.

- Meike, A., and Wittwer, C., 1993, "Formation of Colloids from Introduced Materials in the Post-Emplacement Environment: A Report on the State of Understanding," Proceedings of the Topical Meeting on Site Characterization and Model Validation, Focus '93, September 26-29, 1993, Las Vegas, NV, Amer. Nuc. Soc., Inc., La Grange Park, Illinois, p. 95-102.
- Meike, A., C. J. Bruton, M. Onofrei, and B. Viani, 1994. "Progress in Understanding the Structure and Thermodynamics of Calcium Silicate Hydrates," Proceedings of the Fifth Annual International Conference on High Level Radioactive Waste Management, Las Vegas, Nevada, pp. 2590-2596.
- Mercer, A. D., I. R. Jenkins, and J. E. Rhoades-Brown, 1968. "Comparative Study of Factors Influencing the Action of Corrosion Inhibitors for Mild Steel in Neutral Solution. III. Sodium Nitrite," British Corrosion Journal, Vol. 3, pp. 136-144.
- Mifflin, M. D., and J. W. Hess, 1979. "Regional Carbonate Flow Systems in Nevada," W. Back and D. A. Stephenson (Guest-Editors), Contemporary Hydrogeology, The Goerge Burke Maxey Memorial Volume, Journal of Hydrology, Vol. 43, pp. 217-237.
- Miller, D. G., 1982. "Estimation of Tracer Diffusion Coefficients of Ions in Aqueous Solution," UCRL-53319, Lawrence Livermore National Laboratory, Livermore, California.
- Miller, I., R. Kossik and M. Cunnane, 1992. "A New Methodology for Repository Site Suitability Evaluation," Proceedings of the Third International Conference for High Level Radioactive Waste Management, Las Vegas, Nevada, April 12-16, 1992.
- Minai, Y., G. R. Choppin, and D. H. Sisson, 1992. "Humic Material in Well Water from the Nevada Test Site," Radiochimica Acta, Vol. 56, pp. 195-199. (NNA. 930607.0076)
- M&O (Civilian Radioactive Waste Management System, Management and Operating Contractor [CRWMS M&O]), 1993a. "A Comparative Application of the Repository Integration Program (RIP) to Total System Performance Assessment-1991," B00000000-AA-09-00010-00, Las Vegas, Nevada.
- M&O (Civilian Radioactive Waste Management System, Management and Operating Contractor [CRWMS M&O]), 1993b. "Repository Subsurface Layout Options and ESF Interface," B00000000-01717-5705-00009, Rev. 00, Las Vegas, Nevada, December .
- M&O (Civilian Radioactive Waste Management System, Management and Operating Contractor [CRWMS M&O]), 1993c. "Characteristics Database: LWR Radiological PC Database," A00000000-02268-1200-20002, V1.0, VA-M04-20002.021.C014, Vienna, Virginia

- M&O (Civilian Radioactive Waste Management System, Management and Operating Contractor [CRWMS M&O]), 1994a. "Additional Sensitivity Analyses Extending the Total System Performance Assessment (TSPA)-1993 Results," B00000000-01717-0200-00122, Rev. 00, CRWMS M&O, Las Vegas, Nevada.
- M&O (Civilian Radioactive Waste Management System, Management and Operating Contractor [CRWMS M&O]), 1994b. "Initial Summary Report for Repository/Waste Package Advance Conceptual Design," B00000000-01717-5705-00015, Rev. 01, Las Vegas, Nevada.
- M&O (Civilian Radioactive Waste Management System, Management and Operating Contractor [CRWMS M&O]), 1994c. "Generic Repository Layouts for Various Thermal Loadings," B00000000-01717-5705-00002, Rev. 00, Las Vegas, Nevada, August.
- M&O (Civilian Radioactive Waste Management System, Management & Operating Contractor [CRWMS M&O]), 1995a. "Thermomechanical Analyses," B00000000-01717-5705-00013, Rev. 00, Las Vegas, Nevada.
- M&O (Civilian Radioactive Waste Management System, Management and Operating Contractor [CRWMS M&O]), 1995b. "Estimation of the Extent of the Disturbed Zone Around a Repository Drift Caused by Excavation and Thermal Loading," Las Vegas, Nevada, letter report transmitted to DOE via transmittal LV.RL.SEL.06/30-138 on June 30.
- M&O (Civilian Radioactive Waste Management System, Management and Operating Contractor [CRWMS M&O]), 1995c. "Controlled Design Assumption Document," B00000000-01717-4600-00032, Rev. 01, Las Vegas, Nevada, April 28.
- M&O (Civilian Radioactive Waste Management System, Management and Operating Contractor [CRWMS M&O]), 1995d. "Systems Study of Options for Characterizing the Calico Hills Nonwelded Hydrogeologic Unit at Yucca Mountain, Nevada," B00000000-01717-5705-00021, Rev. 01., Las Vegas, Nevada.
- M&O (Civilian Radioactive Waste Management System, Management and Operating Contractor [CRWMS M&O]), 1995e. "White Paper: Proposed Thermal Loading Strategy," A00000000-01717-1710-00001, Rev. 00, Las Vegas, Nevada.
- M&O (Civilian Radioactive Waste Management System, Management and Operating Contractor [CRWMS M&O]), 1995f. "Emplacement Mode Evaluation Report," BCA000000-01717-5705-00002, Rev. 00, Las Vegas, Nevada, May.
- Montazer, P., and W. E. Wilson, 1984. "Conceptual Hydrologic Model of Flow in the Unsaturated Zone, Yucca Mountain, Nevada," Water-Resources Investigation Report 84-4345, U.S. Geological Survey, Lakewood, Colorado.

- Murphy, W. M., 1991. "Performance Assessment Perspectives with Reference to the Proposed Repository at Yucca Mountain, Nevada," Proceedings from the Technical Workshop on Near-Field Performance Assessment for High-Level Waste Held in Madrid, October 15-17, 1990, SKB Technical Report 91-59, P. Sellen, M. Apted, and J. Gago (eds)., Swedish Nuclear Fuel and Waste Management Co., Stockholm, Sweden, pp. 11-22.
- Murphy, W. M., 1993. "Geochemical Models for Gas-Water-Rock Interactions in a Proposed Nuclear Waste Repository at Yucca Mountain," Proceedings of the Topical Meeting on Site Characterization and Model Validation, Focus '93, September 26-29, 1993, Las Vegas, Nevada, American Nuclear Society, Inc., La Grange Park, Illinois, pp. 115-121.
- NAS, (National Research Council), 1983. "A Study of the Isolation System for Geological Disposal of Radio Active Waste," Board on Radioactive Waste Management - Waste Isolation Panel, National Academy Press, Washington, D.C.
- NAS, (National Research Council), 1995. "Technical Bases for Yucca Mountain Standards," National Academy of Science, Washington, D.C.
- Neall, F., P. Smith, T. Sumerling, and H. Umeki, 1995. "Putting HLW Performance Assessment Results in Perspective," NAGRA Bulletin, No. 25, pp 47-55.
- Nelson, R. W., 1995. "Testing of Abstractions Used in Total System Performance Assessments," Proceedings of the Sixth Annual International Conference on High Level Radioactive Waste Management, Las Vegas, Nevada, pp. 255-257.
- Nevada Bureau of Mines and Geology and the Nevada Department of Minerals, 1993. "Major Mines of Nevada," University of Nevada-Reno, MacKay School of Mines, Special Publication P-4.
- Nichols, W. D., and J. P. Akers, 1985. "Water-Level Declines in the Amargosa Valley Area," Nye County, Nevada, 1962-84, USGS-WRI-85-4273.
- Nitao, J. J., 1989. "V-TOUGH - An Enhanced Version of the TOUGH Code for the Thermal and Hydrologic Simulation of Large-Scale Problems in Nuclear Waste Isolation," UCID-21954, Lawrence Livermore National Laboratory, Livermore, California.
- Nitao, J. J., 1988. "Numerical Modeling of the Thermal and Hydrological Environment Around a Nuclear Waste Package Using the Effective Continuum Approximation: Horizontal Emplacement," UCID-21444, Lawrence Livermore National Laboratory, Livermore, California.

- Nitsche H., R. C. Gatti, E. M. Standifer, S. C. Lee, A. Muller, T. Prussin, R. S. Deinhammer, H. Maurer, K. Becraft, S. Leung, and S. A. Carpenter, 1993. "Measured Solubilities and Speciations of Neptunium, Plutonium and Americium in a Typical Groundwater (J-13) from the Yucca Mountain Region," Milestone Report 3010-WBS 1.2.3.4.1.3.1. LA-12562-MS UC-802, Los Alamos National Laboratory, Los Alamos, New Mexico, 127 pp.
- Nitsche H., K. Roberts, T. Pussin, A. Muller, K. Becraft, D. Keeney, S. A. Carpenter, and R. C. Gatti, 1994. "Measured Solubilities and Speciations from Oversaturation Experiments of Neptunium, Plutonium, and Americium in UE-25p #1 Well Water from the Yucca Mountain Region," Milestone Report 3329-WBS 1.2.3.4.1.3.1. LA-12563-MS UC-802, Los Alamos National Laboratory, Los Alamos, New Mexico, 95 pp.
- Nitsche H., Roberts, K., Becraft, K., Pussin, T., Keeney, D., Carpenter, S. A., and Hobart, D. E., 1995, "Comparison of Solubilities and Speciations from Oversaturation and Undersaturation Experiments of Neptunium, Plutonium, and Americium in UE-25p #1 Well Water at 60° C from the Yucca Mountain Region," Milestone Report 3412, WBS 1.2.3.4.1.3.1, LA-LBL-TIP-94-001, January, 1995, Lawrence Berkeley Laboratory, Berkeley, California, 85p.
- NRC (U. S. Nuclear Regulatory Commission), 1981. Estimates of Internal Dose Equivalent to 22 Target Organs for Radionuclides Occurring in Routine Releases from Fuel-cycle Facilities, Vol. III., Dunning D. Killough G., Bernard S., Pleasant J., and Walsh P., NUREG/CR-150 Vol. 3, (ORNL/GUREG/TM-190/V3, US NRG, Washington, D.C.
- NRC (U. S. Nuclear Regulatory Commission), 1993. "Disposal of High-Level Radioactive Wastes in Geologic Repositories," Part 60, Title 10, Chapter 1, Code of Federal Regulations, Washington, D.C.
- NRC (U. S. Nuclear Regulatory Commission), 1995. "Iterative Performance Assessment: Phase II", Draft report. Washington, D.C.
- Nuttall, H. E., R. Jain, and Y. Fertelli, 1991. "Radiocolloid Transport in Saturated and Unsaturated Fractures," Proceedings of the Second Annual International Conference on High Level Radioactive Waste Management, Las Vegas, Nevada, April 28-May 3, Vol. 1, pp. 189-196. (NNA.930625.0031)
- Ogard, A. E., and J. F. Kerrisk, 1984. "Groundwater Chemistry Along Flow Paths Between a Proposed Repository Site and the Accessible Environment," LA-10188-MS, UC-70, Los Alamos National Laboratory, Los Alamos, New Mexico.
- Ogard, A. E., 1987. "Importance of Radionuclide Transport by Particulates Entrained in Flowing Groundwaters," Groundwater Chemistry at Yucca Mountain, Nevada, and Vicinity," J. F. Kerrisk, LA-10929-MS, Los Alamos National Laboratory, Los Alamos, New Mexico, pp. 114-118. (NNA.83067.0078)

- Ortiz, T. S., R. L. Williams, F. B. Nimick, B. C. Whittet, and D. L. South, 1985. "A Three-Dimensional Model of Reference Thermal/Mechanical and Hydrological Stratigraphy at Yucca Mountain, Southern Nevada," SAND84-1076, Sandia National Laboratories, Albuquerque, New Mexico.
- Pei-Lin, T., M. D. Siegel, C. D. Updegraf, K. K. Wahi, and R. V. Guzowski, 1985. "Repository Site Data Report for Unsaturated Tuff, Yucca Mountain, Nevada," NUREG/CR-4410, U.S. Nuclear Regulatory Commission, Washington, D.C. (HQS.880517.1853)
- Penrose, W. R., W. L. Polzer, E. H. Essington, D. M. Nelson, and K. A. Orlandini, 1990. "Mobility of Plutonium and Americium Through a Shallow Aquifer in a Semiarid Region," Environmental Science and Technology, Vol. 24, pp. 228-234. (NNA.830607.0058)
- Pereira D., O. Nobre, and E. Almeida, 1993. "Atmospheric Corrosion of Mild Steel: What Can We Do?," Progress in the Understanding and Prevention of Corrosion, J. M. Costa and A. D. Mercer (eds.), Vol. 1, pp. 66-75.
- Peters, C. A., Yang, I. C., Higgins, J. D., and Burger, P. A., 1992. "A Preliminary Study of the Chemistry of Pore Water Extracted from Tuff by One-Dimensional Compression," Proceedings of the Seventh International Symposium on Water-Rock Interaction, Vol. 1, pp. 741-745, Y. K. Kharaka and A. Maest (eds.), U.S. Geological Survey, Menlo Park, California.
- Phipps, P. B., and D. W. Rice, 1979. "The Role of Water in Atmospheric Corrosion," Corrosion Chemistry, G. R. Brubaker, and P. B. Phipps (eds.), ACS Symposium Series 89, American Chemical Society, pp. 235-261.
- Pigford, T. H., 1993. "The Engineered Barrier System: Performance Issues," Scientific Basis for Nuclear Waste Management XVI, Materials Research Society Symposium Proceedings, Vol. 294, pp. 657-662, C.G. Interrante and R.T. Pabalan (eds.), Materials Research Society, Pittsburgh, Pennsylvania.
- Pourbaix, M., 1966. "Atlas of Electrochemical Equilibrium in Aqueous Solutions," Pergamon Press, 644 pp.
- Prowell, G., 1994. Personal communication to J. H. Lee, December 28.
- Pruess, K., 1987. "TOUGH User's Guide," NUREG/CR-4645, Nuclear Regulatory Commission, Washington, D.C.
- Pruess, K., 1991. "TOUGH2 - A General -Purpose Numerical Simulator for Multiphase Fluid and Heat Flow," Lawrence Berkeley Laboratory, LBL-29400.

- Pruess, K., and Y. W. Tsang, 1993. "Modeling of Strongly Heat-Driven Flow Processes at a Potential High-Level Nuclear Waste Repository at Yucca Mountain," Proceedings of the Fourth International High Level Radioactive Waste Management Conference, Las Vegas, Nevada, April 26-30.
- Pruess, K., and Y. W. Tsang, 1994. "Thermal Modeling for a Potential High-Level Nuclear Waste Repository at Yucca Mountain, Nevada," LBL-35381, Lawrence Berkeley Laboratory, Berkeley, California.
- Pruess, K., Y. W. Tsang, and J. S. Y Wang, 1985. "Modeling of Strongly Heat-Driven Flow in Partially Saturated Fractured Porous Media," *Memoirs, International Association of Hydrogeologists*, XXVII, pp. 486-497.
- Pryor, M. J., and M. Cohen, 1953. "The Inhibition of the Corrosion of Iron by Some Anodic Inhibitors," Journal of the Electrochemical Society, Vol. 100, No. 5, pp. 203-215.
- Pyke, R., and M. Cohen, 1948. "Rate of Breakdown and Mechanism of Nitrite Inhibition of Steel Corrosion," Transaction of Electrochemical Society, Vol. 93, No. 3, pp. 63-78.
- Ramsay, J. D., 1988. "The Role of Colloids in the Release of Radionuclides from Nuclear Waste", Radiochimica Acta, Vol. 44/45, pp. 165-170. (NNA.930701.0050)
- Reeves, M., N. A. Baker, and J. O Duguid, 1994. "Review and Selection of Unsaturated Flow Models," B00000000-01425-2200-00001, Rev. 00, CRWMS M&O, Las Vegas, Nevada.
- Robinson, B. A., A. V. Wolfsberg, G. A. Zyvoloski, and C. W. Gable, 1995. "An Unsaturated Zone Flow and Transport Model of Yucca Mountain," Draft Report, Milestone 3468, Los Alamos National Laboratory, Los Alamos, New Mexico.
- Ruijini, G., S. C. Srivastava, and M. B. Ives, 1989. "Pitting Corrosion Behavior of UNS No. 8904 Stainless Steel in a Chloride/Sulfate Solution," Corrosion, Vol. 45, No. 11, pp. 874-882.
- Rush, F. E., 1970. "Regional Ground-Water Systems in the Nevada Test Site Area, Nye, Lincoln, and Clark Counties, Nevada," Department of Conservation and Natural Resources Water Resources Reconnaissance Report 54, State of Nevada, 25 pp
- Rush, F. B., B. R. Scott, A. S. Van Denburgh, and B. J. Vasey, 1971. "State of Nevada Water Resources and Interbasin Flows," Nevada Division Water Research Map, 1:750,000, State of Nevada.
- Ryder, E. E., 1993. "Comparison of Predicted Far-field Temperatures for Discrete and Smeared Heat Sources", Proceedings of the Fourth International High-Level Radioactive Waste Management Conference, Las Vegas, Nevada.

- SAIC (Science Applications International Incorporated), 1986. "Preliminary Socioeconomic Profile of Nye County, Nevada: Community Services," DOE/NV/10270-3, Las Vegas, Nevada.
- Santanam, L., S. Raghavan, and B. A. Chin, 1992. "Zircaloy Cladding Rupture During Repository Storage," Nuclear Technology, Vol. 97, pp. 316-322.
- Sassani, D. C., 1992. "Petrologic and Thermodynamic Investigation of the Aqueous Transport of Platinum-Group Elements During Alteration of Mafic Intrusive Rocks," Ph.D. Dissertation, Washington University, St. Louis, Missouri, University Microfilms, 1100 p.
- Saterlie, S. F., 1994. "Integration of Thermal Calculations," TRW IOC LV.SEA.SFS.12/94-134, TRW Environmental Safety Systems, Las Vegas, Nevada.
- Scanlon, B. R., 1995. "Review of Unsaturated Zone Studies in Arid Sites and Implications for Contaminant Transport," Presented to Nuclear Waste Technical Review Board, San Francisco, California, June.
- Schenker, A. R., D. C. Guerin, T. H. Robey, C. A. Rautman, and R. W. Barnard, 1995. "Stochastic Hydrogeologic Units and Hydrogeologic Properties Development for Total System Performance Assessments," SAND94-0244, Sandia National Laboratories, Albuquerque, New Mexico.
- Scott, R. B., and J. Bonk, 1984. "Preliminary Geologic Map of Yucca Mountain with Geologic Sections, Nye County, Nevada," Open-file Report 84-494, U.S. Geological Survey, Las Vegas, Nevada.
- Siegel, M. D., D. B. Ward, W. C. Cheng, C. Bryant, C. S. Chocas, and C. G. Reynolds, 1993. "Preliminary Characterization of Materials for Reactive Transport Model Validation Experiment," High Level Radioactive Waste Management. Proceedings of the Fourth Annual International Conference, Las Vegas, Nevada, April 26-30, American Nuclear Society, La Grange Park, Illinois. (NNA.870519.0076)
- Sinnock, S., 1995. "The Many Barriers of Yucca Mountain," Proceedings of the Sixth International High Level Radioactive Waste Management Conference, Las Vegas, Nevada, pp. 281-283.
- SNL (Sandia National Laboratories), 1987. "Nevada Nuclear Waste Storage Investigations Project, Site Characterization Plan Conceptual Design Report," SAND84-2641, Sandia National Laboratories, Albuquerque, New Mexico, September.
- Southwell, C. R., and A. L. Alexander, 1970. "Corrosion of Metals in Tropical Waters. Structural Ferrous Metals," Materials Protection, pp. 14-23, January.

- Southwell, C. R., and J. D. Bultman, 1982. "Atmospheric Corrosion Testing in the Tropics," Atmospheric Corrosion, W. H. Ailor (ed.), Wiley-Interscience, pp. 943-967.
- Southwell, C. R., J. D. Bultman, and A. L. Alexander, 1976. "Corrosion of Metals in Tropical Environments - Final Report of 16-Year Exposures," Materials Performance, pp. 9-26, July.
- Stahl, D., 1993. "Waste Package Corrosion Inputs," CRWMS M&O Interoffice Correspondence, IOC LV.WP.DS.06/93.107, June 21.
- Stahl, D., 1995. "Demonstrating Compliance with the Controlled Release Requirements," Presentation at the DOE/NRC Technical Exchange on EBS Release Rates and Waste Form Testing, June 28-29, Las Vegas, Nevada.
- Statistical Sciences, 1993. "A Gentle Introduction to S-PLUS for Windows, Version 3.2," StatSci, a Division of MathSoft, Inc., Seattle, Washington.
- Steward, S. A., and W. J. Gray, 1994. "Comparison of Uranium Dissolution Rates from Spent Fuel and Uranium Dioxide," Proceedings of the Fifth International Conference on High-Level Radioactive Waste Management, Las Vegas, Nevada, May 22-26, 1994, American Nuclear Society, La Grange Park, Illinois, and American Society of Civil Engineers, New York, New York, Vol. 4, pp. 2602-2608.
- Stumm, W., and Morgan, J. J., 1981, Aquatic Chemistry, 2nd edition, John Wiley & Sons Inc., New York, 780 p.
- Strum, M. J., H. Weiss, J. C. Farmer, and D. B. Bullen, 1988. "Survey of Degradation Modes of Candidate Materials for High-Level Radioactive-Waste Disposal Containers. Vol. 7: Weldability of Austenitic Alloys," UCID-21362, Lawrence Livermore National Laboratory, Livermore, CA, June.
- Strutt, J. E., J. R. Nichols, and B. Barbier, 1985. "The Prediction of Corrosion by Statistical Analysis of Corrosion Profiles," Corrosion Science, Vol. 25, pp. 305-315.
- Szklarska-Smialowska, Z., 1986. "Pitting Corrosion of Metals", National Association of Corrosion Engineers, Houston, Texas.
- Taylor, P., R. J. Lemire, and D. D. Wood, 1993. "The Influence of Moisture on Air Oxidation of UO₂: Calculations and Observations," Nuclear Technology, Vol. 104, pp. 164-170.
- Taylor, P., D. D. Wood, A. M. Duclos, and D. G. Owen, 1989. "Formation of Uranium Trioxide Hydrates on UO₂ Fuel in Air-Steam Mixtures Near 200 °C," Journal of Nuclear Materials, Vol. 168, pp. 70-75.

- Thompson, J. L., 1989. "Actinide Behavior on Crushed Rock Columns," Journal of Radioanalytical and Nuclear Chemistry, Vol. 130, No. 2, pp. 353-364. (NNA.920131.0401)
- Townsend, H. E., and J. C. Zoccola, 1982. "Eight-Year Atmospheric Corrosion Performance of Weathering Steel in Industrial, Rural and Marine Environments," Atmospheric Corrosion of Metals, ASTM STP 767, S.W. Dean, Jr. and E.C. Rhea (eds.), American Society for Testing and Materials, pp. 45-59.
- Tri, N. Q., V. D. Huy, L. V. Cuong, and P. Th. San, 1993. "Atmospheric Corrosion Testing in Vietnam," Progress in the Understanding and Prevention of Corrosion, J.M. Costa and A.D. Mercer (eds.), Vol. 1, pp. 105-114.
- Triay, I. R., D. E. Hobart, A. J. Mitchell, T. W. Newton, M. A. Ott, P. D. Palmer, R. S. Rundberg, and J. L. Thompson, 1991. "Size Determinations of Plutonium Colloids Using Autocorrelation Photon Spectroscopy," Radiochimica Acta, Vol. 52/53, pp. 127-131.(NNA.930607.0060)
- Triay, I. R., C.R. Cotter, M.H. Huddleston, D.E. Leonard, S.C. Weaver, S.J. Chipera, D.L. Bish, A. Meijer, and J.A. Canepa, 1995a. "Neptunium Transport through Yucca Mountain Tuffs I: Batch Sorption Results," Milestone #3349, Los Alamos National Laboratory, Los Alamos, New Mexico.
- Triay, I. R., C.R. Cotter, S.M. Kraus, M.H. Huddleston, S.J. Chipera, and D.L. Bish, 1995b. "Report on Radionuclide Sorption in Yucca Mountain Tuffs with J-13 Well Water: Neptunium, Uranium and Plutonium," Milestone # 3338, Los Alamos National Laboratory, Los Alamos, New Mexico.
- Triay, I. R., A. Furlano, S.C. Weaver, S.J. Chipera, and D.L. Bish, 1995c. "Report on the Study of Kinetic Effects using crushed Tuff Columns: Neptunium in Sodium Bicarbonate Waters," Milestone # 3041, Los Alamos National Laboratory, Los Alamos, New Mexico.
- Triay, I., Simmons, A., Levy, S., Nelson, S., Nuttal, H., Robinson, B., Steinkampf, W., and Viani, B., 1995a, "Colloid-Facilitated Radionuclide Transport at Yucca Mountain", Los Alamos National Laboratory Report LA-12779-MS, UC-802, April, 1995.
- Triay, I., Degueldre, C., Wistrom, A., Cotter, C., and Lemons, W., 1995b, "Progress Report on Colloid-Facilitated Transport at Yucca Mountain," Milestone Report 3383, Draft #2, (LA000000000128.001).
- Tsang, Y. W., and K. Pruess, 1989. "Preliminary Studies of Gas Phase Flow Effects and Moisture Migration at Yucca Mountain, Nevada," LBL-28819, Lawrence Berkeley Laboratory, Berkeley, California.

- Tsang, Y. W., and K. Pruess, 1990. "Further Modeling Studies of Gas Phase Flow Effects and Moisture Migration at Yucca Mountain, Nevada," LBL-29127, Lawrence Berkeley Laboratory, Berkeley, California.
- van Genuchten, M. Th., 1980. "A Closed-Form Equation for Predicting the Hydraulic Conductivity of Unsaturated Soils," Soil Science Society American Journal, Vol. 44, pp. 892-898.
- van Genuchten, M. Th., and D. R. Nielsen, 1985. "On Describing and Predicting the Hydraulic Properties of Unsaturated Soils," Annales Geophysicae, Vol. 3, No. 5, pp. 615-628.
- Van Konynenburg, R. A., C. Smith, H. Culham, and C. Otto, Jr., 1986. "Behavior of Carbon-14 in Waste Packages for Spent Fuel in a Repository in Tuff," Scientific Basis for Nuclear Waste Management VIII, J. Jantzen, J. Stone, and R. Ewing (eds.), pp. 405-412.
- Van Konynenburg, R. A., C. F. Smith, H. W. Culham, and H. D. Smith, 1987. "Carbon-14 in Waste Packages for Spent Fuel in a Tuff Repository," Scientific Basis for Nuclear Waste Management X, J.K. Bates and W.B. Seefeld, (eds.), Vol. 84, Materials Research Society, Pittsburgh, Pennsylvania.
- Van Konynenburg, R. A., R. D. McCright, A. K. Roy, and D. A. Jones, 1995. "Engineered Materials Characterization Report for the Yucca Mountain Site Characterization Project: Volume 1. Introduction, History, and Current Candidates," UCRL-ID-119564, Vol. 1, Lawrence Livermore National Laboratory, Livermore, California, August.
- Van Konynenburg, R. A., 1995. Personal communication to J.H. Lee, August 21.
- Vernon, W. H., 1933. "The Role of the Corrosion Product in the Atmospheric Corrosion of Iron," Transactions of the Electrochemical Society, Vol. 64, pp. 31-41.
- Vilks, P., 1994. "The Role of Colloids and Suspended Particles in Radionuclide Transport in the Canadian Concept for Nuclear Fuel Waste Disposal," AECL-10280, Whiteshell Laboratory, Atomic Energy of Canada, Ltd., Pinawa, Manitoba.
- Vinsome, P. K., and J. Westerveld, 1980. "A Simple Method for Predicting Cap and Base Rock Heat Losses in Thermal Reservoir Simulators," Journal of Canadian Petroleum Technology, pp. 87-90, July-September.
- Waddel, R. K., 1982. "Two-Dimensional, Steady-State Model of Ground-Water Flow, Nevada Test Site and Vicinity," USGS-WRI-82-4085, U.S. Geological Survey, 72 pp.
- Waddel, R. K., J. H. Robison, and R. K. Blankennagel, 1984. "Hydrology of Yucca Mountain and Vicinity," Nevada-California--Investigative Results Through Mid-1983, USGS-WRI-84-4267, U.S. Geological Survey.

- Walker, G. E., and T. E. Eakin, 1963. "Geology and Ground Water of Amargosa Desert," Nevada-California, Department of Conservation and Natural Resources, Ground-Water Resources Reconnaissance Series Report 14, State of Nevada, Carson City, Nevada.
- Wan, J., and J. L. Wilson, 1994, "Colloid Transport in Unsaturated Porous Media," *Water Resources Research*, v. 30(4), pp. 857-864.
- Wang, J. S., and T. N. Narasimhan, 1993. "Processes, Mechanisms, Parameters and Modeling Approaches for Partially Saturated Flow in Soil and Rock Media," SAND88-7054, Sandia National Laboratories, Albuquerque, New Mexico.
- Wanner, H., and Forest, I., 1992, "Chemical Thermodynamics of Uranium Vol. 1", North-Holland Elsevier Science Publishers, The Netherlands.
- Was, G. S., R. Christensen, C. Park, and R. W. Smith, 1985. "Statistical Patterns of Fuel Failure in Stainless Steel Clad Light Water Reactor Fuel Rods," *Nuclear Technology*, Vol. 71, pp. 445-457.
- Wasywich, K. M., W. H. Hocking, D. W. Shoesmith, and P. Taylor, 1993. "Differences in Oxidation Behavior of Used CANDU Fuel During Prolonged Storage in Moisture-Saturated Air and Dry Air at 150 °C," *Nuclear Technology*, Vol. 104, pp. 309-329.
- Wei, F. I., 1991. "Atmospheric Corrosion of Carbon Steels and Weathering Steels in Taiwan," *British Corrosion Journal*, Vol. 26, No. 3, pp. 209-214.
- West, K. A., 1988. "Nevada Nuclear Waste Storage Investigations Exploratory Shaft Facility Fluids and Materials Evaluation," LA-11398-MS, November 1988.
- Westinghouse Electrical Co., 1982. "Conceptual Waste Package Designs for Disposal of Nuclear Waste in Tuff," Report AESD-TME-3138, Appendix B, pp. 353-380, September.
- Wilson, C. N., 1987, "Results from Cycles 1 and 2 of NNWSI Series 2 Dissolution Tests", HEDL-TME85-22, May, 1985.
- Wilson, C. N., 1990, "Results from the NNWSI Series 3 Spent Fuel Dissolution Tests", Pacific Northwest Laboratory Report PNL-7170, June 1990.
- Wilson, M. L., J. H. Gauthier, R. W. Barnard, G. E. Barr, H. A. Dockery, E. Dunn, R. R. Eaton, D. C. Guerin, N. Lu, M. J. Martinez, R. Nilson, C. A. Rautman, T. H. Robey, B. Ross, E. E. Ryder, A. R. Schenker, S. A. Shannon, L. H. Skinner, W. G. Halsey, J. Gansemer, L. C. Lewis, A. D. Lamont, I. R. Triay, A. Meijer, and D. E. Morris, 1994. "Total System Performance Assessment for Yucca Mountain - SNL Second Iteration (TSPA-1993)," SAND93-2675, Sandia National Laboratories, Albuquerque, New Mexico.

- Winograd, I. J., and I. Friedman, 1972. "Deuterium as a Tracer of Regional Ground-Water Flow, Southern Great Basin, Nevada-California," Geological Society America Bulletin, Vol. 83, No. 12, pp. 3691-3708.
- Winograd, I. J., and W. Thordarson, 1975. "Hydrogeologic and Hydrochemical Framework, South-Central Great Basin, Nevada-California, with Special Reference to the Nevada Test Site," U.S. Geological Survey Professional Paper 712-C, U.S. Government Printing Office, Washington, D.C., pp. C1-C126.
- Wittwer, C., G. Chen, G. S. Bodvarsson, M. Chornack, A. Flint, L. Flint, E. Kwicklis, and R. Spengler, 1995. "Development of the LBL-USGS Three-Dimensional Site-Scale Groundwater Flow Model of Yucca Mountain, Nevada," LBL-37356/UC-814, Lawrence Berkeley Laboratory, Berkeley, California.
- Xiang, Y., S. Mishra, and B. Dunlap, 1995. Hydrologic Sensitivity Analyses for the Unsaturated Zone at Yucca Mountain, Nevada, B00000000-01717-2200-00099, Rev. 00, Civilian Radioactive Waste Management System, Management and Operating Contractor, Las Vegas, Nevada.
- Yang, I. C., A. K. Turner, T. M. Sayre, and P. Montazer, 1988. "Triaxial-Compression Extraction of Pore Water from Unsaturated Tuff, Yucca Mountain, Nevada," USGS Water-Resources Investigations Report 88-4189, U.S. Geological Survey.
- Yang, I. C., G. S. Davis, and T. M. Sayre, 1990. "Comparison of Pore-Water Extraction by Triaxial Compression and High-speed Centrifugation Methods," Proceedings of Conference on Minimizing Risk to the Hydrology Environment," American Institute of Hydrology, pp. 250-259.
- Yunker, J. L., W. B. Andrews, G. A. Fasano, C. C. Herrington, S. R. Mattson, R. C. Murray, L. B. Ballou, M. A. Revelli, A. R. Ducharme, L. E. Shephard, W. W. Dudley, D. T. Hoxie, R. J. Herbst, E. A. Patera, B. R. Judd, J. A. Docka, and L. D. Rickertsen, 1992. "Report of Early Site Suitability Evaluation of the Potential Repository Site at Yucca Mountain, Nevada," SAIC-91/8000, Technical and Management Support Services, Science Applications International Corporation, Las Vegas, NV.
- Yunker, J. L., 1995. "Waste Containment and Isolation Strategy for the Yucca Mountain Site," Presentation at the Nuclear Waste Technical Review Board Meeting, October 17-18, Arlington, Virginia.
- Zyvoloski, G., Z. Dash, and S. Kelkar, 1995. "FEHM 1.0, Finite Element Heat and Mass Transfer Code," LA-12062-MS, Rev.1, Los Alamos National Laboratory, Los Alamos, New Mexico.

CODES AND REGULATIONS

40 CFR Part 191, "Environmental Standards for the Management and Disposal of Spent Nuclear Fuel, High-level and Transuranic Radioactive Wastes," Federal Register, Vol. 50, No. 182, September 19, 1985, pp. 38066-38089.

ACRONYM LIST

AE	Accessible Environment
APD	Areal Power Density
AECL	Atomic Energy of Canada Limited
AML	Areal Mass Loading
BWR	Boiling Water Reactor
CAM	Corrosion Allowance Material
CCDF	Complementary Cumulative Distribution Function
CDA	Controlled Design Assumption
CFR	Code of Federal Regulations
CIDP	Center In Drift On Pedestal
CH _n	Calico Hills nonwelded
CH _v	Calico Hills nonwelded-vitric (also Ch _{nv})
CH _z	Calico Hills nonwelded-zeolitic (also Ch _{nz})
CRM	Corrosion Resistant Material
1-D	One-dimensional
2-D	Two-dimensional
3-D	Three-dimensional
DF	Degree of Freedom
DHLW	Defense High-Level Waste
DOE	Department of Energy
EBS	Engineered Barrier System
ECM	Equivalent Continuum Model
EPA	Environmental Protection Agency
EPRI	Electric Power Research Institute
ESF	Exploratory Studies (Shaft) Facility
FEHM	Finite Element Heat and Mass Transfer
FEP	Features, Events, and Processes
GAI	Golder Associates, Inc.
GWd	Giga Watt days
HLW	High-Level Waste
IAEA	International Atomic Energy Agency
ICRP	International Commission on Radiation Protection
LBL	Lawrence Berkeley Laboratory
LANL	Los Alamos National Laboratory
LLNL	Lawrence Livermore National Laboratory

MCRM	Moderately Corrosion Resistant Material
MIC	Microbiologically Influenced Corrosion
M&O	Management & Operating Contractor
MGDS	Mined Geologic Disposal System
MPC	Multi-Purpose Canister
MTHM	Metric Tons Heavy Metal
MTU	Metric Tons of Uranium
MWd	Mega Watt days
NAGRA	Swiss National Cooperative for the Disposal of Radioactive Waste
NAS	National Academy of Science
NRC	Nuclear Regulatory Commission
OCRWM	Office of Civilian Radioactive Waste Management
PNC	Power Reactor and Nuclear Fuel Development Corporation (Japan)
PNL	Pacific Northwest Laboratory
PPn	Prow Pass nonwelded
PTn	Paintbrush nonwelded
PWR	Pressurized Water Reactor
RH	Relative Humidity
RIP	Repository Integration Program
RSS	Residual Sum of Squares
SKB	Svensk Karnbranslehantering AB (Sweden)
SNF	Spent Nuclear Fuel
SNL	Sandia National Laboratory
SZ	Saturated Zone
SolWoG	Solubility Working Group
T	Temperature
TCw	Tiva Canyon welded
TSA	Total System Analyzer
TSPA	Total System Performance Assessment
TSv	Topopah Spring welded-vitrophyre
TSw	Topopah Spring welded
TVO	Teollisuuden Voima Oy (Finland)
USGS	U.S. Geological Survey
UZ	Unsaturated Zone
VG	Van Genuchten
WIPP	Waste Isolation Pilot Plant
WP	Waste Package
Yr	Year

Prepared - 10/31/95:17:16:32

P&S Account No.	- 1.2.5.4.1 TR	BASELINE Start Date - 10/01/95 BASELINE Finish Date - 09/30/96 Element ID - TR541
P&S Account Title	- Total System Performance Assessment	
WBS No.	- 1.2.5.4.1	
WBS Title	- Total System Performance Assessment	

Annual Budget	Fiscal Year Distribution												At Complete 2088
	Prior 0	FY1996 2088	FY1997 0	FY1998 0	FY1999 0	FY2000 0	FY2001 0	FY2002 0	FY2003 0	FY2004 0	FY2005 0	Future 0	

Statement of Work:

In FY 1996, perform preliminary, pre-decisional work that will allow the performing of analyses that demonstrate with reasonable assurance that the total containment system designs will meet the regulatory requirements. Assist in the review and further development of total system performance allocations utilizing input from waste package, site and repository performance assessment activities. Develop, verify, validate, benchmark, and document codes for assessing the performance of the repository, as needed. Identify and prioritize data required for performance assessment, utilizing appropriate uncertainty-analysis techniques. Maintain awareness of international technical advances in the area of performance assessment, and integrate into appropriate. Coordinate and manage the total system PA activity performed by subcontractors and other participant organizations.

ALL DELIVERABLES ACCEPTED IAW DOE PROCEDURES FOR ACCEPTANCE REVIEWS, UNLESS OTHERWISE NOTED.

Integrate physical process submodels and data into computational models for prediction of total system postclosure performance (including uncertainties). Assess whether the Yucca Mountain MGDS will meet the overall system performance objective of 10 CFR 60.112 and the protection requirements of EPA 40 CFR 191.15 and 191.16.

DESCRIPTION OF WORK:

- o Develop a methodology for performance assessment.
- o Conduct preliminary identification of significant events.
- o Conduct preliminary identification of release-scenario classes (Performance Assessment Activity 1.1.2.1).
- o Conduct preliminary assessments of total-system performance.
- o Develop preliminary models for releases along aqueous pathways.
- o Develop preliminary model for gas-phase releases.
- o Develop preliminary model for releases through basaltic igneous activity.
- o Develop preliminary model for releases through tectonic activity.
- o Develop preliminary model for releases through human intrusion.
- o Screen preliminary scenario classes (Performance Assessment Activity 1.1.2.2).
- o Develop preliminary simplified mathematical models (Performance Assessment Activity 1.1.3.1).
- o Develop preliminary formulation of simplified radionuclide source term (Performance Assessment Activity 1.1.3.1).
- o Select release-scenario classes (Performance Assessment Activity 1.1.4.1).
- o Develop model for releases along water pathways.
- o Develop model for gas-phase releases.
- o Develop model for releases through basaltic igneous activity.
- o Develop model for releases through tectonic activity.
- o Develop model for releases through human intrusion.
- o Perform final screening of scenario classes (Performance Assessment Activity 1.1.4.1).
- o Provide final versions of simplified mathematical models (Performance Assessment Activity 1.1.4.2).
- o Calculate transport through and doses from the ground-water pathway (Performance Assessment Activity 1.2.1.1).
- o Calculate transport through and doses from the gaseous-release pathway (Performance Assessment Activities 1.2.2.1 and

Prepared - 10/31/95:17:16:32

P&S Account No. - 1.2.5.4.1 TR -Total System Performance Assessment

Statement of Work (cont.):

- 1.2.2.2).
- o Calculate the quantity of waste products that could be transported to a special source of ground water during the first 1000 years after disposal (Performance Assessment Activity 1.3.2.1.1).
 - o Construct a total-system simulator (Performance Assessment Activity 1.1.5.1.1).
 - o Construct joint probability distributions (Performance Assessment Activity 1.1.5.1.2).
 - o Perform iterative calculations to produce empirical complementary cumulative distribution functions (Performance Assessment Activity 1.1.5.1.3).
 - o Refine the formulation of a simplified radionuclide source term using information from the ESF and advanced conceptual design of the waste package.
 - o Develop methods for the use of expert judgement.

DELIVERABLES

Deliv ID	Description/Completion criteria.	Due Date
T6520	Seismic Activity Scenarios Criteria - Submit draft report on seismic activity scenarios to DOE.	29-Mar-96
T6521	CRWMS M&O/TRW Total System Performance Assessment- Criteria - Final Total System Performance Assessment-1995 report submitted to DOE for review.	10-Nov-95
T6522	Total System Performance Assess. Invest. Analysis Criteria - Provide presentation on assumptions, module development, uncertainties, and approach for the Total System Performance Assessment - Investment Analysis.	13-Sep-96
T6523	CRWMS M&O Test Model Abstractions for Total System Criteria - Complete draft white paper discussing development of total-system models from subsystem and process-level models for the Investment Analysis.	30-May-96

Participant M0567

Yucca Mtn. Site Char. Project-Planning & Control System
PACS Participant Work Station (PPWS)
Participant Planning Sheet (PSA03)

01-Sep-95 to 30-Sep-95
Page - 3
Inc. Dollars in Thousands

Prepared - 10/31/95:17:16:32

P&S Account No. - 1.2.5.4.1 TR -Total System Performance Assessment

DELIVERABLES

Deliv ID	Description/Completion criteria	Due Date
T6526	Description of Performance Allocation Criteria - This work will be documented in a draft white paper quantifying the relative contribution of each barrier to the overall system performance and focus on those aspects of the waste isolation and containment strategy that are most robust and where additional information should be expected to reduce the uncertainty in the predicted results.	13-Sep-96

Approvals

Jean L. Younker 10-31-95
Preparer - print name Date

Technical Reviewer - print name Date

QA Reviewer - print name Date

Jean Younker
Preparer - Signature

Technical Reviewer - Signature

QA Reviewer - Signature Date